Hashemite Kingdom of Jordan

Jordan Journal of Biological Sciences

An International Peer-Reviewed Scientific Journal

Financed by the Scientific Research and Innovation Support Fund

This title is indexed in Scopus

http://jjbs.hu.edu.jo/

المجلة الأردنية للعلوم الحياتية
Jordan Journal of Biological Sciences (JJBS)
http://jjbs.hu.edu.jo

Jordan Journal of Biological Sciences (JJBS) (ISSN: 1995–6673 (Print); 2307-7166 (Online)): An International Peer- Reviewed Open Access Research Journal financed by the Scientific Research and Innovation Support Fund, Ministry of Higher Education and Scientific Research, Jordan and published quarterly by the Deanship of Scientific Research , The Hashemite University, Jordan.

Submission Address
Professor Atoum, Manar F
The Hashemite Universit y
P.O. Box 330127, Zarqa, 13115, Jordan
Phone: +962-5-3903333 ext.4147
E-Mail: jjbs@hu.edu.jo

المجلة الاردنية للعلوم الحياتية
Jordan Journal of Biological Sciences (JJBS)
http://jjbs.hu.edu.jo

International Advisory Board (Arranged alphabetically)

Instructions to Authors

Scopes

Study areas include cell biology, genomics, microbiology, immunology, molecular biology, biochemistry, embryology, immunogenetics, cell and tissue culture, molecular ecology, genetic engineering and biological engineering, bioremediation and biodegradation, bioinformatics, biotechnology regulations, gene therapy, organismal biology, microbial and environmental biotechnology, marine sciences. The JJBS welcomes the submission of manuscript that meets the general criteria of significance and academic excellence. All articles published in JJBS are peer-reviewed. Papers will be published approximately one to two months after acceptance.

Type of Papers

The journal publishes high-quality original scientific papers, short communications, correspondence and case studies. Review articles are usually by invitation only. However, Review articles of current interest and high standard will be considered.

Submission of Manuscript

Manuscript, or the essence of their content, must be previously unpublished and should not be under simultaneous consideration by another journal. The authors should also declare if any similar work has been submitted to or published by another journal. They should also declare that it has not been submitted/ published elsewhere in the same form, in English or in any other language, without the written consent of the Publisher. The authors should also declare that the paper is the original work of the author(s) and not copied (in whole or in part) from any other work. All papers will be automatically checked for duplicate publication and plagiarism. If detected, appropriate action will be taken in accordance with International Ethical Guideline. By virtue of the submitted manuscript, the corresponding author acknowledges that all the co-authors have seen and approved the final version of the manuscript. The corresponding author should provide all co-authors with information regarding the manuscript, and obtain their approval before submitting any revisions. Electronic submission of manuscripts is strongly recommended, provided that the text, tables and figures are included in a single Microsoft Word file. Submit manuscript as e-mail attachment to the Editorial Office at: JJBS@hu.edu.jo. After submission, a manuscript number will be communicated to the corresponding author within 48 hours.

Peer-review Process

It is requested to submit, with the manuscript, the names, addresses and e-mail addresses of at least 4 potential reviewers. It is the sole right of the editor to decide whether or not the suggested reviewers to be used. The reviewers' comments will be sent to authors within 6-8 weeks after submission.
Manuscripts and figures for review will not be returned to authors whether the editorial decision is to accept, revise, or reject. All Case Reports and Short Communication must include at least one table and/ or one figure.

Preparation of Manuscript

The manuscript should be written in English with simple lay out. The text should be prepared in single column format. Bold face, italics, subscripts, superscripts etc. can be used. Pages should be numbered consecutively, beginning with the title page and continuing through the last page of typewritten material.

The text can be divided into numbered sections with brief headings. Starting from introduction with section 1. Subsections should be numbered (for example 2.1 (then 2.1.1, 2.1.2, 2.2, etc.), up to three levels. Manuscripts in general should be organized in the following manner:

Title Page

The title page should contain a brief title, correct first name, middle initial and family name of each author and name and address of the department(s) and institution(s) from where the research was carried out for each author. The title should be without any abbreviations and it should enlighten the contents of the paper. All affiliations should be provided with a lower-case superscript number just after the author's name and in front of the appropriate address.
The name of the corresponding author should be indicated along with telephone and fax numbers (with country and area code) along with full postal address and e-mail address.

Abstract

The abstract should be concise and informative. It should not exceed **350 words** in length for full manuscript and Review article and **150 words** in case of Case Report and/ or Short Communication. It should briefly describe the purpose of the work, techniques and methods used, major findings with important data and conclusions. No references should be cited in this part. Generally non-standard abbreviations should not be used, if necessary they should be clearly defined in the abstract, at first use.

Keywords

Immediately after the abstract, **about 4-8 keywords** should be given. Use of abbreviations should be avoided, only standard abbreviations, well known in the established area may be used, if appropriate. These keywords will be used for indexing.

Abbreviations

Non-standard abbreviations should be listed and full form of each abbreviation should be given in parentheses at first use in the text.

Introduction

Provide a factual background, clearly defined problem, proposed solution, a brief literature survey and the scope and justification of the work done.

Materials and Methods

Give adequate information to allow the experiment to be reproduced. Already published methods should be mentioned with references. Significant modifications of published methods and new methods should be described in detail. Capitalize trade names and include the manufacturer's name and address. Subheading should be used.

Results

Results should be clearly described in a concise manner. Results for different parameters should be described under subheadings or in separate paragraph. Results should be explained, but largely without referring to the literature. Table or figure numbers should be mentioned in parentheses for better understanding.

Discussion

The discussion should not repeat the results, but provide detailed interpretation of data. This should interpret the significance of the findings of the work. Citations should be given in support of the findings. The results and discussion part can also be described as separate, if appropriate. The Results and Discussion sections can include subheadings, and when appropriate, both sections can be combined

Conclusions

This should briefly state the major findings of the study.

Acknowledgment

A brief acknowledgment section may be given after the conclusion section just before the references. The acknowledgment of people who provided assistance in manuscript preparation, funding for research, etc. should be listed in this section.

Tables and Figures

Tables and figures should be presented as per their appearance in the text. It is suggested that the discussion about the tables and figures should appear in the text before the appearance of the respective tables and figures. No tables or figures should be given without discussion or reference inside the text.

Tables should be explanatory enough to be understandable without any text reference. Double spacing should be maintained throughout the table, including table headings and footnotes. Table headings should be placed above the table. Footnotes should be placed below the table with superscript lowercase letters. Each table should be on a separate page, numbered consecutively in Arabic numerals.

Each figure should have a caption. The caption should be concise and typed separately, not on the figure area. Figures should be self-explanatory. Information presented in the figure should not be repeated in the table. All symbols and abbreviations used in the illustrations should be defined clearly. Figure legends should be given below the figures.

References

References should be listed alphabetically at the end of the manuscript. Every reference referred in the text must be also present in the reference list and vice versa. In the text, a reference identified by means of an author's name should be followed by the year of publication in parentheses (e.g.(Brown,2009)). For two authors, both authors' names followed by the year of publication (e.g.(Nelson and Brown, 2007)). When there are more than two authors, only the first author's name followed by "*et al*." and the year of publication (e.g. (Abu-Elteen *et al*., 2010)). When two or more works of an author has been published during the same year, the reference should be identified by the letters "a", "b", "c", etc., placed after the year of publication. This should be followed both in the text and reference list. e.g., Hilly, (2002a, 2002b); Hilly, and Nelson, (2004). Articles in preparation or submitted for publication, unpublished observations, personal communications, etc. should not be included in the reference list but should only be mentioned in the article text (e.g., Shtyawy,A., University of Jordan, personal communication). Journal titles should be abbreviated according to the system adopted in Biological Abstract and Index Medicus, if not included in Biological Abstract or Index Medicus journal title should be given in full. The author is responsible for the sccuracy and completeness of the references and for their correct textual citation. Failure to do so may result in the paper being withdraw from the evaluation process. Example of correct reference form is given as follows:-

Reference to a journal publication:

Bloch BK. 2002. Econazole nitrate in the treatment of *Candida vaginitis*. *S Afr Med J.* , **58**:314-323.

Ogunseitan OA and Ndoye IL. 2006. Protein method for investigating mercuric reductase gene expression in aquatic environments. *Appl Environ Microbiol*., **64**: 695-702.

Hilly MO, Adams MN and Nelson SC. 2009. Potential fly-ash utilization in agriculture. *Progress in Natural Sci.*, **19**: 1173-1186.

Reference to a book:

Brown WY and White SR.1985. **The Elements of Style**, third ed. MacMillan, New York.

Reference to a chapter in an edited book:

Mettam GR and Adams LB. 2010. How to prepare an electronic version of your article. In: Jones BS and Smith RZ (Eds.), **Introduction to the Electronic Age**. Kluwer Academic Publishers, Netherlands, pp. 281–304.

Conferences and Meetings:

Embabi NS. 1990. Environmental aspects of distribution of mangrove in the United Arab Emirates. Proceedings of the First ASWAS Conference. University of the United Arab Emirates. Al-Ain, United Arab Emirates.

Theses and Dissertations:

El-Labadi SN. 2002. Intestinal digenetic trematodes of some marine fishes from the Gulf of Aqaba. MSc dissertation, The Hashemite University, Zarqa, Jordan.

Nomenclature and Units

Internationally accepted rules and the international system of units (SI) should be used. If other units are mentioned, please give their equivalent in SI.

For biological nomenclature, the conventions of the *International Code of Botanical Nomenclature, the International Code of Nomenclature of Bacteria,* and the *International Code of Zoological Nomenclature* should be followed.
Scientific names of all biological creatures (crops, plants, insects, birds, mammals, etc.) should be mentioned in parentheses at first use of their English term.

Chemical nomenclature, as laid down in the *International Union of Pure and Applied Chemistry* and the official recommendations of the *IUPAC-IUB Combined Commission on Biochemical Nomenclature* should be followed. All biocides and other organic compounds must be identified by their Geneva names when first used in the text. Active ingredients of all formulations should be likewise identified.

Math formulae

All equations referred to in the text should be numbered serially at the right-hand side in parentheses. Meaning of all symbols should be given immediately after the equation at first use. Instead of root signs fractional powers should be used. Subscripts and superscripts should be presented clearly. Variables should be presented in italics. Greek letters and non-Roman symbols should be described in the margin at their first use.

To avoid any misunderstanding zero (0) and the letter O, and one (1) and the letter l should be clearly differentiated. For simple fractions use of the solidus (/) instead of a horizontal line is recommended. Levels of statistical significance such as: $^{*}P < 0.05$, $^{**}P < 0.01$ and $^{***}P < 0.001$ do not require any further explanation.

Copyright

Submission of a manuscript clearly indicates that: the study has not been published before or is not under consideration for publication elsewhere (except as an abstract or as part of a published lecture or academic thesis); its publication is permitted by all authors and after accepted for publication it will not be submitted for publication anywhere else, in English or in any other language, without the written approval of the copyright-holder. The journal may consider manuscripts that are translations of articles originally published in another language. In this case, the consent of the journal in which the article was originally published must be obtained and the fact that the article has already been published must be made clear on submission and stated in the abstract. It is compulsory for the authors to ensure that no material submitted as part of a manuscript infringes existing copyrights, or the rights of a third party.

Ethical Consent

All manuscripts reporting the results of experimental investigation involving human subjects should include a statement confirming that each subject or subject's guardian obtains an informed consent, after the approval of the experimental protocol by a local human ethics committee or IRB. When reporting experiments on animals, authors should indicate whether the institutional and national guide for the care and use of laboratory animals was followed.

Plagiarism

The JJBS hold no responsibility for plagiarism. If a published paper is found later to be extensively plagiarized and is found to be a duplicate or redundant publication, a note of retraction will be published, and copies of the correspondence will be sent to the authors' head of institute.

Galley Proofs

The Editorial Office will send proofs of the manuscript to the corresponding author as an e-mail attachment for final proof reading and it will be the responsibility of the corresponding author to return the galley proof materials appropriately corrected within the stipulated time. Authors will be asked to check any typographical or minor clerical errors in the manuscript at this stage. No other major alteration in the manuscript is allowed. After publication authors can freely access the full text of the article as well as can download and print the PDF file.

Publication Charges

There are no page charges for publication in Jordan Journal of Biological Sciences, except for color illustrations,

Reprints

Ten (10) reprints are provided to corresponding author free of charge within two weeks after the printed journal date. For orders of more reprints, a reprint order form and prices will be sent with article proofs, which should be returned directly to the Editor for processing.

Disclaimer

Articles, communication, or editorials published by JJBS represent the sole opinions of the authors. The publisher shoulders no responsibility or liability what so ever for the use or misuse of the information published by JJBS.

Indexing

JJBS is indexed and abstracted by:

DOAJ (Directory of Open Access Journals)	CABI
Google Scholar	EBSCO
Journal Seek	CAS (Chemical Abstract Service)
HINARI	ETH- Citations
Index Copernicus	Open J-Gat
NDL Japanese Periodicals Index	SCImago
SCIRUS	Clarivate Analytics (Zoological Abstract)
OAJSE	Scopus
ISC (Islamic World Science Citation Center)	AGORA (United Nation's FAO database)
Directory of Research Journal Indexing (DRJI)	SHERPA/RoMEO (UK)
Ulrich's	

المجلة الأردنية للعلوم الحياتية
Jordan Journal of Biological Sciences (JJBS)
ISSN 1995- 6673 (Print), 2307- 7166 (Online)
http://jjbs.hu.edu.jo

The Hashemite University

Deanship of Scientific Research

TRANSFER OF COPYRIGHT AGREEMENT

Journal publishers and authors share a common interest in the protection of copyright: authors principally because they want their creative works to be protected from plagiarism and other unlawful uses, publishers because they need to protect their work and investment in the production, marketing and distribution of the published version of the article. In order to do so effectively, publishers request a formal written transfer of copyright from the author(s) for each article published. Publishers and authors are also concerned that the integrity of the official record of publication of an article (once refereed and published) be maintained, and in order to protect that reference value and validation process, we ask that authors recognize that distribution (including through the Internet/WWW or other on-line means) of the authoritative version of the article as published is best administered by the Publisher.

To avoid any delay in the publication of your article, please read the terms of this agreement, sign in the space provided and return the complete form to us at the address below as quickly as possible.

Article entitled:----------

Corresponding author: ----------

To be published in the journal: Jordan Journal of Biological Sciences (JJBS)

I hereby assign to the Hashemite University the copyright in the manuscript identified above and any supplemental tables, illustrations or other information submitted therewith (the "article") in all forms and media (whether now known or hereafter developed), throughout the world, in all languages, for the full term of copyright and all extensions and renewals thereof, effective when and if the article is accepted for publication. This transfer includes the right to adapt the presentation of the article for use in conjunction with computer systems and programs, including reproduction or publication in machine-readable form and incorporation in electronic retrieval systems.
Authors retain or are hereby granted (without the need to obtain further permission) rights to use the article for traditional scholarship communications, for teaching, and for distribution within their institution.

☐ **I am the sole author of the manuscript**

☐ **I am signing on behalf of all co-authors of the manuscript**

☐ **The article is a 'work made for hire' and I am signing as an authorized representative of the employing company/institution**

Please mark one or more of the above boxes (as appropriate) and then sign and date the document in black ink.

Signed:_____ **Name printed:** _____
Title and Company (if employer representative) : _____
Date: _____

Data Protection: By submitting this form you are consenting that the personal information provided herein may be used by the Hashemite University and its affiliated institutions worldwide to contact you concerning the publishing of your article.

Please return the completed and signed original of this form by mail or fax, or a scanned copy of the signed original by e-mail, retaining a copy for your files, to:

Hashemite University
Jordan Journal of Biological Sciences
Zarqa 13115 Jordan
Fax: +962 5 3903338
Email: jjbs@hu.edu.jo

EDITORIAL PREFACE

Jordan Journal of Biological Sciences (JJBS) is a refereed, quarterly international journal financed by the Scientific Research and Innovation Support Fund, Ministry of Higher Education and Scientific Research in cooperation with the Hashemite University, Jordan. JJBS celebrated its 12th commencement this past January, 2020. JJBS was founded in 2008 to create a peer-reviewed journal that publishes high-quality research articles, reviews and short communications on novel and innovative aspects of a wide variety of biological sciences such as cell biology, developmental biology, structural biology, microbiology, entomology, molecular biology, biochemistry, medical biotechnology, biodiversity, ecology, marine biology, plant and animal biology, plant and animal physiology, genomics and bioinformatics.

We have watched the growth and success of JJBS over the years. JJBS has published 11 volumes, 45 issues and 479 articles. JJBS has been indexed by SCOPUS, CABI's Full-Text Repository, EBSCO, Clarivate Analytics- Zoological Record and recently has been included in the UGC India approved journals. JJBS Cite Score has improved from 0.18 in 2015 to 0.7 in 2019 (Last updated on 1 March, 2021) and with Scimago Institution Ranking (SJR) 0.18 (Q3) in 2019.

A group of highly valuable scholars have agreed to serve on the editorial board and this places JJBS in a position of most authoritative on biological sciences. I am honored to have six eminent associate editors from various countries. I am also delighted with our group of international advisory board members coming from 15 countries worldwide for their continuous support of JJBS. With our editorial board's cumulative experience in various fields of biological sciences, this journal brings a substantial representation of biological sciences in different disciplines. Without the service and dedication of our editorial; associate editorial and international advisory board members, JJBS would have never existed.

In the coming year, we hope that JJBS will be indexed in Clarivate Analytics and MEDLINE (the U.S. National Library of Medicine database) and others. As you read throughout this volume of JJBS, I would like to remind you that the success of our journal depends on the number of quality articles submitted for review. Accordingly, I would like to request your participation and colleagues by submitting quality manuscripts for review. One of the great benefits we can provide to our prospective authors, regardless of acceptance of their manuscripts or not, is the feedback of our review process. JJBS provides authors with high quality, helpful reviews to improve their manuscripts.

Finally, JJBS would not have succeeded without the collaboration of authors and referees. Their work is greatly appreciated. Furthermore, my thanks are also extended to The Hashemite University and the Scientific Research and Innovation Support Fund, Ministry of Higher Education and Scientific Research for their continuous financial and administrative support to JJBS.

Professor Atoum, Manar F.
March, 2021

JJBS

Volume 15, Number 5, December 2022
ISSN 1995-6673

Jordan Journal of Biological Sciences

CONTENTS

Original Articles

JJBS

Volume 15, Number 5,December 2022
ISSN 1995-6673
Pages 717 – 727
https://doi.org/10.54319/jjbs/150501

Jordan Journal of Biological Sciences

Association of Genetic Polymorphisms of *POU1F1* Gene on Twin Production in Egyptian Sheep and Goats

Mohamad M. Aboelenin[§], Hassan R. Darwish[§,*] , Mariam G. Eshak , Ibrahim M. Farag

Cell Biology Department, National Research Centre, Giza, Egypt

Received: November 28, 2021; Revised: March 26, 2022; Accepted: April 11, 2022

Abstract

The expression of POU1F1 gene is necessary for the normal survival, differentiation and development of several hormones' secretory cells such as somatotrophs, lactotrophs and thyrotrophs which produce growth hormone, prolactin, and thyrotropin releasing hormone, respectively. Several studies indicated that the POU1F1 gene can act as a potent candidate gene to enhance important traits such as growth, development reproduction and production in different mammals' species. The aim of this investigation was to verify the genetic polymorphisms in POU1F1 gene and to declare their effects on litter size (twin production) in Egyptian sheep and goat breeds. For DNA extraction, blood samples were collected from 139 females (113 ewes/doe at the first, second, third and fourth parity and 26 were a yearling ewe/doe). PCR amplification and PCR-SSCP were carried out using six pairs of primers. The nucleotide sequence genotyping analysis was performed to confirm banding patterns of PCR-SSCP, and to identify associated SNPs with twin production trait. Only primers 5 and 6 detected genetic polymorphisms by PCR-SSCP. The nucleotide sequence analyses between the observed patterns of POUlF1 gene revealed variable nucleotide substitutions at different positions in coding regions on charts. These nucleotide substitutions identified additional POU1F1 alleles and showed further sequence polymorphisms. The sequence analysis showed that "A" allele was more frequent in animals that have high production of offspring. In contrast, the high frequencies of C and T alleles were revealed to induce decrease in prolificacy trait in sheep and goats. The observed different alleles may cause alterations in deduced amino acid sequences that affect litter size and lamb production. The genetic analysis in this study proved that the allele A of POU1F1gene would be considered the favorable gene, and thus could utilized into a breeding program based on gene assisted selection strategy for selection ewes of high prolificacy and twin lambs.

Keywords: POU1F1 gene, PCR- SSCP, Marker assisted selection, Prolificacy, small ruminant.

1. Introduction

The POU domain, class 1, transcription factor 1 (POU1F1) gene (also named Pituitary-specific positive transcription factor 1, PIT-1 or growth hormone factor 1 (GHF-1)) was revealed to be a member of the tissue – specific POU-containing transcription factor family. In ovine and caprine, the POU1F1 genes were all detected to be located on chromosome $1q^{21-22}$ and include six exons involving the POU domain and homeodomain (Woollard *et al.*, 2000). The expression of POU1F1 gene is necessary for the normal survival, differentiation and development of three adenohypophysis cell types including somatotrophs, lactotrophs and thyrotrophs (Li *et al.*, 1990; Simmons *et al.*, 1990). Also, its expression was found to be required for the transcription of the genes encoding growth hormone (GH) (Nelson *et al.*, 1988; Mullis, 2007), prolactin (PRL) (Nelson *et al.*, 1988; Ben-Batalla *et al.*, 2010) and thyroid – stimulating hormone (TSH) (Li *et al.*, 1990). These genes (GH, PRL and TSH) and their coding proteins were observed to be closely related with reproduction in mammals (Hull *et al.*, 2001; Sun *et al.*, 2002; Yasuo *et al.*, 2010). Several studies indicated that the SNPs within POU1F1 gene can act as genetic markers to enhance several important traits such growth, development reproduction and production in different mammals' species. For example, Giordano (2016) observed in humans that the mutations of POU1F1 gene resulted in deficiency in pituitary hormone leading to impairment of growth and development of individuals. Genetic polymorphisms of POU1F1 gene in pig were revealed to have significant effects on litter size as a reproduction trait (Sun *et al.*, 2002).In sheep, four splicing forms of POU1F1 gene had been identified and showed different trans-activation of GH and PRL promoters (Bastos *et al.*, 2006b).Also, Jalil-Sarghale *et al.* (2014)and Ozmen *et al.* (2014) found that the genetic polymorphisms in POU1F1 gene have significant association with milk production and weaning weight traits in some Iranian sheep breeds. In goats, a lot of Single Nucleotide Polymorphisms (SNPs) in POU1F1 gene were observed to be significantly associated with milk performance, cashmere production, growth traits (Lan *et al.*, 2007a; Lan

* Corresponding author e-mail: drhrhdarwish@gmail.com.
§These authors have contributed equally to this work and share first authorship

et al., 2009; Nazari-Ghadikolaei *et al.*, 2018; Zhu *et al.*, 2019) and litter size rates (Lan *et al.*, 2007a; Feng *et al.*, 2012; Zhu *et al.*, 2019). Based on previous findings, the investigation on exploring potential genetic polymorphisms (SNP -Single Nucleotide Polymorphism-markers) to improve the twin production or enhance the litter size trait in the Egyptian small ruminants is worthy of in-depth study. So far, no researches have detected the SNP polymorphisms of POU1F1 gene in such Egyptian animal species. Therefore, the main aim of this investigation was to verify the genetic polymorphisms in POU1F1 gene (by using PCR- Single Strand Conformation Polymorphism (SSCP) and DNA sequencing) and to declare their effects on litter size (twin production) in Egyptian sheep and goat breeds.

2. Materials and Methods

2.1. Experimental animals

The blood samples were collected from one hundred and thirty-nine healthy females of sheep and goats. The samples were collected from Animal Production Farms belonging to Faculty of Agriculture (Cairo University), New Nubaria Farms belonging to NRC and Governmental Halayieb, Egypt. The sheep females consisted of ninety-five animals (belong to Barki, Osseimi, Rahmani, Saudanez and Awassi breeds) comprised of eighty-three adult ewes and twelve young ewes. On the other hand, the goat females consisted of forty-four animals (belong to Zaraiby, Damascus, Boer, Saanine and Barki breeds) comprised of thirty adult does and fourteen young does. Both the adult ewes and does were at first, second, third and fourth parity.

The animals were not subject to any treatments during this study, and only blood samples were collected from sheep and goats under veterinary supervision. Since the studied animals were a part of the herds of the farms mentioned above at the time of blood collection and were not subject to any treatments, the animals were kept in the same herds after blood sampling for this study.

2.2. Blood sample collection and DNA extraction

The all procedures that carried out on the animals were approved by the Institutional Animal Care and Use Committee (IACUC), Faculty of Science, Cairo University, Egypt with Permit (Reference) Number: CUFS F Mol. Biol. 50 15. The collection of blood samples had been carried out aseptically from jugular vein of the animal and in vacutainer tubes containing EDTA. Genomic DNA was extracted from white blood cells using salting out method (Aboelenin *et al.*, 2017a; Aboelenin *et al.*, 2017b; Mahrous *et al.*, 2020c)**.** DNA concentration and quality had been assessed, and then stored at -20°C until used into amplification process.

2.3. Primers and PCR amplification

Based on the genomic sequence available in GenBank of POU1F1gene, the following primers sequences (Table1) were designed using Primer-BLAST software (www.ncbi.nlm.nih.gov/tools/primer-blast) based on the sequence of GenBank record NC_019458. The annealing temperature of each pair was optimized using a conventional PCR to exclude the presence of unspecific products or primer dimer, and the PCR products were analyzed by 2% agarose gel electrophoresis as described previously (Madkour *et al.*, 2020; Mahrous *et al.*, 2020a; Mahrous *et al.*, 2020b; Mahrous *et al.*, 2020d; Sroor *et al.*, 2020; Madkour *et al.*, 2021a; Madkour *et al.*, 2021b; Mahrous *et al.*, 2021; Aboelenin *et al.*, 2022; Sroor et al., 2022)#The Polymerase chain reaction had been carried out in 25µl volume involving 2.5 µl of 10 x PCR buffer (50 mmol/L KCL, 10 mmol/L Tris-HCl (pH 8.0), 0.1% Triton X-100) 1.5 mmol/L $MgCl_2$, 200µmol/L each dNTP, 1µmol/L each primer, 50 ng genomic DNA, and 1 U Taq DNA polymerase. The conditions of PCR were denaturation at 94ºC for 6 min; followed by 32 cycles of denaturation at 94ºC for 30s, annealing at 55-62ºC for 30s, extension at 72ºC for 30s; with a final extension at 72ºC for 10 min.

2.4. Single Strand conformational polymorphism (SSCP)

For SSCP analysis, the PCR products were resolved. 10 µl of PCR product were diluted in denaturing solution that consisted of A and B types. “A” type solution included 95% of Formamide, 10 mM NaOH, 0.05% Xylene-Cyanol and 0.05% bromophenol blue. “B” type solution same as “A” solution, plus 20 mM of EDTA (pH 8.0). A 10% SSCP gel mixture (30 ml) was prepared through acrylamide- -bisacrylamide (37.5: 1), TEMED (30 µl) and 10% ammonium persulfate (0.8 ml) in a 1x TBE (90 mM Tris-borate at pH 8.3, 4 mM EDTA), and a voltage of 300 V, running time (6- 8 h) and running temperature at 4ºC. Each PCR reaction had been diluted in denaturing solution, denatured at 95ºC for 5 min, chilled on ice and resolved on non-denaturing polyacrylamide gel. Electrophoresis was performed in a vertical unit (Hoefer Scientist SE600, 160 x 140 x 1 mm) in a 1x TBE buffer. The gels had been stained with 0.1% silver nitrate and visualized through 2% NaOH solution (containing 0.1% formaldehyde). Homozygous and Heterozygous genotypes from different SSCP patterns in different breeds had been photographed and analyzed using Gel Documentation system.

The reactions of PCR were conducted in 25 ul volume containing 0.5 ul of 10 u Mol/1 each primer, 2.5 ul of 10 x PCR buffer [50 mMol/1 KCL, 10 mMol/1 Tris – HCL (pH8.0), 0.1 % TritonX- 100], 1.5 – 1.8ul of 25 mMol/1 Mg Cl_2, 2.0 µl of 2.5 mMol/ 1 each dNTP, 2.0 ul of 50 ng/µl genomic DNA, 1.0 ul of 2.5 U/µl Taq DNA polymerase. The PCR conditions were as follows: initial denaturation at 95ºC for 5 min, followed by 34 cycles of denaturation at 94ºC for 30s, annealing at 55-62 for 30s, extension at 72ºC for 45s; with a final extension at 72 for 10 min.

Table 1. The sequences of primers and product size of PCR amplification of POU1F1 gene.

Primer		Product Size
POU1F1-1-F	GGGCATGGATTGTGTTTGGGTAAG	459 bp
POU1F1-1-R	TTCAAAGCACCCATCCTGACATCTT	
POU1F1-2-F	AAGGCTTTAGTCCACTGTGATG	430 bp
POU1F1-2-R	CACTCTGGTCAAGATTCCCTTTG	
POU1F1-3-F	ACTAAGCTACACTGACTTCTACTTC	470 bp
POU1F1-3-R	GGATTTCTGAGCAGCGTGTAA	
POU1F1-4-F	ATGTTCCTATCTGAATTCTTTTGAC	475 bp
POU1F1-4-R	TTCAACCGAGGGAAACCATT	
POU1F1-5-F	TATAAGTGTAGCCAGACCATT	494 bp
POU1F1-5-R	TCTTCTCCACTAACTTTTAATATC	
POU1F1-6-F	TTTCAGAGTCTTTAGGTTTCCTTTT	456 bp
POU1F1-6-R	AGAGAAACACTTCTGCAAACATTAC	

F stands for forward primer; R stands for reverse primer.

2.5. Sequence analysis

The PCR products of all different patterns forPOU1F1 gene had been purified and sequenced by special Company (Macrogen Incorporation, Seoul, Korea). Sequence analysis and alignment had been performed by cluster wide analysis using Codon Code Aligner Software V. 10.0.2; CodonCode Corporation, Centerville, USA (https://www.codoncode.com/aligner/index.htm).

2.6. Statistical Analysis

The different PCR-SSCP patterns (due to using primers 5 and 6) and allele frequencies (by using primer 5) that were revealed in the present study had been statistically analyzed by one way ANOVA followed by two-way ANOVA. The differences among pattern and allele groups had been determined significantly according to the method of Waller *et al.* (1969). Moreover, the allele frequencies that were identified by using primer 6 had been statistically analyzed using T-Test. The values are expressed as mean±SE. All statements of significance had been based on probability of ($P \leq 0.05$).

3. Results

3.1. Results of PCR amplification of POU1F1 gene:

Genomic DNA of 139 sampled animals had been amplified using six pairs of primers for POU1F1 gene. PCR products were detected by running a 2% Agarose gel electrophoresis (Figures 1 to 6 shows example of 7 genotyped animals). The sizes of PCR products of primers 1, 2, 3, 4, 5 and 6 were 459 bp, 430 bp, 470 bp, 475 bp, 494 bp and 456 bp, respectively. These amplified products were consistent with the target fragments and had good specificity, which could be directly analyzed by SSCP.

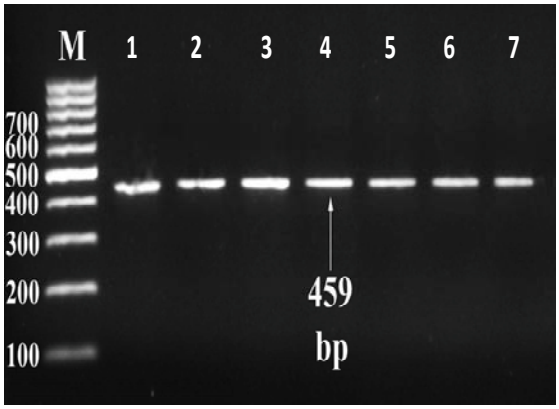

Figure 1. PCR products (Lanes 1-7) of POU1F1 gene at size 459 bp using primer 1. Lane M:100 bp ladder.

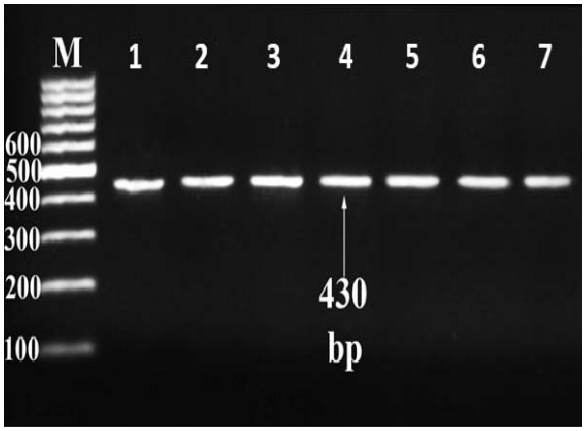

Figure 2. PCR products (Lanes 1-7) of POU1F1 gene at size 430 bp using primer 2. Lane M:100 bp ladder.

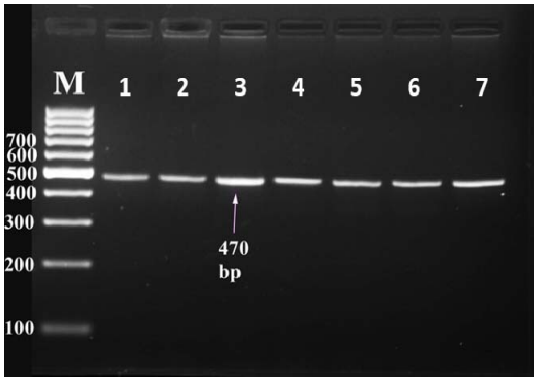

Figure 3. PCR products (Lanes 1-7) of POU1F1 gene at size 470 bp using primer 3. Lane M:100 bp ladder.

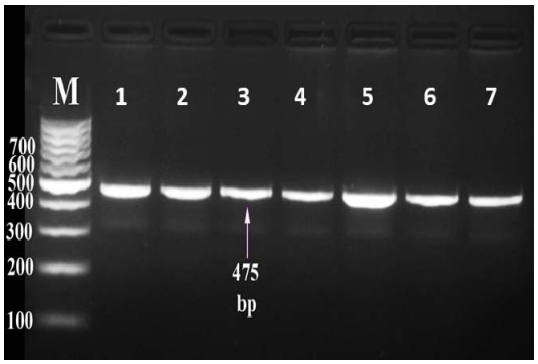

Figure 4. PCR products (Lanes 1-7) of POU1F1 gene at size 475 bp using primer 4. Lane M:100 bp ladder.

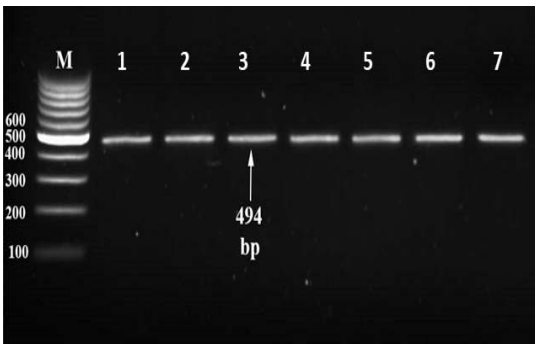

Figure 5. PCR products (Lanes 1-7) of POU1F1 gene at size 494 bp using primer 5. Lane M:100 bp ladder.

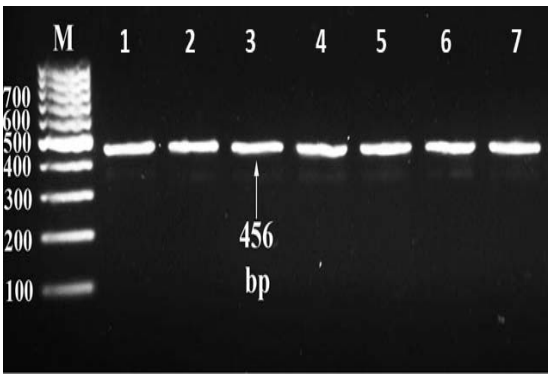

Figure 6. PCR products (Lanes 1-7) of POU1F1 gene at size 456 bp using primer 6. Lane M:100 bp ladder.

3.2. Results of PCR-SSCP analysis:

3.2.1. PCR-SSCP of primers 1,2, 3 and 4 of POU1F1gene:

PCR-SSCP analyses of 459 bp product size (bp) of primer 1 or 430 bp product size of primer 2, or 470 bp of primer 3 and 475 bp of primer 4 were shown in Figures 7, 8, 9 and 10, respectively. No polymorphisms were found and thus all animals (sheep and goats) were monomorphic.

Figure 7. Shows monomorphic type of PCR-SSCP analysis of POU1F1 gene using primer 1.

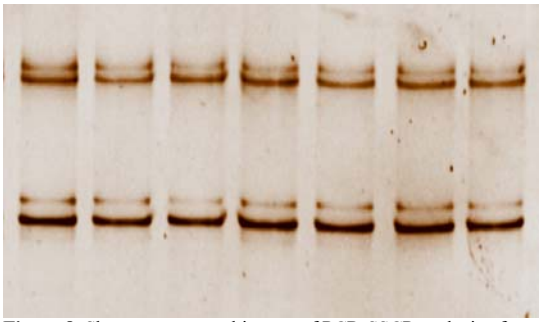

Figure 8. Shows monomorphic type of PCR-SSCP analysis of POU1F1 gene using primer 2.

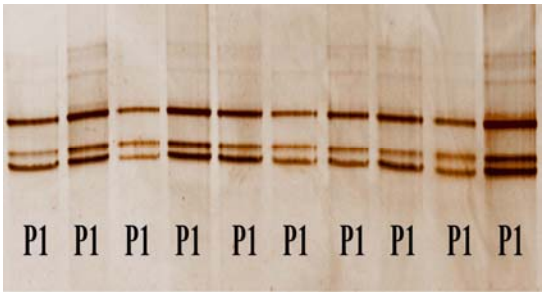

Figure 9. Shows monomorphic type of PCR-SSCP analysis of POU1F1 gene using primer 3.

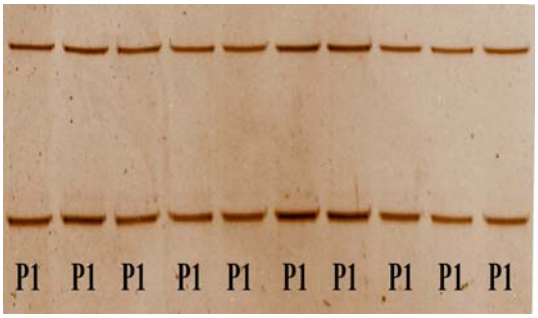

Figure 10. Shows monomorphic type of PCR-SSCP analysis of POU1F1 gene using primer 4.

3.2.2. PCR-SSCP of primer 5 of POU1F1 gene:

PCR-SSCP analysis of 494 bp PCR product size was shown in Figure 11 and Table 2. The results detected genetic polymorphisms in all small ruminant breeds. Three banding patterns (P1, P2 and P3 in sheep and P1, P2 and P4 in goats) were identified. The banding patterns of P1 and P2 in both sheep and goats were identical. However, the banding patterns P3 (in sheep) and P4 (in goats) were different.

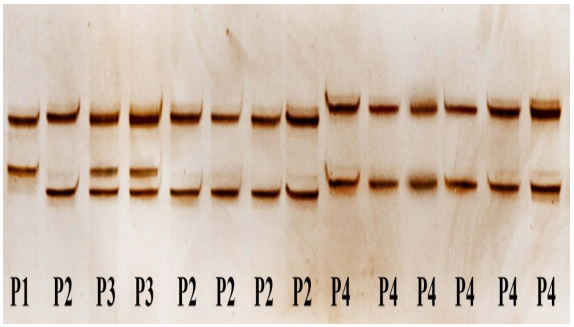

Figure 11. Shows four SSCP different patterns of POU1F1 gene using primer 5.

Table 2. Shows genetic polymorphisms of POU1F1gene using primer 5 and their effects on litter size in different Egyptian sheep and goat breeds:

Species	No. of animals	SSCP patterns (Ps)	No. of animals at age of sexual maturation	No. of mothers	No. of single births (S.b)	No. of twin births (T.b)	% S.b	% T.b	Mean No. of lambing	Mean No. of litter size (Twin production)
		P1	4	34	35	15	1.03	0.44	1.9±0.24a	1.47±0.12ab
Sheep	95	P2	6	42	45	31	1.07	0.74	2.55±0.19ab	1.81±0.1bc
		P3	2	7	6	3	0.86	0.43	1.7±0.47a	1.29±0.28ab
		P1	1	10	13	17	1.3	1.7	4.7±0.49c	3.0±0.38c
Goats	44	P2	1	11	10	14	0.91	1.27	3.45±0.34b	2.18±0.23c
		P4	12	9	6	4	0.67	0.44	1.56±0.47a	1.11±0.3a

Data expressed as mean ± SE. values followed by different superscript letters are significantly different from one another within the same columns ($P \leq 0.05$).

In sheep, pattern 1 (P1) was revealed in 38 females, 34 of them were mothers and the remaining 4 females were at age of sexual maturity, whereas pattern 2 (P2) was observed in 48 animals including 42 mothers and 6 females were at age of sexual maturity. Moreover, pattern 3 was detected in 9 females; these females involved 7 mothers and 2 females were at age of sexual maturity. The results showed that the mothers of P2 had high rates of each litter size and the mean number of lambing in comparison with the mothers of P1 or the mothers of P3. So, this genotype (P2) is considered to be a fecundity gene marker.

In goats, pattern 1 (P1) was found in 11 females, 10 of them were mothers and one female was at age of sexual maturity. Pattern 2 (P2) was detected in 12 females, that included 11 mothers and one female was at age of sexual maturity, whereas pattern 4 (P4) was observed in 21 females involving 9 mothers and 12 females were at age of sexual maturity. The mothers of P1 followed by mothers of P2 had high rates of litter size and increase of mean number of lambing as compared to mothers of P4. The mothers of P1 had the highest rates of each of mean number of lambing and mean number of twin production. So, this genotype (P1) is considered to be a prolificacy gene marker.

3.2.2. PCR-SSCP of primer 6 of POU1F1gene

PCR-SSCP analysis of the 456 bp PCR product size was shown in Figure/Fig. 12 and Table 3. The results detected genetic polymorphisms in sheep and goat breeds. In sheep, the genetic polymorphisms were represented by the presence of 2 banding patterns (P1 and P2). Pattern 1 (P1) was found in 93 animals involving 81 mothers and 12 females were at age of sexual maturity. Pattern 2 (P2) was only identified in two mothers.

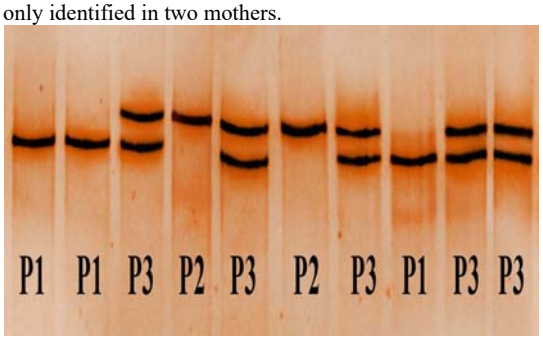

Figure 12. Shows three SSCP different of patterns of POU1F1 gene using primer 6.

Table 3. Shows genetic polymorphisms of POU1F1 gene using primer 6 and their effects on litter size in different Egyptian sheep and goat breeds:

Species	No. of animals	SSCP patterns (Ps)	No. of animals at age of sexual maturation	No. of mothers	No. of single births (S.b)	No. of twin births (T.b)	% S.b	% T.b	Mean No. of lambing	Mean No. of litter size (Twin production)
Sheep	**95**	**P1**	12	81	82	46	1.01	0.57	2.15±0.12a	1.58±0.1ab
		P2	0.0	2	4	3	2.0	1.5	5.0±0.9b	3.5±0.5c
Goats	**44**	**P1**	1	2	3	4	1.5	2.0	5.5±1.4b	3.5±0.5c
		P2	8	25	25	29	1.0	1.16	3.32±0.22ab	2.16±0.14b
		P3	5	3	1	2	0.33	0.67	1.67±0.24a	1.0±0.57a

Data expressed as mean ± SE. values followed by different superscript letters are significantly different from one another within the same columns (P≤0.05).

The mothers of P2 had high rates of each of mean number of litter size and the mean number of lambing as compared to mothers of P1. So, this genotype (P2) is considered to be as a fecundity gene marker. In goats, the genetic polymorphisms were revealed by the presence of three banding patterns (P1, P2 and P3). Pattern 1 and pattern 2 in both goats and sheep were identical. Pattern 1 of goats was observed in three animals including 2 mothers and one female was at age of sexual maturity. Whereas pattern (P2) was shown in 33 females, these females consisted of 25 mothers and 8 animals were at age of sexual maturity. Moreover, Pattern 3 (P3) was found in 8 animals involving 3 mothers and 5 females were at age of sexual maturity. The results indicated that the mothers of P1 followed by the mothers of P2 had high rates of litter size and increase of mean number of lambing in comparison with the mothers of P3. The mothers of pattern 1 had the highest rates of each of litter size and mean number of lambing. So, this genotype (P1) is considered as a prolificacy gene marker.

3.3. Nucleotide sequence analysis of POU1F1 gene:

In the present study, genetic polymorphisms had been identified in POU1F1 gene only by using primers 5 and 6. However, PCR-SSCP analysis showed no genetic polymorphisms by using primers 1, 2 ,3 and 4, where all animals were monomorphic, and nucleotide sequence analyses in these animals were recorded in Figures (13-16).

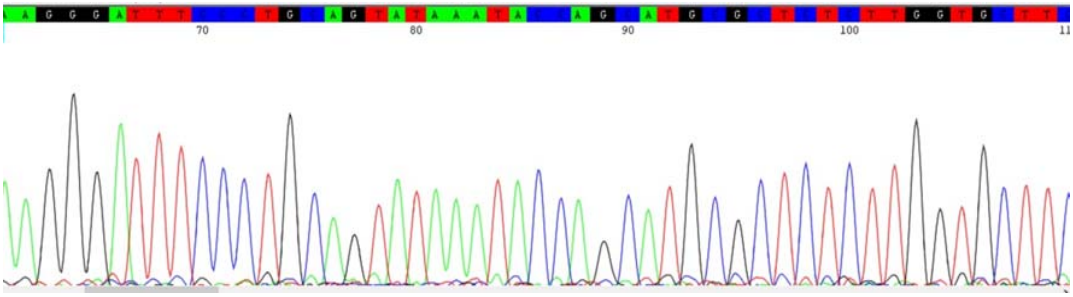

Figure 13. Sequence analysis of monomorphic type of PCR-SSCP analysis of POU1F1 gene using primer 1 (Showed no any of SNPs).

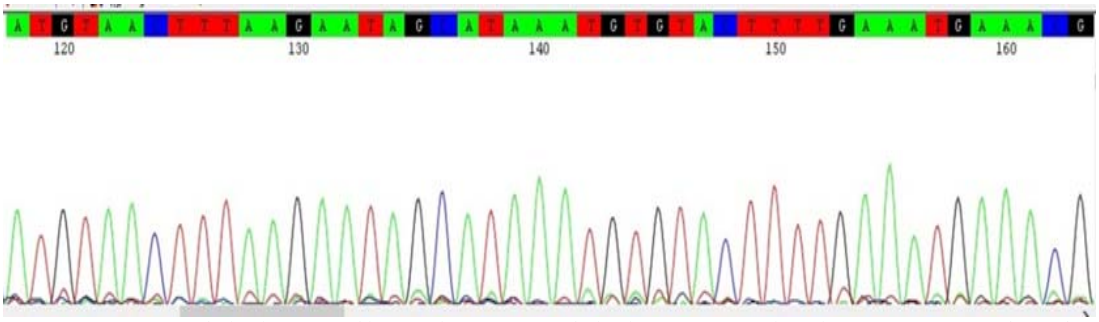

Figure 14. Sequence analysis of monomorphic type of PCR-SSCP analysis of POU1F1 gene using primer 2 (no SNPs were detected).

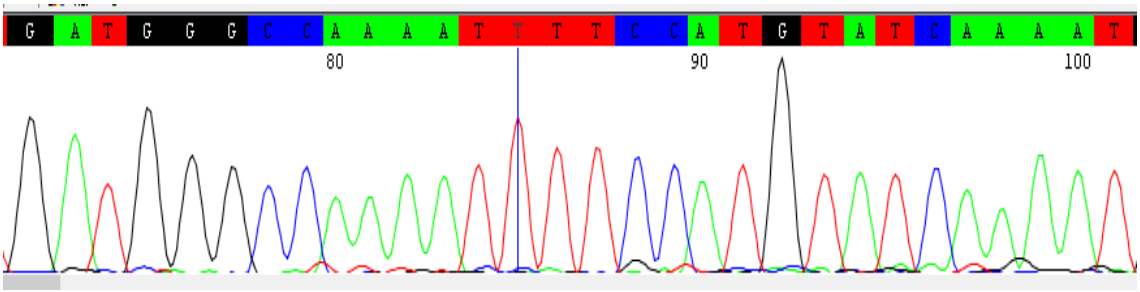

Figure 15. Sequence analysis of monomorphic type of PCR-SSCP analysis of POU1F1 gene using primer 3 (Showed no any of SNPs).

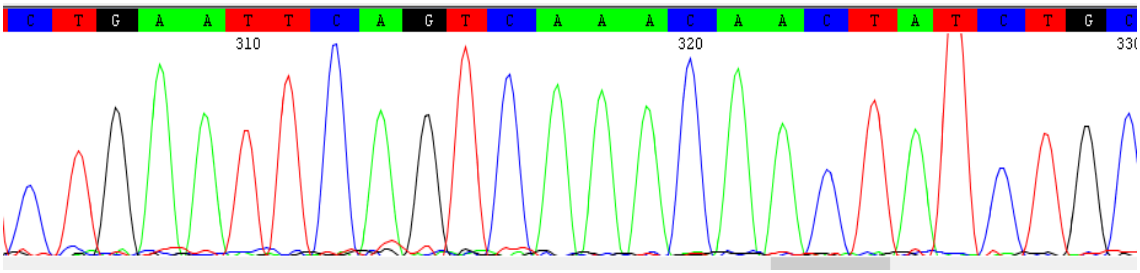

Figure 16. Sequence analysis of monomorphic type of PCR-SSCP analysis of POU1F1 gene using primer 4 (no SNPs were detected).

By using primer 5, the PCR-SSCP results showed four patterns. Nucleotide sequence analysis (Fig.17 and Tables4 and 5) of PCR products detected differences between the four patterns, where several nucleotide substitutions were observed in coding regions on charts in the positions 30, 172, 232 and 257. At position 30, pattern 1 had "A" nucleotide, while patterns 2 and 4 had "G" nucleotide. Whereas at pattern 3, "G" nucleotide was replaced by "A" nucleotide (A/G). In position 172, patterns 1 and 2 were discriminated with "A" nucleotide, while patterns 3 and 4 were discriminated with "C" nucleotide. On the other hand, at position 232, nucleotide sequence analysis showed the presence of "A" nucleotide in patterns 1,2 and 3 and they differed than pattern 4 at the same position, where P4 had "G" nucleotide. Moreover, in position 275, "C" nucleotide was replaced by "T" nucleotide (T/C) in each of patterns 1 and 3; however, "C" nucleotide was found in patterns 2 and 4.

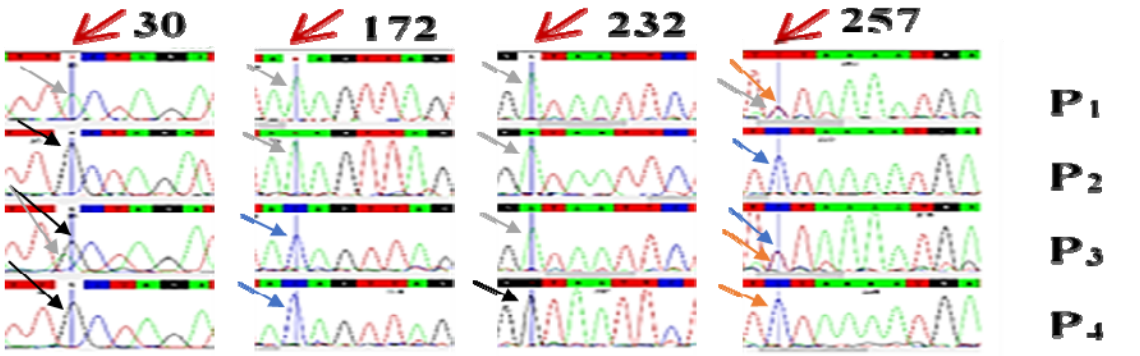

Figure 17. Sequence analysis of PCR-SSCP patterns (P1, P2, P3 and P4) using primer 5. P1 has A, A, A, T nucleotides at the specified positions; P2 has G, A, A, C; P3 has G, G, A, T and P4 has G, C, G, C of POU1F1 gene.

Table 4. Nucleotide sequence analysis of POU1F1 gene using primer 5 showing different alleles and genotypes in Egyptian domestic sheep and goats.

Patterns (P)	Species	Nucleotide sequences in the positions				Genotypes
		30	172	232	257	
P1	Sheep and goats	"A" allele(A/A)	"A" allele(A/A)	"A" allele(A/A)	"T/C" allele	AA, TC
P2	Sheep and goats	"G" allele(G/G)	"A" allele(A/A)	"A" allele(A/A)	"C" allele(C/C)	GG, AA, CC
P3	Sheep	allele "A/G"	"C" allele (C/C)	"A" allele(A/A)	"T/C" allele	AG, CC, AA, TC
P4	Goats	"G" allele(G/G)	"C" allele (C/C)	"G" allele(G/G)	"C" allele(C/C)	GG, CC

Table 5. Nucleotide sequence analyses of POU1F1 gene in Egyptian sheep and goats showing genotype and allele frequencies (using primers 5):

The used primer	Species	T. No. of animals	Type of patterns (P_s) of SSCP analysis	Genotype	No. of animals with SSCP patterns	Genotype frequencies	Allele frequencies
Primer 5	**Sheep**	**95**	P1	AA, TC	AA (29) + TC (9)	AA (0.31) + TC (0.09)	A (0.31±0.14)^a T (0.045± 0.03)^a C (0.045± 0.28)^a
			P2	AA, CC, GG	AA (24) + CC (12) + GG (12)	AA (0.25) + CC (0.126) + GG (0.126)	A (0.25± 0.114)^a C (0.126± 0.096)^a G (0.126± 0.088)^a
			P3	AA, CC, AG, TC	AA (3) + CC (3) +AG (1) + TC (2)	AA (0.03) + CC (0.03) + AG (0.01) + TC (0.02)	A (0.035± 0.02)^a C (0.04± 0.025)^a G (0.005± 0.002)^a T (0.01± 0.007)^a
	Goats	**44**	P1	AA, TC	AA (8) + TC (3)	AA (0.18) + TC (0.07)	A (0.18± 0.091)^a T (0.035± 0.019)^a C (0.035± 0.02)^a
			P2	AA, CC, GG	AA (6) + CC (3) + GG (3)	AA (0.14) + CC (0.07) + GG (0.07)	A (0.14± 0.076)^a C (0.07± 0.042)^a G (0.07± 0.038)^a
			P4	CC, GG	CC (11) + GG (10)	CC (0.25) + GG (0.23)	C (0.25± 0.081)^a G (0.23± 0.79)^a

Data expressed as mean ± SE. values followed by different superscript letters are significantly different from one another within the same columns (P≤0.05).

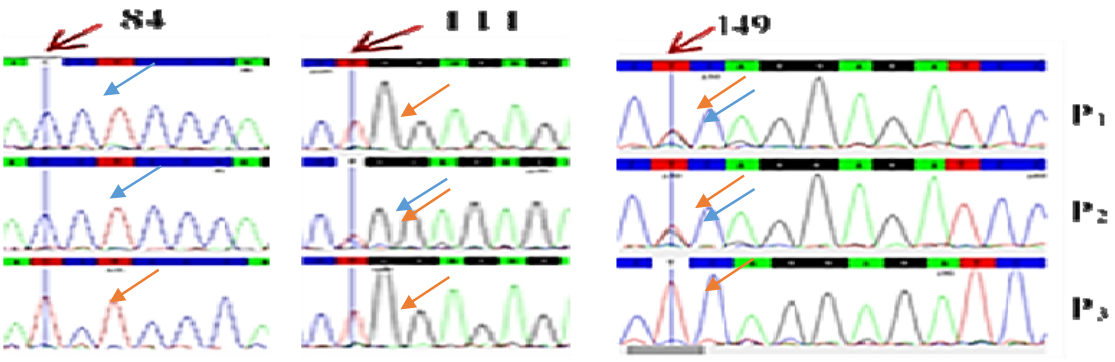

Figure 18. Sequence analysis of PCR-SSCP patterns (P1, P2 and P3), P1 has C, T, T nucleotides at the specified positions; P2 has C, C, T; and P3 has T, T, T of POU1F1 gene using primer 6.

By using primer 6, the PCR-SSCP results clarified 3 patterns. Nucleotide sequence analysis of PCR products (Fig. 18 and Tables6 and 7) identified differences between the three patterns, where several nucleotide substitutions were revealed in coding regions on charts in the positions 84, 111 and 149.

Table 6. Nucleotide sequence analysis of POU1F1 gene using primer 6 showing different alleles and genotypes in Egyptian domestic sheep and goats.

Patterns (P)	Species	Nucleotide sequences in the positions			Genotypes
		84	111	149	
P1	Sheep and goats	"C" allele (C/C)	"T" allele (T/T)	"T/C" allele	CC, TT, TC
P2	Sheep and goats	"C" allele (C/C)	"T/C" allele	"T/C" allele	CC, TC
P3	Goats	"T" allele "T/T"	"T" allele (T/T)	"T" allele (T/T)	TT

At position 84, patterns 1 and 2 were discriminated with "C" nucleotide (C/C), whereas pattern 3 had "T" nucleotide (T/T). Also, at position 111, the sequence analysis showed the presence of "T" nucleotide in each of pattern 1 and pattern 3 (T/T), while in pattern 2, "C" nucleotide was replaced with "T" nucleotide (T/C). Moreover, in position 149 "C" nucleotide was replaced with "T" nucleotide in patterns 1 and 2 (T/C), whereas in the same position (149) pattern 3 was discriminated with "T" nucleotide (T/T).

Table 7. Nucleotide sequence analyses of POU1F1 gene in Egyptian sheep and goats showing genotype and allele frequencies (using primers 6):

The used primer	Species	T. No. of animals	Type of patterns (P_s) of SSCP analysis	Genotype	No. of animals with SSCP patterns	Genotype frequencies	Allele frequencies
Primer 6	**Sheep**	**95**	P1	CC, TT, TC	CC (40) + TT (40) + TC (13)	CC (0.42) + TT (0.42) + TC (0.14)	C (0.49±0.145)[a] T (0.49±0.127)[a]
			P2	CC, TC	CC (1) + TC (1)	CC (0.01) + TC (0.01)	C (0.015±0.0115)[a] T (0.005±0.0052)[a]
	Goats	**44**	P1	CC, TT, TC	CC (1) + TT (1) + TC (1)	CC (0.02) + TT (0.02) + TC (0.02)	C (0.03±0.017)[a] T (0.03±0.015)[a]
			P2	CC, TC	CC (11) + TC (22)	CC (0.25) + TC (0.5)	C (0.5±0.109)[a] T (0.25±0.076)[a]
			P3	TT	TT (8)	TT (0.18)	T (0.18)

Data expressed as mean ± SE. values followed by different superscript letters are significantly different from one another within the same columns ($P \leq 0.05$).

4. Discussion

The results revealed genetic polymorphisms and different patterns (Polymorphic types) in POU1F1 gene of Egyptian sheep and goats. Moreover, nucleotide sequence analyses between the observed patterns revealed variable nucleotide substitutions causing different alleles (or different genotypes). The genetic analysis in this study noted that the high frequency of A allele (or AA genotype) was more frequent than other alleles or genotypes in animals that have the highest rates of litter size (twin production). In contrast, the high frequencies of C and T alleles or (CC and TT genotypes) were found to be induced the reduction of fecundity rates. Using the PCR-SSCP, PCR-RFLP and DNA sequencing methods, Lan *et al.* (2007c) detected several genetic polymorphisms in nine Chinese domestic caprine breeds. Their results observed four genetic variations, two mutations of them (T-to-G and T-to-C) were detected in the exon 6 and the other remaining two mutations of them (T-to-C) and (G-to-A) were found in the 3`UTR. Also, the using of ALuI PCR-RFLP and nucleotide sequence analysis detected a T to C silent mutation (Ser 279 Ser) in the 174th nucleotide of exon 6. Furthermore, in another study by Lan *et al.* (2007a) on genetic polymorphism in POU1F1 gene of eight Chinese local caprine breeds (Sa, LS, GZ, GB, MT, BJ, GW and LZ) by using DdeI PCR-RFLP and DNA sequence analysis, the results showed two mutations, the first mutation was T to G which located at the 60th base of exon 6 resulting in no amino acid change at the 241st of mature protein. In another study by Lan *et al.* (2007b) a mutation G to A transition was identified at the 92nd position of the 3`UTR region. Also, Lan *et al.* (2009) observed by using PstI PCR-RFLP a mutation T to C transition at position 110 of the 3`UTR region of POU1F1 gene in Inner Mongolia White Cashmere (IMWC) goats. The same authors (Lan *et al.*, 2009) used PCR-SSCP and nucleotide sequence analyses to screen the genetic polymorphism of the exons 1 to 5 and 5`UTR region in mentioned gene. Their results identified different 12 SNPs. In Jining Grey goats, (Feng *et al.*, 2012) showed by using PCR-SSCP, PCR-RFLP and nucleotide sequence analyses, the presence of genetic polymorphisms in POU1F1gene. Six mutations were detected including C 256 T in exon 3, C 53 T and T 123 G in intron 3 and G 682 T (A 228 S), T 723 G and C 837 T in exon 6.

In ovinePOU1F1 gene, (Bastos *et al.*, 2006a) revealed four mutations of 100 Portuguese indigenous "Churro da Terra Quents" sheep, these mutations included one G to A transition at codon 58 (Cys 58 Tyr) in exon 2, two G to A transitions in exon 3 (leading to the changes in amino acids such Gly 89 Asn and Ala 105 Thr), and an "A" to "G" transition in intron 4. Also, in another study, (Bastos *et al.*, 2006b) identified in ovine POU1F1 gene four alternative variants. These variants involved POU1F1-wild –type (wt), POU1F1-β (a 78 bp insert in the trans- activation domain), POU1F-γ (lacking exon 3) and POU1F1- δ (lacking exons 3,4 and 5), respectively.

Concerning the effect of genetic polymorphism of POU1F1 gene on reproductive performance including litter size, the findings of our results revealed that the presence of genetic polymorphisms in POU1F1 gene affected the litter size in Egyptian sheep and goat breeds. Similarly, in Chinese goats, (Lan *et al*., 2007a) observed that the DdeI RFLP Polymorphism T 241 G of POU1F1 gene was significantly (P<0.05) associated with litter size. Also, (Feng *et al*., 2012) identified that the two mutations (C 256 T and G 682 T out of six ones (C 256 T in exon 3, C 53 T and T 123 G in intron 3 and G 682 T (A 228 S), T 723 G and C 837 T in exon 6) in the POU1F1 gene were found to be significantly (P<0.05) affected litter size in Jining Grey goats. In Shaanbei White Cashmere goats (SBWC), (Zhu *et al*., 2019) found by direct DNA sequencing in POU1F1gene three important nucleotide polynorphisms (SNPs), c.682 G>T,c.723 T>G and c.837 >C. Two of these mutations, c.682 G>T and c..837 T>C loci were associated with litter size and the individuals that carry these mutations were found to have more offspring than the individuals that carry other mutation such c.723 T>G.

The association between genetic polymorphism in POU1F1 gene and reproductive traits was explained in previous studies**:**(Sun *et al*., 2002) reported that the polymorphisms in POU1F1 gene were investigated to have significant effects on the levels of both growth hormone (GH) and prolactin (PRL) in the neonates of Chinese Meishan pig. The lower levels of GH and the higher levels of PRL were observed in the neonates with MspI- DD genotype than other genotypes. Their results showed significant correlations between POU1F1 – α mRNA and both GH mRNA and GH plasma concentration levels. As mentioned in the above discussion, (Bastos *et al*., 2006a) detected four variants of POU1F1 ovine gene including POU1F1–wt, POU1F1 – β, POU1F1 γ– and POU1F1 δ. These variants displayed different trans –activation of GH and PRL promoters. The γ and δ variants significantly reduced the trans – activation of GH (P<0.001) and PRL (P<0.05). However, β variant increased 10% in a trans – activation capacity for GH promoter than wt. Moreover, β variant presented 12% in a trans-activation capacity for PRL promoter than those found in wt trans – activation capacity. These results confirm that fertility traits are regulated by several genes in which some SNPs affect the reproduction performance (Farag *et al*., 2018).

5. Conclusion

The present data proved that "A" allele of POU1F1 gene was more frequent in animals that have high production of offspring. In contrast, the high frequencies of C and T alleles were revealed to induce decrease in prolificacy trait in sheep and goats. Therefore, the genetic polymorphisms in POU1F1gene could contribute in performing the successful breeding program. This program could determine the favorable genomic to select a herd with high prolificacy or with greater litter size (twin production).

Acknowledgements

We acknowledge the financial support of the National Research Center to cover all the materials which was provided as a “Internal project (No. 11020104) and under title”: “Use of gene markers and Ca2+ regime for improving production of twins in Egyptian domestic sheep and goats”, PI: Dr. Ibrahim Farag.

Ethics approval and consent to participate

Blood samples were collected form sheep and goats under veterinary supervision and comply with local and international guidelines, international recommendations for the care and use of animals.The Blood samples were collected (after a written approval) from Animal Production Farm in Faculty Agriculture, Cairo University and Nubaria Farm belonging to National Research Centre, in addition to cooperating with the Governmental Halayieb Farm, Egypt). All procedures carried out on the animals were approved by the Institutional Animal Care and Use Committee (IACUC), Faculty of Science, Cairo University, Egypt with Permit (Reference) Number: CUFS F Mol. Biol. 50 15.

References

Aboelenin MM, Mahrous KF, Elkerady A and Rashed MA 2017a. Molecular characterization of cytochrome P450 aromatase (cyP19) gene in Egyptian river buffaloes. *Egypt J Genet Cytol*, **46:** 305-311.

Aboelenin MM, Mahrous KF, Rashed MA and Sallam MA 2017b. Molecular characterization of tumor necrosis factor- A (TNFA) gene in Egyptian river buffaloes. *Arab Univ J Agric Sci*, **25:** 367-375.

Aboelenin MM, Darwish HR, Abd El-Aziz KB, Farag IM 2022. Genetic polymorphisms of Inhibin-βA (INHβA) gene and their association with twin production trait in Egyptian Small Ruminants. *Jordan J Biol Sci*, accepted.

Bastos E, Avila S, Cravador A, Renaville R, Guedes-Pinto H and Castrillo JL 2006a. Identification and characterization of four splicing variants of ovine POU1F1 gene. *Gene*, **382:** 12-19.

Bastos E, Santos I, Parmentier I, Castrillo JL, Cravador A, Guedes-Pinto H and Renaville R 2006b. Ovis aries POU1F1 gene: cloning, characterization and polymorphism analysis. *Genetica*, **126:** 303-314.

Ben-Batalla I, Seoane S, Macia M, Garcia-Caballero T, Gonzalez LO, Vizoso F and Perez-Fernandez R 2010. The Pit-1/Pou1f1 transcription factor regulates and correlates with prolactin expression in human breast cell lines and tumors. *Endocr Relat Cancer*, **17:** 73-85.

Farag I, Darwish H, Aboelhassan D, Aboelenin M and Shakweer W 2018. Study of genetic polymorphism in BMPRIB gene and its association with improving twin production in Egyptian sheep and goats. *Res J Anim Vet* Sci, **10:** 1-5.

Feng T, Chu MX, Cao GL, Tang QQ, Di R, Fang L and Li N 2012. Polymorphisms of caprine POU1F1 gene and their association with litter size in Jining Grey goats. *Mol Biol Rep*, **39:** 4029-4038.

Giordano M 2016. Genetic causes of isolated and combined pituitary hormone deficiency. *Best Pract Res Clin Endocrinol Metab*, **30:** 679-691.

Hull KL and Harvey S 2001. Growth hormone: roles in female reproduction. *J Endocrinol*, **168:** 1-23.

Jalil-Sarghale A, Moradi Shahrbabak M, Moradi Sharbabak H, Sadeghi M and Mura MC 2014. Association of pituitary specific transcription factor-1 (POU1F1) gene polymorphism with growth and biometric traits and blood metabolites in Iranian Zel and Lori-Bakhtiari sheep. *Mol Biol Rep,* **41:** 5787-5792.

Lan XY, Pan CY, Chen H and Lei CZ 2007a. A DdeI PCR-RFLP detecting genetic variation of goat POU1F1 gene. *Can J Anim Sci*, **87:** 13-14.

Lan XY, Pan CY, Chen H, Lei CZ, Hua LS, Yang XB, Qiu GY, Zhang RF and Lun YZ 2007b. DdeI Polymorphism in Coding Region of Goat POU1F1 Gene and Its Association with Production Traits. *Asian-Australas J Anim* Sci, **20:** 1342-1348.

Lan XY, Pan CY, Chen H, Zhang CL, Li JY, Zhao M, Lei CZ, Zhang AL and Zhang L 2007c. An AluI PCR-RFLP detecting a silent allele at the goat POU1F1 locus and its association with production traits. *Small Rumin Res*, **73:** 8-12.

Lan XY, Shu JH, Chen H, Pan CY, Lei CZ, Wang X, Liu SQ and Zhang YB 2009. A PstI polymorphism at 3′UTR of goat POU1F1 gene and its effect on cashmere production. *Mol Biol Rep*, **36:** 1371-1374.

Li S, Crenshaw EB, 3rd, Rawson EJ, Simmons DM, Swanson LW and Rosenfeld MG 1990. Dwarf locus mutants lacking three pituitary cell types result from mutations in the POU-domain gene pit-1. *Nature*, **347:** 528-533.

Madkour M, Aboelenin MM, Aboelazab O, Elolimy AA, El-Azeem NA, El-Kholy MS, Alagawany M and Shourrap M 2021a. Hepatic expression responses of DNA methyltransferases, heat shock proteins, antioxidant enzymes, and NADPH 4 to early life thermal conditioning in broiler chickens. *Ital J Anim Sci*, **20:** 433-446.

Madkour M, Aboelenin MM, Shakweer WME, Alfarraj S, Alharbi SA, Abdel-Fattah SA and Alagawany M 2021b. Early life thermal stress modulates hepatic expression of thermotolerance related genes and physiological responses in two rabbit breeds. *Ital J Anim Sci*, **20:** 736-748.

Madkour M, Aboelenin MM, Younis E, Mohamed MA, Hassan H, Alagawany M and Shourrap M 2020. Hepatic acute-phase response, antioxidant biomarkers and DNA fragmentation of two rabbit breeds subjected to acute heat stress. *Ital J Anim Sci*, **19:** 1568-1576.

Mahrous KF, Abd El - Kader HAM, Mabrouk DM, Aboelenin MM, Osman NM, Khalil WKB and Hassanane MS 2020a. Molecular characterization and expression analysis of hepc1 and hepc2 in three tilapia species collected from Lake Manzala. *Bull Natl Res Cent*, **44:** 36.

Mahrous KF, Aboelenin MM, Abd El-Kader HAM, Mabrouk DM, Gaafar AY, Younes AM, Mahmoud MA, Khalil WKB and Hassanane MS 2020b. Piscidin 4: Genetic expression and comparative immunolocalization in Nile tilapia (Oreochromis niloticus) following challenge using different local bacterial strains. *Dev Comp Immunol*, **112:** 103777.

Mahrous KF, Aboelenin MM, Rashed MA, Sallam MA and Rushdi HE 2020c. Detection of polymorphism within leptin gene in Egyptian river buffalo and predict its effects on different molecular levels. *J Genet Eng Biotechnol*, **18:** 6.

Mahrous KF, Mabrouk DM, Aboelenin MM, Abd El-Kader HAM, Gaafar AY, Younes AM, Mahmoud MA, Khalil WKB and Hassanane MS 2020d. Molecular characterization and immunohistochemical localization of tilapia piscidin 3 in response to Aeromonas hydrophila infection in Nile tilapia. *J Pept Sci*, **26:** e3280.

Mahrous KF, Mabrouk DM, Aboelenin MM, Abd El kader HAM and Hassanane MS 2021. Identification and characterization of antimicrobial peptide genes in Clarias gariepinus and Chelon ramada. *Jordan J Biol Sci*, **14:** 51-64.

Mullis PE 2007. Genetics of growth hormone deficiency. *Endocrinol Metab Clin North Am*, **36:** 17-36.

Nazari-Ghadikolaei A, Mehrabani-Yeganeh H, Miarei-Aashtiani SR, Staiger EA, Rashidi A and Huson HJ 2018. Genome-Wide Association Studies Identify Candidate Genes for Coat Color and Mohair Traits in the Iranian Markhoz Goat. *Front Genet*, **9:** 105.

Nelson C, Albert VR, Elsholtz HP, Lu LI and Rosenfeld MG 1988. Activation of cell-specific expression of rat growth hormone and prolactin genes by a common transcription factor. *Science*, **239:** 1400-1405.

Ozmen O, Kul S and Unal EO 2014. Polymorphism of sheep POU1F1 gene exon 6 and 3'UTR region and their association with milk production traits. *Iran J Vet Res*, **15:** 331-335.

Simmons DM, Voss JW, Ingraham HA, Holloway JM, Broide RS, Rosenfeld MG and Swanson LW 1990. Pituitary cell phenotypes involve cell-specific Pit-1 mRNA translation and synergistic interactions with other classes of transcription factors. *Genes Dev*, **4:** 695-711.

Sroor FM, Aboelenin MM, Mahrous KF, Mahmoud K, Elwahy AHM and Abdelhamid IA 2020. Novel 2-cyanoacrylamido-4,5,6,7-tetrahydrobenzo[b]thiophene derivatives as potent anticancer agents. *Arch Pharm (Weinheim)*, **353:** e2000069.

Sroor FM, Othman AM, Aboelenin MM and Mahrous KF. 2022. Anticancer and antimicrobial activities of new thiazolyl-urea derivatives: gene expression, DNA damage, DNA fragmentation and SAR studies. *Med Chem Res*, **31(3):** 400-415.

Sun HS, Anderson LL, Yu TP, Kim KS, Klindt J and Tuggle CK 2002. Neonatal Meishan pigs show POU1F1 genotype effects on plasma GH and PRL concentration. *Anim Reprod Sci*, **69:** 223-237.

Waller RA and Duncan DB 1969. A Bayes Rule for the Symmetric Multiple Comparisons Problems. *J Am Stat Assoc*, **64:** 1484-1503.

Woollard J, Tuggle CK and Ponce de Leon FA 2000. Rapid communication: localization of POU1F1 to bovine, ovine, and caprine 1q21-22. *J Anim Sci*, **78:** 242-243.

Yasuo S, Yoshimura T, Ebihara S and Korf HW 2010. Photoperiodic control of TSH-beta expression in the mammalian pars tuberalis has different impacts on the induction and suppression of the hypothalamo-hypopysial gonadal axis. *J Neuroendocrinol*, **22:** 43-50.

Zhu H, Zhang Y, Bai Y, Yang H, Yan H, Liu J, Shi L, Song X, Li L, Dong S, Pan C, Lan X and Qu L 2019. Relationship between SNPs of POU1F1 Gene and Litter Size and Growth Traits in Shaanbei White Cashmere Goats. *Animals (Basel)*, **9(3):**114.

JJBS

Volume 15, Number 5,December 2022
ISSN 1995-6673
Pages 729 – 738
https://doi.org/10.54319/jjbs/150502

Jordan Journal of Biological Sciences

In silico Tools and Techniques for Screening and Development of Peptide-Based Spike Protein Inhibitors against Novel Coronavirus (Sars-CoV-2)

Raghunath Satpathy*

School of Biotechnology, Gangadhar Meher University, Amruta Vihar, Sambalpur Odisha, 768004, India

Received: December 17, 2021; Revised: March 13, 2022; Accepted: April 27, 2022

Abstract

The recent pandemic situation created by the novel coronavirus (SARS-CoV-2) across the globe is a great concern. So, the discovery of novel antiviral agents is desirable to address this challenge. In this context, the antiviral peptides (AVPs) possess an enormous potential and can be considered to develop novel therapeutic strategies to combat SARS-CoV-2 infection. The anti-viral peptides are mostly preferable over small inhibitor molecules for having high target specificity and lower side effects. The spike protein is an important structural protein of SARS-CoV-2 that binds with the human angiotensin-converting enzyme-2 leading to host entry of the virus. Hence, the activity of the anti-viral peptides will be based on the interference of the peptide inhibitor between the binding site of spike protein, and the ACE2 protein ultimately will prevent the virus invasion process. Several database resources are available that contain many anti-viral peptides from natural sources. However, the experimental basis of establishing the therapeutic importance of every protein from the database is a difficult and time-consuming task. Hence the available bioinformatics tools and techniques can be suitably used to screen, structure prediction, evaluation of ant-viral peptide- SARS-CoV-2 spike protein interaction, toxicity prediction, molecular dynamics simulation, and so on. In this review, the implementation of some of the major computational tools, their availability, and effectiveness in predicting the peptides against the Spike protein have been discussed.

Keywords: Antiviral peptides**,** novel coronavirus, Spike Protein, Bioinformatics, Screening Methods, Binding Affinity

1. Introduction

The novel coronavirus disease was first identified in China during the last month of 2019. Further, this novel virus (SARS-CoV-2) infection continued to outbreak globally at an alarming rate. The genomic sequence study of the virus has been observed to share some homology with the related virus such as (Middle East respiratory syndrome-CoV) and the coronavirus (SARS-CoV) [1-3]. High infection, as well as the death rate of the novel coronavirus in comparison to other previously known coronaviruses, created the research challenge to discover the potential drug candidates for the pharmacological treatments. From the beginning of the pandemic, several molecules have been repurposed and proposed to prevent the infection of the virus; however, till yet, no such effective drug is available for the treatment [4-6]. Some of the repurposed drugs including remdesivir, favipiravir, lopinavir, ritonavir, ribavirin for the inhibitor of viral RNA- replication have been approved but there is no evidence regarding their clinical efficacy [7-11]. In the host-virus interaction process of SARS-CoV-2, the Spike glycoproteins (molecular weight 180-200 kDa) play a major role. The Spike glycoproteins (S) contain an N-terminus region (extracellular), transmembrane (TM) anchored region, and a short C-terminal region (Figure 1). It was studied that, the *open* conformation of the S-protein facilitates the virus interaction with ACE2 protein of host (human) and further leads to the fusion process with the host cell membrane. The S protein also contains the polysaccharide coating that prevent the virus from the host immune system recognition process [12-14].

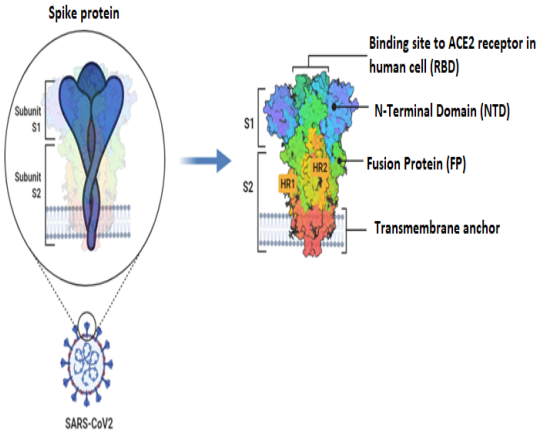

Figure 1. Structural components of the spike glycoprotein (SARS-CoV-2)

* Corresponding author. e-mail: rnsatpathy@gmail.com.

Table 1. Target regions of the Sars -CoV-2 spike glycoprotein

Subunit of Spike Protein	S. No	Specific target region of S protein	Sequences regions	Function
S1	1	N-terminal domain (NTD)	13-305	Helps in attachment and recognition of virus
	2	Receptor binding domain (RBD)	319-541	Binds to the cell receptor hACE2
	3	Receptor binding motif (RBM)	437-508	Binds to the cell receptor of hACE2
S2	1	Fusion peptide (FP)	788-806	Helps in anchoring the target membrane with the S protein, and play important role in mediating membrane fusion
	2	Heptad repeat 1 (HR1)	912-984	Essential for the viral fusion and cell entry mechanism
	3	Heptad repeat 2 (HR2)	1163-1213	Essential for the viral fusion and entry function of the S2 subunit
	4	Transmembrane domain (TM)	1213-1237	The downstream TM domain anchors the S protein to the viral membrane

The length of the spike protein of the SARS-CoV-2 virus comprises 1273 amino acids long, and it is further divided into two subunits, S1and S2, which are actively involved in the host cell entry process. The spike protein is trimeric in its native form and the S1 and S2 subunits of the virus form a "crown" structure from which the term "corona" is originated in the Latin language translation. The S1 subunit is classified into N-terminal domain (NTD), the receptor-binding domain (RBD), and the carboxy-terminal domain (CTD). The CTD domain also contains two subdomains such as SD1 and SD2. Similarly, the S2 subunit consists of two regions such as heptapeptide repeat 1 (HR1) and heptapeptide repeat 2 (HR2). The HR1 act as a fusion peptide and the HR2 act as the transmembrane domain (TM) (Figure 1). In the viral entry process, the S protein directly interacts with the cell surface receptor, human angiotensin-converting enzyme-2 (hACE2). Particularly, the open conformation state of the RBD domain is accessible for binding with the hACE2. After the binding event to the human ACE2 receptor, S1 and S2 cleavage sites are accessed by the host protease due to the conformational change in the S protein [15-21]. The detailed sequence position and the function of the different components of the spike protein have been shown in Table 1, and the mechanism is shown in Figure 2.

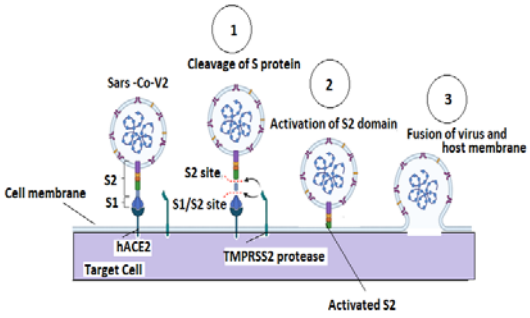

Figure 2. Basic entry mechanism of SARS-CoV-2 into the host cell

Soon after the process, the proteolytic cleavage occurs at the position of S1 and S2 subunit junction site as well as at the S2 subunit region with the help of a serine protease enzyme TMPRSS2. Following this cleavage event, HR1 and HR2 regions of the S2 subunit interact to form a structural arrangement known as *fusion core*. The *fusion core* formation further enhances the entry of the virus into the host cell by the cellular endocytic mechanism. Finally, the viral RNA is released into the host cell and the viral replication process is initiated. Interestingly, research has established that the SARS-CoV-2 shows an enhanced affinity towards binding (about 10 to 20-fold) with hACE2, as compared to another related virus such as SARS-CoV [22-23].

Recently, efforts have been given to discover potential antiviral therapeutic molecules. The traditional biochemical approach of small molecule inhibitors is associated with several obstacles like drug resistance, huge cost, time-consuming as well as toxicity [24-25]. In this context, the antiviral peptides (AVPs) are considered as one of the important therapeutic molecules due to their *specificity*, *efficacy, potency,* and desirable *pharmacokinetic properties* [26]. For the last 50 years, Antiviral peptides (AVPs) have shown their effectiveness, hence generating a perspective for treating viral infections such as novel coronavirus. The key feature of antiviral peptides are, they are involved in the specific interaction and inhibition of target protein. Therefore, targeting the AVPs in the form of novel therapeutics against the pathogenic virus-like SARS-CoV-2 might be established as a promising tool to develop an effective treatment process. Prediction and application of effective anti-viral peptides against respiratory disease-causing viruses like SARS-CoV, SARS-CoV2, MERS-CoV have been described and reported by many researchers [27-33].

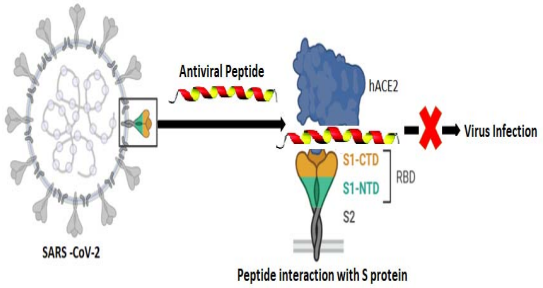

Figure 3. Possible mechanism of action of the anti-viral peptides with the spike protein

The potential AVPs are to be identified, hence they can be targeted specifically to the RBD domains in the S protein of novel coronavirus so that, the interference will restrict the host cell receptor-mediated viral entry. The possible mechanism of AVP- based inhibition of spike protein is presented in Figure 3. The binding features of the Spike protein of SARS-CoV-2 with ACE2 have been studied, and it was revealed several charged amino acids of ACE2 are important for its interaction [34]. Li et al. also studied the binding affinity of peptides that binds to the

specific hotspot area of the spike protein by computing the rate of inhibition [35].

The objective of the review is to provide a basic methodology that is involved in the searching and development of an effective spike inhibitor peptide molecule. Additionally, the challenges and scope of the process have been discussed.

2. In-silico development process of peptide molecules against the SARS-CoV-2 spike protein

An experimental basis for searching for novel and effective anti-viral peptide molecules that can specifically block the S protein function of the novel coronavirus is a challenging task. However, the computational approach facilitates the process for searching and predicting an effective antiviral peptide. This method will also lead to discovering and understanding the mechanism behind the spike protein-peptide interaction that corresponds to the antiviral effects [36-39]. Several steps are to be followed in the in-silico based novel effective peptide discovery against the spike protein inhibitor are schematically presented in Figure 4 and described in the sections below.

3. Retrieval of peptide sequence information

The information about the antiviral peptide sequence information from natural sources can be obtained from several available databases. Searching the literature regarding the specific peptides that can inhibit the spike protein of the virus may also help to explore the potential one. Along with the amino acid sequences, several databases also contain an analytical tool for peptide analysis. Some of the important databases and their availability that contains anti-viral peptides are represented in Table 2.

Table 2. Important databases contain information about anti-viral peptides

S.No	Name of the database	Availability
1	AVPdb Database	https://webs.iiitd.edu.in/raghava/satpdb/catalogs/avpdb
2	Antimicrobial Peptide Database (APD)	https://aps.unmc.edu/database/anti
3	Database of Antimicrobial Activity and Structure of Peptides (DBAASP)	https://dbaasp.org/
4	LAMP2	http://biotechlab.fudan.edu.cn/database/lamp/
5	CAMPR3 (Collection of Anti-Microbial Peptides)	http://www.camp.bicnirrh.res.in/index.php
6	DRAMP (Data repository of antimicrobial peptides)	http://dramp.cpu-bioinfor.org/

4. Screening criteria for the peptides

After retrieval of the anti-viral peptide sequences from the database search, it is essential to screen the spike binding activity of these peptide sequences based on a certain feature. For example, Mustafa et al. studied several features of the probable active peptides against the MERS-CoV spike protein [40]. As the MERS-CoV spike protein resembles the SARS-CoV-2 spike protein, hence similar type of criteria can be used to screen the potential peptides [41-42]. In addition to this, several strategies have been employed by many researchers for screening probable spike peptides having spike binding characteristics [43-46]. Some of the criteria for screening of potential peptide molecules are:

(i) *length of amino acids* should be 20aa to 55aa (length of the peptide sequence is proportional to the antiviral activity)

(ii) *positively charged residues* should be more abundant

(iii) *net charge* of the peptide > 0 as the spike protein of Sars- CoV-2 is neutral and less negatively charged in nature

(iv) the peptide should be *non-toxic* to human cells

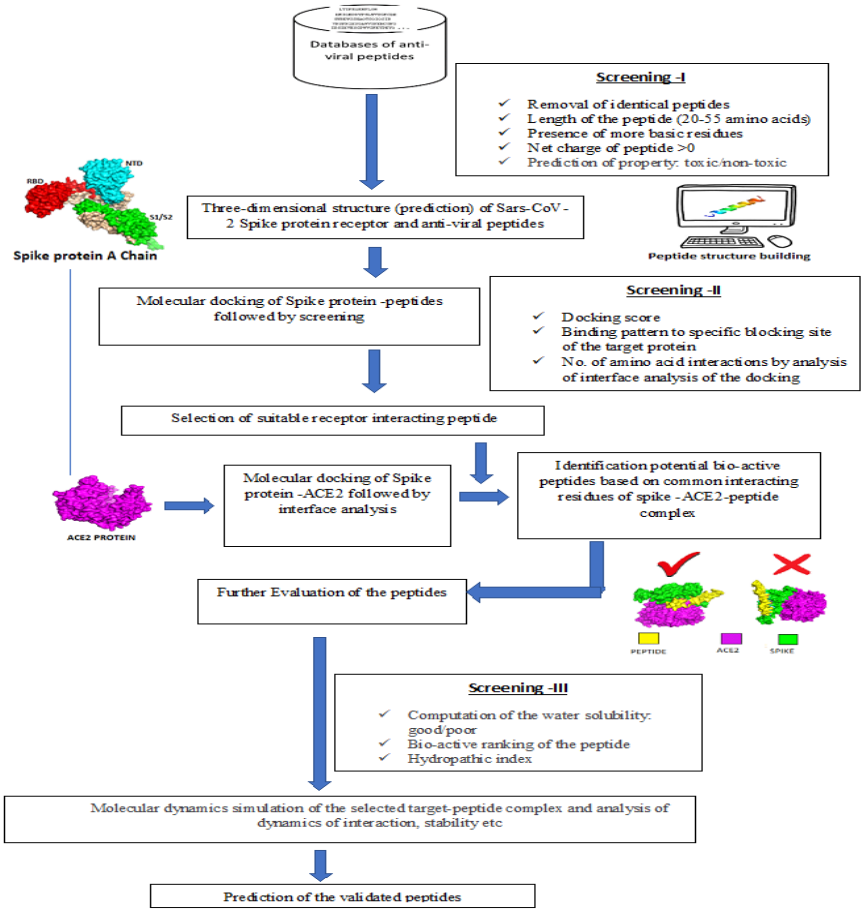

Figure 4. steps for *in silico* prediction of novel bioactive peptides against spike proteins

5. Prediction of the 3D structure of spike glycoproteins and anti-viral peptides

The protein data bank (PDB) available at https://www.rcsb.org/ may be searched for the availability of the three-dimensional structure of the (SARS-CoV-2) spike proteins as well as for the small peptides. Recently, Gowthaman et al. developed a database Cov 3D (available at https://cov3d.ibbr.umd.edu), which contains coronavirus structural data from the PDB including the spike protein [47]. Also, the 3D structure prediction of the spike protein as a target can be performed from the amino acid sequence followed by validation. UniProt database (https://www.uniprot.org) is usually used to retrieve the amino acid sequence information of the spike protein. Several tools available for the 3D structure prediction of spike protein, are being used by many researchers (Table 3).

Table 3. Popular 3D structure prediction tools for peptide molecules

S. No	Name of the tool	Availability	Recently used by researchers for spike protein structure prediction
1	SWISS MODEL	https://swissmodel.expasy.org/	(Padilla-Sanchez 2020; Allam et al. 2020)
2	Modeller	https://salilab.org/modeller/	(Hall et al. 2020; Martin et al. 2020; Hassanzadeh et al. 2020)
3	Phyre 2	http://www.sbg.bio.ic.ac.uk/phyre2/html/page.cgi?id=index	(Jaimes et al. 2020)
4	RaptorX	http://raptorx.uchicago.edu/	(King et al. 2021; Awadelkareem et al. 2020)
5	I Tasser	https://zhanggroup.org/I-TASSER/	(Prashantha et al. 2021; Ibrahim et al. 2020)

Similarly, for the small peptide sequences, the 3D structure can be predicted by using online server like pepfold (available at https://bioserv.rpbs.univ-paris-diderot.fr/services/PEP-FOLD/). This web-based tool predicts the 3D structure of linear peptides sequences from 5 to 50 amino acid range. Also, other open-source stand-alone programs like open Chimera (https://www.cgl.ucsf.edu/chimera/) can be used to build peptide structure from the sequences. Many of the protein-protein docking programs take the peptide sequence along with the target protein sequence as input and automatically predict the 3D structure thereby preparing the structural

file for the docking simulation. After the prediction of the 3D structure of the peptide, the energy minimization should be performed till it attains negative free energy. Evaluation of the predicted structure can be performed by computing the Ramachandran plot, side-chain placement, and so on. For the structure verification of the predicted structures, the SAVES servers may be used (https://saves.mbi.ucla.edu/).

6. Molecular docking and molecular dynamics (MD) simulation study of anti-viral peptides with SARS-CoV-2 spike proteins

To compute the binding affinity as well as the binding pose of the selected potential anti-viral peptide with the virus spike protein, molecular docking is to be performed. Molecular docking is a computational approach in which the affinity, pose of the ligand is evaluated along with the receptors. Mainly two types of algorithms are involved in this process, searching algorithm and scoring algorithms. Based on the implementation of the combinations of algorithms, different types of docking programs are available [48-49].

The protein-peptide docking programs are broadly classified into three categories. The first one is template-based docking (a protein-peptide input structure is searched for a known template structure from the database followed by comparative analysis). The second method is known as local docking (the peptide binding site is searched on the given input receptor by the user given peptides). The third method is global docking in which the peptide behaves as rigid in nature and binding pose and position are evaluated by the exhaustive search on the receptor. Also, in the molecular docking process of protein and peptide, the number of flexible bonds, size, a loop structure, and terminal charges in the peptide structure are the important parameters on which the accuracy of the prediction depends [50-51]. In this process, the Spike protein is behaving as the receptor and the peptide sequence as the ligand and the binding affinity, the binding pose can be computed from the receptor-ligand complex by application of suitable searching and scoring functions in several docking programs [52-60], presented in Table 4.

Table 4. Molecular docking programs that are frequently used for protein-peptide interaction study

S. No	Name of the server	Availability
1	GalaxyPepDock	http://galaxy.seoklab.org/pepdock
2	Rosetta FlexPepDock	http://flexpepdock.furmanlab.cs.huji.ac.il
3	PepCrawler	http://bioinfo3d.cs.tau.ac.il/PepCrawler
4	HADDOCK peptide docking	http://milou.science.uu.nl/services/HADDOCK2.2/haddock.php
5	GRAMM-X	http://vakser.compbio.ku.edu/resources/gramm/grammx
6	DINC 2.0	http://dinc.kavrakilab.org
7	pepATTRACT	http://bioserv.rpbs.univ-paris-diderot.fr/services/pepATTRACT
8	CABS-dock	http://biocomp.chem.uw.edu.pl/CABSdock
9	ClusPro PeptiDock	https://peptidock.cluspro.org
10	PIPER-FlexPepDock	http://piperfpd.furmanlab.cs.huji.ac.il
11	HawkDock server	http://cadd.zju.edu.cn/hawkdock
12	Z dock server	https://zdock.umassmed.edu
13	SwarmDock server	https://bmm.crick.ac.uk/~svc-bmm-swarmdock
14	pyDockWEB	https://life.bsc.es/pid/pydockweb
15	3D garden	http://www.sbg.bio.ic.ac.uk/3dgarden
16	Hex server	http://hexserver.loria.fr
17	DOCKSCORE	http://caps.ncbs.res.in/dockscore
18	FRODOCK	https://chaconlab.org/modeling/frodock
19	HPEPDOCK Server	http://huanglab.phys.hust.edu.cn/hpepdock
20	MDockPeP	https://zougrouptoolkit.missouri.edu/mdockpep
21	ClusPro 2.0	https://cluspro.org

In the computational procedure, after molecular docking simulation, the implementation of a reliable specific scoring function is the basic requirement for the prediction of the correct binding nature of the protein-peptide complex. In this context, theoretically calculation of the end-point binding free energy by the methods such as Molecular mechanics Poisson–Boltzmann surface area (MM/PBSA) is used. By using this method, the binding affinities, as well as the binding conformations, are obtained for protein-peptide complex systems [61]. In the MM-PBSA method, the free energy (ΔG) of receptor-ligand (protein-peptide) binding is estimated by deducting the free energy between the complex and the unbound form. Previously, the MM-PBSA method has been successfully used to analyze and evaluate the protein-protein docking complexes [62-65]. A significant number of specific viral protein-peptide interactions is used for the determination of affinity of the potential AVPs and used for the in-depth understanding of the behaviour towards the target molecule. To investigate the spike protein-peptide interaction, it is essential to study the interface region of the docked complex. The interface analysis results from the numbers of amino acid interactions with the specific binding domains. This also leads to evaluating

the different types of interaction such as cation–π, hydrogen bonding, and electrostatic interaction essential to describe the anti-viral inhibition property of the peptide [66-67].

Molecular dynamics (MD) simulation is a computational method used for understanding and prediction of the structure as well as the function of biological macromolecules. This method is based on the physical principles (Newton's equations of motion). The macromolecular conformation is represented by the dynamic model from which the motion of the individual atoms and subsequent conformational changes are calculated from a trajectory file. Specifically, by the MD simulation, the macroscopic behaviour from various microscopic interactions present in molecular systems is computed. The MD simulation methods are frequently used in the drug discovery process to study the receptors (targets) and their association with ligand (drug) molecules after docking to discover the novel molecules by computing various parameters. MD simulation can also be used to study the configuration change in the protein structure that involves the monomeric or the trimeric form of the spike glycoprotein. In addition to this, a comparative structural analysis of the ligand-bound state of spike protein and native (unbound) state can be performed. Currently, the MD simulation techniques are used in the case of spike protein to study the proper binding of the ligand, total energy variation profile of the complex, dynamicity of protein domain, variation of hydrogen bonds, dynamics of actively interacting residues of the spike protein throughout the simulation period and so on [68-69].

Table 7. Molecular dynamics simulation software and their availability

7. Identification of bioactive peptide molecules

Along with the docking score and the *pose* of the binding peptide and several physicochemical screenings are also essential to select the potential peptide inhibitor molecules. The major problem is in the therapeutic use of peptides is their toxicity. Hence the peptide features like toxicity, bioavailability, in *vivo* instability, half-life, and ability to cross the membrane are to be evaluated carefully. These factors obtained from the peptide evaluation output can be utilized further in the specific rational design process of novel peptides with enhanced stability and other required physicochemical properties [70-71]. Some of the important bioinformatics tools used to compute such peptide properties are given in Table 6.

Table 6: Peptide designing and screening tools and their availability

Several scientific studies on the peptide-based inhibitors against the pathogenic virus have been developed and proposed in the last few years. The finding of small effective peptides was considered to be one of the best molecules that can be targeted to the spike protein [72]. Wong et al., in 2020 conducted *in silico* study to identify potential SARS-CoV-2 cell entry inhibitors from peptides derived from different edible insects. In-silico-based gastrointestinal (GI) digestion of the insect protein was performed to generate peptide molecules. Subsequent molecular docking study with the spike protein resulted that, a tri-peptide generated from the source mealworm can act as the effective inhibitor [73]. Allam et al. analyzed the peptide and polyphenol-based inhibitor that can block the SARS-CoV-2 spike protein by inhibiting the glucose-regulating protein 78 receptors. The in-silico screening process was conducted by taking the available databases of bioactive peptides. Protein-peptide docking analysis resulted in five potential peptides that can inhibit the GRP78 binding site [74]. Salman et al., conducted the computational protein-protein interaction study to obtain the effective peptides from the inhalers that can bind the spike protein. Molecular docking simulation of S protein (receptor) with different compounds such as alpha-1-antitrypsin, dornase-alfa, angiotensin-converting enzyme-2 (ACE-2), human palate were analyzed. The peptide molecules obtained were further predicted as the potential anti- SARS-CoV-2 agents [75]. Protein peptide docking followed by the interface analysis study also showed that the amphibian derived peptides such as Dermaceptin-9 from the amphibian genus *Phyllomedusa* is an effective spike protein inhibitor of Sars- CoV-2 [76-77]. In 2020, Barh et al. implemented three different *in silico* strategies to design the potential novel peptide inhibitors that can interact and inhibit the Sars CoV-RBD - hACE2 interaction. The key binding residues were identified from the interaction study followed by identifying the peptide binders from the bacterial peptide database. Then a chimeric peptide was designed that is capable of binding the key residues of the SARS-CoV-2 -RBD - hACE2 complex. For the screening of the best potential peptides, the parameters like physiochemical properties, numbers, and positions of key residues binding, binding energy, and antiviral properties were considered [78]. Alibakhshi et al. conducted a computational study to design the effective peptides by targeting the RBD of SARS-CoV-2 spike protein and human ACE2 interaction. The analysis was based on taking stretches of peptides from the ACE2 protein. Further, the different mutants were designed by computational method, and interaction of the peptides with spike protein was studied by using the molecular docking simulation method. As a subsequent study, molecular dynamics simulation was carried out to evaluate the best mutant peptide that interacts with the S protein in comparison to the wild peptide [79]. A similar study was conducted by Panda et al., to design a peptide having a resemblance to human ACE-2 protein. The non-interacting residues of ACE2 were mutated to generate a mutant peptide library. The molecular docking by HADDOCK server followed by molecular dynamics simulation (150 nanoseconds) by Gromacs tool was used to identify the novel mutant peptide developed the enhanced binding affinity about three times [80].

8. Challenges and Future research scope

There is a continuous increasing trend in the knowledge level in the experimental data related to the structure of SARS-CoV-2 and its entry process to the host cell. Much of the information is available now in the form of published literature and databases. This data provides a solid background to apply the computational techniques such as modeling, identification, and characterization of novel antiviral peptides that would interfere with spike-ACE2 binding and the membrane fusion process. Although

the peptide molecules are advantageous over other small molecules, properties of the peptides like toxicity, immunogenicity, and stability of peptides remain as the major issues and need to be addressed in the development process of peptide-based inhibitors [81-85].

Moreover, the following specific challenges are associated with the discovery process of potential peptide inhibitors against the spike protein of SARS-CoV-2 and need to be addressed.

- S1 RBD domain of Spike glycoprotein is part of a highly mutable region, hence targeting to inhibit the domain is challenging, however, specifically targeting the peptide molecules to the HR region of the S2 subunit, with enhanced affinity might be effective to prevent the SARS-CoV-2 infections.
- Other than binding affinity property of AVPs to S-protein, prediction of several important parameters such as penetration capacity to the tissue, stability in the plasma, protease enzyme degradation potential, immunological interference, and toxicity is necessary.
- The full-length wild-type S protein structure of SARS-CoV-2 is still not available in the database. Hence important missing amino acid residues and loops might affect the in-silico results regarding peptide-protein binding. Hence, the complete form of the crystal structure of the spike protein (both wild-type as well as variants) is to be determined.

9. Conclusions

SARS-CoV-2 is evolved as a novel pathogenic virus with a significantly enhanced infection rate. Due to the deadliest nature of this coronavirus, it is essential to search for an effective medication to respond to this infectious disease to avoid pandemic situations. Specifically, the interaction of the spike glycoprotein of the virus with the human ACE2 receptor causes the viral entry into the host cell. So, the use of peptide-based inhibitor molecules against the spike protein will be a promising approach to inhibit the process. Currently, the therapeutic application of peptide molecules is implemented against many diseases. Anti-viral peptides are most often preferred over small molecules due to their specific, few side effects, and no drug resistance activity. So, the study about targeting the spike glycoprotein of the virus with the potential novel anti-viral peptides will create a milestone in this emerging area. However, the mutation acquired by the virus, *in vivo* bioavailability, toxicity, and stability of anti-viral peptides are the major limitations. The available sophisticated bioinformatics tools and databases can be implemented for structure prediction of peptides, binding affinity study, validation, and dynamics analysis, *in silico* toxicity, bioactivity, and stability prediction, and so on. Furthermore, these results obtained from the *in-silico* analysis can be further combined along with *the experimental* results, for the development of proper validated peptide-based inhibitors by targeting the SARS-CoV-2 glycoprotein.

*Created with BioRender.com.

Conflict of interest

Nothing

References

Santos-López G, Cortés-Hernández P, Vallejo-Ruiz V, Reyes-Leyva J. SARS-CoV-2: basic concepts, origin and treatment advances. Gac Med Mex. 2021;157(1):84-9. doi: 10.24875/GMM.M21000524, PMID 34125824.

Hu B, Guo H, Zhou P, Shi ZL. Characteristics of SARS-CoV-2 and COVID-19. Nat Rev Microbiol. 2021;19(3):141-54. doi: 10.1038/s41579-020-00459-7, PMID 33024307.

Yang J, Petitjean SJL, Koehler M, Zhang Q, Dumitru AC, Chen W, Derclaye S, Vincent SP, Soumillion P, Alsteens D. Molecular interaction and inhibition of SARS-CoV-2 binding to the ACE2 receptor. Nat Commun. 2020;11(1):4541. doi: 10.1038/s41467-020-18319-6, PMID 32917884.

V'kovski P, Kratzel A, Steiner S, Stalder H, Thiel V. Coronavirus biology and replication: implications for SARS-CoV-2. Nat Rev Microbiol. 2021;19(3):155-70. doi: 10.1038/s41579-020-00468-6, PMID 33116300.

Murgolo N, Therien AG, Howell B, Klein D, Koeplinger K, Lieberman LA, Adam GC, Flynn J, McKenna P, Swaminathan G, Hazuda DJ, Olsen DB. SARS-CoV-2 tropism, entry, replication, and propagation: considerations for drug discovery and development. PLOS Pathog. 2021;17(2):e1009225. doi: 10.1371/journal.ppat.1009225, PMID 33596266.

Trougakos IP, Stamatelopoulos K, Terpos E, Tsitsilonis OE, Aivalioti E, Paraskevis D, Kastritis E, Pavlakis GN, Dimopoulos MA. Insights to SARS-CoV-2 life cycle, pathophysiology, and rationalized treatments that target COVID-19 clinical complications. J Biomed Sci. 2021;28(1):9. doi: 10.1186/s12929-020-00703-5, PMID 33435929.

Martinez MA. Compounds with therapeutic potential against novel respiratory 2019 coronavirus. Antimicrob Agents Chemother. 2020;64(5):e00399-20. doi: 10.1128/AAC.00399-20, PMID 32152082.

Martinez MA. Clinical trials of repurposed antivirals for SARS-CoV-2. Antimicrob Agents Chemother. 2020;64(9):e01101-20. doi: 10.1128/AAC.01101-20, PMID 32631826.

Doi Y, Hibino M, Hase R, Yamamoto M, Kasamatsu Y, Hirose M, Mutoh Y, Homma Y, Terada M, Ogawa T, Kashizaki F, Yokoyama T, Koba H, Kasahara H, Yokota K, Kato H, Yoshida J, Kita T, Kato Y, Kamio T, Kodama N, Uchida Y, Ikeda N, Shinoda M, Nakagawa A, Nakatsumi H, Horiguchi T, Iwata M, Matsuyama A, Banno S, Koseki T, Teramachi M, Miyata M, Tajima S, Maeki T, Nakayama E, Taniguchi S, Lim CK, Saijo M, Imai T, Yoshida H, Kabata D, Shintani A, Yuzawa Y, Kondo M. A prospective, randomized, open-label trial of early versus late favipiravir therapy in hospitalized patients with COVID-19. Antimicrob Agents Chemother. 2020;64(12):e01897-20. doi: 10.1128/AAC.01897-20, PMID 32958718.

Cao B, Wang Y, Wen D, Liu W, Wang J, Fan G, Ruan L, Song B, Cai Y, Wei M, Li X, Xia J, Chen N, Xiang J, Yu T, Bai T, Xie X, Zhang L, Li C, Yuan Y, Chen H, Li H, Huang H, Tu S, Gong F, Liu Y, Wei Y, Dong C, Zhou F, Gu X, Xu J, Liu Z, Zhang Y, Li H, Shang L, Wang K, Li K, Zhou X, Dong X, Qu Z, Lu S, Hu X, Ruan S, Luo S, Wu J, Peng L, Cheng F, Pan L, Zou J, Jia C, Wang J, Liu X, Wang S, Wu X, Ge Q, He J, Zhan H, Qiu F, Guo L, Huang C, Jaki T, Hayden FG, Horby PW, Zhang D, Wang C. A trial of lopinavir–ritonavir in adults hospitalized with severe Covid-19. N Engl J Med. 2020;382(19):1787-99. doi: 10.1056/NEJMoa2001282, PMID 32187464.

Martinez MA. Lack of effectiveness of repurposed drugs for COVID-19 treatment. Front Immunol. 2021;12:635371. doi: 10.3389/fimmu.2021.635371, PMID 33777024.

Du L, He Y, Zhou Y, Liu S, Zheng BJ, Jiang S. The spike protein of SARS-CoV—a target for vaccine and therapeutic

development. Nat Rev Microbiol. 2009;7(3):226-36. doi: 10.1038/nrmicro2090, PMID 19198616.

Koley T, Madaan S, Chowdhury SR, Kumar M, Kaur P, Singh TP, Ethayathulla AS. Structural analysis of COVID-19 spike protein in recognizing the ACE2 receptor of different mammalian species and its susceptibility to viral infection. 3 Biotech. 2021;11(2):109. doi: 10.1007/s13205-020-02599-2, PMID 33552834.

Li F. Structure, function, and evolution of coronavirus spike proteins. Annu Rev Virol. 2016;3(1):237-61. doi: 10.1146/annurev-virology-110615-042301, PMID 27578435.

Henderson R, Edwards RJ, Mansouri K, Janowska K, Stalls V, Gobeil SMC, Kopp M, Li D, Parks R, Hsu AL, Borgnia MJ, Haynes BF, Acharya P. Controlling the SARS-CoV-2 spike glycoprotein conformation. Nat Struct Mol Biol. 2020;27(10):925-33. doi: 10.1038/s41594-020-0479-4, PMID 32699321.

Tang T, Bidon M, Jaimes JA, Whittaker GR, Daniel S. Coronavirus membrane fusion mechanism offers a potential target for antiviral development. Antiviral Res. 2020;178:104792. doi: 10.1016/j.antiviral.2020.104792.

Ke Z, Oton J, Qu K, Cortese M, Zila V, McKeane L, Nakane T, Zivanov J, Neufeldt CJ, Cerikan B, Lu JM, Peukes J, Xiong X, Kräusslich HG, Scheres SHW, Bartenschlager R, Briggs JAG. Structures and distributions of SARS-CoV-2 spike proteins on intact virions. Nature. 2020;588(7838):498-502. doi: 10.1038/s41586-020-2665-2, PMID 32805734.

Wrapp D, Wang N, Corbett KS, Goldsmith JA, Hsieh CL, Abiona O, Graham BS, McLellan JS. Cryo-EM structure of the 2019-nCoV spike in the prefusion conformation. Science. 2020;367(6483):1260-3. doi: 10.1126/science.abb2507, PMID 32075877.

Xia S, Liu M, Wang C, Xu W, Lan Q, Feng S, Qi F, Bao L, Du L, Liu S, Qin C, Sun F, Shi Z, Zhu Y, Jiang S, Lu L. Inhibition of SARS-CoV-2 (previously 2019-nCoV) infection by a highly potent pan-coronavirus fusion inhibitor targeting its spike protein that harbors a high capacity to mediate membrane fusion. Cell Res. 2020;30(4):343-55. doi: 10.1038/s41422-020-0305-x, PMID 32231345.

Sakkiah S, Guo W, Pan B, Ji Z, Yavas G, Azevedo M, Hawes J, Patterson TA, Hong H. Elucidating interactions between SARS-CoV-2 trimeric spike protein and ACE2 using homology modeling and molecular dynamics simulations. Front Chem. 2020;8:622632. doi: 10.3389/fchem.2020.622632, PMID 33469527.

Walls AC, Park YJ, Tortorici MA, Wall A, McGuire AT, Veesler D. Structure, function, and antigenicity of the SARS-CoV-2 spike glycoprotein. Cell. 2020;181(2):281-292.e6. doi: 10.1016/j.cell.2020.02.058, PMID 32155444.

Kang S, Peng W, Zhu Y, Lu S, Zhou M, Lin W, Wu W, Huang S, Jiang L, Luo X, Deng M. Recent progress in understanding 2019 novel coronavirus (SARS-CoV-2) associated with human respiratory disease: detection, mechanisms and treatment. Int J Antimicrob Agents. 2020;55(5):105950. doi: 10.1016/j.ijantimicag.2020.105950, PMID 32234465.

Letko M, Marzi A, Munster V. Functional assessment of cell entry and receptor usage for SARS-CoV-2 and other lineage B betacoronaviruses. Nat Microbiol. 2020;5(4):562-9. doi: 10.1038/s41564-020-0688-y, PMID 32094589.

Chang KY, Yang JR. Analysis and prediction of highly effective antiviral peptides based on random forests. PLOS ONE. 2013;8(8):e70166. doi: 10.1371/journal.pone.0070166, PMID 23940542.

Castel G, Chtéoui M, Heyd B, Tordo N. Phage display of combinatorial peptide libraries: application to antiviral research. Molecules. 2011;16(5):3499-518. doi: 10.3390/molecules16053499, PMID 21522083.

Charoenkwan P, Anuwongcharoen N, Nantasenamat C, Hasan MM, Shoombuatong W. In silico approaches for the prediction and analysis of antiviral peptides: a review. Curr Pharm Des. 2021;27(18):2180-8. doi: 10.2174/1381612826666201102105827, PMID 33138759.

Kaspar AA, Reichert JM. Future directions for peptide therapeutics development. Drug Discov Today. 2013;18(17-18):807-17. doi: 10.1016/j.drudis.2013.05.011, PMID 23726889.

Bruno BJ, Miller GD, Lim CS. Basics and recent advances in peptide and protein drug delivery. Ther Deliv. 2013;4(11):1443-67. doi: 10.4155/tde.13.104, PMID 24228993.

Schütz D, Ruiz-Blanco YB, Münch J, Kirchhoff F, Sanchez-Garcia E, Müller JA. Peptide and peptide-based inhibitors of SARS-CoV-2 entry. Adv Drug Deliv Rev. 2020;167:47-65. doi: 10.1016/j.addr.2020.11.007, PMID 33189768.

Mahendran ASK, Lim YS, Fang CM, Loh HS, Le CF. The potential of antiviral peptides as COVID-19 therapeutics. Front Pharmacol. 2020;11:575444. doi: 10.3389/fphar.2020.575444, PMID 33041819.

Sharma A, Pant K, Pande A, Sinha S, Pant B. Modeling novel anti-viral peptides (AVPs) with in-silico docking simulations against corona virus. Mater Today Proc. 2021;46:11169-76. doi: 10.1016/j.matpr.2021.02.377, PMID 33680868.

Agarwal G, Gabrani R. Antiviral peptides: identification and validation. Int J Pept Res Ther. 2021;27:149-68.

Mahmud S, Biswas S, Kumar Paul G, Mita MA, Afrose S, Robiul Hasan M, Sharmin Sultana Shimu M, Uddin MAR, Salah Uddin M, Zaman S, Kaderi Kibria KM, Arif Khan M, Bin Emran T, Abu Saleh M. Antiviral peptides against the main protease of SARS-CoV-2: A molecular docking and dynamics study. Arab J Chem. 2021;14(9). doi: 10.1016/j.arabjc.2021.103315, PMID 103315.

Dai C, Ma Y, Zhao Z, Zhao R, Wang Q, Wu Y, Cao Z, Li W. Mucroporin, the first cationic host defense peptide from the venom of Lychas mucronatus. Antimicrob Agents Chemother. 2008;52(11):3967-72. doi: 10.1128/AAC.00542-08, PMID 18779362.

Li Q, Zhao Z, Zhou D, Chen Y, Hong W, Cao L, Yang J, Zhang Y, Shi W, Cao Z, Wu Y, Yan H, Li W. Virucidal activity of a scorpion venom peptide variant mucroporin-M1 against measles, SARS-CoV and influenza H5N1 viruses. Peptides. 2011;32(7):1518-25. doi: 10.1016/j.peptides.2011.05.015, PMID 21620914.

Mitra D, Pandey J, Jain A, Swaroop S. In silico design of multi-epitope-based peptide vaccine against SARS-CoV-2 using its spike protein. J Biomol Struct Dyn. 2021:1-14. doi: 10.1080/07391102.2020.1869092, PMID 33403946.

Stoddard SV, Wallace FE, Stoddard SD, Cheng Q, Acosta D, Barzani S, Bobay M, Briant J, Cisneros C, Feinstein S, Glasper K, Hussain M, Lidoski A, Lingareddy P, Lovett G, Matherne L, McIntosh J, Moosani N, Nagge L, Nyamkondiwa K, Pratt I, Root E, Rutledge MR, Sawyer M, Singh Y, Smith K, Tanveer U, Vaghela S. In silico design of peptide-based SARS-CoV-2 fusion inhibitors that target WT and mutant versions of SARS-CoV-2 HR1 domains. Biophysica. 2021;1(3):311-27. doi: 10.3390/biophysica1030023.

Ling R, Dai Y, Huang B, Huang W, Yu J, Lu X, Jiang Y. In silico design of antiviral peptides targeting the spike protein of SARS-CoV-2. Peptides. 2020;130:170328. doi: 10.1016/j.peptides.2020.170328.

Alibakhshi A, Ahangarzadeh S, Beikmohammadi L, Soltanmohammadi B, Bahrami AA, Ranjbar MM, Mohammadi E. Computational design of a potential therapeutic peptide against

spike protein of SARS-CoV-2. J Comput Biophys Chem. 2021;20(4):337-46. doi: 10.1142/S2737416521500162.

Mustafa S, Balkhy H, Gabere M. Peptide-protein interaction studies of antimicrobial peptides targeting middle east respiratory syndrome coronavirus spike protein: an in-silico approach. Adv Bioinformatics. 2019;2019:6815105. doi: 10.1155/2019/6815105, PMID 31354813.

Bangaru S, Ozorowski G, Turner HL, Antanasijevic A, Huang D, Wang X, Torres JL, Diedrich JK, Tian JH, Portnoff AD, Patel N, Massare MJ, Yates JR, Nemazee D, Paulson JC, Glenn G, Smith G, Ward AB. Structural analysis of full-length SARS-CoV-2 spike protein from an advanced vaccine candidate. Science. 2020;370(6520):1089-94. doi: 10.1126/science.abe1502, PMID 33082295.

Fikriani CN, Ardana IKKG, Listyorini D. The comparison of SARS-CoV-2, SARS-CoV, and MERS-CoV genome and spike protein variations. J Riset Biologi Aplikasinya. 2021;3(1):38-44. doi: 10.26740/jrba.v3n1.p38-44.

Wang G, Li X, Wang Z. APD3: the antimicrobial peptide database as a tool for research and education. Nucleic Acids Res. 2016;44(D1):D1087-93. doi: 10.1093/nar/gkv1278, PMID 26602694.

Du L, Yang Y, Zhou Y, Lu L, Li F, Jiang S. MERS-CoV spike protein: a key target for antivirals. Expert Opin Ther Targets. 2017;21(2):131-43. doi: 10.1080/14728222.2017.1271415, PMID 27936982.

Zhao H, Zhou J, Zhang K, Chu H, Liu D, Poon VKM, Chan CC, Leung HC, Fai N, Lin YP, Zhang AJ, Jin DY, Yuen KY, Zheng BJ. A novel peptide with potent and broad-spectrum antiviral activities against multiple respiratory viruses. Sci Rep. 2016;6(1):22008. doi: 10.1038/srep22008, PMID 26911565.

Wang G. Natural antimicrobial peptides as promising anti-HIV candidates. Curr Top Pept Protein Res. 2012;13:93-110. PMID 26834391.

Gowthaman R, Guest JD, Yin R, Adolf-Bryfogle J, Schief WR, Pierce BG. CoV3D: a database of high resolution coronavirus protein structures. Nucleic Acids Res. 2021;49(D1):D282-7. doi: 10.1093/nar/gkaa731, PMID 32890396.

Morris, G. M.; Lim-Wilby, M. Molecular Docking. In. Methods in Molecular Biology; Humana Press 2008, (365–382). DOI: 10.1007/978-1-59745-177-2_19

Satpathy, R. Application of Molecular Docking Methods on Endocrine Disrupting Chemicals: A Review. J. Appl. Biotechnol. Rep. 2020; 7: 74–80.

Wang, J.; Alekseenko, A.; Kozakov, D.; Miao, Y. Improved Modeling of Peptide-Protein Binding Through Global Docking and Accelerated Molecular Dynamics Simulations. Front. Mol. Biosci. 2019; 6: 112. DOI: 10.3389/fmolb.2019.00112

Ciemny, M.; Kurcinski, M.; Kamel, K.; Kolinski, A.; Alam, N.; Schueler-Furman, O.; Kmiecik, S. Protein–Peptide Docking: Opportunities and Challenges. Drug Discov. Today 2018, 23: 1530–37. DOI: 10.1016/j.drudis.2018.05.006

Padilla-Sanchez V, Padilla-Sanchez V, Padilla-Sanchez V, Padilla-Sanchez V, Padilla-Sanchez V, Padilla-Sanchez V, Padilla-Sanchez V. In silico analysis of SARS-CoV-2 spike glycoprotein and insights into antibody binding. Res Ideas Outcomes. 2020;6:e55281. doi: 10.3897/rio.6.e55281.

Allam M, Ismail A, Khumalo ZTH, Kwenda S, Van Heusden P, Cloete R, ... & Bhiman JN 2020. Whole genome sequence of the severe acute respiratory syndrome coronavirus 2 SARS-COV-2 obtained from A South African coronavirus Disease 2019 Covid19 patient. *Accessed on*, *2*.

Hassanzadeh K, Perez Pena H, Dragotto J, Buccarello L, Iorio F, Pieraccini S, Sancini G, Feligioni M. Considerations around the SARS-CoV-2 Spike Protein with particular attention to COVID-19 brain infection and neurological symptoms. ACS Chem Neurosci. 2020;11(15):2361-9. doi: 10.1021/acschemneuro.0c00373, PMID 32627524.

Martin WR, Cheng F. Repurposing of FDA-approved toremifene to treat COVID-19 by blocking the Spike glycoprotein and NSP14 of SARS-CoV-2. J Proteome Res. 2020;19(11):4670-7. doi: 10.1021/acs.jproteome.0c00397, PMID 32907334.

Jaimes JA, André NM, Chappie JS, Millet JK, Whittaker GR. Phylogenetic analysis and structural modeling of SARS-CoV-2 spike protein reveals an evolutionary distinct and proteolytically sensitive activation loop. J Mol Biol. 2020;432(10):3309-25. doi: 10.1016/j.jmb.2020.04.009, PMID 32320687.

King M, Dinulos A, DaMota J, Walton E, Dahlquist K. A bioinformatics approach to investigating the structural and functional consequences of SNPs in TMPRSS2 for COVID-19 infection. FASEB J. 2021;35(S1). doi: 10.1096/fasebj.2021.35.S1.04753.

Awadelkareem EA, Ali SA. Vaccine design of coronavirus spike (S) glycoprotein in chicken: immunoinformatics and computational approaches. Transl Med Commun. 2020;5(1):13. doi: 10.1186/s41231-020-00063-0, PMID 32869000.

Prashantha CN, Gouthami K, Lavanya L, Bhavanam S, Jakhar A, Shakthiraju RG, Suraj V, Sahana KV, Sujana HS, Guruprasad NM, Ramachandra R. Molecular screening of antimalarial, antiviral, anti-inflammatory and HIV protease inhibitors against spike glycoprotein of coronavirus. J Mol Graph Model. 2021;102:107769. doi: 10.1016/j.jmgm.2020.107769.

Ibrahim IM, Abdelmalek DH, Elshahat ME, Elfiky AA. COVID-19 spike-host cell receptor GRP78 binding site prediction. J Infect. 2020;80(5):554-62. doi: 10.1016/j.jinf.2020.02.026, PMID 32169481.

Weng G, Wang E, Chen F, Sun H, Wang Z, Hou T. Assessing the performance of MM/PBSA and MM/GBSA methods. 9. Prediction reliability of binding affinities and binding poses for protein–peptide complexes. Phys Chem Chem Phys. 2019;21(19):10135-45. doi: 10.1039/c9cp01674k, PMID 31062799.

Massova I, Kollman PA. Computational alanine scanning to probe protein−protein interactions: a novel approach to evaluate binding free energies. J Am Chem Soc. 1999;121(36):8133-43. doi: 10.1021/ja990935j.

Hou T, Wang J, Li Y, Wang W. Assessing the performance of the MM/PBSA and MM/GBSA methods. I. The accuracy of binding free energy calculations based on molecular dynamics simulations. J Chem Inf Model. 2011;51(1):69-82. doi: 10.1021/ci100275a, PMID 21117705.

Spiliotopoulos D, Kastritis PL, Melquiond AS, Bonvin AM, Musco G, Rocchia W, Spitaleri A. dMM-PBSA: a new HADDOCK scoring function for protein-peptide docking. Front Mol Biosci. 2016;3:46. doi: 10.3389/fmolb.2016.00046, PMID 27630991.

Genheden S, Ryde U. The MM/PBSA and MM/GBSA methods to estimate ligand-binding affinities. Expert Opin Drug Discov. 2015;10(5):449-61. doi: 10.1517/17460441.2015.1032936, PMID 25835573.

Lim H, Baek A, Kim J, Kim MS, Liu J, Nam KY, Yoon J, . Hot spot profiles of SARS-CoV-2 and human ACE2 receptor protein interaction obtained by density functional tight binding fragment molecular orbital method. Sci Rep. 2020;10(1):16862. doi: 10.1038/s41598-020-73820-8, PMID 33033344.

Ortega JT, Serrano ML, Pujol FH, Rangel HR. Role of changes in SARS-CoV-2 spike protein in the interaction with the human ACE2 receptor: an in silico analysis. Excli J. 2020;19:410-7. doi: 10.17179/excli2020-1167, PMID 32210742.

Dror RO, Dirks RM, Grossman JP, Xu H, Shaw DE. Biomolecular simulation: a computational microscope for molecular biology. Annu Rev Biophys. 2012;41:429-52. doi: 10.1146/annurev-biophys-042910-155245, PMID 22577825.

Justino GC, Nascimento CP, Justino MC. Molecular dynamics simulations and analysis for bioinformatics undergraduate students. Biochem Mol Biol Educ. 2021;49(4):570-82. doi: 10.1002/bmb.21512, PMID 33844418.

Ali R, Rani R, Kumar S. New peptide based therapeutic approaches. In: Ashraf GMd, Sheikh IA, editors. Advances in protein chemistry. Jeddah: OMICS Group eBooks; 2013.

Gentilucci L, De Marco R, Cerisoli L. Chemical modifications designed to improve peptide stability: incorporation of non-natural amino acids, pseudo-peptide bonds, and cyclization. Curr Pharm Des. 2010;16(28):3185-203. doi: 10.2174/138161210793292555, PMID 20687878.

Pomplun, S. Targeting the SARS-CoV-2-spike Protein: From Antibodies to Miniproteins and Peptides. R.S.C. Med. Chem. 2020; 12:197–202. DOI: 10.1039/d0md00385a

Wong, F. C.; Ong, J. H.; Chai, T. T. Identification of Putative Cell-Entry-Inhibitory Peptides Against SARS-CoV-2 from Edible Insects: An in-Silico Study. EFOOD 2020; 1 : 357–68. DOI: 10.2991/efood.k.200918.002

Allam, L.; Ghrifi, F.; Mohammed, H.; El Hafidi, N.; El Jaoudi, R.; El Harti, J.; Lmimouni, B.; Belyamani, L.; Ibrahimi, A. Targeting the GRP78-Dependant SARS-CoV-2 Cell Entry by Peptides and Small Molecules. Bioinformatics Biol. Insights 2020; 14: 1177932220965505. DOI: 10.1177/1177932220965505

Salman, S.; Shah, F. H.; Chaudhry, M.; Tariq, M.; Akbar, M. Y.; Adnan, M. In Silico Analysis of Protein/Peptide-Based Inhalers Against SARS-CoV-2. Future Virol. 2020; 15 : 557–64. DOI: 10.2217/fvl-2020-0119.

Fakih, T. M. Dermaseptin-Based Antiviral Peptides to Prevent COVID-19 through In Silico Molecular Docking Studies Against SARS-Cov-2 Spike Protein. Pharm. Sci. Res. 2020; 7: 65–70. DOI: 10.7454/psr.v7i4.1079

Satpathy, R. In Silico Prediction of Anti-SARS-CoV-2 Effect of Dermaseptin Peptides from Amphibian Origin. Trends Pept. Protein Sci. 2020; 5: 1–9.

Barh, D.; Tiwari, S.; Silva Andrade, B.; Giovanetti, M.; Almeida Costa, E.; Kumavath, R.; Ghosh, P.; Góes-Neto, A.; Carlos Junior Alcantara, L.; Azevedo, V. Potential Chimeric Peptides to Block the SARS-CoV-2 Spike Receptor-Binding Domain. F1000Res. 2020; 9: 576. DOI: 10.12688/f1000research.24074.1

Alibakhshi, A.; Ahangarzadeh, S.; Beikmohammadi, L.; Soltanmohammadi, B.; Bahrami, A. A.; Ranjbar, M. M.; Mohammadi, E. Computational Design of a Potential Therapeutic Peptide Against Spike Protein of SARS-CoV-2. J. Comput. Biophys. Chem. 2021; 20 (4): 337–46. DOI: 10.1142/S2737416521500162

Panda, S. K.; Sen Gupta, P. S.; Biswal, S.; Ray, A. K.; Rana, M. K. ACE-2-derived Biomimetic Peptides for the Inhibition of Spike Protein of SARS-CoV-2. J. Proteome Res. 2021; 20 (2): 1296–1303. DOI: 10.1021/acs.jproteome.0c00686.

Efaz FM, Islam S, Talukder SA, Akter S, Tashrif MZ, Ali MA, Sufian MA, Parves MR, Islam MJ, Halim MA. Repurposing fusion inhibitor peptide against SARS-CoV-2. J Comp Chem. 2021;42(32):2283-93. doi: 10.1002/jcc.26758, PMID 34591335.

Chowdhury AS, Reehl SM, Kehn-Hall K, Bishop B, Webb-Robertson BM. Better understanding and prediction of antiviral peptides through primary and secondary structure feature importance. Sci Rep. 2020;10(1):19260. doi: 10.1038/s41598-020-76161-8, PMID 33159146.

Vlieghe P, Lisowski V, Martinez J, Khrestchatisky M. Synthetic therapeutic peptides: science and market. Drug Discov Today. 2010;15(1-2):40-56. doi: 10.1016/j.drudis.2009.10.009, PMID 19879957.

Thotakura N, Kaushik L, Kumar V, Preet S, Babu PV. Advanced approaches of bioactive peptide molecules and protein drug delivery systems. Curr Pharm Des. 2018;24(43):5147-63. doi: 10.2174/1381612825666190206211458, PMID 30727874.

Uusna J, Langel K, Langel Ü. Toxicity, immunogenicity, uptake, and kinetics methods for CPPs Cell-Penetrating Peptides. Methods Mol Biol. 2015;1324:(133-48). doi: 10.1007/978-1-4939-2806-4_9, PMID 26202267.

JJBS

Volume 15, Number 5,December 2022
ISSN 1995-6673
Pages 739 – 762
https://doi.org/10.54319/jjbs/150503

Jordan Journal of Biological Sciences

Delavirdine and Dolutegravir as Potential Inhibitors of SARS-CoV-2 Main Protease (M^{pro}): An *In-Silico* Study

Fadi G. Saqallah [1,2], Abdulsalam Q. Almashhadani [3], Belal O. Al-Najjar [4,*] and Habibah A. Wahab [2,3,*]

1 Discipline of Pharmaceutical Chemistry, School of Pharmaceutical Sciences, Universiti Sains Malaysia, 11800 Penang, Malaysia; 2 Pharmaceutical Design and Simulation (PhDS) Laboratory, School of Pharmaceutical Sciences, Universiti Sains Malaysia, 11800 Penang, Malaysia; 3 Discipline of Pharmaceutical Technology, School of Pharmaceutical Sciences, Universiti Sains Malaysia, 11800 Penang, Malaysia; 4 Department of Pharmaceutical Sciences, Faculty of Pharmacy, Al-Ahliyya Amman University, 19328, Amman, Jordan

Received: December 30, 2021; Revised: February 9, 2022; Accepted: February 19, 2022

Abstract

SARS-CoV-2 is a recently discovered member of coronaviruses (CoVs) family that is very contagious and has a high infectivity rate. Expanding the search for antivirals which act against SARS-CoV-2 would allow more treatment options for infected patients, accelerate their recovery time, and avoid some serious adverse effects that the limited number of approved medications might cause. In this study, we assess 74 antiviral agents, chloroquine, and hydroxychloroquine inhibitory activity against the virus's main protease (M^{pro}), which is essential for its replication. Virtual screening of the compounds has been conducted where the screened ligands were assessed according to their binding energy to the main binding pocket of M^{pro}. Ten antivirals, in addition to chloroquine and hydroxychloroquine were further studied through molecular docking simulations and assessed for their binding conformations and interactions with the protein's catalytic dyad residues. Furthermore, molecular dynamics simulations were established to study delavirdine, dolutegravir, raltegravir and vicriviroc for 100 ns. Results show that delavirdine and dolutegravir are excellent candidates that can inhibit the catalytic activity of M^{pro}. This could significantly reduce patients' hospitalisation time and the need for secondary measures.

Keywords: SARS-CoV-2, CoVID-19, main protease, delavirdine, dolutegravir

1. Introduction

Coronaviruses (CoVs) are a broad family of single-stranded RNA viruses. They can infect animals and humans, causing respiratory, gastrointestinal, hepatic, and neurological disorders (Zimmermann & Curtis, 2020). CoVs can be classified into four genera; alpha-CoV, beta-CoV, gamma-CoV, and delta-CoV, according to their protein sequences. To date, seven human coronaviruses (HCoVs) have been identified, including two alpha-CoVs; HCoV-NL63 and HCoV-229E, and five beta-CoVs; HCoV-OC43, HCoV-HKU1, the Severe Acute Respiratory Syndrome-CoV (SARS-CoV), the Middle East Respiratory Syndrome-CoV (MERS-CoV), and the Severe Acute Respiratory Syndrome-CoV-2 (SARS-CoV-2, also called CoVID-19) (Ye *et al.*, 2020; Zaki *et al.*, 2012). SARS-CoV-2 is a recently identified CoV discovered by the end of December 2019. It was identified after several Chinese health authorities observed clusters of unknown-cause pneumonia-like symptoms in Wuhan City, China (Lu *et al.*, 2020; Zhou *et al.*, 2020).

Computer-aided modelling reveals a high degree of resemblance between SARS-CoV-2 and the well-known SARS-CoV from 2002, with identical receptor-binding domain structures that maintain van der Waals forces (Zhang *et al.*, 2020). SARS-CoV-2 recognises human ACE2 more efficiently with a stronger spike (S) protein binding affinity to human ACE2 than SARS-CoV. This increases the SARS-CoV-2 ability to spread between people (Wan *et al.*, 2020). CoVs have been identified to contain four essential proteins that can be targeted in drug discovery. These targets include spike (S), membrane (M), envelope (E), and nucleocapsid (N) proteins. However, a serine-type 3-chymotrypsin protease, also known as the main protease, $3CL^{pro}$ or M^{pro} (33.8 kDa), has also been identified. This enzyme is encoded by the non-structural protein 5 (NSp5). M^{pro} is an essential protein in the replication cycle of the virus. It carries out the proteolytic activity of two overlapping polyproteins; pp1a and pp1ab encoded by the replicase enzyme, and digests them into polypeptides (Fehr & Perlman, 2015; Hegyi & Ziebuhr, 2002). Today, about 353 crystal structures of SARS-CoV-2 M^{pro} are deposited in the Protein Data Bank (RCSB PDB) (Berman *et al.*, 2000). These crystal structures vary between being in their apo state or complexed with various inhibitors. A potent peptide-like irreversible inhibitor (N3P) (Figure 1) is a known inhibitor of SARS and MERS proteases which has been studied extensively for its inhibitory activity against SARS-CoV-2 M^{pro} (Jin, Du, Xu, Deng, Liu, Zhao, Zhang, Li, Zhang, Peng, *et al.*, 2020).

* Corresponding authors. e-mail: b.najjar@ammanu.edu.jo (B.O.A.-N.), habibahw@usm.my (H.A.W.).

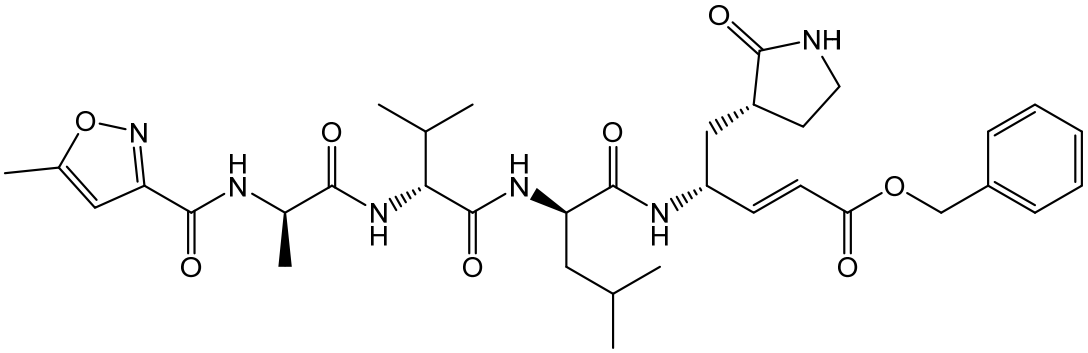

Figure 1. Irreversible peptide-like inhibitor (N3P) of coronavirus M^{pro} (sequence: 02J-ALA-VAL-LEU-PJE-010).

Patients with confirmed CoVID-19 infections show symptoms like respiratory distress, fever, cough, and shortness of breath. The incubation period seems to be between two days and up to two weeks after exposure (Carlos *et al.*, 2020). Therefore, early diagnosis of CoVID-19 is important for treating the disease and preventing it from spreading further. Many studies have found that chest computed tomography (CT) offers high sensitivity for early CoVID-19 diagnosis. However, real-time polymerase chain reaction (RT-PCR) detection of viral nucleic acid remains the reference test. Compared to RT-PCR, chest CT imaging can be a more accurate, practical, and rapid method of diagnosing and assessing the infection, especially in epidemic areas. Other diagnosis procedures of CoVID-19 include but are not limited to, clinical, physical, and laboratory diagnosis (Ai *et al.*, 2020; Zu *et al.*, 2020).

At the same time, intensive efforts by many researchers are being pushed into investigating different potential medications, including antivirals (anti-influenza and anti-HIV-1), combinations of antivirals, and anti-malaria drugs to treat SARS-CoV-2 infections. Many antiviral medications have been studied and suggested to treat SARS-CoV-2, such as lopinavir/ritonavir, ribavirin, indinavir, maraviroc, and simeprevir (Chu *et al.*, 2004; Dong *et al.*, 2020; Li & De Clercq, 2020). Recently, the US Food & Drug Administration (FDA) agency discouraged the use of these antivirals for the management of CoVID-19 infections (NIH, 2021). It is noteworthy that the use of lopinavir/ritonavir combination therapy has been found not to decrease the mortality rate or demonstrate any clinical evidence of improvement in hospitalised patients in two clinical trials (Horby, Mafham, Bell*, et al.*, 2020; Pan *et al.*, 2021). To date, the only approved antivirals for managing severe SARS-CoV-2 infections are remdesivir, Paxlovid, and molnupiravir. Remdesivir was approved in October 2020 for those above 12 years old and weighing ≥40 kg. Clinical trials showed a significant decrement in recovery time for patients with moderate to severe symptoms (FDA, 2020). On the other hand, Paxlovid, a trade name by Pfizer for a combination of nirmatrelvir tablets and ritonavir tablets, co-packaged for oral use, was approved recently (December 2021) by the FDA (FDA, 2021b). Paxlovid was shown to significantly decrease the need for hospitalisation and the number of deaths among severely SARS-CoV-2 infected patients (Mahase, 2021). Lastly, molnupiravir, an antiviral developed by Merck, was approved by the FDA around the same time of approving Paxlovid. Molnupiravir was announced to be restrictively administered for patients older than 18 and at high risk for developing severe symptoms that would require hospitalisation or might lead to death (FDA, 2021a).

In this study, we focus on the potential activity of 74 antiviral agents, as well as chloroquine and hydroxychloroquine as M^{pro} inhibitors of SARS-CoV-2. This investigation aims to examine the mechanisms of binding and interactions of these antivirals, chloroquine, and hydroxychloroquine with SARS-CoV-2 M^{pro} using molecular docking, molecular dynamics, and mechanics calculations. Furthermore, exploring new antiviral agents for the management of SARS-CoV-2 infections would allow a wider choice of medications for patients with certain medical conditions which would prevent them from taking the currently approved antivirals, and for patients whom would suffer intolerable or allergic adverse reactions to the approved antivirals. The choice of M^{pro} as the target of interest comes after realising its importance in the virus life cycle and the fact that there are no correlated homologues proteins in humans.

2. Methodology

2.1. Virtual Screening

SARS-CoV-2 M^{pro} crystal structure was downloaded from Protein Data Bank (PDB) (PDB ID: 6LU7) (Berman *et al.*, 2000; Jin, Du, Xu, Deng, Liu, Zhao, Zhang, Li, Zhang, & Peng, 2020). The protease was cleaned and prepared using BIOVIA Discovery Studio 16.1 (BIOVIA, 2017). Further preparations by adding Kollman charges and polar hydrogens were done with the help of AutoDockTools 1.5.6 (Morris *et al.*, 2009) and then saved in PDBQT format (Sanner, 1999). Two-dimensional chemical structures of chloroquine, hydroxychloroquine, and the 74 antivirals were downloaded from National Institutes of Health (NIH) PubChem (Table S1, Supplementary Information) (Kim *et al.*, 2018). All compounds were compiled into one PDBQT with the help of OpenBabel 3.0.0 (O'Boyle *et al.*, 2011). Virtual screening of 500 runs among all target compounds was achieved using AutoDock Vina 1.1.2 (Trott & Olson, 2010) (Grid size: 80×80×80, Coordinates: -9.732, 11.403, 68.925, as *x*, *y*, *z*, respectively). However, the peptide-like internal ligand (N3P) from the crystal structure of the enzyme was employed as a control inhibitor.

2.2. Molecular Docking

The top ten antivirals with the lowest binding energies determined by AutoDock Vina were selected for this step besides chloroquine, hydroxychloroquine, and the control peptide; N3P. Gasteiger charges were added. Grid and docking parameters files were prepared using AutoDockTools 1.5.6 with the same grid size and coordinates as aforementioned for 250 Genetic Algorithm runs. Docking simulations were performed using AutoDock 4.2.6 (Morris *et al.*, 2009).

2.3. Molecular Dynamics

Four antivirals with the highest affinities towards M^{pro} were selected for this part of the study. The selection of the compounds was accomplished after evaluating the docked compounds' binding energies and conformations, and the type of interactions at the binding pocket of M^{pro}, especially with the catalytic dyad residues. Molecular dynamics studies have been established with the help of AMBER 18.0 (Case *et al.*, 2018). Simulation systems were prepared by subjecting the protein crystal structure to the ff14SB forcefield and checking residues' protonation states. Ligands' topology files were prepared using Antechamber, AM1-BCC charge model, and the general AMBER force field (GAFF). Simulations were carried out in TIP3P water while adding four natrium ions to neutralise the systems. First, minimisation of the simulation systems for 10,000 steepest descent steps and 5,000 conjugate gradient steps was done. Then, gradual heating of the systems using NVT and NPT ensembles was done for 3 ns. Equilibration was further carried out for 6 ns using the NPT ensemble. Finally, a multistep production run of the systems for 100 ns was conducted using Particle Mesh Ewald Molecular Dynamics (PMEMD) engine while applying SHAKE algorithm and constant pressure periodicity (Götz *et al.*, 2012; Le Grand *et al.*, 2013; Salomon-Ferrer *et al.*, 2013). Later, MDAnalysis (Gowers *et al.*, 2019; Michaud-Agrawal *et al.*, 2011) was employed to analyse the pairwise Root Mean Square Deviation (RMSD). Further, CPPTRAJ (Roe & Cheatham III, 2013) was used to analyse the Root Mean Square Fluctuation (RMSF) of the protein, the hydrogen bonds between the binding pocket's residues and the interacting ligand, and the mass-weighted radius of gyration (RadGyr) of the non-hydrogen atoms of these residues for the last 10 ns of the simulation of each system.

2.4. Molecular Mechanics Free Energy of Binding

To calculate the free energy difference ($\Delta G_{binding}$) between the bound and unbound states of each complex, and to estimate the dynamic binding affinity, the Generalized Born Surface Area (MM-GBSA) calculations were employed (Miller III *et al.*, 2012). Energy values were calculated for the last 10,000 frames with an interval of 100 frames, salt concentration of 0.150 M, and no quasi-harmonic entropy approximation. Runs were performed with the help of the solvated, complex, receptor, and ligand topology files.

3. Results & Discussion

3.1. Virtual Screening

Virtual screening of the 74 antivirals, chloroquine, and hydroxychloroquine against SARS-CoV-2 M^{pro} crystal structure (PDB: 6LU7) was accomplished using AutoDock Vina. The peptide-like inhibitor showed a decently low binding energy of -9.3 kcal/mol. Evaluation of the binding affinities was based on the estimated binding energies of the molecules and their binding conformations at the binding pocket. Both chloroquine and hydroxychloroquine showed low binding energies of -5.1 and -5.9 kcal/mol, respectively, suggesting that their interactions at the main pocket of M^{pro} are comparatively weak (Table 1). Moreover, their binding conformations show that the quinoline ring system of chloroquine protrudes out of the pocket groove and does not interact strongly with the surrounding amino acid residues. In contrast, hydroxychloroquine fitted nicely inside the pocket (Figure 2-a). Among the 74 antivirals, dolutegravir, maraviroc, daclatasvir, simeprevir, vicriviroc, delavirdine, lopinavir, raltegravir, indinavir, and sofosbuvir were the top antiviral molecules which bound with energy values that are very comparable to the control ($\leq$ -8.0 kcal/mol) (Table 1). At the same time, their binding conformations occupy the active site in a way which resembles that of N3P (Figure 2-b). It should be noted that the virtual screening results are consistent with previously reported findings (Ibrahim *et al.*, 2021; Khater & Nassar, 2021). The top ten antivirals with the lowest binding energies, in addition to chloroquine and hydroxychloroquine were selected for further assessment against SARS-CoV-2 M^{pro}.

Remdesivir has been studied extensively for its inhibitory activity against M^{pro} (Daoud *et al.*, 2021; Naik *et al.*, 2020). Later studies have stated that the official target of this antiviral medication is the RNA-dependent RNA-polymerase (RdRp) (Kokic *et al.*, 2021). Nevertheless, a double-blind, randomised, placebo-controlled clinical trial was conducted to confirm the effectiveness of remdesivir, which has been found to reduce hospitalisation time and lower the chances of respiratory tract infections (Beigel *et al.*, 2020). However, another study group found that GS-441524 and its phosphorylated analogue are active metabolites of remdesivir, which act on the non-structural protein 3 (NSp3) of CoVID-19 (Ni *et al.*, 2021). These findings would explain the moderate activity of remdesivir towards M^{pro}.

Table 1. Estimated binding energies of the 74 antivirals (sorted ascendingly), chloroquine, and hydroxychloroquine in comparison with the peptide-like control (N3P) as a result of virtual screening

Compound	*Binding Energy (kcal/mol)*	*Compound*	*Binding Energy (kcal/mol)*
N3P (Control)	*-9.3*		
Chloroquine	*-5.1*	*Cocaine*	*-6.7*
Hydroxychloroquine	*-5.9*	*Imiquimod*	*-6.7*
Dolutegravir	*-8.9*	*Valganciclovir*	*-6.7*
Maraviroc	*-8.5*	*Nitazoxanide*	*-6.6*
Daclatasvir	*-8.3*	*Telbivudine*	*-6.6*
Simeprevir	*-8.3*	*Edoxudine*	*-6.5*
Vicriviroc	*-8.2*	*Famciclovir*	*-6.5*
Delavirdine	*-8.1*	*Nelfinavir*	*-6.5*
Lopinavir	*-8.1*	*Nevirapine*	*-6.5*
Raltegravir	*-8.1*	*Cidofovir*	*-6.4*
Indinavir	*-8.0*	*Stavudine*	*-6.4*
Sofosbuvir	*-8.0*	*Vidarabine*	*-6.4*
Baloxavir marboxil	*-7.9*	*Arbidol*	*-6.3*
Loviride	*-7.9*	*Ganciclovir*	*-6.3*
Podophyllotoxin	*-7.9*	*Tenofovir*	*-6.3*
Darunavir	*-7.8*	*Viramidine*	*-6.3*
Fosamprenavir	*-7.8*	*Adefovir*	*-6.2*
Remdesivir	*-7.8*	*Didanosine*	*-6.2*
Tipranavir	*-7.8*	*Penciclovir*	*-6.2*
Elvitegravir	*-7.7*	*Valaciclovir*	*-6.2*
Ritonavir	*-7.7*	*Ribavirin*	*-6.1*
Amprenavir	*-7.6*	*Tromantadine*	*-6.0*
Efavirenz	*-7.6*	*Oseltamivir*	*-5.9*
Pleconaril	*-7.6*	*Peramivir*	*-5.9*
Boceprevir	*-7.5*	*Rimantadine*	*-5.9*
Letermovir	*-7.5*	*Zalcitabine*	*-5.9*
Cobicistat	*-7.4*	*Zanamivir*	*-5.9*
Rilpivirine	*-7.3*	*Ibacitabine*	*-5.8*
Telaprevir	*-7.3*	*Methisazone*	*-5.8*
Doravirine	*-7.2*	*Acyclovir*	*-5.7*
Etravirine	*-7.0*	*Idoxuridine*	*-5.7*
Saquinavir	*-7.0*	*Amantadine*	*-5.5*
Entecavir	*-6.9*	*Emtricitabine*	*-5.5*
Trifluridine	*-6.9*	*Lamivudine*	*-5.1*
Abacavir	*-6.8*	*Moroxydine*	*-5.1*
Atazanavir	*-6.8*	*Fosfonet*	*-4.5*
Inosine	*-6.8*	*Foscarnet*	*-4.3*
Zidovudine	*-6.8*	*Docosanol*	*-4.0*

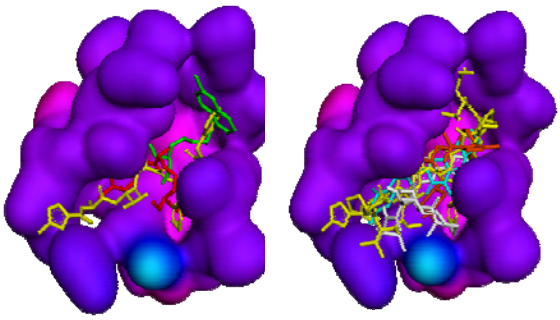

(a) ***(b)***

Figure 2. 3D representations of the binding conformations of the virtually screened compounds at the binding pocket of SARS-CoV-2 M^{pro}. **(a)** Peptide-like control (yellow), chloroquine (green), and hydroxychloroquine (red). **(b)** Peptide-like control (yellow), dolutegravir (light blue), maraviroc (orange), daclatasvir (light green), and simeprevir (white).

3.2. Molecular Docking

Relying on virtual screening results, molecular docking simulations of the top ten antivirals (based on their binding energies and conformations), chloroquine and hydroxychloroquine were performed using AutoDock 4.2.6. Similarly, the SARS-CoV-2 M^{pro} crystal structure (PDB: 6LU7) was chosen as a target. The crystal structure suggests that THR25, THR26, LEU27, HIS41, SER46, MET49, TYR54, PHE140, LEU141, ASN142, GLY143, CYS145, HIS163, MET165, GLU166, LEU167, PRO168, PHE185, ASP187, GLN189, THR190, ALA191, and GLN192 are the residues which build its active site. The internal bound ligand (N3P) was used as a control molecule. The lowest energies of binding and interacting amino acid residues are charted and summarised in Figure 3 and Table 2. The control inhibitor showed a quite low binding energy of -9.88 kcal/mol, which agrees with the energy value from the virtual screening. Interaction-wise, N3P was shown to interact through five hydrogen bonds with CYS145, HIS163, GLU166, GLN189, and THR190, among other various van der Waals (vdW) and Pi-interactions. It is noteworthy that N3P binds with both catalytic residues, CYS145 and HIS41, with one hydrogen bond and two Pi-sigma interactions, respectively (Table 2, Figure S1-a, Supplementary Information). The re-docked conformation of N3P was similar to its native conformation with a root mean square deviation (RMSD) of 0.92 Å (Figure 4). In comparison with the virtual screening results, chloroquine and hydroxychloroquine appeared to have higher binding affinities towards the protease; -6.96 kcal/mol, for both molecules (Table 2) which are in agreement with the previously reported values (Shivanika *et al.*, 2020; Srivastava *et al.*, 2020). Both molecules' quinoline ring systems occupy the S2 subsite at the binding pocket with a difference in their RMSDs of 0.58 Å. Chloroquine was found to interact with CYS145 and HIS41 through three Pi-interactions, whereas only one hydrogen bond can be noticed between the hydrogen atom of its secondary amine and GLN189, which can be considered as a weak interaction (Figure S1-b, Supplementary Information). In contrast, hydroxychloroquine was found to interact through four hydrogen bonds with LEU141, GLY143, SER144, and GLN189, while only interacting with the CYS145 through

a vdW interaction (Figure S1-c, Supplementary Information).

Although chloroquine and hydroxychloroquine moderately bind to M^{pro}, other studies were conducted earlier to support these findings (Mengist *et al.*, 2021; Nimgampalle *et al.*, 2020). However, it was found that other derivatives of these two ligands can *in-silico* inhibit the activity of this protein with higher affinities (Nimgampalle *et al.*, 2020). Few clinical trials were conducted to study the effectiveness of chloroquine and hydroxychloroquine in CoVID-19-infected patients. The use of hydroxychloroquine was found of no benefit in decreasing the mortality rate of hospitalised patients, in spite, its use in clinical practice increased the probability of needing to intubate in comparison to patients who received the standard of care (Horby, Mafham, Linsell, *et al.*, 2020). Another two studies found that using chloroquine with or without azithromycin was associated with prolonged QTc intervals in CoVID-19 patients (Arshad *et al.*, 2020; Nguyen *et al.*, 2020). Furthermore, Torsade de Pointes, ventricular arrhythmia, and cardiac deaths were also associated with the use of the earlier combination therapy (Nguyen *et al.*, 2020). Thus, the FDA panel discourages using chloroquine or hydroxychloroquine to treat CoVID-19 patients (NIH, 2021).

Among the docked antivirals, simeprevir, maraviroc and indinavir displayed the lowest binding energy values of -11.98, -11.82, and -10.58 kcal/mol, respectively (Table 2). Simeprevir was found to form three hydrogen bonds with HIS163, HIS164, and GLU166 while interacting with CYS145 through two aromatic Pi-sulphur bonds (Figure S1-k, Supplementary Information). Maraviroc, in contrast, was found to interact only through one hydrogen bond with GLU166 while maintaining three Pi-alkyl interactions with both catalytic residues (Figure S1-I, Supplementary Information). Still, indinavir interacted with GLU166 and GLN189 through conventional hydrogen bonds while only interacting with the catalytic residues through one vdW and one Pi-alkyl interactions (Figure S1-g, Supplementary Information). Although that vicriviroc displayed a higher binding energy (-8.22 kcal/mol) which is still comparable to that of N3P, it managed to interact using its fluorine atoms with both CYS145 and HIS41 through hydrogen bonds. Moreover, two halogen interactions with THR26 and GLY143, and an aromatic interaction with the CYS145 residue can be noticed, suggesting a strong affinity towards the binding pocket (Table 2, Figure S1-m, Supplementary Information). Furthermore, daclatasvir, delavirdine, dolutegravir, and raltegravir displayed binding energies similar to vicriviroc (Table 2) while maintaining at least one hydrogen bond with one of the catalytic residues and several hydrophobic interactions with the other (Table 2, Figure S1-d-f and j, Supplementary Information). Finally, lopinavir and sofosbuvir were found to bind with relatively higher binding energies of -7.72 and -7.37 kcal/mol, respectively (Table 2). Interaction-wise, lopinavir did not form any hydrogen bond with the catalytic dyad, only two Pi-interactions (Figure S1-h, Supplementary Information). In contrast, sofosbuvir had five hydrogen bonds with ASN142, CYS145, HIS163, GLU166, and GLN189 and an unfavourable interaction between its sulphur atom and HIS41 (Figure S1-l, Supplementary Information). Interestingly, all the docked antiviral molecules were found to fit into the binding pocket of M^{pro} in a similar way to that of the control molecule (Figure 5), except for daclatasvir where only half of the dimeric symmetric molecule fits within the pocket, while the other half protrudes out of it towards the S4 subsite (Figure 5-c).

Based on the analyses above, only four antivirals were chosen for further investigations using molecular dynamics. Vicriviroc was chosen as it forms two hydrogen bond interactions with both residues of the catalytic dyad. Delavirdine, dolutegravir and raltegravir were chosen as they bind through one hydrogen bond with a catalytic residue while maintaining at least one hydrophobic interaction with the other. Daclatasvir was excluded as it does not fit into the active site, whereas indinavir, lopinavir, maraviroc and simeprevir could not form any hydrogen bonding with neither of the catalytic residues. Sofosbuvir was excluded from any additional assessments as it showed the highest binding energy among its peers. Similarly, chloroquine and hydroxychloroquine were disqualified from being proceeded into any further calculations.

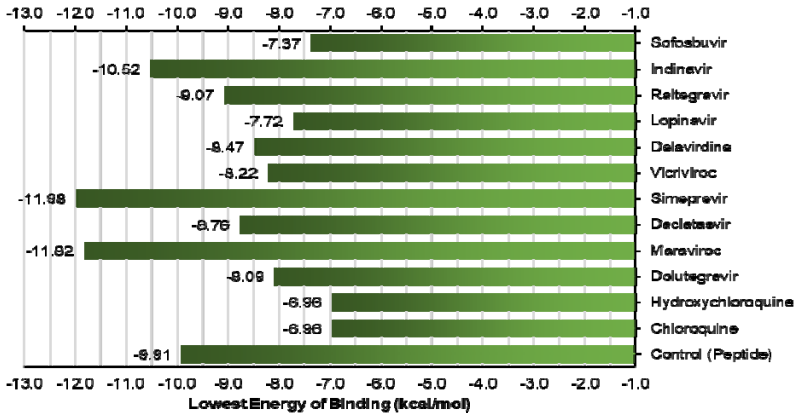

Figure 3. Histogram of the lowest binding energies (kcal/mol) of the ten antivirals, chloroquibe, hydroxychloroquine, and the peptide-like control which were docked against the catalytic site of SARS-CoV-2 M^{pro}.

Table 2. The lowest energy of binding (LEB), estimated inhibition constant (K_i), and the types of interactions and their corresponding amino acids of the peptide-like inhibitor (N3P), chloroquine, hydroxychloroquine, and ten different antivirals as a result of molecular docking against SARS-CoV-2 M^{pro}.

Compound	***LEB (kcal/mol)***	***Estimated K_i***	***Hydrogen-bond Interactions***	***Pi-Interactions***	***Aromatic Interaction***
N3P (Control)	*-9.91*	*54.10 nM*	*CYS145, HIS163, GLU166, GLN189, THR190*	*THR25, HIS41, MET49, MET165, PRO168, ALA191*	*THR25, PRO168, ALA191*
Chloroquine	*-6.96*	*7.86 uM*	*GLN189*	*HIS41, CYS145, HIS163, MET165, HIS172*	*HIS41, MET165, GLN189*
Hydroxychloroquine	*-6.96*	*7.96 uM*	*LEU141, GLY143, SER144, GLN189*	*HIS163, MET165, HIS172*	*MET165*
Daclatasvir	*-8.76*	*377.64 nM*	*CYS145, GLU166, PRO168, THR169, GLN189*	*HIS41, MET49, MET165*	*PRO168*
Delavirdine	*-8.47*	*621.04 nM*	*HIS41, MET165, ARG188*	*MET49*	*CYS145, MET165*
Dolutegravir	*-8.09*	*1.17 uM*	*LEU141, GLY143, SER144, CYS145, GLU166, GLN189, THR190, GLN192*	*LEU27, HIS41, MET165*	*MET165*
Indinavir	*-10.52*	*19.59 nM*	*GLU166, GLN189*	*HIS41, LEU141, MET165*	*HIS41, LEU141, MET165*
Lopinavir	*-7.72*	*2.21 uM*	*ASN142, GLN189*	*LEU27, HIS41, MET49, MET165, PRO168*	*HIS41, GLY143, MET165, PRO168*
Maraviroc	*-11.82*	*2.17 nM*	*GLU166*	*HIS41, MET49, CYS145, HIS163, MET165*	*MET165*
Raltegravir	*-9.07*	*225.93 nM*	*LEU141, CYS145, GLU166, GLN192*	*LEU27, MET165*	*MET165, PRO168*
Simeprevir	*-11.98*	*1.67 nM*	*HIS163, HIS164, GLU166*	*MET49, CYS145*	*MET49, CYS145*
Sofosbuvir	*-7.37*	*3.94 uM*	*ASN142, CYS145, HIS163, GLU166, GLN189*	*HIS41, MET165, GLU166*	*LEU27, HIS41*
Vicriviroc	*-8.22*	*945.16 uM*	*HIS41, CYS145, GLU166*	*LEU27, MET165, PRO168, THR190*	*GLY143, CYS145, THR90, ALA191*

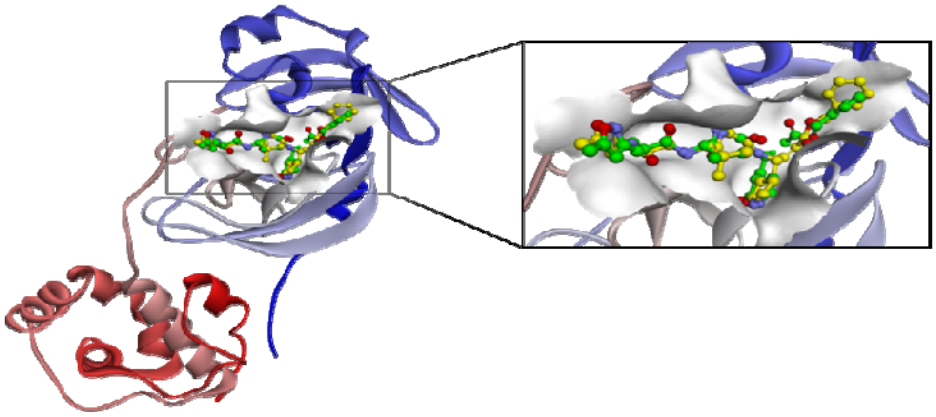

Figure 4. A 3D ribbon representation of SARS-CoV-2 M^{pro} crystal structure (PDB: 6LU7) showing the main binding pocket (white open surface) and the superimposed conformations of its internal ligand (N3P) in its native state (green) and after docking (yellow).

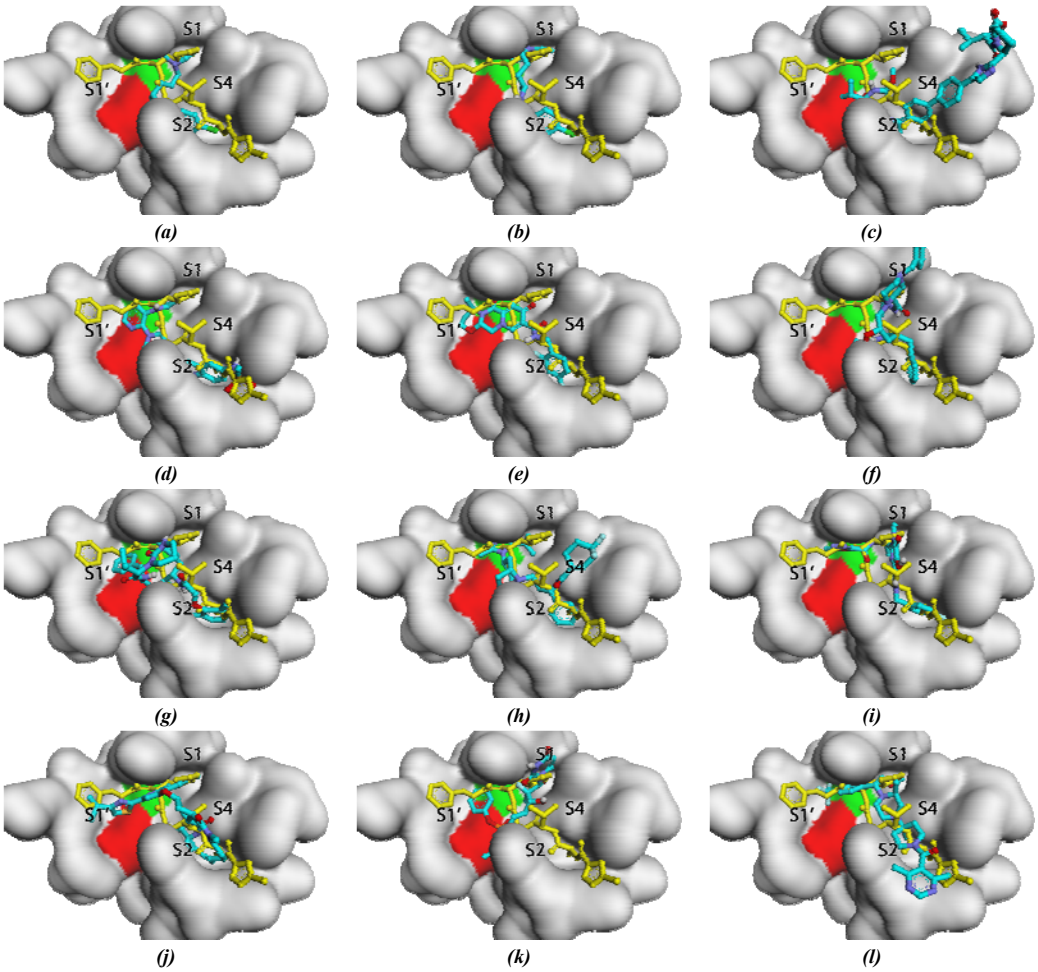

Figure 5. Binding conformations of the peptide-like control molecule (yellow), **(a)** chloroquine, **(b)** hydroxychloroquine, **(c)** daclatasvir, **(d)** delavirdine, **(e)** dolutegravir, **(f)** indinavir, **(g)** lopinavir, **(h)** maraviroc, **(i)** raltegravir, **(j)** simeprevir, **(k)** sofosbuvir and **(l)** vicriviroc at the binding pocket of SARS-CoV-2 M^{pro} (PDB: 6LU7) showing the catalytic residues; HIS41 (red) and CYS145 (green), and the subsites (S1', S1, S2, and S4).

3.3. Molecular Dynamics

Each of delavirdine, dolutegravir, raltegravir and vicriviroc, which showed the best comprehensive interactions with the catalytic residues and binding conformations from molecular docking simulations, were employed in this part of the study, while the N3P was employed as a control inhibitor of M^{pro}.

The native form of SARS-CoV-2 M^{pro} bound to each of the four antiviral drugs was simulated through 100 ns. All four antivirals displayed a comparable resilience

interacting with the active site of the protease (Figure 6). Mean RMSD values of delavirdine-, dolutegravir-, raltegravir-, vicriviroc- and N3P-M^{pro} complexes are 2.59, 2.93, 2.38, 3.01 and 3.24 Å, respectively (Figure 7). Pairwise RMSD values of delavirdine, dolutegravir, and raltegravir are coherent and within the range of 1.0 to 3.0 Å (Figure 6-a-c). This indicates consistent stabilities of the ligand-M^{pro} complexes. Delavirdine took about 20 ns to stabilise within the binding pocket of M^{pro} (2.5-3.0 Å) (Figure 6-a), whereas it only took 10 ns for dolutegravir to achieve it (2.7-3.0 Å) (Figure 6-b). Raltegravir, on the other hand, achieved its M^{pro}-complex stability gradually without any sharp elevation in its RMSD values (Figure 6-c). In contrast, vicriviroc's RMSD values were slightly elevated towards 4.0 Å for the most part during the first 62 ns (Figure 6-d). Whereas during the next 38 ns, it was noticed that vicriviroc leaves the main binding pocket and interacts with a distant site that is out of the scope and near the S2 and S4 subsites (data not shown). Overall, these RMSD values are significantly lower than those of the N3P-M^{pro} complex, where it was seen to elevate towards 7.5 Å, especially after 77 ns.

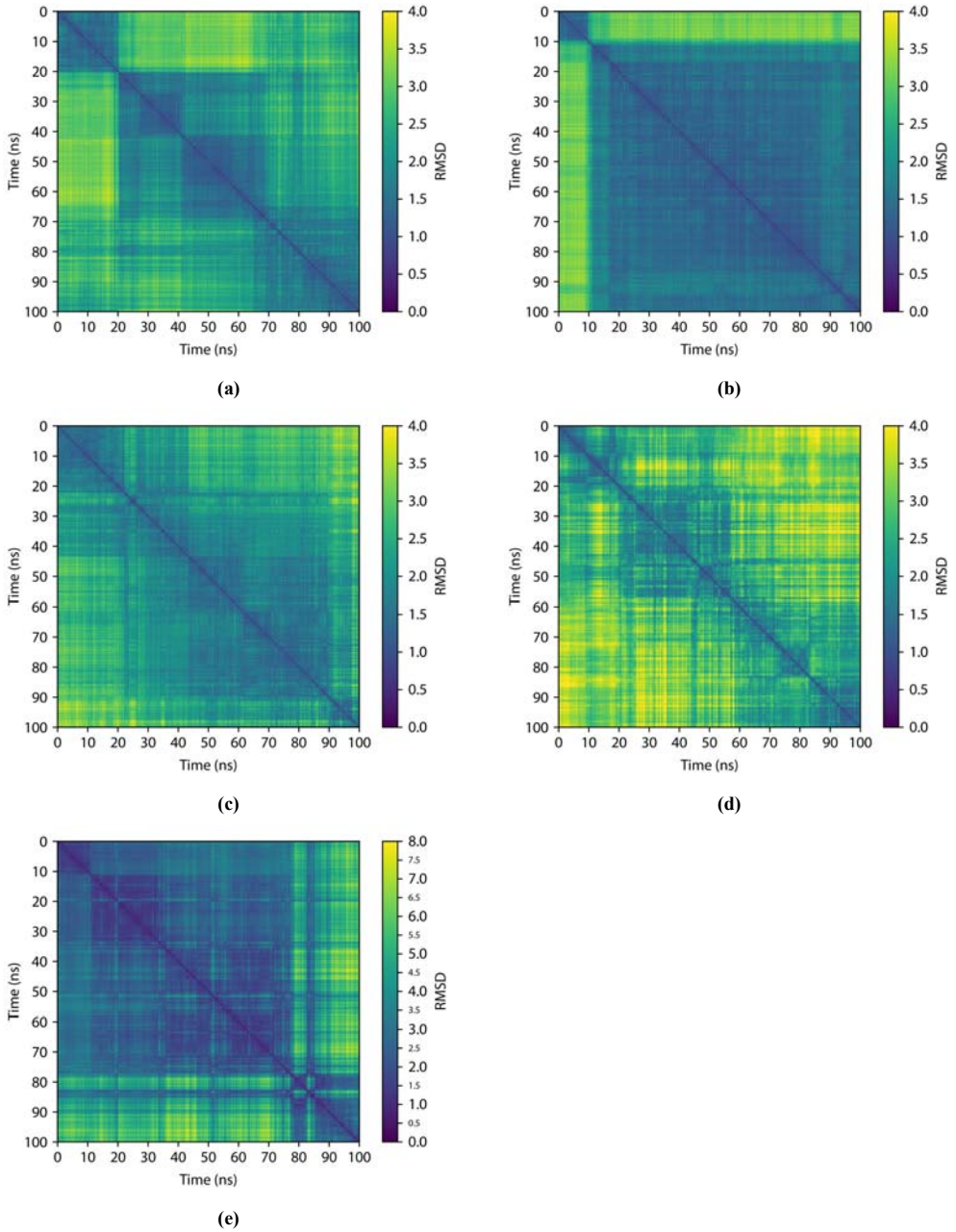

Figure 6. Heatmaps of the pairwise root mean square deviations (RMSDs) of **(a)** delavirdine-M^{pro}, **(b)** dolutegravir-M^{pro}, **(c)** raltegravir-M^{pro}, **(d)** vicriviroc-M^{pro}, and **(e)** N3P-M^{pro} complexes.

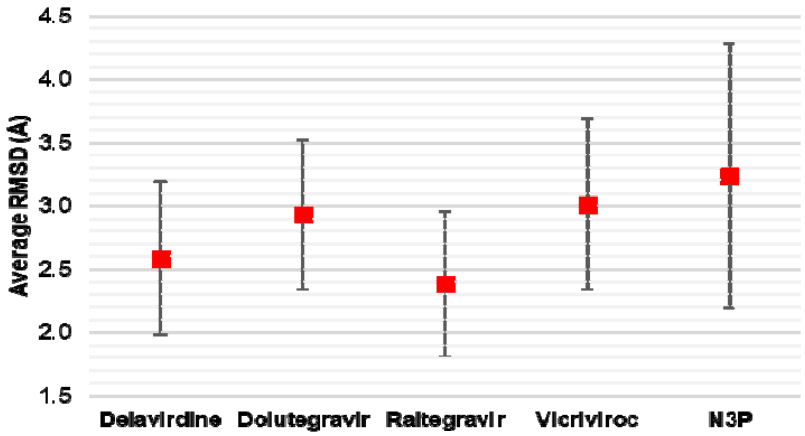

Figure 7. Average RMSD values of delavirdine-, dolutegravir-, raltegravir-, vicriviroc- and N3P-M^{pro} complexes.

The RMSF values of the ligand-M^{pro} represent fluctuated protein regions during molecular dynamics simulations. As illustrated in Figure 8, high levels of fluctuations can be noticed in the SER46, GLU47, ASP48, MET49, LEU50, ASN51, PRO52, SER139, PHE140, LEU141, ASN142 from β-turn region, ASP153, TYR154, ASP155 from the β-hairpin region, GLN189, THR190, ALA191, GLN192, ALA193 residues, and ASN274, GLY275, MET276, ASN277, GLY278, ARG279, THR280, SER301, GLY302, VAL303, THR304, PHE305, GLN306 from β-turn region, in comparison to the rest of the amino acid residues. Each of delavirdine-, dolutegravir-, and raltegravir-M^{pro} complexes displayed similar shifts in their RMSF values. However, vicriviroc-M^{pro} showed higher and less consistent fluctuations of all residues compared to the earlier-mentioned complexes, indicating higher flexibility of the protein structure. The N3P control had the highest fluctuations, indicating that the N3P-M^{pro} complex has a more flexible nature than the other complexes.

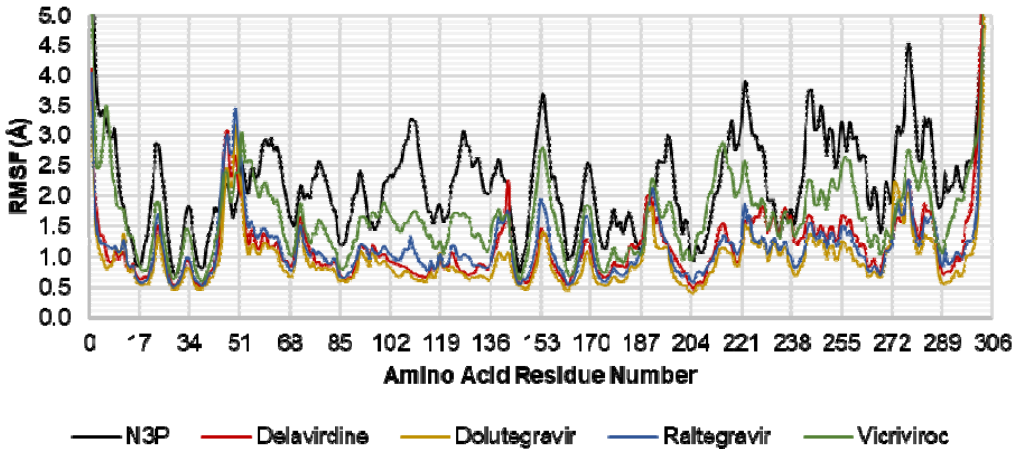

Figure 8. Root mean square fluctuations (RMSFs) of SARS-CoV-2 M^{pro} amino acid residues when in complex with delavirdine, dolutegravir, raltegravir, vicriviroc, and N3P.

Moreover, Table 3 shows the hydrogen bond analysis of protein residues and the studied ligands. In the case of delavirdine-M^{pro}, three hydrogen bonds are formed between GLU166 and the ligand for 52.23, 14.04 and 6.60% of the simulation time. Also, ASP187, ARG188 and ASN142 form hydrogen interactions with delavirdine for 26.51, 19.08 and 12.38%, respectively. Lower hydrogen bonding incidences can also be noticed with THR190 and GLN192 with shorter lifetimes. Overall, delavirdine can successfully maintain hydrogen bonding at the active site of the protease during the whole simulation time (Figure 9). Furthermore, in dolutegravir-M^{pro} complex, two hydrogen bond interactions can be seen between GLU166 and the ligand for 45.16 and 8.55%. GLY143, HIE41 and CYS145 are also residues involved in the ligand's hydrogen bonding, with occupancies of 41.90, 20.84 and 15.12%, respectively. A lower hydrogen bond interaction lifetime is additionally seen between dolutegravir and GLN189 (Table 3). Likewise, dolutegravir can maintain hydrogen interactions with M^{pro} during the whole 100 ns of the simulation (Figure 9). In contrast, raltegravir and vicriviroc had lower overall incidences of hydrogen bonds at M^{pro} active site. Both ligands were only capable of forming two hydrogen bond interactions for each system with very short lifetimes (Table 3). Figure 9 shows a gap in the consistency of hydrogen bond interactions between raltegravir and M^{pro} (67-74 ns). This is due to the change of raltegravir's binding conformation where the *p*-fluorobenzene ring protruded outwards, while only the 2-methyloxodiazole ring occupies the binding pocket (data

not shown). Comparably, vicriviroc could not interact with the binding pocket residues after 62 ns of the simulation time. This refers to the fact that it left the main binding pocket of M^{pro} and headed towards a distant region of the protein structure, as explained earlier. In the N3P-M^{pro} complex, the ligand was found to interact with GLU166 through two hydrogen bonds with occupancies of 61.61 and 51.42%. GLN189 is another residue that is also involved through five hydrogen bond interactions of 20.88, 6.59, 5.93, 5.59 and 5.27%. Similarly, THR190 and GLY143 form hydrogen bond interactions with N3P for 13.45 and 9.69%, respectively (Table 3).

Table 3. Hydrogen bond analyses of delavirdine-, dolutegravir-, raltegravir-, vicriviroc- and N3P-M^{pro} complexes during the 100 ns molecular dynamics simulations.

Complex	*Acceptor*	*Donor H*	*Donor*	*Occupancy (%)*	*Average Distance (Å)*	*Average Angle*
DEL-M^{pro}	*GLU166@O*	*DEL307@H*	*DEL307@N*	*52.23*	*2.82*	*160.83*
	ASP187@O	*DEL307@H*	*DEL307@N*	*26.51*	*2.85*	*157.11*
	ARG188@O	*DEL307@H*	*DEL307@N*	*19.08*	*2.84*	*153.71*
	GLU166@O	*DEL307@H*	*DEL307@N*	*14.04*	*2.83*	*158.33*
	DEL307@O	*ASN142@H*	*ASN142@N*	*12.38*	*2.85*	*158.09*
	DEL307@O	*GLN192@H*	*GLN192@N*	*9.88*	*2.88*	*160.38*
	DEL307@O	*GLU166@H*	*GLU166@N*	*6.60*	*2.89*	*162.50*
	THR190@O	*DEL307@H*	*DEL307@N*	*6.39*	*2.83*	*157.07*
DOL-M^{pro}	*DOL307@O*	*GLU166@H*	*GLU166@N*	*45.16*	*2.87*	*162.45*
	DOL307@O	*GLY143@H*	*GLY143@N*	*41.90*	*2.82*	*149.01*
	DOL307@O	*HIE41@H*	*HIE41@N*	*20.84*	*2.87*	*154.27*
	DOL307@O	*CYS145@H*	*CYS145@N*	*15.12*	*2.91*	*160.84*
	DOL307@O	*GLU166@H*	*GLU166@N*	*8.55*	*2.89*	*152.36*
	GLN189@O	*DOL307@H*	*DOL307@N*	*5.24*	*2.86*	*155.96*
RAL-M^{pro}	*HIE164@O*	*RAL307@H*	*RAL307@N*	*18.76*	*2.88*	*162.62*
	RAL307@O	*GLN189@H*	*GLN189@N*	*8.96*	*2.84*	*159.05*
VIC-M^{pro}	*VIC307@N*	*GLN189@H*	*GLN189@N*	*11.55*	*2.92*	*161.27*
	VIC307@O	*GLU166@H*	*GLU166@N*	*10.74*	*2.89*	*162.94*
N3P-M^{pro}	*GLU166@O*	*N3P307@H*	*N3P307@N*	*61.61*	*2.86*	*161.29*
	N3P307@O	*GLU166@H*	*GLU166@N*	*51.42*	*2.88*	*161.79*
	GLN189@O	*N3P307@H*	*N3P307@N*	*20.88*	*2.84*	*161.12*
	THR190@O	*N3P307@H*	*N3P307@N*	*13.45*	*2.89*	*154.48*
	N3P307@O	*GLY143@H*	*GLY143@N*	*9.69*	*2.86*	*155.62*
	GLN189@O	*N3P307@H*	*N3P307@N*	*6.59*	*2.90*	*163.36*
	N3P307@O	*GLN189@H*	*GLN189@N*	*5.93*	*2.87*	*159.67*
	N3P307@O	*GLN189@H*	*GLN189@N*	*5.59*	*2.85*	*159.30*
	N3P307@O	*GLN189@H*	*GLN189@N*	*5.27*	*2.84*	*161.64*

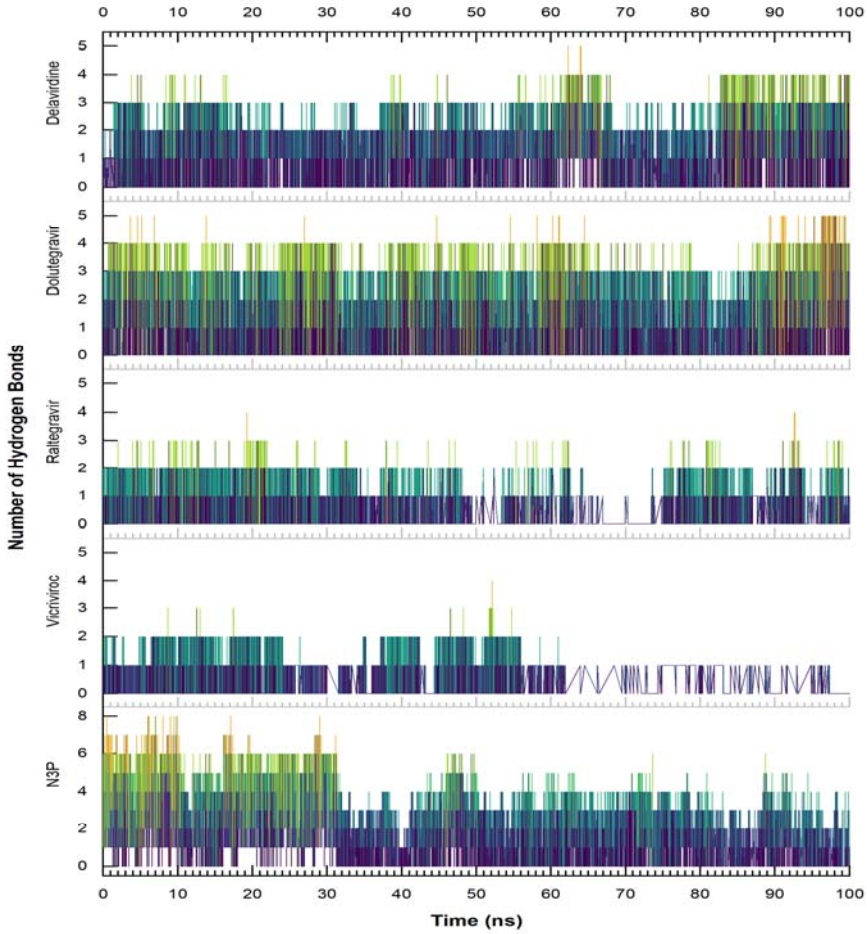

Figure 9. The frequency of hydrogen bond interactions between delavirdine, dolutegravir, raltegravir, vicriviroc and N3P within the active site of M^{pro} during the molecular dynamics simulations.

The degree of rigidity, compactness and folding of protein of the simulated systems was measured by analysing the RadGyr for the last 10 ns of the simulations time. Mean RadGyr of delavirdine-, dolutegravir-, raltegravir-, vicriviroc- and N3P-M^{pro} complexes are 11.61, 11.76, 12.39, 12.31 and 11.73 Å, respectively. It can be observed from Figure 10 that delavirdine and dolutegravir complexes with the protein have almost similar RadGyr values and a nearly similar profile to that of N3P-M^{pro}. This indicates that the protein structure in these complexes is stable. However, the binding of raltegravir and vicriviroc to M^{pro} seems to have a higher effect on the protein compactness. RadGyr results indicate that both of the latter ligands show higher RadGyr values and fluctuations, translated into lower levels of structural rigidity.

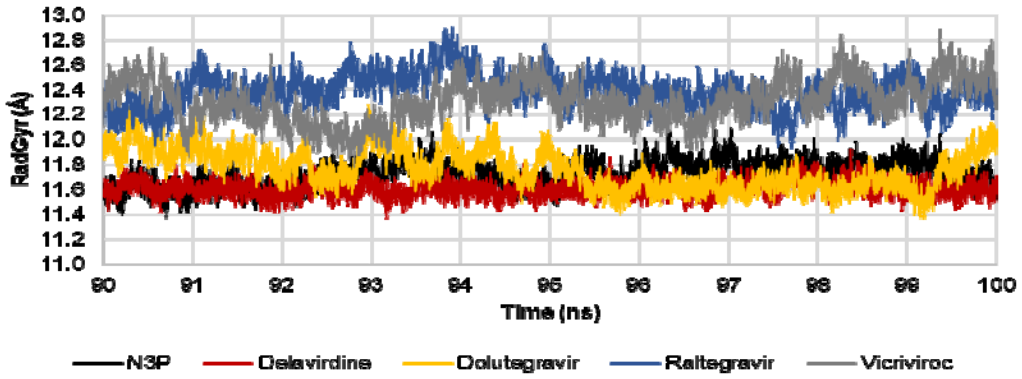

Figure 10. Time series analysis of all the simulated systems for the degree of rigidity and compactness through measuring the radius of gyrations (RadGyr) for the last 10 ns of the simulations time.

3.4. Molecular Mechanics Free Energy of Binding

MM-GBSA analyses were done for the last 10 ns of each trajectory of the simulated complexes to predict the binding free energies for the ligand-receptor. According to the energy components of the binding free energies, the major favourable contributions to the ligands binding are the van der Waals (ΔE_{vdW}) and electrostatic (ΔE_{ELE}) energies for all complexes. On the contrary, the term polar solvation-free energy (ΔE_{GB}) is largely unfavourable for binding in the five complexes. The terms ΔE_{vdW} and ΔE_{ELE} promote binding and can offset the negative effect of ΔE_{GB}. MM-GBSA values for vdW and ELE correlate with the number of hydrogen bonds. Thus, the more hydrogen bonding, the lower the ELE energy and the more favourable the vdW interactions, i.e. lower vdW energy. The total calculated free binding energy ($\Delta G_{binding}$) against M^{pro} for delavirdine is greater than the other antivirals and N3P (Table 4, Figure 11). Dolutegravir, however, showed a similar $\Delta G_{binding}$ to that of N3P. On the other hand, $\Delta G_{binding}$ of raltegravir and vicriviroc were significantly higher compared to the earlier mentioned ligands and the control peptide. It is noteworthy that these energy values are consistent with the hydrogen bonding analyses of the systems. Moreover, as raltegravir and vicriviroc are known to have higher water solubilities, this would explain the more favourable total solvation-free energy (ΔG_{solv}). At the same time, delavirdine and dolutegravir have much lower aqueous solubility levels, which explains how their energy values are mainly driven by vdW and ELE interactions.

Table 4. MM-GBSA binding energy analyses in kcal/mol of the last 10 ns for the simulated systems trajectories.

Complex	ΔE_{vdW}	ΔE_{ELE}	ΔE_{GB}	ΔE_{SURF}	ΔG_{gas}	ΔG_{solv}	$\Delta G_{binding}$
DEL-M^{pro}	*-37.14±2.54*	*-26.08±5.64*	*27.00±3.90*	*-4.42±0.31*	*-63.22±6.18*	*22.57±3.84*	*-40.65±3.80*
DOL-M^{pro}	*-37.46±3.19*	*-23.90±5.86*	*30.07±4.07*	*-4.60±0.25*	*-61.36±6.29*	*25.48±3.97*	*-35.88±4.31*
RAL-M^{pro}	*-28.93±4.73*	*-6.38±6.58*	*22.65±7.26*	*-3.45±0.51*	*-35.31±8.94*	*19.21±6.98*	*-16.11±3.84*
VIC-M^{pro}	*-24.93±6.54*	*-3.38±4.07*	*10.56±4.41*	*-2.96±0.67*	*-28.31±8.65*	*7.60±4.00*	*-20.71±6.09*
N3P-M^{pro}	*-49.27±3.99*	*-24.06±6.45*	*44.63±5.33*	*-6.12±0.55*	*-73.34±7.96*	*38.51±4.99*	*-34.83±4.34*

ΔE_{vdW}, van der Waals contribution. ΔE_{ELE}, electrostatic contribution. ΔE_{GB}, polar solvation-free energy. ΔE_{SURF}, nonpolar solvation free energy. ΔG_{gas}, gas-phase energy; $\Delta G_{gas} = \Delta E_{vdW} + \Delta E_{ELE}$. ΔG_{solv}, total solvation free energy; $\Delta G_{solv} = \Delta E_{SURF} + \Delta E_{GB}$. $\Delta G_{binding}$, total free energy of binding; $\Delta G_{binding} = \Delta G_{gas} + \Delta G_{solv}$.

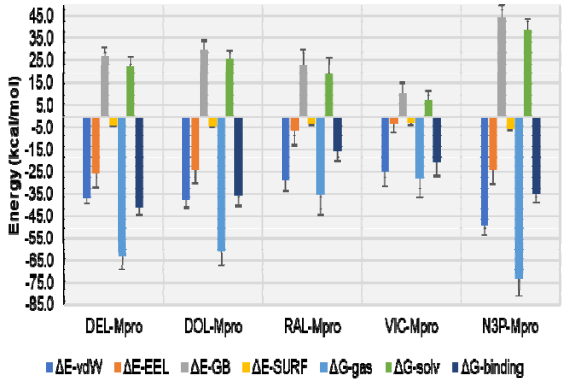

Figure 11. Histogram of the MM-GBSA binding energy analyses in kcal/mol of the last 10 ns for the simulated systems trajectories.

ΔE_{vdW}, van der Waals contribution. ΔE_{ELE}, electrostatic contribution. ΔE_{GB}, polar solvation free energy. ΔE_{SURF}, nonpolar solvation free energy. ΔG_{gas}, gas-phase energy; $\Delta G_{gas} = \Delta E_{vdW} + \Delta E_{ELE}$. ΔG_{solv}, total solvation free energy; $\Delta G_{solv} = \Delta E_{SURF} + \Delta E_{GB}$. $\Delta G_{binding}$, total free energy of binding; $\Delta G_{binding} = \Delta G_{gas} + \Delta G_{solv}$.

Overall, each of delavirdine and dolutegravir in complex with M^{pro} were found to have almost similar profiles to that of N3P, suggesting a potential inhibitory activity of the enzyme's catalytic activity, thus blocking the virus life cycle.

Delavirdine is a potent non-nucleoside reverse transcriptase inhibitor (NNRTI) of HIV-1 reverse transcriptase. It has an excellent pharmacokinetic profile and is metabolised through CYP3A4 and CYP2D6 (Tran *et al.*, 2001). On the other hand, dolutegravir is an integrase inhibitor (INI) of HIV-1 and HIV-2 integrases. Similarly, it has an excellent pharmacokinetic profile; nonetheless, it does not induce or inhibit any of the CYP isozymes (Katlama & Murphy, 2012). Both molecules showed excellent RMSD values, which are lower than that of N3P. This suggests consistent stability of delavirdine- and dolutegravir-M^{pro} complexes which the RMSF of the receptor residues can also measure. In the N3P-M^{pro} complex, it is apparent that the amino acids lining the binding pocket showed higher RMSF fluctuations signifying the flexibility of the protein in general. However, $M^{pro,}$ when bound to either delavirdine or dolutegravir, these residues had much fewer fluctuations throughout the 100 ns of simulation time and an apparent less flexibility of the whole protein crystal structure. These findings were furtherly supported by the degree of compactness of the systems (RadGyr). Both molecules, delavirdine and dolutegravir, had very comparable values of RadGyr to that of N3P, which indicates a sustainable degree of rigidity and protein folding. On the other hand, only delavirdine and dolutegravir managed successfully to sustain hydrogen bond interactions with the amino acid residues of the active site with occupancies and frequencies comparable to that of N3P. Moreover, molecular mechanics calculations show that both antivirals can bind through excellent binding energies, which are also comparable to N3P.

The chemical structures of delavirdine and dolutegravir provides amide bonds which resemble that of the peptide scissile bond. This would provide an excellent feature for both ligands where the catalytic dyad residues can digest this bond and in turn inhibit any further catalytic activity of the protease. However, a very limited number of studies discussed the inhibitory activity of delavirdine and dolutegravir towards SARS-CoV-2 M^{pro}. In an *in-silico* study, Al-Khafaji et al. suggested that delavirdine can be a potential inhibitor of the protease by binding irreversibly and covalently to its active site (Al-Khafaji *et al.*, 2021). In

contrast, a virtual screening conducted by Indu and co-workers suggested that dolutegravir can act as a potential inhibitor of M^{pro} and RdRp of CoVID-19 (Indu *et al*., 2020). Similarly, a molecular dynamics study of both antivirals found that dolutegravir is an excellent candidate that might inhibit CoVID-19 M^{pro} by showing RMSD and RMSF fluctuations that agree with our findings. However, in the same study, although delavirdine was found to have a similar RMSD profile to our results, it caused higher shifts and fluctuations of the protein RMSF and a lower binding energy than that of dolutegravir (Sharma & Deep, 2020).

4. Conclusion

In conclusion, our results validate the ability of the N3P peptide-like molecule to irreversibly inhibit SARS-CoV-2 M^{pro} despite it having some major fluctuations in its RMSF values. Comparably, chloroquine and hydroxychloroquine do not provide a good enough inhibitory activity towards the protease, although the FDA panel now does not recommend the use of both medications for CoVID-19 infections. Among the 74 antivirals, remdesivir; an FDA-approved antiviral for controlling CoVID-19 infections, was confirmed not to act by inhibiting M^{pro}. In spite, it acts as an RdRp inhibitor. Therefore, only delavirdine and dolutegravir are proposed as excellent inhibitors of M^{pro}. However, more investigations are required to confirm and validate the inhibitory activity of these two antivirals towards M^{pro} through *in-vitro*, *in-vivo* and clinical studies. This would provide a wider range of options to treat and control CoVID-19 infections in patients by minimising hospitalisation and recovery time and probably eliminate the need for ventilators, intubation, and oxygen supplies.

Acknowledgement

This research was supported by USM RU TOP-DOWN for the project titled Catalogue of USM-RIKEN Natural Product (CURINaP) Library for the Discovery of Bioactive molecules on Ageing and Ageing Related Diseases (1001/PFARMASI/870031).

Data Availability

Data that support this study are available in the article and accompanying the supplementary material provided after the References section.

References

Ai, T., Yang, Z., Hou, H., *et al.* 2020. Correlation of chest CT and RT-PCR testing in coronavirus disease 2019 (COVID-19) in China: a report of 1014 cases. *Radiology*, **296(2)**: 200642.

Al-Khafaji, K., Al-Duhaidahawi, D., & Taskin Tok, T. 2021. Using integrated computational approaches to identify safe and rapid treatment for SARS-CoV-2. *J Biomol Struct Dyn*, **39(9)**: 3387-3395.

Arshad, S., Kilgore, P., Chaudhry, Z. S., *et al.* 2020. Treatment with hydroxychloroquine, azithromycin, and combination in patients hospitalized with COVID-19. *Int J Infect Dis*, **97**: 396-403.

Beigel, J. H., Tomashek, K. M., Dodd, L. E., *et al.* 2020. Remdesivir for the Treatment of Covid-19 — Final Report. *N Engl J Med*, **383(19)**: 1813-1826.

Berman, H. M., Westbrook, J., Feng, Z., *et al.* 2000. The Protein Data Bank. *Nucleic Acids Res*, **28(1)**: 235-242.

BIOVIA. 2017. Discovery Studio Modeling Environment, *San Diego*.

Carlos, W. G., Dela Cruz, C. S., Cao, B., *et al.* 2020. Novel wuhan (2019-nCoV) coronavirus. *Am J Respir Crit Care Med*, **201(4)**: 7-8.

Case, D. A., Ben-Shalom, I. Y., Brozell, S. R., *et al.* 2018. AMBER 2018. *University of California, San Francisco*.

Chu, C. M., Cheng, V. C. C., Hung, I. F. N., *et al.* 2004. Role of lopinavir/ritonavir in the treatment of SARS: initial virological and clinical findings. *Thorax*, **59(3)**: 252-256.

Daoud, S., Alabed, S. J., & Dahabiyeh, L. A. 2021. Identification of potential COVID-19 main protease inhibitors using structure-based pharmacophore approach, molecular docking and repurposing studies. *Acta Pharm*, **71(2)**: 163-174.

Dong, L., Hu, S., & Gao, J. 2020. Discovering drugs to treat coronavirus disease 2019 (COVID-19). *Drug Discov Ther*, **14(1)**: 58-60.

FDA. 2020. FDA Approves First Treatment for COVID-19. *US Food & Drug Administration* Retrieved 08-02-2022 from https://www.fda.gov/news-events/press-announcements/fda-approves-first-treatment-covid-19

FDA. 2021a. Coronavirus (COVID-19) Update: FDA Authorizes Additional Oral Antiviral for Treatment of COVID-19 in Certain Adults. *US Food & Drug Administration* Retrieved 08-02-2022 from https://www.fda.gov/news-events/press-announcements/coronavirus-covid-19-update-fda-authorizes-additional-oral-antiviral-treatment-covid-19-certain

FDA. 2021b. Coronavirus (COVID-19) Update: FDA Authorizes First Oral Antiviral for Treatment of COVID-19. *US Food & Drug Administration* Retrieved 08-02-2022 from https://www.fda.gov/news-events/press-announcements/coronavirus-covid-19-update-fda-authorizes-first-oral-antiviral-treatment-covid-19

Fehr, A. R., & Perlman, S. 2015. Coronaviruses: an overview of their replication and pathogenesis. *Methods in molecular biology (Clifton, NJ)*, **1282**: 1-23.

Götz, A. W., Williamson, M. J., Xu, D., *et al.* 2012. Routine microsecond molecular dynamics simulations with AMBER on GPUs. 1. Generalized born. *J Chem Theory Comput*, **8(5)**: 1542-1555.

Gowers, R. J., Linke, M., Barnoud, J., *et al.* 2019. MDAnalysis: a Python package for the rapid analysis of molecular dynamics simulations. *Proc of the 15th Python in Science Conf*: 98-105.

Hegyi, A., & Ziebuhr, J. 2002. Conservation of substrate specificities among coronavirus main proteases. *J Gen Virol*, **83(3)**: 595-599.

Horby, P. W., Mafham, M., Bell, J. L., *et al.* 2020. Lopinavir-ritonavir in patients admitted to hospital with COVID-19 (RECOVERY): a randomised, controlled, open-label, platform trial. *Lancet*, **396(10259)**: 1345-1352.

Horby, P. W., Mafham, M., Linsell, L., *et al.* 2020. Effect of Hydroxychloroquine in Hospitalized Patients with Covid-19. *N Engl J Med*, **383(21)**: 2030-2040.

Ibrahim, M. A. A., Abdelrahman, A. H. M., Allemailem, K. S., *et al.* 2021. In silico evaluation of prospective anti-COVID-19 drug candidates as potential SARS-CoV-2 main protease inhibitors. *The Protein Journal*, **40(3)**: 296-309.

Indu, P., Rameshkumar, M. R., Arunagirinathan, N., *et al.* 2020. Raltegravir, Indinavir, Tipranavir, Dolutegravir, and Etravirine against main protease and RNA-dependent RNA polymerase of SARS-CoV-2: A molecular docking and drug repurposing approach. *J Infect Public Health*, **13(12)**: 1856-1861.

Jin, Z., Du, X., Xu, Y., *et al.* 2020. Structure of Mpro from COVID-19 virus and discovery of its inhibitors. *Nature*, **582**: 289-293.

Katlama, C., & Murphy, R. 2012. Dolutegravir for the treatment of HIV. *Expert Opin Investig Drugs*, **21(4)**: 523-530.

Khater, I., & Nassar, A. 2021. In silico molecular docking analysis for repurposing approved antiviral drugs against SARS-CoV-2 main protease. *Biochem Biophys Rep*, **27**: 101032.

Kim, S., Chen, J., Cheng, T., *et al.* 2018. PubChem 2019 update: improved access to chemical data. *Nucleic Acids Res*, **47(D1)**: 1102-1109.

Kokic, G., Hillen, H. S., Tegunov, D., *et al.* 2021. Mechanism of SARS-CoV-2 polymerase stalling by remdesivir. *Nat Commun*, **12(1)**: 1-7.

Le Grand, S., Götz, A. W., & Walker, R. C. 2013. SPFP: Speed without compromise—A mixed precision model for GPU accelerated molecular dynamics simulations. *Comput Phys Commun*, **184(2)**: 374-380.

Li, G., & De Clercq, E. 2020. Therapeutic options for the 2019 novel coronavirus (2019-nCoV). *Nat Rev Drug Discov*, **19**: 149-150.

Lu, H., Stratton, C. W., & Tang, Y. W. 2020. Outbreak of Pneumonia of Unknown Etiology in Wuhan China: the Mystery and the Miracle. *J Med Virol*, **94(4)**: 401-402.

Mahase, E. 2021. Covid-19: Pfizer's paxlovid is 89% effective in patients at risk of serious illness, company reports. *BMJ*, **375**: 2713.

Mengist, H. M., Dilnessa, T., & Jin, T. 2021. Structural basis of potential inhibitors targeting SARS-CoV-2 main protease. *Front Chem*, **9**: 622898.

Michaud-Agrawal, N., Denning, E. J., Woolf, T. B., *et al.* 2011. MDAnalysis: a toolkit for the analysis of molecular dynamics simulations. *J Comput Chem*, **32(10)**: 2319-2327.

Miller III, B. R., McGee Jr, T. D., Swails, J. M., *et al.* 2012. MMPBSA.py: an efficient program for end-state free energy calculations. *J Chem Theory Comput*, **8(9)**: 3314-3321.

Morris, G. M., Huey, R., Lindstrom, W., *et al.* 2009. AutoDock4 and AutoDockTools4: Automated docking with selective receptor flexibility. *J Comput Chem*, **30(16)**: 2785-2791.

Naik, V. R., Munikumar, M., Ramakrishna, U., *et al.* 2020. Remdesivir (GS-5734) as a therapeutic option of 2019-nCOV main protease - in silico approach. *J Biomol Struct Dyn*, **39(13)**: 4701-4714.

Nguyen, L. S., Dolladille, C., Drici, M.-D., *et al.* 2020. Cardiovascular toxicities associated with hydroxychloroquine and azithromycin: an analysis of the World Health Organization Pharmacovigilance Database. *Circulation*, **142(3)**: 303-305.

Ni, X., Schröder, M., Olieric, V., *et al.* 2021. Structural Insights into Plasticity and Discovery of Remdesivir Metabolite GS-441524 Binding in SARS-CoV-2 Macrodomain. *ACS Med Chem Lett*, **12(4)**: 603-609.

NIH. 2021. COVID-19 Treatment Guidelines: Antiviral Drugs That Are Approved or Under Evaluation for the Treatment of COVID-19. *National Institutes of Health*. Retrieved 29-06-2021 from https://www.covid19treatmentguidelines.nih.gov/therapies/antiviral-therapy/

Nimgampalle, M., Devanathan, V., & Saxena, A. 2020. Screening of Chloroquine, Hydroxychloroquine and its derivatives for their binding affinity to multiple SARS-CoV-2 protein drug targets. *J Biomol Struct Dyn*, **39(14)**: 4949-4961.

O'Boyle, N. M., Banck, M., James, C. A., *et al.* 2011. Open Babel: An open chemical toolbox. *J Cheminform*, **3(1)**: 33.

Pan, H., Peto, R., Henao-Restrepo, A. M., *et al.* 2021. Repurposed Antiviral Drugs for Covid-19 - Interim WHO Solidarity Trial Results. *N Engl J Med*, **384(6)**: 497-511.

Roe, D. R., & Cheatham III, T. E. 2013. PTRAJ and CPPTRAJ: software for processing and analysis of molecular dynamics trajectory data. *J Chem Theory Comput*, **9(7)**: 3084-3095.

Salomon-Ferrer, R., Götz, A. W., Poole, D., *et al.* 2013. Routine microsecond molecular dynamics simulations with AMBER on GPUs. 2. Explicit solvent particle mesh Ewald. *J Chem Theory Comput*, **9(9)**: 3878-3888.

Sanner, M. F. 1999. Python: a programming language for software integration and development. *J Mol Graph Model*, **17(1)**: 57-61.

Sharma, S., & Deep, S. 2020. *In-silico* drug repurposing for targeting SARS-CoV-2 main protease (M^{pro}). *J Biomol Struct Dyn*, **40(7)**: 3003-3010.

Shivanika, C., Kumar, D., Ragunathan, V., *et al.* 2020. Molecular docking, validation, dynamics simulations, and pharmacokinetic prediction of natural compounds against the SARS-CoV-2 main-protease. *J Biomol Struct Dyn*, **40(2)**: 585-611.

Srivastava, A. K., Kumar, A., Tiwari, G., *et al.* 2020. In silico investigations on the potential inhibitors for COVID-19 protease. *arXiv Preprint*: 1-12.

Tran, J. Q., Gerber, J. G., & Kerr, B. M. 2001. Delavirdine. *Clin Pharmacokinet*, **40(3)**: 207-226.

Trott, O., & Olson, A. J. 2010. AutoDock Vina: improving the speed and accuracy of docking with a new scoring function, efficient optimization, and multithreading. *J Comput Chem*, **31(2)**: 455-461.

Wan, Y., Shang, J., Graham, R., *et al.* 2020. Receptor recognition by the novel coronavirus from Wuhan: an analysis based on decade-long structural studies of SARS coronavirus. *J Virol*, **94(7)**.

Ye, Z.-W., Yuan, S., Yuen, K.-S., *et al.* 2020. Zoonotic origins of human coronaviruses. *Int J Biol Sci*, **16(10)**: 1686.

Zaki, A. M., Van Boheemen, S., Bestebroer, T. M., *et al.* 2012. Isolation of a novel coronavirus from a man with pneumonia in Saudi Arabia. *N Engl J Med*, **367(19)**: 1814-1820.

Zhang, H., Penninger, J. M., Li, Y., *et al.* 2020. Angiotensin-converting enzyme 2 (ACE2) as a SARS-CoV-2 receptor: molecular mechanisms and potential therapeutic target. *Intensive Care Med*, **46(4)**: 586-590.

Zhou, P., Yang, X.-L., Wang, X.-G., *et al.* 2020. A pneumonia outbreak associated with a new coronavirus of probable bat origin. *Nature*, **579(7798)**: 270-273.

Zimmermann, P., & Curtis, N. 2020. Coronavirus Infections in Children Including COVID-19 - An Overview of the Epidemiology, Clinical Features, Diagnosis, Treatment and Prevention Options in Children. *The Pediatric Infectious Disease Journal*, **39(5)**: 355-368.

Zu, Z. Y., Jiang, M. D., Xu, P. P., *et al.* 2020. Coronavirus disease 2019 (COVID-19): a perspective from China. *Radiology*, **296(2)**: E15-E25.

SUPPLEMENTARY INFORMATION

Table S1. Chemical structures of chloroquine, hydroxychloroquine and the 74 antiviral compounds which were utilised for the virtual screening against SARS-CoV-2 Mpro.

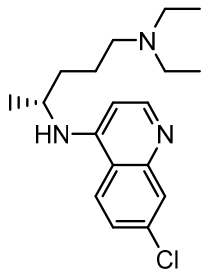	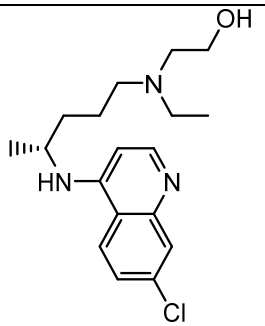	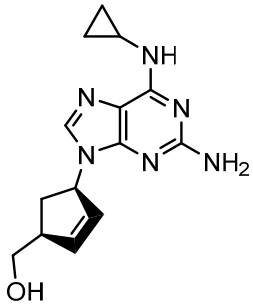	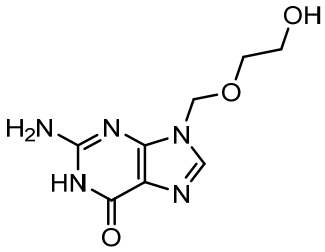
Chloroquine	Hydroxychloroquine	Abacavir	Acyclovir
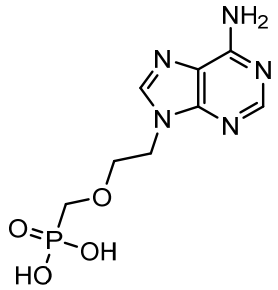	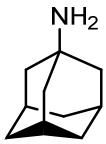	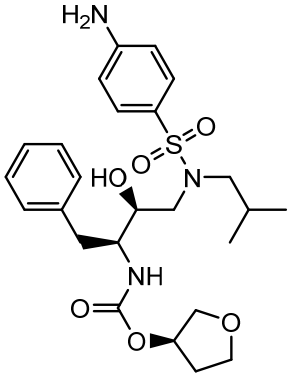	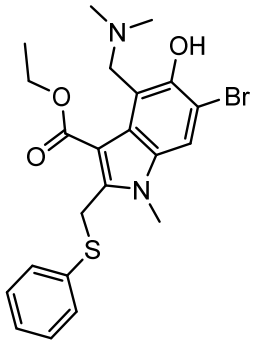
Adefovir	Amantadine	Amprenavir	Arbidol
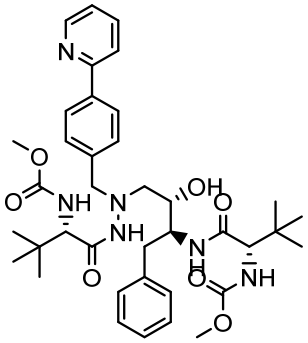	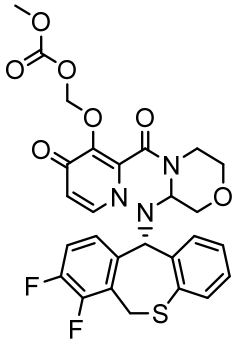	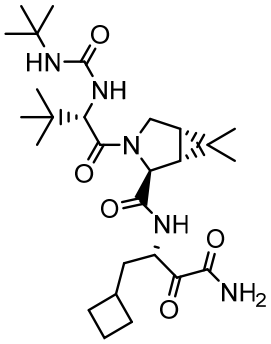	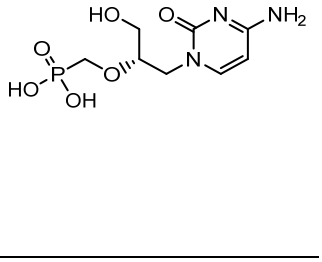
Atazanavir	Baloxavir marboxil	Boceprevir	Cidofovir

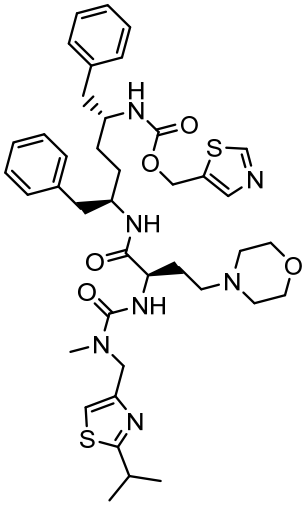	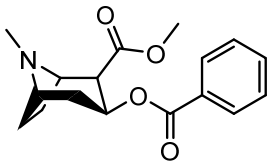	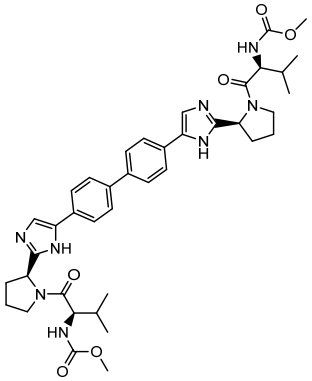	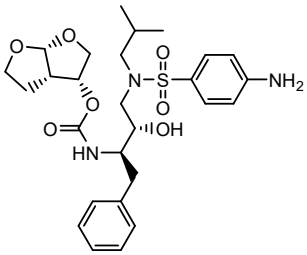
Cobicistat	Cocaine	Daclatasvir	Darunavir
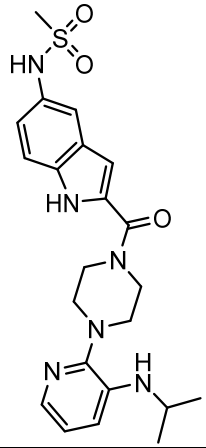	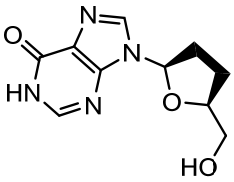	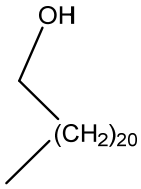	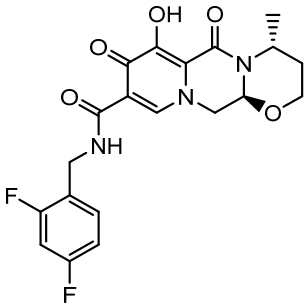
Delavirdine	Didanosine	Docosanol	Dolutegravir
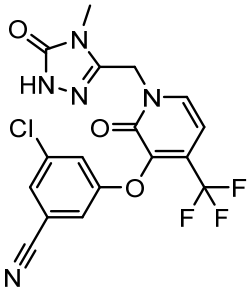	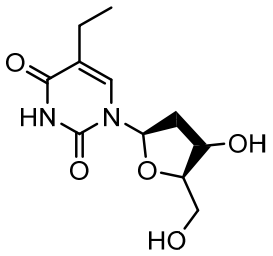	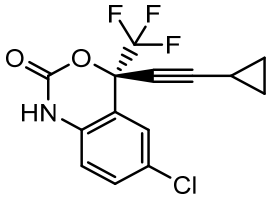	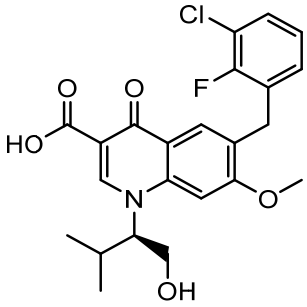
Doravirine	Edoxudine	Efavirenz	Elvitegravir
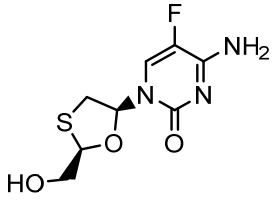	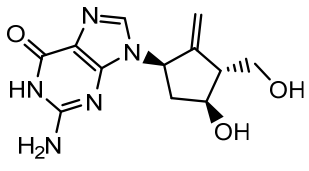	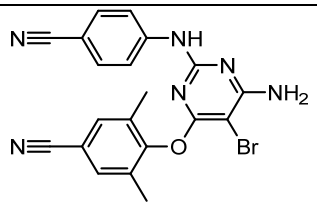	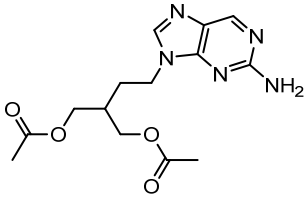
Emtricitabine	Entecavir	Etravirine	Famciclovir

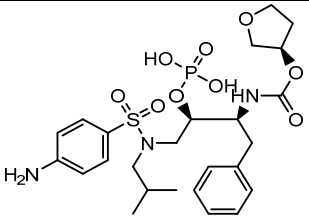	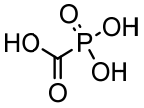	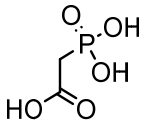	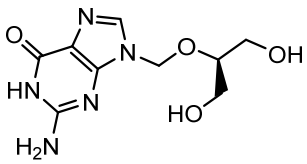
Fosamprenavir	Foscarnet	Fosfonet	Ganciclovir
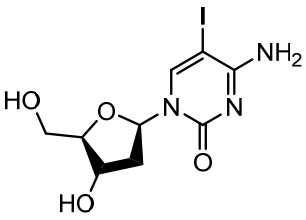	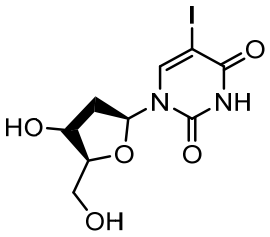	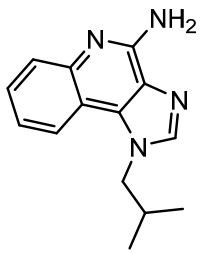	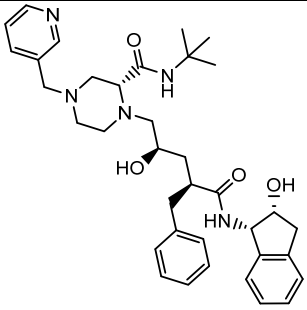
Ibacitabine	Idoxuridine	Imiquimod	Indinavir
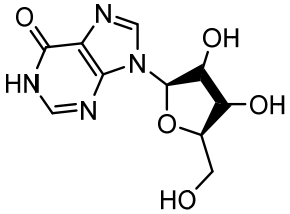	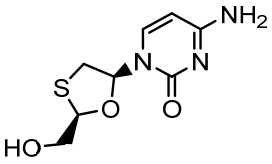	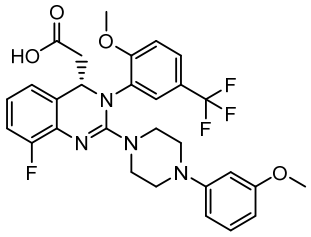	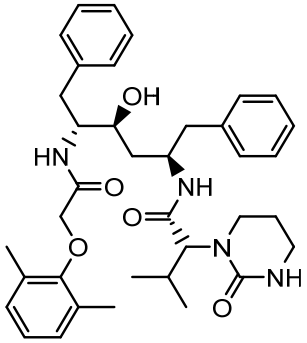
Inosine	Lamivudine	Letermovir	Lopinavir
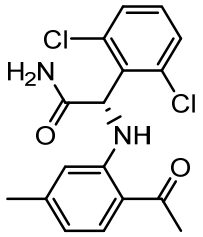	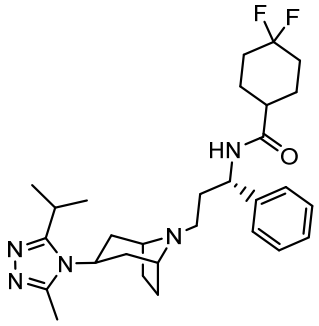	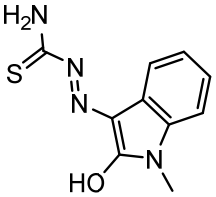	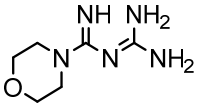
Loviride	Maraviroc	Methisazone	Moroxydine
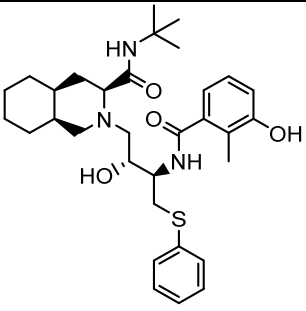	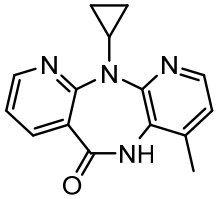	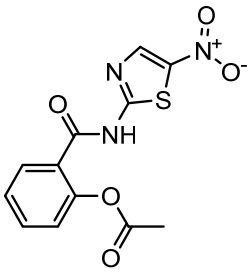	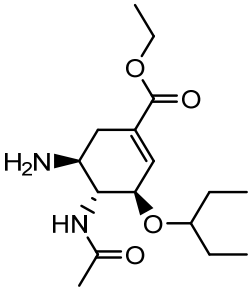

Nelfinavir	Nevirapine	Nitazoxanide	Oseltamivir
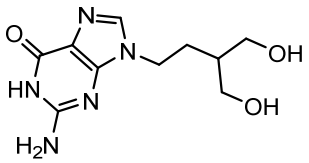	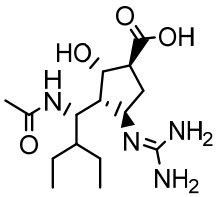	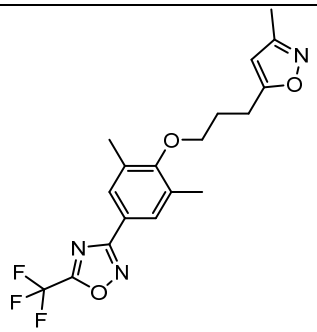	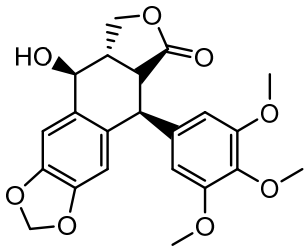
Penciclovir	**Peramivir**	**Pleconaril**	**Podophyllotoxin**
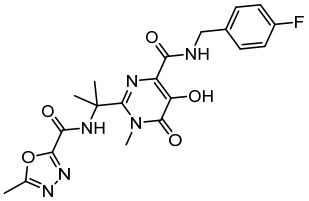	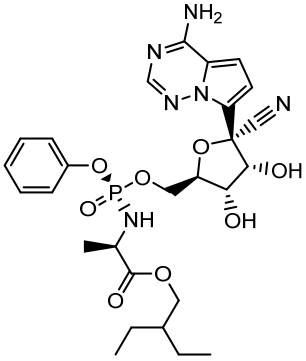	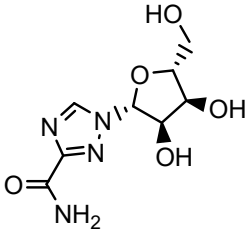	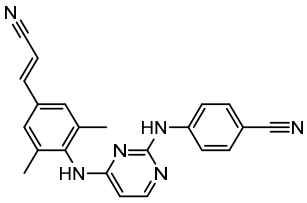
Raltegravir	**Remdesivir**	**Ribavirin**	**Rilpivirine**
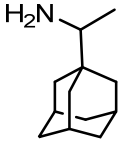	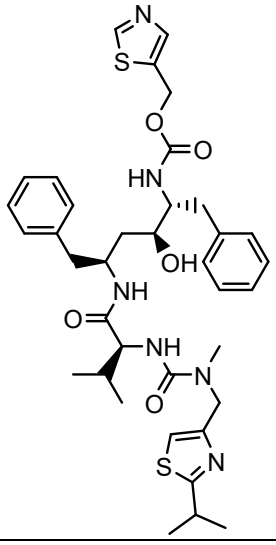	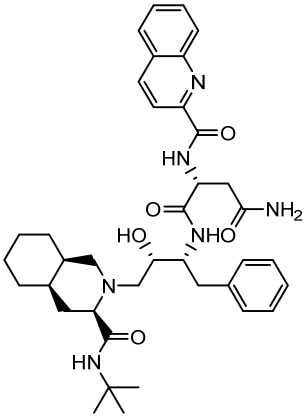	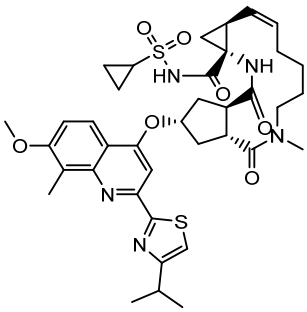
Rimantadine	**Ritonavir**	**Saquinavir**	**Simeprevir**
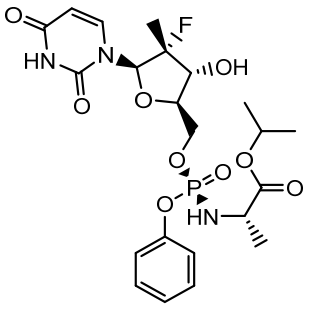	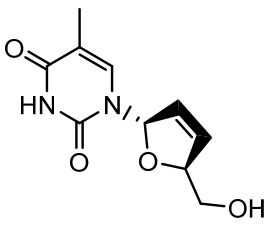	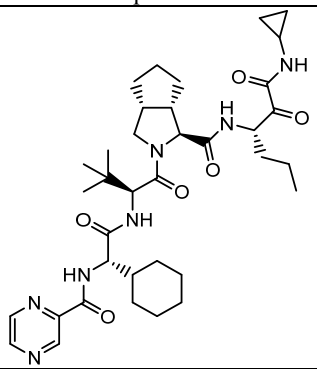	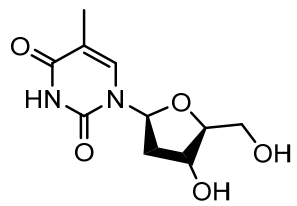

Sofosbuvir	Stavudine	Telaprevir	Telbivudine
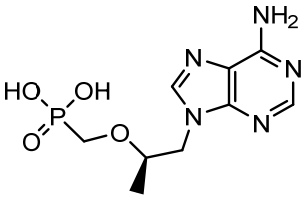	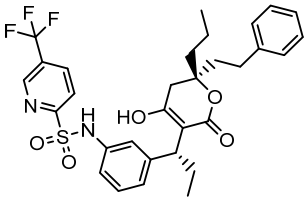	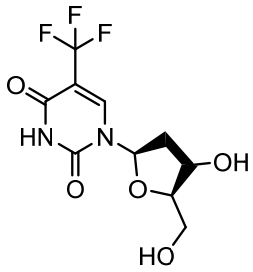	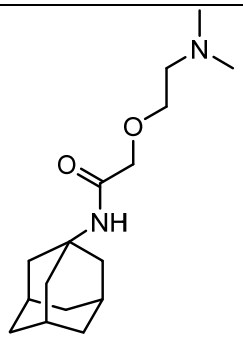
Tenofovir	**Tipranavir**	**Trifluridine**	**Tromantadine**
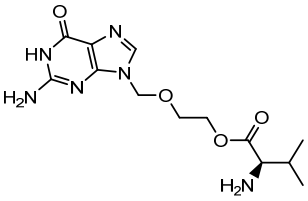	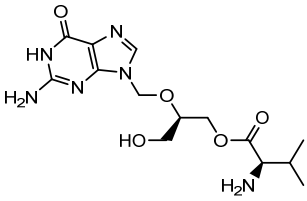	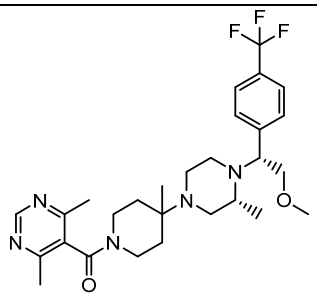	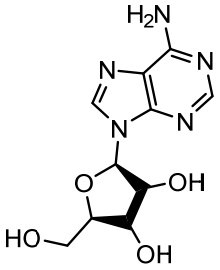
Valaciclovir	**Valganciclovir**	**Vicriviroc**	**Vidarabine**
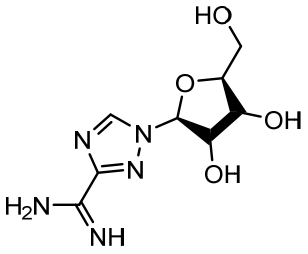	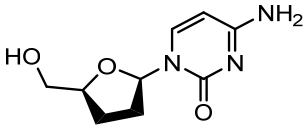	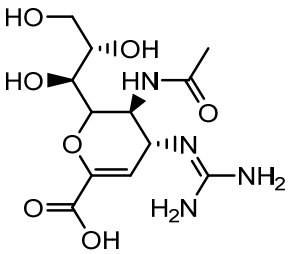	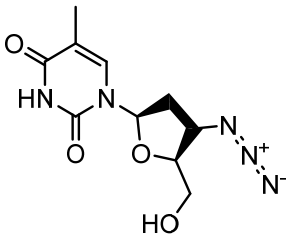
Viramidine	**Zalcitabine**	**Zanamivir**	**Zidovudine**

a. N3P (Control)

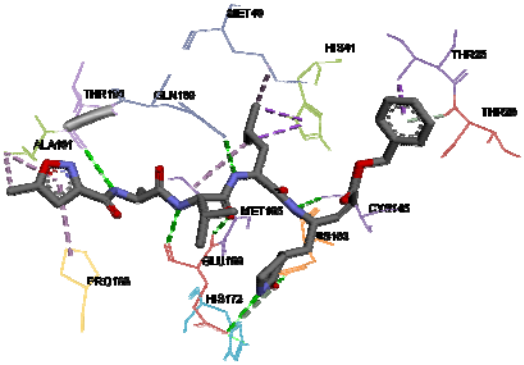

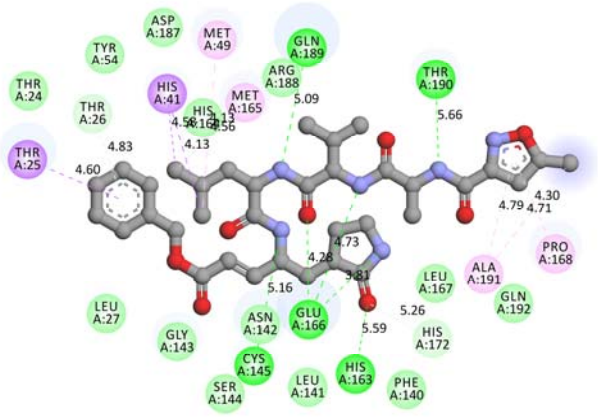

b. Chloroquine

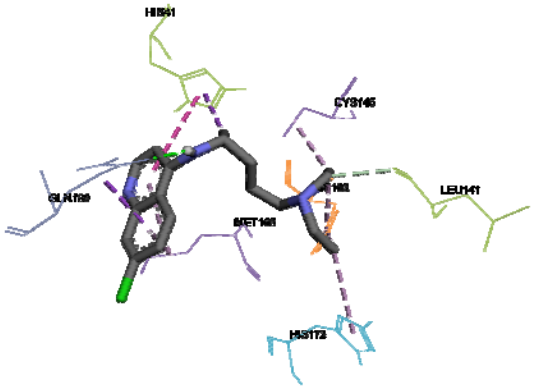

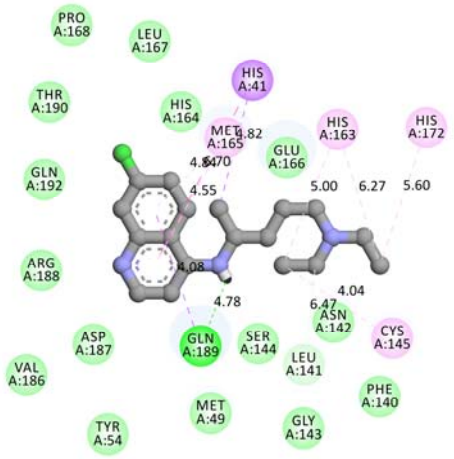

c. Hydroxychloroquine

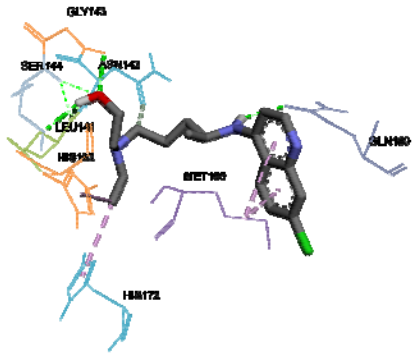

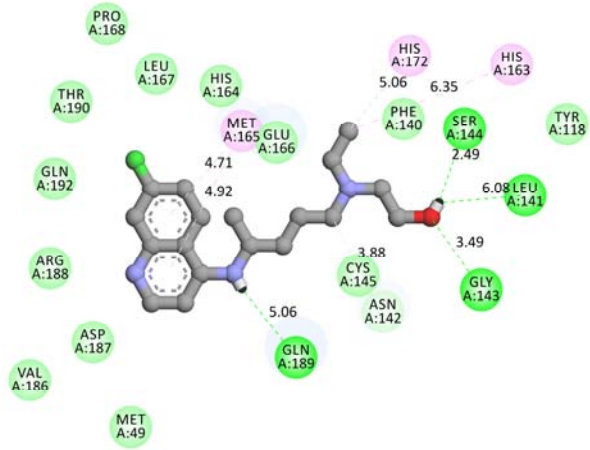

d. Daclatasvir

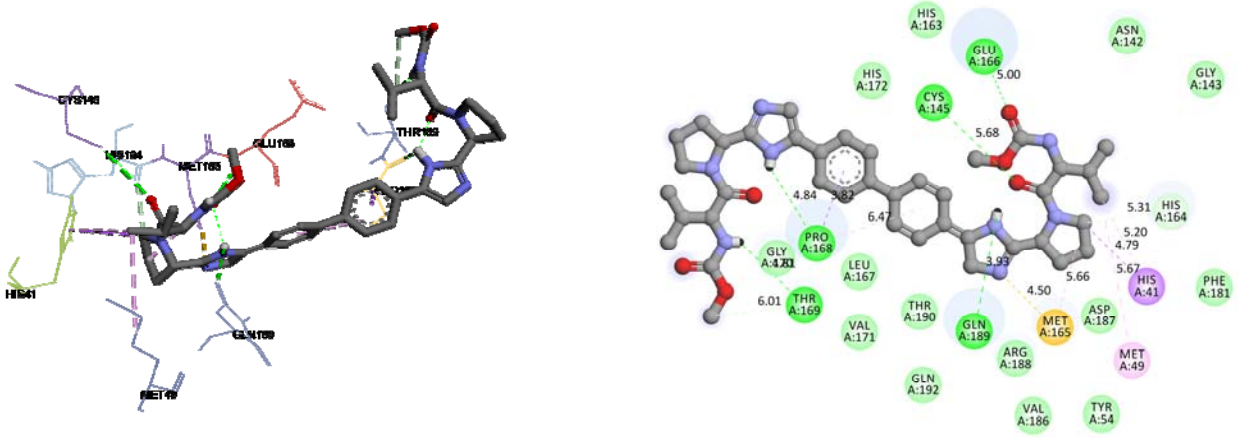

e. Delavirdine

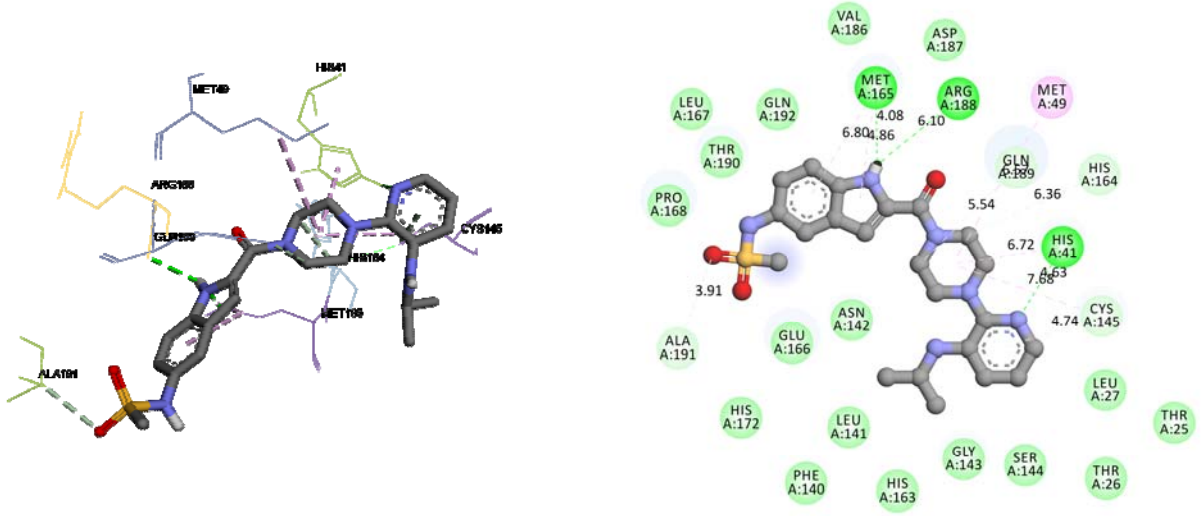

f. Dolutegravir

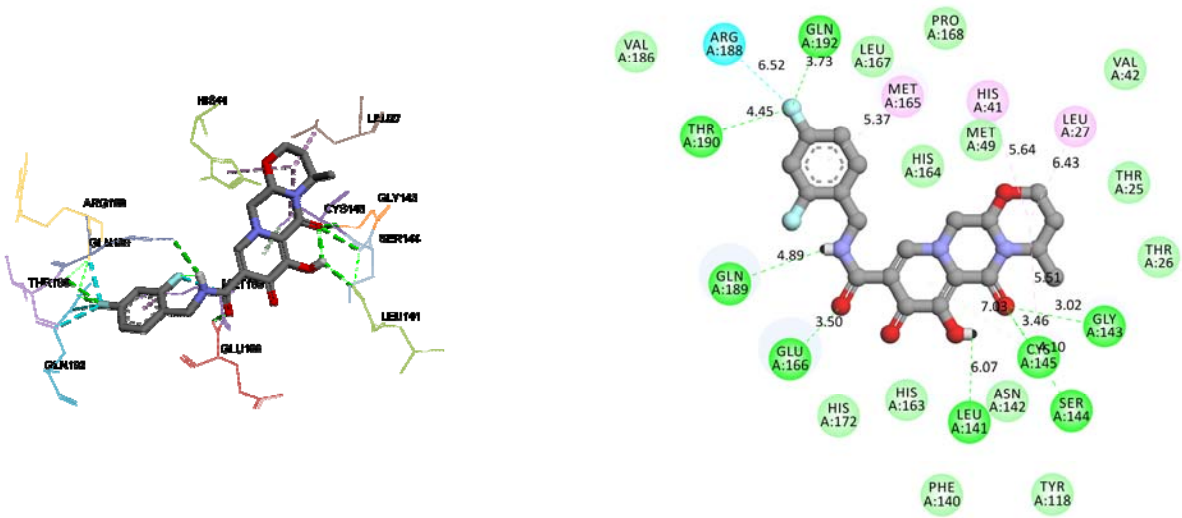

g. Indinavir

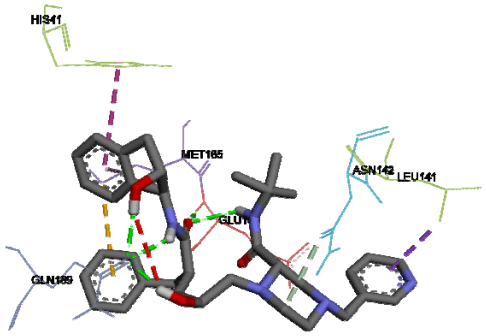

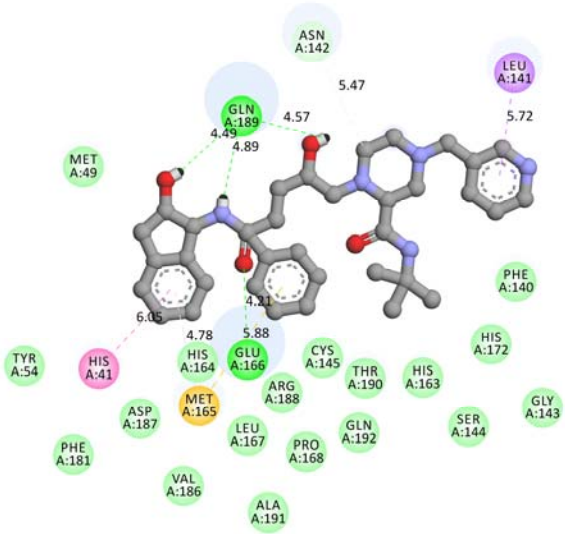

h. Lopinavir

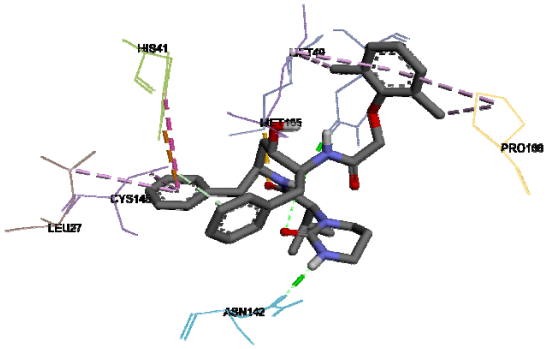

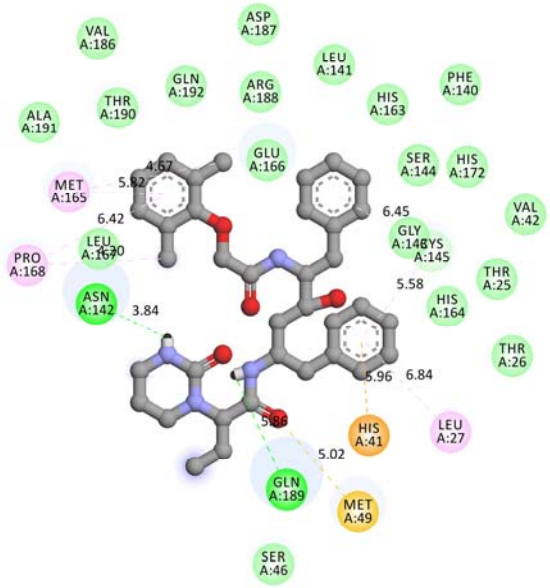

i. Maraviroc

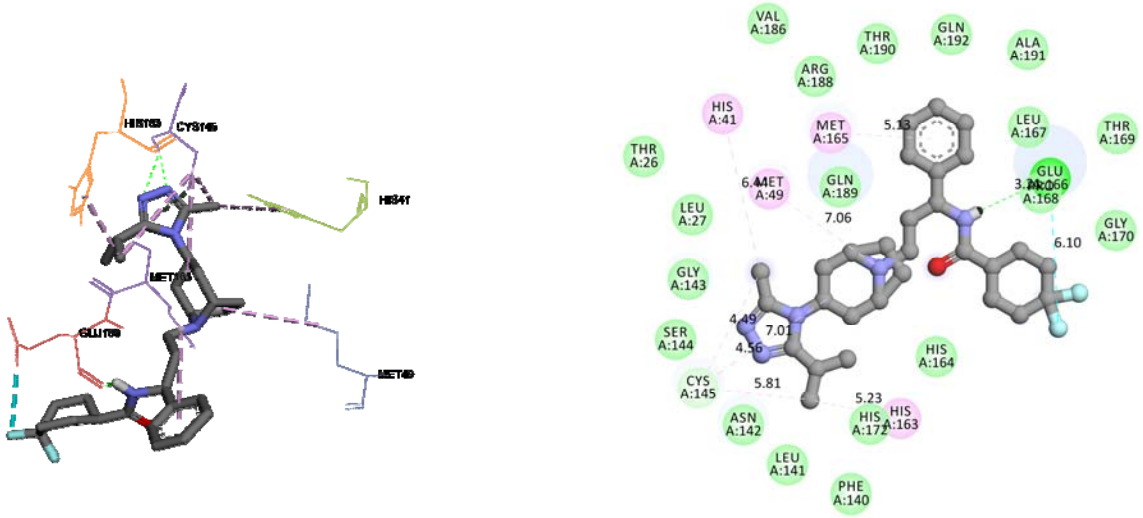

j. Raltegravir

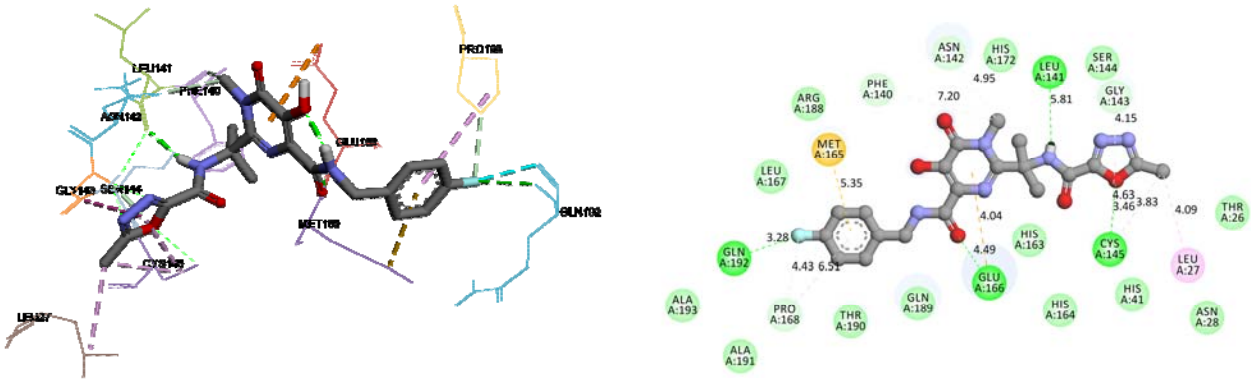

k. Simeprevir

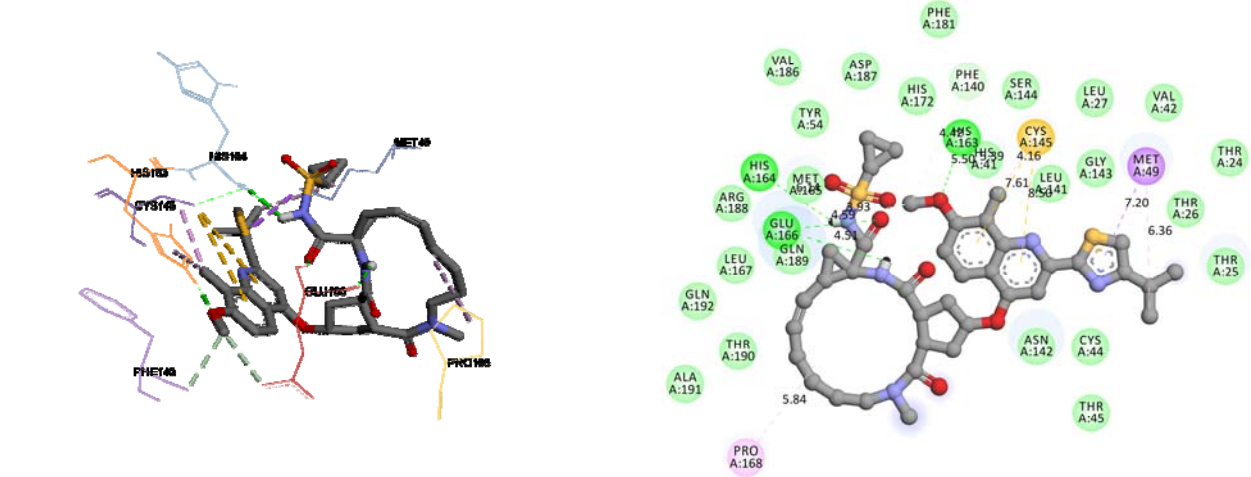

l. Sofosbuvir

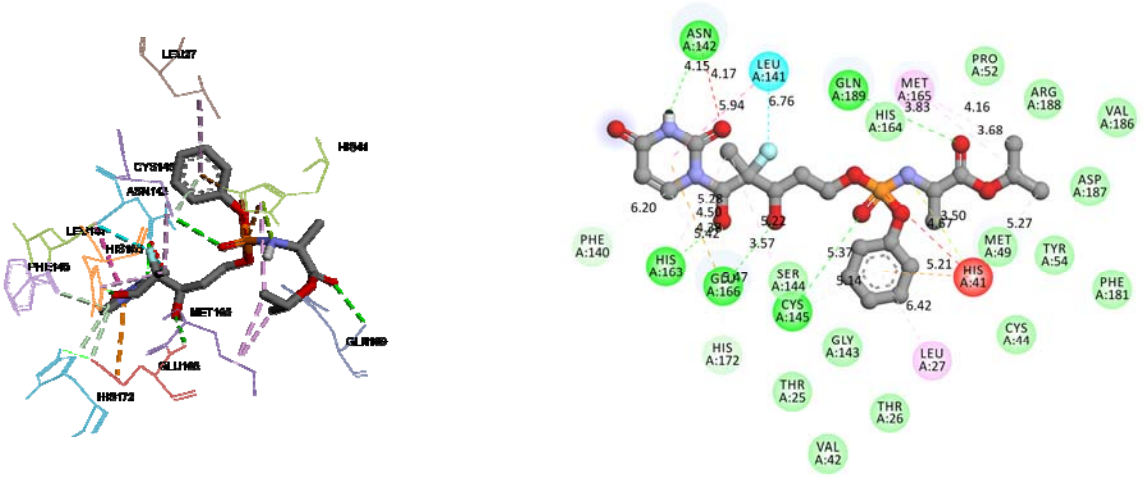

m. Vicriviroc

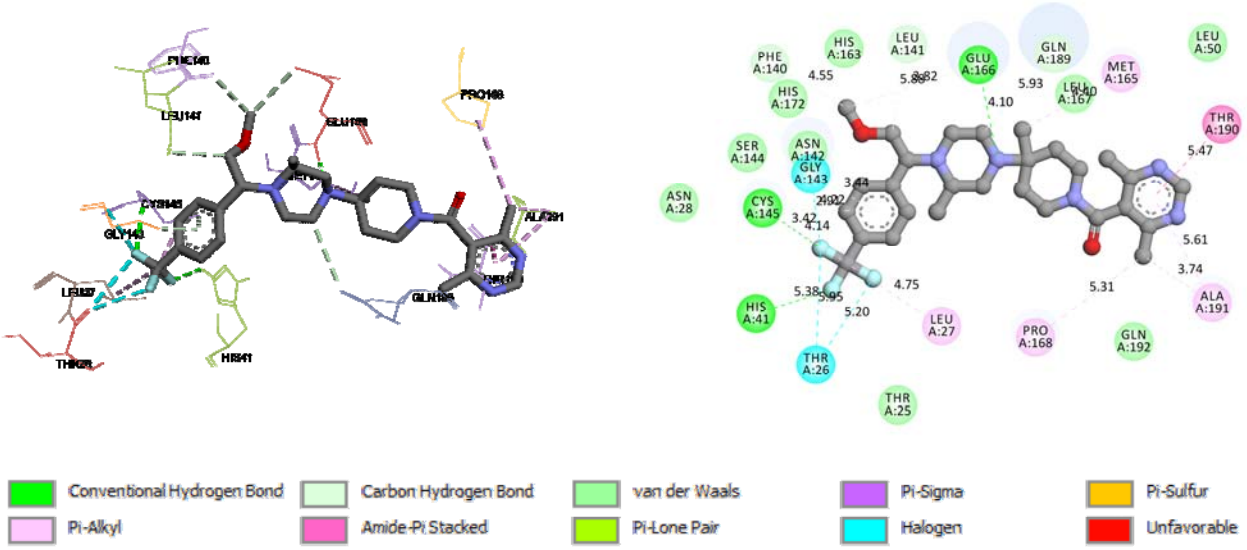

Figure S1. 3D and 2D representations of the binding poses and interactions of the docked control peptide (N3P), chloroquine, hydroxychloroquine, daclatasvir, delavirdine, dolutegravir, indinavir, lopinavir, maraviroc, raltegravir, simeprevir, sofosbuvir, and vicriviroc as a result of molecular docking simulations.

JJBS

Volume 15, Number 5,December 2022
ISSN 1995-6673
Pages 763 – 770
https://doi.org/10.54319/jjbs/150504

Jordan Journal of Biological Sciences

Blood Characteristics and Tissue Histology of *Oreochromis niloticus* Fed *Ipomoea batatas* Leaf

Diomerl Edward B. Baldo[1,5,6]*, Patricia M. Candelaria[2], Francis N. Baleta[3], Love Joy P. Baleta[4], Mylene C. Navarro[2], Lander C. Plantado[2]

[1]*Partido State University Caramoan Campus, Caramoan, Camarines Sur 4429, Philippines;* [2]*Partido State University Sagñay Campus, Sagñay, Camarines Sur 4421, Philippines;* [3]*Philippine Council for Industry, Energy and Emerging Technology Research and Development, DOST Complex, Bicutan, Taguig City 1631, Philippines;* [4]*College of Business and Management, Partido State University Goa Campus Goa, Camarines Sur, 4422, Philippines;* [5]*Biological Sciences Division, National Research Council of the Philippines, DOST Complex, Bicutan, Taguig City 1631, Philippines;* [6]*Applied Biological Sciences Program, Chulabhorn Graduate Institute, 54 Kamphaeng Phet 6 Road, Lak Si, Bangkok 10210, Thailand*

Received: January 9, 2022; Revised: April 21, 2022; Accepted: May 3, 2022

Abstract

Clinical hematology and tissue histoarchitecture are prognostic indicators of pathological conditions in fish. Using *Oreochromis niloticus*, a 12-week feeding experiment assessed the hematology and histopathology of ammonia-exposed tissues of gills, kidney and liver. Four treatments were used in the experiment. Fish in the control group was fed the practical diet (T1), while others received diet supplemented with *Ipomoea batatas* in powder (T2), hot water extract (T3), and crude extract (T4). Hematological profiling was conducted for 12 weeks. Results indicated significant differences at week 6 in neutrophils and lymphocytes, at week 8 in erythrocytes, lymphocytes, eosinophils, and platelets, and at week 12 in hemoglobin (P<0.05). Liver of T1 and T4 illustrated histoarchitecture at normal limits, while erythrocyte infiltration and vacuolation of hepatocytes were observed in T2 and T3. All groups fed *I. batatas*-supplemented diets showed beneficial effect on the kidney as evidenced by notable decrease in the melanomacrophages. Gill tissues displayed no prominent signs of improvement against widespread infiltration of inflammatory cells in both primary and secondary lamella. The results of the present study demonstrated that incorporation of crude extracts of *I. batatas* can boost early enhancement of lymphocyte and neutrophil production and improve ammonia-induced kidney and liver histopathology.

Keywords: *Ipomoea batatas,* hematology, histology, *Oreochromis niloticus*, ammonia

1. Introduction

Aquaculture is observed to be rapidly growing in production volume and economic impact. By 2030, it is predicted to be the primary source of fish mainly due to consumption demands and reduced captured of common wild species (FAO, 2016). Expectedly, aquaculture production can feed the growing population in every part of the world. However, challenges in successful and effective expansion in aquaculture sector is faced by culture farmers (Abbas *et al.,* 2019). Important factors in this endeavor include its ability to expand sustainably, coping with changes in ecosystem, and profitable aquafeed industry (Fazio, 2019). Prices of animal protein ingredients have been increasing (Olsen and Hasan, 2012), which led to increase in the cost of fish raising, and subsequently elevated the fish product cost.

Nile tilapia (*Oreochromis niloticus)* is one of the main and accepted farmed species around the globe. While, the dietary requirement of tilapia is well reported (Wilson, 1994), alternative feed for more sustainable production, affordable sale prices and promising nutritional values is still warranted. Fish nutritionists all over the world are continuously searching for natural dietary source, which can maximize the fish production in a time-bound and at low cost manners.

Protein is now considered as the most expensive component in aquaculture diet. Thus, feed manufacturers search for alternative sources of carbohydrate and fat-rich sources (Yones *et al.,* 2019). As potential non-protein energy sources, lipids and carbohydrates are among the choices tapped in today's aquaculture development. A number of studies have shown that most cultured fish can efficiently utilize both these macromolecules for better growth (Boujard *et al.,* 2004; Darias *et al.,* 2015). Currently, there is a dearth of reported studies to unmask natural products of non-protein substitutes that could maximize the use of costly protein and increase feed efficiency.

Sweet potato (*Ipomoea batatas)* is a dicotyledonous plant, which belongs to the morning-glory or convolvulaceae family. Locally, it is known as *camote.* It is an herbaceous creeping plant with smooth, lightly moderate green leaves sometimes with a considerable amount of purple pigmentation along its veins (Arifina *et al.,* 2020). Sweet potato leaves contain 4.90% crude fat; 24.85% crude protein; 51.95% carbohydrate; 7.20% crude

* Corresponding author. e-mail: debbaldo@parsu.edu.ph.

fiber; and the caloric value is estimated at 351.30 ME kcal/g (Antia *et al.,* 2006). However, the plant's potential as economic source is unrecognized due to its concept as food to the common population and traditional feed to domestic animals (Oyenuga, 1968). Sweet potato is dominantly found in the tropics like the Philippines. The abundance of this plant source provide justification to its possible use as meal ingredient in aquaculture. Therefore, the present study assessed the effects of *I. batatas* feed supplementation on blood profile and tissue histoarchitecture of ammonia-exposed *O. niloticus*. Specifically, it aims to determine the weekly hematological response in red blood cells (RBCs), white blood cells (WBCs), and blood platelets components, besides examine the histological alterations in the liver, kidney, and gills of experimental fish.

2. Materials and Methods

2.1. Plant preparation

Sweet potato red shoots were purchased at Goa public markets in Camarines Sur, Philippines with a total number of 305 bundles. Samples were stationed at the Science Laboratory of Partido State University Natural Science Laboratory. Leaves were washed and air-dried for 72 hours. Thereafter, the leaves were reduced to fine powder using mechanical blender. Powdered sweet potato leaves are stored for extraction procedures.

2.2. Preparation of hot water extract

Hot water extraction was performed according to Kim *et al.* (2011). Pulverized sweet potato leaves at 50 g were added to 500 mL of pure distilled water. The solution was boiled in a hot plate for 3 hours at temperature not exceeding 100°C. The suspension was passed through a nylon mesh. The filtered hot water extract was frozen and maintained in a storage until the feed formulation.

2.3. Preparation of crude extract

Pulverized sweet potato leaves at 500 g were soaked in 5 L of analytical grade ethanol for 72 hours. Thereafter, the samples were filtered using Whatman paper no. 42. The filtrate was collected and concentrated using rotary evaporator (IKA-100) under reduced pressure at 45°C in 100 rpm. The extract was refrigerated at 4°C until the feed formulation.

2.4. Fish culture and feeding experiment

A total of 240 male and female *O. niloticus* with mean weight 14.91 ± 1.59g were collected at PSU-Sagnay Multi-species Hatchery and were acclimated for 1 week in 1 m^3 concrete tanks. Experimental fish were randomly distributed in four treatments with three replications, each replicate was assigned with 20 fish. During the acclimatization period, fish fed the basal diet. The water was aerated with electric pumps and was renewed once every three days. Water quality parameters such as dissolved oxygen (DO), and temperature were monitored regularly and maintained using DO-meter and tank thermometer, respectively.

2.4.1. Diets and experimental design

Fish in the control group (T1) fed a practical diet described by FAO (2021) with 0% of sweet potato leaves. Other groups received the practical diet (95%), supplemented with 5% of either sweet potato leaves powder (T2), hot-water extract (T3) and crude extract (T4). Diet ingredients were grounded, mixed, and pelleted using animal feed pellet machine. The respective diets were provided twice on a daily basis (8:00 AM and 4:00 PM) and consisted with 5% of the live body weight of the fish.

2.5. Blood collection and hematological analysis

Twelve fish were randomly collected from each treatment. Blood samples at 0.5 ml per fish were collected at weeks 2, 4, 6, 8, 10 and 12, from the caudal peduncle region using 1 cc (25 g × 5/8) syringe rinsed with ethylenediaminetetraacetic acid (EDTA) as anti-coagulant. The samples were analyzed using Rayto Auto Hematological Analyzer (RT-7600) to determine various hematological parameters such as red blood cells (RBCs), hemoglobin, hematocrit, mean corpuscular volume (MCV), mean corpuscular hemoglobin (MCH), mean corpuscular hemoglobin concentration (MCHC), white blood cells (WBCs), neutrophils, lymphocytes, monocytes, eosinophil, platelet, mean platelet volume (MPV) and platelet distribution width (PDW).

2.6. Ammonia toxicity experiment

A range finding test was conducted to determine the sub-lethal dose of ammonia following the methods described by El-Shafai *et al.* (2004), with few modifications. After the 12-week feeding experiment, the fish were exposed to 6 mg L^{-1} concentration of ammonia (Loba Chemie, India) continuously supplied with aeration. The fish were observed in a 24-hour duration (Küçük, 2014). Fish demonstrating morbidities and mortalities were sacrificed. Ice was added incrementally, and was used as a non-chemical anesthesia (Coyle *et al.,* 2004). Kidney, liver and gills were harvested for histopathological examination.

2.7. Histological analysis

A total of four random fish from each group were sacrificed. In brief, fragments from target organs such as kidney, liver and gills were harvested. The samples were then fixed in 95% formaldehyde solution. Subsequently, samples were dehydrated, cleared using xylene and embedded in paraffin. Segments were cut at 3 µm via a microtome. Samples were stained with hematoxylin and eosin (H&E) for histopathological analysis.

2.8. Statistical analysis

Data are shown as mean ± standard error of the means (SEM). One-way analyses of variance (ANOVA) was performed using IBM SPSS Statistics 26.0 software. Differences between treatment means were compared by Tukey's test. The significant differences between mean were statistically considered at $P<0.05$.

3. Results

In this study, the effect of sweet potato incorporation in feeding diets on blood profile and tissue histomorphology of *O. niloticus* was evaluated. The latter effect was achieved by ammonia exposure within 24 hours. Data on the changes in hematological parameters are presented separately in Tables 1, 2, and 3. While, the histological

characterization of tissues from liver, kidney and gills are shown in Figures 1, 2 and 3, respectively.

3.1. Changes in RBCs, WBCs and Platelet count

In Table 1, the data suggest no significant difference in hematocrit throughout the feeding duration. At week 2, significant (P<0.05) difference was observed in the three formulated diets in terms of MCV. At week 8, RBCs recorded significant difference among treatments, where T4 and T2 displayed the lowest and highest count, respectively. This record is inverse with those of MCHC in the same week. At week 12, T2 significantly showed a high level of hemoglobin (P<0.05).

Table 1. Record of erythrocyal components of *Oreochromis niloticus* fed *Ipomoea batatas* for the 12-week feeding experiment

	Treatment	Culture period (week)					
		2	4	6	8	10	12
Red blood cells (10^6 mL^{-1})	T1	1.81±0.08	1.97±0.05	2.05±0.10	2.00±0.06^{ab}	2.00±0.12	1.73±0.09
	T2	1.78±0.14	2.00±0.08	2.11±0.14	2.08±0.06^{b}	1.95±0.17	1.88±0.13
	T3	1.93±0.07	1.93±0.13	1.96±0.12	1.84±0.08^{ab}	1.99±0.15	1.94±0.13
	T4	1.67±0.11	1.59±0.23	1.85±0.11	1.78±0.08^{a}	1.73±0.14	1.85±0.12
Hematocrit (%)	T1	24.4±1.32	23.68±0.83	28.38±1.09	31.07±1.41	28.97±1.09	26.23±1.74
	T2	28.22±2.78	26.97±0.93	29.75±1.40	31.47±1.04	26.60±1.99	30.37±1.51
	T3	28.62±0.66	26.60±0.99	27.77±1.61	28.13±0.59	30.15±1.27	28.47±1.34
	T4	26.80±1.54	22.07±3.10	27.75±1.04	28.05±1.27	25.90±2.16	26.25±1.16
Hemoglobin (g dL^{-1})	T1	105.33±6.87	104.33±3.19	116.17±5.18	124.17±2.37	114.33±5.38	113.67±5.42^{a}
	T2	115.33±7.63	117.67±3.74	112.83±5.11	121.50±8.01	119.00±5.33	136.00±4.22^{b}
	T3	118.00±1.62	119.33±3.45	105.17±5.51	123.00±2.81	132.17±2.60	129.50±2.27^{ab}
	T4	109.00±5.19	100.00±13.5	114.33±6.07	126.17±3.44	107.17±9.36	119.67±4.07^{a}
Mean Corpuscular Volume (fl)	T1	134.95±5.99^{a}	119.93±3.03	140.17±8.13	155.38±3.14	146.33±4.19	151.05±4.16
	T2	157.63±3.89^{b}	119.10±20.14	142.33±5.10	151.02±2.70	138.82±6.60	153.28±7.88
	T3	149.23±3.53^{b}	139.80±6.40	142.07±3.54	153.82±4.80	154.80±8.15	144.57±4.60
	T4	161.10±3.08^{b}	137.25±5.13	142.88±4.29	157.88±1.54	149.55±4.11	147.20±6.83
Mean Corpuscular Hemoglobin Concentration (g dL^{-1})	T1	431.67±10.44	441.33±7.32	401.67±10.72	412.50±8.63^{ab}	393.50±5.92	436.33±17.98
	T2	476.50±48.73	438.0±6.11	380.83±11.26	385.0±18.87^{a}	426.83±8.83	453.0±14.91
	T3	412.50±4.65	451.83±16.25	380.83±10.60	437.83±13.26^{ab}	441.83±12.96	450.50±13.61
	T4	413.67±22.32	458.17±21.61	411.17±7.72	451.67±13.26^{b}	416.50±17.50	438.0±.28

Values are presented as mean±SEM; n=12
Different letters indicate significant difference, P<0.05

For leukocytal records, no significant difference was observed in the white blood cells and monocytes (Table 2). At week 6, leukocytes level from the three formulated diets of *I. batatas* revealed significant increase. In the same week, neutrophil count presented the opposite trend with T1 showing significant increase (T2,>T4>T3). At week 8, T1 and T3 showed significant elevations in lymphocytes. Also, T2 group showed significant increase in eosinophils levels (P<0.05).

Table 2. Record of leukocytal components of *Oreochromis niloticus* fed *Ipomoea batatas* for the 12-week feeding experiment

	Treatment	Culture period (Week)					
		2	4	6	8	10	12
White blood cells (10^3 mL^{-1})	T1	60.18±3.82	65.91±6.87	80.11±6.47	76.77±5.80	63.26±4.58	76.76±5.83
	T2	70.39±7.09	63.91±2.54	85.67±3.82	84.42±3.26	66.63±7.79	78.36±5.06
	T3	62.40±1.99	68.06±2.89	86.27±5.71	92.44±7.83	75.09±3.11	85.60±4.50
	T4	61.55±4.85	59.81±10.77	88.29±4.51	70.14±2.84	59.50±8.77	68.85±3.93
Neutrophils (10^3 mL^{-1})	T1	19.14±3.00	11.85±3.47	15.96±3.43^{b}	12.09±7.66	5.14±2.89	7.62±3.86
	T2	16.80±2.49	16.10±3.26	6.77±2.67^{ab}	14.84±3.72	9.13±4.72	13.69±8.01
	T3	12.56±3.24	15.54±2.52	2.37±0.99^{a}	13.29±5.08	7.58±2.34	14.90±3.45
	T4	17.15±4.42	12.30±4.31	6.60±2.06^{ab}	25.57±3.74	6.60±2.19	8.17±2.96
Lymphocytes (10^3 mL^{-1})	T1	16.67±2.66	35.78±14.42	38.47±6.93^{a}	50.89±12.01^{ab}	54.64±7.26	43.20±9.41
	T2	20.68±5.47	19.63±3.35	70.06±5.78^{b}	41.31±10.7^{b}	51.66±8/86	48.95±7.60
	T3	28.20±8.62	18.34±2.29	74.60±6.91^{b}	64.82±12.74^{ab}	61.43±5.89	60.06±4.54
	T4	20.86±8.31	29.06±11.43	66.81±6.49^{b}	8.66±1.37^{b}	43.70±7.41	54.88±2.26
Monocytes (10^3 mL^{-1})	T1	22.29±2.54	17.06±6.05	21.10±4.18	11.93±6.84	1.95±1.66	11.10±4.52
	T2	30.54±6.12	26.59±1.44	6.22±5.48	25.46±8.19	6.38±3.65	7.95±3.47
	T3	22.16±6.39	32.32±4.42	5.64±3.93	12.90±6.73	3.40±2.59	13.44±4.04
	T4	22.91±5.46	16.69±5.14	11.78±4.89	32.80±1.61	6.59±2.25	7.19±4.43
Eosinophils (10^3 mL^{-1})	T1	1.99±0.48	1.23±0.16	4.55±1.62	1.84±0.52^{ab}	1.52±0.31	1.06±0.20
	T2	2.39±1.14	1.60±0.25	2.58±1.21	2.82±0.34^{b}	2.78±1.06	2.27±0.56
	T3	1.26±0.27	1.84±0.41	0.82±0.24	1.39±0.25^{a}	2.66±0.51	2.16±0.69
	T4	0.61±0.13	1.77±0.42	3.11±0.94	0.89±0.18^{a}	2.56±0.93	2.20±0.21

Values are presented as mean±SEM; n=12
Different letters indicate significant difference, P<0.05

For platelet monitoring (Table 3), no significant difference was observed from weeks 2 to 12 in the MPV. Platelet and PDW were shown to present early changes in the three *I. batatas* supplemented feeds as compared to those fed the practical diet (T1) at week 2 (P<0.05). At week 8, platelet level significantly accelerated in T3 (P<0.05). At week 12, T1 and T2 showed significant increase in the PDW.

Table 3. Record of thrombocytal components of *Oreochromis niloticus* fed *Ipomoea batatas* for the 12-week feeding experiment

	Treatment	Culture period (week)					
		2	4	6	8	10	12
Platelet (10^6 mL^{-1})	T1	9.00±0.94^a	12.17±3.03	12.17±1.44	42.83±10.59^a	20.17±3.23	58.83±28.68
	T2	16.17±2.13^b	12.67±1.48	18.83±4.09	118.17±10.59^b	35.67±14.85	94.83±39.87
	T3	16.17±2.13^b	15.67±3.33	36.00±16.14	44.00±9.84^a	22.00±3.23	21.83±6.07
	T4	14.33±0.87^b	14.50±1.88	19.33±3.08	27.83±4.04^a	17.00±3.55	85.33±40.72
Mean platelet volume (fl)	T1	7.35±0.37	6.82±0.37	9.17±0.54	9.55±0.46	10.10±0.44	10.63±1.29
	T2	8.43±0.38	8.33±0.61	9.18±0.39	11.30±0.98	10.63±1.01	11.72±1.4
	T3	8.30±0.35	8.78±0.44	8.98±0.79	9.32±0.55	10.67±0.29	9.55±0.4
	T4	8.43±0.27	7.90±0.75	9.20±0.58	10.18±0.29	9.30±0.62	10.38±1.46
Platelet distribution width (fl)	T1	16.22±0.46^a	16.22±0.49	18.10±0.36	17.60±0.46	17.37±0.54	16.82±0.60^{ab}
	T2	17.83±0.30^b	17.48±0.45	17.92±0.31	16.85±1.22	18.15±0.32	16.20±0.58^{ab}
	T3	18.02±0.32^b	17.62±0.37	17.78±0.67	18.52±0.43	17.60±0.50	17.58±0.58^b
	T4	17.68±0.35^b	17.33±0.49	18.25±0.36	18.58±0.16	17.40±0.47	15.13±0.49^a

Values are presented as mean±SEM; n=12
Different letters indicate significant difference, P<0.05

3.2. Histopathological alterations of organs

3.2.1. The gills tissues

Gills tissues (Figure 1 A-D) show no notable amelioration in any of the experimental groups. All samples demonstrated destruction in the histomorphology of gills as observed by the infiltration of inflammatory cells, predominantly lymphocytes in the primary and secondary lamella. However, more tissue anomalies are exhibited in the T2 and T3 such as hyperplasia with foci of necrosis. Gills from T4 displayed foci of congestion in primary and secondary lamella, primary lamellar epithelial lifting, fusion and clubbing of lamellar tips.

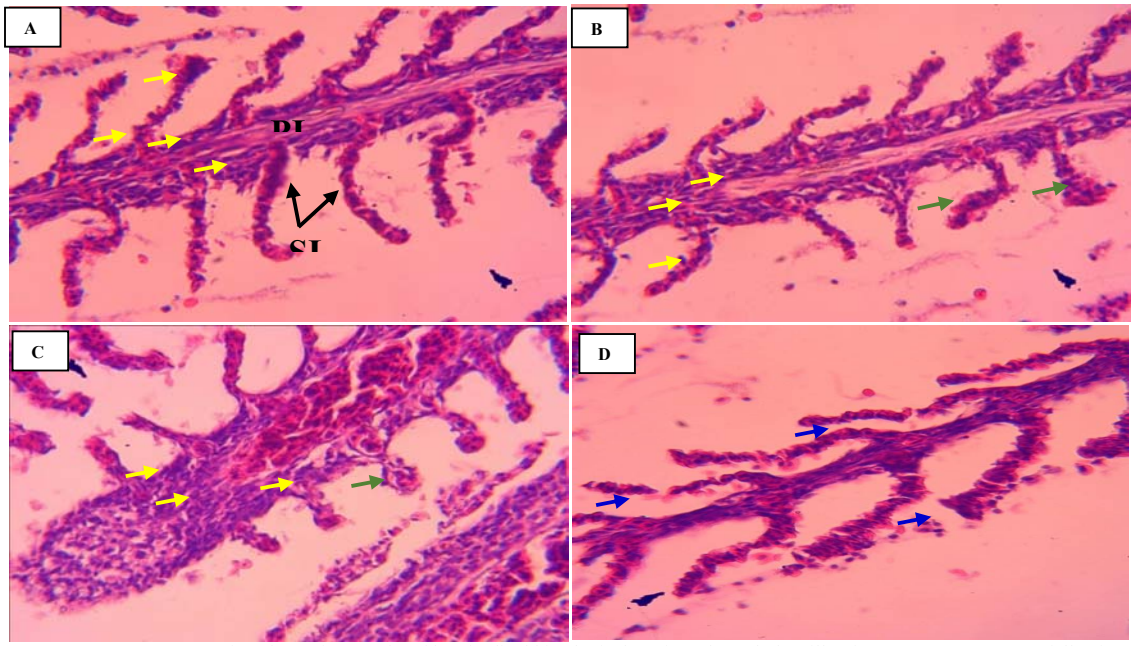

Figure 1 (A-D). Representative photomicrographs of longitudinal histological sections through the gills of *Oreochromis niloticus* following 24-hr exposure to ammonia from experimental fish fed the practical diet (A), sweet potato powder (B), sweet potato hot water extract (C), and sweet potato crude extract (D), showing primary lamellar epithelium (PLE), secondary lamellae (SL), widespread infiltration of inflammatory cells in the primary and secondary lamella (yellow arrow), hyperplasia with foci of necrosis (green arrow), epithelial lifting and fusion of lamellar tips (blue arrow). (H&E, 400×).

3.2.2. The kidney tissues

The histological alterations in kidney tissues of all treatments are briefly illustrated in Figure 2 (A-D). The feeding supplementation demonstrated no significant effect in the histopathology of kidney tissues except for the decrease of melanomacrophages (MMC), compared to control group. T2 and T3 illustrated prominent necrosis of tubular epithelium and hepatic cord disorder accompanying with hepatocyte hypertrophy and cloudy swelling. Also spotted are foci of mineralization in some tubules. T4 group showed aggregates of lymphocytes around blood vessels.

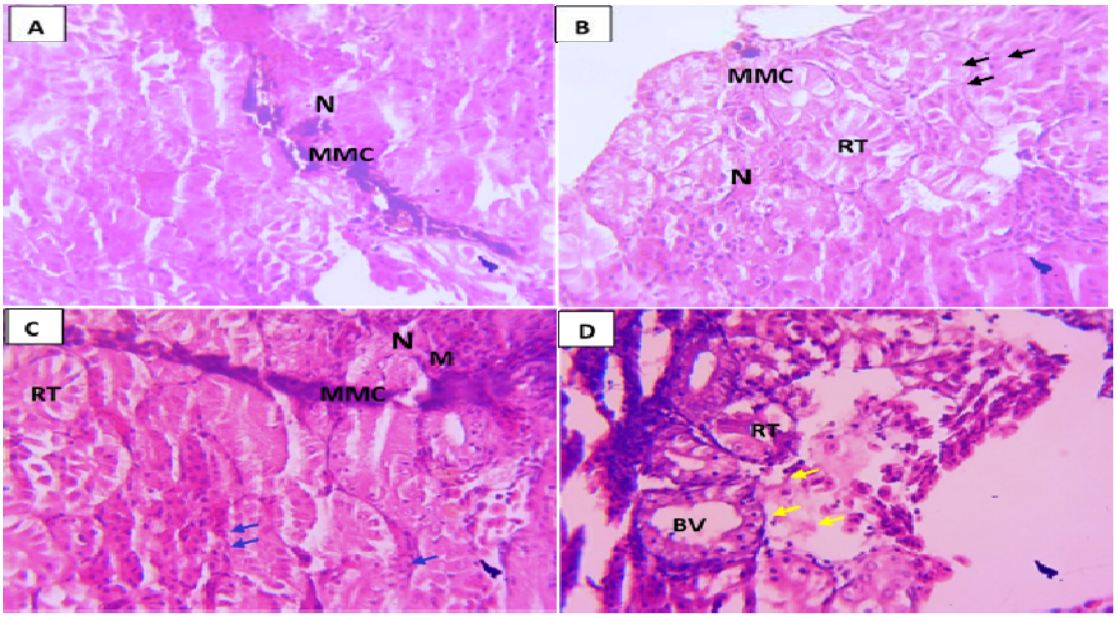

Figure 2 (A-D). **Representative photomicrographs of kidney tissues of *Oreochromis niloticus* following 24-hr exposure to ammonia** from experimental fish fed the practical diet (A), sweet potato powder (B), sweet potato hot water extract (C), and sweet potato crude extract (D), showing moderate depletion of hemopoietic tissues in the interstitium surrounding the tubules (black arrow), increased numbers of melanomacrophages (MMC) within the interstitium, prominent necrosis of tubular epithelium (N), hepatic cord disorder accompanying with hepatocyte hypertrophy and cloudy swelling (blue arrow), foci of mineralization in some tubules (M), few aggregates of lymphocytes (yellow arrow) around blood vessels (BV), renal tubules (RT). (H&E, 400×).

3.2.3. The liver tissues

Surprisingly, histopathology of liver (Figure 3 A-D) showed normalized liver in the control group receiving the practical diet for 12-week of the feeding trial. There were no pathological abnormalities, with hepatocytes presenting a homogenous cytoplasm, and a large central or sub-central spherical nucleus. In both of T2 and T3, moderately damaged liver was exposed. The histopathological changes found in the liver of examined fish included irregular arrangements of hepatocytes, vacuolation, and erythrocyte infiltration in the hepatic tissues. Comparable to the control group, T4 showed nearly normalized liver histology characterized by prominent normal size hepatocytes with central and sub-central spherical nucleus.

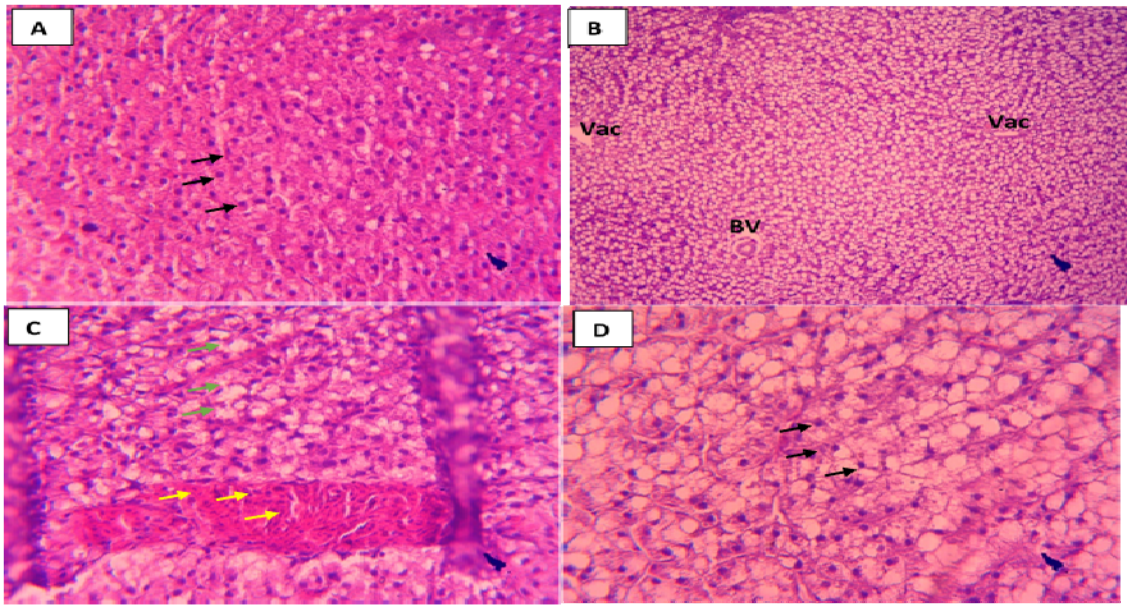

Figure 3 (A-D). Representative photomicrographs of liver tissues of *Oreochromis niloticus* following 24-hr exposure to ammonia, from experimental fish fed the practical diet (A), sweet potato powder (B), sweet potato hot water extract (C), and sweet potato crude extract (D), showing normal hepatocytes (black arrow), mild loss of cytoplasmic vacuolations (vac), blood vessels containing proteinaceous fluid (BV), erythrocyte infiltration into blood sinusoids (yellow arrow) and increased vacuolation of hepatocytes (green arrow). (H&E, 400×)

4. Discussion

Hematological parameters are important indicators of the fish's physiological and health status. According to Sahan *et al.* (2016) WBCs, RBCs, hematocrit and hemoglobin monitoring is instrumental in maintaining the stock in fish farms. More authors prove that botanical immunostimulants have bioactive substances that can cause increase in blood cell counts, thereby triggering immunity and enhance natural defense in fish species (Ajeel and Al-Faragi, 2013; Haghighi and Rohani, 2013; Talpur *et al.,* 2013).

In this study, significant increase has been reported in the MCV, and PDW at week 2, as all formulated diets exhibited significant increase compared to the practical diet. This trend was further shown at week 6 in the levels of lymphocytes. These elevations determined increase in the natural defense cells number. Neutrophils significantly increased in the practical diet–fed group. These results are indicative of early enhancement of immune cells. Indistinct pattern on week 8 has been recorded as blood components in the group receiving T4 significantly decrease (lymphocytes, eosinophils, RBCs and platelet) compared to other groups. The increase in RBCs can be a result of an improved oxygen supply, mirroring a more efficient blood circulation supply of the organism (Ruiz *et al.,* 2020).

Formulated feeds from sweet potato effected to no significant difference in terms of WBCs at any monitoring week. This result is in corroboration with the findings reported by Yones *et al.* (2019), where increasing levels of carbohydrates from wheat bran, corn and sorghum was used as alternative source of carbohydrates to tilapia culture. Lowest WBCs can be observed in T4 or crude extract supplemented feed group, indicative of immunosuppression in the experimental fish.

In the present study, histological alterations in three important organs was studied, gills for examining respiration in respect to exposure to toxins, liver for metabolism of toxicants, and kidney for its involvement in the elimination process. After the 24-hour exposure to 6 mg ammonia L^{-1}, samples from all experimental set-ups revealed notable anomalies in the gill histoarchitecture. According to the study of Le Ruyet *et al.* (1998) ammonia enters the fish 15 minutes following exposure. Initial effects of such contaminants are evidenced in the cellular and sub-cellular levels starting from the first hour of exposure. There are also reports mentioning that chronic exposure to nitrate results to change in the swimming patterns and more importantly to the health of the fish (Davidson *et al.,* 2014). In this study, histological effects in gill tissues agrees to findings of previous authors (Yones *et al.,* 2019; Ruiz *et al.,* 2020), where hyperplasia of the lamella, widespread infiltration of inflammatory cells and epithelial lifting and fusion of lamellar tips were observed after exposure to ammonia. No evidence of gills histology normalization in any of the treatment were demonstrated by all the formulated feed diets, suggesting the inability of the feed components to secrete and continuously replace their mucus layer as a biological barrier (Yoon *et al.,* 2015). For kidney tissue examination, evident decrease in MMCs was observed in all fish receiving sweet potato-incorporated diets. MMCs are aggregates of highly pigmented phagocytes found primarily in the head kidney and spleen, and occasionally on livers (Steinel and Bolnick, 2017). The decline in the numbers of MMCs could be related to an adaption of fish to the recirculation system, allowing a decline of natural stress conditions. MMCs are developed in cases involving chronic inflammatory lesions, in the destruction, detoxification and recycling of endogenous and exogenous materials. Also, it could be indicative of environmental stress and mirrors activity immune response to microbial antigens (Agius and Roberts, 2003). On the other hand, the liver is a vital organ involved in the physiological processes of metabolism, and excretion. Thus, it plays a pivotal role in the removal of toxic substances from the bloodstream and final excretion. In the current study, histoarchitecture of the fish liver tissue was damaged in T2 and T3 groups, as revealed by the increase in hepatocellular basophilia, moderate loss of cytoplasmic vacuolations and few blood vessels containing proteinaceous fluid. Vacuolation may indicate stored energy in the form of glycogen or lipid, and may also express a degenerative change in cellular organelles like the endoplasmic reticulum and Golgi apparatus (Braunbeck, 1998). Furthermore, observable vacuolations may be reflective of an accumulation of free fluid in the cytoplasm (Stehr *et al.,* 1998). Fluid build-up causes distention of the liver cell cytoplasm resulting to ballooning degeneration or cloudy swelling, which was evident in the T3 group. On the other hand, crude extract of sweet potato when added as feed ingredient was able to display normalized liver histoarchitecture. These formulated feeds were mentioned to contain high amounts of total carbohydrates with the crude extract presenting the highest value of 34.94% compared to 34.20% and 34.63% of hot water extract and sweet potato powder, respectively (Pallaya-Baleta *et al.,* 2021). Thus, the possible mechanism that may have occurred as result of normalized liver tissue in T4-fed group is the optimal amounts of carbohydrates present. Metabolism of such may have improved the liver histology after the toxicant contamination. The consequence of this study agrees with the findings communicated by Ishak *et al.* (2016) who concluded that fish fed carbohydrates at 30% show minor histological alterations with increased occurrence of lipid vacuolization in hepatocytes and reduced expression of nucleus that would indicate disintegrated liver cells.

The current findings are early confirmed with reports on high levels of protein and non-protein energy source of sweet potato (An, 2004; Ekenyem and Madubuike, 2006). Furthermore, Ishida *et al.* (2000) and Ekenyem and Madubuike (2006) indicated that the leaf of sweet potato has high protein content (26% to 35%) and ideal minerals quantities of vitamins such as A, B2, C, and E. The present study further supports the early claim of Oyenuga (1968) on the rich nutrient qualities of sweet potato leaves and recommends the use of sweet potato leaves as source of feed supplement in aquaculture.

5. Conclusion

From the obtained findings, it could be concluded that supplementation of the crude extracts of sweet potato leaves in practical diets of *Oreochromis niloticus* can significantly improve hematological profile and eventually

the fish immune response. Similarly, the incorporation of the crude extracts displayed activity in the enhancement of liver and kidney histopathology against ammonia as an environmental toxicant. Finally, sweet potato is warranted as preferable feed additive supplement, capitalizing on its non-protein source such as carbohydrates as bioactive component.

Acknowledgement

This work was funded by Partido State University Research and Development Office though the unit's research exploration fund. The authors likewise acknowledge the technical assistance of Mr. Jericho L. Encinas for the feeding experiment. The authors also acknowledge the National Research Council of the Philippines (NRCP) through the Research Dissemination in Local and International Platforms (RDLIP) for the publication support.

References

Abbas WT, Abumourad IM, Mohamed LA, Abbas HH, Authman M, Soliman WS, and Elgendy MY. 2019. The Role of the Dietary Supplementation of Fenugreek Seeds in Growth and Immunity in Nile Tilapia with or without Cadmium Contamination. *Jordan J. Biol. Sci,* **12(5)**: 649 – 656.

Agius C, and Roberts RJ. 2003. Melano-macrophage centres and their role in fish pathology. *J Fish Dis,* **26(9)**: 499-509. doi:https://doi.org/10.1046/j.1365-2761.2003.00485.x.

Ajeel SG, and Al-Faragi JKH. 2013. Effect of ginger (*Zingiber officinale*) and garlic (*Allium sativum*) to enhance health of common carp, *Cyprinus carpio* L. *Iraqi J Vet Sci,* **37**: 59-62.

An LV. 2004. Sweet Potato Leaves for Growing Pigs Biomass Yield , Digestion and Nutritive Value. PhD Dissertation, Swedish University of Agricultural Sciences, Uppsala, Sweden.

Antia BS, Akpan EJ, Okon PA, and Umoren IU. 2006. Nutritive and anti-nutritive evaluation of sweet potatoes (*Ipomoea batatas*) leaves. *Pak J Nutr*, **5**: 166-168.

Arifina EV, Rahmawati N, and Lahay RR. 2020. Analysis of physiological characters and yield quality of several sweet potato (*Ipomoea batatas* L.) genotypes at various watering levels in rainfed paddy field. *IOP Conf. Ser.: Earth Environ Sci,* **454(1)**: 012173. doi:10.1088/1755-1315/454/1/012173.

Boujard T, Gélineau A, Covés D, Corraze G, Dutto G, Gasset E, and Kaushik SJ. 2004. Regulation of feed intake, growth, nutrient and energy utilisation in European sea bass *(Dicentrarchus labrax)* fed high fat diets. *Aquac,* **231**: 529-545.

Braunbeck T. 1998. Cytological alterations in fish hepatocytes following *in vivo* and *in vitro* sublethal exposure to xenobiotics — structural biomarkers of environmental contamination (Vol. EXS, 86). Birkhäuser, Basel: S61pringer Book Archive.

Coyle SD, Durborow RM, and Tidwell JH. 2004. Anesthetics in aquaculture (Vol. 3900): Southern Regional Aquaculture Center Stoneville.

Darias MJ, Castro-Ruiz D, Estivals G, Quazuguel P, Fernández-Méndez C, Núñez-Rodríguez J, Clota F, Gilles S, García-Dávila C, Gisbert E, and Cahu C. 2015. Influence of dietary protein and lipid levels on growth performance and the incidence of cannibalism in *Pseudoplatystoma punctife*r (Castelnau, 1855) larvae and early juveniles. *J Appl Ichthyol,* **31(4):** 74-82. doi:https://doi.org/10.1111/jai.12978.

Davidson J, Good C, Welsh C, and Summerfelt ST. 2014. Comparing the effects of high vs. low nitrate on the health, performance, and welfare of juvenile rainbow trout, *Oncorhynchus mykiss* within water recirculating aquaculture systems. *Aquacult Eng,* **59**: 30-40. doi:https://doi.org/10.1016/j.aquaeng.2014.01.003.

Ekenyem BU, and Madubuike FN. 2006. An assessment of *Ipomoea asarifolia* leaf meal as feed ingredient in broiler chick production. *Pak J Nutr*, **5**:46-50.

El-Shafai SA, El-Gohary FA, Nasr FA, van der Steen NP, and Gijzen HJ. 2004. Chronic ammonia toxicity to duckweed-fed tilapia (*Oreochromis niloticus*). *Aquac,* **232(1-4)**: 117-127.

Fazio F. 2019. Fish hematology analysis as an important tool of aquaculture: A review. *Aquac,* **500**: 237-242. doi:https://doi.org/10.1016/j.aquaculture.2018.10.030.

Food and Agriculture Organization of the United Nations. (2016). "The State of World's Fisheries and Aquaculture 2016". https://www.fao.org/publications/sofia/2016/en/ (Jan. 21, 2021).

Food and Agriculture Organization of the United Nations. (2021). "Aquaculture Feed and Fertilizer Resources Information System". https://www.fao.org/fishery/affris/species-profiles/nile-tilapia/faqs/en/ (Nov. 3, 2021).

Haghighi MK, and Rohani MS. 2013. The effects of powdered ginger *(Zingiber officinale)* on the haematological and immunological parameters of rainbow trout, *Oncorhynchus mykiss. J Medicinal Plant and Herb Ther Res*, **1**: 8-12.

Ishak SD, Kamarudin MS, Ramezani-Fard E, Saad CR, and Yusof YA. 2016. Effects of varying dietary carbohydrate levels on growth performance, body composition and liver histology of Malaysian mahseer fingerlings (*Tor tambroides). J Environ Biol*. **37(4)**: 755-764.

Ishida H, Suzuno H, Sugiyama N, Innami S, Tadokoro T, and Maekawa A. 2000. Nutritive evaluation on chemical components of leaves, stalks and stems of sweet potatoes (*Ipomoea batatas* poir). *Food Chem,* **68(3)**: 359-367. doi:10.1016/s0308-8146(99)00206-x.

Kim I-S, Yang M-R, Lee O-H, and Kang S-N. 2011. Antioxidant activities of hot water extracts from various spices. *Int J Mol Sci,* **12(6)**: 4120-4131. doi:10.3390/ijms12064120.

Küçük S. 2014. Acute toxicity of ammonia to blue tilapia, *Oreochromis aureus* in saline water. *Afr J Biotechnol,* **13**: 1550-1553.

Le Ruyet JP, Boeuf G, Infante JZ, Helgason S, and Le Roux A. 1998. Short-Term Physiological Changes in Turbot and Seabream Juveniles Exposed to Exogenous Ammonia. *Comparative Biochemistry and Physiology Part A: Molecular & Integrative Physiology*. **119(2)**: 511-518. doi:https://doi.org/10.1016/S1095-6433(97)00458-3.

Olsen RL, and Hasan MR. 2012. A limited supply of fishmeal: Impact on future increases in global aquaculture production. *Trends Food Sci Technol,* **27(2)**: 120-128. doi:https://doi.org/10.1016/j.tifs.2012.06.003.

Oyenuga VA. 1968. Nigeria's Foods and Feeding-stuffs; Their Chemistry and Nutritive Value: Ibadan University Press.

Pallaya-Baleta LJ, Baleta F, Magistrado-Candelaria P, Plantado L, Baldo DE, Navarro M, and Encinas J. 2021. Growth performance and economic viability of dietary inclusion of *Ipomoea batatas* L. shoot powder and extracts in the practical diets of *Oreochromis niloticus* L. *Egypt J Aquat Res*, **48(3)**: 273-279. doi:https://doi.org/10.1016/j.ejar.2021.11.005.

Ruiz ML, Owatari MS, Yamashita MM, Ferrarezi JVS, Garcia P, Cardoso L, Martins ML, and Mouriño JLP. 2020. Histological effects on the kidney, spleen, and liver of Nile tilapia *Oreochromis niloticus* fed different concentrations of probiotic *Lactobacillus plantarum. Trop Anim Health Prod*, **52(1)**: 167-176. doi:10.1007/s11250-019-02001-1.

Sahan A, Özütok S, and Kurutb_ EB. 2016. Determination of some hematological parameters and antioxidant capacity in Nile tilapia *(Oreochromis Niloticus* Linnaeus, 1758) fed ginger (*Zingiber Officinale* Roscoe) to *Aeromonas hydrophila. Turkish J Fish Aquat Sci,* **16**: 197-204.

Stehr CM, Johnson LL, and Myers MS. 1998. Hydropic vacuolation in the liver of three species of fish from the U.S. West Coast: lesion description and risk assessment associated with contaminant exposure. *Dis Aquat Organ,* **32(2)**: 119-135. doi:10.3354/dao032119.

Steinel NC, and Bolnick DI. 2017. Melanomacrophage centers as histological indicator of immune function in fish and other poikilotherms. *Front Immunol,* **8**: 827. doi:10.3389/fimmu.2017.00827.

Talpur AD, Ikhwanuddin M, and Ambok Bolong A-M. 2013. Nutritional effects of ginger (*Zingiber officinale* Roscoe) on immune response of Asian sea bass, *Lates calcarifer* (Bloch) and disease resistance against *Vibrio harveyi*. *Aquac,* **400-401**: 46-52. doi:https://doi.org/10.1016/j.aquaculture.2013.02.043.

Wilson RP. 1994. Utilization of dietary carbohydrate by fish. *Aquac*, **124(1)**: 67-80. doi:https://doi.org/10.1016/0044-8486(94)90363-8.

Yones A-Mas, Eissa IA-M, Ghobashy MAE-F, and Marzok SS. 2019. Effects of different dietary carbohydrate sources on growth performance and liver histology of Nile tilapia (*Oreochromis niloticus*) fingerlings. *Egypt J Histol.* **42(3)**: 599-607. doi:10.21608/ejh.2019.12234.1115.

Yoon G, Al-Saadi N, and Ambuali A. 2015. Gill histology of Nile tilapia, *Oreochromis niloticus* following chronic and acute exposure to ammonia. *J Agric Mar Sci*, **20**: 66-72. doi:10.24200/jams.vol20iss0pp66-72.

JJBS

Volume 15, Number 5,December 2022
ISSN 1995-6673
Pages 771 – 777
https://doi.org/10.54319/jjbs/150505

Jordan Journal of Biological Sciences

DPPH Free Radical Scavenging Activity of *Citrus aurantifolia* Swingle Peel Extracts and their Impact in Inhibiting the Browning of *Musa Paradisiaca* L. Var. Kepok Tanjung Explants

Mohamad Nurzaman[1,*], Nandang Permadi[1], Tia Setiawati[1], Rusdi Hasan[1], Yulia Irawati[2], Euis Julaeha[3] and Tati Herlina[3]

[1]*Department of Biology, Faculty of Mathematics and Natural Sciences, Universitas Padjadjaran. Jl. Raya Bandung Sumedang Km 21, Sumedang, West Java 45363, Indonesia;* [2] *IP2TP Subang, Indonesian Tropical Fruits Research Institute, Ministry of Agriculture. Jl. Garuda III, Subang, West Java 41212, Indonesia;*[3]*Department of Chemistry, Faculty of Mathematics and Natural Sciences, Universitas Padjadjaran. Jl. Raya Bandung Sumedang Km 21, Sumedang, West Java 45363, Indonesia*

Received: January 25, 2022; Revised: April 28, 2022; Accepted: June 6, 2022

Abstract

Musa paradisiaca var. Kepok Tanjung is a popular banana cultivar that is widely consumed by the majority of the Indonesia's population. However, the browning of explants caused by the polyphenol oxidase (PPO) enzyme is becoming a major constraint for its production which can lead to the low productivity of seedlings. Therefore, this research aims to determine the antioxidant activity of Citrus aurantifolia peel extracts and their ability in inhibiting the browning of Kepok Tanjung bananas explants at the shoot initiation stage under in vitro condition. The extracts were obtained through the maceration of C. aurantifolia peel residue using n-hexane, ethyl acetate, and ethanol solvents which were added to the culture medium. Furthermore, the 50% inhibitory concentration (IC_{50}) was determined by the 2,2-diphenyl-1-picrylhydrazyl (DPPH) method, while enzyme activity was assessed by spectrophotometric method using catechol substrate. The results showed that the ethyl acetate extract of C. aurantifolia peel from day 6 at concentration of 0.3 mg/mL can inhibit oxidation, as shown by the reduced browning index of the explants. Meanwhile, the highest antioxidant activity was discovered at day 9 with PPO enzyme activity of 80.261 U/mL at the same concentration.

Keywords: DPPH, antioxidant, C. aurantifolia, browning, M. paradisiaca

1. Introduction

Musa paradisiaca var. Kepok Tanjung is a popular banana cultivar that is widely used as an ingredient in flour production due to its sweet taste and distinctive aroma (Putri *et al.,* 2015). The increase in demand for Kepok Tanjung bananas has become an obstacle for farmers, especially for propagation using seeds. Meanwhile, one of the best alternatives for producing its seedlings is through *in vitro* plant propagation techniques (Mose *et al.,* 2020; El-Sayed *et al.,* 2021). This method is able to produce high quality banana explants in large quantities, uniformly, within a short time, and also support vigorous plants' development during their subsequent growth cycles(Ferdous *et al.,* 2015).However, the browning of the explants becomes a major constraint that often occurs when they are injured due to the high polyphenols exposure (Puspitasari and Syauqy, 2014).

Research indicated that the browning of the explants was caused by the activity of residual peroxidase (POD), polyphenol oxidase (PPO) (Xu *etal.,* 2015;Wu *et al.,* 2018), and phenylalanine ammonia lyase (PAL) (Sun *et al.,* 2015).PPO is a group of oxidoreductase enzymes containing two Cu atoms, and it is located in the chloroplast of the plants. This enzyme catalyzes the hydroxylation of monophenols to o-diphenols and the oxidation of o-diphenols to o-quinones with molecular oxygen as a co-substrate (Oliveira *et al.,* 2011; Al-Gabbiesh *et al*., 2015). O-quinone is a highly reactive molecule that passes through non-enzymatic secondary reactions to form a brown complex polymer known as melanin and a crosslinked polymer with protein functional groups (Taranto *et al.,* 2017). Meanwhile, loss of subcellular compartmentalization that is due to aging, injury, interaction with pests or pathogens, mishandling during postharvest processing, and storage gave contact between PPO and vacuolar phenolic substrates (Taranto *et al.,* 2017). The presence of reactive oxygen species (ROS) such as superoxide anions (O_2^-), hydrogen peroxide (H_2O_2), and hydroxyl radicals ($^{\cdot}OH$) also play an important role in causing the browning of explants. Moreover, research also showed that proteins, phospholipids, and pigments are degraded by free radicals during the browning process (Misra *etal.,* 2010). When the browning of explants was not properly treated, it can cause a decrease in regenerative ability, reduction of callus

* Corresponding author. e-mail: m.nurzaman@unpad.ac.id.

growth, inhibition of adventitious shoot growth, and death of culture tissue (Xu *et al.,* 2015).

Previous studies showed that browning in explants can be reduced by graphene oxide (GO) for Chinese orchid (Wu *et al.,* 2018), pretreatment using potassium citrate antioxidant solution of plantain (Onuoha *et al.,* 2011), and application of ascorbic acid, citric acid, and activated charcoal in the media to banana explants (*Musa spp*. cv. Grand Naine) (Safwat *et al.,* 2015).

Antioxidants compounds can delay oxidation reaction by capturing excess of free radicals and preventing chain reactions. Chemical compounds such as carotenoids, ascorbic acid, tocopherols, glutathione, cysteine, phenolics, and flavonoids, as well as several other enzymes, namely superoxide dismutase (SOD), guiacol peroxidase (GPX), catalase-peroxidase (APX), catalase (CAT), and glutathione reductase (GR) may become paramount importance in catalyzing the cleavage of O_2 into H_2O_2 and O_2(Zou *et al.,* 2016). The conversion of H_2O_2 to water is carried out in the cytosol and chloroplast by the glutathione ascorbate cycle, which involves APX and GR enzymes (Misra *et al.,* 2010).

Citrus aurantifolia peel contains various chemical compounds such as molasses, pectin, polyphenols, vitamins, minerals, essential oils, and dietary fiber(Rafiq *et al.,* 2018), which can be used for applications in industrial or agriculture. The presence of phenol and flavonoid makes the peels to pose the ability as a natural antioxidant where they can produce semipolar and polar compounds that can be extracted with various solvents such as ethyl acetate and ethanol (Okubgo and Oriakhi, 2015).

Loizzo *et al.* (2012) reported that antioxidant activity of *C. aurantifolia* peel that was extracted with polar (methanol) and non-polar (n-hexane) solvents indicated that methanol extract was more active than n-hexane when using the 2,2-diphenyl-1-picrylhydrazyl (DPPH) method. *C. aurantifolia* contains polyphenolic compounds possessing antioxidant properties that can capture free radicals, so that the oxidation process will be reduced by the addition of *C. aurantifolia* extract. The presence of polyphenolic compounds was traced by extracting *C. aurantifolia* peel using a variety of non-polar, semi-polar, and polar solvents such as n-hexane, ethyl acetate and ethanol.

Antioxidant has been used for inhibiting the browning of explant in tissue culture, as discussed above. So far, efforts to inhibit browning of explant were conducted by the application of synthetic antioxidants (e.g., Wu *et al.,*2018; Safwat *et al.,* 2015;Onuoha *et al.,* 2011). Research using natural antioxidants from *C. aurantifolia* peel extract in tissue culture has not yet been reported. Therefore, this current research is carried out to determine the presence of antioxidants and their suspected active compounds for reducing the browning of *M. paradisiaca* var. Kepok Tanjung explants. This research will become an important contribution in sustainable banana productions.

2. Materials and Methods

2.1. Materials

The materials used in this research include lime *(C. aurantifolia)* from Cibodas Village, West Bandung Regency, Indonesia, while explants of *M. paradisiaca* var. Kepok Tanjung was taken from the Indonesian Tropical Fruits Research Institute (IP2TP), Ministry of Agriculture, Subang Regency, Indonesia.

2.2. Preparation of non-volatile extract of C. aurantifolia peel

A 400 g of *C. aurantifolia* peel chopped into pieces of about 2 cm in size and put into a distillation flask, soaked with distilled water for 3 hours to separate the essential oils. The residue was extracted by maceration in succession using n-hexane, ethyl acetate, and ethanol solvents. Extraction was carried out for 3 days, where each extract was collected and concentrated with a rotary evaporator to remove the solvent. Subsequently, the concentrated extract was used for further purposes. The*C. aurantifolia* extraction preparation step was done by three replications.

2.3. DPPH free radical scavenging activity of C. aurantifolia peel extract

The antioxidant activity test was assessed using the 2,2-diphenyl-1-picrylhydrazyl (DPPH) method, as a highly reactive free radical chromogen. The concentration of the tested substance varied based on the ability to scavenge DPPH free radicals,

A total of 0.1 mL of n-hexane extract, ethyl acetate, and ethanol with a concentration of 100-4000 ppm was added to 2 mL of DPPH (0.21 mM in 95% ethanol). The mixture was shaken and kept for 60 minutes in a dark room and ambient temperature. Subsequently, light absorbance was measured with a UV-Vis spectrometer at 517 nm and the DPPH inhibition was calculated using the equation by (Safdar *et al.,* 2016).

$$\text{Inhibition } (\%) = \frac{A_c - A_s}{A_c} \times 100\%$$

Description: A_c and A_s are control and sample absorbance, respectively

IC_{50} was measured with,

$$IC_{50} = (50 - b)/a$$

Description: IC_{50} is obtained from regression equation of inhibition percentage against extract concentrations.

2.4. Liquid vacuum column chromatography (KVC)

The stationary phase used was silica gel G60 with a size of ± 200 mesh, while the mobile phase was graded between the ratio of n-hexane: ethyl acetate: ethanol. Before the separation process with KCV, the sample was impregnated using silica gel with a size of 50-100 mesh. The sample was inserted at the top of the column which is spread evenly and was covered with filter paper. Furthermore, it was eluted from low polarity, increased by 10%, and the column was sucked dry at each fraction collection (Maro *et al.,* 2015). The combination of the same fraction was monitored by thin-layer chromatography (TLC) using a silica gel plate GF254, n-hexane: ethyl acetate in a ratio of 7:3, and the eluent was observed at 254 nm and 366 nm UV lamps, respectively.

2.5. Identification of active compound of extract

Identification of compounds using liquid chromatography-mass spectrometry (LC-MS) was carried out on the fraction with the highest antioxidant activity. A total of 0.5 g of extract was dissolved in 50 mL of methanol p.a. and the solution was filtered using a 0.22-micron syringe filter, put into a 2 mL vial, and injected into the LC-MS system.

2.6. Treatment and maintenance of explants

C. aurantifolia peel extract with the highest activity obtained based on the antioxidant activity test was treated with three levels of concentration of 0.1, 0.2, and 0.3 mg/mL *C. aurantifolia* peel extracts. As positive controls, the 0.1 mg/mL ascorbic acid and PVP were used. Each extract concentration was added to Murashige and Skoog (MS) culture media with 2.5 ppm benzyl amino purine (BAP) and 0.1 ppm thidiazuron (TDZ). The banana explants were incubated in a room with a light intensity of 1,000 – 4,000 lux, a temperature of 25±2°C, 80% humidity with 16 hours of irradiation for 15 days of shoot initiation stage.

2.7. Browning index

Visual observation of browning was carried out every 3 days for 15 days of the shoot initiation stage. Browning level was recorded as follows: level 0: no browning, level 1: browning only in the explant incision, level 2: browning appeared in culture media with an area of fewer than 0.5 cm^2 where the explant was the center, level 3: browning appeared in culture media with an area of more than 0.5 cm^2, where the explant was the center (Wu *et al.,* 2018). Meanwhile, the browning index was calculated using formula below:

$$\text{Browning Index} = \sum \frac{(a) \times (b)}{(A) \times (b')} \times 100\%$$

Description: a is the number of browning explants, A is the total number of explants, b is the browning level, and b' is the highest level of browning.

2.8. Extraction of polyphenol oxidase enzymes (PPO)

M. paradisiaca explants were taken randomly on days 0, 3, 6, 9, and 12 for each treatment and kept at frozen temperature of -18°C. All treatments were replicated three times. The explants (5 g) were cut into small pieces, dissolved in 5 mL 50 mM citrate buffer, which contain 0.5% (w/v) tritone X-100, 2 mM EDTA, 1 M NaCl, and 0.5% (w/ v) PVP, and homogenized for 10 minutes at 4°C and pH 7.0. Subsequently, the supernatant was filtered using cheesecloth and centrifuged at 12,000 rpm for 20 minutes. The supernatant that contained PPO was used as a crude extract of PPO, which was incubated for 30 minutes at 17°C (Murniati *et al.,* 2018).

2.9. Polyphenol oxidase enzyme (PPO) activity test

The PPO activity was observed using the spectrophotometric method with catechol substrate and modified according to the Sigma procedure. The units were measured at initial rates using a UV-Vis-nir scanning double beam spectrophotometer (UV-Vis 1800, Shimadzu).

Subsequently, 0.1 mL of crude extract of PPO was mixed with the substrate at various concentrations of 0.20 - 0.40 mM and dissolved in 3 mL of 50 mM citrate buffer, which contained 2.1 mM ascorbic acid and 0.65 mM EDTA. The optimal PPO activity was determined by varying the pH from 6.8 to 7.2 and incubation temperature from 10 to 30°C. The PPO activity (U/mL) obtained in the assay was estimated by the initial reaction rate and expressed as absorbance curve (A) vs time (minutes) (Gauillard *et al.,* 1993). Meanwhile, the total activity (U) was obtained by multiplying the activity (U/mL) and the total volume (mL) (Dennison, 2002). The calculation of PPO activity is explained as follows:

$$\text{PPO Activity} = \frac{1}{sb} \cdot \frac{V_{total}}{V_{enzyme}} \cdot \frac{d\,[substart]}{dt}$$

Description:

$\frac{1}{sb}$ = absorbance slope vs [substrate] substrate standard curve

$\frac{d\,[substart]}{dt}$ = absorbance slope vs time (minute) from initial speed

2.10. Data analysis

The obtained data were analyzed using SPSS 25.0, and the Shapiro-Wilk test was conducted to evaluate the data normality. When the analysis of variance (ANOVA) with a 95% confidence level (P= 0.05) has a significant effect, it was continued with Duncan's test at a 95% confidence level (P= 0.05).

3. Results and Discussion

3.1. C. aurantifolia peel extract

The yield percentage of *C. aurantifolia* peel extract through different solvent polarity levels reveals that the highest extraction yield was obtained with nonpolar solvent of ethanol (4.76%) followed by semi polar solvent of ethyl acetate (2.28%) and nonpolar solvent of hexane (0.37%). This result can be explained partly due to that the semi-polar and polar chemical components of *C. aurantifolia* peel such as polyphenols and flavonoids are more in abundance than non-polar components. Differences in polarity and concentration among the extraction solvents may influence the variation in the extraction yield. Hegazy and Ibrahium (2012) investigated various organic solvents for extracting flavonoid and polyphenol compounds from orange peel and found that the extraction yields ranged from 8.27% to 28.32%, with hexane and methanol extraction, respectively. Likewise, Safdar *et al.* (2016) who extracted *C. retuculate* peel using different techniques and solvents found that ethanol extraction yielded more extract (18.46%) than ethyl acetate extraction (5.12%).

3.2. DPPH free radical scavenging activity of C. aurantifolia peel

In measuring antioxidant activity, IC_{50} was defined as the amount of substance concentration that can inhibit 50% of the oxidation reaction by DPPH. Figure 1 shows the percentage of inhibition as a function of the substance concentration. Antioxidant activity test showed that each extract had a different percentage of inhibition (IC_{50}). It showed a positive correlation between the concentration of the extract and the percentage of inhibition of 2.78 mg/mL with a correlation value of 0.992 for n-hexane, 0.19 mg/mL with a correlation value of 0.991 for ethyl acetate,

and 2.45 mg/mL with a correlation value of 0.994 for ethanol.

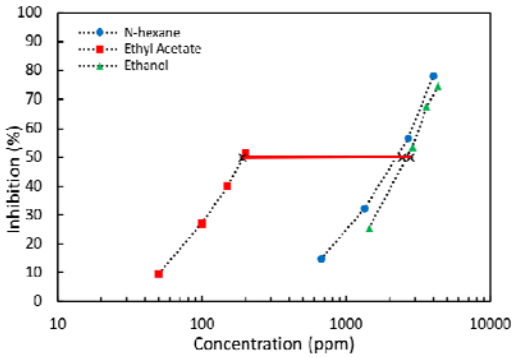

Figure 1. The inhibition percentage of n-hexane, ethyl-acetate, and ethanol extract of *C. aurantifolia* peel in various concentration. The value of IC_{50} is shown by the red horizontal line. The values of line regression approximation for each extract denoted by black cross.

Positive correlation between the concentrations of all extracts and the percentage of inhibition (0.992 for n-hexane, 0.991 for ethyl acetate, and 0.994 for ethanol) indicates the effectiveness of the inhibition caused by the increase in the number of polyphenols contained in the extract. Furthermore, the highest inhibitory activity was shown by ethyl acetate extract by giving the highest percentage of inhibition. It is indicated by the smallest IC_{50}value of ethyl acetate extract of 0.19 mg/mL, followed by n-hexane extract of 2.45 mg/mL, and ethanol extract of 2.78 mg/mL. The result is in an agreement with previous research, which recorded that the antioxidant activity of flavonoids is contained in the ethyl acetate extract of *C. aurantium* (Shen *et al.*, 2019).

3.3. Ethyl acetate extract fractionation

Fractionation of the ethyl acetate extract by vacuum liquid chromatography was carried out to trace the most active fraction and obtain six combined fractions (A-F fraction), with antioxidant activity as shown in Table 1.

Table 1. Antioxidant activity of six fractions, from ethyl acetate extract

Combined Fraction	Concentration (ppm)	Inhibition (%)	IC_{50} (mg/mL)
	0	0.00 □ 0.00	
	1377	9.50 □ 0.18	
A	4590	21.07 □ 0.32	13.42 □ 0.001[a]
	9180	34.96 □ 0.49	
	18360	66.38 □ 0.86	
	0	0.00 □ 0.00	
	463	24.84 □ 0.27	
B	1158	46.45 □ 0.23	1.30 □ 0.001[b]
	1853	69.01 □ 0.96	
	2317	84.35 □ 0.46	
	0	0.00 □ 0.00	
	118	20.82 □ 0.23	
C	157	35.43 □ 1.95	0.23 □ 0.002[c]
	235	51.14 □ 1.44	
	313	69.02 □ 0.95	
	0	0.00 □ 0.00	
	20	9.94 □ 0.60	
D	39	15.45 □ 0.99	0.15 □ 0.005[e]
	78	22.79 □ 4.86	
	156	52.96 □ 1.41	
	0	0.00 □ 0.00	
	11	13.03 □ 0.18	
E	33	28.97 □ 1.13	0.05 □ 0.001[f]
	55	51.42 □ 0.62	
	66	62.71 □ 0.22	
	0	0.00 □ 0.00	
	117	36.43 □ 0.67	
F	176	50.73 □ 0.60	0.18 □ 0.005[d]
	234	62.75 □ 1.87	
	293	76.62 □ 2.06	

[*]Statistical test of significant difference with 95% confidence level. The mean value followed by the same letters showed no significant difference (P <0.05).

Based on the Table1, fraction E gave the highest activity with an IC_{50} value of 0.05 mg/mL, which was included in the strong category, followed by fractions D and F with moderate categories of 1.5 and 0.18 mg/mL, respectively. Meanwhile, the other fractions were in the weak category according to Molyneux (2004).

3.4. Identification of active compounds

The LC chromatogram and its mass fraction were analyzed to predict the compounds with a role in the E fraction, as shown in Figures 2, 3, and 4.

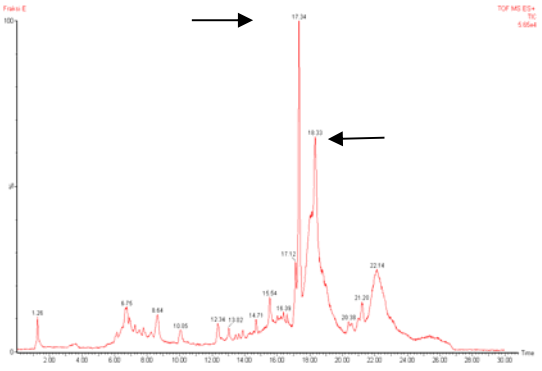

Figure 2. LC chromatogram of fraction E inverted phase with C-18 column, methanol solvent: water gradient

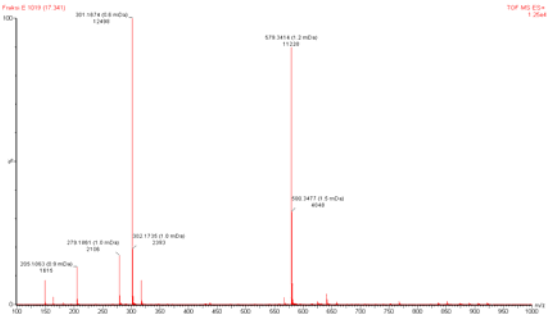

Figure 3. Peak MS experience pattern with a retention time of 17.34 minutes

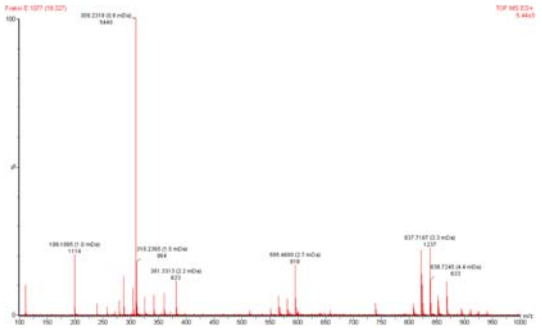

Figure 4. Peak MS experience pattern with a retention time of 18.33 minutes

Figure 2 shows the LC-MS chromatogram profile of fraction E at several peaks. The main component was estimated to play an important role in antioxidant activity with retention times of 17.34 and 18.33 minutes. According to the mass spectrum on the TOP MS ES+ technique, the m/z molecular ion (M+) for the main peak (tr 17.34 min) was 580.3477, while the second peak (tr 18.33 min) was 838.7245. Based on the molbase.com database approach, m/z 580.3477 was derived from the mass of the formula $C_{39}H_{50}O_{20}$, which is assumed to be a naringin compound (Figure 5). Meanwhile, m/z 838.7245 was derived from the mass of the formula $C_{39}H_{50}O_{20}$ which is an epimedin A1 compound (Figure 6). These compounds are effective antioxidants and are often present in citrus peels, naringin (Chen *et al.,* 2008; Chen *et al.,* 2017; Safdar *et al.,* 2016; Xu *et al.,* 2015).

The main flavonoid components in the *Citrus* genus, such as naringin, naringenin, hesperidin, quercetin, and rutin are also discovered in the *C. aurantifolia* peel (Loizzo *et al.,* 2012). Meanwhile, flavonoids function directly in capturing ROS and reducing the formation of hydrogen peroxide (H_2O_2) (Nakao *et al.,* 2011). It was also reported that naringin increases the activity of antioxidant enzymes, such as superoxide dismutase (SOD), guaiacol peroxidase (GPX), catalase-peroxidase (APX), catalase (CAT), and glutathione reductase (GR). Furthermore, hesperidin reduced free radicals by inhibiting XO, as a key mechanism of antioxidant action, while other flavonoids such as naringenin, quercetin, and rutin capture hydroxyl radicals (·OH) directly (Zou *et al.,* 2016).

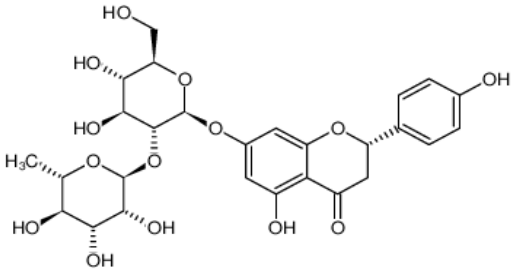

Figure 5. The chemical structure of naringin

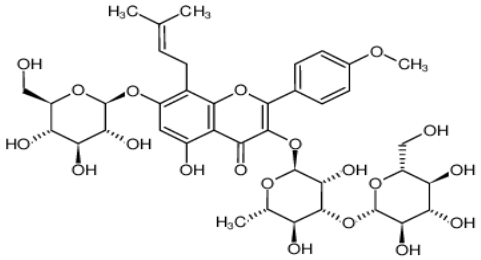

Figure 6. Chemical structure of epimedin A1

Naringin and epimedin A1 are polyphenolic compounds, meanwhile, the large number of hydroxyl groups bound to the compounds made them function as antioxidants by donating hydrogen atoms bonded to oxygen atoms in DPPH reagents. The activity of the E fraction was stronger (0.05 mg/mL) than the ethyl acetate extract (0.46 mg/mL), which indicated the antagonistic action of other compounds in the ethyl acetate extract.

3.5. Browning index

The increase in incubation time was followed by a higher browning index in all samples (Figure 7). Meanwhile, the additional treatment on day 3 had no significant effect on the browning index of *C. aurantifolia* peel extract compared to the negative control (ethyl acetate solvent). After 6 days, the browning index was significantly lower than the control because the positive control ascorbic acid and PVP were pure compounds at the same concentration (0.1 mg/mL). Similarly, the active substance in the ethyl acetate extracts was mixed with other chemical compounds contained in the extract. After 6 days, the browning index of 0.3 mg/mL of *C. aurantifolia* peel extract was slightly lower than 0.1

mg/mL and 0.2 mg/mL, respectively. It showed that the application of antioxidant extract can significantly reduce the browning index. Specifically, the 0.3 mg/mL treatment which has a better effect at the shoot initiation stage after 6 days as visualized in Figure 8a and 8b that contrasted to the control in Figure 8c and 8d.

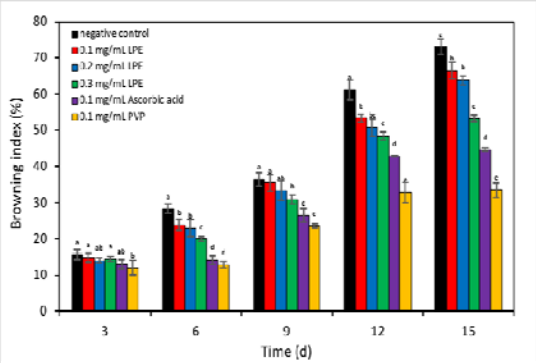

Figure 7. Effect of *C. aurantifolia* peel extract concentration on the browning index (%) of *M. paradisiaca* explants at the shoot initiation stage. Each value is expressed as mean ± SD (n=7).*The mean value followed by the same letters showed no significant difference (P <0.05).

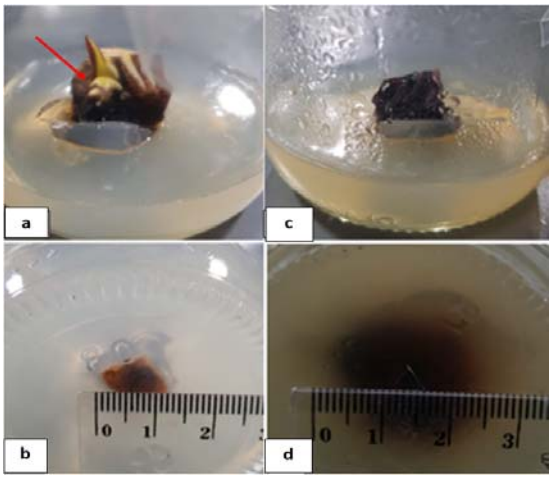

Figure 8. Shoot initiation stage of *M. paradisiaca* tissue culture.

a. The upper view of shoot initiation (red arrow) of explant that had slightly browned on culture treated with *C. aurantifolia* extract. b. The bottom view of explant that have slightly browned in culture treated with *C. aurantifolia* extract. c. The upper view of the explant that shows large browning and did not grow buds in the culture without *C. aurantifolia* extract treatment. d. The bottom view of the explant that shows large browning in the culture without *C. aurantifolia* extract treatment.

The treatment of *C. aurantifolia* peel extract can reduce browning in *M. paradisiaca* explants as indicated by a lower browning index and shoot growth initiation (Figure 8a,b). Whilst the treatments without *C. aurantifolia* peel extract showed a higher browning index, stunted growth, and no shoots appeared as shown in Figure 8c,d. It assumes that oxidation process which leads to a cell death is inhibited by polyphenols contained in the peel extract of *C. aurantifolia* (Taranto *et al.*, 2017).

3.6. The activity of polyphenol oxidase enzyme (PPO)

After 3 and 6 days, there was no significant change in the PPO activity in explants cultured compared to controls. However, the PPO activity of the sample was significantly lower than the control. This occurred because a longer incubation time increases the interaction between the active substances contained in the extract of *C. aurantifolia* peel with banana explants. The PPO activity with 0.3 mg/mL peel extract of *C. aurantifolia* was slightly lower than 0.1 mg/mL and 0.2 mg/mL after 3 days. Therefore, the administration of antioxidants significantly inhibited PPO activity, specifically treatment 0.3 mg/mL which had a better effect on inhibiting PPO activity after 9 days (Figure 9).

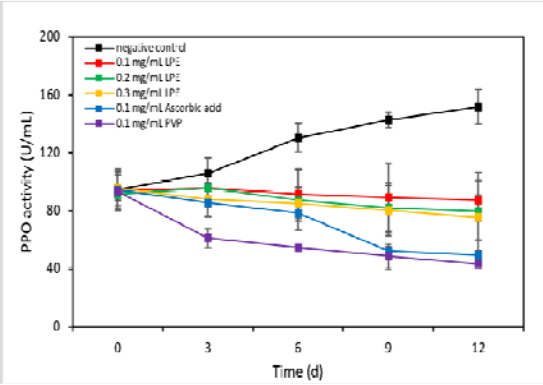

Figure 9. Effect of *C. aurantifolia* peel extract concentration on the PPO enzyme activity (U/mL) of *M. paradisiaca* explants at the shoot initiation stage. Each value is expressed as mean ± SD (n = 3).

The antioxidant compounds extracted from the *C. aurantifolia* peel extracts play a salient role in scavenging the ROS produced when *M. paradisiaca* explants are injured. Furthermore, the presence of ROS explosion affected membrane integrity and led to a loss of cellular compartmentalization, which caused the accumulation and oxidation of phenolic compounds (Xu *et al.*, 2015). The released phenolic acts as a signaling molecule and promotes an increase in PPO levels through feedback regulation. Similarly, bioactive compounds contents also can inhibit the function of oxidant enzymes such as nitric oxide synthase (NOS), lipoxygenase (LOX), xanthine oxidase (XO), cyclooxygenase (COX), NADPH oxidase (NOX), and myeloperoxidase (MPO), which are the main promoters of ROS formation (López-Alarcón and Denicola, 2013).

4. Conclusion

This research shows that ethanol solvent produces the highest extract yield for *C. aurantifolia*. However, the highest yield quantity obtained does not have the highest antioxidant activity. The best IC_{50} value (0.19 mg/mL) obtained in the ethyl acetate extract was higher compared to ethanol and n-hexane extracts. It is assumed that naringin ($C_{27}H_{32}O_{14}$) and epimedin A1 ($C_{39}H_{50}O_{20}$) are the compounds that contribute to the antioxidant activity of ethyl acetate extract. Ethyl acetate extract of *C. aurantifolia* peel with various concentrations affected the browning index inhibition and PPO enzyme activity. The treatment that gave the best response to the inhibition of

the browning index and PPO enzyme activity was 0.3 mg/mL ethyl acetate extract concentration. Therefore, *C. aurantifolia* peel can be used as an antioxidant for reducing the browning in banana propagation.

Acknowledgements

The authors are grateful to the Ministry of Research and Technology/National Research and Innovation Agency for funding through the Basic Research Grants for Higher Education (PDUPT) scheme (No. 1207/UN6.3.1/PT.00/2021) and the Universitas Padjadjaran for ALG of Prof. Tati Herlina (No. 1959/UN6.3.1/PT.00/2021) and Prof. Euis Julaeha (No: 2203/UN6.3.1/PT.00/2022).

References

Al-Gabbiesh A, Kleinwächter M and Selmar D. 2015. Influencing the contents of secondary metabolites in spice and medicinal plants by deliberately applying drought stress during their cultivation. *Jordan J Biol Sci.*, **8(1)**: 1-10.

Chen XJ, Ji H, Zhang QW, Tu PF, WangYT, Guo BL and Li SP. 2008. A rapid method for simultaneous determination of 15 flavonoids in Epimedium using pressurized liquid extraction and ultra-performance liquid chromatography. *J Pharm Biomed Anal.*, **46(2)**: 226–235.

Chen XM, Tait AR and Kitts DD. 2017. Flavonoid composition of orange peel and its association with antioxidant and anti-inflammatory activities. *Food Chem.*, **218**: 15–21.

Dennison C. 2002. A Guide to Protein Isolation. In **A Guide to Protein Isolation**. Kluwer Academic Publisher.

El-Sayed IM, Salama WH, Salim RG and Taha LS. 2021. Relevance of nanoparticles on micropropagation, antioxidant activity and molecular characterization of *Sequoia sempervirens* L. Plant. *Jordan J Biol Sci.*, **14(2): 374–382.**

Ferdous MH, Masum Billah AA, Mehraj H, Taufique T and Jamal Uddin AFM. 2015. BAP and IBA pulsing for in vitro multiplication of banana cultivars through shoot-tip culture. *J Biosci Agric Res.*, **3(2)**: 87–95.

Gauillard F, Richard-Forget F and Nicolas J. 1993. New sprectrophotometric assay for polyphenol oxidase activity. *Anal Biochem.*, **215(1)**: 59–65.

Hegazy A and Ibrahium M. 2012. Antioxidant Activities of Orange Peel Extracts. *World Appl Sci J*., **18(5)**:684-688.

Loizzo MR, Tundis R, Bonesi M, Menichini F, De Luca D, Colica C and Menichini F. 2012. Evaluation of Citrus aurantifolia peels and leaves extracts for their chemical composition, antioxidant and anti-cholinesterase activities. *J Sci Food Agric.*, **92 (15)**: 2960–2967.

López-Alarcón C and Denicola A. 2013. Evaluating the antioxidant capacity of natural products: A review on chemical and cellular-based assays. *Anal Chim Acta*, **763**: 1–10.

Maro JP, Alimuddin HA and Harlia. 2015. Aktivitas antioksidan hasil kromatografi vakum cair fraksi metanol kulit batang ceria (*Baccaurea hookeri*). *J Kajian Kom.*, **4**: 35–40.

Misra P, Toppo DD, Gupta N, Chakrabarty D and Tuli R. 2010. Effect of antioxidants and associate changes in antioxidant enzymes in controlling browning and necrosis of proliferating shoots of elite Jatropha curcas L. *Biomass and Bioenergy*, **34 (12)**: 1861–1869.

Molyneux P. 2004. The Use of the Stable Free Radical Diphenylpicryl-hydrazyl (DPPH) for Estimating Antioxidant Activity. *Songklanakarin J Sci Technol.*, **26(2)**: 211–219.

Mose W, Daryono BS, Indrianto A, Purwantoro A and Semiarti E. 2020. Direct Somatic Embryogenesis and Regeneration of an Indonesian orchid Phalaenopsis amabilis (L.) Blume under a Variety of Plant Growth Regulators, Light Regime, and Organic Substances. *Jordan J Biol Sci*., **13(4):** 509- 518**.**

Murniati A, Buchari B, Gandasasmita S, Nurachman Z and Nurhanifah N. 2018. Characterization of polyphenol oxidase application as phenol removal in extracts of rejected white oyster mushrooms (pleurotus ostreatus). *Orien J Chem.*, **34(3)**: 1457–1468.

Nakao K, Murata K, Itoh K, Hanamoto Y, Masuda M, Moriyama K, Shintani T and Matsuda H. 2011. Anti-hyperuricemia effects of extracts of immature Citrus unshiu fruit. *J Trad Med.,* **28**: 10–15.

Okubgo T and Oriakhi K. 2015. A comparative study of in vitro antioxidant activity and phytochemical constituents of methanol extract of Aframomum melegueta and Costus afer leaves. *Jordan J Biol Sci.***, 8(4):** 273–279**.**

Oliveira C.M, Ferreira ACS, De Freitas V and Silva AMS. 2011. Oxidation mechanisms occurring in wines. *Food Res Int.*, **44(5)**: 1115–1126.

Onuoha IC, Eze CJ and Unamba CIN. 2011. In vitro prevention of browning in plantain culture. *OnLine J Biol Sci.*, **11(1)**: 13–17.

Puspitasari S and Syauqy A. 2015. Pengaruh pemberian pisang kepok (Musa Paradisiaca Forma Typical) terhadap kadar Malondialdehyde (MDA) tikus Sprague Dawley pra-sindrom metabolik. *J Nut Coll*., **4(4)**: 314–322.

Putri TK, Veronika D, Ismail A, Karuniawan A, Maxiselly Y, Sutari A and Irwan W. 2015. Utilization kind of local West Java bananas (banana and plantain) based figs and flour product. *J Kultivasi*, **14**: 63–70.

Rafiq S, Kaul R, Sofi SA, Bashir N, Nazir F and Ahmad Nayik G. 2018. Citrus peel as a source of functional ingredient: A review. *J Saudi Soc Agric Sci.*, **17(4)**: 351–358.

Safdar MN, Kausar T, Jabbar S, Mumtaz A, Ahad K and Saddozai AA. 2016. Extraction and quantification of polyphenols from kinnow (*Citrus reticulate* L.) peel using ultrasound and maceration techniques. *J Food Drug Anal*., **25(3)**: 488–500.

Safwat G, Abdul-Rahman F and Sharbasy ASEl. 2015. The effect of some antioxidants on blackening and growth of in vitro culture of banana (*Musa spp*. cv. grand naine). *J Genet Cytol*., **44(1)**: 47–59.

Shen CY, Wan L, Wang TX and Jiang JG. 2019. Citrus aurantium L. var. amara Engl. inhibited lipid accumulation in 3T3-L1 cells and Caenorhabditis elegans and prevented obesity in high-fat diet-fed mice. *Pharmacol Res.,* **147**: 1-12.

Sun Y, Zhang W, Zeng T, Nie Q, Zhang F and Zhu L. 2015. Hydrogen sulfide inhibits enzymatic browning of fresh-cut lotus root slices by regulating phenolic metabolism. *Food Chem.*, **177**: 376–381.

Taranto F, Pasqualone A, Mangini G, Tripodi P, Miazzi M, Pavan S and Montemurro C. 2017. Polyphenol Oxidases in Crops: Biochemical, Physiological and Genetic Aspects. *Int J Mol Sci.*, **18(2)**: 377.

Wu T, Li J, Zhang J, Lin M, Wu Z, Cai X, Xiang W, Tan S and Zhang Z. 2018. Graphene oxide inhibits the lethal browning of Cymbidium sinense by reducing activities of enzymes. *J Plant Biotechnol Microbiol.*, **1**: 11–20.

Xu C, Ru Z, Li L, Zeng B, Huang J, Huang W and Hu O. 2015. The Effects of Polyphenol Oxidase and Cycloheximide on the Early Stage of Browning in Phalaenopsis Explants. *Horti Plant J.*, **1(3)**: 172–180.

Zou Z, Xi W, Hu Y, Nie C and Zhou Z. 2016. Antioxidant activity of Citrus fruits. *Food Chem.*, **196**: 885–896.

JJBS

Volume 15, Number 5,December 2022
ISSN 1995-6673
Pages 779 – 786
https://doi.org/10.54319/jjbs/150506

Jordan Journal of Biological Sciences

Cloning and Expression of Gene Encoding Lipase from Local Isolate *Bacillus cereus* Isolated from Compost Jambangan Indonesia

Retno Rahayu Puspita Ningsih[1], Sri Sumarsih[1], Sofijan Hadi[1], Wiwin Retnowati[2], and Purkan Purkan[1,*]

[1].Chemistry Department, Faculty of Science and Technology, Airlangga University. Jl. Mulyorejo, Surabaya 60115, Indonesia.; [2] Microbiology Division, Faculty of Medicine, Airlangga University, Jl Prof Dr. Moestajab, Surabaya, Indonesia

Received: January 28, 2022; Revised: April 27, 2022; Accepted: May 15, 2022

Abstract

Bacillus cereus from Jambangan compost showed lipolytic activity and produce the thermostable lipase. Cloning and expression of lipase gene from the local bacteria was done to increase the enzyme production to support its use in many fields. In this research, the lipase gene was isolated from *Bacillus cereus* by PCR method using a pair of F-Lip and R-Lip primers, then cloned in *E. coli* using the pGemT vector and expressed with pCold II DNA vector. The amplification of lip gene by PCR could produce DNA fragments measuring 0.9 kb. The DNA fragment was then inserted into the pGemT cloning vector and resulted in pGemT-*lip*recombinant at 3.9 kb. The DNA fragment 3.9 kb represented a combination of pGemT size (3.0 kb) with lip gene (0.9 kb). The expression of the lipase gene in the *E. coli* BL21 (DE3) host was carried out with the pCold II DNA expression vector resulting in recombinant DNA at 5.2 kb. The 4.3 kb DNA fragment corresponds to the empty pCod II-DNA plasmid DNA, while the 0.9 kb fragment corresponds to lip gene. The production of recombinant lipase was carried out by cold shock technique at 15 °C when the culture reached OD 600 0.4-0.5 and was followed by induction of 0.1 mM IPTG. The results of SDS-PAGE analysis showed the presence of protein band 30 kDa at SDS PAGE electroforegram. The enzyme showed specific activity of as46.03 U/mg. The results indicated the lip gene encoding lipase from*Bacillus cereus* could be expressed well in the host of *E. coli* BL21 (DE3).

Keyword : Lipase, Bacillus cereus, cloning, gene expression

1. Introduction

Enzymes have been used for decades in various chemical industrial processes (Pliego et al., 2015). In general, enzymes are proteins that catalyze chemical reactions. The lipase enzyme (triacylglycerol acylhydrolase, E.C.3.1.1.3) has a characteristic structure consisting of α/β hydrolase folding which is commonly found in hydrolase enzymes (Kapoor & Gupta, 2012). Lipase has eight parallel folds except in the ß2 region. The β3-β8 folds are connected byα helical bonds arranged on both sides of the fold. The active site of α/β hydrolase has a part called the catalytic triad. Lipase can be used in several reactions such as transesterification, alcoholysis, interesterification, esterification, and aminolysis (Choudhary, 2017). Research on lipase is developed for biodiesel production because it is able to catalyze the hydrolysis reaction of triacylglycerol into glycerol, diacylglycerol, monoglycerol, and free fatty acids (Treich et al., 2010). In biodiesel, the lipase enzyme is used as an enzyme that has high thermostability. The ability of thermostability makes lipase more stable at high temperatures, thermostable enzymes are generally produced from thermophilic microbial strains which are basically resistant to heat (Hama et al., 2018, Purkan et al., 2017).

Thermostable lipase from compost bacteria has been reported to be able to work at temperature of 60-75°C (Maruwka et al., 2009). Shaini and Jayasree, (2016) reported the presence of 24 strains of lipase-producing bacteria from compost. The existence of this bacterial strain can be used for recombinant DNA technology. The use of recombinant DNA technology can be used as effort to provide enzymes quickly, easily and in large quantities and about 90% of industrial enzymes are recombinant products (Adrio & Demain, 2014). Purkan, et al. (2018) have screened lipolytic bacteria producing lipase enzymes from compost and found *Bacillus cereus* bacteria capable to produce thermophilic lipases that are resistant to temperatures of 60-70°C. In an effort to overexpress the enzyme that can support the provision of abundant and superior lipase, cloning and expression of the gene encoding the lipase enzyme from local isolates of *Bacillus cereus* was carried out. Several stages that were carried out in this study include genomic DNA isolation, primer design, PCR, lipase gene cloning, analysis with restriction enzymes, sequencing, gene expression and enzyme activity tests.

* Corresponding author. e-mail: purkan@fst.unair.ac.id.

2. Materials and Methods

2.1. Bacteria sample and chemical

Bacillus cereus was obtained from the research results of Purkan et al., 2018. *E. coli* Top10, *E. coli* BL21 (DE3), pGemTand pCold II DNA were obtained from the Biochemistry Laboratory, FST Unair. Ampicillin, T4 DNA ligase, Taq DNA polymerase, *Nde*I, *Xba*I, and IPTG. PCR primers were synthesized at Macrogen, Singapore. The primers used were F-Lip and R-Lip which were designed based on the lipase gene *Bacillus cereus* ATCC 14579 (NC-004722) as a reference taken from Genbank (www.ncbi.nlm.nih.gov/). Other chemicals used are reagents commonly used in chemistry and molecular biology laboratories such as materials forcompetent cell manufacture,electrophoresis, lipase enzyme activity testing and SDS-PAGE.

Table 1 Primers designed based on lipase gene*Bacillus cereus* ATCC 14579(NC-004722)

No	Primer Name	Primer Sequence (5'→ 3')
1	F-Lip	TCGCTCCATATGAAGCGATTTAGC TATTTTATGG
2	R-Lip	TAGGTCTCTAGATTATTTTTCAA CTTTGATCGGATTTG

Liquid LB medium was made from a mixture of 0.5% (w/v) yeast extract, 1% (w/v) NaCl, and 1% (w/v) triptone. Solid LB medium has the same composition as liquid LB medium, but contains 2% (w/v) Bacto agar. Preparation of LB-ampicillin medium was carried out by adding 100 µg/mL into sterile LB medium.

2.2. Cloning of lip geneinto pGemT vector

Thegenomic DNA of*Bacillus cereus* was extracted by using Wizard Genomic DNA Purification kit Promega. The product then was used as template for amplification of lip gene with PCR technique using F-Lip and R-Lip primers. The PCR process was carried out on a DNA-thermal cycler machine for 30 cycles. The conditions for each cycle consisted of a predenaturation step at 94 ºC for 7 minutes and the denaturation of the PCR process at 94 ºC for 1 minute. Annealing of primers in the PCR process was set on 55-65 ºC for 1 minute, extension at 72 ºC for 1.5 minutes, then final extension process at 72 ºC for 5 minutes. The PCR products were checked on agarose gel (1%) by electrophoresis. Purification of PCR product DNA from agarose gel was carried out using a Geneiad PCR/Gel purification kit column. The purified PCR results were ligated using T4 DNA ligase according to the Promega procedure into pGemT plasmids and transformed into *E. coli* Top10 competent cells. The results of the transformation were then checked using the blue-white screening method with solid LB media containing ampicillin/X-Gal/IPTG. Isolation of pGemT-lip recombinant plasmid from positive clones was performed with the QIAprep Spin Miniprep Kit (Qiagen). The recombinant plasmids were cut using restriction enzymes (*Nde*I and *Xba*I) and examined on agarose gel (1%) by electrophoresis. Subsequently, DNA lip sequences were performed in the pGemT-lip recombinant plasmid using the dideoxy-Sanger method with an automatic sequencer (ABI PRISM) in Macrogen, Singapore.

2.3. Sequence Analysis

The nucleotide alignment of the sequencing resultsingsequence of lipase *Bacillus cereus* ATCC 14579NC-004722 as referencethan were performed using the SeqMan programDNA Star Software (Lasergen). The results of in-silico translation of lip gene nucleotides were carried out using the EditSeq Software DNA Star program between the *Bacillus cereus* reference lipase and local strain lipase from Jambangan Surabaya.

2.4. Insertion of lip gen to pCold II DNAvector

DNA lipase fragments were cut from the pGemT-lip recombinant plasmid using restriction enzymes (*Nde*I and *Xba*I) and examined on agarose gel (1%) by electrophoresis. Then it was purified using the Geneiad PCR/Gel purification kit column. The DNA fragments were then ligated using T4 DNA ligase according to the Promega procedure into pCold II DNA plasmids and transformed into competent *E. coli* BL21 (DE3) cells. Isolation of the pCold-lip recombinant plasmid from a positive clone of *E. coli* BL21 (DE3)-lip was carried out with the QIAprep Spin Miniprep Kit (Qiagen). The recombinant plasmids were then cut using restriction enzymes (*Nde*I and *Xba*I) and examined on agarose gel (1%) by electrophoresis.

2.5. Lipase expression

E. coli BL21 (DE30 [pCold II-lip] was grown in 25 mL of liquid LB medium containing 100 µg/mL ampicillin, then incubated with 150 rpm shaking at 37ºC for 5-6 hours, to obtain OD_{600} 0,4-0,5. The culture was then cooled by means of incubation at 15 ºC for 30 minutes without shaking. To express protein lipase, culture was induced with the addition of 0,1 mM IPTG, then incubated again at 15 ºC with 150 rpm shaking for 24 hours. Subsequently, the culture was centrifuged at 5000 rpm for 10 minutes at 4ºC to obtain cell pellets, the lysed by untrasonicator waves. The isolated protein was then analyzed by SDS-PAGE to determine its molecular weight focusing the lipase protein.

2.6. Lipase activity assay

The lipase activity test was carried out in several stages, including making standard curves of p-NP with concentrations of 20, 40, 60, and 80 µM and measuring the absorbance value using a UV-Vis spectrophotometer at a maximum wavelength (λmax) of 410 nm.

Determination of lipase activity was performed by using p-nitrophenylpalmitate (p-NPP) as a substrate. Substrate solution was prepared by adding 1800 µL of substrate mixture and 100 µL of enzyme solution and 100 µL of Tris-HCl buffer. The solution was incubated at 45 °C for 15 min. Then 250 µL Na2CO3 (0,1 M) was added to the solution. The absorbance was determined after 15 minutes at λ= 410 nm using a spectrophotometer.

One unit of activity (U) was expressed as the amount of enzyme required to produce 1µM of the p-nitrophenol (p-NP) product released every minute under assay conditions (Ertugul,et al., 2007). The unit of enzyme activity is calculated using the

$$\text{Unit activity (U/mL)} = \frac{[\text{p-NP}]\ (\mu\text{M}) \times 1000 \times \text{Fp}}{\text{Time}}$$

The p-NP, time, the number of 1000 and Fp in the formula shows respectively to the p-nitrophenol, time for

enzyme reaction, unit conversion from mM to uM, and the dilution factor of enzyme.

Determination of protein levels in this research was detected by Bradford method with a standard solution using Bovine Serum Albumin (BSA). Detection of absorbance was carried out at 595 nm.

3. Results and Discussion

3.1. Insertion of the PCR-Resulted Lipase gene into the pGemT Vector

The purified DNA lip from the PCR was inserted into the pGemT plasmid. The splicing of the two DNA fragments can take place properly through the insertion mechanism as shown in Fig 1.

Transformation of *E. coli* Top10 bacteria with the product of ligation process resulted 2 white colonies and 7 blue colonies were obtained. The white colonies obtained were thought to carry recombian plasmid, so that they were further characterized. While the blue colonies are transformant cells that have no recombinant DNA. The results of the transformation can be seen in Fig 2.

The data in Fige 2.C as a negative control in LB-ampicillin media showed that no colonies grew, so it can be ascertained that the media was positive for ampicillin which was active in killing wild type microbes. In Figure 2.D, the *E. coli* Top10 competent cells grow well on LB media without ampicillin, this reflects that the cells performance for transformation process is good. Inserted DNA as a positive control in LB-ampicillin media obtained many colonies of *E. coli* Top 10 (Figure 2.B) with blue and white color, this indicates that *E. coli* Top10 has inserted with empty pGemT plasmid or pGemT-DNA insert positive control. Therefore, these bacteria can grow on media containing ampicillin. Fig 2A showed the presence of blue colonies and white colonies; this indicates that there are colonies containing empty pGemT and recombinant pGemT.

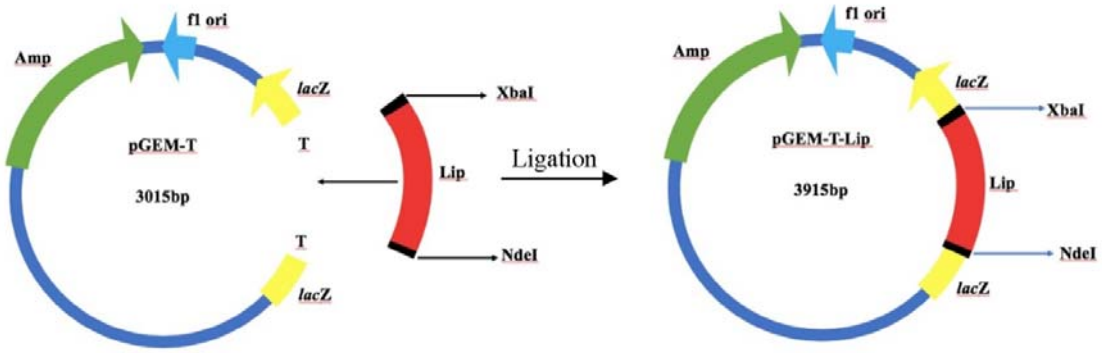

Figure 1. The process of ligation of the lipase gene into pGemTvector

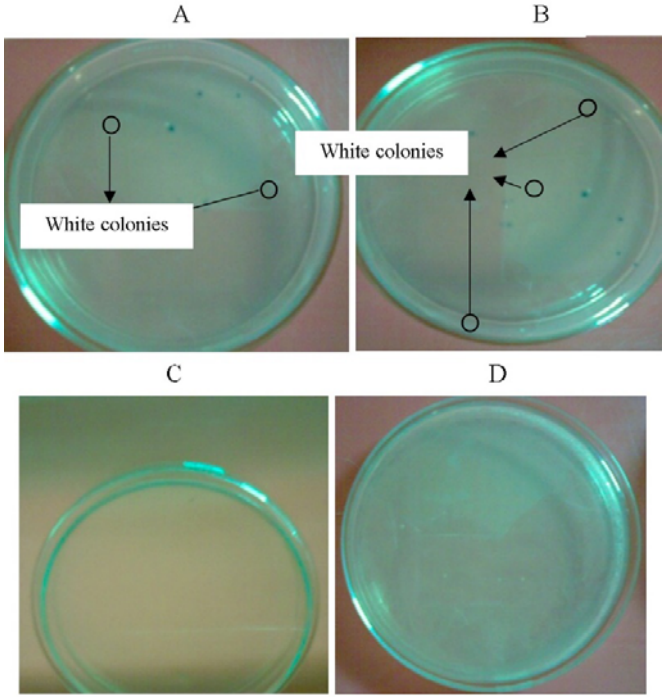

Figure 2. Plating results of *E. coli* cells of Top 10 transformants on LB amphicilin media. A) transformed with pGemT-lip, produced blue and white colonies; B) the result of the transformation with positive control insertion DNA, resulted in blue and white colonies; C) competent cells in LB media with ampicillin; D) competent cells in media LB without ampicillin.

The isolated recombinant plasmids were detected by agorase gel electrophoresis, and the results were shown in Fig 3. The isolated recombinant plasmids were characterized by cutting with restriction enzymes *Nde*I and *Xba*I, and the results can be seen in Fig 4. Cutting of pGemT plasmids with restriction enzyme EcoRv resulted in one band at 3 kb (Fig 4 lane 2). This restriction enzyme has one truncation site on the pGemT plasmid map. The size of the 3 kb band that was cut with the EcoRv enzyme was in accordance with the size of the pGemT plasmid DNA. Cutting of the recombinant pGemT-lip plasmid with *Nde*I and *Xba*I enzymes each produced one DNA band of 3.9 kb in size (Lane 4 and 5). The pGemT vector has *Nde*I and *Xba*I enzyme cleavage sites. The appearance of this 3.9 kb band represents a combination of the size of pGemT (3.0 kb) with DNA lip (0.9 kb). With these results, it can be stated that the DNA lip has been inserted properly in the pGemT vector. Further characterization of DNA lip was carried out by sequencing technique.

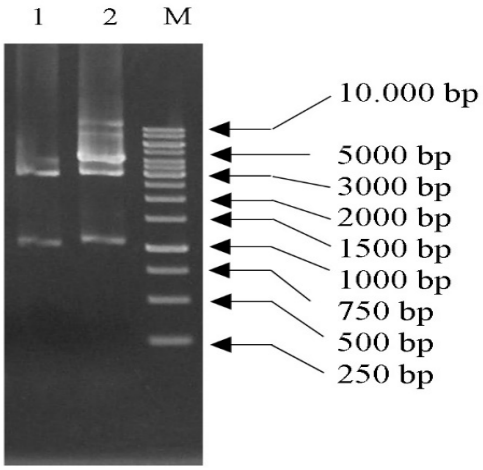

Figure 3. Electrophoregram of isolated recombinant plasmids from two white colonies. Lane 1, the results of the isolation plasmid from colony one, and lane 2, from colony two.

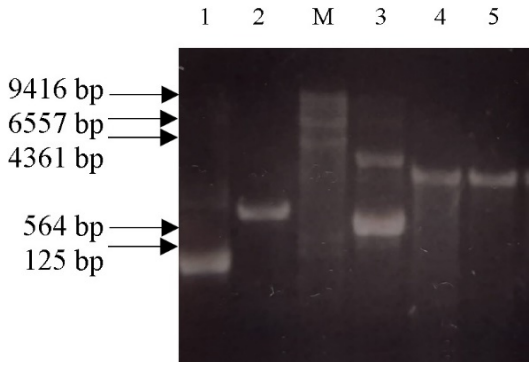

Figure 4. Electrophoregram of pGemT-lip recombinant DNA cutting with several restriction enzymes. Lane1, pGemT uncut; lane 2, pGemT/EcoRv (3 kb size); M, marker /*Hind*IIII; lane 3, pGemT-lip uncut; lane 4, pGemT-lip/*Nde*I (3.9 kb size); lane 5, pGemT-lip/*Xba*I (3.9 kb size)

3.2. Ligation lipasegene into pCold II-DNA expression vector

The lipase gene contained in the pGemT-lip recombinant plasmid was subcloned in the pCold II-DNA expression vector (Fig 5). Lip DNA was removed from the recombinant pGemT by cutting with two restriction enzymes *Nde*I and *Xba*I than it purified by PCR/Gel Purification kit Geneaid and ligated into the pCold II DNA expression vector. Prior to insertion, the pCold II DNA vector was cut with restriction enzymes *Nde*I and *Xba*I.

In the transformation of pCold-lip ligation mixture into competent cells of *E. coli* BL21(DE3) bacteria, 5 white bacterial colonies were obtained (Figure 6.A). Meanwhile, pCold II DNA emptyplasmid was transformed*into E. coli* BL21(DE3) which was cut with *Nde*I and *Xba*I enzymes did not produce cell colonies (Fig 6.E). This indicates that the restriction of the pCold II DNA plasmid by the two enzymes has been carried out perfectly. From the comparison of two data (Fig 6.A and E), it can be assumed that the cell colonies in Figure 6.A are *E. coli* carrying the recombinant pCold II-lip plasmid. Further characterization of this recombinant plasmid was carried out by plasmid isolation and cutting with restriction enzymes. The negative control on LB-ampicillin media (Fig 6.D) had no colonies grew, it could be ascertained that the media containing ampicillin kills the wild type bacteria. In Fig 6.C, the *E. coli* BL21 (DE3) grew well in the medium without ampicillin, this represent that the condition of competent cells for transformation step was health. The positive control in LB-ampicillin media was overgrown with recombinant *E. coli* BL21(DE3); the bacteria cells showed resistant to the antibiotic. Each white colony shown in Figure 6.A was then grown in LB-ampicillin media for plating duplication and then plasmid isolation and cutting with restriction enzymes were performed.

Digestion of the pCold II-lip recombinant plasmid with restriction enzymes was performed to characterize the recombinant plasmid. In addition, it was also used to confirm the successful process of ligation between DNA lip with the pCold II-DNA vector. Cutting the recombinant pCold II-lip plasmid (5.2 kb) using *Nde*I and *Xba*I enzymes could produce two DNA bands measuring 4.3 kb and 0.9 kb, respectively (Fig 7.C). The 4.3 kb DNA fragment corresponded to the pCod II-DNA (Fig. 7.A), while the 0.9 kb DNA fragment corresponded to the lip size (Fig. 7.B). The appearance of 2 bands from this double-cut result indicates that the insertion of the lip gene into the pCold II DNA vector was successful.

3.3. Sequencingof lip gene

Determination of lip gene nucleotideswere carried out by using the dideoxy-Sanger method with F-Lip and R-Lip primers. The entire ORF sequence of the lipase gene was sequenced. The results of the analysis of nucleotide alignment results from sequencing with reference lipases carried out with the SeqMan program on DNA Star Software (Lasergen) showed that the sample lipase gene had an identity (percent match) of 87-89% against the reference lipase *Bacillus cereus* ATCC 14579 (NC-004722). The electrophoregram of the nucleotide alignment results from this sequence is shown in Fig 8. The in silico translation of lipase gene nucleotides resulted in 295 amino acid residues. Alignment results between amino acid residues of protein lipase samples with reference are listed in Table 2. The analysis of the alignment results showed that there were 13 amino acid variants between the reference *Bacillus cereus* lipase and local strain lipase from Jambangan Surabaya. The 3D structure image of the recombinant lipase protein shown in

Fig 9 was predicated using the Swiss Model online software.The structural model constructed by using 2qtx.pdb template from *Bacillus subtilis* lipase that revealed an identity score of 36.1%. The model exhibited the Ramachandran favoured as 94.94% with structural α-helix and ß-sheet appeared dominantly (Fig 9).

Table 2. CLUTAL 2.1 multiple alignment of lipase amino acid residues

LipF	MKRFSYFMVGCLTLTLLVGCSAAEKPVEQVKQVKNTLTAKLATEEKMIEIDGQTIYFKKI
LipaseR	MKRFSYFMVGCLTLTLLVGCSAAEKPVEQVKQVTNTLTAKLATEEKMIEIDGQTIYFKKI
Reference	MKRFSYFMVGCLTLTLLVGCSAAEKPVEQVKQVKNTITAKLATEEKMVEIDGQTIYFKKI
LipF	GNEKPPLLMIHGFGGSSDGFRKIYSDLAKDHTIISVDALGFGRSSKPMDFYYSFPTHANL
LipaseR	GNEKPPLLMIHGFGGSSDGFRKIYSDLAKDHTIISVDALGFGRSSKPMDFYYSFPTHANL
Reference	GNEKPPLLMIHGFGGSSDGFQKIYSDLAKDHTIISVDALGFGRSSKPMDFYYSFPTHANL
LipF	YYKLMKKLGYDSFAILGHSMGGEISLNLTYLYPEAVTHLILTDATGGAHTLVNKQGSPKP
LipaseR	YYKLMKKLGYDSFAILGHSMGGEISLNLTYLYPEAVTHLILTDATGGAHTLVNKQGSPKP
Reference	YYKLMKKLGYDSFAILGHSMGGEISLNLTYLYPEAVTHLILTDATGGPHTFVTKQGSPKP
LipF	QLSTDLHTVSAIADYDESKVKFKRNDEEHYNKMKLWPRRLQINANEIQQPTLIIWGRNDS
LipaseR	QLSTDLHTVSAIADYDESKVKFKRNDEEHYNKMKLWPRRLQINANEIQQPTLIIWGRNDS
Reference	QLSTDLNAVSSITDYDESKVKFKRNDEEHYNKMKLWPRRLKINANEIKQPTLIIWGRNDS
LipF	SVSWKEGETYHQFLKNSTFHIIEKGYHAPFRQEPQEFVGYVKDFFKNNPIKVEK
LipaseR	SVSWKEGETYHQFLKNSTFHIIEKGYHAPFRQEPQEFVGYVKDFFKNNPIKVEK
Reference	SVSWKEGETYHQFLKNSTLHIIEKGYHAPFRQEPQEFVGYVKDFFKNNPIKVEK

Table 3. Amino acid residues variance between reference lipase (Genbank) and sample

Residual number	Amino acids		
	Lipase GenBank	Lipase F	Lipase R
37	I	L	L
48	V	I	I
81	Q	R	R
168	P	A	A
171	F	L	L
173	T	N	N
187	N	H	H
188	A	T	T
191	S	A	A
193	T	A	A
221	K	Q	Q
228	K	Q	Q
260	L	F	F

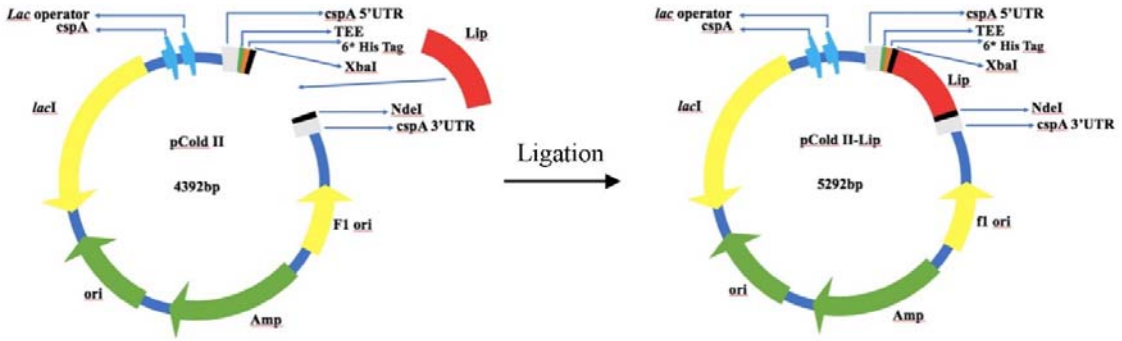

Figure 5. The process of ligation of the lipase gene to the pCold II-DNA vector.

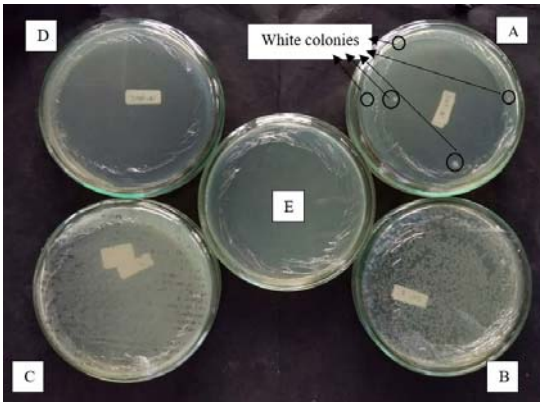

Figure 6. Product of transforman cells when *E. coli* BL21 (DE3) transformed with pCold II-lip. A. transformants with mixed pCold-lip ligation on LB-Ampicillin media (some colonies); B. transformants with pCold in LB-Ampicillin media (many colonies); C. Competent cells in LB media without ampicillin (many calonies); D. Competent cells in LB-ampicillin media (no colonies); E. transformants with pCold II/*Nde*I/*Xba*Iplasmid (no clonies)

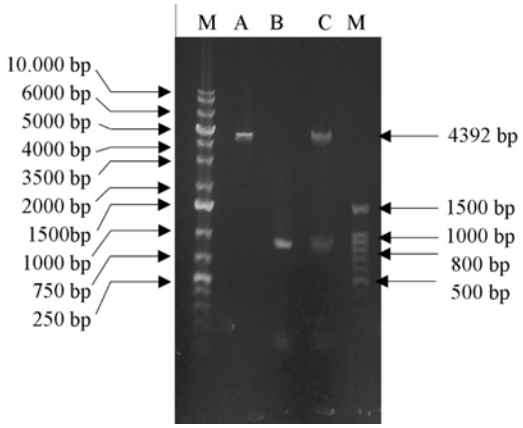

Figure 7. Electrophorogram of pCold-lip recombinant DNA cutting with restriction enzymes. M Lane, Marker; Lane A, cut pCold II with *Nde*I and *Xba*I enzymes (4392 bp); column B, insert, DNA lip (0.9 kb); lane C, cut pCold-lip with *Nde*I and *Xba*I enzymes, resulted in 2 bands measuring 4.392 kb and 0.9 kb

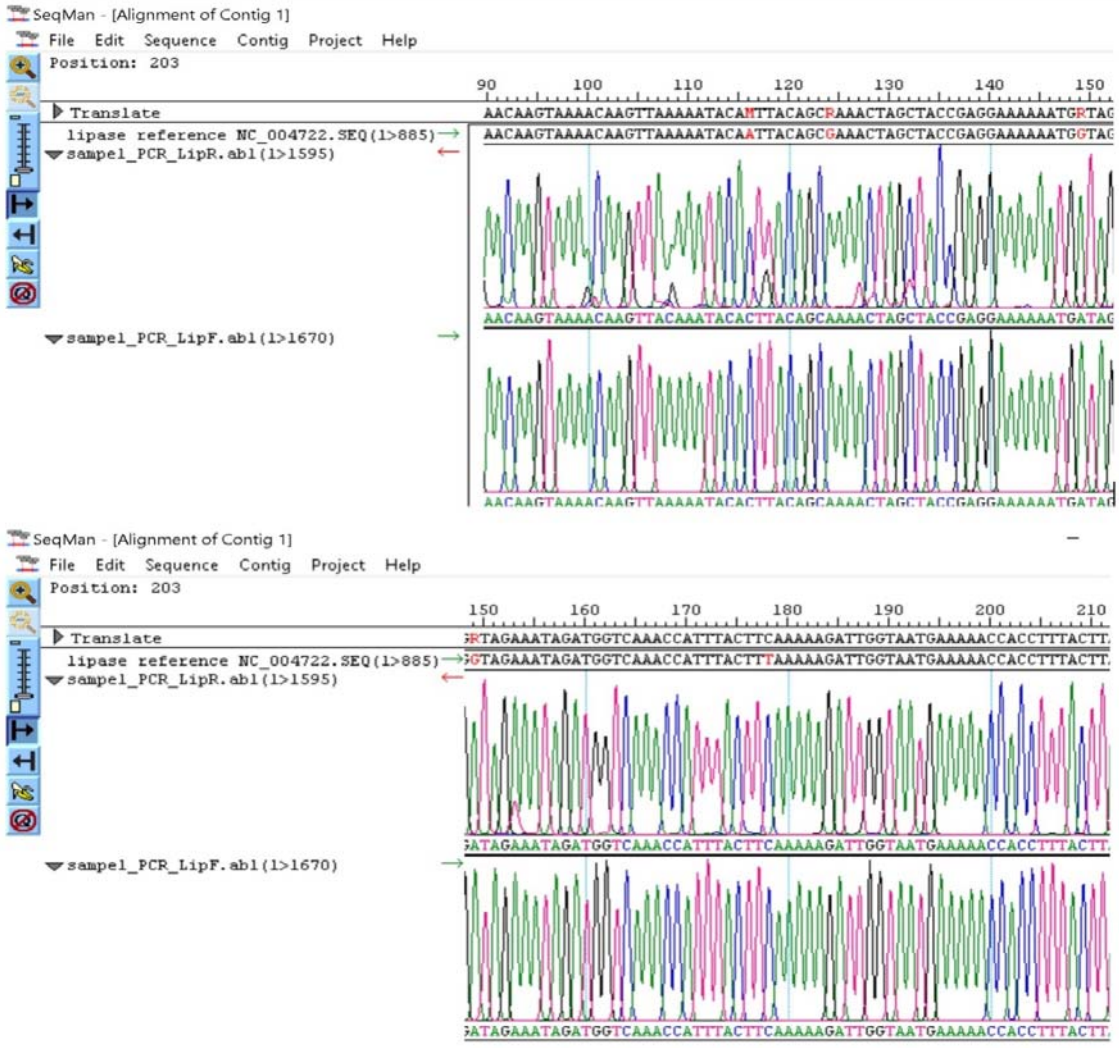

Figure 8. The results of this alignment of DNA lip nucleotides against the reference lipase from GenBank.

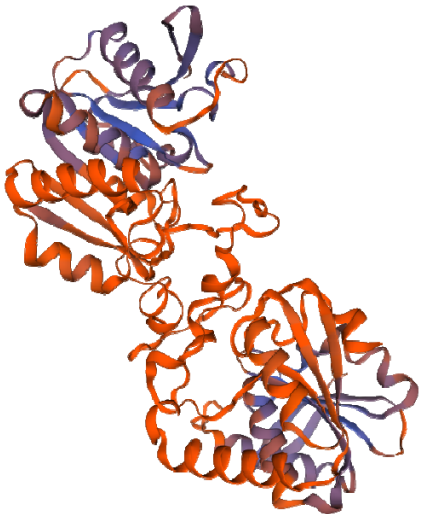

Figure 9. The model structure drawing of recombinant lipase of *Baccillus cereus* local strain of Jambangan origin

3.4. Lipase Gene Expression

Gene expression is an important step in protein production. *E. coli* cell is widely used as host for gene expression because they are easy to treat and the cost of culture is relatively cheap. Gene expression in *E. coli* host cells often results in insoluble proteins. This constraint can be minimized by using a low-temperature expression system.

Plasmid pCold II DNA is a cold shock expression vector; therefore, the expression of the lipase gene coding region was carried out at low temperatures. In the pCold II DNA vector, the expression of the inserted gene was controlled by the promoter derived from the cold shock gene (cspA) derived from *E. coli*. This can be advantageous in the process of lipase expression because the promoter can be well recognized by the host cell. The presence of a lac operator in the pCold II DNA vector that is inserted downstream of the cspA promoter allows the insertion gene to be expressed precisely. Another consideration designed with the expression system in the pCold II DNA vector is obtaining the lipase protein in a soluble state.

Expression of the lipase gene in the pCold II DNA vector was done to look at whether the protein lipase can be produced by *E. coli* BL21 (DE3)[pCold II-lip]. Extracts obtained from *E. coli* BL21 (DE3)[pCold II-lip] was analyzed by SDS-PAGE. The results of SDS-PAGE protein extract showed that *E. coli* carrying pCold II-lip and induced with IPTG, produced protein bands with a molecular mass of 30 kDa (Fig. 10, lane 1 and 2). The band was not appearfrom extract of *E. coli* that had nopCold II-lip (Fig 10,lane 3). The result showed that the lipase protein was expressed well.

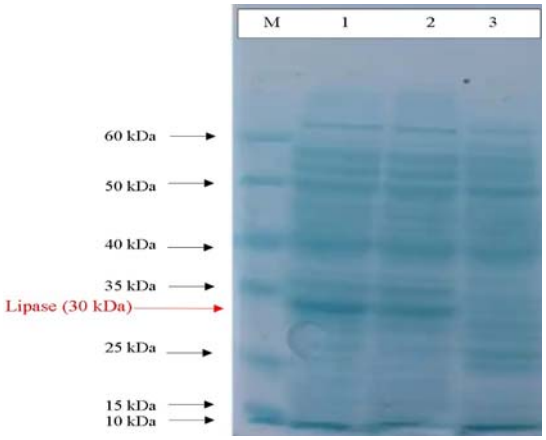

Figure 10. Results of SDS-PAGE protein expression results. M lane, marker; lane 1, sonicated protein; lane 2, protein extracted with SDS; lane 3, protein BL21 (DE3) without plasmid as a negative control

3.5. Lipase activity

Lipase activity test was carried out using p-nitrophenyl palmitate (pNPP) as a substrate. Lipase activity was measured based on changes in absorbance at a wavelength of 410 nm which indicated the release of p-nitrophenol compounds (pNP) from the substrate. Based on the results of the enzym activity test, it was obtained that was 0.083 U/mL with a total activity of 0.83 U.The specific activity of the lipase produced was 46.03 U/mg.The lipase activity of non recombinant E. *coli* BL21(*DE3*) in spectrophotometry was almost not detected; the absorbance was very low, so far from Beer-Lambert Law.

A number of studies have also reported the activity of recombinant lipases, including *Pyrococcus furiosus* which has an activity of 8.9 U/mg with a molecular weight of 48.8 kDa (Alqueres at al., 2011) and recombinant lipase from isolate S4-01 which has relatives with *Bacillus amyloliquefacies*has an activity of 3.91 U/mg with a molecular weight of 53.2 kDa (Sembiring at al., 2015).

The production of recombinant proteins is growing every year, leading to the emergence of new host cells, vectors, and cloning and expression techniques that are more diverse and of higher quality. Various recombinant lipase enzymes have been produced and studied by a number of researchers. Lipase is an enzyme that has a molecular weight in the range of 19–60 kDa, belonging to the α/β hydrolase family. This enzyme has an active site formed by the catalytic triad Ser, Asp/Glu and His. Protein Lipases have a unique sequence consensus, namely GXSXG in their primary structure, where X is an amino acid residue (Balan A et al., 2012). Lipase properties from various sources have been reported in several publications. The expression of the lipase gene from *Bacillus subtilis* strain IFFI10210 using plasmid vector pBSR2 that had a strong lipase promoter in the host cell *Bacillus subtilis* A.S.1.1655 was able to produce lipase with 100 times higher activity than the original source. The obtained lipase has a molecular weight of 24 kDa (Yapin L et al., 2010, Jisheng Ma et al., 2006). The lipase production has also been reported to increase after the yeast of *Sporobolomyces salmonicolor*was developed by mutagenesis and molecular expression. The research could provide the mutant OVS8 yeast with capacity on lipase production 3.2 time greater than its wild typestrain (Thabit

et al, 2012).*Geobacillus thermodenitrificans* IBRL-nra has also been reported to produce thermostable lipases capable of being active at 65ºC. The resulting lipase has a BM of 30 kDa (Balan A et al., 2012).

In this study, the lipase gene expression of *Bacillus cereus* was carried out in *E. coli* BL21(DE3) cells. The results of the study obtained protein lipase with a molecular weight of 30 kDa and had good enzyme activity. The recombinant lipase showed a high lipolytic activity, therefore in the future it is necessary to develop its production on a large scale to support its further application for many purposes.

4. Conclusion

The conclusions of this research were that the construction results of pGemT-lip and pCold-lip recombinant plasmids respectively could produce 3.9 kb and 5.2 kb recombinant DNA. The 3.9 kb recombinant DNA band represents the combination of pGemT (3 kb) with DNA lip (0.9 kb). Meanwhile, 5.2 kb recombinant DNA showed a combination of pCold II DNA vector (4.3 kb) with DNA lip (0.9 kb).The lipase gene had an identity percent (percent match) of 87-89% against the lipase reference *Bacillus cereus* ATCC 14579 (NC-004722). Alignment analysis showed that there were 13 amino acid variants between the *Bacillus cereus* reference lipase and local strain lipase from Jambangan Surabaya.The result of lip gene expression in *E. coli* BL21 (DE3) host cells was able to produce 30 kDa protein on SDS PAGE electrophoregram. The protein showed a specificlipase activity of 46.03 U/mg protein.Referring to the high activity, the scale up production on the recombinant enzyme is important, developed to support its further application for many purposes.

Acknowledgment

This work was supported by Basic Research of Superior Universities (PDUPT) project from The Ministry of Education and Culture, Republic of Indonesia No. 8/E1/KPT/ 2021, followed by contract Number 4/E1/KP.PTNBH/2021 and 480/UN3.15/PT/2021

References

Adrio JL and Demain AL. 2014. Microbial Enzymes: Tools For Biotechnological Processes. *Biomolecules*., **4**:117–139.

Sylvia MCA, Roberta VB, Denise MGF, Tito LMA, Orlando BM and Rodrigo VA. 2011. Characterization of the Recombinant Thermostable Lipase (Pf2001) from Pyrococcus furiosus : Effects of Thioredoxin Fusion Tag and Triton X-100. *Enzyme Res*., **2011**:1-7.

Balan A, Darah I, Rashidah ARand Fatimah AAR. 2012. Purification and Characterization of a Thermostable Lipase from Geobacillus thermodenitrificans IBRL-nra. *Enzyme Res*., **2012**: 987523

Choudhry R. 2017. Isolation and Screening of Lipase Production Bacteria From Oil Mill efluent. *Indian J. Sci. Res*., **13(2)**:192-194.

Hama Sand Kondo A. 2013. Enzymatic Biodiesel Production: An Overview Of Potential Feedstocks And Process Development. *Bioresour Technol*., **135**:386-395.

Kapoor Mand Gupta MN. 2012. Lipase Promiscuity And Its Biochemical Applications. *Process Biochem*., **47**:555-569.

MaruwkaAW, Dach J and Sawicka A. 2009. Effect Of Temperature On The Number Of Selected Microorganism Groups and Enzymatic Activity Of Sewage Sludge Composted With Different Addition In Cybernetic Bioreactor. *Agron. Res*., **7(2):**1634-16457.

Purkan P, Huruniawati E, Sumarsih S. 2017. Xylanase enzyme from a local strain of Pseudomonas stutzeri. *J. Chem. Technol. Metall*., **52(6)**:1079-1085

Purkan P, Indah TL, Rizky A, Retno RPN, Wiwin A, Hamidah N, Sri S, Sofijan H, Wiwin R and Seung W.K. 2018. Isolation of lipolytic bacteria from domestic waste compost and its application to biodiesel production. *Rasayan J. Chem*., **13(4)**:2074-2084.

Pliego J, Mateos JC, Rodriguez J, Valero F, Baeza M, Femat R, Camacho R, Sandoval G and Herrera-Lopez EJ. 2015. Monitoring Lipase/Esterase Activity By Stopped Flow In A Sequential Injection Analysis System Using P-Nitrophenyl Butyrate. *Sensors (Basel)*., **(2):**2798-811.

Shaini PV and Jayasree S. 2016. Isolation and Characterization of Lipase Producing Bacteria from Windrow Compost. *Int. J. Curr*., *Microbiol. App. Sci*., **15(5)**, 926-933.

Sembiring A, Suwanto A and Mubarik NR. 2015. Isolation of Cloned Thermophilic Lipase-Producing Bacteria and Expression of Lipase-Coding Genes. Master Theses, Bogor Agricultural Institute, Bogor, Indonesia.

Treich H, de Oliveira D, Mazutti M, Di Luccio M and Oliveira JV. 2010. A Review On Microbial Lipases Production.*Food Bioprocess Technol*., **3**:182–196.

Yaping L, Qian L, Jin W, Yufan W, Wuyundalai B, Fengxia L, Zhaoxin L. 2010. Overexpression and characterization in *Bacillus subtilis* of a positionally nonspecific lipase from Proteus vulgaris. *J Ind Microbiol Biotechnol.,* **37**:919–925.

Thabit HM, Pasha C, Ahmad MDM and Linga VR. 2012. Isolation of novel lipase producing *Sporobolomyces salmonicolor* OVS8 from oil mill spillage and enhancement of lipase production. *Jordan J. Biol. Sci*., **5(4)**:301-306.

Jisheng M, Zuoming Z, Baijing W, Xiangju K, Yuguo W, Shugui C, Yan F.2006. Overexpression and characterization of a lipase from *Bacillus subtilis*. *Protein Expr Purif*., **45(1)**:22-9.

JJBS

Volume 15, Number 5, December 2022
ISSN 1995-6673
Pages 787 – 796
https://doi.org/10.54319/jjbs/150507

Jordan Journal of Biological Sciences

A simple and cost Effectively Method for Production of Recombinant of Full Length of Human Placenta-Specific Protein using *E. coli* BL21 strain

Eva Mohammad[1*], Chadi Soukkarieh[1**]

[1] Department of animal biology, Faculty of Science, Damascus University, Damascus-Syria.

Received: February 1, 2022; Revised: April 11, 2022; Accepted: May 15, 2022

Abstract

Placenta-specific protein 1 (PLAC1) is one of the most significant cancer/testis antigens with restricted expression in the placenta and testis and high expression in a wide range of human cancers. PLAC1 has fundamental roles in cancer progression and is suggested as a diagnostic biomarker and therapeutic target for many cancers. However, producing full length of recombinant PLAC1 (rPLAC1) in *E. coli* BL21 strain as soluble form with maintaining its efficacy is still limited. Yet, major issues such as inclusion bodies (IBs) formation must be overcome. Here, we try to address this issue by optimizing rPLAC1 expression conditions. We purified rPLAC1 by immobilized metal affinity chromatography (IMAC) without using urea and detected the production of rPLAC1 by SDS-PAGE and western blot (WB). Our results demonstrated that the optimum conditions for the production of the full length of rPLAC1 in *E. coli* BL21 are induction at the early-log phase of growth ($O.D_{600nm}$=0.3-0.5) using 0.5 mM IPTG at induction temperature of 22 °C for 7-8 hours. Moreover, we indicated that optimization of induction conditions probably increases protein-soluble form yield without needing to use urea or any denaturing buffer in purification later. Taken together, we have introduced a simple and cost effectively method for the production of the full length of human rPLAC1 and increasing its soluble form without using urea.

Keywords: Placenta-specific protein 1; Cancer/Testis antigen; Recombinant protein; *E.coli* BL21.

1. Introduction:

Placenta-specific protein 1 (PLAC1) is a type II membrane protein with 212 amino acids (aa) (Cocchia et al., 2000; Koslowski et al., 2007). It consists of three main parts: a short N-terminal intracellular component as a conserved signal peptide about 23 aa, a single transmembrane domain from 5-22 aa, and a large extracellular domain from 23-212 aa (Cocchia et al., 2000; Roldán, 2012; Mahmoudian et al., 2019). The extracellular domain contains a homolog part to the N-terminal sub-domain of the zona pellucida (ZP3) glycoprotein that ranges from 29–119 aa (Mahmoudian et al., 2019). PLAC1 is a cell membrane-associated protein (Fant et al., 2007; Koslowski et al., 2007; Silva et al., 2007; Liu et al., 2008; Ghods et al., 2014a; Ghods et al., 2014b; Nejadmoghaddam et al., 2017; Wu et al., 2017). It could be cytoplasmic (Liu et al., 2008; Ghods et al., 2014b; Liu et al., 2015; Wu et al., 2017; Yin et al., 2017) or nuclear protein (Liu et al., 2014; Liu et al., 2015). However, PLAC1 has different molecular weights, which range from 24 kDa to 30 kDa, depending on multiple factors like posttranslational modification (PTM) especially glycosylation (Mahmoudian et al., 2019; Mahmoudian et al., 2020). At the gene level, the PLAC1 gene is located on Xq26.3 containing 6 exons, the last exon (number 6) contains an open reading frame (ORF) with a length of about 639 bp (Cocchia et al., 2000; Chen et al., 2011; Caballero and Chen, 2012; Devor et al., 2014; Devor, 2016). PLAC1 is concerned with restricted expression type on the apical region of Syncytiotrophoblast, the too limited expression on Cytotrophoblast (CTB) and testis (Fant et al., 2007; Silva et al., 2007; Fant et al., 2010; Roldán, 2012; Wagner, 2014; Chang et al., 2016; Mahmoudian et al., 2019). PLAC1 is not detectable in other normal cells in normal status (Ghods et al., 2014a; Ghods et al., 2014b; Mahmoudian et al., 2019). In addition, it is considered an essential component for proper placental and embryonic development (Jackman et al., 2012; Devor, 2014; Chang et al., 2016; Mahmoudian et al., 2019). Nevertheless, PLAC1 is an important member of the cancer/testis antigens (CTAs) family (Cocchia et al., 2000). Recent studies confirmed its expression in more than 74 cancer cell lines (Silva et al., 2007; Mahmoudian et al., 2019). Including prostate (Ghods et al., 2014a; Nejadmoghaddam et al.,

* Corresponding author. e-mail: evaredcrescent@hotmail.com.
** Corresponding co-author. e-mail:Soukkarieh@gmail.com.

Abbreviations used in this article: aa; amino acids, APS; Ammonium persulfate, bp; Base pair, E. coli; Escherichia coli, sfGFP; super folding Green Fluorescent Protein, IB; Inclusion Body, IPTG; Isopropyl-β-D-Thiogalactothiopyronoside, ORF; Open reading frame, PBS; Phosphate-buffered Saline, PCR; Polymerase Chain Reaction, PLAC1; Placenta specific-protein1, plac1; Placenta specific-protein1 coding gene, SDS; Sodium Dodecyl Sulfate, SDS-PAGE; SDS-Poly Acrylamide Gel Electrophoresis, PTM; posttranslational modification, TBST; Tris-buffered Saline-Tween20, TEMED; Tetramethylethylenediamine, WB; Western Blot.

2017), breast (Koslowski et al., 2007; Li et al., 2018), uterus (Devor et al., 2014), cervix (Chen et al., 2021), ovary (Devor et al., 2017). In addition to, lung (Yang et al., 2018), liver (Wu et al., 2017), colon (Ren et al., 2020), gastric (Liu et al., 2021), pancreatic cancers (Yin et al., 2017), nasopharyngeal carcinomas (Lin et al., 2021), melanoma (Mahmoudi et al., 2020), and osteosarcoma (Yu et al., 2021). PLAC1 has important roles in cancer progression and maintenance including transforming normal cells into cancer cells, growing, resistance to apoptosis, immortalization, proliferation, migration, invasion, metastasis, and angiogenesis (Koslowski et al., 2007; Li et al., 2018; Mahmoudian et al., 2019; Ma et al., 2020; Ren et al., 2020; Roldán et al., 2020). PLAC1 has differential expression in many cancers such as prostate cancer, which shows a correlation of PLAC1 expression level with the Gleason score (Ghods et al., 2014a). Furthermore, PLAC1 is an important diagnostic and prognostic biomarker for multiple cancers and an attractive candidate target for cancer immunotherapy especially prostate cancer (PCa) (Nejadmoghaddam et al., 2017).

Recombinant protein (RP) production technology is one of the most important pharmaco- medico-biotechnology techniques that aim to use engineered biological tools for the production of pharmacological benefit proteins (Rosano and Ceccarelli, 2014; Pham, 2018; Puetz and Wurm, 2019). The most remarkable class of RPs is recombinant membrane proteins like PLAC1 that form about 20–30 % of all genes encode products (Schlegel et al., 2014). Nevertheless, isolating membrane proteins from their natural sources suffers from many difficulties due to their low abundance leading to a low isolated amount, which does not meet the needs of structural and functional studies (Schlegel et al., 2014). In addition, the use of natural sources excludes the potential of genetically manipulating proteins to ease their detection and/or purification (Schlegel et al., 2014). *E. coli* strains are the most widely used bacterial host to produce RPs, thus 80% of proteins with their solved three-dimensional structures were submitted to the protein data bank (PDK), and more than 29 engineered antibodies were produced by *E. coli* strains (Frenzel et al., 2013; Kaur et al., 2018). However, many challenges are facing it in the production of multiple proteins, especially membrane proteins, like miss-folding, expression of proteins in insoluble form owing to its hydrophobic nature and tendency to aggregate in inclusion bodies (IBs), and digestion by proteases (Gopal and Kumar, 2013; Rosano and Ceccarelli, 2014; Nazari et al., 2017; Kaur et al., 2018). Several studies have produced rPLAC1 since some of them have used eukaryotic systems (Mahmoudian et al., 2020). However, the expression in eukaryotic systems is very expensive compared to prokaryotic systems. Others have used different prokaryotic systems mainly focused on *E. coli* strains. Thus, most of them have employed expensive genetically modified strains and molecular tools (Silva et al., 2007; Dong et al., 2008; Nazari et al., 2017; Nejadmoghaddam et al., 2017). In addition, others have used the *E.coli* BL21 strain, which is known for its cost-effectivity with different gene constructions (full length or the truncated form/without the Transmembrane part) (Nazari et al., 2017). Nevertheless, they have not obtained the expression of this recombinant protein (rPLAC1), neither the soluble form nor insoluble form in this strain, unless fusing it with high relative molecular weight protein tags (Nazari et al., 2017), which may affect the protein functional three-dimensional structure (Gopal and Kumar, 2013; Kaur et al., 2018). In addition, the main challenges facing the production of full length rPLAC1, in other genetically modified *E.coli* strains, have not been solved completely, especially the formation of insoluble proteins and aggregation in IBs (Silva et al., 2007; Nazari et al., 2017; Nejadmoghaddam et al., 2017)**.** However, optimization studies have indicated the importance of optimizing the expression conditions to obtain the correct form of recombinant protein (Gopal and Kumar, 2013; Rosano and Ceccarelli, 2014; Kaur et al., 2018). Therefore, we focused in our present study on optimization production conditions of rPLAC1 in full length, using specific strain (*E.coli* BL21), as using this efficient expression system in the expression of rPLAC1 has multiple advantages especially easy to handle and cost/time effective(Gopal and Kumar, 2013; Rosano and Ceccarelli, 2014; Kaur et al., 2018). We used simple strategies depending on the reference studies (Gopal and Kumar, 2013; Kaur et al., 2018). First, we have induced the BL21 at decreased-gradient induction temperatures for increased-gradient induction periods in the first log phase with 0.5 mM IPTG (phase-1). Second, we tested the optimum condition from phase-1 using gradient optical densities (O.D) at the early-log phase of the bacterial growth curve, followed by testing it using gradient concentrations of inducer and time course expression. Here, we have produced rPLAC1 in full length and soluble form (as half amount of produced rPLAC1) in the BL21 strain by optimization of four-cultivation conditions (inducer concentration, bacterial-growth phase, temperature, and time course expression) without using any urea or denaturing agents in purification later.

2. Materials and Methods

2.1. Bacterial strain, growth media, plasmid, and ladders.

E. coli strain; top10 (Invitrogen, USA) and BL21 (DE3) (Novagen, Germany) were used in cloning and protein expression, respectively, and transformed with the pRSET vector (Invitrogen). For general maintenance, pre-culturing, cloning, and protein expression, *E. coli* was cultured in Luria Bertani Broth (LB Broth) (Sigma-Aldrich, USA), and LB Agar (Sifin, Germany) with 100 µg/ml ampicillin (amp) (Cytogen, Korea), in an orbit-rotating incubator at 37 °C. Two DNA ladders; 1kb Ladder and 100 pb Ladder (Vivantis, Malaysia), and two protein molecular weight ladders (INTRON Biotechnology, Korea) were used too.

2.2. Plasmid construction and cloning ORF plac1.

ORF plac1 was amplified from human genomic DNA by PCR using two specific primers; plac1-for-*Xho1* (5`-AT ATA CTC GAG CAA AGT CCA ATG ACT GTG CTG TG-3`) and plac1-rev-*Kpn1* (5`-A TAT GGT ACC TCA CAT GGA CCC AAT CAT ATC ATC-3`). These primers were designed for amplifying ORF plac1 without signal peptide coding sequence (ss), and to add *XhoI* restriction site at the 5` end and *KpnI* at the 3` end of the PCR amplicon (inserted gene) (Figure 1A). The PCR amplification program was been optimized. Thus, it

consisted of 5 min of denaturation step at 94 °C followed by 35 cycles of short denaturation step at 94 °C for 30 sec, annealing at gradient temperature of melting for 30 sec, and final extension at 72 °C for 2 min. Finally, 72 °C for 5 min. In addition, the amplification was done using PFU polymerase (Thermos scientific, USA). Both amplified ORFplac1 fragment and the pRSET vector (Figure 1B) were digested with *XhoI* and *KpnI* restriction enzymes (New England Biolabs, USA). Then, they were ligated with each other using DNA Ligase T4 (Thermo scientific). *E. coli* top10 was transformed with this recombinant vector pRSET–ORF plac1 (Figure 1C), by heat shock. The transformed colonies with recombinant vector (positive colonies) were screened by colony-PCR using T7 universal primers. After that, the extracted plasmids from these positive colonies were digested with the same enzymes and were confirmed by sequencing. Then the confirmed construction was cloned in *E. coli* BL21 using the same procedure. In addition to transformation BL21with pRSET-sfGFP construction as a positive control (Al-Homsi et al., 2012; Al-jaghasi et al., 2021). *Geneious v4.8* software was used to design recombinant construction schematics.

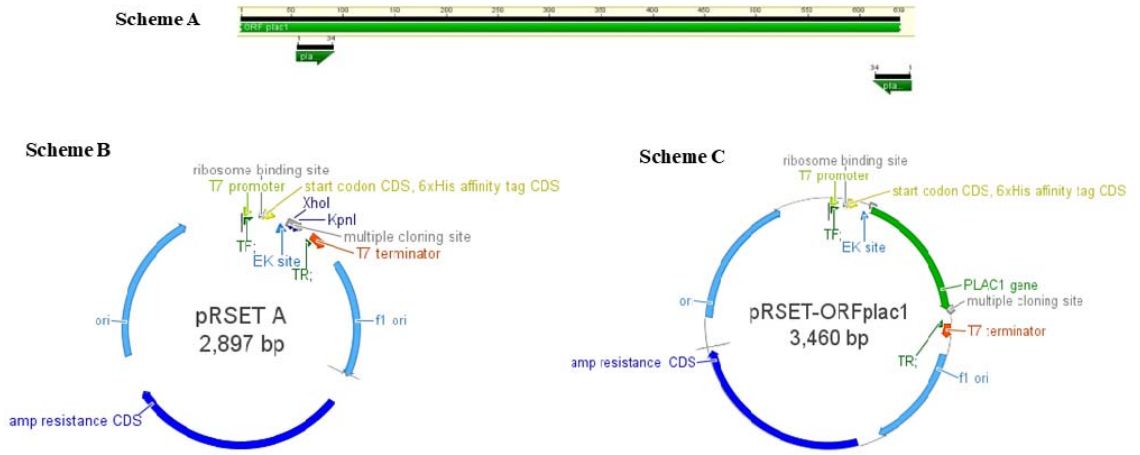

Figure 1: Schematic of ORFplac1 and pRSET before and after ligation. Scheme A; ORFplac1 with specific primers, Scheme B; pRSET construction, &Scheme C; pRSET-ORFplac1 construction.

2.3. Expression and purification of rPLAC1 protein.

Fresh transformed *E. coli* BL21 with recombinant vector (pRSET–ORFplac1) was grown overnight in a small culture volume (3ml of LB broth with amp), in an orbit-rotating incubator at 37 °C. The next day, 1.5 ml from this pre-culture was transferred into 10-50 ml of LB broth with amp (for small scale expression) or into 400-1000 ml of LB broth with amp (for large scale expression). Then, cultures were incubated at 37 °C until obtaining $O.D_{600nm}$ in the range 0.3-0.9. The expression was induced using a gradient of IPTG concentrations (Thermo scientific, USA), at gradient induction temperatures (37 °C, 22 °C, 16 °C) for gradient periods of expression induction time (3-4 h, 7-8 h, and overnight 16-20 h), respectively. After that, the culture was harvested by centrifuging at 4000 rpm for 15 min. The expression of sfGFP was induced as positive control by induction BL21 transformed with (pRSET-sfGFP) with 0.5 m IPTG at 16 °Covernight as mentioned in (Al-jaghasi et al., 2021). Later, pallets were manually purified by re-suspending with phosphate-buffered saline (PBS) and cells were lysed by repeated freezing and thawing on ice with a vortex. Then, solutions were centrifuged at 4000 rpm at 4 °C for 2 min, the supernatant was diluted with binding buffer to the final concentration; 20 mM sodium phosphate, 300 mM NaCl, 20 mM imidazole, and 200 µl Nickle charged Nitrilotiace acid (Ni-NTA) agarose beads 50 % slurry (Qiagen, Germany); 1 ml binding buffer /200 µl Ni-NTA /1 ml supernatant with rolling for 1h. Later, rPLAC1 was purified from the cytoplasmic extract by IMAC using a PD-10 column of NTA super sepharose (Qiagen, Germany), and washed with 10 volumes of binding buffer (after incubating for 1h). After that, bound protein (rPLAC1) was eluted by 300 µl elution buffer consisting of 20 mM sodium phosphate, 300 mM NaCl, and 250 mM imidazole after incubating for 1 h. Then, the eluted fraction was detected by SDS-PAGE followed by WB. The concentration of the purified protein was determined according tothe Bradford method (Bradford, 1976) using the Bradford reagent (Sigma-Aldrich, USA). In addition, the percentage of the purifiedrPLAC1 was estimated by ImageJ software.

2.4. SDS- PAGE of PLAC1 Protein.

The presence of rPLAC1 whole-cell lysate and purity of rPLAC1 was evaluated by Comassie-stained SDS-PAGE. Protein samples were diluted with 5X sample buffer consisting of 0.01 % bromophenol blue, 25 % glycerol, 10 % SDS, 5 % β-mercaptoethanol, and 16 mM Tris-HCl PH 6.8), and incubated at 95 °Cwater bath for 5 min. Then, they were separated by SDS-PAGE using a Bio-Rad Mini-Protean Tetra Cell system following the manufacturer's instruction in a gel that was prepared using stacking gel 4.5% and resolving gel 15%. Then, electrophoresis was applied using 100 V in electrophoresis buffer (25 mM Tris-base, 192 mM Glycine, 0.1 % SDSfor 1L d H_2O). The gel was stained in Comassie brilliant blue buffer (0.25 % Comassie R250, 10 % acetic acid, 40 % methanol) for 45-60 min and then washed several times in distaining buffer (30 % methanol, 10 % acetic acid).

2.5. Immunoblotting of PLAC1 Protein

Firstly, protein samples were separated in acrylamide gel, blotted onto 0.2 µm nitrocellulose membrane (Whatman, Germany) using 1X transfer buffer (25 mM Tris-base, 192 mM Glycine, 20 % Methanol for 1L d H_2O). Then, the membrane was blocked overnight at 4 °Cin 8 % skimmed milk diluted in T-BST buffer (10 mM Tris-HCl, 154 mM NaCl, 0.1 % Tween 20, pH=7.5). Then, incubated with Rabbit anti-HIS antibodies; 1/500 dilution (Bethyl laboratories USA) for 1 h with shaking at room temperature, washed again with T-BST buffer, and incubated with secondary antibody antibodies (Goat anti-Rabbit antibodies conjugated with alkaline phosphatase (AP); 1/1000 dilution), (Bethyl laboratories) for 1 h with shaking at room temperature. Finally, this membrane was incubated in darkness with chromogen substrate 33 µl Nitro blue tetrazolium (NBT) and 33 µl 5-Bromo-4-chloro-3-Indolyl phosphate (BCIP) (Sigma-Aldrich); diluted in 10 ml of substrate buffer (100 mM Tris-base, 100 mM NaCl, and 5 mM $MgCl_2$, pH=9.5) for 2-3 min.

3. Results

3.1. Cloning of ORF plac1 into pRSET vector

The amplified ORFplac1 fragment (about 593 bp in length) was identified by agarose gel-electrophoresis following PCR (Figure 2A), digested (Figure 2B), and ligated with the digested pRSET vector (Figure 2C). Transformed *E. coli* top10 with ligated products were screened by colony-PCR approach, which enabled comparing between empty pRSET containing colonies (negative colonies), which gave a fragment of 276 bp and pRSET–ORFplac1 containing colonies (positive colonies), which gave a longer fragment of 860 bp due to the existence of the inserted gene within them (Figure 2D). Plasmid constructs were extracted from positive PCR colonies and digested to ensure these positive colonies, where the pRSET–ORFplac1 containing colonies gave two fragments of 584 bp and 2877 bp after digestion due to the existence of the inserted gene within them (Figure 2E). Finally, this construction pRSET–ORFplac1was sequenced and compared with sequences in the Gene Bank, whereas results confirmed that no alteration or base substitution in the ORFplac1 sequence which was 100 % identical with that of *Homo sapience* (Genbank accession number:10761) and has been sent to NCBI and provided with (GenBank accession number:OK880267).

3.2. Expression and Purification of rPLAC1 Protein

Production of rPLAC1 was obtained after the transformation of BL21cells with the confirmed pRSET–ORFplac1 plasmid construction (Figure 1C). The protein expression was induced at decreased-gradient induction temperatures for increased-gradient induction periods (37 °C/3-4h, 22 °C/7-8h, 16 °C/16-20) in the first log phase ($O.D_{600nm}$=0.3-0.5) with 0.5 mM IPTG (phase-1) (Figure 3A). Then, we tested the optimum condition from phase-1 using gradient O.D at the early-log phase of the bacterial growth curve ($O.D_{600nm}$=0.3-0.5, and $O.D_{600nm}$=0.9) (Figure 3B), followed by testing it using gradient concentrations of inducer (0.5-1 mM IPTG) (Figure 3C), and gradient time course expression (Figure 3D). Then, protein expression was induced on a large scale (Figure 4A). The optimum condition for rPLAC1 production in soluble form was to induce bacteria at the first log phase ($O.D_{600nm}$=0.3-0.5), using 0.5 mM IPTG at 22°C for an incubation period of about 7-8 h and rPLAC1 was obtained as ~29 kDa band on SDS-PAGE (Figures 3A, B, C &D). The expression on a large scale was not different from a small scale since rPLAC1 was obtained as ~29 kDa band on SDS-PAGE within the same optimum expression conditions (Figure 4A). rPLAC1 was purified from the cytoplasmic extract by IMAC and the purification product was separated in SDS-PAGE, which has obtained a clear main band of about ~29 kDa presenting the pure rPLAC1 in the soluble fraction (Figure 4B). However, there was a remaining part of rPLAC1 in the insoluble fraction (Figure 4B). Although rPLAC1 was partially purified from bacteria cytoplasmic extract, the purification has been done without using any reducing /denaturing agents like urea, and the yield of pure rPLAC1was about half the total amount of rPLAC1 in the extract as mentioned in the purification recovery table (Table 1). The purity of the soluble form of rPLAC1was estimated at 37.76% (Table 2) as there were some non-specific bands besides rPLAC1 (Figure 4B).

Table 1. Purification recovery table, S; soluble form, I; insoluble form.

Procedure	Yield (mg)	Percentage (%)	Recovery
Total protein in extract (S, I)	18.1	100	
Nickle column	10	55.24	55.24% of total

Supplementary Data:

Table 2. Percentage of purified protein (Soluble form of rPLAC1), which was estimated depending on intensity rPLAC1 band in SDS-PAGE analysis of purification stage, by ImageJ software

	Percentage of purified protein
The soluble form of rPLAC1	37.76%

3.3. Immunoblotting of rPLAC1 Protein.

Detection of rPLAC1 was done after migration of total sample extract and pure rPLAC1 in SDS-PAGE (acrylamide 15%), blotting on nitrocellulose membrane and incubating with primary antibodies followed by secondary antibodies, and substrate. The location of rPLAC1 on nitrocellulose membrane was detected and defined as ~29 kDa compared to the protein molecular weight ladder (Figure 4C).

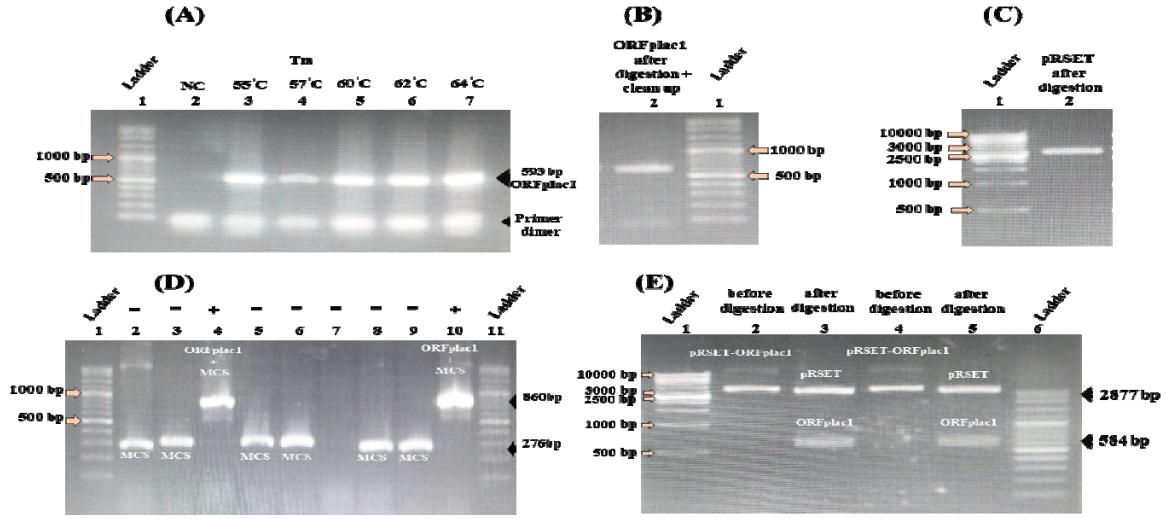

Figure 2. Electrophoresis of multiple stages of the Cloning (ORF PLAC1 into pRSET vector) products in 1 % agarose gel. **(A)** PCR product using gradient Tm; from the left; lane 1 DNA Ladder 100pb, lane 2 negative control (NC) (without genomic DNA), lane 3 Tm=55°C, lane 4 Tm=57°C, lane 5 Tm=60°C, lane 6 Tm=62°C & lane 7 Tm=64°C, Tm; Temperature of melting (annealing). **(B)**ORFplac1 after digestion and clean up; from the right; lane1 DNA Ladder 100pb, lane 2 ORFplac1 after digestion with *XhoI* and *Kpn1* enzymes and clean up. **(C).** pRSET plasmid extracted from *E. coli* top10; from the left; lane 1 DNA Ladder1kb, lane 2 extracted pRSET after digestion with *XhoI* and *Kpn1* enzymes. **(D)** Colony-PCR products of transformed *E. coli* top10 colonies with pRSET-ORFplac1; from the left; lanes 1&11 DNA Ladder 100pb, lanes 4&10 positive colonies (+), lanes 2, 3, 5, 6, 7, 8&9 negative colonies (-). **(E)** Extracted plasmid from the two positive colonies; from the left; lane 1 DNA Ladder 1 kb, lanes 2&4 extracted pRSET–ORFplac1 constructions before digestion, lanes 3&5 extracted pRSET–ORFplac1 constructions after digestion with *XhoI*, and *Kpn1* enzymes, &lane 6 DNA Ladder100bp.

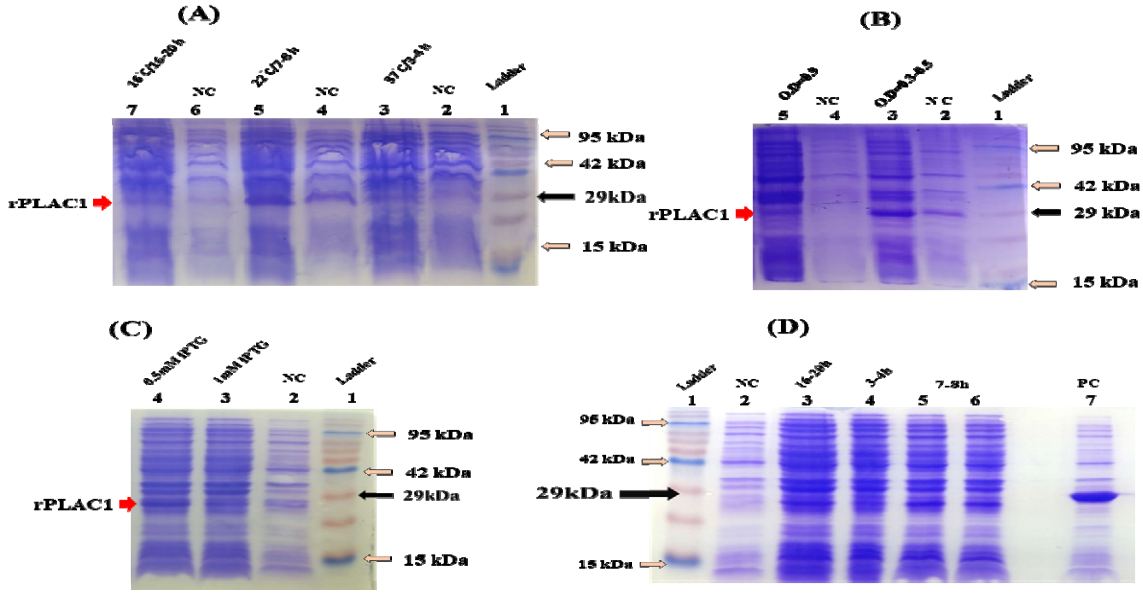

Figure 3.SDS-PAGE of *E. coli* BL21 transformed with (pRSET-ORFplac1) extracts before and after induction in optimized culture cultivation conditions and processing with 5X sample processing buffer and 1X PBS. **(A)** Optimization of induction temperature/period. From the right; lane1 protein molecular weight ladder, lanes 2, 4 &6 extracts before induction NC. Lane 3 extract after induction with 0.5 mM IPTG at O. D_{600nm}= 0.3-0.5 of bacterial growth phase in **37 °C** for **3-4h**. Lane5 extract after induction with 0.5 mM IPTG at O.D_{600nm}=0.3-0.5 of the bacterial growth phase at**22 °C** for **7-8h** (*). Lane 7 extract after induction with 0.5mM IPTG at O.D_{600nm}= 0.3-0.5 of bacterial growth phase in **16 °C** for **16-20h**. **(B)** Optimization of O.D in induction time. From the right; lane1 protein molecular weight ladder, lanes 2&4 extracts before induction NC, lane 3 extract after induction with same conditions (*), lane 5 extracts after induction with same conditions (*), except O.D_{600nm}, thus the used was O.D_{600nm}=0.9. **(C)** Optimization of IPTG concentration. From the right; lane1 protein molecular weight ladder, lane 2 extract before induction NC, lane 3 extract after induction with same conditions (*), except IPTG concentration, thus the used was 1mM IPTG, lane 4 extract after induction with same conditions (*). **(D)** Optimization of time course induction. From the left; lane1 protein molecular weight ladder, lane 2 extract before induction NC, lane 3 extract after induction with same conditions (*), except the period of induction, thus the used was 16-20h, lane 4 extract after induction with same conditions (*), except the period of induction, thus the used was 3-4, lanes 5&6 extracts after induction with same conditions (*). &Lane 7 PC (*E. coli* BL21 transformed with (pRSET-sfGFP) after induction at 16 °C overnight).

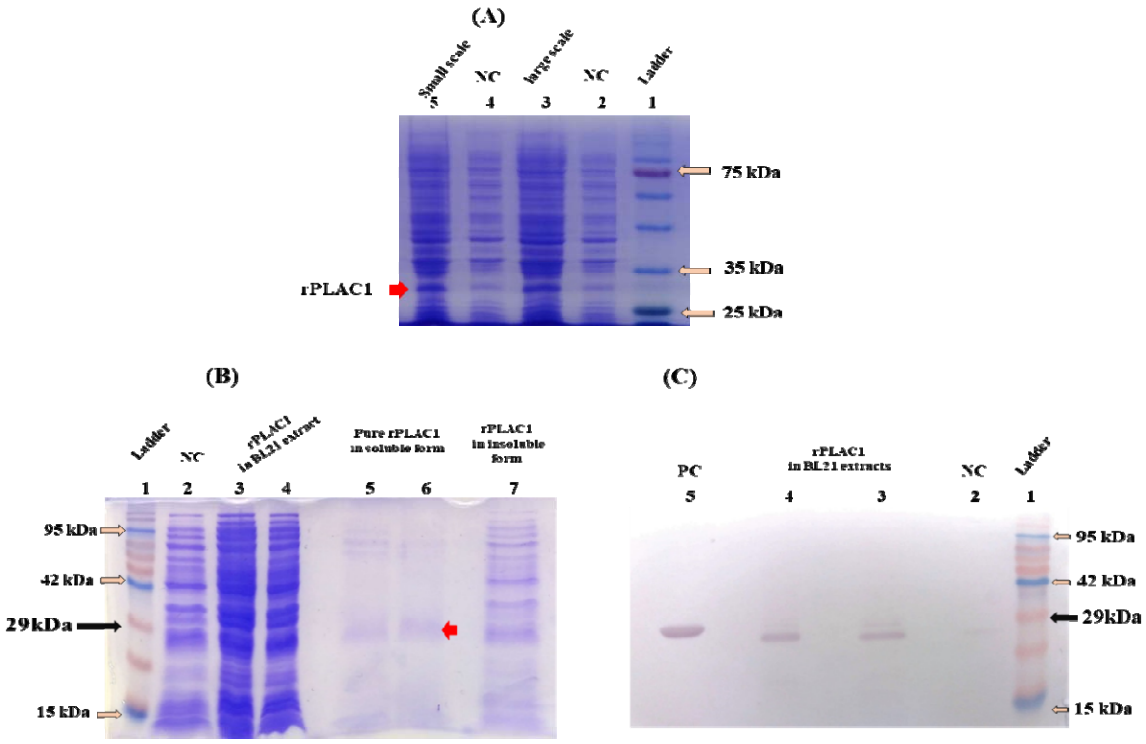

Figure 4.SDS-PAGE &WB analysis of *E. coli* BL21 transformed with (pRSET-ORFplac1) extracts in small and large scales before and after induction with optimum conditions (0.5mM IPTG in O.D= 0.3-0.5 at 22°C for 7-8h) and purification**. (A)** SDS-PAGE analysis for large &small scales extracts. From the right; lane 1 protein molecular weight ladder, lanes 2 &4 NC (extract before induction), lane 3 extract after expression on a large scale, &lane 5 extract after expression on a small scale. **(B)**SDS-PAGE analysis for extracts before and after induction with Optimum condition (*) and purification. From the left; lane1 protein molecular weight Ladder, lane 2 NC (extract before expression), lanes 3 &4 extract after expression and before purification, lanes 5 &6 extracts after expression and purification (soluble form) without using urea, &lane 7 extract after expression (insoluble form). **(C)** WB analysis; From the right; lane 1 protein molecular weight ladder, lane 2 NC (extract before induction), lanes 3 &4 extracts after expression in optimum conditions (0.5mM IPTG in O.D= 0.3-0.5 at 22°C for 7-8h), &lane 5 PC (*E. coli* BL21 transformed with (pRSET-sfGFP) after induction in 16 °C for overnight).

4. Discussion

PLAC1 is an important member of the CTAs family, serves as a prognostic and diagnostic cancer biomarker, and is a promising therapeutic target for many cancers (Cocchia et al., 2000; Nejadmoghaddam et al., 2017; Mahmoudian et al., 2019). *E.coli* BL21 is a strong expression system that presents a high productivity yield in a short time (Gopal and Kumar, 2013; Kaur et al., 2018). However, producing rPLAC1 in *E.coli* BL21 strain has faced many obstacles, especially no expression at all or accumulation of rPLAC1 in IBs needing urea or other denaturing agents for purification, which denatures its structure and alters its function, despite employing many strategies (Ghods et al., 2014b; Nazari et al., 2017; Nejadmoghaddam et al., 2017; Mahmoudian et al., 2019). Since there are no universal strategies for protein production as each specific protein needs its specific strategies for proper production (Gopal and Kumar, 2013; Kaur et al., 2018), hence it is suggested to employ efficient strategies to produce rPLAC1 in soluble form without compromising the correct form. In our study, we have amplified ORFplac1 without ss. Because it is a cleavable domain and its only function is to direct protein through secretory pathway in eukaryotes (Roldán, 2012). Besides, recent studies in prokaryotes proved that removing of ss increased the stability of RPs without changing its biochemical characteristics (Gopal and Kumar, 2013). We also concentrated on optimizing the conditions that affect rPLAC1 expression in a soluble form depending on recent studies (Gopal and Kumar, 2013; Kaur et al., 2018). First, we induced the *E. coli* BL21 strain at different induction temperatures and for different induction periods (37 °C/3-4h, 22 °C/7-8h, 16 °C/16-20) in the first log phase ($O.D_{600nm}$=0.3-0.5) with 0.5 mM IPTG (phase-1). Our results showed that low induction temperature, about 22 °C, with an induction period of about 7-8h are optimal conditions for soluble expression. However, hydrophobic interactions are the main cause of IBs formation and they decreased when the temperature is lowered. So the lower temperature, the less amount of IBs, and the more soluble form of protein (Gopal and Kumar, 2013; Kaur et al., 2018). Moreover, both short and too long induction periods are inefficient for the expression of RPs as bacteria need a period to adapt to culture conditions and their metabolic activity is decreased, respectively (Gopal and Kumar, 2013; Kaur et al., 2018). Second, we induced BL21 in gradient O.Ds at the early-log phase (about $O.D_{600nm}$=0.3-0.9) (phase-2). We found that the optimum phase for induction bacteria is the first log phase ($O.D_{600nm}$=0.3 -0.5) as it is reported that bacterial cultures

that are induced at the early-log phase presented a low endogenous protein production of about 30%, and high exogenous RPs, which leads to efficient protein purification (Gopal and Kumar, 2013; Kaur et al., 2018). whereas the induction at the late-log phase decreased the RPs due to the high density of bacteria that reduced its metabolic efficacy (Gopal and Kumar, 2013; Kaur et al., 2018). Our results also revealed that using a low concentration of IPTG (about 0.5 mM IPTG) is the optimum. The high amount of inducer leads to the accumulation of RPs in IBs because the rate of protein synthesis overwhelms the folding machinery whereas lower concentration leads to inefficient induction (Gopal and Kumar, 2013; Kaur et al., 2018). In this study, we obtained pRSET–ORFplac1 construction without any mutation or frame-shift, and achieved the expression of the full length of rPLAC1 in soluble form in *E. coli* BL21 strain, as ~29 kDa molecular weight after separating and detecting rPLAC1 using 15% SDS-PAGE and WB, respectively. Our results agree with different studies reporting the molecular weights of rPLAC1 around 27 kDa (Nejadmoghaddam et al., 2017), 27.2 kDa (Nazari et al., 2017), and 28-30 kDa (Fant et al., 2007). Nevertheless, some reports obtained different molecular weights such as 25kDa (Mahmoudian et al., 2020), 26kDa (Koslowski et al., 2007; Dong et al., 2008), and 35kDa (Silva et al., 2007), which can be attributed to several factors like PTM and existence of different isoforms (Mahmoudian et al., 2019). Besides, the length of PLAC1 (truncated, full length, or fused with tags) (Silva et al., 2007; Nazari et al., 2017; Mahmoudian et al., 2020). Some studies used the His tag (Fant et al., 2007; Dong et al., 2008; Nazari et al., 2017; Nejadmoghaddam et al., 2017; Mahmoudian et al., 2020), and others used Enhanced-GFP (EGFP) (Mahmoudian et al., 2020) and Glutathione S-transferase (GST) (Silva et al., 2007). In addition, some of them produced PLAC1 without ss (Fant et al., 2007; Nazari et al., 2017; Nejadmoghaddam et al., 2017), and others expressed it with ss (Dong et al., 2008; Mahmoudian et al., 2020). Even some reporters used other *E. coli* strains like *E. coli* M13 (Dong et al., 2008), or eukaryotic expression systems like CHO-K1 cells (Mahmoudian et al., 2020)and baculovirus expression systems with Sf9 cells (Fant et al., 2007) (Table3). Here, we produced a full length rPLAC1 in soluble form as half amount of produced protein with 12.44 µg of purePLAC1/ml of bacteria culture, and ~10mg in 1L of bacteria culture, after purifying with IMAC and without using denaturing agents. However, we have not overcome the IBs completely as the half amount of protein in extracts was insoluble form, which maybe attributed to a lack of chaperons, codon usage, and a reducing state of bacterial cytoplasm (Baneyx, 1999; Nazari et al., 2017). In comparison with other studies, neither the soluble truncated nor the full length rPLAC1 was produced using BL21 as an expression system, except in one study, which produced rPLAC1 fused with thioredoxin (Trx) tag (Nazari et al., 2017) (Table3). The full length of rPLAC1 was expressed as the insoluble form as IBs in all strains, and the soluble form was only obtained after PLAC1 had been expressed with a large size fusion tag like Trx (Nazari et al., 2017). Our rPLAC1 had good purity; nevertheless, some of the non-specific bands were still obtained, which may be attributed to the tendency of some *E. coli* endogenous proteins to strongly bind to metal ions like Nickel or the presence of superficial groups of His residues (Bolanos-Garcia and Davies, 2006). Purification of full length rPLAC1 in our study, and using 5% of deoxycholic acid for purification of fused rPLAC1 with Trx tag in recent studies. We successfully optimized expression conditions for the production of the full length of rPLAC1 in soluble form, using *E. coli* BL21.

Table 3. Comparison between different expression systems that have been used for the production of Human rPLAC1. HCC; Human hepatocellular carcinoma, GST; Glutathione-s-transferase, SA of TFR1; signal anchor of transferrin receptor 1, NI; no information has been told in the article.

Reference studies	Expression in an insoluble form	Expression in soluble form	Urea Or any denaturing agent	Purification technique	ss	tags	Cultivation conditions	Protein concentration	Protein KDa	Protein aa	Inserted gene Bp	Expression vector	Host strain	Host systems
(Nazari et al., 2017)	-	Expression only in Origami TM and Shuffle T7 with no expression in BL21 at all	2M urea & 12pH for denaturing for purification of truncated or full lengthPLAC1 Or 5% of deoxycholic (DOC) acid for purification of Trx-PLAC1	IMAC & gel filtration chromatography with 95% purity technical estimated	-	6X HIS tag and Trx tag at N-terminal in protein level and 5´end in gene level	The optimum condition for T-plac1 is Induction at $O.D_{600nm}$=0.6-0.9 with 0.1, 1 mM IPTG and induction temperatur15 °C for 24 hours	10mg/L Using Far-UV CD spectrum	22KDa & 18KDa	117-212aa	Truncated-plac1 (T-plac1) 351-636pb	p- cold vector	OrigamiTM (DE3)	Prokaryotes
													Shuffle T7 (DE3)	
	All strains express as IBs with the high amount in OrigamiTM and Rosetta2with no observed expression in BL21 using WB	No expression at all strains including BL21						35mg/L Using Far-UV CD spectrum	27.2KDa	23-212aa	Full length-plac1 (F-plac1) 69-636bp		Rosetta2 (DE3)	
	Little amount	The main part in all strains with the high amount in Rosetta2 with noobserved expression in BL21 in WB					Induction at $O.D_{600nm}$=0.6-0.9 Witno observedM IPTG and induction temperature 22 °C for 12 hours	25mg/L Using Far-UV CD spectrum	45KDa	23-212aa Fused with trx tag	Fused plac1 with trx (Trx-plac1)	pET32-a	Rosettagami (DE3) pLysS	E.coli
													BL12 (DE3)	
Our study	half of the total amount	There is Obvious expression in BL21 with an amount of about half of total rPLAC1 in the lysate	urea or any denaturing agent hasn't been used at all	Manually IMAC using Nickel-charged NTA column with about 37.76% purity	-	6X HIS tag at N-terminal in protein level and 5´end in gene level	Induction at $O.D_{600nm}$=**0.3-0.5** with **0.5** mM IPTG and induction temperature 22 °C for **7-8** hours	10mg/L Using spectrophotometer with Bradford method	~29KDa	21-212aa	ORFplac1 63-636bp 573bp from Human genomic DNA	pRSET	BL12DE3)	
(Nejadmoghaddam et al., 2017)	+	-	2M urea & 12pH for denaturing for purification	Same(Nazari et al., 2017)					~27 kDa	23-212aa	Full length-plac1 (F-plac1) 69-636bp	Same (Nazari et al., 2017)	Same(Nazari et al., 2017)	
(Dong et al., 2008)		NI		IMAC using Nickel-charged NTA agarose risen	+	6X HIS tag	Induction at temperature 37 °C for **5** hours	NI	26KDa	212aa	196bp from Human HCC cDNA	pQE30 vector	M13	
(Silva et al., 2007)		NI		IMAC with Glutathione-sepharose Beads	-	GST tag in C-terminal	NI		35KDa	125-212aa Fused with GST tag	The coding sequence of PLAC1 125-212aa	pGEX-4T	E. coli strain	
(Fant et al., 2007)		NI		IMAC using Nickel-charged NTA	-	6X HIS tag at N-terminal	Induction for **7-8** hours	NI	28-30KDa	23-212aa	PLAC1 Coding sequence	pAcGP67 transfer vector	Baculovirus with Sf9 cells	Eukaryotes
(Mahmoudian et al., 2020)	Cytoplasmic protein			NI	+	6X HIS tag at C-terminal	Induction at temperature 37 °C for **24-48** hours	NI	25KDa	1-212aa	mRNA 291bp converted to cDNA	LeGo-iG2 vector	CHO-K1	
									39KDa	50-212aa With SA of TFR1	The coding sequence of PLAC1 50-212aa With SA of TFR1	pIRES2-EGFP vector		

5. Conclusion

PLAC1 is one of the important CTAs, which serve as prognostic, diagnostic, and immunotherapeutic targets for many cancers. In our study, we have partially optimized the production conditions of rPLAC1 in a simple and cost effectively method. We found that the optimum conditions to produce the full length of rPLAC1 are induction of *E.coli* BL21 at the early-log phase of growth ($O.D_{600nm}$=0.3-0.5) with 0.5 mM IPTG and induction temperature of 22 °C for 7-8 hours. We obtained a soluble form of rPLAC1 in a concentration equal to 12.44 µg of purePLAC1/ml bacteria culture. Our team tries to produce ScFv antibodies-library against this rPLAC1 for diagnosing prostate cancer later.

Acknowledgments

The author thanks Damascus University for supporting this work, the Department of Molecular Biology and Biotechnology of Atomic Energy Commission in Syria for providing molecular tools, the scientific group of Dr. Chadi Soukkarieh, Dr. Ghmkin Hassan, Dr. Abdul-Qader Abbady, Dr. Tomadher Siam and Dr. Radwan Mohammad for their kind and continuous support through this work.

References

Al-Homsi L, Al-Assad J, Kweider M, Al-Okla S and Abbady A. 2012. Construction of pRSET-sfGFP plasmid for fusion-protein expression, purification and detection. *Jordan J Biol Sci.* **5(4):** 279-288.

Al-jaghasi A, Abbady A-Q, Al-Khatib S and Soukkarieh C. 2021. Cloning, expression and purification of Leishmania major PSA-sfGFP fusion protein. *Jordan J Biol Sci.* **14(2)**.

Baneyx F. 1999. Recombinant protein expression in Escherichia coli. *Curr Opin Biotechnol.* **10(5):** 411-421.

Bolanos-Garcia V M and Davies O R. 2006. Structural analysis and classification of native proteins from E. coli commonly co-purified by immobilised metal affinity chromatography. *Biochim Biophys Acta.* **1760(9):** 1304-1313.

Bradford M M. 1976. A rapid and sensitive method for the quantitation of microgram quantities of protein utilizing the principle of protein-dye binding. *Anal Biochem.* **72(1-2):** 248-254.

Caballero O L and Chen Y-T. 2012. Cancer/testis antigens: potential targets for immunotherapy. **Innate Immune Regulation and Cancer Immunotherapy**. Springer, pp. 347-369.

Chang W-L, Wang H, Cui L, Peng N-N, Fan X, Xue L-Q and Yang Q. 2016. PLAC1 is involved in human trophoblast syncytialization. *Reprod Biol.* **16(3):** 218-224.

Chen R, Sheng C, Ma R, Zhang L, Yang L and Chen Y. 2021. PLAC1 is an independent predictor of poor survival, and promotes cell proliferation and invasion in cervical cancer. *Mol Med Rep.* **24(5):** 1-12.

Chen Y, Moradin A, Schlessinger D and Nagaraja R. 2011. RXRα and LXR activate two promoters in placenta-and tumor-specific expression of PLAC1. *Placenta.* **32(11):** 877-884.

Cocchia M, Huber R, Pantano S, Chen E Y, Ma P, Forabosco A, Ko M S and Schlessinger D. 2000. PLAC1, an Xq26 gene with placenta-specific expression. *Genomics.* **68(3):** 305-312.

Devor E J. 2014. Placenta-specific protein 1 is conserved throughout the Placentalia under purifying selection. *Sci World J.* **2014**.

Devor E J. 2016. Placenta-specific protein 1 (PLAC1) is a unique onco-fetal-placental protein and an underappreciated therapeutic target in cancer. *Integr Cancer Sci Therap.* **3:** 479-483.

Devor E J, Gonzalez-Bosquet J, Warrier A, Reyes H D, Ibik N V, Schickling B M, Newtson A, Goodheart M J and Leslie K K. 2017. p53 mutation status is a primary determinant of placenta-specific protein 1 expression in serous ovarian cancers. *Int J Oncol.* **50(5):** 1721-1728.

Devor E J, Reyes H D, Santillan D A, Santillan M K, Onukwugha C, Goodheart M J and Leslie K K. 2014. Placenta-specific protein 1: a potential key to many oncofetal-placental OB/GYN research questions. *Obstet Gynecol Int.* **2014**.

Dong X Y, Peng J R, Ye Y J, Chen H S, Zhang L J, Pang X W, Li Y, Zhang Y, Wang S and Fant M E. 2008. Plac1 is a tumor-specific antigen capable of eliciting spontaneous antibody responses in human cancer patients. *Int J Cancer.* **122(9):** 2038-2043.

Fant M, Barerra-Saldana H, Dubinsky W, Poindexter B and Bick R. 2007. The PLAC1 protein localizes to membranous compartments in the apical region of the syncytiotrophoblast. *Mol Reprod Dev.* **74(7):** 922-929.

Fant M, Farina A, Nagaraja R and Schlessinger D. 2010. PLAC1 (Placenta-specific 1): a novel, X-linked gene with roles in reproductive and cancer biology. *Prenat Diagn.* **30(6):** 497-502.

Frenzel A, Hust M and Schirrmann T. 2013. Expression of recombinant antibodies. *Front Immunol.* **4:** 217.

Ghods R, Ghahremani M-H, Madjd Z, Asgari M, Abolhasani M, Tavasoli S, Mahmoudi A-R, Darzi M, Pasalar P and Jeddi-Tehrani M. 2014a. High placenta-specific 1/low prostate-specific antigen expression pattern in high-grade prostate adenocarcinoma. *Cancer Immunol Immunther.* **63(12):** 1319-1327.

Ghods R, Ghahremani M H, Darzi M, Mahmoudi A R, Yeganeh O, Bayat A A, Pasalar P, Jeddi-Tehrani M and Zarnani A H. 2014b. Immunohistochemical characterization of novel murine monoclonal antibodies against human placenta-specific 1. *Biotechnol Appl Biochem.* **61(3):** 363-369.

Gopal G J and Kumar A. 2013. Strategies for the production of recombinant protein in Escherichia coli. *protein J.* **32(6):** 419-425.

Jackman S M, Kong X and Fant M E. 2012. Plac1 (placenta-specific 1) is essential for normal placental and embryonic development. *Mol Reprod Dev.* **79(8):** 564-572.

Kaur J, Kumar A and Kaur J. 2018. Strategies for optimization of heterologous protein expression in E. coli: Roadblocks and reinforcements. *Int J Biol Macromol.* **106:** 803-822.

Koslowski M, Sahin U, Mitnacht-Kraus R, Seitz G, Huber C and Türeci Ö. 2007. A placenta-specific gene ectopically activated in many human cancers is essentially involved in malignant cell processes. *Cancer Res.* **67(19):** 9528-9534.

Li Y, Chu J, Li J, Feng W, Yang F, Wang Y, Zhang Y, Sun C, Yang M and Vasilatos S N. 2018. Cancer/testis antigen-Plac1 promotes invasion and metastasis of breast cancer through Furin/NICD/PTEN signaling pathway. *Mol Oncol.* **12(8):** 1233-1248.

Lin C, Qian P, Zhang Y, Liu Z, Dai K and Sun D. 2021. Plac1 promotes nasopharyngeal carcinoma cells proliferation, migration and invasion via Furin/NICD/PTEN pathway. *Tissue Cell.* **69:** 101480.

Liu D, Shi K, Fu M and Chen F. 2021. Placenta-specific protein 1 promotes cell proliferation via the AKT/GSK-3β/cyclin D1 signaling pathway in gastric cancer. *IUBMB life.* **73(9):** 1131-1141.

Liu F, Shen D, Kang X, Zhang C and Song Q. 2015. New tumour antigen PLAC1/CP1, a potentially useful prognostic marker and

immunotherapy target for gastric adenocarcinoma. *J Clin Pathol.* **68(11):** 913-916.

Liu F, Zhang H, Shen D, Wang S, Ye Y, Chen H, Pang X, Song Q and He P. 2014. Identification of two new HLA-A* 0201-restricted cytotoxic T lymphocyte epitopes from colorectal carcinoma-associated antigen PLAC1/CP1. *J Gastroenterol.* **49(3):** 419-426.

Liu F F, Dong X Y, Pang X W, Xing Q, Wang H C, Zhang H G, Li Y, Yin Y H, Fant M and Ye Y J. 2008. The specific immune response to tumor antigen CP1 and its correlation with improved survival in colon cancer patients. *Gastroenterology.* **134(4):** 998-1006.

Ma J, Li L, Du J, Pan C, Zhang C and Chen Y. 2020. Placenta-Specific Protein 1 Enhances Liver Metastatic Potential and is Associated with the PI3K/AKT/NF-κB Signaling Pathway in Colorectal Cancer. *Eur J Cancer Prev.* **30(3):** 220.

Mahmoudi A-R, Ghods R, Rakhshan A, Madjd Z, Bolouri M-R, Mahmoudian J, Rahdan S, Shokri M-R, Dorafshan S and Shekarabi M. 2020. Discovery of a potential biomarker for immunotherapy of melanoma: PLAC1 as an emerging target. *Immunopharmacol Immunotoxicol.* **42(6):** 604-613.

Mahmoudian J, Ghods R, Nazari M, Jeddi-Tehrani M, Ghahremani M H, Ghaffari-Tabrizi-Wizsy N, Ostad S N and Zarnani A-H. 2019. PLAC1: biology and potential application in cancer immunotherapy. *Cancer Immunol Immunother.* **68(7):** 1-20.

Mahmoudian J, Nazari M, Ghods R, Jeddi-Tehrani M, Ostad S N, Ghahremani M H, Vafaei S, Amiri M M and Zarnani A-H. 2020. Expression of human placenta-specific 1 (PLAC1) in CHO-K1 cells. *Avicenna J Med Biotechnol.* **12(1):** 24.

Nazari M, Zarnani A-H, Ghods R, Emamzadeh R, Najafzadeh S, Minai-Tehrani A, Mahmoudian J, Yousefi M, Vafaei S and Massahi S. 2017. Optimized protocol for soluble prokaryotic expression, purification and structural analysis of human placenta specific-1 (PLAC1). *Protein Expr Purif.* **133:** 139-151.

Nejadmoghaddam M-R, Zarnani A-H, Ghahremanzadeh R, Ghods R, Mahmoudian J, Yousefi M, Nazari M, Ghahremani M H, Abolhasani M and Anissian A. 2017. Placenta-specific1 (PLAC1) is a potential target for antibody-drug conjugate-based prostate cancer immunotherapy. *Sci Rep.* **7(1):** 1-13.

Pham P V. 2018. Medical biotechnology: techniques and applications. **Omics Technologies and Bio-Engineering**. Elsevier, Academic Press, pp. 449-469.

Puetz J and Wurm F M. 2019. Recombinant proteins for industrial versus pharmaceutical purposes: a review of process and pricing. *Processes.* **7(8):** 476.

Ren Y, Lv Y, Li T and Jiang Q. 2020. High expression of PLAC1 in colon cancer as a predictor of poor prognosis: A study based on TCGA data. *Gene.* **763:** 145072.

Roldán D B. 2012. F**unctional characterization of the placenta specific protein PLAC1 and its use for cancer immunotherapy**. Doctoral dissertation, Universitätsbibliothek Mainz, Mainz, Germany.

Roldán D B, Grimmler M, Hartmann C, Hubich-Rau S, Beißert T, Paret C, Cagna G, Rohde C, Wöll S and Koslowski M. 2020. PLAC1 is essential for FGF7/FGFRIIIb-induced Akt-mediated cancer cell proliferation. *Oncotarget.* **11(20):** 1862.

Rosano G L and Ceccarelli E A. 2014. Recombinant protein expression in Escherichia coli: advances and challenges. *Front Microbiol.* **5:** 172.

Schlegel S, Hjelm A, Baumgarten T, Vikström D and de Gier J-W. 2014. Bacterial-based membrane protein production. *Biochim Biophys Acta.* **1843(8):** 1739-1749.

Silva W A, Gnjatic S, Ritter E, Chua R, Cohen T, Hsu M, Jungbluth A A, Altorki N K, Chen Y-T and Old L J. 2007. PLAC1, a trophoblast-specific cell surface protein, is expressed in a range of human tumors and elicits spontaneous antibody responses. *Cancer Immun.* **7(1)**.

Wagner M. 2014. **Molecular and functional characterization of the candidate tumor antigens placenta specific 1 and claudin 6**. Johannes Gutenberg-Universität, Mainz, Germany.

Wu Y, Lin X, Di X, Chen Y, Zhao H and Wang X. 2017. Oncogenic function of Plac1 on the proliferation and metastasis in hepatocellular carcinoma cells Corrigendum in/10.3892/or. 2019.6955. *Oncol Rep.* **37(1):** 465-473.

Yang L, Zha T-Q, He X, Chen L, Zhu Q, Wu W-B, Nie F-Q, Wang Q, Zang C-S and Zhang M-L. 2018. Placenta-specific protein 1 promotes cell proliferation and invasion in non-small cell lung cancer. *Oncol Rep.* **39(1):** 53-60.

Yin Y, Zhu X, Huang S, Zheng J, Zhang M, Kong W, Chen Q, Zhang Y, Chen X and Lin K. 2017. Expression and clinical significance of placenta-specific 1 in pancreatic ductal adenocarcinoma. *Tumor Biol.* **39(6):** 1010428317699131.

Yu Y, Xu Y, Cai W and Zuo W. 2021. Expression level of PLAC1 in osteosarcoma patients and its regulatory effect on the development of osteosarcoma. *J BUON.* **26(2):** 592-598.

JJBS

Volume 15, Number 5, December 2022
ISSN 1995-6673
Pages 797 – 804
https://doi.org/10.54319/jjbs/150508

Jordan Journal of Biological Sciences

Pharmacognostical Evaluation and *In vitro* Antioxidant and Anti-inflammatory Activity of *Exacum bicolor* Roxb.

Rajisha K[1], Jennifer Fernandes[2,*]

[1]*Department of Pharmacognosy, P.A. College of Pharmacy, Rajiv Gandhi University of Health Sciences, Kairangala village, Mangalore – 574199;* [2]*Department of Pharmaceutical Chemistry, NGSM Institute of Pharmaceutical Sciences, Nitte (Deemed to be University), Paneer, Deralakatte, Mangalore – 575018*

Received: April 1, 2022; Revised: August 1, 2022; Accepted: September 12, 2022

Abstract

The primary goal of this research was to investigate the morphological and microscopical characteristics of various parts of *Exacum bicolor* Roxb, as well as the antioxidant and anti-inflammatory activity of different extracts. The morphology and microscopy of leaves, stem, flower and root were studied, along with powder characteristics of the whole plant. The whole plant was powdered and extracted using various solvents such as chloroform, acetone methanol and water. Antioxidant activity of various extracts of the plant was determined by DPPH method and nitric oxide scavenging assay method. The protein denaturation and membrane stabilization methods were used to assess anti-inflammatory activity. Microscopic examination revealed that it is a dorsiventral leaf with covering trichomes. The histology of roots showed the phloem encircles the xylem, and the xylem with distinct vessels and lignified xylem parenchyma. The powder microscopical characteristics are stomata, epidermal cells, trichomes, xylem vessels, xylem fibers, *etc*. These features of the plant can be used as a tool for the development of a monograph. The chloroform extract showed a better antioxidant activity compared with other extracts, while methanolic extract showed good anti-inflammatory activity in comparison between the extracts.

Keywords: *Exacum bicolor* Roxb., morphology, microscopy, antioxidant, anti-inflammatory.

1. Introduction

Plant anatomy is still a valuable tool for resolving perplexing issues in botanical research at the national level. Anyone who works with plants has to understand plant anatomy. When publishing experimental data, many researchers thoroughly neglect the need to understand anatomy (Cutler et al., 2008). Plant anatomy is traditionally considered the microscopic study of plant tissues and cells, and the invention of light, and electron microscopes has greatly aided our understanding of the structure (Crang *et al*., 2018).

Exacum bicolor Roxb. (E.bicolor) is an angiosperm in the *Gentianaceae* family which is a family of flowering plants with 84 genera and 1688 species (Rajisha and Jennifer, 2020a).*E.bicolor Roxb.* is an erect herb that grows in the plains from July to November and in the high mountains from July to January. The whole plant has medicinal properties such as tonic, antipyretic, and promoting appetite. This plant can also be used to produce dye. People use this as traditional medicine in case of elevated glucose levels and skin problems due to its bitter taste. Traditional Kerala practitioners recommend washing the eyes with a decoction of the entire plant. However, due to its limited distribution and accessibility concerns, it is not commonly used. (Sreelatha *et al*., 2007; Rajisha and Jennifer, 2020b).

The presence of specific bioactive components in certain amounts is the main reason for the therapeutic activity of plants. Such issues are often resolved by fixing exact specifications about the pharmacognostic characteristics of plant drugs. Pharmacognostic evaluations drive support in the validation of a plant and guarantee plant drug efficacy and safety.

Chemical composition information on the genus Exacum is limited. Exacum species have enormous pharmacological potential, which has been demonstrated by their widespread use in conventional medicine and has been backed by ethnobotanical research and investigations into particular biological activity. Due to overexploitation, many Exacum species are endemic and frequently in danger of extinction. Micropropagation can assist defend those species and help introduce them to commercial floriculture. (Skrzypczak-Pietraszek E, 2015).

Although the plant has a traditional medicinal value, data on its quality control profile is still unavailable. This study aims to develop a scientific standardization monograph for *E.bicolor* Roxb. and the antioxidant and anti-inflammatory activity of the different plant extracts. This information helps to identify adulterants and to ensure the quality of herbs.

* Corresponding author. e-mail: fernandesj@nitte.edu.in.

2. Methodology

2.1. Plant material

In the month of August-November, plant *E.bicolor* Roxb. was collected from regions of Kerala (Kannur and Kasaragod). It was identified and authenticated taxonomically by Dr. K. Gopal Krishna Bhat, Professor of Botany(Rtd.). A specimen voucher (17PH001R) was preserved in the Department of Pharmacognosy of Nitte Gulabi Shetty Institute of Pharmaceutical Sciences, Mangalore, Karnataka, India.The whole plant was collected, cleaned, and further utilized for the morphological and microscopical studies of leaf, stem, and root. The remaining plants were shade-dried, powdered and used for powder microscopic analysis.

2.2. Extraction of plant material

Prior to Soxhlet extraction, the powder was defatted with petroleum ether, weighed and then placed in the Soxhlet apparatus. The extraction was performed using the method developed by KanikaDulta*et.al.* with slight modification. The Soxhlet extraction was carried out with chloroform, acetone, and methanol by successive solvent Soxhlet extraction (KanikaDulta*et.al,* 2021). The marc, after methanol extraction, was mixed with water and boiled in a water bath. The extracts were filtered, the solvents were distilled, and the pure extract was obtained.

2.3. Morphological studies

The morphological evaluation of the whole plant of *E.bicolor* Roxb. was carried out. Various organoleptic features of different parts of plant like leaves, stem, flowers and fruits (colour, taste, odour, shape, size) were evaluated.

2.4. Microscopical studies

Suitable sections of plant part (root, stem and root) were taken for anatomical evaluation. By using a microtome, transverse sections of leaf, stem and root were taken. The proper sections with a thickness of 10-15 µm were selected and warmed with chloral hydrate solution, which acts as a clearing agent. These clear sections were further stained with phloroglucinol and with 1-2 drops of conc. HCl. After two minutes, these sections were transferred to glass slides and added a drop of glycerine. The transverse sections were enclosed with the help ofa cover slip and observed under a microscope (Biovis IP2000 digital microscope) from both sides (Kandalwal, 2005; Ghaid J.Al-Rabadi, 2014).

2.5. Powder microscopical studies

The whole plant was collected and washed thoroughly with water to remove soil and other adhesive material for powder analysis. The plant was dried under shade, and this was followed by powdering the whole plant; the obtained powder was passed through sieve no. 60. Minimal amount of the powder was boiled with chloral hydrate followed by staining it with conc. HCl (1:1) and phloroglucinol solution to find various kinds of tissues proving authenticity. To find calcium oxalate crystals, one more sample was mounted in water; and to observe starch grains, one sample was mounted in an iodine solution. (Kandalwal,2005;Haeborne,1973).

2.6. Determination of leaf constant

Fully developed leaves were used to quantify the stomatal density and stomatal index. The lower epidermis was pulled off from the middle section of the leaf. In total, 5 distinct leaves were used to calculate the stomatal density. Along with stomatal density, the epidermal layer is also used to determine the stomatal index. The stomatal index was calculated by using the following formula

$SI = S / E + S \times 100$

Where,

SI -Stomatal index

S-Number of stomata cells per unit area

E -number of epidermal cells per unit area.

The vein islet number as well as vein termination number are determined by using the leaves lamina (Paul V*et.al.*2017).

2.7. In vitro biological assays

2.7.1. Antioxidant activity

2.7.1.1. DPPH scavenging activity

A chemical 2, 2-diphenyl-1-picrylhydrazyl (DPPH)since spare electron is delocalized over a entire molecule, preventing dimerization; it is characterized as a persistent free radical as is a case with most other free radicals. The deep violet color is caused by electron delocalization, which is characterized by a 517 nm absorption band in ethanol (Alam *et. al*.,2013).

1 ml of 0.3 mM alcoholic solution of DPPH was added to 2.5 ml of the samples with varying concentrations (6.25-100µg/ml) of *E.bicolor* Roxb. and standard ascorbic acid. Ascorbic acid is a very good antioxidant; it protects the cellular component from free radical damage. After 30 minutes of reaction at room temperature in the dark, the absorbance was measured at 517 nm(Dahiru Daniel and Thagriki Dluya, 2016). The percentage of DPPH radical inhibition was estimated by comparing the test results to those of the control group using the formula below:

Percentage of inhibition = $[(A_0 – A_1) / A_0] \times 100$

Where A_0 = Absorbance of the control,A_1 = Absorbance of the sample/ standard(Muntana and Prasong, 2010).

2.7.1.2. Nitric Oxide Scavenging Assay

0.5 mL phosphate buffer saline (pH 7.4) was used to dilute 2 mL sodium nitroprusside (10 mM) and was treated with 0.5 mL sample at different concentrations (6.25-100µg/ml) and incubated for 2h 30min. 0.5 mL of the reaction mixture was pipetted out after incubation.1 mL of sulfanilic acid was added to it. Further, it was allowed to stand for another 5 minutes to complete diazotization. After that, 1ml of 1-naphthylamine was added, stirred, and set aside for 30 minutes. In diffused light, a pink chromophore was generated. A control was also made with the same solutions without the sample drug or standard drug. The solution's absorbance was measured at 546nm in comparison to a blank solution. Calculation of percentage inhibition of nitric radical was carried out with the formula:

Percentage of inhibition = $[(A_0 – A_1) / A_0] \times 100$

Where A_0 = Absorbance of the control, A_1 = Absorbance of the plant extract/ standard (Marcocci L *et al*., 1994).

2.7.2. Anti-inflammatory activity of whole plant extracts

2.7.2.1. Inhibition of protein denaturation method

The reaction mixture (0.5 ml) comprised of 0.05ml plant extracts (acetone, chloroform, aqueous and methanol) and 0.45 ml of bovine serum albumin (5% aqueous solution) and pH was adjusted to 6.3 with the help of 1N HCl. For 20 min samples were incubated at 37^0C followed by heating it for 3min at 57^0C. Diclofenac was used as a standard drug (6.25-100µg/ml). Diclofenac is a nonsteroidal anti-inflammatory drug, and it inhibits COX-2 enzyme. After cooling, the samples, 2.5ml phosphate buffer saline (pH 6.3) were added to each tube. At 660nm, absorbance was measured. In control testing, 0.05 ml water was used instead of extracts, whereas the product control was devoid of bovine serum albumin. The proportion of inhibition of denaturation of protein was estimated (Shravan,2011) as:

Percentage Inhibition = (Abs Control – Abs Sample)/Abs Control× 100

2.7.2.2. Membrane stabilization method

Sterilized Alsever solution 10ml (0.42% sodium chloride in water, 0.05% citric acid, 0.8% sodium citrate and 2% dextrose) was blended along with equivalent amount of fresh whole human blood. Isosaline was used to wash the packed cells three times after being centrifuged at 3000 rpm for 10 minutes (0.85 percent pH 7.2). Blood volume was measured and reconstituted in suspension of isosaline (10% v/v).

Heat induced hemolysis: Human Red Blood Cell membrane stabilization by membrane lysis induced by hypotonicity is the principle involved. Phosphate buffer 1ml (pH 7.4, 0.15M), HRBC suspension 0.5ml (10% v/v) along with 0.5ml test solution (6.25-100µg/ml) and hyposaline 2ml (0.36%) constituted assay mixture. standard drug used was diclofenac (6.25-100µg/ml). All reaction mixture in the centrifugation tubes were kept at 56°C for 30 min in water bath. After incubation, all tubes were placed under tap water for cooling. At 2500 rpm, centrifugation of reaction mixture was carried out for 5minutes, and at 560nm absorbance of supernatants was measured. Experiment was repeated thrice for all test samples. Percentage membrane stabilization activity was calculated by the formula as shown below (Bag *et al*.,2013).

% Hemolysis = (Absorbance of test/ Absorbance of control) x 100

%Protection = 100 – [(Absorbance of test/ Absorbance of control) x100

2.8. Statistical analysis

All the data were significantly evaluated with graph prism pad 6. the Hypothesis testing methods include ANOVA, P values of less than 0.05 were considered to indicate statistical significance. All the results are reported as the mean ± the standard error of the mean(SEM).

3. Results

3.1. Morphological studies

The morphological evaluation of *E.bicolor* Roxb. was carried out and the observations are given in figure:1. The *E.bicolor* Roxb. has a characteristic odour and bitter taste. In dry grasslands, the plant grows to a height of 25-80cm, while in upper grasslands, it grows to a height of 40-120cm. Stems quadrangular, branched basally and apically, winged (wings 0.2–0.4 cm broad), hard at the base when mature, nodes and internodes are present. Leaves are dark green, sessile-subsessile, glossy, and have broadly elliptic-ovate, spathulate or linear-lanceolate or broadly oblong lamina, 4–16 × 1.5–2.5 cm in size, 3–5 nerved at base, cuneate at base, acute apex and thick root and perennating structure.

Flowers are dichasial cyme inflorescence, terminal or axillary. At any given moment, there will be 10-20 buds to bloom and at an average there will be 40 flowers per plant. Flowering periods last for 30-45 days; pedicels 0.5–3 cm long. The flower bears a green calyx which is dorsally winged. The wings are 3-5mm broad, the calyx has 4 ovate-lanceolate lobes with 1–1.5 × 0.3–0.5 cm size and acute-acuminate apex. The corolla tube is 0.5–1 cm long yellowish white colour. The flower has 4 petals and the petals are violet colour at apex and white the rest, yellow at the throat. Stamens-4; pale green-yellow short filament, 0.3–1.5 cm long; yellowish orange anthers, linear, curved, sagittate, 1–1.8 cm long. Green ovate ovary, 0.5–1.5 × 0.3–0.8 cm; greenish white style, 1–2 cm long, deflexed; simple, rounded stigma, faintly 2-lobed; lobes are 0.15 cm long.

Fruits are capsule and brown, oblong-ovate, 1–2 × 0.8–1 cm, unilocular. Numerous, minute tetrahedral seeds, 0.2–0.35 × 0.1–0.2 mm in size with reddish brown testa. All these parameters were recorded for this plant, and these were helpful in the primary identification of *E.bicolor*.

Figure1. a) *E.bicolor* Roxb. b) Leaf of *E. bicolor* Roxb. c) Flower of *E.bicolor* Roxb.

3.2. Microscopical studies

The *E.bicolor* Roxb. leaf is dorsiventrally differentiated. Epidermal cells were present on both the upper and lower surface of the leaf. The cells in the upper epidermis are larger than those in the lower epidermis. The upper and lower epidermal cells are continuous over the midrib region. Uniseriate, multicellular covering trichomes and anomocytic stomata are present in the leaf epidermis. The laminar region of the plant has palisade cells and spongy parenchyma cells. Palisade cells were only found under the upper epidermis. The spongy parenchyma

comprises loosely arranged parenchymatous cells with vascular strands. The midrib region consists of strips of collenchyma present above the lower epidermis and below the upper epidermis. Arc-shaped collateral closed vascular bundles is more pronounced towards the midribs ventral surface. A well-developed phloem and xylem tissues are present in the dorsal and ventral surface of midrib respectively. The microscopical images were given in figure2.

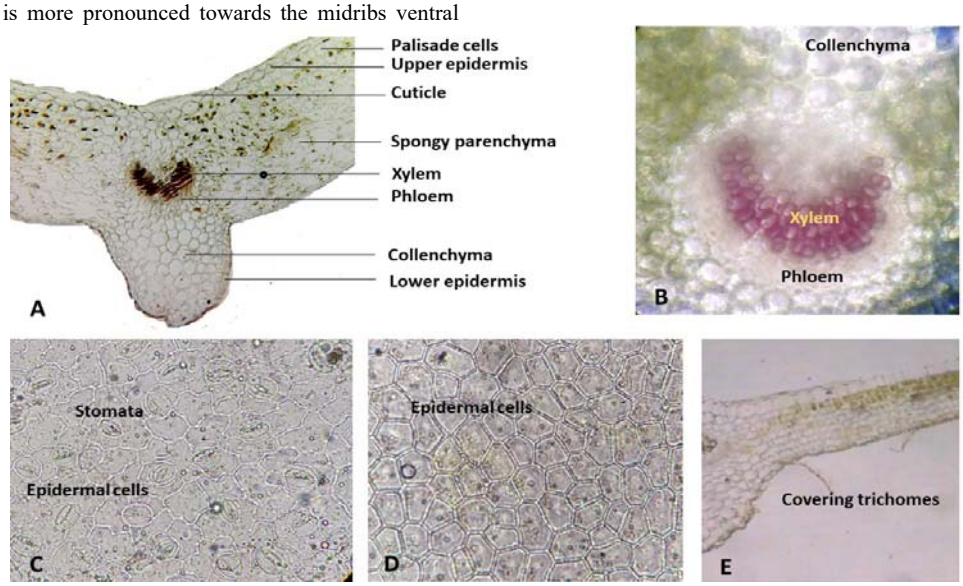

Figure 2. A) Transverse section of *E.bicolor* Roxb. leaf(60X), B) Vascular bundle(270X) C) Stomata(60X) D) Epidermal cells(60X) E) Uniseriate multicellular covering trichomes(60X)

The transverse section of the stem is quadrangular in shape without any hairs. The microscopy of the stem showed the presence of four stem wings. The outer most part is with single-layered rectangular epidermal cells with a very thick and smooth cuticle, next to the epidermis cortex is present and cortex is composed of 3-5 layers of parenchymatous cells which are loosely arranged with abundant starch grains. Thick-walled, elongated, single-layer endodermis cells without any intercellular spaces were present. The vascular bundles are present below the single-layered endodermis. The phloem is situated on the peripheral side of the xylem and is distinct. Xylem is more prominent and inhabits the chief part of the stem. The xylem possesses xylem fibres, xylem vessels and xylem parenchyma. The vascular bundles form a ring around the central pith. The large polygonal parenchymatous cells make a central pith and these cells contain calcium oxalate crystals. The microscopical images were given in figure 3.

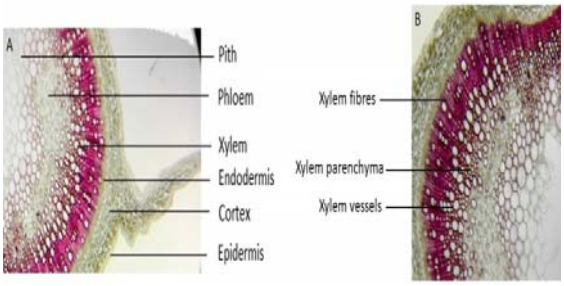

Figure 3: A) Transverse section of *E. bicolor*Roxb. stem (60X)B) Transverse section shows xylem vessels, xylem parenchyma and xylem fibres(100X)

The root of *E.bicolor* Roxb. consist of distinct, lignified cork, and below the cork few layers of phellogen and phelloderm are present. The cortex is relatively large, thick-walled parenchymatous cells containing abundant starch. The phloem encircles the xylem, and the xylem is developed with distinct vessels and lignified xylem parenchyma. Medullary rays are running between the xylem. The microscopical images were given in figure:4.

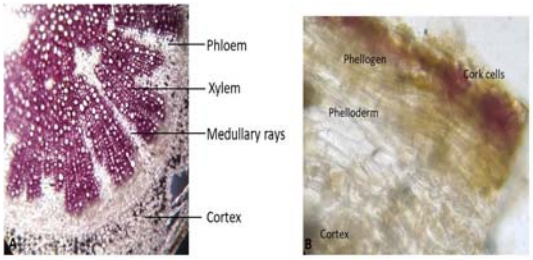

Figure 4:a) Trasverse section of periderm of *E.bicolor*Roxb. (60X)b) Transverse section of root of *E.bicolor*Roxb.(100X)

3.3. Powder microscopical studies

The microscopical evaluation of powdered *E.bicolor* Roxb. was carried out. The microscopy showed the presence of anomocytic stomata; the guard cells advance a lenticular pore in between and become bean-shaped. Polygonal, isodiametric, or elongated epidermal cells but were not arranged in a definite pattern. Uniseriate multicellular trichomes are present in the plant. The pollen grains which produce male gametes. Spiral and reticulate xylem vessels, xylem parenchyma and parenchymatous cells are also present in the powder of *E.bicolor* Roxb.. The images of different characters were given in figure:5.

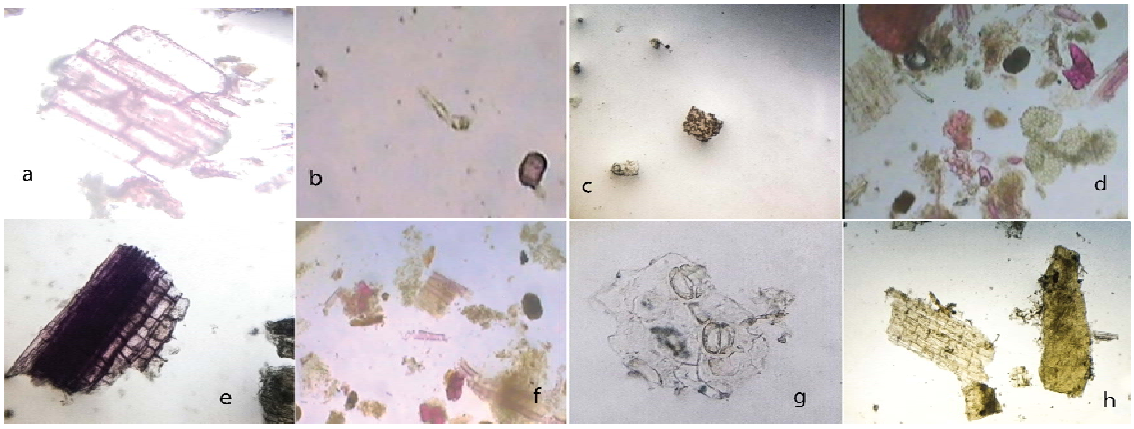

Figure 5: a)Parenchymatouscells(60X) b)Covering trichomes(60X) c)Epidermal cells(60X)d) Pollen grains(60X) e) Xylem fibres with xylem vessels(60X) f) Spiral xylem vessels(60X) g) Stomata(270X) h) Epidermal cells(60X)

3.4. Determination of leaf constant

The constants like a stomatal number, stomatal index, vein islet number and vein termination number of *E.bicolor* were determined, and the results were given in the table 1

Table 1. Leaf constant of *E.bicolor* Roxb.

Sl.no:	Leaf constant	Value per square mm
1	Stomatal number	82.2±4.970
2	Stomatal Index	24.4±3.050
3	Vein islet no	12±1.871
4	Vein termination no	7.4±1.140

Each column represents as means ± SD (n = 5)

3.5. In vitro biological assays

3.5.1. Antioxidant activity

3.5.1.1. DPPH scavenging activity

The DPPH radical scavenging activity of a plant extract is one of the most broadly used methods for determining its antioxidant activity. DPPH is a protonated radical with a characteristic absorption peak at 517 nm that lowers as the proton radical is scavenged by natural plant extracts. The ability of various extracts of *E. bicolor* to scavenge DPPH free radicals was assessed by measuring the decrease in DPPH absorbance at 517 nm. The activity of DPPH radical scavenging was measured in percentage inhibition. The chloroform extract showed a better antioxidant activity compared to other extracts. Ascorbic acid was used as standard. Ascorbic acid(standard) IC_{50} value was found to be 14.09±0.636µg/ml followed by chloroform extract 67.46±0.916µg/ml, acetone extract 88.52±2.431µg/ml, methanol extract 96.60±3.516µg/ml and aqueous extract 176.09±8.934µg/ml. The results were given in figure 6.

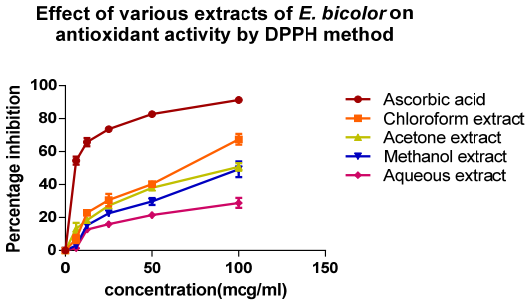

Figure 6. Effect of various extracts of *E.bicolor*Roxb. on antioxidant activity by DPPH method.

3.5.1.2. Nitric oxide scavenging assay

Nitric oxide scavenging activity was carried out with various extracts (chloroform, acetone, methanol and aqueous) of *E.bicolor* and ascorbic acid as standard compound. The reductive potential of all extracts and standard preparations exhibited dose-dependent activity. Ascorbic acid(standard)IC_{50} value was found to be 21.94±0.478µg/ml followed by chloroform extract 63.92±0.916µg/ml, acetone extract 92.52±1.987µg/ml, methanol extract 106.85±2.035µg/ml and aqueous extract 121.50±2.512µg/ml. The results are given in figure 7.

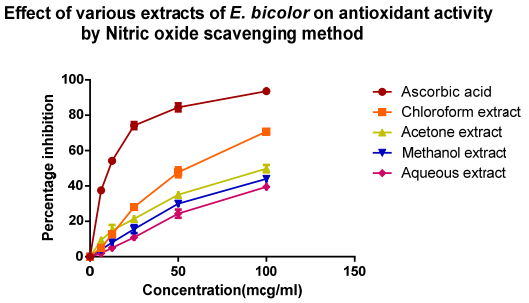

Figure 7. Effect of various extracts of *E.bicolor*Roxb.on antioxidant activity by nitric oxide scavenging method.

3.5.2. Anti-inflammatory activity of whole plant extracts

3.5.2.1. Inhibition of protein denaturation method

In this regard, the chloroform, acetone, methanolic and aqueous extracts of the whole plant of *E.bicolor* displayed significant activity. The methanolic extracts at a concentration of 100µg/ml showed maximum activity among all extracts. The IC_{50} value of standard diclofenac sodium was found to be 26.56±1.100µg/ml followed by methanol extract 56.06±0.735µg/ml, chloroform extract 74.99±1.972µg/ml, acetone extract 88.63±2.459µg/ml and aqueous extract 119.89±4.891µg/ml. The results are given in figure 8.

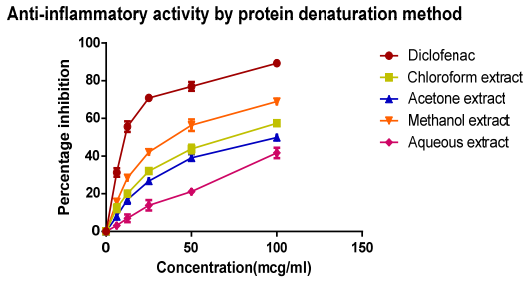

Figure 8. Effect of various extracts of *E.bicolor*Roxb. on anti-inflammatory activity by protein denaturation method.

3.5.2.2. Membrane stabilization test

Human red blood cell membrane lysis inhibition induced by hypotonicity,i.e. stabilization of HRBC membrane, was taken as a degree of the anti-inflammatory activity. The percentage of membrane stabilization for various (chloroform, acetone, methanol and aqueous) extracts of *E.bicolor* was done. Diclofenac sodium was used as standard, and it showed a percentage protection of 83.95±1.487 at 100µg/ml. The methanolic extract was effective in inhibiting the heat-induced hemolysis of HRBC at different concentrations compared to other extracts. The percentage protection of methanolic extract was found to be 67.85±1.113 at 100µg/ml, chloroform 49.67±1.068 at 100µg/ml, 46.83±2.801 at 100µg/ml and acetone 45.39±1.391 at 100µg/ml. The results are given in figure 9.

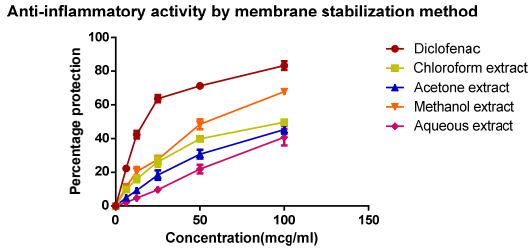

Figure 9. Effect of various extracts of *E.bicolor*Roxb.on anti-inflammatory activity by membrane stabilization method.

4. Discussion

Despite the extensive medicinal uses of *E. bicolor* Roxb., there is little information on the morphological and microscopical parameters that would justify the quality control profile of this plant. Herbal drug standardization is critical for confirming the safety and efficacy of herbal drugs. Organoleptic and microscopical evaluation are the parameters for standardizing crude drugs. Morphological studies are the quickest means to evaluate the identity and purity of any crude drug. In addition to morphology, microscopic features that can be easily distinguished are equally important in the confirmation of the identity and purity of the plant. The leaf of *E.bicolor* Roxb.is dorsiventral type; it consists of covering trichomes and anomocytic stomata. The stem is quadrangular in shape and shows the presence of four wings. Besides, the stem consists of the epidermis, cortex, endodermis, phloem, xylem, and pith. Xylem is more prominent and occupies a significant portion of the stem. The *E.bicolor* Roxb. root consists of evident, lignified cork, and a few layers of phellogen, and phelloderm is present beneath the cork. The cortex is relatively large, and the phloem encircles the xylem. The xylem is developed with distinct vessels and lignified xylem parenchyma. Medullary rays are running between the xylem.

Free radicals are recognized to play a significant role in a wide range of clinical manifestations. By combating various free radicals, antioxidants protect us from a multiple ailment. They either work by conserving antioxidant defense systems or scavenging reactive oxygen species (Umamaheswari and Chatterjee, 2008). The ability of natural products to donate electrons can be assessed using the 2, 2′-diphenyl-1-picrylhydrazyl radical (DPPH) purple-colored solution bleaching method (Nunes*et al* 2012. Al-Ghamdi*et al.*, 2020). Chloroform extracts had a substantially higher inhibitory percentage than the other fractions evaluated in this study. This study implies that phytochemical elements in the plant extract can donate hydrogen to a free radical to scavenge potential harm, as given in figure 6.

Endothelial cells, macrophages, and neurons all produce nitric oxide, which is involved in the control of a variety of physiological processes, including inflammation. Excessive nitric oxide generation and release have been linked to several disorders such as cardiovascular and inflammatory diseases, cancer and cataract. Specific nitric oxide synthase (NOSs) produces nitric oxide in biological tissues by metabolizing arginine to citrulline and forming nitric oxide via a five-electron oxidative process. These substances alter many cellular component's structures and functional behavior (Knowles, 1986). The drop in absorbance at 546 nm caused by a reduction in nitric acid generation was used to measure the extract's nitric oxide scavenging potency.

The anti-inflammatory action of medicinal plants was investigated using protein denaturation and stabilization of human red blood cell membranes. Protein denaturation is commonly related to inflammation (Naz*et al*.,2017). The current research found that methanolic extract considerably reduced protein/albumin denaturation.

The erythrocyte membrane is identical to the lysosomal membrane; hence, the extract may also be able to stabilize lysosomal membranes. This stabilization is critical in restraining the inflammatory response because it prevents the extracellular release of lysosomal contents of activated neutrophils such as proteases and bactericidal enzymes, which induce additional tissue inflammation and damage (Azeem*et al*.,2010). Hypotonicity-induced hemolysis can be caused by cell shrinkage caused by osmotic loss of intracellular electrolytes and fluid components. The extract

may inhibit or promote mechanisms stimulating or enhancing intracellular component efflux. (Kumar *et al*.,2012).

Furthermore, the findings by Rajisha *et.al* 2020a., alkaloids, glycosides, phenolic compounds, flavonoids, sterols, carbohydrates, terpenoids, saponins and gums, and mucilage are present in *E.bicolor* Roxb. The flavonoids and phenolic compounds in the extract may be responsible for this antioxidant and anti-inflammatory activity.

5. Conclusion

According to Ayurvedic Pharmacopoeia of India, morphological and microscopical studies are vital parameters for standardizing crude drugs. Morphological studies are the quickest means to ensure the identity and purity of any crude drug. Distinguishable microscopical characters are also very helpful for confirmation of the identity and purity of the plant. The authenticity of any crude drug needs to be standardized using a suitable method to prevent adulteration. *E.bicolor* Roxb. is a dicot plant. This study can be an essential tool for the botanical identification of the plant *E.bicolo r*Roxb. since no comprehensive standardized work has been stated in the literature for this plant so far. Therefore, this study gives exclusive authenticity parameters, which will help conscript a monograph of this plant. The present study also supports the antioxidant and anti-inflammatory activity of *E.bicolor* Roxb.

Acknowledgment

Authors are grateful to Dr. K. Gopalkrishna Bhat, Department of Botany, Poorna prajna College, Udupi for authenticating the plant and NGSM Institute of Pharmaceutical Sciences, Nitte (Deemed to be University) in Mangaluru, Karnataka, for providing the requisite laboratory facilities.

References

Al-Ghamdi AY, Fadlelmula AA and Abdalla MO. 2020. Total phenolic content, antioxidant and antimicrobial activity of *Rutachalepensis L*. leaf extract in Al-Baha Area, Saudi Arabia. *Jordan J. Biol. Sci.*, **13**: 675-680.

Alam MN, Bristi NJ andRafiquzzaman M. 2013. Review on in vivo and in vitro methods evaluation of antioxidant activity. *Saudi Pharm J.*, **21(2):**143-152. doi: https://doi.org/10.1016/j.jsps.2012.05.002

Al-Rabadi GJ. 2014. Microscopic analysis of in vitro digested milled barley grains: influence of particle size heterogeneity. *Jordan J. Biol. Sci.*, ***147*(1572):** 1-5.

Azeem AK, Dilip C, Prasanth SS,Shahima VJH, Sajeev K, and Naseera C. 2010. Anti–inflammatory activity of the glandular extracts of *Thunnusalalunga*. *"Asian Pac. J. Trop. Med., **3*(10):** 794-796. https://doi.org/10.1016/S1995-7645(10)60190-3

Bag A, Kumar Bhattacharyya S, Kumar Pal N andRanjanChattopadhyay R. 2013. Anti-inflammatory, anti-lipid peroxidative, antioxidant and membrane stabilizing activities of hydroalcoholic extract of *Terminaliachebula* fruits. *Pharm Biol.*, ***51*(12):** 1515-1520. DOI: 10.3109/13880209.2013.799709

Crang R, Lyons-Sobaski S and WiseR. 2018. *Plant anatomy: a concept-based approach to the structure of seed plants*. Springer. DOI:10.1007/978-3-319-77315-5

Cutler DF, BothaT and Stevenson DW. 2008. Plant anatomy. *An applied approach. Malden, MA: Blackwell Publishing*.

Daniel D and Dluya T. 2016. In vitro biochemical assessments of methanol stem bark extracts of Ficussycomorus plant. *Jordan J. Biol. Sci., **147*(3384):** 1-6.

Dulta K, ThakurK, VirkAK, Thakur A, Chauhan P, Kumar V and Chauhan PK. 2021. Comparison of different solvents for antioxidant and antibiogrampattern of Bergeniaciliata rhizome extract from Shimla district of Himachal Pradesh. *Jordan J Biol Sci.,**14*(1):** 23-29. doi: 10.54319/jjbs/140105

Harborne AJ. 1998. *Phytochemical methods a guide to modern techniques of plant analysis*. springer science & business media.

KandalwalKR. 2005. **Practical Pharmacognosy**, thirteenth ed. NiraliPrakashan, Pune.

Knowles RG, PalaciosM, Palmer RM andMoncada S. 1989. Formation of nitric oxide from L-arginine in the central nervous system: a transduction mechanism for stimulation of the soluble guanylatecyclase. *Proc. Natl. Acad. Sci., **86*(13):** 5159-5162. doi: 10.1073/pnas.86.13.5159

Kumar V, Bhat ZA, Kumar D, Khan NA andChashoo IA. 2012. Evaluation of anti-inflammatory potential of leaf extracts of Skimmiaanquetilia. *Asian Pac. J. Trop. Biomed., **2*(8):** 627-630. doi: 10.1016/S2221-1691(12)60109-9

Marcocci L, Maguire JJ, Droylefaix, MT and Packer L. 1994. The nitric oxide-scavenging properties of Ginkgo biloba extract EGb 761. *Biochem. Biophys. Res. Commun., **201*(2):** 748-755. doi: 10.1006/bbrc.1994.1764

MuntanaN andPrasong, S. 2010. Study on total phenolic contents and their antioxidant activities of Thai white, red and black rice bran extracts. *Pak J Biol Sci.,**13*(4):** 170-174. doi:10.3923/pjbs.2010.170.174

Bekbolatova N,Kurbatova EV, Sakipova NB,IbragimovaZN,Alpysbayeva LI, KabdenovaST andBoylan F. 2018. Macroscopic and microscopic diagnostic features of the potential herbal drug *Crataegusalmaatensis*Pojark endemic in Kazakhstan. *Iran. J. Pharm. Sci., **14*(2):** 39-50. doi: 10.22034/IJPS.2018.33737

NazR, AyubH, NawazS, Islam ZU, YasminT, BanoAand RobertsTH. 2017. Antimicrobial activity, toxicity and anti-inflammatory potential of methanolic extracts of four ethnomedicinal plant species from Punjab, Pakistan. *BMC Complement Altern. Med.*, ***17*(1):** 1-13. doi: 10.1186/s12906-017-1815-z.

NunesXP, Silva FS, Almeida JRGDS, Barbosa FilhoJM, de Lima JT, de AraújoRibeiroLA andJúnior LJQ.2012. *Biological oxidations and antioxidant activity of natural products* (pp. 1-20). New York: INTECH Open Access Publisher. doi: 10.5772/26956.

Paul V, Sharma L, Pandey R and Meena RC. 2017. Measurements of stomatal density and stomatal index on leaf/plant surfaces. *Manual of ICAR Sponsored Training Programme for Technical Staff of ICAR Institutes on—Physiological Techniques to Analyze the Impact of Climate Change on Crop Plants*, *27*.DOI:10.13140/RG.2.2.13426.40646

Rajisha K andFernanadesJ. 2020. Pharmacognostic and Preliminary Phytochemical Investigation of Exacum bicolor Roxb. *Res J Pharm Technol., **13*(4):**1752-1756. **DOI:** *10.5958/0974-360X.2020.00316.9*

Rajisha K andFernanadesJ. 2020. Identificationof compounds from different fractions of*Exacum bicolor*Roxb. byGC-MS analysis. *Plant archives*., 20(2): 4531-4536.

Shravan KN, Kishore G, Siva KG andSindhu PES. 2011. In vitro anti-inflammatory and anti-arthritic activity of leaves of Physalisangulata L. *Int J Pharm Ind Res.*, ***1*(3):** 211-213.

Singh D, Aeri V andAnanthanarayanaDB. 2018. Development of internet technology TIPHAM (Tool for identity of Powdered Herbals through Analytical Microscopy) for microscopic identification of crude herbal drugs. *Pharmacogn. Mag.*, ***14*(55):** 213. **DOI:** 10.4103/pm.pm_563_17

Skrzypczak-Pietraszek E. 2015. Phytochemistry and biotechnology approaches of the genus Exacum. In *The Gentianaceae-Volume 2: Biotechnology and Applications* Springer, Berlin, Heidelberg, pp. 383-40.

Sreelatha, U, BaburajTS, KuttyCN, NazeemPA and BhaskarJ. 2007. Cultivation prospects of Exacum bicolor Roxb.—an endangered, ornamental and anti-diabetic herb. *Nat. prod. Radiance.*,**6(5):** 402 – 404. DOI:10.22159/ajpcr.2021.v14i5.40966

Umamaheswari M and Chatterjee TK. 2008. In vitro antioxidant activities of the fractions of Coccinniagrandis L. leaf extract. *Afr. J. Tradit. Complement. Altern. Med.*,**5:** 61-73. DOI:10.4314/AJTCAM.V5I1.31258

JJBS

Volume 15, Number 5, December 2022
ISSN 1995-6673
Pages 805 – 811
https://doi.org/10.54319/jjbs/150509

Jordan Journal of Biological Sciences

Molecular Phylogeny and Deep Origins of the Hybrid *Mokara* Dear Heart (Orchidaceae)

Dang Chien Ha[1], Phi Bang Cao[2], Van Dinh Nguyen[1], Chi Toan Le[1,*]

[1] *Hanoi Pedagogical University 2, 32 Nguyen Van Linh, Xuan Hoa, Phuc Yen, Vinh Phuc, Vietnam;* [2]*Faculty of Natural Sciences, Hung Vuong University, Nong Trang, Viet Tri, Phu Tho, Vietnam*

Received: March 28, 2022; Revised: July 11, 2022; Accepted: August 25, 2022

Abstract

Hybridization has played a significant influence in the evolution of plants. The hybrids orchid genus *Mokara* Dear Heart is a cut orchid with beautiful flowers, and it is economically important. Both maximum likelihood (ML) and Bayesian inference (BI) methods were used to construct the phylogeny of *Mokara* Dear Heart to explore the phylogenetic relationships of *Mokara*Dear Heart and its parents based on the molecular data from ITS and *matK* sequences. Our molecular results supported that *Mokara* Dear Heart is closely related to the genus *Vanda*, but far from *Arachnis*. The genetics of chloroplast a type of the plastid and nucleus of *Moraka* Dear Heart could be derived from the *Vanda* lineage. The hybrid orchid *Mokara* Dear Heart is a bigeneric hybridization and originated from *Arachnis* and *Vanda*. In the hybridization scenario of *Mokara* Dear Heart, the *Vanda* Yip Sum Wah acted as the father's parent and crossed with *Arachnis* Maggie Oei's maternal lineage, resulting in paternal transmission of the chloroplast to the *Mokara* Dear Heart. The commercial name *Mokara* Dear Heart should be corrected to *Aranda* Dear Heart.

Keywords: molecular phylogeny, hybrid, chloroplast, nucleus, *Vanda*, *Mokara* Dear Heart, *Aranda* Dear Heart

1. Introduction

Exploring the molecular phylogenetic relationship between taxa can help scientists discover novel findings. Plant evolution has been aided by hybridization, and imperfect lineage sorting is believed to have occurred during several rapid radiations. As a result, there are several examples of accordance and discordance between phylogenetic trees from chloroplast and nuclear genes in plants. Much of the backbone phylogeny of angiosperm has been resolved using a molecular phylogenetic approach (see Soltis *et al*., 2009, 2011; Ruhfel *et al*., 2014) as well as clarified longstanding questions in relationships of major clades of the plant.

Orchidaceae is the largest angiosperm family, with almost 25000 species and 800 genera (Chen *et al*., 2009). The family members were distributed across the whole world except Antarctica (Chen *et al*., 2009; Zhang *et al*., 2013). The species of Orchidaceae play a significant role in economy, ornamental, and medicine. In several tribes of Orchidaceae, Vandeae is a large horticulturally important group with almost 2000 species. *Mokara* the "Smile Orchid", is popularin Asia, where it has been first hybridized and cultivated (Soon, 1989; Dalayap *et al*., 2011). *Mokara* is Vandaceous orchid, which is the result of the trigeneric hybridization of *Ascocentrum*, *Arachnis*, and *Vanda* genera (Dalayap *et al*., 2011; Peyachoknagul *et al*., 2014). Currently, several varieties of *Mokara* were produced with unique and highly variable star-shaped flowers, and flowers with a large number of colors compared to other orchids such as pink, purple, blue, yellow, orange, and red (Dalayap *et al*., 2011). The *Mokara* species are cut orchids with beautiful flowers, and they are economically important. The economic *Mokara* Dear Heart is an orchid hybrid that was registered by Mizuta in 1972 (Woo and Nakamoto, 1990). However, the *Mokara* Dear Heart lineage was hybridized from *Arachnis* Maggie Oei and *Vanda* Yip Sum Wah, in which *Arachnis* Maggie Oei is the seed parent and *Vanda* Yip Sum Wah pollen parent (https://orchidroots.com). Moreover, the accepted name of this lineage was corrected to *Aranda* Dear Heart. Therefore, there are disagreements over the commercial and scientific names for this lineage, which can be resolved by molecular phylogeny.

Several molecular phylogenetic studies for Vandeae members were performed (Carlsward *et al*., 2006; Gardiner *et al*., 2013; Zhang *et al*., 2013; Szlachetko *et al*., 2014; Zou *et al*., 2015). In these studies, the three genera *Ascocentrum*, *Vanda*, and *Arachnis* were included to investigate the phylogenetic relationship and monophyly of the three genera. However, the phylogenetic position and molecular relationship of the hybrids orchid *Mokara* are absent.

Lee (1994) conducted a study on the genetics of *Mokara*, and the results of the study indicated that the lineages of *Mokara* have genetic diversity. The triploid *Mokara* cultivars generally outperform their diploid counterparts in various horticultural characteristics and are more desirable for commercial cut-flower production.

The monophyly of Vandeae was investigated by Carlsward *et al*. (2006) using molecular data from ITS,

* Corresponding author. e-mail: Lechitoan@hpu2.edu.vn.

*trn*L-F, and *mat*K; however, the samples of *Mokara*'s three parents are limited. Gardiner *et al*. (2013) presented a molecular study using a sequence of three DNA regions. Results of the study showed that the genus *Vanda* s.l. forms a clade including approximately 73 species, containing some members of *Euanthe*, *Christensonia*, *Ascocentrum*, *Neofinetia*, and *Trudelia*, and the species *Aerides flabellata*. However, the genetic relationships within *Vanda* s.l. remain a mystery, and morphological classifications for the species are inconsistent with the findings.

Zhang *et al*. (2013) elucidated the molecular relationship between 14 genera of the *Aerides*–*Vanda*clade. The *Aerides*–*Vanda* clade was supported as a monophyletic group. The molecular data from five plastid DNA and ITS regions proved that *Ascocentrum* is non-monophyletic. *Pendulorchis* was treated as a new genus; some other treatments were provided for the *Aerides*–*Vanda* clade.

Recently, the close relationship between *Vanda* and *Ascocentrum* was reconstructed by Zou *et al*. (2015) based on five DNA regions (*atp*I-H, *mat*K, *psb*A-*trn*H, *trn*L-F, and ITS) of 211 individuals from 74 genera. In this study, the subtribe Aeridinae was supported as monophyletic, and 10 major clades were recognized in the Aeridinae. Additionally, within the Aeridinae, most genera were strongly supported as monophyletic, and only several genera were found to be polyphyletic.

Thus, in order to investigate the phylogenetic position and molecular relationship between *Aranda*, *Mokara*, and its parents, we conducted the phylogenetic analyses using molecular data from chloroplast and nuclear DNA regions. Our major aims are to (1) construct the phylogenetic placement of *Mokara* Dear Heart and (2) investigate the patterns of phylogenetic relationship consistent with the hybridization of *Mokara* Dear Heart.

2. Materials and Methods

2.1. Taxon sampling

To determine the phylogenetic position of *Mokara* Dear Heart, we assembled sequences of all the three parents genera *Ascocentrum*, *Vanda*, and *Arachnis* that are available in GenBank (NCBI). The duplication and uncertain sequences were excluded. For the *Vanda* genus, all phylogenetic clades of the genus were included following Gardiner *et al*. (2013). In total, 113 sequences that represented 84 species for both ingroups and outgroups were included in the molecular analyses. Two DNA regions including ITS, and *mat*K were used for molecular analyses.

We sampled three individuals of *Mokara* Dear Heart that were collected from Vietnam. The *Mokara* Dear Heart samples were obtained from a nursery of Hanoi Pedagogical University 2. Our *Mokara* Dear Heart samples belong to the *Aranda* variety of *Mokara*. *Mokara* Dear Heart samples were planted in pots of sand in growth chambers. (http://www.orchidsasia.com/mhyblist.htm).

2.2. DNA extraction, polymerase chain reactions (PCR), and sequencing

For the three individuals of *Mokara*Dear Heart collected from Vietnam, we extracted genomic DNA from silica gel dried leaves using the CTAB procedure as previously described (Raskoti and Ale, 2021), and the i-genomic Plant DNA extraction mini kit (iNtRON), following the manufacturer's recommended protocol. The PCR and sequencing were conducted using the primers presented by Gardiner *et al*. (2013). PCR products were separated and visualized using an ABI3730 automated sequencer (Applied Biosystems, USA). All sequences were aligned in Geneious v.8.0.5 (Kearse *et al*., 2012). Voucher information and GenBank accession numbers are listed in AppendixS1. To test the topological incongruence between the nuclear and plastid DNA regions, the incongruence length difference (ILD) test was conducted (Farris *et al*., 1995). The results of the ILD test showed no significant incongruence between the nuclear and the plastid datasets in this study. Consequently, we concatenated them into one dataset.

2.3. Phylogeneticanalyses

The molecular phylogenetic analyses of *Mokara* Dear Heart were performed using both the Bayesian inference (BI) and Maximum likelihood (ML) methods. The ML trees were generated by performing a rapid bootstrap analysis in RAxML v.8.2.12 (Stamatakis, 2006; Stamatakis *et al*., 2008) with the GTR + I + G substitution model generated by jModeltest 2.1.6 (Darriba *et al*., 2012) and applying 1,000 bootstrap replicates. The BI analysis was performed on MrBayes 3.2.6 (Ronquist and Huelsenbeck, 2003) on the CIPRES using the best-fitting models that estimated separately each gene region (*matK*: GTR+G, ITS: GTR+I+G) (Miller *et al*., 2010). We ran the Markov chain Monte Carlo (MCMC) for 10 million generations, and trees were sampled every 1000 generations. Tracer v.1.4 was used to check the effective sample sizes (ESSs) of all relevant parameters (>200) (Rambaut and Drummond, 2007). The obtained trees were visualized using FigTree v.1.4.0 (Rambaut, 2009).

3. Results and Discussion

3.1. Molecular phylogenetic placement of Mokara Dear Heart: Congruence among nuclear and chloroplast phylogenetic analyses

The lengths of the two single data sets *mat*K and ITS were 1642 bps, and 710 bps, respectively. The combined dataset included 84 individuals with lengths of matrix 2352 bps. The topologies from two single data sets *mat*K, ITS, and the combined dataset from ML and BI analyses were highly congruent, and we thus presented the results from the three data sets (*mat*K, ITS, and the combined datasets) in the ML tree with bootstrap values from ML and BI analyses in Figs. 1. 2 and 3, respectively.

Our molecular data well supported that *Mokara* Dear Heartis placed in Vandeae by both single data sets (*mat*K and ITS) and combined dataset (Figs. 1, 2, 3). Our results indicate that the genus *Vanda* forms a clade containing some members of the genera *Ascocentrum*, *Christensonia*, and *Mokara* Dear Heart also seen in Zou *et al*. (2015), in spite of the fact that the species *Vanda malipoensis* is placedwith *Ascocentrum christensonianum* and *Ascocentrum pusillum* in a separate clade (Fig. 3).

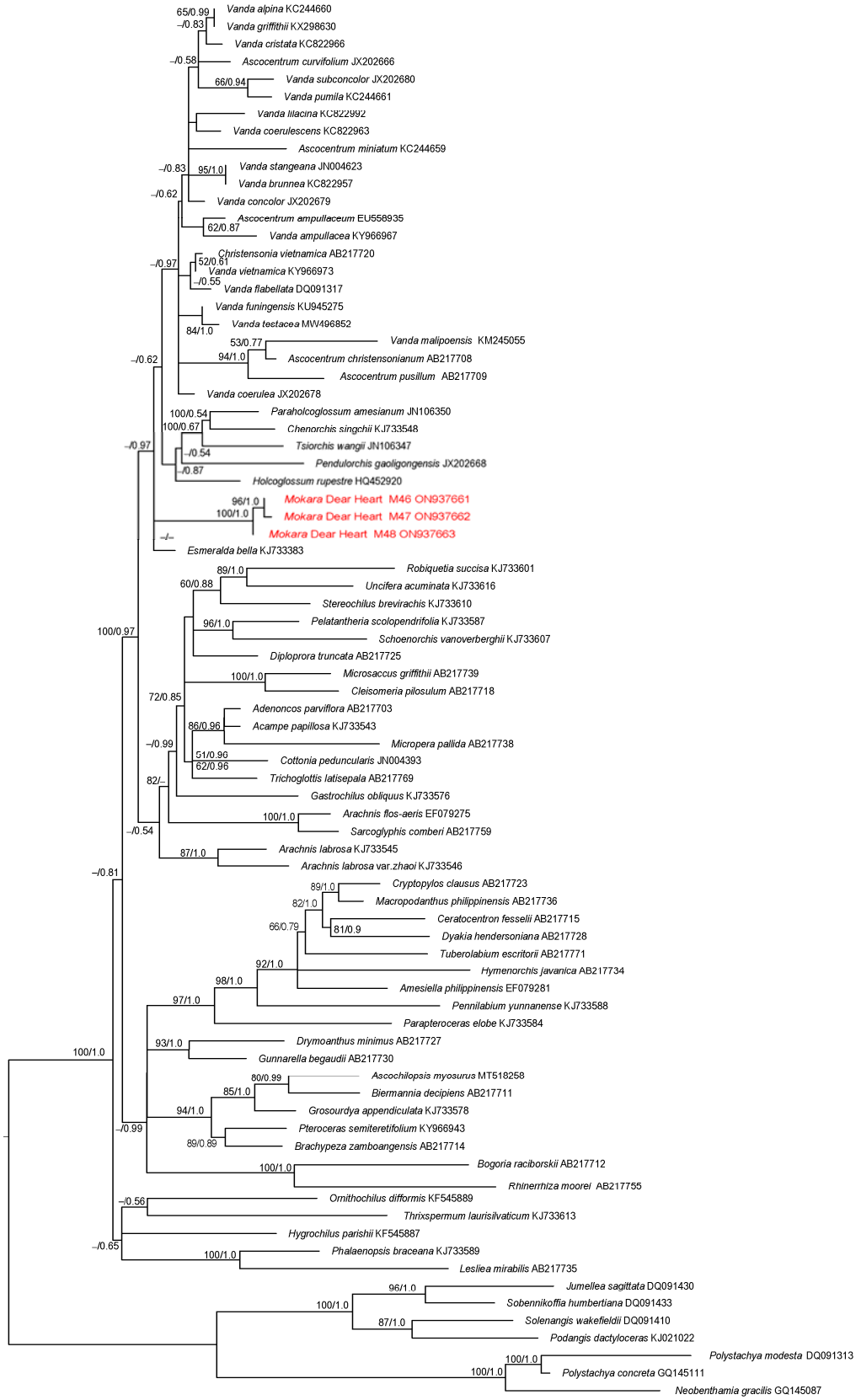

Figure 1. Maximum likelihood tree of *Mokara* Dear Heart based on the *matK* datasets. The bootstrap values from ML and BI analyses are displayed on the nodes. The symbol "–" denotes support values less than 50%.

Figure 2. Maximum likelihood tree of *Mokara* Dear Heart based on the ITS datasets. The bootstrap values from ML and BI analyses are displayed on the nodes. The symbol "–" denotes support values less than 50%.

The ITS sequences strongly supported *Mokara* Dear Heart placed within the *Vanda* genus. The three individuals of *Mokara* Dear Heart formed a clade with strongly supported (Bootstrap value (BS) = 100%; Posterior probability (PP) = 1.0). The genus *Ascocentrum* is non-monophyletic, two clades were recognized for *Ascocentrum*, and they are both placed within *Vanda* (Fig. 1). The first clade includes *A. ampullaceum*, *A. curvifolium*, *A. miniatum*, and *A. aurantiacum*, while another clade consists of *A. christensonianum* and *A. pusillum* formed as sister to *Vanda* with weakly supported (Fig. 2). Whereas, one of the three *Mokara*'s parent the genus *Arachnis* placed far from the *Vanda* clade. Thus, molecular analysis of ITS supported the non-monophyletic of *Vanda*, and *Mokara* Dear Heart is closely related to *Vanda*, while the *mat*K data indicated that *Mokara* Dear Heart formed as a sister to *Vanda* and *Ascocentrum*. However, the genus *Ascocentrum* is polyphyletic and placed within *Vanda* (Gardiner *et al*., 2013). The genus *Arachnis* was weakly placed far from the three genera (Fig. 2), and this genus was also recognized as non-monophyletic.

The results from the combined dataset strongly supported the placement of *Mokara* Dear Heart within the

Vanda genus (Fig. 3). Similarity is a situation of *Ascocentrum* and *Christensonia* genera. However, our results also indicated that *Ascocentrum* is non-monophyletic with *A. pusillum*, *A. christensonianum*, and *Vanda malipoensis* formed in a separate clade (Fig. 3). The nest of *Ascocentrum* within *Vanda* seems to result from the pollination of ancestors between the two genera through time and space.

Therefore, our molecular data supported that *Mokara* Dear Heart is closely related to its parent the genus *Vanda*, but it is far from *Arachnis*.

3.2. Genetic traits of Mokara suggested by molecular data

The *Mokara* is a Vandaceous member that is the result of a trigeneric cross between *Ascocentrum*, *Arachnis*, and *Vanda*. However, questions on the commercial and scientific names especially genetics of the hybrid lineages are needed to resolve. Based on the molecular results, we see that the similar position of *Mokara* in phylogenetic trees from nuclear (ITS) and chloroplast (*mat*K) data suggests that the genetics of the organelle plastid and nucleus of *Moraka* are linked (Figs. 1, 2), with the chloroplast a type of plastid and much of the genetic materials in the nucleus of *Moraka* derived from the *Vanda* lineage.

Figure 3. Maximum likelihood tree of *Mokara* Dear Heart based on the combined datasets from ITS and *matK*. The bootstrap values from ML and BI analyses are displayed on the nodes. The symbol "–" denotes support values less than 50%.

The molecular results supported that the hybrid orchid *Mokara* Dear Heart is a bigeneric hybridization and likely originated from *Arachnis* and *Vanda*. In which, *Arachnis* is the seed parent and *Vanda* is the pollen parent.

Indeed, angiosperms normally inherit both the chloroplast and mitochondrial genomes from their mothers (Camus *et al.*, 2022; Birky, 2008). However, for the hybrid orchid *Mokara* Dear Heart, we find that the chloroplast genome seems derived from the *Vanda* lineage (Fig. 1). Thus, this result is unexpected. Biparental inheritance of organellar genomes has been reported in several studies (Fauré *et al*., 1994; Testolin and Cipriani, 1997; Havey *et al*., 1998; Yang *et al*., 2000). Furthermore, in angiosperms, we find that several paternal inheritances of chloroplast genomes were discovered such as *Helianthus verticillatus* (Ellis *et al*., 2008) Celastrales–Oxalidales–Malpighiales (COM) clade (Sun*et al*., 2015), four Australian *Callitris* species (Cupressaceae) (Sakaguchi *et al*., 2012), and *Larrea* (Yang *et al*., 2000). Sun *et al.* (2015) mentioned the possibility of paternal chloroplast transmission to the COM clade's ancestor, but mitochondria are still maternally inherited. Moreover, the hybrid lineage may exhibit strong paternal chloroplast inheritance. For the *Mokara* Dear Heart case, in spite of the mitochondrial sequences being absent in previous and the current study, however, it is likely maternally inherited as other taxa in angiosperms (Fig. 4). Thus, it is possible that a complex hybridization event resulted in the chloroplast and mitochondrial genomes divergence of *Mokara* Dear Heart.

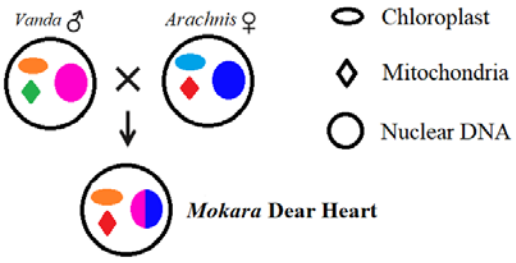

Figure 4. Mapping simulation of the hybrids orchid genus *Mokara* Dear Heart from *Arachnis* and *Vanda*. Plant lineages are represented by large circles, while nuclear DNA types are represented by small circles, chloroplasts are represented by ovals, and mitochondria are represented by diamonds. During the hybridization, the chloroplast genome is paternally inherited from the *Vanda*, while the mitochondrion genome is maternally inherited from the *Arachnis*.

In this hybridization scenario of *Mokara* Dear Heart, the *Vanda* Yip Sum Wah acted as the father parent and hybridized with *Arachnis* Maggie Oei's maternal lineage, resulting in paternal chloroplast transfer to the *Mokara* Dear Heart (Fig. 4). Thus, the hybridization event could be a reason for the conflict between the chloroplast and mitochondrial genomes, as well as competition among nuclear loci with half of the alleles in offspring contributed by each parent. That resulted in the close relationship between hybrid lineage and the paternal parent of Mokara based on chloroplast and nuclear data. Additionally, the commercial name *Mokara* Dear Heart should be corrected to *Aranda* Dear Heart.

4. Conclusions

This study represents a comprehensive phylogenetic relationship of the hybrids orchid genus *Mokara* Dear Heart. *Mokara* Dear Heart is closely related to its parent the genus *Vanda*, but far from *Arachnis*. The genetics of the organelles chloroplast and nucleus of *Moraka* are linked, with the chloroplast of *Mokara* Dear Heart apparently derived from the *Vanda* lineage. The hybrid orchid *Mokara* Dear Heart is a bigeneric hybridization originated from *Arachnis* and *Vanda*. In the hybridization scenario of *Mokara* Dear Heart, the *Vanda* Yip Sum Wah acted as the father parent and crossed with *Arachnis* Maggie Oei's maternal lineage, resulting in paternal transmission of the chloroplast to the *Mokara* Dear Heart. The commercial name *Mokara* Dear Heart should be corrected to *Aranda* Dear Heart.

Acknowledgments

We thank Dr. Wyckliffe Omondi Omollo from State Key Laboratory of Systematic and Evolutionary Botany, Institute of Botany, Chinese Academy of Sciences, China, and Dr. Viet Hong La from Hanoi Pedagogical University 2, Vietnam for their help in initiating this study.

Author Contributions

C.T.L. P.B.C and V.D.N designed the study. V.C.H. collected the data. V.C.H., C.T.L. and P.B.C analyzed the data. All authors wrote and gave final approval for publication.

References

Birky CW. 2008. Uniparental inheritance of organelle genes. *Curr Biol*., **18**: R692–695.

Camus MF, Alexander-Lawrie B, Sharbrough J and Hurst GDD. 2022. Inheritance through the cytoplasm. *Heredity*, 1–13.

Carlsward BS, Whitten, WMark, Williams NH and Bytebier B. 2006. Molecular phylogenetics of Vandeae (Orchidaceae) and the evolution of leaflessness. *Am J Bot.*, **93**: 770–786.

Chen X, Liu Z, Zhu G, Lang K, Ji Z, Luo Y, Jin X, Cribb PJ, Wood JJ, Gale SW, Ormerod P, Vermeulen JJ, Wood HP, Clayton D and Bell A. 2009. Orchidaceae. In: Wu ZY, Raven PH and Hong DY (Eds.), **Flora of China**. Vol. 25. Science Press, Beijing, and Missouri Botanical Garden Press, St. Louis.

Dalayap RM, Torres, MAJ and Demayo CG. 2011. Landmark and outline methods in describing petal, sepal and labellum shapes of the flower of mokara orchid varieties. *Int J Agric Biol.*, **13**: 652–658.

Darriba D, Taboada GL, Doallo R and Posada D. 2012. JModelTest 2: more models, new heuristics and high-performance computing. *Nature Methods*, **9**: 772.

Ellis JR, Bentley KE and McCauley DE. 2008. Detection of rare paternal chloroplast inheritance in controlled crosses of the endangered sunflower *Helianthus verticillatus*. *Heredity*, **100:** 574–580.

Farris JS, Källersjö M, Kluge AG and Bult C. 1995 Constructing a significance test for incongruence. *Syst Biol.*, **44:** 570–572.

Fauré S, Noyer JL, Carreel F, Horry JP, Bakry F and Lanaud C. 1994. Maternal inheritance of chloroplast genome and paternal inheritance of mitochondrial genome in bananas (*Musa acuminate*). *Curr Genet.*, **25**: 265–269.

Gardiner LM, Kocyan A, Motes M, Roberts DL and Emerson BC. 2013. Molecular phylogenetics of *Vanda* and related genera (Orchidaceae). *Bot J Linn Soc*, **173**: 549–572.

Havey MJ, McCreight JD, Rhodes B and Taurick G. 1998. Differential transmission of the *Cucumis organellar* genomes. *Theor Appl Genet.*, **97**: 122–128.

Kearse M, Moir R A, Wilson S, Stones-Havas M, Cheung S, Sturrock S, Buxton A, Cooper S, Markowitz C, Duran T, Thierer B, Ashton M and Drummond A. 2012. Geneious basic: an integrated and extendable desktop software platform for the organization and analysis of sequence data. *Bioinformatic*, **28**: 1647–1649.

Lee YH. 1994. Genomic and meiotic analysis of *Mokara* orchids. *J. Hered*., **85(1):** 39–43.

Miller MA, Pfeiffer W and Schwartz T. 2010. Creating the CIPRES Science Gateway for inference of large phylogenetic trees. In: Proceedings of the gateway computing environments workshop (GCE). Pp. 1–8. New Orleans: Institute of Electrical and Electronics Engineers (IEEE).

Peyachoknagul S, Nettuwakul C, Phuekvilai P, Wannapinpong S and Srikulnath K. 2014. Development of microsatellite markers of vandaceous orchids for species and variety identification. *Genet Mol Res.*, **13**: 5441–5445.

Rambaut A. 2009. FigTree v.1.4. Available at: http://tree.bio.ed.ac.uk/software/figtree/

Rambaut A and Drummond AJ. 2007. Tracer. Version 1.4. Available at:http://beast.bio.ed.ac.uk/Tracer

Raskoti BB and Ale R. 2021. DNA barcoding of medicinal orchids in Asia. *Sci Rep.*, **11:** 23651.

Ronquist F. 1997. Dispersal-vicariance analysis: a new approach to the quantification of historical biogeography. *Syst Biol.*, **46**: 195–203.

Ronquist F and Huelsenbeck JP. 2003. MrBayes 3: Bayesian phylogenetic inference under mixed models. *Bioinformatics*, **19**: 1572–1574.

Ruhfel BR, Gitzendanner MA, Soltis DE, Soltis PS and Burleigh JG, 2014. From algae to angiosperms – inferring the phylogeny of green plants (Viridiplantae) from 360 plastid genomes. *BMC Evol Biol.*, **14**: 23.

Sakaguchi S, Tsumura Y, Crisp MD, Bowman DMJS and Isagi Y. 2014. Genetic evidence for paternal inheritance of the chloroplast in four Australian *Callitris* species (Cupressaceae). *J For Res.*, **19**: 244–248.

Soltis DE and Soltis PS. 2009. The role of hybridization in plant speciation. *Annu Rev Plant Biol.*, **60**: 561–588.

Soltis DE, Smith SA, Cellinese N, Wurdack KJ, Tank DC, Brockington SF, Refulio-Rodriguez NF, Walker JB, Moore MJ, Carlsward BS, Bell CD, Latvis M, Crawley S, Black C, Diouf D, Xi Z, Rushworth CA, Gitzendanner MA, Sytsma KJ, Qiu YL, Hilu KW, Davis CC, Sanderson MJ, Beaman RS, Olmstead RG, Judd WS, Donoghue MJ and Soltis PS. 2011. Angiosperm phylogeny: 17 genes, 640 taxa. *Am J Bot.*, **98**: 704–730.

Soon TE. 1989. Orchids of Asia. Times Book International, Times Center, Singapore.

Stamatakis A. 2006. RAxML-VI-HPC, maximum likelihood-based phylogenetic analyses with thousands of taxa and mixed models. *Bioinformatics*, **22**: 2688–2690.

Stamatakis A, Hoover P and Rougemont J. 2008. A rapid bootstrap algorithm for the RAxML Web servers. *Syst Biol.*, **57**: 758–771.

Sun M, Soltis DE, Soltis PS, Zhu X, Burleigh JG and Chen ZD. 2015. Deep phylogenetic incongruence in the angiosperm clade Rosidae. *Mol Phylogenet Evol.*, **83**: 156–166.

Szlachetko DL, Górniak M, Kolanowska M, Mytnik-Ejsmont J, Kowalkowska AK, Rutkowski P and Kolinski T. 2014. Taxonomic position and phylogeny of the genus *Vargasiella* (Orchidaceae, Vandoideae) based on molecular and morphological evidence. *PLoS ONE*, **9**: e98472.

Testolin R and Cipriani G. 1997. Paternal inheritance of chloroplast DNA and maternal inheritance of mitochondrial DNA in the genus *Actinidia*. *Theor App Genet*, **94**: 897–903.

Woo T D, Nakamoto W K. 1990. Do orchids grow in Hawaii? and how!. The Hawaii orchid foundation for the American orchid society, Hawaii.

Yang TW, Yang YA and Xiong Z. 2000. Paternal inheritance of chloroplast DNA in interspecific hybrids in the genus *Larrea* (Zygophyllaceae). *Am J Bot.*, **87**: 1452–1458.

Zhang GQ, Liu KW, Chen LJ, Xiao XJ, Zhai JW, Li Q, Cai J, Hsiao YY, Rao WH, Huang J, Ma XY, Chung SW, Huang LQ, Tsai WC and Liu ZJ. 2013. A new molecular phylogeny and a new genus, *Pendulorchis*, of the *Aerides–Vanda* Alliance (Orchidaceae: Epidendroideae). *PLoS ONE*, **8**: e60097.

Zou LH, Huang JX, Zhang GQ, Liu J and Zhuang XY. 2015. A molecular phylogeny of Aeridinae (Orchidaceae: Epidendroideae) inferred from multiple nuclear and chloroplast regions. *Mol Phylogenet Evol.*, **85**: 247–254.

Supporting Information

AppendixS1. GenBank accession numbers for DNA sequences generated or used in this study. The sequences generated in this study begin with ON. "–" indicates missing data.

JJBS

Volume 15, Number 5, December 2022
ISSN 1995-6673
Pages 813 – 824
https://doi.org/10.54319/jjbs/150510

Jordan Journal of Biological Sciences

Insight Towards Induction of Reproductive-Metabolic Phenotypes of Polycystic Ovarian Syndrome

Shaimaa Nasr Amin [1,2,*] , Fida Asali[3,] Mohamed Fathi Mohamed Elrefai[1,4,] Walaa Bayoumie El Gazzar[1,5], Sherif Ahmed Shaltout[6,7], Dalia Azmy Elberry[2], Samaa Samir Kamar[8,9], Noha Samir Abdel Latif [10], Marwa Nagi Mehesen[10,11], Mai Mohammed Ayoub[1], Khaled Anwer Albakri[12] , Asmaa Mohammed ShamsEldeen[2,13]

[1] Department of Anatomy, Physiology, and Biochemistry, Faculty of Medicine, The Hashemite University, PO Box 330127, Zarqa 13133, Jordan; [2] Department of Medical Physiology, Faculty of Medicine, Cairo University, Cairo, Egypt; [3] Department of Obstetrics and Gynaecology, Faculty of Medicine, The Hashemite University, PO Box 330127, Zarqa 13133, Jordan; [4] Department of Anatomy and Embryology, Faculty of Medicine, Ain Shams University, Cairo, Egypt; [5] Department of Medical Biochemistry and Molecular Biology, Faculty of Medicine, Benha University, Benha, Egypt;[6] Department of Pharmacology, Public Health and Clinical skills, The Hashemite University, PO Box 330127, Zarqa 13133, Jordan; [7] Department of Pharmacology, Faculty of Medicine, Benha University, Benha, Egypt;[8] Department of Histology, Faculty of Medicine, Cairo University, Egypt; [9] Department of Histology Armed Forces College of Medicine, Egypt; [10]Department of Medical Pharmacology, Faculty of Medicine, Cairo University, Cairo, Egypt;[11] Department of Pharmacy Practice and Clinical Pharmacy, Faculty of Pharmacy, Future University in Egypt, Cairo, Egypt; [12] Faculty of Medicine, The Hashemite University, PO Box 330127, Zarqa 13133; [13]Physiology department, Faculty of medicine, October 6 University,Giza,Egypt

Received: May 11, 2022; Revised: August 18, 2022; Accepted: August 18, 2022

Abstract

Hormonal disturbances, multiple ovarian cysts, and oligo-anovulation are the key features of the polycystic ovarian syndrome (PCOS). Consistently, without a directly hormone-regulated animal model, we developed three phenotypes of PCOS in rats to simulate the reproductive-metabolic disturbances of human PCOS. Twenty-four female Sprague-Dawley rats underwent vaginal smears for two sequential cycles to exclude any PCOS-like rats. Rats were divided into the following groups: healthy control, PCOS induced by a high-fat, high-sugar (HFHS) diet, PCOS induced by HFHS diet +monosodium glutamate (MSG), and PCOS induced by continuous light exposure (L/L). At the end of the study, an abdominal ultrasound revealed multiple ovarian cysts, and a vaginal smear documented the arrest of the estrous cycle. Serum samples showed hyperinsulinemia and hyperandrogenism in all PCOS-induced groups, but with superiority of the L/L group in developing higher insulin levels, insulin resistance, and anti-Müllerian hormone (AMH). Although the frequency of isolated uterine contractions increased in all modeling groups compared to the control, the contraction amplitude was higher in HFHS than in L/L and HFHS-MSG groups. The three animal models manifested the key features of PCOS and symptoms of metabolic syndrome. Disturbed circadian rhythm and HFHS diet are more in line with the increased risk of PCOS.

Keywords: PCOS, Circadian rhythm, HFHS, AMH, Testosterone.

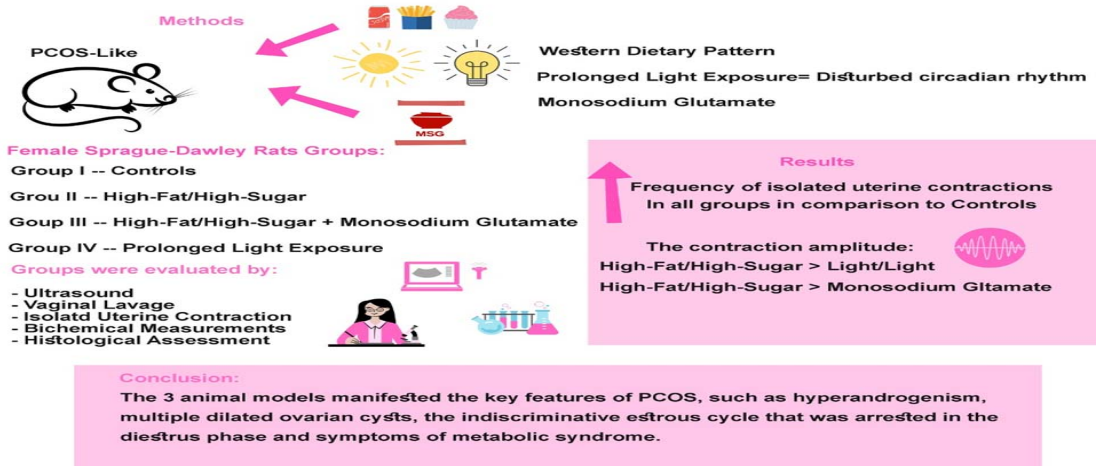

* Corresponding author. e-mail: shaimaa@hu.edu.jo.

1. Introduction

Polycystic ovarian syndrome (PCOS) is the most prevalent metabolic and hormonal dysfunction among reproductive-aged females (Goodarzi et al., 2011) and one of the main contributors to infertility in this age group (Kutcher et al., 2009). It is associated with polycystic ovarian morphology, rarity or lacking ovulation, hyperandrogenism, dyslipidemia, and insulin resistance. The collection of these abnormalities has long-term sequelae like fatty liver, cardiovascular diseases, diabetes, and cancer (Anagnostis et al., 2018).

Although the pathophysiology and etiology of PCOS have not been thoroughly demonstrated, multiple factors can influence women's hormones and metabolic processes during intrauterine and prepuberty life (Anagnostis et al., 2018).

Obesity-induced by diet may contribute to the pathophysiology of PCOS as it causes irregular cycles, hormonal imbalances, and ovarian signaling impairments (Volk et al., 2017). Moreover, the available evidence promotes the importance of substituting diet for pharmacological therapy to alleviate PCOS symptoms and reduce weight and metabolic abnormalities (Toscani et al.,2011).

Almost all food additives function as either palatability enhancers or preservatives. One of these salts is monosodium glutamate (MSG) (Moore, 2003). MSG is a hydrated sodium salt of naturally occurring L-glutamic acid, sold commercially, consisting of glutamate, sodium, contaminants, and water. The harmless endogenously produced glutamate also can be found in natural food, while synthetic glutamate is toxic and found in industrial foods (Chakraborty, 2019). MSG diminishes the functions of the ovary by boosting the production of estradiol, follicle-stimulating hormone (FSH), and luteinizing hormone (LH), which results in enhancing follicular development and oxidative defense (Mondal et al., 2018).

The circadian rhythm allows metabolism to adapt and predict the day's light-dark cycle, ensuring the best physiological functioning. Accordingly, the disruption in this rhythm may lead to several diseases, such as metabolic syndrome and obesity (Moustafa, 2020). On the other hand, PCOS women experience multiple sleep and related psychological problems that decrease sleep quality (Kang et al., 2015). The cyclic light-dark circadian rhythm controls LH surges on which ovulation depends (McCORMACK, 1973). Therefore, any change in these light-dark photoperiods can disturb the normality of the cycle and decrease ovulation, which is a PCOS essential character (Weber and Adler, 1979).

Based on the previous reports on the impact of diet and circadian rhythm disturbances on PCO development, this study aimed to evaluate and compare the impact of diet changes versus circadian rhythm disturbances on ovarian and uterine functions in female rats and correlate the resulting changes to the known picture of PCOS.

2. Materials and Methods

"The Institutional Review Board of The Hashemite University" approved (15/2020) the experimental steps, animal handling, sampling, and euthanasia. The handling of animals followed the "Care and Use of Laboratory Animals guide" (NIH publication no. 85-23, revised 2011).

2.1. A-Experimental design and study groups:

This research followed a randomized controlled animal experimental design including twenty-four female Sprague-Dawley rats whose weight ranged from 150 to 180 g (70 days old). All were subjected to vaginal smears, which were examined by light microscopy for two successive cycles (around 8–10 days), and any PCOS-like rats that showed long estrous cycles (more than 5 days) have been excluded (Hu et al., 2018). The animals were kept in stainless steel cages as three rats per cage to prevent isolation-induced stress, exposed to a 25 °C environmental temperature under a 12:12 h light: dark cycle except for group IV, which was exposed to a 12:12 h light: light cycle (continuous illumination). Rats were categorized into four groups:

Group I- healthy control had free access to water, a regular chow diet (7% simple sugars, 3% fat, 50% polysaccharide, 15% protein), and energy of 3.5 kcal/g (Samuelsson et al., 2008).

Group II-PCOS induced by a high-fat, high-sugar (HFHS) diet had free access to water, a 32% sucrose solution, and high-fat chow (5.24 kcal/g, 60% of calories derived from fat) for 14 weeks (Volk et al., 2017, Nurullahoglu-Atalik et al., 2020).

Group III-PCOS induced by HFHS diet +monosodium glutamate (MSG) had a similar diet to the previous group in addition to MSG daily 0.8 gm/kg BW/day orally by gavage (Mondal et al., 2018) for 14 weeks.

Group IV-PCOS induced by prolonged light exposure were kept in the light experiment box where they were subjected to a continuously illuminated environment (L/L, lights for 24 hours/day) for 14 weeks. The dimensions of the light experiment box were 120 cm in length, 45 cm in width, and 180 cm in height. Furthermore, it is vertically divided into four equal and separated compartments (length, width, and height of 120 cm, 45 cm, and 45 cm per compartment). Each compartment has its ventilation and fluorescent lamp (color temperature: 6500 k, illumination: 600 lux) (Kang et al., 2015).

At week fourteen of the study, an ultrasound was performed to assess ovarian size. Then cervical dislocation was used to euthanize rats. Abdomens were dissected, and blood samples were obtained from the aorta for measurement of serum LH; FSH; Anti-Müllerian Hormone (AMH); Testosterone (T), glucose, insulin, triglycerides (TG); Total Cholesterol (TC); High-density lipoprotein (HDL); Low-density lipoprotein (LDL).

Ovaries were dissected and weighed, then prepared for histopathological examination. The uterus has been separated from all surrounding fat and connective tissue and dissected into two parts; the first recording isolated contractions by Powerlab, and the second was fixed for histopathological examination.

2.2. B-Estrus cycle monitoring:

Vaginal lavage was done daily during weeks 8 to 14 of the study, identifying stages of the estrous cycle through cytological examination. The vaginal cells were flushed with a small amount of distilled water or saline through a

pipette. Then few drops of cell suspension were spread on a glass slide for microscopic examination, allowed to air dry, and subsequently stained with crystal violet stain (McLean et al., 2012).

2.3. C-Abdominal Ultrasound:

Prior to the imaging study, anesthetizing of the rats was done by administration of combined ketamine (100 mg/kg) and xylazine (10 mg/kg) intraperitoneally (Wellington et al., 2013). The fur was removed from the costal margin to the caudal abdomen; next, the anesthetized rat was placed supine on a warmed table to keep the rat safe and comfortable. We used Edan DUS 60 ultrasound diagnostic system with a linear transducer (8.5 MHz) (CA, USA). Female rat ovaries are in fat pads at the end of the uterine horn, lateral to the kidneys bilaterally. (Wang et al., 2017). Ovaries were first measured in the largest sagittal plane as the longest possible diameter (D1) and the second-longest possible ovarian diameter (D2**)** at a right angle to the first measurement. Finally, the mean ovarian diameter (MOD) was calculated using a two-dimensional formula to evaluate ovarian size (Vladimir et al., 2004):

$$MOD = [\{MOD_{\text{left ov.}} = (D1 + D2)/2\} + \{MOD_{\text{right ov.}} = (D1 + D2)/2\}]/2.$$

2.4. D-Isolated Uterine contractions:

The right uterine horn was excised and sliced into longitudinal strips of 5 mm length to record uterine contractility. Each strip was placed vertically in an organ bath containing about 10ml of Krebs–Heinseleit (KH) buffer composed of (mM): NaCl 115.0; KCl 4.6; CaCl2.2H2O 2.5; KH2PO4 1.2; MgSO4.7H2O 2.5; NaHCO3 25 and glucose 11.0 at 37 °C, ventilated with 95% O2/ 5% CO2 throughout the experimental period and solution was replaced every 15 minutes (Darios et al., 2012).

The uterine contractions' changes in isometric force, including amplitude, frequency, and rhythmicity, were recorded using an isometric transducer (Lab Chart software, AD instruments, power lab, New South Wales, Australia). One gm of resting tension was applied first, and the strips were allowed to equilibrate for 60 minutes (Sajadi et al., 2018). Then, recording a 10 min continuous curve was done.

2.5. E-Biochemical measurements & calculations:

Blood samples were left for two hours at room temperature to clot, centrifuged for 10 minutes (4°C) at 1000×g; then serum samples were collected and kept at -20°C till further assessment of the following parameters as per manufacturer's guidelines (MyBioSource, San Diego, CA, USA). Rat ELISA Kits were used for the measurement of serum LH (Catalog No: MBS764675), FSH (Catalog No: MBS2502190), AMH (Catalog No: MBS701712), and Testosterone (Catalog No: MBS282195). Quantitative insulin and fasting serum glucose were measured using Rat Insulin ELISA Kit (Catalog No: MBS045315), and Rat glucose ELISA Kit (Catalog No: MBS7233226) purchased from MyBioSource, San Diego, CA, USA.

The following formula was used to calculate the homeostasis model assessment-estimated insulin resistance (HOMA-IR) index; (HOMA-IR): HOMA−IR = Fasting insulin (μU/mL) × fasting glucose (mmol/L)/22.

Rat Total Cholesterol ELISA Kit (Catalog No: MBS722885), Rat Triglyceride ELISA Kit (Catalog No: MBS726298), and Rat HDL ELISA Kit (Catalog No: MBS704516) purchased from MyBioSource, San Diego, CA, USA was used for Serum total cholesterol (TC), triglycerides (TG) and HDL levels, respectively. Low-density lipoprotein cholesterol (LDLc) levels were estimated using the Friedewald formula: LDL = TC – TG/5 – HDL (Friedewald et al., 1972).

2.6. F-Histological study:

At the end of the experiment, uterine and ovarian tissues were retrieved, fixed in 10% formol saline, processed into paraffin blocks, and seven um serial sections were cut and put on glass slides. Haematoxylin and Eosin were used to stain the sections. (Kiernan, 2001)**.**

2.7. G-Statistical analysis:

Data were analyzed by "SPSS 21" (IBM SPSS Statistics 21; IBM Corporation, New York, USA) and expressed as mean ± standard deviation (Mean ± SD). Normality of distribution was evaluated by Shapiro-Wilk's test. Quantitative variables between the groups were compared using analysis of variance (ANOVA) with the Bonferroni post hoc test. Results were statistically significant at $p \leq 0.05$ (Chan, 2003).

3. Results

3.1. A-Changes in body weight in all studied groups:

There is no significant difference among the rats of the four studied groups at the beginning of the study, as shown in Table 1. However, by the end of the work, there was a significant increase (P-value ≤0.05) in body weight in groups fed on HFHS and HFHS+MSG compared to the control group, while the difference between the L/L group and the control group remained insignificant. The % change in body weight was significantly greater in groups fed on HFHS and HFHS +MSG (26.4% and 28.184%, respectively) compared to the control group and L/L group (12.7% and 13.22%, respectively).

Table 1. Bodyweight and ovarian weight in the studied groups:

	CONTROL	HFHS	HFHS+MSG	L/L
BW1(gm)	146±8.170	146.330±10.230	150.830±14.280	157.500± 8.800
BW2(gm)	164.600±15.380	185±8.366 [a]	193.340±10.320 [a]	178.330±7.500
% Change of Bodyweight	12.700%	26.400%	28.184%	13.220%
Absolute Ovarian weight (mg)	53±8	125±20 [a]	160±32 [a b]	140±7 [a]
Relative Ovarian Weight (*Ovarian Weight / 100 gm of final body weight)* (mg%)	32.3±5.2	67.56±2.4 [a]	82.9±22.2 [a b]	78.5±9.3 [a]

HFHS: High Fat High Sugar; **MSG:** Monosodium Glutamate**; L/L:** Light/Light cycle, **BW1:** Body Weight at the start of the work, **BW2:** Body Wight at the end of the work.

[a]: Significant compared to control group, [b:] significant compared to HFHS group, [c:] significant compared to HFHS+MSG group at P-value≤0.05.

3.2. B- Comparison of ovarian weight and diameter in all groups:

Table 1 shows a significant increase (P-value ≤0.05) of absolute and relative ovarian weight in HFHS, HFHS+MSG, and L/L groups in comparison with the control group, noting that this ovarian weight is significantly higher (P-value ≤0.05) in HFHS+MSG fed group compared to the group fed on HFHS only. As shown in (figure 1), the abdominal Ultrasound revealed a significant expansion (P-value ≤0.05) in the *mean ovarian diameter* in HFHS, HFHS+MSG, L/L groups compared to the control group.

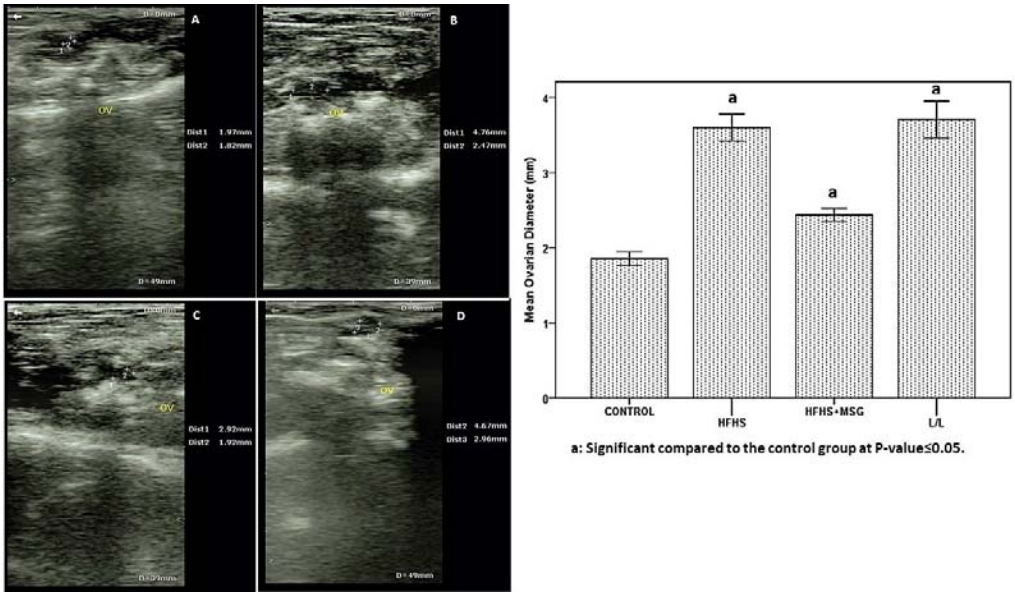

Figure 1. Mean Ovarian Diameter in the studied groups in abdominal Ultrasound. Abdominal Ultrasound: the longest possible diameter (D1) and the second-longest possible ovarian diameter (D2) to be at a right angle to the first measurement.

The mean ovarian diameter (MOD) = [{MOD $_{\text{left ov.}}$ = (D1 + D2)/2} + {MOD $_{\text{right ov.}}$ = (D1 + D2)/2}]/2.

[A: Control group; B: PCO group induced by HFHS; C: PCO group induced by HFHS+MSG; D: PCO group induced by L/L]

3.3. C-Functional assessment of isolated uterine Contractions:

-As shown in **(**table 2) and (figure 2): there is a significant rise (P-value ≤0.05) in the frequency of isolated uterine contractions in HFHS, HFHS+MSG, L/L rats in comparison with the control rats, with its value significantly exceeding (P-value ≤0.05) those in the HFHS+MSG and L/L groups compared to the HFHS group and also significantly higher (P-value ≤0.05) in the L/L group compared to HFHS+MSG group.

While the amplitude of isolated uterine contractions increased significantly in HFHS and L/L groups compared to the control group, its value is significantly lower in the L/L group than in the HFHS group (the highest amplitude recorded). On the other hand, the HFHS+MSG group revealed a significant reduction (P-value ≤0.05) in the contraction amplitude compared with the other three groups. Moreover, figure 2 demonstrated irregular contractions in the HFHS+MSG group compared to the regular contractions recorded in the other three groups.

Table 2. Functional assessment of isolated uterine Contractions in the studied groups:

	CONTROL	HFHS	HFHS+MSG	L/L
Frequency of uterine contractions (contraction/10 minutes)	11.670±1.370	12.330±1.370 [a]	17+.890 [a b]	14.330±.510 [a b c]
The amplitude of uterine contractions (gm tension)	0.490±.030	1.23±.044 [a]	0.160±.030 [a b]	0.780±.020 [a b c]

HFHS: High Fat High Sugar; **MSG:** Monosodium Glutamate**; L/L:** Light/Light Cycle

[a]: Significant compared to the control group, [b:] significant compared to HFHS group, [c:] significant compared to HFHS+MSG group at P-value≤0.05.

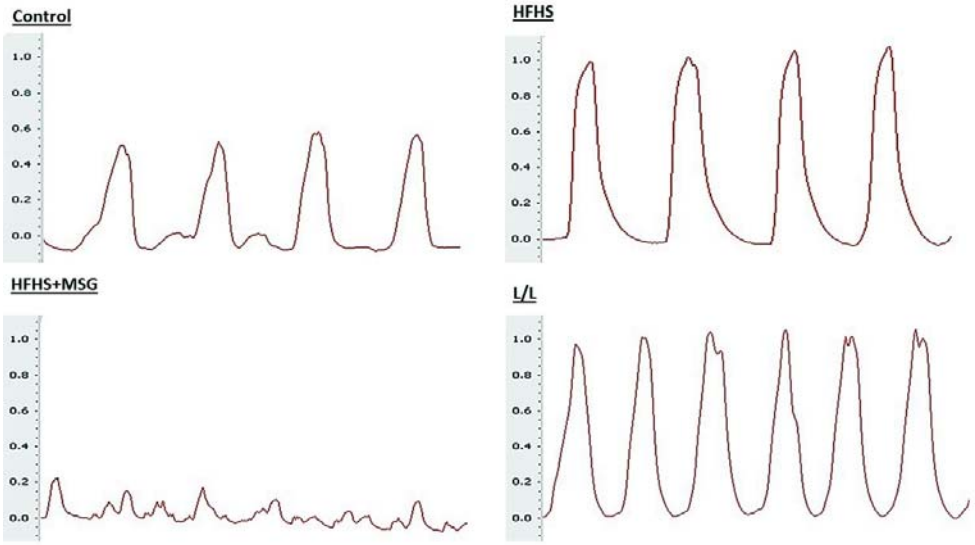

Figure 2. Isolated Uterine Contractions in the studied groups. Increased frequency of isolated uterine contractions in HFHS, HFHS+MSG, L/L groups compared to the control group. The amplitude of isolated uterine contractions increased in HFHS, and L/L groups compared to the control group, noting that its value is lower in the L/L group than in the HFHS group. The HFHS+MSG group showed a decreased contraction amplitude compared to the other three groups with an irregular pattern of contractions.

3.4. D-Biochemical results:

Table 3 shows a significant rise (P-value ≤0.05) in serum levels of LH and Testosterone in HFHS, HFHS+MSG, and L/L groups in comparison with the control group, noting that LH levels are significantly higher (P-value ≤0.05) in the HFHS+MSG group in comparison with the HFHS group. On the contrary, the serum level of FSH decreased significantly (P-value ≤0.05) in HFHS, HFHS+MSG, and L/L groups in comparison with the control group. These findings led to a significant elevation (P-value ≤0.05) in LH/FSH ratio in HFHS, HFHS+MSG, and L/L groups in comparison with the control group, also noting that this ratio is significantly higher (P-value ≤0.05) in the HFHS+MSG and L/L groups in comparison with the HFHS group.

AMH was significantly increased (P-value ≤0.05) in HFHS and L/L groups compared to the control group this increase was not significant in HFHS+MSG compared to control, HFHS, L/L groups.

Serum glucose levels and HOMA-IR were significantly increased (P-value ≤0.05) in HFHS, HFHS+MSG, and L/L groups compared to the control group. Serum glucose or HOMA-IR showed no significant difference among the three model groups (HFHS, HFHS+MSG, L/L groups). In comparison, serum insulin level was significantly increased (P-value ≤0.05) only in the L/L group in comparison with the control and the other two model groups (HFHS, HFHS+MSG), among which there is no significant difference in this serum insulin.

There is a significant elevation (P-value ≤0.05) in serum TG and TC in HFHS, HFHS+MSG, and L/L groups compared to the control group. TC only shows a significant rise (P-value ≤0.05) in the HFHS+MSG and L/L groups compared to the HFHS group.

Serum LDL in HFHS+MSG and L/L groups show a significant elevation (P-value ≤0.05) in comparison with the control and HFHS groups, while there is no significant difference in serum HDL among the studied groups.

Table 3. Biochemical Measurements and calculations in the studied groups:

	CONTROL	HFHS	HFHS+MSG	L/L
Serum LH	13.530± .740	17.250±.520 [a]	19.540±1.480 [a b]	18.150±.450 [a]
Serum FSH (MIU/ml)	9.830±.620	6.010±.450 [a]	5.630±.440 [a]	5.100±.610 [a b]
LH: FSH	1.380±.140	2.890±.300 [a]	3.480±.370 [a b]	3.590±.470 [a b]
Serum Testosterone (ng/ml)	6.400±1.120	8.780±1 [a]	8.400±.840 [a]	8.930±.710 [a]
AMH (ng/ml)	10.980±1.020	12.270±.770 [a]	11.230±.810	12.350±.3100 [a]
Serum Glucose (mmol/ml)	5.150±.680	6.850±.500 [a]	7.590±.450 [a]	6.890±.700 [a]
Serum Insulin (UIU/ml)	7.850±.350	8.320±.360	8.580±.500	9.580±.830 [a b c]
HOMA-IR	1.820±.250	2.560±.120 [a]	2.900±.300 [a]	2.960±.540 [a]
Serum TG (mg/dl)	77±5.800	98.170±5.500 [a]	99±2.960 [a]	103.500±4.700 [a]
Serum TC (mg/dl)	146±5.650	166.660±9.400 [a]	178.830±7.270 [a b]	182.300±3.380 [a b]
Serum HDL (mg/dl)	59±5.290	59.500±5.010	58.300±6.500	55.170±2.780
Serum LDL (mg/dl)	73.160±11.920	87.340±11.130	103.600±6.950 [a b]	106.660±3.900 [a b]

HFHS: High Fat High Sugar; **MSG:** Monosodium Glutamate**; L/L:** Light/Light cycle**; LH**: Luteinizing Hormone**; FSH:** Follicle-stimulating hormone**; AMH:** Anti-Müllerian Hormone**; HOMA-IR:** Homeostatic Model Assessment for Insulin Resistance**; HOMA-B**: Homeostasis model assessment of β-cell function**; TG:** Triglycerides**; TC:** Total Cholesterol**; HDL:** High-density lipoprotein**; LDL:** Low-density lipoprotein; **S100P:** S100 calcium-binding protein P**; ADAMTS19:** A Disintegrin-Like And Metalloprotease With Thrombospondin Type 1 Motif 19; **FLCs:** Free Light Chains.[a]: Significant compared to control group, [b]: significant compared to HFHS group, [c]: significant compared to HFHS+MSG group at P-value≤0.05.

3.5. E-Histopathological results:

3.5.1. -H&E staining of ovarian and uterine sections:

In Figure 3, ovarian sections in the control group showed typical structures of primordial follicles, follicles at different stages, and corpus luteum. However, the PCO group induced by HFHS exhibited multiple degenerated follicles with desquamated cells in the lumen and multiple dilated cysts lined with flattened cells and multiple atretic follicles. In addition, the PCO group induced by HFHS+MSG revealed multiple dilated cysts lined with flattened cells and degenerated follicles. Moreover, the PCO group induced by L/L showed multiple dilated cysts.

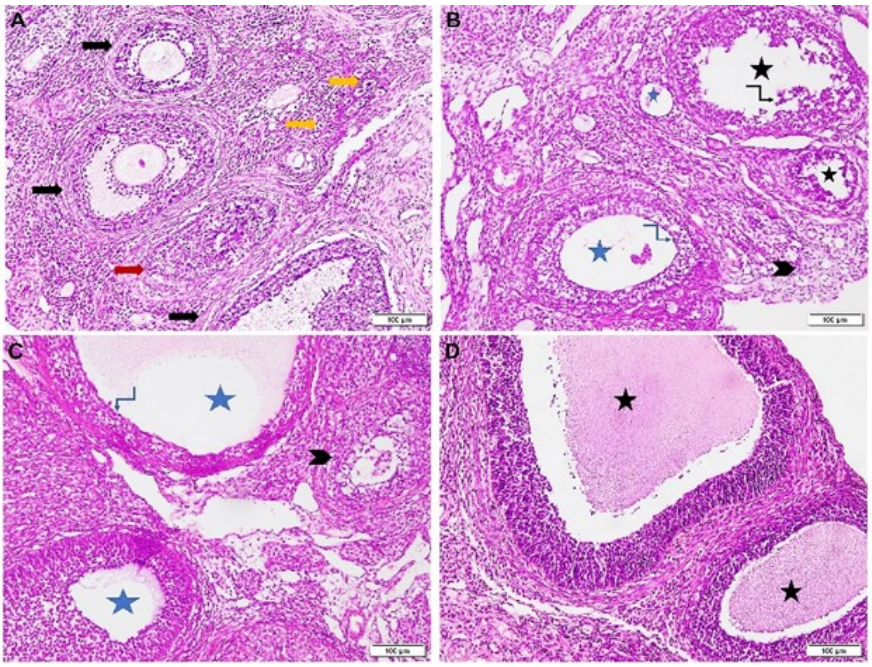

Figure 3: A photomicrograph of sections in the ovary (H&E x100).**A**: Control group showing typical ovarian structure, including primordial follicles (yellow arrows), follicles at different stages (black arrows), and corpus luteum (red arrow).**B**: PCO group induced by HFHS exhibiting multiple degenerated follicles (black asterisk) with desquamated cells in the lumen (kinked arrow) and multiple dilated cysts (blue asterisk) lined with flattened cells (blue kinked arrow) and multiple atretic follicles (arrowhead).**C**: PCO group induced by HFHS+MSG revealing multiple dilated cysts (blue asterisk) lined with flattened cells (blue kinked arrow) and degenerated follicle (arrowhead).**D**: PCO group induced by L/L showing multiple dilated cysts (asterisk).

In (Figure 4), the uterine morphology of control rats revealed a typical uterine structure lined with simple columnar epithelium with underlying connective stroma containing uterine glands. In comparison, the PCO group induced by HFHS revealed a uterus lined with stratified columnar epithelium with underlying connective stroma

rich in eosinophils and contains dilated uterine glands. PCO group induced by HFHS+MSG showed hypertrophied elongated columnar epithelium with underlying connective stroma rich in eosinophils, dilated congested blood vessels, and contains hypertrophied uterine glands. PCO group induced by L/L exhibited stratified columnar epithelium with underlying connective stroma rich in eosinophils and dilated congested blood vessels.

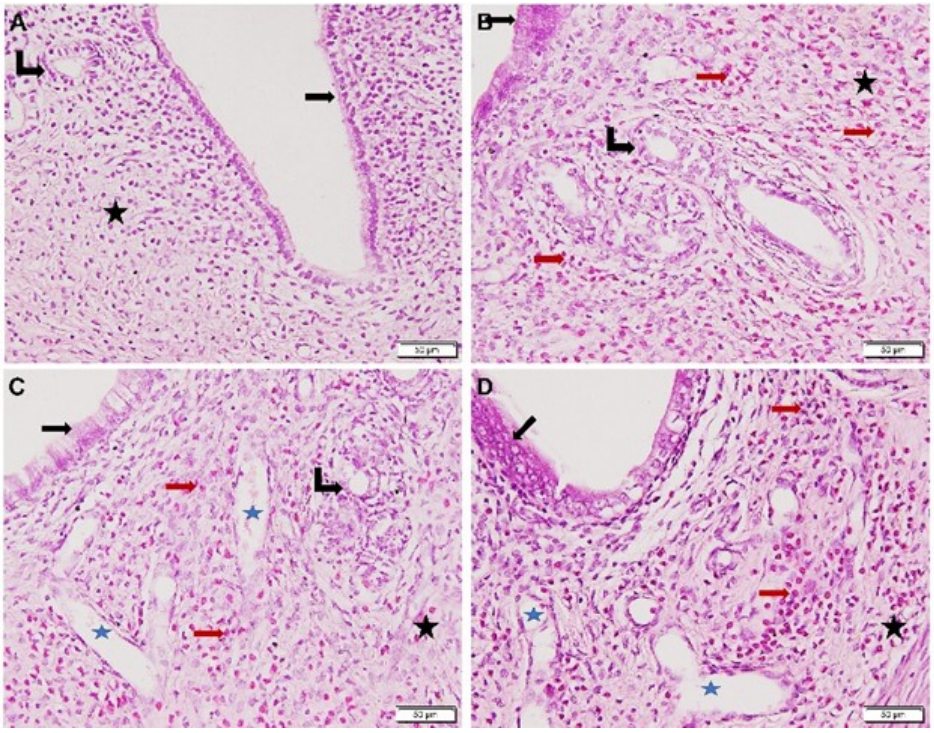

Figure 4. A photomicrograph of uterine sections (H&E x200).**A**: Control group showing typical uterine structure lined with simple columnar epithelium (black arrow) with underlying connective stroma (asterisk) containing uterine glands (kinked arrow).**B**: PCO group induced by HFHS showing uterus lined with stratified columnar epithelium (black arrow) with underlying connective stroma (asterisk) rich in eosinophils (red arrows) and contains dilated uterine glands (kinked arrow).**C**: PCO group induced by HFHS+MSG exhibiting uterine tissue lined with hypertrophied elongated columnar epithelium (black arrow) with underlying connective stroma (asterisk) rich in eosinophils (red arrows), dilated congested blood vessels (blue asterisk), and contains hypertrophied uterine glands (kinked arrow).**D**: PCO group induced by L/L revealing uterus lined with stratified columnar epithelium (black arrow) with underlying connective stroma (asterisk) rich in eosinophils (red arrows) and dilated congested blood vessels (blue asterisk).

Estrus cycle phases in studied groups evaluated by vaginal smear as shown in (figure 5); the vaginal smear of the control group revealed a regular estrus cycle formed of four phases: proestrus, estrus, metestrus, and diestrus. The proestrus phase is characterized by clusters of small, rounded, nucleated cells with central rounded nuclei. The Estrus phase exhibited clusters of cornified non-nucleated squamous epithelial cells. Many cornified epithelial cells with a few darkly stained leucocytes were observed during the metestrus phase. However, the darkly stained leucocytes predominated with few cornified epithelial cells in the diestrus phase, and rarely nucleated cells could be seen. In the PCO group**s** (induced by HFHS, HFHS+MSG, and L/L), the estrus cycle was delayed, and most rats remained in the diestrus phase.

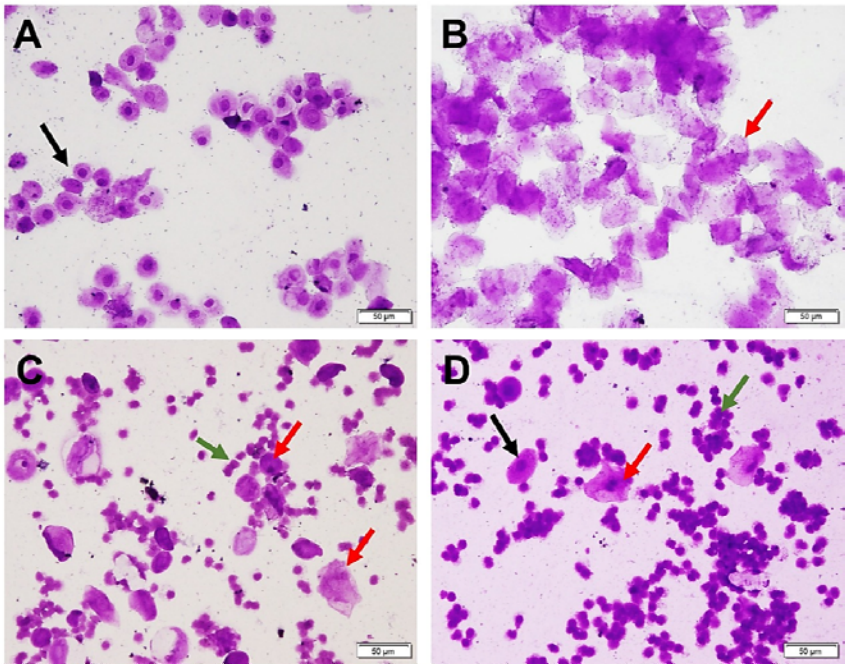

Figure 5. A photomicrograph of vaginal smear showing the different stages of the estrus cycle.

A) Proestrus phase exhibits small, rounded, nucleated cells with central rounded nuclei (black arrow).

B) Estrus phase showing clusters of cornified non-nucleated squamous epithelial cells (red arrow).

C) Metestrus phase reveals a large number of cornified epithelial cells (red arrows) with few darkly stained leucocytes (green arrow).

D) Diestrus phase showing darkly stained leucocytes (green arrow) with few cornified epithelial cells (red arrow). NB, one nucleated cell (black arrow) can be seen.

4. Discussion

Many studies have demonstrated that genetic anomalies, lifestyle, hormonal imbalance before birth, and other environmental causes may give rise to PCOS (Wen et al., 2020). The current study compared the functional, biochemical, and morphological changes in response to dietary changes and circadian rhythm disturbance via continuous light exposure and loss of the normal light-dark cycles.

In the present study, the estrus cycle was delayed in the model groups (induced by HFHS, HFHS+MSG, and L/L), and most rats remained in the diestrus phase. Roberts et al. (2017) showed reproductive abnormalities in HFHS animals. The distribution of estrous cycles varied in a fraction of the time terms spent in proestrus, estrus, and diestrus (Volk et al., 2017).

Previous studies demonstrated that HFHS-fed animals had disrupted estrous cyclicity, with a shorter period in proestrus and longer in estrus than in the controls. A more significant fraction of time recognized in estrus is accompanied by ovulation failure and infertility (Brawer et al., 1986). Another study showed that in MSG treated group, the vaginal mucosa was lined with vacuolated or pyknotic cells with infiltration of leukocytes, and this demonstrates the estrus cycle disturbance in PCO groups induced by MSG (El-Beltagy and Elghaweet, 2016).

Prolonged light exposure can also disturb the estrus cycle in female rats and explain one of the PCO induction theories in females. Kang et al. (2015) reported an indiscriminative estrous cycle in two-thirds of female rats 4 weeks after continuous light exposure and in all L/L rats following 16 weeks of continuous exposure to light, confirmed by daily vaginal smears.

Several studies showed that high-fat, high-sucrose diet rats revealed hyperphagia, rapidly developing obesity, and impaired glucose tolerance (la Fleur et al., 2011; Apolzan and Harris, 2012). That was in accordance with changes in body weight in HFHS and HFHS+MSG compared to the control group.

One environmental factor contributing to PCOS is circadian rhythm disruption (Farhud and Aryan, 2018). Some studies have demonstrated that females subjected to night-light shifts showed irregularity in their menstrual cycles, dysmenorrhea, insulin resistance, and glucose metabolism dysregulation, all of which are recognized risk factors for PCOS (Lim et al., 2018). The continuous light exposure was evidenced to produce PCOS changes and high androgen secretion in rodents (Kang et al., 2017, Chu et al., 2020), which is concomitant with our results.

Besides increased body weight, the present work showed that absolute and relative ovarian weights remarkably increased in rats fed on HFHS and HFHS+MSG compared to the control rats. This is concomitant with Akin tayo et al.'s study (2021), where ovarian weights significantly increased in PCOS animals with or without a fructose-enriched diet. Our results also agree with Hilal et al. (2020), who showed an increase in ovarian weight in mice fed with a HF diet, suggesting that this was due to the rise in their body weights.

Moreover, absolute and relative ovarian weights of rats exposed to L/L environment increased significantly without a significant rise in body weight. This partially

follows Kang et al.'s (2015) study, which revealed ovarian and uterine enlargement associated with weight loss in female rats exposed to continuous light. A significant rise in mean values of ovarian diameter calculated by the abdominal Ultrasound in all PCOS phenotypes was documented compared to the control group. In agreement with our results, enlarged ovaries are also observed in Kang et al.'s study (2015); the authors reported this observation in the L/L group of PCOS in rats induced by a continuous light environment. Another study observed no remarkable rise in the total ovarian volume. However, there was a significant elevation in ratios of volume of the cortex to the medulla volume in the ovaries of HFD mice, suggesting a rise in the number and diameters of cortical follicles (Hilal et al., 2020).

We also noted a significant rise in the frequency and amplitude of the regularity of uterine contractions in HFHS and L/L groups compared to the control. The significant frequency increase was accompanied by a remarkable reduction of amplitude and irregularity of contraction in the HFHS+MSG group compared with the control. Aktas et al. (2019) showed that uterine contractile responses in PCOS showed a significant rise compared to the control group and explained increased myometrium thickness. Another research has demonstrated uterine contractions' irregularities with variant mechanical responses of isolated uteri in PCOS rats (Sajadi et al., 2018).

Other researchers have demonstrated a remarkable increase in myometrium thickness and myometrium area in hyperandrogenised rats (Bracho et al., 2019). Moreover, Sajadi et al. (2018) reported more irregularity in uterine contractions of PCOS rats than in control rats following administration of carbachol and oxytocin.

It is known that preovulation surge needs estradiol's positive feedback that induces kisspeptin expression. Hypothalamus' kisspeptin neurons that project directly to the gonadotropin-releasing hormone may be the feedback mediators. However, it was reported that a fat diet decreased the kisspeptin expression, and decreased sensitivity between the feedback and kisspeptin is also correlated with reduced LH (Zhou et al., 2014). Additionally, HFHS rats show higher estradiol concentrations at proestrus, which may correlate with LH levels' alternation.

Further, saturated fatty acids reduce adenylate cyclase activity, stimulating LH (Cano et al., 2008). This could explain the result of a previous work done by Volk et al. (2017) that showed reduced LH levels at a diestrus among high-fat diet-fed rats compared with those fed a control diet which disagrees with our study. Another study revealed that LH levels have slightly decreased, but there was no significant difference between the two diet patterns (standard and HFHS) (Cano et al., 2008). This disagreement could be explained by the differences in the calories and fats fed to the mice

Moreover, our study revealed a significant increase in anti-Müllerian hormone (AMH) and LH levels in HFHS rats compared to control rats, which is not compatible with the other studies that reported no statistical difference between both diet types (Volk et al., 2017; Roberts et al., 2020). These disagreements could be due to the different sampling times.

The release of the early predictor for ovarian reserve, AMH (Visser et al., 2006), begins after the development from the primordial to the primary follicle. The low FSH reduces this initial recruitment. On the other hand, FSH stimulates the differentiation of antral follicles to reach ovulation requested for cyclic recruitment. Further, AMH may decrease the granulosa cells' receptors of FSH. Accordingly, the absence of AMH increases the number of recruited follicles for growth, which results in depletion of the pool of primordial follicles over time(Roberts et al., 2020).

Continuous light exposure could induce AMH elevation. The identical change in AMH level revealed that in the absence of steroid hormone administration, continuous light environment principally participated in AMH increase, and circadian rhythm disturbance might be critical in the pathology of ovulation abnormality in PCOS (Chu et al., 2020). This is also in line with our results. Among PCOS women, there was a positive association between the number of antral follicles and AMH level in serum; thus, elevated serum levels of AMH are used as a diagnostic way in PCOS. These findings indicate the role of AMH in the pathogenesis of PCOS. However, our study reported an insignificant difference between the HFHS+MSG and control groups regarding AMH levels, which is compatible with a previous study conducted by Gaspar et al. (2016). Based on what we mentioned, any factor that can induce AMH elevation may be considered pathogenic and participate in PCOS development. Our result revealed that the L/L cycle group has a higher AMH level than the control group, which agrees with a previous study (Chu et al., 2020).

The result reported by Volk et al. (2017) revealed that T level was higher in the high-fat diet group in comparison with the control group, which is concomitant with our finding. The suggested explanation is that the increased T level is related to elevated LH within the estrus cycle's negative feedback phase. Moreover, insulin signaling abnormality may alternate the basal releasing of hormones.

On the other hand, previous studies reported no statistical difference between the two diet types regarding the free serum T levels (Cano et al., 2008; Roberts et al., 2017). However, one of these studies demonstrated a linear correlation between the T levels and the number of cysts in the ovary of individual rats in the HFHS group (Roberts et al., 2017).

Our results showed that rats fed on MSG manifested elevated LH and androgen levels. These findings agree with the results of Mondal et al. (2018). Their suggested explanation is that MSG can initiate a positive feedback mechanism on the anterior pituitary by increasing LHRH, which augments LH secretion. Creanga et al. (2008) reported that around one-five of serum T level is released by hyperinsulinemia, increasing LH secretion. Previous studies reported that LH and T levels were significantly increased in light-exposed rats (Zhang et al., 2021). The suggested explanation is that prolonged light exposure may decrease melatonin, which functions directly on the hypothalamus cells and reduces the secretion of the gonadal releasing hormone, leading to increased LH and T levels. These findings align with our study results that showed a significant increase in LH and T levels.

In many ways, obesity participates in PCOS development through insulin resistance and producing

Testosterone from androstenedione in the circulation while decreasing gonadotropin secretion (Arner, 2005). Visceral fat significantly contributes to developing PCOS insulin resistance (Rosen and Spiegelman, 2014). Testosterone and a high-calorie diet probably promote visceral fat accumulation and insulin resistance in women by suppressing lipolysis and enhancing lipogenesis (Rosenfield and Ehrmann, 2016). Dunaif et al., 1992 found that most hyperandrogenic women had androgenic ovarian dysfunction that had nothing to do with elevated serum LH or polycystic ovarian morphology.

Hyperinsulinemia enhances LH stimulation of androgen production from ovaries through up-regulating LH-binding sites and promoting androgen secretion in response to LH at the cytochrome $P450C_{17}$ (Rosenfield and Ehrmann, 2016). Thus, all management ways that decrease serum insulin remarkably improve ovulation and hyperandrogenaemia in PCOS (Turkmen et al., 2016). Both significant increases in serum testosterone in the three PCOS groups and significant hyperinsulinism (especially in the L/L group) were demonstrated by our results, which may explain this increase in the mean ovarian diameter.

Animals in all groups had significantly higher blood glucose levels and showed insulin resistance, as concluded by their high HOMA-IR scores compared to controls. Our results support what was previously reported by Roberts et al., 2017 who demonstrated that animals in the HFHS group had more glucose levels than controls and exhibited insulin resistance.

Our current study also revealed that a continuous light environment caused a significant rise in fasting insulin and glucose levels with elevated HOMA-IR scores. Albreiki et al., (2017) demonstrated that bright light at night was accompanied by a marked increase in plasma glucose and insulin, suggesting glucose intolerance and insulin insensitivity, concomitant with our results. This finding supports what was previously reported by Skinner et al. (2019), who also reported that the increased blood glucose levels induced by the disrupted light cycle exceeded that of the HFD. They suggested that circadian misalignment negatively affects neuroendocrine regulation of body weight and central regulation of glucose homeostasis.

Assessment of lipid profile in the current work revealed higher TG and total cholesterol in all experimental groups compared to controls. Serum LDL significantly increased in HFHS+MSG and L/L groups compared to the control. These results could be related to the apparent insulin resistance and the development of dyslipidemia in these groups. Insulin resistance could also alter systemic lipid metabolism and the development of dyslipidemia (Ormazabal et al., 2018).

Surprisingly, no significant difference was found in HDL levels in the studied groups. This contradicts the work done by Collison et al. (2009), who demonstrated that MSG significantly elevated serum HDL-C, and several studies have reported that circadian misalignment is accompanied by low HDL-cholesterol levels (Ferraz-Bannitz et al., 2021).

Histologically, our study revealed degenerative follicles with desquamated cells in the lumen and dilated cysts lined with flattened cells, more atretic follicles, and a reduction in the number of CL, indicating ovulatory interruption in the HFHS group (Volk et al., 2017). This also agrees with Roberts et al. (2017), who observed the presence of substantial numbers of follicular cysts in HFHS ovaries and a considerable elevation of cystic counts compared to controls. In addition, Ko et al., 2017 found that changes in ovarian histology indicate that female reproductive function may be changed due to high sugar intake.

Following Eweka et al.'s (2011) study, the extracted ovarian specimens from MSG-treated animals showed hypertrophy of the theca folliculi cells, complete distortion, and destruction of the basement membrane between the theca folliculi from the zona granulosa. Degenerative changes with pyknotic nuclei and vacuolated cytoplasm were demonstrated in the oocyte and granulosa cells (Ali et al., 2014). Moreover, the higher dose of MSG led to degenerative and atrophic changes in the ovaries with either apoptotic or necrotic cell death (Eweka and Om'Iniabohs, 2007). Our histopathological results in the MSG group also agreed with those of Bojanić et al., 2009 who reported cystic degenerative effects in the ovary with many atretic follicles and no corpora lutea. In the L/L group, increased number of cystic dilated follicles, thickening of the tunica albuginea in many phases, atretic follicles, fewer granular cell layers, and absent layers of oocytes agreed with Kang et al.'s findings (2015).

Compared to control, the PCO group induced by HFHS revealed a uterus lined with stratified columnar epithelium with underlying connective stroma containing dilated uterine glands. O'Connor et al., 1996 demonstrated that hyperplasia was principally demonstrated in the luminal and glandular epithelium of endometrium and myometrium of the HFD group, which agrees with our results. Kayode et al. (2021) recommended that a high-fat diet may induce some bioactive agents that induce endometrial hyperplasia and protect the uterus against elevated levels of hormones, lipids, and oxidative stress.

Currently, the HFHS+MSG group showed uterine hypertrophied changes. The increase in estrogen levels in the MSG-fed animals may indicate an increase in aromatase enzyme activity that turns Testosterone into estradiol, resulting in elevated estradiol synthesis and the related endometrial changes (Ebbeling et al., 2018, El-Beltagy and Elghaweet, 2016).

In conclusion, to study PCOS with laboratory animals, we have conducted three phenotypes of animal models depending on either diet regimens or altered circadian rhythm. Herein, the continuous light exposure simulates the human sleep disorder, and the intake of HFHS diet simulates the western dietary pattern. The three animal models manifested the key features of PCOS, such as hyperandrogenism, multiple dilated ovarian cysts, the indiscriminative estrous cycle that was arrested in the diestrus phase, and symptoms of metabolic syndrome. Disturbed circadian rhythm and HFHS diet are more consistent with an increased risk of PCOS.

Further research is required to investigate the effect of combined intake of HFHS and the external impacts of continuous light environment on the trait of PCOS and evaluate the potential molecular processes underlying the developed phonotype. More cellular investigations are needed with other techniques like immunohistochemistry and ultrastructural description using an electron microscope; these investigations formed the limitations for

the current study that we will try to elucidate in the following parts of our project.

Funding:

This work received funds from The Hashemite University, Jordan (Research ID:59/2020).

Acknowledgement:

We are grateful to Ms. Yasmeen Jamal Alabdallat for her help in the present study.

Conflict of Interest:

The authors declare the absence of any conflicts of interest.

Statement of Data Availability:

On reasonable request, the supporting data of this study's findings can be provided by the corresponding author, [SN. Amin].

References:

Akintayo, C.O., Johnson, A.D., Badejogbin, O.C., Olaniyi, K.S., Oniyide, A.A., Ajadi, I.O., Ojewale, A.O., Adeyomoye, O.I., Kayode, A.B., 2021. High fructose-enriched diet synergistically exacerbates endocrine but not metabolic changes in letrozole-induced polycystic ovarian syndrome in Wistar rats. Heliyon, 7: e05890.

Aktas, S., Un, I., Barlas, I.O., Ozturk, A.B., Karagul, M.I., 2019. Evaluation of the Rho A/Rho-kinase pathway in the uterus of the rat model of polycystic ovary syndrome. Reprod. Biol, 19: 45–54.

Albreiki, M.S., Middleton, B., Hampton, S.M., 2017. A single night light exposure acutely alters hormonal and metabolic responses in healthy participants. Endocr. Connect, 6: 100–110.

Ali AA, El-Seify GH, El Haroun HM, Mohammed Soliman MA.2014. Effect of monosodium glutamate on the ovaries of adult female albino rats and the possible protective role of green tea. Menoufia Med J, 27:793-800

Anagnostis, P., Tarlatzis, B.C., Kauffman, R.P., 2018. Polycystic ovarian syndrome (PCOS): Long-term metabolic consequences. Metabolism, 86: 33–43.

Apolzan, J.W., Harris, R.B. 2012. Differential effects of chow and purified diet on the consumption of sucrose solution and lard and the development of obesity. Physiol. Behav, 105: 325–331.

Arner, P., 2005. Effects of Testosterone on fat cell lipolysis. Species differences and possible role in polycystic ovarian syndrome. Biochimie, 87: 39–43.

Bojanić, V., Bojanić, Z., Najman, Stevo, Savić, T., Jakovljević, V., Najman, Staša, Jančić, S., 2009. Diltiazem prevention of toxic effects of monosodium glutamate on ovaries in rats. Gen Physiol Biophys, 28: 149–154.

Bracho, G.S., Altamirano, G.A., Kass, L., Luque, E.H., Bosquiazzo, V.L. 2019. Hyperandrogenism induces histo-architectural changes in the rat uterus. Reprod. Sci, 26: 657–668.

Brawer, J.R., Munoz, M., Farookhi, R. 1986. Development of the Polycystic Ovarian Condition (PCO) in the Estradiol Valerate-Treated Rat. Biol. Reprod. 35:647–655.

Cano, P., Jiménez-Ortega, V., Larrad, Á., Toso, C.F.R., Cardinali, D.P., Esquifino, A.I. 2008. Effect of a high-fat diet on 24-h pattern of circulating levels of prolactin, luteinizing hormone, Testosterone, corticosterone, thyroid-stimulating hormone and glucose, and pineal melatonin content, in rats. Endocrine, 33: 118–125.

Chakraborty, S.P. 2019. Patho-physiological and toxicological aspects of monosodium glutamate. Toxicol. Mech. Methods. 29: 389–396.

Chan, Y., 2003. **Biostatistics 102**: quantitative data–parametric & non-parametric tests. Blood Press.

Chu, W., Zhai, J., Xu, J., Li, S., Li, W., Chen, Z.-J., Du, Y. 2020. Continuous light-induced PCOS-like changes in reproduction, metabolism, and gut microbiota in Sprague-Dawley rats. Front. Microbiol, 10: 3145.

Collison, K.S., Maqbool, Z., Saleh, S.M., Inglis, A., Makhoul, N.J., Bakheet, R., Al-Johi, M., Al-Rabiah, R., Zaidi, M.Z., Al-Mohanna, F.A. 2009. Effect of dietary monosodium glutamate on trans-fat-induced nonalcoholic fatty liver disease. J. Lipid Res, 50: 1521–1537.

Creanga, A.A., Bradley, H.M., McCormick, C., Witkop, C.T. 2008. Use of metformin in polycystic ovary syndrome: a meta-analysis. Obstet. Gynecol, 111: 959–968.

Darios, E.S., Seitz, B., Watts, S.W. 2012. Smooth muscle pharmacology in the isolated virgin and pregnant rat uterus and cervix. J. Pharmacol. Exp. Ther, 341: 587–596.

Dunaif A, Givens J, Haseltine F, Merriam G, 1992. **Polycystic Ovary Syndrome.** Cambridge, MA: Blackwell Scientific Publications.

Ebbeling, C.B., Feldman, H.A., Klein, G.L., Wong, J.M.W., Bielak, L., Steltz, S.K., Luoto, P.K., Wolfe, R.R., Wong, W.W., Ludwig, D.S. 2018. Effects of a low carbohydrate diet on energy expenditure during weight loss maintenance: randomized trial. BMJ, 363: k4583.

El-Beltagy, A.E.-F.B.M., Elghaweet, H.A. 2016. Adverse effects of monosodium glutamate on the reproductive organs of adult Female albino rats and the possible ameliorated role of carob (Ceratonia Siliqua). J. Biosci. Appl. Res. 2: 170–184.

Eweka, A., Igbigbi, P., Ucheya, R. 2011. Histochemical studies of the effects of monosodium glutamate on the liver of adult Wistar rats. Ann. Med. Health Sci. Res, 1: 21–30.

Eweka, A., Om'Iniabohs, F. 2007. Histological studies of the effects of monosodium glutamate on the small intestine of adult Wistar rat. Electron J Biomed, 2: 14–18.

Farhud, D., Aryan, Z., 2018. Circadian rhythm, lifestyle and health: a narrative review. Iran. J. Public Health, 47: 1068.

Ferraz-Bannitz, R., Beraldo, R.A., Coelho, P.O., Moreira, A.C., Castro, M., Foss-Freitas, M.C. 2021. Circadian Misalignment Induced by Chronic Night Shift Work Promotes Endoplasmic Reticulum Stress Activation Impacting Directly on Human Metabolism. Biology, 10: 197.

Friedewald, W.T., Levy, R.I., Fredrickson, D.S. 1972. Estimation of the concentration of low-density lipoprotein cholesterol in plasma, without use of the preparative ultracentrifuge. Clin. Chem, 18: 499–502.

Gaspar, R.S., Benevides, R., Fontelles, J., Vale, C.C., França, L.M., Barros Pde, T., Paes, A. 2016. Reproductive alterations in hyperinsulinemic but normoandrogenic MSG obese female rats. J Endocrinol, 229: 61–72.

Goodarzi, M.O., Dumesic, D.A., Chazenbalk, G., Azziz, R. 2011. Polycystic ovary syndrome: etiology, pathogenesis and diagnosis. Nat. Rev. Endocrinol, 7: 219–231.

Hilal, G., Fatma, T., Ferruh, Y., Sabire, G., Yüksel, A. 2020. Effect of high-fat diet on the various morphological parameters of the ovary. Anat. Cell Biol, 53:58-67.

Hu, M., Zhang, Y., Feng, J., Xu, X., Zhang, J., Zhao, W., Guo, X., Li, J., Vestin, E., Cui, P. 2018. Uterine progesterone signaling is a target for metformin therapy in PCOS-like rats. J. Endocrinol, 237: 123–137.

Kang, X., Jia, L., Li, Y., Zhang, X., 2017. Acupuncture attenuates hyperglycaemia and improves ovarian function in female rats subjected to continuous light exposure. Acupunct. Med. 35: 352–359.

Kang, X., Jia, L., Shen, X., 2015. Manifestation of hyperandrogenism in the continuous light exposure induced PCOS rat model. BioMed Res. Int. 2015:943694.

Kayode, O., Kayode, A., Mgbojikwe, I., Rotimi, D. 2021. Effect of Ketogenic Diet on Monosodium Glutamate-Induced Uterine Fibroids in Female Wistar Rats. J. Babol Univ. Med. Sci, 23: 1–8.

Kiernan JK. 2001.**Histological and Histochemical Methods. In: Theory and practice. 3rd ed.,** Arnold Publisher, London, New York, and New Delhy.

Ko, E.-A., Kim, H.-R., Kim, Y.-B., Kim, H.-S., Lee, S.-H..2017. Effect of High Fructose Corn Syrup (HFCS) intake on the female reproductive organs and lipid accumulation in adult rats. Dev. Reprod. 21:151-156

la Fleur, S., Luijendijk, M., Van Rozen, A., Kalsbeek, A., Adan, R.2011. A free-choice high-fat high-sugar diet induces glucose intolerance and insulin unresponsiveness to a glucose load not explained by obesity. Int. J. Obes. 35: 595–604.

Lim, Y.C., Hoe, V.C., Darus, A., Bhoo-Pathy, N. 2018. Association between night-shift work, sleep quality and metabolic syndrome. Occup. Environ. Med, 75: 716–723.

McCORMACK, C.E., 1973. Acute Effects of Altered Photoperiods on the Onset of Ovulation in Gonadotropin-Treated Immature Rats. Endocrinology, 93: 403–410.

McLean, A.C., Valenzuela, N., Fai, S., Bennett, S.A. 2012. Performing vaginal lavage, crystal violet staining, and vaginal cytological evaluation for mouse estrous cycle staging identification. JoVE, 15: e4389.

Mondal, M., Sarkar, K., Nath, P.P., Paul, G., 2018. Monosodium glutamate suppresses the female reproductive function by impairing the functions of ovary and uterus in rat. Environ. Toxicol, 33:198–208.

Moore, K., 2003. **Congenital malformations due to environmental factors. 2nd Ed** Saunders, Philadelphia.

Moustafa, A. 2020. Effect of light-dark cycle misalignment on the hypothalamic-pituitary-gonadal axis, testicular oxidative stress, and expression of clock genes in adult male rats. Int. J. Endocrinol, 2020:1426846.

Nurullahoglu-Atalik KE, Yerlikaya Humeyra, Oz Mehmet, Esen Hasan. 2020. Determining the Response to Statins in Rat Aorta Using High Fat Diet.JJBS, 13(1):1-6.

Ormazabal, V., Nair, S., Elfeky, O., Aguayo, C., Salomon, C., Zuñiga, F.A. 2018. Association between insulin resistance and the development of cardiovascular disease. Cardiovasc. Diabetol, 17: 1–14.

Roberts, J.A., Carpenter, R.M., Blythe, S.N., Toporikova, N. 2020. FSH/AMH ratio and adipocyte size are linked to ovarian dysfunction. Endocr. Res, 45: 174–189.

Roberts, J.S., Perets, R.A., Sarfert, K.S., Bowman, J.J., Ozark, P.A., Whitworth, G.B., Blythe, S.N., Toporikova, N. 2017. High-fat high-sugar diet induces polycystic ovary syndrome in a rodent model. Biol. Reprod, 96: 551–562.

Rosen, E.D., Spiegelman, B.M. 2014. What we talk about when we talk about fat. Cell, 156: 20–44.

Rosenfield, R.L., Ehrmann, D.A., 2016. The pathogenesis of polycystic ovary syndrome (PCOS): the hypothesis of PCOS as functional ovarian hyperandrogenism revisited. Endocr. Rev, 37: 467–520.

Sajadi, M., Noroozzadeh, M., Bagheripour, F., Tehrani, F.R. 2018. Contractions in the isolated uterus of a rat model of polycystic ovary syndrome compared to controls in adulthood. Int. J. Endocrinol. Metab, 16: e63135.

Samuelsson, A.-M., Matthews, P.A., Argenton, M., Christie, M.R., McConnell, J.M., Jansen, E.H., Piersma, A.H., Ozanne, S.E., Twinn, D.F., Remacle, C., 2008. Diet-induced obesity in female mice leads to offspring hyperphagia, adiposity, hypertension, and insulin resistance: a novel murine model of developmental programming. Hypertension, 51: 383–392.

Skinner, N.J., Rizwan, M.Z., Grattan, D.R., Tups, A., 2019. Chronic light cycle disruption alters central insulin and leptin signaling as well as metabolic markers in male mice. Endocrinology, 160:2257–2270.

Toscani, M. K., Mario, F. M., Radavelli-Bagatini, S., Wiltgen, D., Matos, M. C., & Spritzer, P. M. 2011. Effect of high-protein or normal-protein diet on weight loss, body composition,hormone, and metabolic profile in southern Brazilian women with polycystic ovary syndrome: a randomized study. Gynecol Endocrinol, 27: 925-930.

Turkmen, S., Ahangari, A., Bäckstrom, T. 2016. Roux-en-Y gastric bypass surgery in patients with polycystic ovary syndrome and metabolic syndrome. Obes. Surg. 26: 111–118.

Visser JA, de Jong FH, Laven JS, Themmen AP.2006. Anti-Müllerian hormone: a new marker for ovarian function. Reproduction, 131:1-9.

Volk, K.M., Pogrebna, V.V., Roberts, J.A., Zachry, J.E., Blythe, S.N., Toporikova, N., 2017. High-fat, high-sugar diet disrupts the preovulatory hormone surge and induces cystic ovaries in cycling female rats. J. Endocr. Soc. 1: 1488–1505.

Wang, T., Oltra-Rodríguez, L., García-Carrillo, N., Nieto, A., Cao, Y., Sánchez-Ferrer, M.L., 2017. Ultrasonography in Experimental Reproductive Investigations on Rats. J Vis Exp. 130:56038.

Weber, A.L., Adler, N.T., 1979. Delay of Constant Light-Induced Persistent Vaginal Estrus by 24-Hour Time Cues in Rats. Science, 204:323-325.

Wellington, D., Mikaelian, I., Singer, L., 2013. Comparison of ketamine–xylazine and ketamine–dexmedetomidine anesthesia and intraperitoneal tolerance in rats. J. Am. Assoc. Lab. Anim. Sci. 52: 481–487.

Wen, L., Liu, Q., Xu, J., Liu, X., Shi, C., Yang, Z., Zhang, Y., Xu, H., Liu, J., Yang, H. 2020. Recent advances in mammalian reproductive biology. Sci. China Life Sci. 63, 18–58.

Zhang, L., Liu, Y., Li, M., Zhu, X., Shi, Y., 2021. Effect of a high-calorie diet and constant light exposure on female reproduction, metabolism and immune inflammation: A comparative study of different mouse models. Am. J. Reprod. Immunol,86: e13479.

Zhou Q, Chen H, Yang S, Li Y, Wang B, Chen Y, Wu X.2014. High-fat diet decreases the expression of Kiss1 mRNA and kisspeptin in the ovary and increases ovulatory dysfunction in postpubertal female rats. Reprod Biol Endocrinol, 12:127.

JJBS

Volume 15, Number 5, December 2022
ISSN 1995-6673
Pages 825 – 831
https://doi.org/10.54319/jjbs/150511

Jordan Journal of Biological Sciences

Gelatin-Fibroin Sponges as Scaffolds in Cancer Tissue Engineering

Hoang Viet Le[1,3], Tham Thi Hong Nguyen[2,3], Vu Nguyen Doan[1,2,3], Ha Le Bao Tran[1,2,3*]

[1]*Laboratory of Tissue Engineering and Biomedical Materials, University of Science, Ho Chi Minh City, Vietnam;*[2]*Department of Physiology and Animal Biotechnology, Faculty of Biology and Biotechnology, University of Science, Ho Chi Minh City, Vietnam;* [3]*Vietnam National University, Ho Chi Minh City, Vietnam*

Received: May 4, 2022; Revised: June 12, 2022; Accepted: August 18, 2022

Abstract

Cancer tissue engineering using three-dimensional (3D) cell culture scaffolds has been reported to handle the limitations of two-dimensional (2D) cell culture in vitro and in vivo cancer models. In this paper, the scaffolds were produced via the freeze-drying technique and chemical cross-linking. 1-ethyl-3(3-dimethylamino propyl) carbodiimide hydrochloride (EDC) has been used as a crosslinker for conjugation between gelatin and silk fibroin (SF). The gelatin-fibroin (GF) scaffold evaluated the physicochemical characteristics such as microstructure, functional groups, swelling rate, degradability as well as some biological characteristics including in vitro cytotoxicity,for physicochemical characteristics such as microstructure, functional groups, swelling rate, degradability, and some biological characteristics including in vitro cytotoxicity and cell adhesion, cell proliferation and the spheroid forming capacity of MCF-7 cells on this scaffold. The results showed that the GF scaffold with the uniform pore size demonstrated suitable physicochemical properties that controlled swelling and degradation characteristics. The GF scaffold had no toxicity on human fibroblast cells (hF), and supported MCF-7 cells' adhesion, proliferation, and spheroid formation. In conclusion, this study successfully considered the potential of the GF scaffold as an in vitro 3D cell-culture scaffold in cancer tissue engineering in particular and tissue engineering in general.

Keywords: gelatin, silk fibroin, scaffold, cancer tissue engineering

1. Introduction

According to the GLOBOCAN 2020 estimates of cancer incidence and mortality provided by the International Agency for Research on Cancer, cancer is considered the leading cause of death and the main cause of reducing life expectancy worldwide. From 2015 to 2020, Breast cancer was commonly diagnosed cancer worldwide(Rashan *et al*., 2018; Youssry *et al*., 2019; Al-Momany *et al*., 2020; Sung *et al*., 2021; Ferlay *et al*., 2021). This shows the urgency in studying tumor formation, tumor invades and metastasizing, and the primary cause of cancer-related death. Human tumors consist of many different types of cells, such as cancer cells, fibroblasts, immune cells, etc., which function and are affected differently by many factors such as chemical, physical, and biological factors in the microenvironment. These components contribute to the growth of different regions within the same tumor (Thoma *et al*., 2014). However, the production of therapeutic drugs has encountered difficulties when entering the clinical trial stage because a suitable drug test model similar to tissue mass in vivo has not been found (Ibrahim *et al*., 2010; Aliwaini *et al*., 2020).

Typically, most of the experimental experiments were done in 2D cultures. Cells in the human body grow in an organized 3D matrix, surrounded by other cells. Individual cells are examined through their authors with neighboring cells and extracellular matrix (Smalley *et al*., 2006; Castells-Sala *et al*., 2013; Ha *et al*., 2013; Wu *et al*., 2014; Trivedi *et al*., 2021). Mono-layer culture in cancer research is a simple model that can be performed with many different concentrations and cell lines. If cultured for a long time, it will affect the cells inside.

Therefore, researchers only use mono-layer cell cultures to carry out simple studies in a short, not long, time. A significant drawback of this method is the misalignment of cell-cell, cell-ECM interactions, leading to the failure to form a tissue-like structure in the body. Since the tissue mass does not have the same system as the body's tissue mass, it will significantly affect the evaluation of the effectiveness of cancer treatments, therapies, and drugs. Given the limitations of mono-layer culture, animal models are quite common in the study of tumor growth and drug screening trials. Using animals in research, especially rats, often has the advantages of genetic similarity with humans, small size, ease of manipulation, and short reproduction time to observe the process performance. There are three types: mouse tumor-bearing mice, immunocompromised mice carrying human

* Corresponding author. e-mail: tlbha@hcmus.edu.vn.

List of abbreviations : Silk fibroin SF; Gelatin-fibroin GF ;Human fibroblast HF

tumors, and humanized mice bearing human tumors. Besides the advantages, there are also many disadvantages when investing in research using this model is relatively high. The immune response and growth factors in mice differ from humans. Although the animal body carries a human tumor, that tumor is still modified to fit the animal body. However, the issue of bioethics is one of the leading issues when using this model.

One of the simplest 3D tissue mass models is the cluster cell consisting of the hanging drop and hydrogel methods to generate spherical tumors. Using gels to model cell clusters that can simulate the extracellular matrix, spherical tumor structures also helps simulate cell-cell, cell-ECM interactions, and extracellular signals of a mass of tissue in vivo. However, the use of this gel suffers from the disadvantages of biodegradability and porosity, which may affect cell distribution (Tung *et al*., 2011). Therefore, creating a suitable drug test model will speed up the drug testing process and reduce production costs.

Tissue engineering, which overcomes the limitations of traditional methods, offers new treatment opportunities for several diseases and is a new method for modeling human physiology. To restore a new tissue by tissue engineering, three components are required: cells, biological material (scaffolds), and bioactive molecules. Among them, biomaterials (scaffolds) play a significant role. The scaffold substrates can be highly efficient in loading and delivering cells to specific sites. Therefore, the scaffolds play an essential role in protecting and facilitating the interaction of the cell with the surrounding environment (Ma *et al*., 2005).

Recently, the combination of gelatin and fibroin has been examined for creating a new scaffold with suitable properties for cell culture and overcomes the disadvantages of both gelatin and fibroin. The gelatin-fibroin scaffolds have a porous structure, are highly biodegradable, non-toxic to cells, and support cell adhesion, and proliferation. When combined with cell culture, the tissue will be produced. The in vitro 3D cancer tissue mass is similar to the in vivo tissue mass (Jetbumpenkul *et al*., 2012; Lu *et al*., 2010; Petrenko *et al*., 2011; Asuncion *et al*., 2016; J *et al*., 2015; Pan *et al*., 2016; Dong *et al*., 2019; Nguyen-Thi *et al*., 2018; Nguyen *et al*., 2018).

This study aims to create gelatin-fibroin (GF) sponges based on the freeze-drying technique and chemical cross-linking EDC. The GF was generated with suitable properties as a scaffold for application in the cancer tissue engineering on microstructure, functional groups, swelling rate, and degradation properties; and investigated for its effects on hF in terms of cytotoxicity, cell adhesion, cell proliferation, and the spheroid forming capacity of MCF-7 cells on this scaffold.

2. Materials and Methods

2.1. Creating GF scaffolds

Fibroin solution from silk used for this study was provided by TEBM lab, University of Science, VNU-HCM. The solution of 3.5% fibroin and 0.24% EDC (Sigma-Aldrich, USA) with a ratio of 8:1 (v/v) was mixed, left for 15 minutes at room temperature, and then added 9% gelatin (Merck, USA) with a ratio of 9:8 (v/v) to the above mixture, left for 2 hours at room temperature. Gelatin-fibroin mixture was frozen at -86°C (Panasonic, Japan) overnight and freeze-dried (SP Scientific, England) at 100 mT pressure, -73°C temperature for 12 hours. Sponges were washed with distilled water for 7 hours, changed the water every 20 minutes. The soaked sponges were frozen at -86°C and freeze-dried a second time with a pressure of 100 mT and a temperature of -73°C for 8 hours. Finally, these sponges were sterilized by gamma irradiation dose 25kGy and evaluated some characteristics as scaffolds in tissue engineering.

2.2. Structure of scaffolds

Images were taken using an inverted microscope (Olympus, Japan) equipped with a DP2-BSW digital camera, and a scanning electron microscope (SEM, JSM-6510, JEOL, Japan).

2.3. Functional groups

The chemical compounds of the GF scaffold were identified by PerkinElmer Fourier transform infrared (FTIR) and diode array (DA) spectrometers (Nicolet 5700, USA).

2.4. Swelling rate

According to BS EN 13726-1:2002 standard, the change of a GF scaffold weight in solution A (8.298g of sodium chloride and 0.368g of calcium chloride dihydrate in deionized water and making up to 1 liter) after incubating at 37°C for 30 minutes, was used to observe the swelling rate (%):

Swelling rate (%) = (W1 -W0)/W0 x 100%,

W0 is the weight of the GF scaffold, and W1 is the weight of the GF scaffold after incubating in solution A.

2.5. Degradation rate

The weights of GF scaffold before (D) and after incubating in PBS (Gibco, USA) solution at 37°C; then dried for 15 minutes at 60°C and weighed at 1; 2; 3; 4; 5; 6; 7; 8; 9 days (L) were used to calculate the degradation ratio as per the equation:

The degradation ratio (%) = (D - L)/D x100%

2.6. In vitro cytotoxicity

Human fibroblast cells (hFs) used for cytotoxicity testing are available in the Laboratory of Tissue engineering and Biomedical Materials. The level of cytotoxicity of GF scaffolds was performed by measuring the relative viability of this according to the ISO 10993-5:2009 instruction. The test sample (GF scaffold) and the positive control (latex) were incubated in a complete medium (DMEM-F12 (Sigma–Aldrich, USA), which supplemented with 10% Fetal Bovine Serum (FBS, Sigma–Aldrich, USA) and 1X antibiotics (Sigma–Aldrich, USA) at 37°C for 24 hours. The negative control was the complete medium. The GF and latex were collected and placed on the subconfluent monolayer of the cells and incubated at 37 °C for 24 hours. The forms of cells were captured with an inverted microscope equipped with a DP2-BSW microscope digital camera.

2.7. Cell seeding

MCF-7 cells ($1.5x10^4$cells per milliliter) were seeded into a GF scaffold of 3x3x3mm by incubating in the

culture medium at 37 °C, 5% CO_2 for 24 hours. The non-adherent cells were collected and used to calculate the cell seeding efficiency as per the formula:

The cell seeding efficiency (%) = (Total cells were seeded into scaffolding - The non-adherent cells)/Total cells were seeded into scaffold x 100%

2.8. Cell proliferation

MCF-7 cells were cultured in the GF scaffold at 37 °C, 5% CO_2 for 0; 2; 4; 6; 8 days and evaluated proliferation by an in vitro DNS (3,5-dinitrosalicylic acid) assay. The culture medium was collected, and 100 µl of DNS (1%) (Sigma–Aldrich, USA) was added and mixed at 80 °C for 20 minutes. The color of this liquid was quantified by measuring the absorbance at 570 nm using a microplate reader (Biochrom, USA) (Pepper S. *et al*, 2006).

2.9. Histological evaluation

After seeding into the GF scaffold, MCF-7 cells were cultured in the scaffold with the culture medium at 37°C, 5% CO_2, and replaced the medium every 2 days. The MCF-7-GF scaffold complex was collected after 7 days cultured and fixed with 10% formalin at 4°C for 24 hours. This complex after dehydrating by ethanol and immersing in xylene was embedded in paraffin. These paraffin sections were cut at 4 µm, and stained with H&E (Hematoxylin and Eosin). The inverted microscope equipped with a DP2-BSW microscope digital camera was used to take a photo of this complex after staining.

2.10. Statistical analysis

Each treatment was repeated 3 times. GraphPad Prism version 8.0.2 (GraphPad Software, Inc., San Diego, CA) was used to perform all statistical analyses.

3. Results

3.1. Creating GF scaffolds

The GF scaffolds consisted of 3.5% fibroin, 9% gelatin, cross-linked by 0.24% EDC. Fig.1 showed many pores of the GF scaffolds that can allow cells to adhere inside.

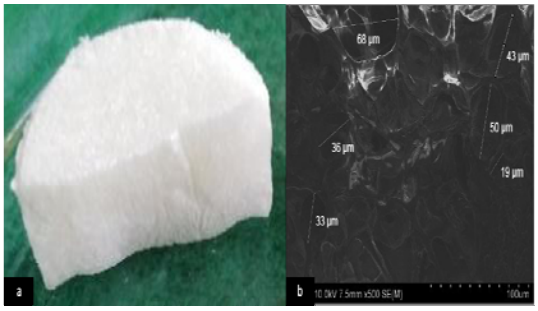

Figure 1. A GF scaffold (a), Structure of a GF scaffold under SEM (b)

3.2. Chemical structure of GF scaffolds

The FTIR spectra in Fig.2 showed an absorption peak at 1,637cm^{-1}, which belongs to the wavelength of the β-sheets form (1,620 – 1,640 cm^{-1}). Besides, the FTIR spectra also showed another absorption peak at 3,435cm^{-1}, which belongs to the wavelength of the form of the N-H bonds (3,200 – 3,400 cm^{-1}). This proved that the GF scaffolds also retain the distinctive properties of gelatin (Hermanto *et al*., 2013). In addition, another absorption peak belongs to the wavelength of the form of the CO-NH bonds (1,550 – 1,650 cm^{-1}), indicating that EDC cross-linked fibroin and gelatin. The FTIR spectra did not show any absorption peaks which belong to the wavelength of the form of the N=C=N bonds (2,120 – 2,145 cm^{-1}) significantly of EDC.

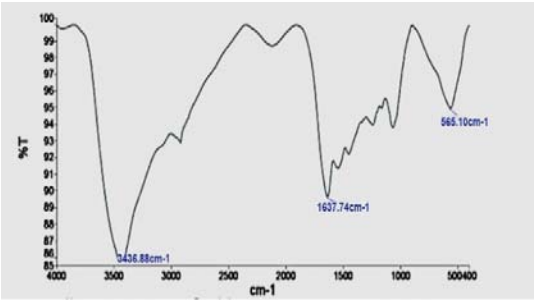

Figure 2.FTIR spectra of GF scaffolds

3.3. Swelling rate of GF scaffolds

The Fig.3 showed that the swelling rate of the GF scaffold is 714.7 ± 61.10% which is more than the swelling rate of scaffolds that use a glutaraldehyde cross-linking method (TK1, 400%) (Dong *et al*., 2019) and other scaffolds which do not use any cross-linking methods (TK2, 127%) (Lu *et al*., 2019). The swelling rates of the GF scaffolds, the glutaraldehyde cross-linking scaffolds and the non-cross-linking scaffolds have a statistical difference (P-value < 0.05).

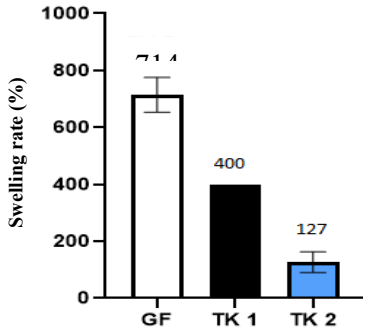

Figure 3. Swelling rate of GF scaffolds

3.4. Degradation rate of GF scaffolds

The degradability of GF scaffolds was investigated within nine days in PBS solution. The results showed that the GF scaffolds degraded by 11.4% by weight in the PBS solution in nine days, the scaffolds remained around 90% after seven days.

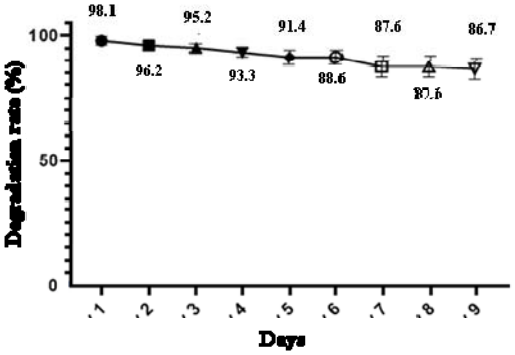

Figure 4. Degradation rate of GF scaffolds

3.5. In vitro cytotoxicity of GF scaffolds

The latex, employed as the positive control, caused severe cell death. Meanwhile, the cells had the standard appearance and could proliferate typically around and under the GF scaffolds. It could be concluded GF scaffolds did not cause toxicity to hFs that is level 0 according to ISO 10993-5. Therefore, the GF scaffolds could be used in cell culture.

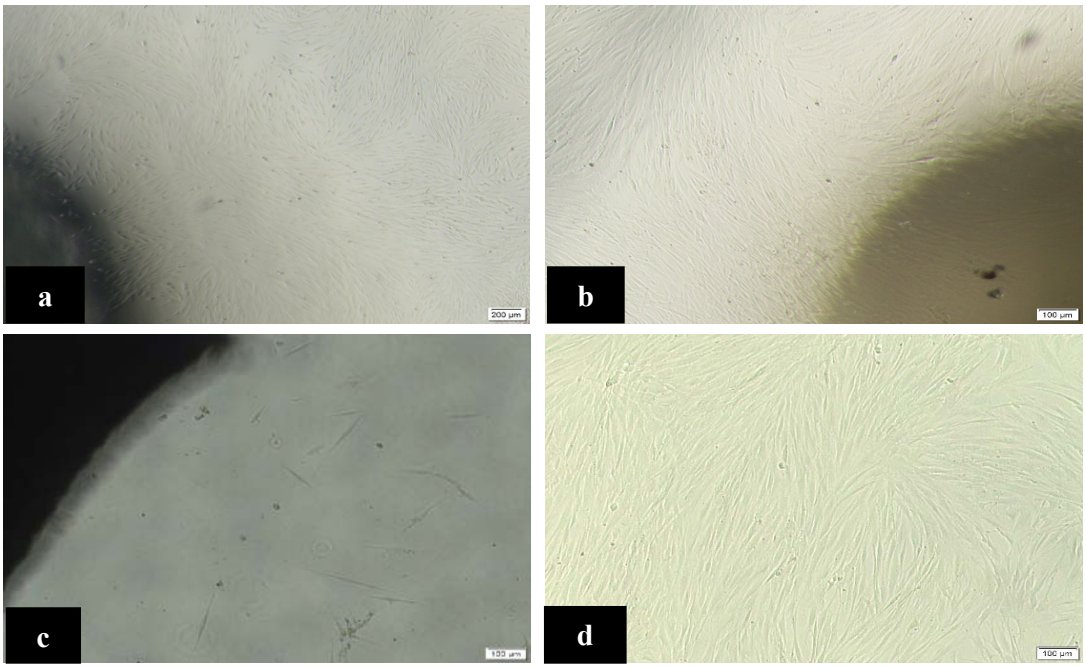

Figure 5. In vitro cytotoxicity of GF scaffolds (a, b), positive control (c), and negative control (d) (n = 3)

3.6. Cell proliferation in GF scaffolds

The MCF-7 cells could adhere and form spheres in the GF scaffolds. At 570 nm, the OD value is inversely proportional to the cell density (Fig.6). These results showed that the GF scaffolds could make the MCF-7 cells adhesion and proliferation. From D-0 to D-2, the OD value has no statistical difference. From D-0 to D-4, the OD value decrease and have a statistical difference (P-value < 0.001). However, from D-4 to D-8, the OD values were in the stable stage.

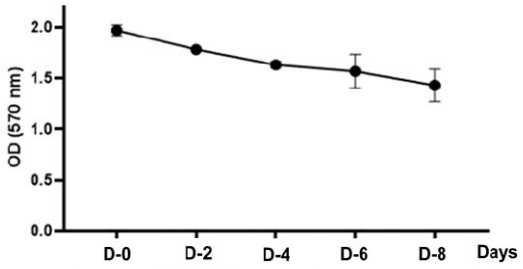

Figure 6. The OD value of the DNS experiment from D-0 to D-8

Fig.7 showed MCF-7 cells could adhere and form spheres inside GF scaffolds. These spheres increased from D-1 (d-31.82 µm) to D-7 (d-119.44 µm) while being cultured by the incubation method.

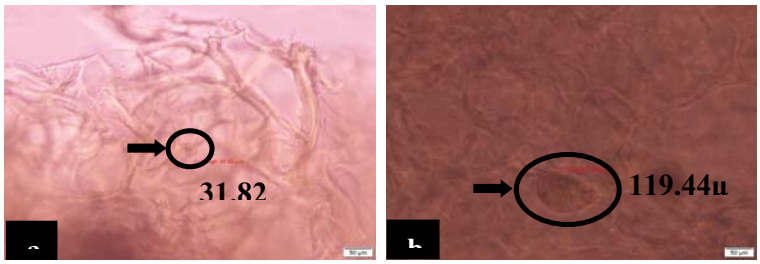

Figure 7. The MCF-7 cells in GF scaffolds on D-1 (a), and D-7 (b)

The MCF-7 cells were seeded into the GF scaffolds with a $1.5x10^4$ cells/mL density. The efficiency of this seeding process was 94.2%. The GF scaffolds could absorb the cell solution and keep them inside. After that, the cells could adhere stably to the GF scaffolds.

On D-7, the complex of MCF-7 cells and a GF scaffold included many cells in the extracellular matrix. Fig.8 showed that the nuclear area of MCF-7 cells got dark purple. The nucleus became clumped.

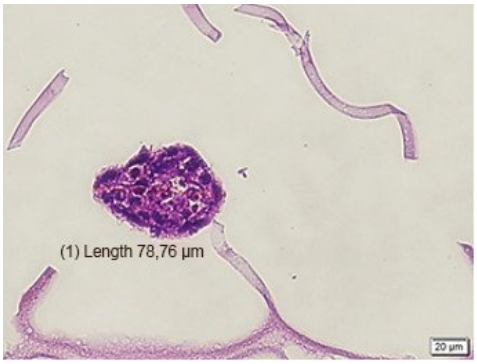

Figure 8. H&E staining of MCF-7 cells on D-7

4. Discussion

Cancer tissue engineering uses scaffolds for culturing cancer cells to study the proliferation, invasion, and metastasis of tumors. In addition, a three-dimensional scaffold is a temporary structure that supports cells to grow in each environment, which can eventually integrate to become tissue (Asghar *et al*., 2015). The supporting scaffold has a porous structure, the ability to provide adequate nutrients to meet the metabolic needs of the cell; it also supports the formation and distribution of vessels. Therefore, cancer tissue engineering has shown great potential when it is possible to simulate the mass of cancer tissue *in vivo* (Ehsan *et al*., 2014).

The combination of gelatin and fibroin by crosslinking not only inherits the superior properties of these two materials but also creates a new scaffold with suitable properties for cell culture and overcomes the disadvantages of both gelatin and fibroin (Jetbumpenkul *et al*., 2012, Wang *et al*., 2016). The scaffolds formed by pure fibroin solution could only make a layer-by-layer structure rather than a porous structure. The properties of durability and compression of scaffolds were lost. By supplementing gelatin in the mixture, the number of layers decreased, and more porous structures formed in the scaffolds because of the interaction of fibroin-gelatin, ultimately decreasing the tendency of the solid from the freezing liquid phase(Lu *et al*., 2010; Asuncion *et al*., 2016). The porous were formed while the ratios of fibroin-gelatin in weight were above 20%. The pore size depended on the concentration of fibroin and crosslinking method (Lu *et al*., 2010). The pore would be enlarged inside the crosslinked scaffolds because carboxyl side groups in gelatin are needed for fibroin-gelatin crosslinking by EDC (Asuncion *et al*., 2016). EDC molecules do not participate in cross-linking and rapidly degrade to non-toxic products, so EDC is less toxic to the body (Ha *et al*., 2013). The glass transition temperature (Tg) is the temperature at which the amorphous regions experience the transition from a rigid state to a more flexible state making the temperature at the border of the solid-state a rubbery state. This temperature in fibroin occurs between -20°C and -30°C, which affects the pore size of the GF scaffold. Faster freezing (-86°C) will reduce the formation of ice crystals inside the scaffold, so when freeze-drying, the GF scaffold has a small pore size with an average size of 100.6 ± 47.84 µm, which is very suitable for cell growth, allowing the diffusion of nutrients from the outside into the core of the scaffold and the removal of waste products. In addition, the FTIR spectra result with the absorption peaks at 1,637cm^{-1}, and 3,435cm^{-1} proved that the GF scaffold's structure is a combination of gelatin and fibroin (Hermanto *et al*., 2013, Kolev *et al*., 2017).

GF scaffolds were demonstrated to absorb and diffuse the culture medium nutrients into the scaffolds by the swelling rate. The holes structures of the GF scaffolds could increase the water absorption capacity of the scaffolds.

In the process of scaffolds creation, the α-helix forms and random coils forms reconstruct into β-sheets forms to achieve high-strength structures (Kolev *et al*., 2017), suitably for the degradable rate of GF scaffolds. The result is similar to another study (Jetbumpenkul *et al*., 2017), after incubating in PBS for 9 days, our GF scaffolds had a degradable rate of 88.6% the same as the results of Jetbumpenkul *et al*. (2012) after 7 days with the remaining weight being 90%. That is one of the essential characteristics of scaffolds which shows that the strength of the scaffold is sufficient to conduct *in vitro* studies.

We confirmed our GF scaffolds as a non-cytotoxicity scaffold regarding the *in vitro* on hF, and its ability to stimulate MCF-7 adhesion with the efficiency of this seeding process more than 90% while another research showed that the efficiency was 80% (Jetbumpenkul *et al*., 2012). The proliferation processes of the MCF-7 cells in the GF scaffolds were investigated by DNS. A yellow compound could be produced while the remaining glucose in the medium reacts with DNS. Because of the proliferation of the MCF-7 cells, the amount of glucose in the medium gradually decreases. The results of the DNS experiment and the microscope image showed that size of MCF-7 spheres increases while culturing by incubation for eight days. HE staining at 7 days showed that there were multiple cells bound together in a matrix scaffold.

However, the proliferation of the MCF-7 cells in the DNS experiment is not clear from day 4 to day 8 of cultured. Besides, this study required the co-culture of many cell types on the GF scaffold and increased incubation time to evaluate forming of a mass and determine the stage of the descriptor block to conduct drug testing. The results show that the GF scaffold is functional in 3D research *in vitro*.

5. Conclusion

The GF scaffolds were entirely created by freeze-drying and cross-linking with EDC. The pores of these scaffolds were 52.76 - 148.44µm. The average swelling rate was 653.6 - 775.8%. These scaffolds degraded by 11.4% by weight in PBS solution in nine days. GF scaffolds did not cause toxicity to fibroblasts. They could make the MCF-7 cell adhesion and proliferation. Therefore, the GF scaffolds could be used in cancer cell culture.

Acknowledgment

This research is funded by the University of Science, VNU-HCM under grant number T2021-66.

References

Al-MomanyB. Z., HammadH. M. and Ahram M. 2020. Regulation of chemoresponsiveness in triple-negative breast cancer: androgen receptor, ABCG2, and microRNA. *Jordan J. Biol. Sci.*, **13(3)**: 257-265

AliwainiS., El-Bashiti T. and Mortaja K. 2020. Pitavastatin Enhances Doxorubicin-induced Apoptosis in MCF7 Breast Cancer Cells. *Jordan J. Biol. Sci., **13(1)**: 101-105*

Asghar W., El Assal R., Shafiee H. and Pitteri S. 2015. Engineering cancer microenvironments for in vitro 3-D tumor models.*Mater.Today*, **18(10)**: 539-553.

Asuncion M. C. T., Goh J. C.-H. and Toh S.-L. 2016. Anisotropic silk fibroin/gelatin scaffolds from unidirectional freezing.*Mater. Sci. Eng.C,* **(67)**:646-656.

Bhattacharjee P., Kundu B., Naskar D. and Kim H.-W. 2017. Silk scaffolds in bone tissue engineering: An overview.*Biomater.*, **63**: 1-17.

Brizzi M. F., Tarone G. and Defilippi P. 2012. Extracellular matrix, integrins, and growth factors as tailors of the stem cell niche.*Curr. Opin. Cell. Biol.*, **24(5)**: 645-651.

Camarillo I. G., Xiao F., Madhivanan S., Salameh T., Nichols M., Reece L. M. and Sundararajan, R. 2014. Low and high voltage electrochemotherapy for breast cancer: An in vitro model study. In: Sundararajan, R.,**Electroporation-Based Therapies for Cancer: from bascis to clinical applications**, Elsevier Limited 55-102.

Chen J., Venkatesan H. and Hu J. 2018. Chemically Modified Silk Proteins.*Adv. Eng. Mater.*, **20(7)**: 1700961

Comșa Ș., Cimpean A. M. and Raica M. 2015. The story of MCF-7 breast cancer cell line: 40 years of experience in research.*Anticancer Res.*, **35(6)**: 3147-3154.

Cuadros T. R., Erices A. A. and Aguilera J. M. 2015. Porous matrix of calcium alginate/gelatin with enhanced properties as scaffold for cell culture.*J. Mech. Behav. Biomed. Mater.*, **46**: 331-342.

Dong Y. and Mohammadzademoghadam S. 2019.Fabrication and characterisation of electrospun silk fibroin/gelatin scaffolds crosslinked with glutaraldehyde vapour.*Front. Mater. Sci.*, **6**: 1-12.

Egeblad M. and Werb Z. 2002. New functions for the matrix metalloproteinases in cancer progression.*Nat. Rev. Cancer.*, **2(3)**:161.

Ehsan S. M., Welch-Reardon K. M., Waterman M. L., Hughes C. C. and George S. C. 2014. A three-dimensional in vitro model of tumor cell intravasation.*Integr. Biol.,***6(6)**: 603-610.

Erez N., Truitt M., Olson P. and Hanahan D. 2010.Cancer-associated fibroblasts are activated in incipient neoplasia to orchestrate tumor-promoting inflammation in an NF-κB-dependent manner.*Cancer Cell*, **17(2)**: 135-147.

Fernandes M., Rosel D. and Brabek J. 2015. Translation in solid cancer: are size-based response criteria an anachronism?.*Clin. Transl. Oncol.*, **17(1)**: 1-10.

Giussani M., Merlino G., Cappelletti V., Tagliabue E. and Daidone M. G. 2015. Tumor-extracellular matrix interactions: Identification of tools associated with breast cancer progression. *Semin. Cancer. Biol.*, **35**: 3-10.

Hermanto S. and Fatimah W. 2013.Differentiation of bovine and porcine gelatin based on spectroscopic and electrophoretic analysis.*J. Food. Pharm. Sci.*, **1(2013)**:68-73

Holle A. W., Young J. L. and Spatz J. P. 2016. In vitro cancer cell–ECM interactions inform in vivo cancer treatment.*Adv. Drug. Deliv. Rev.*, **97**: 270-279.

Ibrahim, A. and Aqel, A. A. 2010. Effect of Salvia triloba L. f. extracts on neoplastic cell lines. *Jordan J. Biol. Sci.*, **3(2)**: 69-76.

Jetbumpenkul P., Amornsudthiwat P., Kanokpanont S. and Damrongsakkul S. 2012. Balanced electrostatic blending approach–An alternative to chemical crosslinking of Thai silk fibroin/gelatin scaffold.*Int. J. Biol. Macromol.*, **50(1)**: 7-13.

Kalluri and Raghu.2016. The biology and function of fibroblasts in cancer.*Nat. Rev. Cancer.*, **16(9)**: 582.

Kim M. H. and Park W. H. 2016. Chemically cross-linked silk fibroin hydrogel with enhanced elastic properties, biodegradability, and biocompatibility.*Int. J. Nanomed.*,**11**: 2967.

Kolev A., Vassileva V. and Georgiev H. 2017. Interaction between fibroin and alginate in the corresponding blended films.*J. Chem. Technol. Metall.*, **52(3)**:449-456

Kondapaka S. B., Fridman R. and Reddy K. B. 1997.Epidermal growth factor and amphiregulin up-regulate matrix metalloproteinase-9 (MMP-9) in human breast cancer cells.*Int. J. Cancer.*, **70(6)**: 722-726.

Levenson, S A. and Jordan. 1997. MCF-7: the first hormone-responsive breast cancer cell line.*Cancer Res.,***57(15)**: 3071-3078.

Li M., Zhang, C. L., S., Wu, Z. and Yan H. 2002.Study on porous silk fibroin materials: 3. Influence of repeated freeze–thawing on the structure and properties of porous silk fibroin materials.*Polym. Adv. Technol.*, **13(8)**: 605-610.

Lu Q., Zhang X. and Hu X. 2010. Green process to prepare silk fibroin/gelatin biomaterial scaffolds.*Macromol. Biosci.*, **10(3)**: 289-298.

Ma, Z., Kotaki, M., Inai, R.and Ramakrishna, S. 2005. Potential of nanofiber matrix as tissue-engineering scaffolds. *Tissue Eng.*, **11(1-2)**, 101-109.

Nguyen N. T., Doan V. N. and Tran H. L. B. 2018. Generating in vitro solid tumor models on gelatin-alginate scaffolds.*Vietnam J. Sci. Tech. Eng.*, **60(4)**: 25-30.

Nguyen-Thi L.-H., Nguyen S. T. and Tran T. 2020. Anti-cancer Effect of Xao Tam Phan Paramignya trimera Methanol Root Extract on Human Breast Cancer Cell Line MCF-7 in 3D Model.*Adv. Exp. Med. Biol.*.**1292**: 13-25

Oskarsson T. 2013. Extracellular matrix components in breast cancer progression and metastasis.*Breast*, **22**: S66-S72.

Pan T., Song W., Cao X. and Wang Y. 2016. 3D bioplotting of gelatin/alginate scaffolds for tissue engineering: influence of crosslinking degree and pore architecture on physicochemical properties.*J. Mater. Sci. Technol.*, **32(9)**: 889-900.

Pepper S. 2006.Pregnancy-associated breast cancer and metastasis.*Nat. Rev. Cancer.*, **6(4)**: 281.

Petrenko and R.V I. 2011. Coupling of gelatin to inner surfaces of pore walls in spongy alginate-based scaffolds facilitates the adhesion, growth and differentiation of human bone marrow mesenchymal stromal cells.*J. Mater. Sci. Mater. Med.*, **22(6)**:1529-1540.

Philip R. and Hansen J. T. 2008. **TNM staging atlas**, Lippincott William & Wilkins.

Qi Y., Wang H., Wei K., Yang Y. and Zheng R.-Y. 2017. A review of structure construction of silk fibroin biomaterials from single structures to multi-level structures.*Int. J. Mol. Sci.*, **18(3)**: 237.

Rashan, L., Hakkim, F. L., Fiebig, H. H., Kelter, G., Merfort, I., Al-Buloshi, M., & Hasson, S. S. 2018. In vitro Anti-Proliferative Activity of the Rubia tinctorum and Alkanna tinctoria Root Extracts in Panel of Human Tumor Cell Lines hasson. *Jordan J. Biol. Sci*, **11(5)**: 489-494.

Rijal G. and Li W. 2016. 3D scaffolds in breast cancer research.*Biomaterials*, **81**: 135-156.

Sweeney E. E., McDaniel R. E., Maximov P. Y. and Fan P. 2012. Models and mechanisms of acquired antihormone resistance in breast cancer: significant clinical progress despite limitations.*Horm. Mol. Biol. Clin. Investig.*, **9(2)**: 143-163.

Thoma C. R., Zimmermann M., Agarkova I., Kelm J. M. and Krek W. 2014. 3D cell culture systems modeling tumor growth determinants in cancer target discovery.*Adv. Drug Deliv. Rev*., **69**: 29-41.

Tung Y.-C., Hsiao A. Y., Allen S. G., Torisawa Y.-s. and Ho M. 2011. High-throughput 3D spheroid culture and drug testing using a 384 hanging drop array.*Analyst*, **136(3)**: 473-478.

Vargo-Gogola, Tracy and Rosen.2007. Modelling breast cancer: one size does not fit all.*Nat. Rev. Cancer*., **7(9)**: 659.

Wang Y., Wang X., Shi J. and Zhu R. 2016. A biomimetic silk fibroin/sodium alginate composite scaffold for soft tissue engineering".*Sci. Rep.*, **6**: 39477.

Youssry, S. A., Hussein, A. E., El-Sheredy, A. G., Ramadan, R., and El-Sheredy, H. G.2019. Clinical Relevance of LC3B, CXCL10, and Bcl-2 in Breast Cancer. *Jordan J. Biol. Sci*, **12(4)**:471-476

JJBS

Volume 15, Number 5, December 2022
ISSN 1995-6673
Pages 833 – 839
https://doi.org/10.54319/jjbs/150512

Jordan Journal of Biological Sciences

Phytochemical Analysis and Biological Activity of *Micromeria fruticosa* (L.) Collected from Northern Jordan

Tareq M. A. Al-Shboul[1,*], Irsal M. Najadat[2], Emad I. Hussein[3,2] , Wesam M. Al Khateeb[2]

[1]*Department of Chemistry and Chemical Technology, Tafila Technical University, Tafila 66110, Jordan ;* [2]*Department of Biological Sciences, Faculty of Science, Yarmouk University, Irbid 21163, Jordan;* [3]*Department of Food Science and Human Nutrition, College of Health and Applied Sciences, A'Sharqiyah University, P.O. Box 42, 400, Ibra, Sultanate of Oman*

Received: June 27, 2022; Revised: August 7, 2022; Accepted: August 15, 2022

Abstract

Different plant-derived bioactive compounds have the potential to be used for medical applications. One of the native medicinal shrub plant species in the Mediterranean area is *Micromeria fruticosa* from the *Lamiaceae* family. In the present work, the antioxidant activity, antimicrobial activity, phytochemical screening analysis, total phenolic content (TPC) and total flavonoid content (TFC) were determined for plant extracts of *M. fruticosa* collected from Jordan. Furthermore, the identification of phenolic compounds was done using liquid chromatography. Results showed that strong antioxidant activity (93.54%) was obtained from butanol extract while water extract exhibited the weakest antioxidant activity (13.7%). The essential oil extract showed the most potent activities against different types of bacteria compared to butanol and aqueous methanol extracts, with minimum inhibitory concentration (MIC) values of 0.2–0.75 mg/ml. The phytochemical analysis of *M. fruticosa* showed the presence of flavonoid, alkaloids, phenols, and tannins in all solvents extract, with maximal phytochemical compounds obtained from butanol extract. The highest TPC, TFC values were measured butanol extract of *M. fruticosa*, whereas the lowest values were measured for water extract. The ions chromatographic analyses (RP-HPLC) for phenolic compounds present in extracts fraction revealed that the most abundant phenolic acids were gallic acid and ellagic acid. Results indicate that *M. fruticosa* extracts may be used in drug industry as a source of effective compounds.

Keywords: Micromeria fruticosa, Antimicrobial, Antioxidants, Phytochemical Screening, Total Phenolic, Phenolic compounds.

1. Introduction

Plants have been used for treatment of several diseases for long time; more than 90% of prescribed medicines are derived from plants. In Jordan, approximately 2100 medicinal plant species were observed. *Micromeria fruticosa* is an aromatic perennial plant native to the rocky area along the Mediterranean, including Palestine and Jordan, known as Qurnya and Ishbitesh-shai (Abu-Rabia, 2012). *Micromeria fruticosa* is derived from the Greek words micro and morose (meaning small and part), referring to the leaves, stalks, and flowers (Quattrocchi,Umberto, 2000) (Figure 1). It is a member of the genus *Micromeria* of *Lamiaceae* family. It grows up to 70 cm high and spread to 60 cm. The essential oil and extracts of this plant contain an important type of monoterpenes. Levels and composition variation of the monoterpene components with season were noted (Dudai *et al*., 2001). Furthermore, several studies suggested that *Micromeria fruticosa* could contain a reasonable amount of antioxidant components (Telci, 2007) and antimicrobial molecules, which could assist in preventing several types of diseases.

Recently, medicinal plants have been studied and investigated to approve their activities and turn the synthetic drug into new safe alternatives (Najadat, 2018; Anand *et al*., 2019; Es-Safi *et al.,* 2020). Medicinal plants pose low-cost production processes and few environmental hazards, side effects, and toxicity that are lesser than synthetic drugs (De Smet, 2004). Plant phenols (flavones, phenolic acids, tannins, and anthocyanins) represent significant natural antioxidant, anticancer, anti-ulcer, antimicrobial, and anti-inflammatory properties (Nikolic *et al.,* 2012). In addition, traditional medicinal plants were used without a scientific background (Strohl, 2000), but in the ancient world and nowadays medicinal plants have been used for treating several diseases. Recently, ensuring the safety, quality and effectiveness of natural medicinal plants and herbal medicine became a key issue in all developing countries by evaluating the potential of plant-derived compounds (Jamshidi-kia, 2018). As a result, it is noteworthy to investigate the effect of medicinal plants on disease, and pathogenic agents and assess the effectiveness of their active ingredients. Several parts of plants can be used for preparing herbal medicine, such as bark or the quinine bark [Cinchona] (Flatie *et al*., 2009). The preparation of medicinal plants can be conducted in several ways including macerations (cold-soaking), infusions (hot teas), tincture (alcohol and water), decoctions (boiled teas) (Handa *et al.,* 2008), soxhelt extraction (Amid *et al*., 2010), microwave-assisted

* Corresponding author. e-mail: tareq92@hotmail.com.

extraction (Trusheva *et al.,* 2007), and sonication extraction (Dhanani *et al.,* 2013).

Recent studies conducted on medicinal plants suggest that active ingredients of these plants are available (Stoyanova *et al*., 2020; Subasi, 2020). Effective extracts of medicinal plants can combat human pathogenic bacteria with the least adverse impacts. Several plants have been investigated regarding antimicrobial and antioxidant activity, total phenolic content, and toxicity effect (Al-Qudah *et al.,* 2022, Imtara *et al.,* 2019; Cock *et al.*, 2017; Diky *et al.,* 2021). *M. fruticosa* is an important plant used worldwide to treat several types of diseases. *M. fruticosa* is a perennial aromatic naturally grown plant used in phytotherapy to treat colds, heart disorders, eye infections, high blood pressure, and abdominal pains. In addition, it is used as a flavoring substance in the food industry. Essential oil of this plant contains different components such as Menthol, Pulegone, Menthofuran, Linalool, 1,8-Cineole, and Piperitenone and other metabolites after oxidation-reduction reaction in the liver (Al-Hamwi *et al*., 2011; Dudai *et al*., 2001; Telci *et al*., 2007). The aim of this study to assess the phytochemical screening, antioxidant and antibacterial activity of *Micromeria fruticosa* plants collected from northern Jordan.

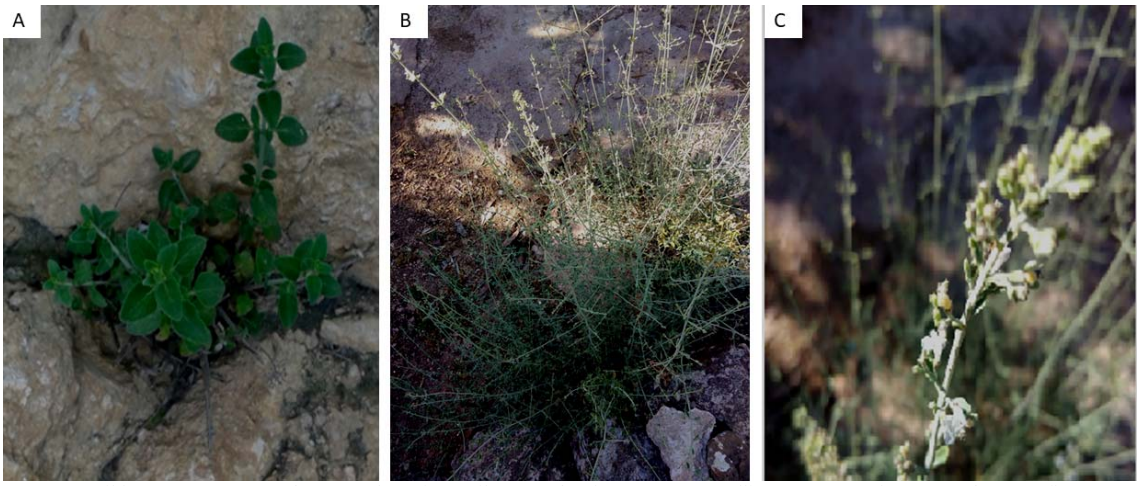

Figure 1. Wild-grown *Micromeria fruticosa* plants from Ajloun area/Jordan. A: young seedling. B: mature plant. C: *M. fruticosa* flowers.

2. Materials and methods

2.1. Plant Materials

Fresh *Micromeria fruticosa* plants were collected from Halawah and the Osarah regions from Ajloun, northern Jordan in April and May 2021. It was identified at the Department of Biological Sciences, Yarmouk University by Professor Ahmad El-Oqlah. *Micromeria fruticosa* samples (leaves and stems) were air dried in the shade for one week, grinded into powder, and stored in the refrigerator in a closed bottle until use.

2.2. Preparation of plant extract

The fine powdered plant material of *Micromeria fruticosa* was defatted with petroleum ether using Soxhlet extraction and then dissolved in methanol. The methanolic extract was evaporated under vacuum to get a crude extract. The obtained extract was steeped in distilled water and was extracted with chloroform by using a separating funnel. The organic layer was partitioned between 10% methanol and hexane. The polar organic species were extracted from the aqueous layer using n-butanol.

2.3. Determination of antioxidant activity of Micromeria fruticosa from Jordan using 1,2-Diphenyl-1-Picrylhydrazyl (DPPH) Radical Capacity Assay

The scavenging activities of different prepared extracts of *Micromeria fruticosa* were screened and tested using 2,2-diphenyl-picrylhydrazyl radical (DPPH) according to the literature (Braca *et al*., 2002; Berset *et al*., 1995; Al-Saleema *et al*., 2019). Different extracts dilutions of the plant extract (0.005, 0.02, 0.04, 0.06, 0.08 and 0.1 mg/ml) were dissolved in 10 ml methanol. Methanol was used for preparing DPPH solution with the addition of 100 ml methanol to 6.0 mg of DPPH for each type of solvent. Briefly, 2 ml of DPPH solution was combined with 1 ml of each dilution of plant extract. The mixtures were incubated shackled and then allowed to settle in a dark area for 30 min and the absorbance was measured at 515 nm after 30 min at room temperature using a spectrophotometer. The scavenging activity of each extract on DPPH radical was calculated using the following equation:

Scavenging activity (%) = (1-Absorbance of sample / Absorbance of control) x 100%

2.4. Antibacterial activity of Micromeria fruticosa extracts

Four Gram-positive strains (*Staphylococcus* aureus ATCC (29213, *Micrococcus luteus* ATCC (9341), *Bacillus cereus* ATCC (11778), and *Staphylococcus epidermidis* ATCC (12228) and five Gram-negative strains (*Serratia marcescens* ATCC (27117), *Escherichia coli* ATCC (25922), *Proteus vulgaris* ATCC (29905), *Salmonella typhimurium* ATCC (13311), and *Klebsiella pneumoniae* ATCC (13883) were used. These bacterial strains were supplied from Laboratory of Microbiology at Yarmouk University in Jordan.

2.4.1. Agar Well Diffusion (AWD) Assay

Bacterial species were fecundated with suspensions of 0.5 McFarland standard and poured on the surface of Mueller-Hinton agar plates (Imtara, 2018). The plates were dried by placing the plates in an incubator for 24 h at 37 °C. The extract of the plant was dissolved in DMSO. Bacterial suspension (100 µL) was then smeared on agar

plates having 2 mm diameter. The plates were incubated at 37°C for 24 hours and the diameters of the inhibition zones were measured after incubation. The minimum inhibitory concentration (MIC) was calculated.

2.5. Phytochemical screening analysis of different extracts of Micromeria fruticosa from Jordan.

The qualitative phytochemical screening of the prepared *Micromeria fruticosa* plant extracts was used to identify the various major groups of chemical constituents such as alkaloids, glycosids, steroids, flavonoids, tannins, phenolic compounds, and saponins present in the extracts using the following standard procedures (Alamzed *et al.,* 2013; Thusa and Mulmi, 2017; Talukdar and Chaudhary, 2010). Results are addressed according to the presence (+) and absence (-) of phytochemical compounds.

2.6. Determination of Total phenolic Content (TPC)

TPC of *Micromeria fruticosa* was determined following Imtara *et al.* (2018) method. Absorbance was measured at 725 nm. The TPC in different extracts was expressed as mg gallic acid equivalents (GAE) per g dry mass.

2.7. Determination of Total Flavonoid Content (TFC)

TFC of different *Micromeria fruticosa* solvent extracts was determined according to the procedure described in the literature (Al-Humaidia *et al.,* 2019). The absorbance was measured at 410 nm. The results were expressed as mg quercetin/g of dry extract.

2.8. RP-HPLC analysis of phenolic compounds

Identification of phenolic compounds in the extract was determined using HPLC Agilent 1100 series HPLC system (Agilent Technologies, Waldbrom, Germany) liquid chromatography on C18 (250 × 4.6 mm,5 µm) analytical column at room temperature with a flow rate of 1.3 ml/min. Gradient elution of two solvents was used: water with 0.2% formic acid (solvent A) and 100% methanol (solvent B), with a linear gradient starting at 10% methanol within 45 min; and were then repeated over 20 min. Rosemerinic acid, caffeic acid, gallic acid, syringic acid, hesperidin, quercetin, rutin, luteolin, and epicatechin were used as reference standard solution to quantify the phenolic compounds in the sample.

3. Results and discussion

3.1. Phytochemical Screening Analysis

The qualitative results of phytochemical analysis for *Micromeria fruticosa* in aqueous methanol, n-butanol, and water extracts revealed that flavonoids, alkaloids, phenols, and tannins were present in all plant extracts. Glycoside and steroids were detected in all extracts except in the water fraction. Additionally, the results of the qualitative phytochemical analysis indicate that the butanol extracts were wealthy in phytochemical species compared to methanol and water extracts. Mucilage was also not present in all crude extracts as shown in Table 1. Flavonoids reduce the risk mostly from cardiovascular diseases and cancer and the high amount could be beneficial as antibacterial agents (Ballard and Marostica, 2019). Plants containing phytochemicals species such as flavonoids, alkaloids, and tannins showed cytotoxic effects (Chowdhury *et al.*, 2017). Moreover, lower cholesterol levels, as well as cytotoxic qualities, anti-bacterial, and anti-viral properties, are valued to the presence of saponin (Bailly and Vergoten, 2020). Tannins play a role as an anticancer agent that is perceptible from its inhibitory activity towards growth (Mazni, *et al*., 2016).

Table 1. Phytochemical screening in different extracts of *Micromeria fruticosa.*

Groups	Aqueous methanol	n-Butanol	Water
Flavonoids	+	++	+
Alkaloids	+	++	+
Glycosids	+	+	-
Phenols	+	++	+
Saponins	+	+	-
Tannins	+	++	+
Steroids	+	+	-
Mucilage	-	-	-

(+) indicated the presence of a small amount of phytochemicals, (++) indicated the presence of a large amount of phytochemicals, and (-) indicated the absence of phytochemicals.

3.2. Antioxidant potential of Micrmeria fruticosa extract

Aqueous Methanol, n-butanol, and water extracts of *M. fruticosa* were used to assess antioxidant activity using 2,2-diphyenyl-picrylhydrazyl radical (DPPH) according to Braca *et al*., (2002). Scavenging activity (%) of Aqueous Methanol, n-butanol, and water extracts of *Micromeria fruticosa* in different concentrations is presented in Table 2. In general, the highest radical scavenging activity was observed in butanol extract. Moreover, the DPPH scavenging power of the butanol extract showed strong scavenging effects (93.54%) compared to other crude plant extracts. Furthermore, an increase in the concentration level for each extract obtained from *M. fruticosa* had a significant increase in radical scavenging activity. *M. fruticosa* extracts contain a large amount of reduction agents, that may react with free radicles to stop the radical chain reaction completely.

Table 2. Antioxidant activity (Radical scavenging %) of *M. fruticosa* aqueous methanol, n-butanol, and water extracts measured by DPPH method.

Concentration (mg/ml)	Aq. Methanol extract	n-butanol extract	Water extract
0.005	14.80±0.35	15.60±0.25	13.70±0.15
0.02	38.07±0.64	40.32±0.70	24.12±0.55
0.04	56.42±1.10	62.56±1.22	33.56±0.92
0.06	77.83±1.52	81.24±2.15	48.40±0.82
0.08	86.24±2.35	89.75±2.28	54.36±1.32
0.1	89.41±2.43	93.54±3.15	61.16±1.35

Values are expressed as means ± SD.

3.3. Antimicrobial activity of different extracts and essential oil of M. fruticosa.

The antimicrobial activities of the hexane, n-butanol, and aqueous methanol fractions and essential oil of *M. fruticosa* were tested by agar well diffusion method against nine bacterial strains. Results from Table 3 showed that Hexane extract did not have any influence on all tested

bacterial strains. However, the butanol and aqueous methanol extracts have moderate antibacterial activity and showed remarkable activity against all Gram-positive (*Bacillus cereus*, *Micrococcus Luteus*, *Staphylococus aureus*, *staphylococus epidermidis*) and three Gram-negative bacteria strains (*Serratia marcescens*, *Escherichia coli*, *Klebsiella pneumoniae*), but both extracts did not have inhibition effect against *Salmonella typhimurium* and *Proteus vulgaris*. The antibacterial activities of both methanol and ethanol extracts were similar. The antibacterial activity of the essential oil was also tested on the nine bacterial species. Moderate activities against all tested strains compared to standard antibiotic Gentamycin were observed. Comparatively, the essential oil extract demonstrated the highest level of inhibition and was shown to be antibacterial against all Gram-positive and all Gram-negative bacteria.

Table 3. Inhibition zones (mm) diameters produced by plant extracts in an agar well diffusion test against bacterial strains.

bacterial strains	Butanol extract	Aq. methanol extract	Essential oil	Hexane extract	Gentamycin
Bacillus cereus	17±2.21	12±1.87	16±2.16	NA	38±3.12
Micrococcus luteus	16±2.16	14±1.88	19±1.88	NA	29±2.98
Staphylococcus aureus	23±2.78	21±1.88	25±2.95	NA	33±3.01
Serratia marcescens	10±1.76	14±1.88	18±2.24	NA	22±1.92
Escherichia coli	21±1.88	23±2.78	28±2.93	NA	35±3.11
Salmonella typhimurium	NA	NA	17±2.21	NA	23±2.78
Klebsiella pneumoniae	16±2.16	18±2.24	23±2.78	NA	30±2.96
Proteus vulgaris	NA	NA	26±2.94	NA	29±2.98
Staphylococcus epidermidis	14±1.88	14±1.88	18±2.24	NA	26±2.94

Inhibition zone (mm), NA: no activity, tested concentration of the standard antibiotic and extracts in (mg/ml)

MIC values for all *M. fruticosa* and essential oil extracts were determined against all bacterial strains as shown in Table 4. MIC values for the butanol fraction ranged from 0.48-0.75 mg/ml, for the butanol fraction, 0.4-0.7 mg/ml for the aqueous methanol portion, and 0.2–0.75 mg/ml for the essential oil portion. Essential oil extract showed the most potent activities against different types of bacteria compared to butanol and aqueous methanol extracts. MIC values obtained are agreed upon and supported by the value findings of the agar well diffusion method. The MIC values of the aqueous methanolic and essential oil extracts revealed the best inhibition influence versus *Staphylococus aureus*, *Escherichia coli, Klebsiella pnuemoniae,* and *Protues vulgeris.* In contrast, none of the bacteria screened were susceptible to hexane extracts at all the tests.

Table 4: Minimal inhibitory concentration (MIC) (mg/ml) of extracts and essential oil of *M. fruticosa*.

Hexane extract	Essential oil	Aq. methanol extract	Butanol extract	bacterial strains
Bacillus cereus	0.70	0.65	0.65	-
Micrococcus luteus	0.65	0.60	0.55	-
Staphylococcus aureus	0.48	0.45	0.30	-
Serratia marcescens	0.75	0.60	0.65	-
Escherichia coli	0.55	0.40	0.20	-
Salmonella typhimurium	-	-	0.60	-
Klebsiella pneumoniae	0.62	0.70	0.35	-
Proteus vulgaris	-	-	0.25	-
Staphylococcus epidermidis	0.64	0.75	0.60	-

Previously published articles inform that extracts with minimum inhibitory concentration lower than 100 µg/ml can be used to have an excellent antibacterial influence (Kuete, 2010). Hence, this principle shows that the essential oil extract showed high activity against *Staphylococcus aureus*, *Escherichia coli, Klebsiella pneumoniae,* and *Proteus vulgaris* bacteria with a range of 0.20-0.35 mg/ml. Aqueous methanol and butanol extracts showed medium influence against all Gram-positive and three Gram-negative bacteria (MIC = 0.40-0.75 mg/ml, 0.48-0.70 mg/ml) respectively. The minimum level of inhibition in all extracts was observed against *Serratia marcescens*, *Staphylococcus epidermidis,* and *Bacillus cereus* with an MIC value of 0.75 mg/ml. The reason could be attributed to the resistance of Gram-negative bacteria because of the complicated structure of their cell wall, which contains a double membrane as opposed to the unique glycoprotein/teichoic acid membrane of Gram-positive bacteria (Ndamane *et al.,* 2013). Antimirobial activity results indicate the potential application of *M. fruticosa* extracts in antibiotic resistance and as a potential replacement of antibiotics to treat drug-resistant infections.

3.4. Determination of Total Flavonoid content (TFC) and total Phenolic content (TPC):

Total phenolic contents in different extracts of *M. fruticosa* were measured by Folin-Ciocalteu technique (Table 5). TPC and TFC values also appeared to have comparable trends in all extracts. The highest TPC and TFC values were noted in the butanol extracts (227.8±1.1, 178.5±3.5) followed by aqueous methanol (184.4±1.2, 94.7±1.4) and then water extracts (133.4±1.5, 72.2 ±1.6) respectively. The obtained results evaluated the lowest values according to both TPC and TFC assays for water extract. In a recent study, TFC and TPC of ethanolic extracts of *M. fruticosa* was 56.78 ± 0.49 mg/g and 8.03 ± 0.01 mg/g, respectively (Sadeq *et al.*, 2021). These values are lower than that of our study. Moreover, these results agree with a recent study that has identified the phenolic and flavonoid compounds in *M. fruticosa* pollens, and they

have been shown to have antioxidant properties (Bakour *et al.,* 2019). In addition, the polarity of the extraction solvents affects the concentration of phenols and flavonoids (Jing *et al.,* 2015). The presence of Flavonoids and Phenolics in *M. fruticosa* extracts indicates the extract's activity as a powerful antioxidant component. These results support the ethno-pharmacological use of *M. fruticosa* in Reactive oxygen species related diseases.

Table 5. TPC and TFC values in different extracts of *M. fruticosa*.

Extracts	TPC (mg/g gallic acid)	TFC (mg/g of quercetin)
n-Butanol	227.8±1.1	178.5±3.5
Aq. methanol	184.7±1.2	94.7±1.4
Water	133.4±1.5	72.2±1.6

3.5. HPLC analysis

In the extraction of *M. fruticosa* using RP-HPLC, nine phenolic compounds were found: Rosemerinic acid, caffeic acid, gallic acid, syringic acid, hesperidin,

quercetin, rutin, luteolin, and epicatechin. All phenolic compounds were present in all solvent extracts. Gallic acid is one of the most important hydroxybenzoic acids, and it was present in large contents in aq. methanol, butanol, and water extracts with percentages of occurrence of 29%, 30%, and 29%, respectively, as shown in Figure 2. Low gallic acid content was observed in the water extract. On the other hand, a high gallic acid amount was observed in samples extracted in aqueous methanol and butanol solvent (Figure 2). A similar trend was observed for syringic acid. Moreover, high caffeic acid amount was observed in water extract and low in aq., methanol and butanol extracts. Rosemerinic acid, quercetin, luteolin and

epicatechin were present in the same amounts in aq. methanol and water extracts with percentage of 3.8%, 14.95, 7.6% and 11.7%, respectively (Figure 2). These phenolic acid results agree with previously published data for other biological samples (Kelebek *et al.,* 2009). Many articles documented the valuable effects of such phenolic compounds on human health, such as their antioxidant properties (Yang *et al.,* 2008; Aytekin *et al.,* 2011; Erkan *et al.*, 2008).

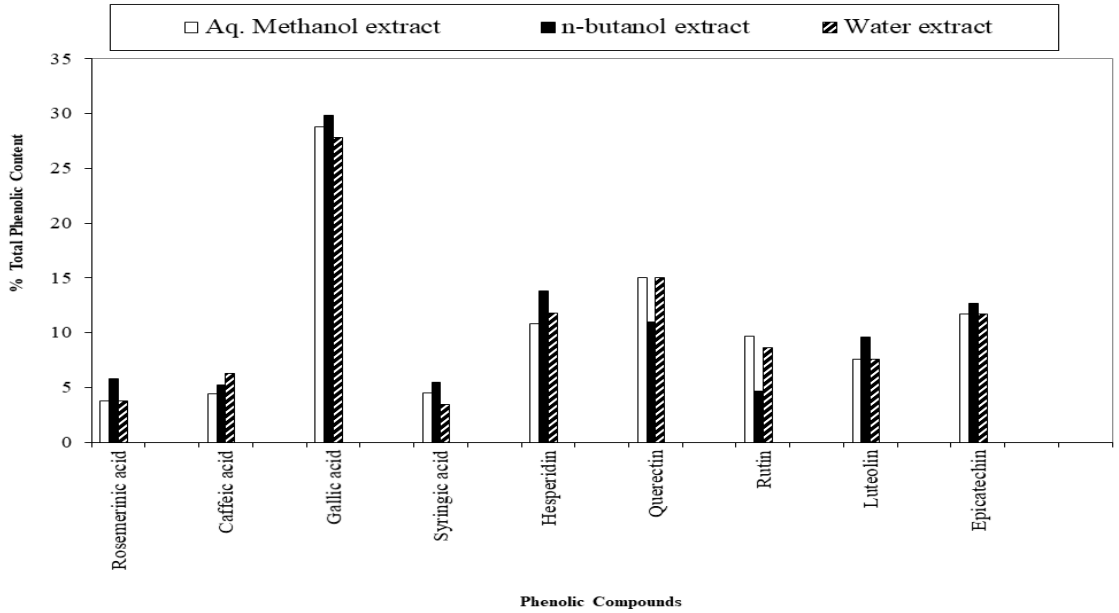

Figure 2: phenolic compounds content of *M. fruticosa* aqueous methanol, butanol, and water extracts using RP-HPLC.

4. Conclusions

The different fractions of *M. fruticosa* showed activities against different strains of bacteria. The minimum inhibition concentration (MIC) values of the *M. fruticosa* extracts were less than the MIC value of the standard, gentamycin. Furthermore, the essential oil extract showed the most potent activities against different types of bacteria compared to butanol and aqueous methanol extracts. The antioxidant data showed that *M. fruticosa* extracts are effective as their antioxidant values are comparable with the standard. Most *M. fruticosa* extracts showed a high antimicrobial activity with high potential to be used in drug industry. This study showed that all Gram- positive and Gram- negative tested bacteria were significantly inhibited by different *M. fruticosa* extracts. No inhibition activity was observed against tested bacteria from hexane extract, due to seasonal variation in the chemical composition of the plant and oil materials. In addition, MIC of *M. fruticosa* were measured for tested microorganisms. The results showed that the essential oil extract manifested the most potent activities against different types of bacteria compared to butanol and aqueous methanol extracts. Identified phenolic compounds separated from *M. fruticosa* extract by HPLC analysis have been tested. With a powerful analytical HPLC technique, the identification and quantification of nine phenolic compounds were achieved for *M. fruticosa.* Findings of this study show that *M. fruticosa* may be used as a safe substitute for food additives and as a potential treatment for diseases caused by antibiotic-resistant bacterial strains and for diseases caused by ROS. Further

study is needed to assess the toxicity of *M. fruticosa* on human and animals.

Acknowledgements:

The authors would like to thank the Deanship of Research and Graduate Studies at Yarmouk University/Jordan for funding this study.

References

Anand U, Jacobo-Herrera NJ, Altemimi AB and Lakhssassi NA. 2019. Comprehensive Review on Medicinal Plants as Antimicrobial Therapeutics: Potential Avenues of Biocompatible Drug Discovery. *Metabolites,* **9(11)**: 258-270.

Amid, Salim RJ and Adenan M. 2010.The Factors Affecting The Extraction Conditions For Newroprotective Activity of *Centellaasiatica* evaluated by Metal Chelating Activity Assay, *J App Sci*., **10**: 837-842.

Al-Dalahmeh Y, Al-Bataineh N, Al-Balawi SS, Lahham JN, Al-Momani IF, Al-Sheraideh MS, Mayyas AS, Abu Orabi ST and Al-Qudah MA. 2022. LC-MS/MS Screening, Total Phenolic, Flavonoid and Antioxidant Contents of Crude Extracts from Three Asclepiadaceae Species Growing in Jordan. *Molecules*, **27**: 859-870.

Al-Hamwi M, Bakkour Y, Abou-Ela M, El-Lakany A, Tabcheh M and El-Omar, F. 2011. Chemical composition and seasonal variation of the essential oil of *Micromeria fruticosa. J Nat Prod.,* **4**: 147-149.

Al-Humaidia JY, Al-Qudah, MA, Al-Saleema, MS and Alotaibia SM. 2019. Antioxidant activity and chemical composition of essential oils of selected cleome species growing in Saudi Arabia. *Jordan J Chem.*, **14**: 29-37.

Alamzeb M, Khan MR, Ali S, Shah SQ and Mamoon UR. 2013. Antimicrobial properties of extracts and compounds isolated from Berberis jaeschkeana, *Bangladesh J Pharmacol.,* **8(2)**: 107-109.

Aytekin A, Morimura S and Kida K. 2011. Synthesis of chitosan caffeic acid derivatives and evaluation of their antioxidant activities. *J Biosci Bioeng.,* **111**: 212-216.

Abu-Rabia, A. 2012. Ethno-Botanic Treatments for Paralysis (Falij) in the Middle East. *Chin Med.,* **3(4)**: 157-166.

Braca A, Sortino C, Politi M, Morelli I and Mendez J. 2002. Antioxidant activity of flavonoids from *Licania licaniaeflora*. *J Ethnopharmacol.*, **79(3)**: 379-381.

Brand-Williams W, Cuvelier E and Berset C. 1995. Use of a free radical method to evaluate antioxidant activity. *LWT - Food Sci Technol.,* **28**: 25-30.

Ballard CR and Marostica, MR. 2019. Health benefts of flavonoid, **Bioactive Compounds**. Woodhead Publishing, United kingdom, pp. 185-201.

Bakour M, Campos MDG, Imtara H and Lyoussi, B. 2019. Antioxidant content and identification of phenolic/flavonoid compounds in the pollen of fourteen plants using HPLC-DAD. *J Apic Res.,* **59**: 35-41.

Cheesman MJ, Ilanko A, Blonk B and Cock IE. 2017. Developing new antimicrobial therapies: Are synergistic combinations of plant extracts/compounds with conventional antibiotics the solution? *Pharmacogn Rev.,* **11**: 57-72.

Chowdhury S, Poddar SK, Zaheen S, Noor FA, Ahmed N, Haque S and Akbar, N. 2017. Phytochemical screening and evaluation of cytotoxic and hypoglycemic properties of *Mangifera indica* Peels. *Asian Pacifc J Trop Biomed*., 7**(1)**: 49-52.

Christian B and Gérard V. 2020. Esculentosides: Insights into the potential health benefts, mechanism of action, and molecular target. *Phytomedicine,* **79**: 153343.

Dhanani T, Shah S, Gajbhiye NA and Kumar S. 2013. Effect of extraction methods on yield, phytochemical constituents and antioxidant activity of *withaniasomnifera*. *Arab J Chem.,***10**: 1193-1199.

De smet and peter AGM. 2004. Health risks of herbal remedies. *Clin Pharmacol Ther.,* **76**: 1-17.

Diky SD, Novita SH, Marsal R,, Zulfahri, Ayu NS and Kusdianti. 2021. Antioxidant and antibacterial activities of Coix lacryma-jobi seed and root oil potential for meningitis treatment. *JJBC*, **14(5)**: 881-887.

Dudai N, Larkov O, Putievsky E and Lewinsohn E. 2001. Developmental control of monoterpene content and composition in *Micromeria fruticosa* (L.) *Druce. Ann Bot London*, **8**: 49-354.

Es-Safi I, Mechchate H, Amaghnouje A, El Moussaoui A, Cerruti P, Avella M, Grafov A and Bousta D. 2020. Marketing and legal status of phytomedicines and food supplements in Morocco. *J Complement Integr Med.*, **18(2)**: 279-285.

Erkan N, Ayranci G and Ayranci E. 2008. Antioxidant activities of rosemary (*Rosmarinus Officinalis* L.) extract, blackseed (*Nigella sativa* L.) essential oil, carnosic acid, rosmarinic acid and sesamol. *Food Chem*., **110**: 76-82.

Flatie T, Gedif T, Asres K and Gebre-Mariam T. 2009. Ethenomedical survey of Berta ethic group Assosa Zone, Benishangul-Gumuz regional state, mid- west Ethiopia. *J Ethnobiol Ethnomedicine*, **5(1)**:1-14.

Handa SS, Khanuja SPS, Longo G and Rakesh DD. 2008. Extraction Technologies for Medicinal and Aromatic Plants, (1stedn),no.66.Italy: United Nations Industrial Development Organization and International Center for science and High Technology.

Imtara H, Elamine Y and Lyoussi B. 2018. Honey Antibacterial Effect Boosting Using Origanum vulgare L. Essential Oil. *Evid Based Complementary Altern Med.*, **2018**: 1-14.

Imtara H, Elamine Y and Lyoussi B. 2018. Physicochemical characterization and antioxidant activity of Palestinian honey samples. *Food Sci Nutr.,* **6**: 2056-2065.

Imtara H, Kmail A, Touzani S, Khader M, Hamarshi H, Saad B and Lyoussi, B. 2019. Chemical Analysis and Cytotoxic and Cytostatic Effects of Twelve Honey Samples Collected from Different Regions in Morocco and Palestine. *Evid Based Complement Altern Med.,***2019**:1-11.

Jamshidi-Kia, F, Lorigooini Z and Amini-Khoei H. 2018. Medicinal Plant: Past history and Future perspective. *J Herb Med Pharmacol*., **7(1)**:1-7.

Jing L, Ma H, Fan P, Gao R and Jia Z. 2015. "Antioxidant potential, total phenolic and total flavonoid contents of Rhododendron anthopogonoides and its protective effect on hypoxia-induced injury in PC12 cells," *BMC complement med ther*., **15(1)**, 287-299.

Kuete V. 2010. Potential of Cameroonian Plants and Derived Products against Microbial Infections: A Review. *Planta Med.*, **76**: 1479-1491.

Kelebek H, Selli S, Canbas A and Cabaroglu T. 2009. HPLC determination of organic acids, sugars, phenolic compositions and antioxidant capacity of orange juice and orange wine made from a Turkish cv. Kozan. *Microchem J.*, **91**: 187-192.

Mollova S, Fidan H, Antonova D, Bozhilov D, Stanev S, Kostova I and Stoyanova A. 2020. Chemical composition and antimicrobial and antioxidant activity of Helichrysum italicum

(Roth) G. Don subspecies essential oils. *Turk J Agric For.,* **44**: 371-378.

Mazni Abu Z, ho Yin W, Azizul I and Nurdin A. 2016. Antioxidant,
antimicrobial and cytotoxic potential of condensed tannin from Leucaena leucocephala Hybrid Rendang. *Food Sci Hum Wellness*, **5(2)**: 65-75.

Ndamane Y, Kambizi L, Songca S and Oluwafemi O. 2013. Antibacterial Effectiveness of *Tetradenia riparia* Extract, a Plant Traditionally Used in the Eastern Cape Province to Treat Diseases of the Respiratory System. *J Med Plant Res.,* **7**: 2755-2760.

Nikolic M, Markovic T, Peric T, Glamoclija J, Stojkovic D, Sokovic M and Markovic D. 2012. Screening of antimicrobial and antioxidant activity of commercial *Melaleuca alternifolia* (tree tea) essential oil. *J Med Plant*, **6(22)**: 3852-3858.

Najadat IM. 2018. In vitro antimicrobial and other activities of Micromeria fruticosa (L) durce collected from northern Jordan. Master dissertation, Yarmouk University, Irbid, Jordan.

Strohl WR. 2000. The role of natural product in modern drug discovery program. *Drug Discov Today*, **5(2)**: 39-41.

Subasi I. 2020. Seed fatty acid compositions and chemotaxonomy of wild Crambe (Brassicaceae) taxa in Turkey. *Turk J Agric For.,* **44**: 662-670.

Sadeq O, Mechchat H, Es-safi I, Bouhrim M, Jawhari FZ, Ouassou H, Kharchoufa L, AlZain MN, Alzamel NM, Al kamaly OM, Bouyahya A, Benoutman A and H. Imtara. 2021. Phytochemical Screening, Antioxidant and Antibacterial Activities of Pollen Extracts from Micromeria fruticosa, Achillea fragrantissima, and Phoenix dactylifera. *Plants*, **10**: 676-691.

Trusheva B,Trunkova D and Bankova V. 2007. Different extraction method components from propolis: a preliminary study. *Chem Cent J.,* 1(13): 1-4.

Telci I and Ceylan M 2007. Essential oil composition of *Micromeria fruticosa* Druce from Turkey. *Chem Nat Compd,*. **43**: 629-631.

Thusa R and Mulmi S. 2017. Analysis of phytoconstituents and biological activities of different parts of Mahonia nepalensis and Berberis aristata, *Nepal J Biotechnol*., **5**: 5-13.

Talukdar A and Chaudhary B. 2010. Phytochemical Screening of ethanolic extracts of Rubia Cordiofolia. *Pharm Biol Sci.,* **1(4)**: 530-536.

Yang J, Guo J and Yuan J. 2008. In vitro antioxidant properties of rutin. *Food Sci Technol*., **41**:1060-1066.

JJBS

Volume 15, Number 5, December 2022
ISSN 1995-6673
Pages 841 – 845
https://doi.org/10.54319/jjbs/150513

Jordan Journal of Biological Sciences

Effectiveness of Flower Extract of *Hibiscus sabdariffa* L. against Anticancer Drug Cyclophosphamide Induced Hepatotoxicity and Oxidative Stress

Rania M. Al-Groom*

Department of Allied Medical Sciences, Zarqa University College, Al-Balqa Applied University.

Received: February 27, 2022; Revised: June 23, 2022; Accepted: August 15, 2022

Abstract

Cyclophosphamide (CP) is an alkylating agent that has been used extensively in medicine as an antineoplastic agent for the treatment of several tumors. Treatment with CP is associated with significant toxicity due to overproduction of reactive oxygen species (ROS) and free radicals resulting in increased levels of oxidative stress (OS) as well as hepatotoxicity. The *Hibiscus sabdariffa L.* Extract (HSE) was given to mice as an antineoplastic agent (CP) at a dose of 250 mg/kg body weight daily for 2 weeks. The degree of liver injury was analysed using several serum parameters including AST, ALT, GGT, total protein and albumin contents. Lipid peroxidation (LPO) which reflects oxidation stress was established by determining catalase and superoxide dismutase in liver homogenate. The biochemical results showed that the administration of CP induced hepatic damage was associated with a significant increase in serum marker enzymes (AST, ALT and GGT) and a decrease in total protein and albumin. In addition, oxidative stress in the liver was also increased, and this was evident from the increase in LPO. In this case MDA , GSH content activities of CAT and SOD were increased. Furthermore, the hepatic cytotoxicity induced by CP treatment was substantiated by the reduction of nucleic acids and protein levels in hepatic cells. Flower extract of HSE administration (250mg/kg) daily improved liver functions and prevented the CP induced hepatocellular injury and oxidative stress. These data presented herein showed that HSE had a protective property against the harmful effects of CP, suggesting that *H. sabdariffa* has the potential to be used as a new therapeutic approach for the treatment of hepatic disorders.

Keywords: *Hibiscus sabdariffa,* extract, cyclophosphamide, oxidative stress, cytotoxicity, hepatotoxicity.

1. Introduction

The increasing demand for nutraceuticals has enhanced attempts to develop new approaches for the treatment of human disease. *Hibiscus sabdariffa* that grows in many countries has many bioactive components as flavonoids (gossiping, sabdaretine, hibicitine, and anthocyanins), phenolic acids (e.g. protocatechuic acid) and rich in vitamin C content (Lin et al., 2011; Pietta, 2000). It was reported that this herb exhibits anticancer, antiseptic, antidepressant and antipyretic activities (Duke, 1985), anti-inflammatory (Dafallah and Al-Mustafa, 1996), antimutagenic effect (Farombi and Fakoya, 2005), antidiabetic, and also jaundice and ulcer treatment properties (Yeşilada et al., 1995). The plant was studied for its effect in hypolipidemia (Hirunpanich et al., 2006), immune protection, cytotoxicity (Okoko and Ere, 2012), atherosclerosis, cardiovascular diseases and diabetes (Farombi and Ige, 2007). HSE has a broad range of pharmacological activities, particularly used as free radical scavenging agent (Oboh and Okhai, 2012) and has antioxidant properties (Olusola et al., 2012) . The health benefits of HSE has attracted scientific interest, and this resulted in several papers published in the last few years. Antioxidants and free radical scavenging are often mentioned as the mechanism leading to the protective benefit of HSE. Antioxidants and anthocyanins were found to be effective hepatoprotective agents against cadmium-induced liver injury in rats (Al-Kubaisy et al., 2016). Acute liver damage can be induced by carbon tetrachloride (CCl4) (Liu et al., 2006). Liu et al. (2010) found that significant protection against acetaminophen-induced liver damage in rats can be achieved using HSE. An investigation conducted by Al-Groom and Al-kubaisy (2016) showed that cadimium chloride ($CdCl_2$) can induce hypochromic microcytic anemia and oxidative stress in rat red blood cells. It was also found that the flower extract of *H. sabdariffa* was proven to be an effective agent against $CdCl_2$-induced depletion of rat hepatic antioxidant system and increase in malondialdehyde (MDA) (Khaled et al., 2016). The supplementation of floral extract partly affects the toxic effect of $CdCl_2$ on oxidative stress and repairs liver tissue. The constituents of *H. sabdariffa* were found to be effective in immune modulation, cholesterol lowering and overall health assistance particularly in cancer treatment. (De Jong *et al.,*2003)

The objective of this study was to determine the effectiveness of flower extract of *Hibiscus sabdariffa* L. in alleviating the side effects of anticancer drug

* Corresponding author. e-mail: raniaalgroom@bau.edu.jo.

Cyclophosphamide (CP) in relation to hepatotoxicity and oxidative stress.

2. Material and Methods

2.1. Preparation of aqueous flower extract (HSE)

H. sabdariffa L. (Rossle) was obtained from a general herbal store in Amman. A botanist from the University of Jordan identified the sample of the plant specimen. The flower was removed and ground with an electric dry mill in to fine powder. An aliquot 100 g ground powder was soaked in 500 ml of distilled water while shaking for 24 hours at 40°C. Subsequently, the sample was filtered through Whatman filter paper No.1 in distilled water. The filtrate was boiled to produce concentration of 250mg/kg when given to the livestock.

2.2. Experimental animals

A combination of 18 healthy albino (20 to 25 g) were obtained from the Al-Ahlyyiah-Amman University and were used throughout this study. Free access to food, water and libitum was permitted for all. The animals were randomly split into three groups of six: A: Group1: Served as control that was treated with corn oil vehicle. B: Group2: Mice were injected with single dose of CP (75 mg/kg) and were used for comparison. C: Group3: Mice were treated with 250mg/kg body weight of (HSE) for two weeks daily and subsequently exposed to a single injection (75mg/kg) of CP, two hours after the last (HSE\vehicle) treatment (Srivastava et al., 2021). All animals were treated in accordance with the rules of the Animal Ethics Committee organizations. Analytical grade chemicals were used throughout this investigation.

2.3. Blood collection

At the end of the testing period animals were subject to etheric anesthesia. Cardiac puncture was conducted to collect the blood which was transferred to EDTA tubes. Then, the samples were centrifuged at 3500 rpm for 15 minutes.

2.4. Blood biochemistry

Serum enzymes: aspirate transaminase (AST), gamma glutamate transaminase (GT), alanine transaminase (ALT), complete protein and albumin were tested on the same day in compliance with the instructions given by the kits manufacture (Randox-UK).

2.5. Hepatic tissue biochemical testing

The mice were sacrificed and their livers were excised and then washed with ice-cold saline and blotted to dryness; samples of liver tissue were homogenized with ice-cold (0.25 M sucrose).

2.6. Assessment of cellular damage (Lipid peroxidation)

The level of lipid peroxides (LPO) served as an index of the intensity of oxidative stress (OS). Malondialdehyde (MDA) was determined in the liver homogenate as described by (Al-Kubaisy et al., 2016), after incubation at 95 °C with thiobarbituric acid to produce pink color. This color has an absorption maxima at 532 nm.

2.7. Estimation of oxidative stress

Estimation of total reduced glutathione (GSH) was determined in the liver homogenates by the method of Ellman (Ohkawa et al., 1979). Yellow color developed when 5.5 dithiol-bis 2 nitrobenzoic acids was added to the supernatant. The intensity of this color was measured by spectrophotometrically at a wavelength of 412 nm against reagent blank with no homogenate. Estimation of catalase (CAT) activity was performed by following the method described by (Beutler, 1963). Catalase activity was determined spectrophotometrically utilizing H_2O_2 as a substrate at the wavelength of 240 nm. The homogeneity of superoxide dismutase (SOD) was estimated by the method described by Johansson and Borg, (1988). This activity was measured under alkaline condition at 325 nm.

2.8. Quantification of nucleic acids and total protein in liver homogenate.

The hepatic homogenate was prepared in cold and hot perchloric acid ($HCLO_4$). The supernatant was used to determine the concentrations of RNA, DNA and total proteins after final extraction, incubation and centrifugation. The RNA was obtained after treating the nucleic acid extract with orcinol reagent. The resultant solution was green in color. The intensity of the color was measured spectrophotometrically at 660 nm. (Kakkar et al., 1984). The diphenylamine extract of hepatic homogenate with the developed blue color was determined using spectrophotometer at wavelength of 600 nm and this reading indicated DNA concentration (Patterson and Mura, 2013). Total protein was determined by the method using the folin-ciocalteu reagent at 750 nm spectrophotometrically (El-Nekeety et al., 2014; Lowry et al., 1951).

2.9. Statistical analysis

Data were expressed as mean ± standard deviation. One-way analysis variance (ANOVA) with the software SPSS version (SPSS version 20) was used. Values below 0.05 (P<0.05) were considered as significant.

3. Result

3.1. Hepatic biochemical markers

The activity of AST, ALT and GGT in the serum of the control and experimental animals are summarized in Table 1. The activity of these enzymes was significantly increased (P<0.05) after injection of Cyclophosphamide (CP) as compared to livestock's in group 1 and 3. Pretreatment of group 3 animals with HSE significantly (P<0.05) reduced the levels of these enzyme markers as compared to group 2. The mean values of total protein and albumin in the serum of control and experimental mice were given in Table 1. Decrease in the values of the biochemical markers was observed in the serum of mice after administration of CP (P<0.05). However, these values relatively increased in group 3, but never reached the value obtained in group 1.

3.2. Effect on lipid peroxidation and oxidative stress in hepatic cells

Table 2 indicates that mice exposure to Cyclophosphamide resulted in hepatic oxidative stress. This study found a significant increase in hepatic tissue in case of (MDA) after CP exposure. HSE supplementation led to substantial lipid peroxidation (LPO) improvement in group 3. Furthermore, a significant decrease in total glutathione content in liver homogenate (P<0.05) was recorded throughout the period of treatment with CP. However, the supplementation with HSE (group3) resulted in a significant elevation in the level of GSH when compared to CP-treated (group 2). The antioxidant enzymes (CAT) and (SOD) in the liver were depleted

significantly when the livestock were treated with CP alone. The activity of these enzymes showed significant protection following treatment with HSE.

Table 1. Effect of pretreatment of HSE on serum biochemical's response of mice to CP

Parameter	Group 1	Group 2	Group 3
AST U/L	61.48 ± 1.81	108.72 ± 3.11 *	81.93 ± 2.98 *
ALT U/L	36.64 ± 1.27	74.75 ± 2.88	57.97 ± 3.77 *
GGT U/L	13.25 ± 1.61	19.23 ± 1.71 *	15.44 ± 1.66 *
T. protein mg/dL	6.69 ± 0.53	4.82 ± 0.66 *	5.59 ± 0.71 *
Albumin mg/dL	4.41 ± 0.78	2.18 ± 0.27*	3.32 ± 0.48*

Results expressed as Means ± SE. for six mice. Comparisons are made between livestock inoculated as follows:
Group 1: mouse treated with corn oil (normal control)
Group 2: mouse treated with corn oil + CP
Group 3: mouse treated with corn oil+ CP+ HSE
(*P <0.05).

Table 2. Effect of pretreatment of HSE on hepatic lipid peroxidation GSH, catalase and superoxide dismutase (SOD) response of mice to CP

Groups	MAD nmol/g liver	GSH nmol/g liver	CAT u/g liver	SOD u/g liver
Group 1	192.40 ± 4.33	71.82 ±2.78	81.52 ± 4.12	73.43 ± 4.87
Group 2	245.72 ± 6.18 *	52.44 ±.18 *	57.28 ± 3.30 *	43.19 ±3.72 *
Group 3	213.85 ± 3.78*	65.61 ±3.11*	68.82 ± 3.61*	61.57 ±4.17 *

Results are expressed as Means ± SE. Comparisons are made between livestock inoculated as follows:
Group 1: mouse treated with corn oil (normal control)
Group 2: mouse treated with corn oil + CP
Group 3: mouse treated with corn oil+ CP+ HSE
(*P <0.05).

3.3. Effect on nucleic acids and proteins levels in hepatic cell's DNA and RNA levels in hepatic cells

Treatment of the experimental animals with CP caused drop in the values of DNA, RNA, and protein. However, when the livestock was treated with CP and HSE the readings of preceding parameters were significantly increased (Table3), they never reached the values obtained for the control group.

Table 3. Effect of pretreatment of HSE on the protein and nucleic acid levels in hepatic cells response of mice to CP

Group	DNA mg/100mg	RNA mg/100mg	protein mg/100mg
Group 1	211.66 ±341	675.22 ±7.91	13.67 ±0.63
Group 2	188.72 ± 4.51 *	563.41 ±9.82*	11.27 ±.37*
Group 3	194.18 ± 5.71 *	639.51 ± 11.18 *	12.10 ± 0.43

Results are expressed as Means ± SE. Comparisons are made between livestock inoculated as follows:
Group 1: mouse treated with corn oil (normal control)
Group 2: mouse treated with corn oil + CP
Group 3: mouse treated with corn oil+ CP+ HSE
(*P <0.05).

4. Discussion

Protective medicines like antioxidants have become increasingly attractive for hepatitis therapeutic illnesses. In this case, scavenging is the major antioxidant mechanism (Lowry et al., 1951). Antioxidant supplementation could affect chemotherapy reactions as well as negative side impacts resulting from antineoplastic agent therapy. These agents have improved toxicity which results from the overproduction of free radicals and reactive oxygen species (ROS) (Ferramosca et al., 2017). CP is an alkylating drug used commonly to treat cancer worldwide (Pramita et al., 2009). Increases peroxidation of the cell membrane and damages many cellular structures. Therefore, many scientists are engaged in finding natural compounds to minimize the negative impacts of CP-induced toxicity. Many crops obtained from natural products can be hepatoprotective to different chronic diseases of the liver. The free radicals and ROS include a range of reactive molecules capable of oxidizing the cell. Oxidative stress may be one of the manifestations of cellular damage in the toxicity of drugs and chemical toxins. Lipid is regarded as a membrane integrity-monitoring index. MAD is commonly used as a lipid peroxidation marker (LPO). The levels of MDA were significantly higher animals treated with CP as compared to the control group. The preventive impact of the HSE administration was noted and tabulated in Table 2. It can be seen from this table that readings were considerably lower and associated with decreased level of MDA. Previous studies demonstrated that HSE is an effective antioxidant and free radical scavenger *in vivo* and *in vitro* conditions. Reduced glutathione is the most abundant antioxidant in hepatic cells, and has a key function in defending tissue oxidation (Franco et al; 2008). In the present study, the depletion in the antioxidative status of the liver was moderately corrected by the use of HSE (Table 2). The reduction of CP in group 2 resulted in the reduction of glutathione by the oxidation of GSH to oxidised glutathione (GSSG). Treatment of the control group inoculated with CP and HSE resulted in an increase of liver GSH as compared to the control group given CP only. The main body defense employs antioxidant enzymes (CAT & SOD), which protects against cell-generated reactive oxygen species (ROS). The plant chemistry assessment of the Hibiscus floral extract revealed the presence of four significant flavonoids; sabdariffa, protocatechuic acid, anthocyanins and vitamin C (Liu et al., 2010). The antioxidant and hepatoprotective molecules activate certain plant-based flavonoids (Olusola et al., 2012;). The relative elevated concentration of polyphenol in floral crude extract of HSE indicates potential antioxidants (Al Groom & Al-Kubaisy, 2016). The DPPH radical scavenging action of HSE was more than vitamin C (Bansal & Simon, 2018). It is reported that the crude extract of HS flowers has total phenolic content of (77-87 mg\g) (Al-Hashimi, 2012). In the current study, CP treatments of the mice resulted in substantial liver damage. This damage is evident from the elevated serum marker activity (ALT, AST, GGT) reduced T. protein and albumin in the mice (Table 1). HSE dose of 250 mg enhanced antioxidant strength (Table 2). These markers were used to signify hepatocellular injury, because they

were situated in the cytoplasm and released into blood circulation after the cell membrane was ruptured. HSE therapy showed a significant protective action against CP-induced hepatotoxicity and modified complete protein and albumin concentration (Table 1).

Herein, the activity of these antioxidant enzymes in the liver tissue was lowered by CP administration. The reduction in the concentrations of these enzymes could be linked to the inactivation of the free radicals, which occurred while CP was metabolized. *H. sabdariffa* floral extract administration has considerably improved the operations of the enzyme by scavenging ROS, as well as the lipid peroxidation that inhibited HSE antioxidant characteristics. Flower extracted compounds showed antioxidant effect against oxidative stress in red blood cells (Al-Groom and Al-Kubaisy, 2016). This study revealed that HSE possesses a potent effect by reducing the resistance to oxidation stress. Damaged markers, and antioxidants including (enzymatic and non-enzymatic) showed that HSE could reduce CP-induced oxidative stress. Administration of free radical scavenging antioxidants can alleviate hepatotoxicity. Stimulation of ribosomal RNA polymerase and protein synthesis can lead to enhanced hepatocyte regeneration (Bhaargavi et al., 2014). HSE works effectively to scavenge ROS and detoxify free radicals produced during metabolic activities of CP. The activity of HSE was estimated to be equivalent to a dose of silymarin drug 20 mg/kg (Jain et al., 2012). Moreover, results obtained in the present study showed that CP-treatment produced a reduction in the DNA, RNA and protein content in hepatic cells. This indicated a significant cytotoxic effect. The treatment of mice with HSE significantly improved these biochemical parameters. One of the mechanisms that can explain the capacity of HSE to stimulate liver tissue regeneration is the increase DNA synthesis, ribosomal RNA, as well as protein synthesis in the injured hepatocytes. The available data suggest that flavonoid contents of HSE might be responsible for these activities. Our finding supports prior studies, particularly the work conducted by Al-Hashimi (2012).

5. Conclusion

Hibiscus sabdariffa L. Extract has significant inhibition of oxidative stress induced by CP. The use of herb resulted in the improvement of hepatocellular injury. Hence, it can be used as adjuvant therapy for preventing the side effects associated with chemotherapy.

Funding statement

This work was supported by the Deanship of Scientific Research at Al-Balqa Applied University.

Conflict of Interest

the author declares that there is no conflict of interests.

References

Al-Hashimi, A. G. (2012). Antioxidant and antibacterial activities of Hibiscus sabdariffa L. extracts. Afr. J. Food Sci, **6(21)**, 506-511.

Al-Kubaisy, K. N., & Al-Essa, L. Y. (2016). Stimulation of Hepatocytes Repair by Fruit Juice of Opuntia ficus indica in Anti Cancer Drug Cyclophosphamide (CP)-Induced Liver Toxicity in Mice. Annu. Res. Rev. Biol., 1-8.

Al-kubaisy, K. N., Al-Groom, R. M., & Al-Amoush, A. (2016). Changes in the Oxidative Stress Biomarkers in Rat Liver Tissue Exposed to Cadmium and Protect with Hibiscus sabdariffa L.(Rossle) Flower Extract. Int. j. curr. microbiol. appl. sci, **5**, 818-824.

Al-Ghamdi, A. Y., Fadlelmula, A. A., & Abdalla, M. O. (2020). Total Phenolic Content, Antioxidant and Antimicrobial Activity of Ruta chalepensis L. Leaf Extract in Al-Baha Area, Saudi Arabia. Jordan J. Biol. Sci., **9(3),** 9-46.

Al Groom, R. M., & Al-Kubaisy, K. (2016). Anthocyanin–rich red dye of Hibiscus sabdariffa L. Calyx Modulates CdCl2-induced hypochromic microcytic anaemia and oxidative stress in rat red blood cells. J. Environ, **5(1)**, 13-18.

Bansal, A., & Simon, M. C. (2018). Glutathione metabolism in cancer progression and treatment resistance. J. Cell Biol., **217(7),** 2291-2298.

Beutler, E. (1963). Improved method for the determination of blood glutathione. J. lab. clin. Med., **61**, 882-888.

Bhaargavi, V., Jyotsna, G., & Tripurana, R. (2014). A review on hepatoprotective activity. Int. J. Pharm. Biol. Sci., 5(3).

Dafallah, A. A., & Al-Mustafa, Z. (1996). Investigation of the anti-inflammatory activity of Acacia nilotica and Hibiscus sabdariffa. Am. J. Chinese Med, **24(03n04)**, 263-269.

de Jong, A., Plat, J., & Mensink, R. P. (2003). Metabolic effects of plant sterols and stanols. J. Nutr. Biochem. **14(7),** 362-369.

Duke, J. (1985). **Handbook of Medicinal Herbs** Livingstone Group Ltd: Edinburgh.

El-Nekeety, A. A., Abdel-Azeim, S. H., Hassan, A. M., Hassan, N. S., Aly, S. E., & Abdel-Wahhab, M. A. (2014). Quercetin inhibits the cytotoxicity and oxidative stress in liver of rats fed aflatoxin-contaminated diet. Toxicol. Rep., **1**, 319-329.

Farombi, E., & Ige, O. (2007). Hypolipidemic and antioxidant effects of ethanolic extract from dried calyx of Hibiscus sabdariffa in alloxan-induced diabetic rats. Fundam. Clin. Pharmacol., **21(6)**, 601-609.

Farombi, E. O., & Fakoya, A. (2005). Free radical scavenging and antigenotoxic activities of natural phenolic compounds in dried flowers of Hibiscus sabdariffa L. Mol. Nutr. Food Res., **49(12)**, 1120-1128.

Ferramosca, A., Di Giacomo, M., & Zara, V. (2017). Antioxidant dietary approach in treatment of fatty liver: new insights and updates. World J. Gastroenterol., **23(23)**, 4146.

Franco, R.; Schoneveld, O. J.; Pappa, A.; Panayiotidis M. I. (2008). The central role of glutathione in the pathophysiology of human diseases. Journal of . Arch. Physiol. Biochem. , **113**:4-5, 234-258,
DOI: 10.1080/13813450701661198.

Hirunpanich, V., Utaipat, A., Morales, N. P., Bunyapraphatsara, N., Sato, H., Herunsale, A., & Suthisisang, C. (2006). Hypocholesterolemic and antioxidant effects of aqueous extracts from the dried calyx of Hibiscus sabdariffa L. in hypercholesterolemic rats. J. Ethnopharmacol., **103(2)**, 252-260.

Jain, A., Dwivedi, N., Bhargava, R., & Flora, S. J. (2012). Silymarin and naringin protects nicotine induced oxidative stress in young rats. Oxid. Antioxid. Med. Sci., **1(1)**, 41-49.

Johansson, L. H., & Borg, L. H. (1988). A spectrophotometric method for determination of catalase activity in small tissue samples. Anal. Biochem., **174(1)**, 331-336.

Kakkar, P., Das, B., & Viswanathan, P. (1984). **A modified spectrophotometric assay of superoxide dismutase.**

Lin, H.-H., Chen, J.-H., & Wang, C.-J. (2011). Chemopreventive properties and molecular mechanisms of the bioactive compounds in Hibiscus sabdariffa Linne. Curr. Med. Chem., **18(8)**, 1245-1254.

Liu, J.-Y., Chen, C.-C., Wang, W.-H., Hsu, J.-D., Yang, M.-Y., & Wang, C.-J. (2006). The protective effects of Hibiscus sabdariffa extract on CCl4-induced liver fibrosis in rats. Food Chem. Toxicol., **44(3)**, 336-343.

Liu, L. C., Wang, C. J., Lee, C. C., Su, S. C., Chen, H. L., Hsu, J. D., & Lee, H. J. (2010). Aqueous extract of Hibiscus sabdariffa L. decelerates acetaminophen-induced acute liver damage by reducing cell death and oxidative stress in mouse experimental models. J. Sci. Food Agric., **90(2)**, 329-337.

Lowry, O., Rosebrough, N., Farr, A. L., & Randall, R. (1951). Protein measurement with the Folin phenol reagent. J. Biol. Chem. , **193(1)**, 265-275.

Oboh, H. A., & Okhai, E. (2012). Antioxidant and free radical scavenging abilities of some indigenous Nigerian drinks. Nigerian Int. j. basic appl. sci., 20(1), 21-26.

Ohkawa, H., Ohishi, N., & Yagi, K. (1979). Assay for lipid peroxides in animal tissues by thiobarbituric acid reaction. Anal. Biochem., **95(2)**, 351-358.

Okoko, T., & Ere, D. (2012). Hibiscus sabdariffa extractivities on cadmium—mediated alterations of human U937 cell viability and activation. Asian Pac. J. Trop. Med., **5(1)**, 33-36.

Olusola, A. O., Olusola, A. O., Bada, S. O., & Obi, F. O. (2012). Comparative study on the effect of Hibiscus sabdariffa calyx anthocyanins and ascorbate on 2, 4-dinitrophenylhydrazine-induced damage in rabbits. Am. J. Biochem., **2(2)**, 1-6.

Patterson, J., & Mura, C. (2013). Rapid colorimetric assays to qualitatively distinguish RNA and DNA in biomolecular samples. J. Vis. Exp.. **72**, e50225.

Pietta, P.-G. (2000). Flavonoids as antioxidants. J. Nat. Prod., **63(7)**, 1035-1042.

Pramita Chakraborty, U. H. S., Murmu, N., Das, J. K., Pal, S., & Bhattacharya, S. (2009). Modulation of cyclophosphamide-induced cellular toxicity by diphenylmethyl selenocyanate in vivo, an enzymatic study. Mol. Cancer., **4(6)**, 183-189.

Rosa, R. M., Moura, D. J., Melecchi, M. I. S., dos Santos, R. S., Richter, M. F., Camarao, E. B., .Saffi, J. (2007). Protective effects of Hibiscus tiliaceus L. methanolic extract to V79 cells against cytotoxicity and genotoxicity induced by hydrogen peroxide and tert-butyl-hydroperoxide. Toxicol. In Vitro, **21(8)**, 1442-1452.

Srivastava, B. D., Srivastava, M., Srivastav, S. K., Urata, M., Suzuki, N., & Srivastav, A. K. (2021). Cypermethrin-Induced Alterations in Serum Calcium and Phosphate of Rats: Protective Role of Jamun Seed and Orange Peel Extracts. J. Biol. Sci., **14(3),** 417 – 422Taylor, J. B. (2007). Comprehensive medicinal chemistry II: Elsevier.

Yeşilada, E., Honda, G., Sezik, E., Tabata, M., Fujita, T., Tanaka, T., Takaishi, Y. (1995). Traditional medicine in Turkey. V. Folk medicine in the inner Taurus Mountains. J. Ethnopharmacol., **46(3)**, 133-152.

JJBS

Volume 15, Number 5, December 2022
ISSN 1995-6673
Pages 847 – 853
https://doi.org/10.54319/jjbs/150514

Jordan Journal of Biological Sciences

Detection of Inherited Thrombophilic Mutations in Jordanian Children Suffering from Thrombotic Events

Haneen H. Al-naimat[1,2], Manal A. Abbas [1,3,*] , Tariq N. Aladily[4], Muna A. ALmahaharmeh[2], Lina M. ALmomani[2]

[1] Department of Medical Laboratory Sciences, Faculty of Allied Medical Sciences, Al-Ahliyya Amman University, 19328, Amman, Jordan;
[2] Department of Hematology and Coagulation,Princess Iman Center for Research and Laboratory Sciences, Amman, Jordan ;
[3] Pharmacological and Diagnostic Research Lab, Al-Ahliyya Amman University, 19328, Amman, Jordan;
[4]Department of Hematopathology, School of medicine, The University of Jordan, Amman 11910, Jordan

Received: April 12, 2022; Revised: July 15, 2022; Accepted: August 11, 2022

Abstract

Inherited thrombophilia is a coagulation condition that is linked to increased risk of thrombosis. This study investigates the prevalence of FV Leiden (G1691A), FV H1299R (HR2), FV Y1702C, MTHFR C677T, MTHFR A1298C, FII G20210A and PAI-1 mutations among children with thrombotic events. This single-center study included 60 Jordanian children of both sexes (4 days-18 years) admitted to hospital and diagnosed with thrombotic event of any type. The control group consisted of 50 healthy subjects. The presence of thrombophilic mutations was detected using polymerase chain reaction strip assay. The majority of thrombotic events (38.3%) were reported in children at school age (6-12 years) and in adolescents (26.7%) (13-18 years). The most common thrombotic events were deep vein thrombosis (35%) followed by cerebrovascular accidents (18.3%) and cerebral vein sinus thrombosis (16.6%). The most common thrombophilic mutations among children diagnosed with thrombotic events were PAI-1(4G/5G), MTHFR A1298C, MTHFR C677T and FV Leiden (G1691A) constituting 63.3%, 56.7%, 48.3%, and 41.7%, respectively. A statistically significant difference in the occurrence of mutations between the control group and children with thrombotic events was found only in FV Leiden (G1691A), MTHFR A1298C and FV H1299R. This study revealed that neither children with thrombotic events nor subjects in the control group carried the FV Y1702C mutation. In conclusion, the presence of FV Leiden (G1691A), MTHFR A1298C and FV H1299R mutations may be considered as a risk factor for thrombosis in children. Genetic testing of children with family history could play an important role in detecting high-risk subjects.

Keywords: Deep vein thrombosis, inherited thrombophilia**,** FV Leiden, thrombophilic mutations**,** venous thromboembolism.

1. Introduction

Pediatric venous thromboembolism (VTE) is a severe health problem with mortality risk and possible complications such as pulmonary embolism, cerebrovascular events, and post-thrombotic syndrome (Monagle and Newall, 2018). Because of its growing recognition in the pediatric population, VTE is no longer considered an adult illness. In the early 1990s, the reported incidence of VTE was just 5.3 occurrences per 10,000 pediatric hospital admissions while in 2017 it had risen substantially to 30-58 incidents per 10,000 hospital admissions (Witmer and Takemoto, 2017). This increased risk in VTE cases may be due to greater survival of critically ill children as a result of increased use of central venous catheters, sophisticated therapies, advanced surgical techniques, and pediatricians' enhanced awareness of VTE (Faustino and Raffini, 2017).

The tendency to develop VTE is genetically determined, acquired or both (Lane et al., 1996). A systematic review on the impact of inherited thrombophilia on VTE in children has shown a significant association between thrombosis and the presence of inherited thrombophilic risk factors (Young et al., 2008). Yet, routine thrombophilia testing is controversial. The criteria for selecting who must be tested should be defined on a scientific basis to increase the chance of discovering a genetic risk factor (Vagdatli et al., 2013). It has been suggested that genetic testing of children is required if there is a family history of thrombophilia (Celkan and Dikme, 2018). In newborns, children, and adolescents with unprovoked and recurrent VTE, diagnostic thrombophilia testing is also advised, especially when no triggering factor is evident (Revel-Vilk et al., 2003). Because the prevalence of inherited thrombophilic mutations varies by population (Roberts et al., 2009), this study was designed to investigate the prevalence of inherited thrombophilia in Jordanian children suffering from any type of thrombotic event.

* Corresponding author. e-mail: m.abbas@ammanu.edu.jo.

2. Materials and Methods

2.1. Population of the study

Children of both sexes (4 days-18 years) admitted to Queen Rania Al-Abdullah Hospital for Children during the period from the 1st of January to 29th of November, 2021 and diagnosed with any thrombotic event with or without any associated disease were included in the study. The ethical approval was obtained from King Hussein Medical Centre, IRB number: 20/2021. The control group included 20 healthy Jordanian children (1 year -18 years) and 30 healthy Jordanian adults (19 - 45 years). Clinical and demographic data of patients (age, sex, thrombotic events, family history and the presence of any associated disease) was extracted from the electronic medical records.

2.2. Testing genetic mutations

Blood samples were collected in EDTA tubes for DNA extraction. Polymerase chain reaction (PCR) was used for genetic testing. The test is based on the reverse-hybridization principle, where specific oligonucleotide probes immobilized as parallel lines on membrane-based strips hybridize with biotinylated PCR products. Genomic DNA was extracted according to a standard procedure using Wizard Genomic DNA Purification kit (Promega, USA, Cat. No. A1125). Thermal Cycler (BIO-RAD iCycler Thermal**)** was used to amplify the DNA. DNA polymerase, PCR mix solution containing oligonucleotides and nitrocellulose membrane strips coated with oligonucleotideswere were obtained from Nuclear Laser Medicine Srl-Viale Delle Industrie, 3 – 20090**,** Settala (MI), Italy. The incidence of factor V (FV) Leiden (G1691A), FV H1299R (HR2), FV Y1702C, methylene-etrahydrofolate reductase (MTHFR) C677T, MTHFR A1298C, Factor II (FII) G20210A and plasminogen-activator inhibitor-1 (PAI-1) (4G/5G) polymorphism was studied.

2.3. Statistical analysis

Using descriptive statistics, the data was presented as numbers (percentages) for categorical variables and mean ± standard deviation for numeric variables. A web-version of Fisher's exact test (Univariate analysis) was used to compare categorical variables (gender and the presence of mutation). SPSS version 22 was used to study the correlation between the type of thrombotic event and age. A p-value of ≤ 0.05 was considered as statistically significant.

3. Results

3.1. Demographic and clinical characteristics of the study population

This study included 60 Arab Jordanian children (32 males and 28 females) admitted to Queen Rania Al-Abdullah Hospital for Children, Amman, Jordan and diagnosed with any thrombotic event. Their ages ranged from 4 days to 18 years with an average of 9 years. The control group included 50 healthy Jordanian subjects (25 males and 25 females). Their ages ranged from 1 year to 45 years: 20 children with a mean age of 9 years and 30 adults with a mean age of 30 years.

A 4-day old male newborn had right ischemic brain lesion and cerebral artery occlusion. The only mutation he had was 4G/4G. The majority of thrombotic events (23 cases; 38.3% of total cases) were at school age (6-12 years) and adolescents (13-18 years) (16 cases; 26.7% of total cases). The most common thrombotic event was deep vein thrombosis (DVT): 21 patients (11 females and 10 males; 35% of total cases). The second most common thrombotic event was cerebrovascular accident (CVA): 11 patients (4 females and 7 males) that constituted 18.3% of the total cases. The third was cerebral vein sinus thrombosis (CVST): 10 patients (4 females and 6 males; 16.6% of the total cases) followed by renal vein thrombosis (RVT) and portal vein thrombosis (PVT) (Table 1). No correlation between the type of thrombotic event and age was found.

Table 1. Thrombotic events reported in the studied children with thrombotic events.

Thrombotic event episode(s)	Sex			
	M	F	Total	Percent (%)
DVT (deep vein thrombosis)	10	9	19	31.6
DVT+ PE **(**pulmonary embolism**)**	0	2	2	3.3
cerebrovascular accident (CVA)	7	4	11	18.3
cerebral vein sinus thrombosis (CVST**)**	6	4	10	16.6
renal vein thrombosis (RVT)	4	3	7	11.6
portal vein thrombosis (PVT)	2	4	6	10
Hepatic vein thrombosis (HVT)	2	0	2	3.3
Thrombosis at AV graft	1	0	1	1.6
Internal jugular vein thrombosis (IJVT)	0	1	1	1.6
Progressed ischemic toes foot and left forearm cubital area	0	1	1	1.6
TOTAL	32	28	60	

None of the children who were diagnosed with thrombotic event died. Forty-three (70% of children with thrombotic events) had a thrombotic event for the first time without a family history or an associated disease except for one child who had a confirmed family history of DVT in several members of his family. Fourteen children (21.7%) had a thrombotic event with an associated disease such as nephritic syndrome (NS) and systemic lupus erythematosus (SLE) (Table 2). Twelve of them were catheterized; one had arteriovenous graft (AV graft) and eleven had central venous catheter (CVC). Five children (8.3%) had recurrent thrombotic episodes: one of them had recurrent DVT and the other child had DVT at the age of 1 year and developed cerebral vein sinus thrombosis at the age of 11 years. The other three children had recurrent thrombotic events with an associated disease (Table 2).

Table 2: Associated diseases with thrombotic events in the studied population of children

Thrombotic event	Associated diseases/Family history	Recurrent thrombosis	Family history	No. cases	Gender	Age
CVA	Single ventricle	-	-	1	M	4Y
CVA	Arthralgia	-	-	1	F	8Y
CVA	Press syndrome	-	-	1	F	9Y
CVA	Down syndrome	-	-	1	M	5Y
CVA	Microcephaly	-	-	1	M	1Y
DVT +PE	Nephrotic syndrome + family history of recurrent thrombosis	√	√	1	F	6Y
DVT	Diagnosed as End-Stage Renal Disease (ESRD)	-	-	1	M	12Y
DVT	systemic lupus erythematosus (SLE)	-	-	1	F	11Y
DVT	Nephrotic syndrome ESRD	-	-	1	M	10Y
DVT	Diagnosed SLE	-	-	1	F	9Y
	Steroid resistant nephrotic syndrome					
DVT	Brain stroke on 12Year old	√	-	1	M	14Y
CVST	CVA on 2-year-old	√	-	1	F	5Y
	Case of arteriovenous Malformation					
IJVT	Case of Acute myeloid leukemia (AML)	-	-	1	F	12y
Thrombosis at AV graft	ESRD	-	-	1	M	13Y
	Dialysis was through AV. Fistula develop thrombosis					
CVA	recurrent stroke complicated by hemiparesis and epilepsy (primary angiitis of the CNS)	√	-	1	M	6Y

3.2.

3.3. Genotyping results of children with thrombotic events vs. control group

Results of this study showed that 85% of the children diagnosed with thrombotic events had at least 2 of the studied thrombophilic genetic variants. The most common thrombophilic mutations in children with thrombotic events were as follows: PAI-1(4G/5G), MTHFR A1298C, MTHFR C677T and FV Leiden (G1691A) constituting 63.3%, 56.7%, 48.3% and 41.7%, respectively. None of the children with any thrombotic event or in the control group carried the FV Y1702C mutation (Figure 1). The prevalence of thrombophilic mutations among the control group was as follows: 22 (44%) had MTHFR C677T mutation, 16 (32%) had MTHFR A1298C mutation, 7 (14%) had PAI-1(4G/4G), 5 (10%) had FV H1299R, 4 (8%) had FV Leiden (G1691A) mutation, 4 (8%) had PAI-1(5G/5G), 39 out of 50 (78%) had PAI-1(4G/5G), 2 (4%) had FII G20210A.

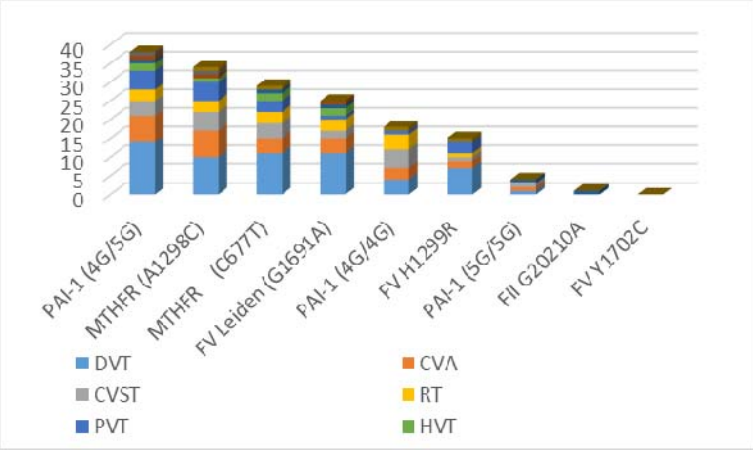

Figure 1: Thrombotic events associated with the studied mutations

The incidence of FV Leiden (G1691A), FV H1299R (HR2), FV Y1702C, MTHFR C677T, MTHFR A1298C, FII G20210A, PAI-1(4G/5G) polymorphism among children diagnosed with thrombotic events compared to the control group is illustrated in Table 3. No statistically significant difference was found between males and females for the presence of any of the seven studied mutations in both control group and children with thrombotic events. A significant difference in the incidence of mutations in the control group and children with thrombotic events was found only in the incidence of FV Leiden (G1691A), MTHFR A1298C and FV H1299R (Table 3). On the other hand, no significant difference in the homozygous/heterozygous ratio was found between the control group and the thrombotic group for the mutations MTHFR A1298C, MTHFR C677T and PAI-1 (Table 3).

Mutation	Frequency in patients	Genotype status HET vs HOMO	Male: female	* P-Value	Frequency in control group	Genotype status HET vs HOMO	Male: female	£P-Value	#P-Value	Ω P-Value
FV Leiden (G1691A)	25 (41.7%)	Heterozygous (GA): 23 Homozygous (AA): 2	11: 14	.295	4 (8%)	Heterozygous	2:2	1.000	**.0001**	-
FV H1299R (HR2)	15 (25%)	Heterozygous (GA): 14 Homozygous (GG): 1	8: 7	1.000	5 (10%)	Heterozygous	2:3	1.000	**.049**	-
FV Y1702C	0	-	-	-	0	-	-	-	-	-
MTHFR C677T	29 (48.3%)	Heterozygous (CT): 25 Homozygous (TT): 4	13: 16	.300	22 (44%)	Heterozygous (CT): 20 Homozygous (TT): 2	10: 12	.776	.703	0.687
MTHFR A1298C	34 (56.7%)	Heterozygous (AC): 31 Homozygous (CC): 3	18: 16	1.000	16 (32%)	Heterozygous (AC): 15 Homozygous (CC): 1	6: 10	.363	**.012**	1.000
PAI-1	56 (93.3%)	Heterozygous 4G/5G:38 Homozygous 4G/4G: 18	29: 27	.615	46 (92%)	Heterozygous 4G/5G:39 Homozygous 4G/4G: 7	24:22	.609	1.000	0.064
FII G20210A	1 (1.7%)	Heterozygous	0: 1	.466	2 (4%)	Heterozygous	1: 1	1.000	0.589	-

Table 3: Frequency, genotype status and sex ratio in the control and thrombotic children groups.

P≤ 0.05 was considered significant

* P- value for gender difference for the presence of the mutation within patients

£ P- value for gender difference for the presence of the mutation within control group

P- value for mutation presence between patients and control group

Ω P- value for homozygous/ heterozygous ratio between patient and control group

4. Discussion

Mutations in genes encoding proteins that activate coagulation process or inactivate anticoagulation play an essential role in predisposition and increase the risk of venous thrombosis (VT) (Nowak-Göttl et al., 2018). In the current investigation, a significant difference in the incidence of mutations was found in FV Leiden (G1691A), MTHFR A1298C and FV H1299R between the control group and children with thrombotic events.

FV Leiden results from the replacement of guanine by adenine at nucleotide 1691 in the FV gene. This leads to the replacement of glutamine by arginine at the activated protein C (APC)-cleavage site resulting in a lack of response to APC. APC is a naturally occurring anticoagulant protein that cleaves and inactivates the procoagulant FVa and FVIIIa, preventing thrombin production (Dahlbäck, 2008). Several studies highlighted the importance of FV Leiden (G1691A) genotype in the development of childhood and adult thrombosis. FV Leiden was found to be a risk factor for ischemic stroke in children (Masri and Al-Ammouri, 2016). In another study, factor V Leiden heterozygozygosity was linked to a seven-fold increased risk of arterial ischemic stroke, neonatal arterial ischemic stroke, and transient ischemic attack (Herak et al., 2009). In adults, the most frequent genetic risk factor for VTE was FV Leiden (G1691A), which was identified in 20- 25 % of VTE patients and 50 % of hereditary thrombophilia patients (Rosendaal et al., 1995). Similarly, FV G1691A mutation was linked to an increased risk of developing thrombosis, including ischemic stroke in children (Ozyurek et al., 2007).

Carrying FV H1299R (A4070G) allele is related to modest APC resistance and a relative excess of the more thrombogenic FV isoform FV1 in plasma (Castoldi et al., 2000a). The prevalence of FV H1299R variant in Jordanian children with thrombotic events was found to be 25% and only 10% in the control group with a significant difference between the two groups. A recent study conducted in Southern Italy on 282 patients (adults and children) with ischemic stroke and 87 patients with transient ischemic attacks, revealed that the prevalence of FV H1299R was 9.9% in ischemic stroke group, 11.5% in transient ischemic attacks group and 9.1% in general population (Cernera et al., 2021). Importantly, it has been reported that the FV H1299R mutation increases the incidence of VT in FV Leiden mutation carriers (Faioni et

al., 1999) and it was considered as a thrombotic risk factor itself (Alhenc-Gelas et al., 1999).

In the present investigation, none of the healthy children or children affected by any thrombotic event carried FV Y1702C mutation. Our study agrees with previous studies that reported a rare prevalence of FV Y1702C mutation in the general population (Castoldi et al., 2000b).

Prothrombin, also known as FII G20210A, is a vitamin K-dependent clotting factor made by the liver which is involved in the conversion of fibrinogen to fibrin. In patients with prothrombin gene mutation plasma, prothrombin is increased due to guanine replacement by adenine at location 20210 in the prothrombin gene (Dahlbäck, 2008). In patients with a family history of venous thrombophilia, FII G20210A mutation was considered to be a moderate risk factor for VT (Poort et al., 1996). In our study, the prevalence of FII G20210A in children diagnosed with thrombotic events was 1.7% with no statistically significant difference from the control group. Similar to our findings, this mutation was not found to be a significant predictor of cerebral thrombosis and arterial ischemic stroke risk in children (Herak et al., 2009; Ozyurek et al., 2007).

The enzyme MTHFR is involved in the methylation of homocysteine to methionine. Mutations in the MTHFR gene may lower enzyme activity, resulting in hyperhomocysteinemia which was associated with a variety of vascular problems, including coronary artery disease and DVT (Liew and Gupta, 2015). In the present investigation, MTHFR had a high prevalence among children diagnosed with thrombotic events. The MTHFR A1298C mutation was present in 56.7% while MTHFR C677T mutation was found in 48.3%. Twenty five percent of children with thrombotic events had both MTHFR A1298C and C677Tmutations. A significant difference in the occurrence of MTHFR A1298C, but not MTHFR C677T mutation, was found between the control group and children with thrombotic events. In an Italian study, the prevalence of MTHFR C677T was 52.1% in ischemic stroke group, 47.7% in transient ischemic attacks group and 43.8% in general population while the prevalence of MTHFR A1298C was 28.3% in ischemic stroke group, 28.2% in transient ischemic attacks group and 29% in the general population (Cernera et al., 2021). Another study showed a correlation between the presence of MTHFR C677T gene polymorphism and the onset of ischemic stroke in young age (Cernera et al., 2021). Moreover, a case-control study comparing 141 childhood patients with VT with 345 healthy controls from Germany revealed that MTHFR C677T mutation is a significant risk factor for venous vascular occlusion in children (Koch et al., 1999).

In our study, the most prevalent mutations among children diagnosed with thrombotic events was PAI-1 (93.3%: 68% 4G/5G and 32% 4G/4G). PAI-1 is the main inhibitor of plasminogen activation, blocking tissue plasminogen activator and urokinase plasminogen activator from converting plasminogen to the fibrinolytic enzyme plasmin (Wiman, 1995). Elevated PAI-I expression that leads to impaired fibrinolytic function is commonly observed in patients with thrombotic disease (Tang et al., 2018). However, the prevalence of PAI-1 mutations was not statistically significant from that of the control group. Endogamy among Jordanian society may explain the high prevalence of these mutations. In a previous study conducted on Jordanian general population, the prevalence of PAI-I 4G/5G polymorphism was 66% (Al-Zoubi et al., 2021). According to recent study, the presence of PAI-1 4G/4G polymorphism increased the risk of arterial and venous thrombosis of varied localization in infants by 48.8% and the likelihood of thrombosis by 9 folds (Filippova et al., 2020). On the other hand, PAI-1 4G/4G and PAI-1 4G/5G genotypes were linked to an elevated risk of VTE in Asian populations (Zhang et al., 2020). Also, the PAI-1 gene 4G/5G genotype was found to be a significant predictor of cerebral thrombosis risk in children in another investigation conducted in Turkey (Ozyurek et al., 2007).

In a previous study, 95% of children with VTE events had an underlying surgical or medical condition such as cardiac disease, cancer, infection or autoimmune disease that triggered thrombosis (Sadiq et al., 2021). In our study 21.7% of the studied children had thrombotic events associated with other diseases such as NS, SLE, acute myeloid leukemia and others. Three children with NS had DVT, and one had thrombosis at AV graft. According to another study NS was associated with a high incidence of VTE (Singhal and Brimble, 2006). Similarly, it was reported that a high prevalence of VTE (28%) is present in patients with primary NS in which 70% of VTE cases were unilateral RVT (Ismail et al., 2020). It has been suggested that the association of haemostatic imbalance secondary to NS (Ismail et al., 2014) with chronic inflammation associated with certain glomerulonephritis along with a genetic predisposition can trigger a VTE (Kerlin et al., 2012). Thus, inherited thrombophilia does not result in a spontaneous VTE, until an acquired hypercoagulable state in NS determines the clinical manifestation of the prothrombotic tendency due to loss of protein in urine that prevents thrombosis and increased synthesis of factors that promote thrombosis (Reich et al., 2003).

In our study, two children had SLE, and it was confirmed that they had DVT. It has been reported earlier that SLE was associated with three times- higher VTE rate compared to the general population (Lee and Pope, 2014). This acquired disease was considered as an independent risk factor for both arterial and venous thrombotic events (Bazzan et al., 2015).

None of the children who were diagnosed with thrombotic event died in this study. Advances in pediatric care may decrease fatality rate in cases of pediatric thrombosis. Long-term follow up of patients especially with recurrence may help in recording the mortality rate. The majority of cases in our cohort suffered from DVT. As reported earlier in literature, young age was a protective factor against developing VTE. Unlike in adults, pulmonary emboli in adolescents were rarely fatal (Spentzouris et al., 2012). In addition, pediatric strokes had better prognosis than adult strokes (Steinlin et al., 2004).

The control group in our study consisted of 20 healthy children and 30 adults. If the control group was composed of children only, one may argue that they may develop thrombotic event in the near future. Thus, including healthy adults in the control group would eliminate this possibility. This was evident in the case of PAI-1 mutations in which a high prevalence was present in both control and thrombotic children indicating that it may not represent a risk factor for thrombosis at later stages in life.

The main aim of the present work was to study the prevalence of thrombophilic mutations among children with thrombotic events. The main limitation of this study was the small number of cases. The reason for that is the rare occurrence of thrombotic events among children. As reported in other studies, thrombotic events in children are rare (Steinlin et al., 2004). Therefore, future longer-term studies are needed.

In conclusion, the present study showed that the most common thrombotic events among children were DVT, followed by CVA and CVST. Eighty five percent of children with thrombotic events had at least 2 mutations among the 7 studied mutations. The presence of FV Leiden (G1691A), MTHFR A1298C and FV H1299R mutations may present a risk factor for thrombosis in children. The findings of this study suggest that genetic testing for inherited thrombophilia in children with family history and/or associated disease such as NS and SLE may play an important role in detecting high-risk patients. The use of prophylactic interventions and life style modifications are recommended in these cases. The gain of knowledge with respect to the pathophysiology of VTE in children is important to correctly assess the need for genetic testing of children with thrombotic events and their family members as well.

Conflict of interest

The authors declare no conflict of interests.

Acknowledgment

This work was published with the support of Al-Ahliyya Amman University.

References

Al-Zoubi N, Alrabadi N, Kheirallah K, Alqudah A. 2021. Prevalence and multiplicity of thrombophilia genetic polymorphisms of fv, mthfr, fii, and pai-i: A cross-sectional study on a healthy jordanian population. *Int. J. Gen. Med*. **14**:5323.

Alhenc-Gelas M, Nicaud V, Gandrille S, van Dreden P, Amiral J, Aubry M-L, Fiessinger J-N, Emmerich J, Aiach M. 1999. The factor v gene a4070g mutation and the risk of venous thrombosis. ***Thromb Haemost***. **81**(02):193-197.

Bazzan M, Vaccarino A, Marletto F. 2015. Systemic lupus erythematosus and thrombosis. *Thromb J.* **13**(1):1-10.

Castoldi E, Rosing J, Girelli D, Hoekema L, Lunghi B, Mingozzi F, Ferraresi P, Friso S, Corrocher R, Tans G. 2000a. Mutations in the r2 fv gene affect the ratio between the two fv isoforms in plasma. ***Thromb Haemost***. **83**(03):362-365.

Castoldi E, Simioni P, Kalafatis M, Lunghi B, Tormene D, Girelli D, Girolami A, Bernardi F. 2000b. Combinations of 4 mutations (fv r506q, fv h1299r, fv y1702c, pt 20210g/a) affecting the prothrombinase complex in a thrombophilic family. *Blood*. **96**(4):1443-1448.

Celkan T, Dikme G. 2018. Thrombosis in children: Which test to whom, when and how much necessary? *Tür Pediatri Arş*. **53**(1):1-9.doi: 10.5152/TurkPediatriArs.2018.2586.

Cernera G, Comegna M, Gelzo M, Savoia M, Bruzzese D, Mormile M, Zarrilli F, Amato F, Micco PD, Castaldo G. 2021. Molecular analysis of prothrombotic gene variants in patients with acute ischemic stroke and with transient ischemic attack. *Medicina.***57**(7):723.

Dahlbäck B. 2008. Advances in understanding pathogenic mechanisms of thrombophilic disorders. *Blood*. **112**(1):19-27.

Faioni E, Franchi F, Bucciarelli P, Margaglione M, De Stefano V, Castaman G, Finazzi G, Mannucci P. 1999. Coinheritance of the hr2 haplotype in the factor v gene confers an increased risk of venous thromboembolism to carriers of factor v r506q (factor v leiden). *Blood.* **94**(9):3062-3066.

Faustino EVS, Raffini LJ. 2017. Prevention of hospital-acquired venous thromboembolism in children: A review of published guidelines. *Front Pediatr*. **5**:9.

Filippova OA, Vakhlova IV, Tsaur GA, Kuznetsov NN, Abolina TB. The role of thrombophilia genes in the clinical implementation of arterial and venous thrombosis in newborns. BIO Web of Conferences; 2020: EDP Sciences.

Herak DC, Antolic MR, Krleza JL, Pavic M, Dodig S, Duranovic V, Brkic AB, Zadro R. 2009. Inherited prothrombotic risk factors in children with stroke, transient ischemic attack, or migraine. *Pediatrics*. **123**(4):e653-e660.

Ismail G, Mircescu G, Ditoiu AV, Tacu BD, Jurubita R, Harza M. 2014. Risk factors for predicting venous thromboembolism in patients with nephrotic syndrome: Focus on haemostasis-related parameters. *Int Urol Nephrol*. **46**(4):787-792.

Ismail G, Obrișcă B, Jurubiță R, Andronesi A, Sorohan B, Hârza M. 2020. Inherited risk factors of thromboembolic events in patients with primary nephrotic syndrome. *Medicina*. **56**(5):242.

Kerlin BA, Ayoob R, Smoyer WE. 2012. Epidemiology and pathophysiology of nephrotic syndrome–associated thromboembolic disease. *CJASN*. **7**(3):513-520.

Koch H, Nabel P, Junker R, Auberger K, Schobess R, Homberger A, Linnebank M, Nowak-Göttl U. 1999. The 677t genotype of the common mthfr thermolabile variant and fasting homocysteine in childhood venous thrombosis. *Eur J Pediatr*. **158**(3):S113-S116.

Lane DA, Mannucci PM, Bauer KA, Bertina RM, Bochkov NP, Boulyjnkov V, Chandy M, Dahlback B, Ginter E, Miletich JP. 1996. Inherited thrombophilia: Part 1. ***Thromb Haemost***. **76**(11):651-662.

Lee JJ, Pope JE. 2014. A meta-analysis of the risk of venous thromboembolism in inflammatory rheumatic diseases. *Arthritis Res Ther*. **16**(5):1-8.

Liew S-C, Gupta ED. 2015. Methylenetetrahydrofolate reductase (mthfr) c677t polymorphism: Epidemiology, metabolism and the associated diseases. *EJMG*. **58**(1):1-10.

Masri A, Al-Ammouri I. 2016. Clinical presentation, etiology, and outcome of stroke in children: A hospital-based study. *Brain Dev*. **38**(2):204-208.

Monagle P, Newall F. 2018. Management of thrombosis in children and neonates: Practical use of anticoagulants in children. *Hematol Am Soc Hemato. Educ Program*. 2018(1):399-404.

Nowak-Göttl U, van Ommen H, Kenet G. 2018. Thrombophilia testing in children: What and when should be tested? *Thromb Res*. **164**:75-78.

Ozyurek E, Balta G, Degerliyurt A, Parlak H, Aysun S, Gürgey A. 2007. Significance of factor v, prothrombin, mthfr, and pai-1 genotypes in childhood cerebral thrombosis. *Clin Appl Thromb Hemost*. **13**(2):154-160.

Poort SR, Rosendaal FR, Reitsma PH, Bertina RM. 1996. A common genetic variation in the 3'-untranslated region of the prothrombin gene is associated with elevated plasma prothrombin levels and an increase in venous thrombosis: *Blood*. **88**:3698-3703.

Reich LM, Bower M, Key NS. 2003. Role of the geneticist in testing and counseling for inherited thrombophilia. *Genet Med*. **5**(3):133-143.

Revel-Vilk S, Chan A, Bauman M, Massicotte P. 2003. Prothrombotic conditions in an unselected cohort of children with venous thromboembolic disease 1. *JTH*. **1**(5):915-921.

Roberts LN, Patel RK, Arya R. 2009. Venous thromboembolism and ethnicity. *Br J Haematol*. **146**(4):369-383.

Rosendaal F, Koster T, Vandenbroucke J, Reitsma P. 1995. High risk of thrombosis in patients homozygous for factor v leiden (activated protein c resistance) *Blood.* **85**(6): 1504-1508.

Sadiq MW, Ukrani RD, Arif A, Akbar I, Altaf S, Moiz B. 2021. Risk assessment and outcome of venous thromboembolism in pediatric population in an academic care center of a low-middle income country. *Clin Appl Thromb Hemost*. **27**:1076029621995895.

Singhal R, Brimble KS. 2006. Thromboembolic complications in the nephrotic syndrome: Pathophysiology and clinical management. *Thromb Res*. **118**(3):397-407.

Spentzouris G, Scriven RJ, Lee TK, Labropoulos N. 2012. Pediatric venous thromboembolism in relation to adults. *J vasc surg*. **55**(6):1785-1793.

Steinlin M, Roellin K, Schroth G. 2004. Long-term follow-up after stroke in childhood. *Eur J Pediatr*. **163**(4):245-250.

Tang J, Zhu W, Mei X, Zhang Z. 2018. Plasminogen activator inhibitor-1: A risk factor for deep vein thrombosis after total hip arthroplasty. *J orthop. surg Res*. **13**(1):1-5.

Vagdatli E, Serafimidou O, Pantziarela E, Tsikopoulou F, Mitsopoulou K, Papoutsi A. 2013. Prevalence of thrombophilia in asymptomatic individuals with a family history of thrombosis. *Hippokratia*. **17**(4):359. PMID: 25031517.

Wiman B. 1995. Plasminogen activator inhibitor 1 (pai-1) in plasma: Its role in thrombotic disease. ***Thromb Haemost***. **74**(07):071-076.

Witmer CM, Takemoto CM. 2017. Pediatric hospital acquired venous thromboembolism. *Front Pediatr*. **5**:198.

Young G, Albisetti M, Bonduel M, Brandao L, Chan A, Friedrichs F, Goldenberg NA, Grabowski E, Heller C, Journeycake J. 2008. Impact of inherited thrombophilia on venous thromboembolism in children: A systematic review and meta-analysis of observational studies. *Circulation*. **118**(13):1373-1382.

Zhang Q, Jin Y, Li X, Peng X, Peng N, Song J, Xu M. 2020. Plasminogen activator inhibitor-1 (pai-1) 4g/5g promoter polymorphisms and risk of venous thromboembolism–a meta-analysis and systematic review. *Vasa*. **49**(2):141-146.

JJBS

Volume 15, Number 5,December 2022
ISSN 1995-6673
Pages 855 – 868
https://doi.org/10.54319/jjbs/150515

Jordan Journal of Biological Sciences

Bioethanol Production from Biologically Pretreated *Prosopis africana* Pods using *Pichia kudriavzevii* SY4

Amina Ahmed El-Imam[1,2], Eromosele Ighalo[2,*], Mardhiyah Sanusi[2], Mushafau Adebayo Oke[3], Patricia Folakemi Omojasola[2]

[1]*Department of Plant and Microbial Biology, North Carolina State University, 27607 USA* [2]*Microbiology Department, The Life Sciences Faculty, University of Ilorin.;* [3]*Independent Researcher, Edmonton, AB, Canada.*

Received: July 30, 2022; Revised: September 29, 2022; Accepted: October 2, 2022

Abstract

High costs and ethical issues have prompted research into novel non-food feedstocks for the fermentation-based manufacture of sustainable fuels. In this study, *Prosopis africana* pods (PAP), an underutilized substrate, was examined for its ability to produce bioethanol. The biomass was pretreated with four mushrooms to delignify it and enhance hydrolysis. A scanning electron microscopy (SEM) was performed on raw and pretreated PAP. The optimum hydrolysis conditions for the pretreated biomass were then determined using the Design of Experiment (DOE) approach. The acid type (HNO_3 and H_3PO_4), concentration (1 %, 3 % and 5 %), solid loading (SL; 5 %, 10 % and 20 %) and contact time (15, 30 and 60 minutes) were optimized using a full-factorial design. The most tolerant yeast isolate from different sources was then molecularly identified after being tested for ethanol tolerance. A half-factorial design was used to screen the fermentation factors, and the Box-Behnken design was used to optimize the relevant components. *Ganoderma lucidum* showed the most luxurious growth during PAP pretreatment and SEM revealed reduction in biomass crystallinity. The hydrolysis conditions of 5 % HNO_3, 20 % SL and 15 minutes contact time were optimal, producing 43.37 ± 0.35 g/L of reducing sugars. The most ethanol-tolerant strain, identified as *Pichia kudriavzevii* SY4, produced 38.26 g/L bioethanol concentration after RSM optimisation. Similarly, optimisation raised bioethanol concentrations from 26.62 ± 0.00 to 38.26 ± 0.18 g/L, a 43.73 % increase. This work is the first report on utilising *Prosopis africana* pods in bioethanol production.

Keywords: Bioethanol, Fermentation, Hydrolysis, Optimisation, *Prosopis africana*, Response Surface Methodology.

1. Introduction

Increasing industrial activities and rapid population increase have caused a boom in energy demand (Raina *et al*., 2020). With more than four-fifths of the global energy market, fossil-derived fuels constitute the main energy source (Branco *et al*., 2019). Over-exploitation has rapidly depleted fossil resources, raising major environmental issues (Milano *et al*., 2016). Consequently, research interest in alternative energy sources has increased drastically (Awoyale and Lokhat, 2019; Rezania *et al*., 2019). One such alternative is biofuels, which can significantly reduce fossil fuel dependence and lower greenhouse gas emissions (Braz *et al*., 2019). The most common biofuel is bioethanol, with 115 billion liters produced in 2019 and it is anticipated to reach 119 billion liters in 2023 (IEA, 2019; Ahmed El-Imam *et al*., 2019).

According to the International Energy Agency (IEA), biofuels should account for 27 % of global transportation fuels by 2050 to satisfy global energy-related CO_2 targets (Ghani *et al*., 2019). First-generation (1G) bioethanol production from carbohydrates (Ibeto *et al*., 2011) like corn starch and sugarcane sugars resulted in the ethical problem of using arable lands to cultivate biofuel crops (Adelabu *et al*., 2018), a negative impact on biodiversity, and contributed to deforestation and desertification (Gerbens-Leenes, 2017; Awoyale and Lokhat, 2021). Thus, the focus shifted to second-generation (2G) or renewable bioethanol, produced by the hydrolysis and fermentation of several feedstocks, including lignocellulosic biomass and industrial and food processing wastes (Ahmed El-Imam *et al*., 2019).

The Russia-Ukraine war, which started in February 2022, has resulted in global spikes in the prices of food and fossil energy sources. Thus, the USA is considering expanding corn-based ethanol production (Gustin, 2022) to reduce dependence on imported oil and lower domestic gasoline prices. However, expanding 1G bioethanol is now even more discouraged due to currently surging food insecurity. An alternative raw material, lignocellulosic biomass, is abundant in nature and affordable, and its utilization in 2G fuel production assures a renewable, self-sufficient and secure supply (Bhatia *et al*., 2017; Branco *et al*., 2019; Wuryantoro *et al*., 2021) at more affordable prices.

Common lignocellulosic materials include agricultural wastes like straw and stover, food processing wastes like bagasse, brans, and pods, and dedicated energy crops like switchgrass and *Miscanthus* sp. These biomasses are composed structurally of hemicellulose, cellulose, and lignin bonded into a stiff matrix that resists hydrolysis into

* Corresponding author. e-mail: eromoseleighalo@gmail.com.

simple sugars and calls for pretreatment techniques (Malik *et al*, 2020; Yildirim *et al*., 2021). The African mesquite (*Prosopis africana*) tree is a perennial leguminous tree found throughout East and West Africa's savanna regions. Its seeds are used to make food condiments, with the empty pods being frequently discarded indiscriminately. These pods are rich in carbohydrates, proteins, and other nutrients, making them ideal for microbial growth and conversion into important and useful products (Pasiecznik *et al*., 2001; Oni *et al*., 2020).

Before utilization, biomass needs to be pretreated, and more than one pretreatment type is commonly employed. Physical pretreatment includes methods like microwave irradiation, ultrasound pretreatment, and size reduction operations. Ionic liquid delignification and acid or alkaline pretreatment are examples of chemical pretreatment methods, whereas CO_2, SO_2, or steam explosion and liquid hot water treatment are examples of physicochemical pretreatment methods (Karimi *et al*., 2013; Beig *et al*., 2021; Yildirim *et al*., 2021). The last pretreatment method is biological, which entails utilizing white-rot fungi and other microbes to break down the dense structure of lignocellulose while leaving the sugars, which can then be hydrolyzed and fermented.

Pretreatment is the most expensive phase of biofuel production, contributing up to 30 % of the total cost (Beig *et al*., 2021). Its advantages include low cost, low severity (Taufikurahman *et al*., 2020), low energy and additive requirements, and the absence of fermentation inhibitors, toxic end-products, and effluents. Biological pretreatment frequently utilizes the white-rot fungi *Trametes versicolor*, *Pleurotus* sp., *Phanerochaete chrysosporium*, and *Lentinus squarrosulus* to delignify the biomass (Sindhu *et al*., 2016; Ahmed El-Imam *et al*., 2021). The residual carbohydrates are then readily depolymerized into sugars and fermented into bioethanol.

Bioethanol production has been reported using *Prosopis juliflora* pods (da Silva *et al*., 2011), but there are no reports using *P. africana* pods (PAP). Here, we report bioethanol production from PAP by optimizing the hydrolysis and fermentation stages using the Full Factorial Design (FFD) and the Response Surface Methodology (RSM), respectively. DOE strategy was employed because it is a multivariate technique widely used to develop products and processes. For the first time, these discoveries point to the optimum conditions for the fermentation-based ethanol generation from the African mesquite tree's pods.

2. Materials and Methods

2.1. Isolation of microorganisms

Yeasts were isolated from different sources (palm wine, sugarcane bagasse, and spoilt oranges) using yeast extract peptone dextrose (YPD) agar (peptone 20 g/L, yeast extract 10 g/L, dextrose 20 g/L, and agar 15 g/L) and incubating at 30 °C for three days. Distinct colonies were selected, purified and pure colonies were maintained on Potato Dextrose Agar (Himedia, India) slants and stored at 4 °C pending use.

2.2. PAP collection and biological pretreatment

Mature pods were obtained from the University of Ilorin campus in North-Central Nigeria. They were dried and milled with a typical locally-fabricated petrol-operated Burr-plate mill and sieved with a 50 mesh sieve. The pods were pretreated biologically using *Ganoderma lucidum*, *Pleurotus eryngii*, *Pleurotus pulmonarius,* and *Hypsizygus ulmarius* obtained from TLC mushrooms Limited, Nigeria. These fungi were chosen because research has shown that members of white rot fungi are the most efficient organisms for delignification as they produce different kinds of lignin-modifying enzymes such as laccase (Lac), manganese peroxidase (MnP), lignin peroxidase (LiP), and versatile peroxidase (VP) (Manavalan *et al*., 2015; Ahmed El-Imam *et al*., 2021). A total of six hundred grams (600 g) of the substrate were put into jute bags, which were then weighed after being moistened to a moisture content of 52 % (w/w) using sterile distilled water. The bags and their contents were sterilized for 30 minutes at 121 °C, and when appropriate, the final moisture contents were adjusted to 52 percent. After being allowed to cool, the bags were inoculated in triplicates with 8 % w/dw of single mushroom spawn and incubated for 21 days at 25 °C ± 2 °C in the dark (Rani *et al*., 2008). The treatment with the most extensive mushroom colonization was selected for hydrolysis and fermentation.

2.3. Analysis of pretreated PAP surface

The structure of the PAP and biologically processed PAP biomasses were examined using Scanning Electron Microscopy (SEM). The samples were placed on carbon tapes and carbon-coated using a carbon coater. Then, using a Phenom ProX desktop SEM (Phenom-World, Netherlands) with a magnification range of 20 – 100,000 x, element detection range of C–Am, and acceleration voltage of 10 kV, the surface characteristics and microstructure of the PAP fibers were examined.

2.4. Ethanol tolerance test

An ethanol tolerance test was performed following a modification of the method described (Iticha, 2016). Using a Neubauer hemocytometer, cell concentrations of suspensions of the isolates were determined, and the cells were inoculated at 1.0×10^7 cells/ml into duplicate 10 ml volumes of a 10 % ethanol (v/v) solution in YPD broth. The OD_{600} of the cultures was measured after three days of incubation at 30 °C. The strain that was most tolerant of ethanol was the one with the highest turbidity.

2.5. Molecular identification of yeast isolate

The most ethanol tolerant isolate was molecularly identified by performing nucleotide sequencing of ITS regions 1 and 2. Genomic DNA was extracted as described (Atalla *et al.,* 2019; Atalla *et al.*, 2020a). The internal transcribed spacer (ITS) 1 and 2 regions were amplified by polymerase chain reaction (PCR) using the primer pairs ITS4: 5-TCCTCCGCTTATTGATATGC-3 and ITS5: 5-GGAAGTAAAAGTCGTAACAAGG-3 (Hamed *et al.,* 2015; Atalla *et al*., 2020b). Initial denaturation at 95 °C for 5 minutes, followed by 35 cycles of denaturation at 95 °C for 1 minute, annealing at 53 °C for 1 minute, extension at 72 °C for 1 minute, and a final extension at 72 °C for 7 minutes, were the PCR conditions. Amplified fragments were visualized on safe view-stained 1.5 % agarose electrophoresis gels and sequenced. Sequence homology was used to identify the strain by comparing the sequences to entries in the NCBI database. After that, phylogenetic analysis was carried out, and the data were clustered using

the neighbor-joining and maximum likelihood methods using the Molecular Evolutionary Genetics Analysis (MEGA) program version 5.2 (Tamura *et al*., 2011).

2.6. Optimisation of Dilute Acid Hydrolysis and reducing sugars estimation

A 3^4 factorial design experiment with 4 factors and 3 levels (Table 1) was conducted to optimize dilute acid hydrolysis of the biologically-pretreated PAP. All hydrolysis were performed in duplicates at 121 ˚C and 15 psi using an autoclave. The total of 108 runs and resultant sugar concentrations are presented in Supplementary Table 1.

The effects of the factors on reducing sugar concentrations were investigated by the second-order polynomial shown below:

$$Y = \alpha_0 + \alpha_1X_1 + \alpha_2X_2 + \alpha_3X_3 + \alpha_4X_4 + \alpha_{1,2}X_1X_2 + \alpha_{1,3}X_1X_3 + \alpha_{1,4}X_1X_4 + \alpha_{2,3}X_2X_3 + \alpha_{2,4}X_2X_4 + \alpha_{3,4}X_3X_4 \quad (1)$$

Where Y is the predicted response (reducing sugars concentration, g/L), α_0 to $\alpha_{3,4}$ are the regression coefficients, and X_1, X_2, X_3 and X_4 are the factors.

Table 1. Independent factors and levels evaluated in the full factorial experimental design in the dilute acid hydrolysis of *Prosopis africana* pods (PAP)

Factors	Levels		
	- 1	0	+ 1
Acid type: (HNO3 and H3PO4) (X1)	-	-	-
Acid conc. (v/v) (X2)	1 %	3 %	5 %
SLR (w/v) (X3)	5 %	10 %	20 %
Hydrolysis time (mins) (X4)	15	30	60

Using Whatman No. 1 filter paper, the hydrolysis slurries were filtered, and the filtrate's pH was then raised to pH 5.5. The DNS method was used to estimate the amount of reducing sugars in the hydrolysate following the method described by Sana *et al*. (2017). 3 ml of DNS reagent was combined with precisely 1 ml of the hydrolysate. Standard and blank samples were created so that the outcomes could be compared. Instead of the hydrolysate, the blank sample included 1 ml of distilled water. Different concentrations (0.02-0.1 %) of glucose standard solutions were prepared. The tubes were incubated at 100 ˚C using a waterbath for 15 minutes. The samples were examined by a UV-spectrophotometer at a wavelength of 540 nm after cooling and the amount of reducing sugars present in the hydrolysate was estimated from a glucose standard curve (Supplementary Figure 1).

2.7. Fermentation

2.7.1. Fermentation conditions

The most ethanol-tolerant yeast strain was employed in the fermentation of the YPD medium and the Dilute Acid Hydrolysate (DAH). The DAH was filter-sterilized using a 0.2 µm Stericup® filter. Triplicate 250 ml flasks containing 25 ml of the medium at pH 5.5 were pitched at stated concentrations and incubated in various conditions (Ahmed El-Imam, 2017; Ahmed El-Imam *et al*., 2019).

2.7.2. Screening of variables using half-factorial experimental design

To ascertain the baseline yield of the given microbe-substrate combination, a preliminary experiment was conducted. The flasks were agitated at 140 rpm for four days at 30 °C with a cell concentration of 1 x 10^7 yeast cells/ml (Adelabu *et al*., 2017; Chang *et al*., 2018). Samples were taken every 24 hours, and the amounts of ethanol and residual glucose were determined.

A two-level and five-factor (2^{5-1}) design was then employed to evaluate five factors and identify which significantly impacted bioethanol production. The range for the fermentation parameters was based on earlier studies (Adelabu *et al*., 2017; Chang *et al*., 2018) and the experimental design is shown in Table 2.

Table 2: Independent factors and levels for half-factorial experimental design in the fermentation of dilute acid hydrolysates of *Prosopis africana* pods (PAP) for ethanol production

Factors	Levels	
	Low	High
Temperature (°C) (X1)	25	35
Inoculum size (cells/ml) (X2)	1 × 105	1 × 107
pH (X3)	3	7
Agitation speed (rpm) (X4)	0	140
Incubation period (h) (X5)	24	96

In order to determine the ideal fermentation conditions, the experimental findings were fitted to the second-order polynomial equation shown below. This way, the influence of the factors and the multiple interaction effects on the observed response were investigated.

$$Y = \alpha_0 + \alpha_1X_1 + \alpha_2X_2 + \alpha_3X_3 + \alpha_4X_4 + \alpha_4X_5 \quad (2)$$

Where Y is the predicted ethanol concentration, X_1, X_2, X_3, X_4, and X_5 are the factors, and α_0 to $\alpha_{4,5}$ are the regression coefficients.

2.7.3. Response Surface Optimisation of factors

To optimize factors identified as significant from the half-factorial screening, Box-Behnken Design (BBD) was used (Table 3).

Table 3: Independent factors and levels for BBD

Factors	Levels		
	-1	0	1
pH	3	5	7
Agitation speed (rpm)	0	70	140
Incubation period (h)	24	60	96

The polynomial quadratic equation was used to evaluate the effects of each factor on the response (Xie *et al*., 2013):

$$Y_i = b_0 + \sum b_iX_j + \sum b_{ij}X_iX_j + \sum b_{ii}X^2_i + e_i \quad (3)$$

Yi is the dependent variable, or predicted response (ethanol concentration, g/L), and Xi and Xj are the independent variables. b*i* and b*ij* are the single and interaction effect coefficients, respectively, and *ei* is the error term.

2.7.4. Bioethanol estimation

The potassium dichromate technique described by Koshy *et al*. (2014) was used to quantitatively estimate the concentration of bioethanol in the hydrolysate. Exactly 30 µl of test sample were taken out of the fermentation broth and placed in test tubes. The volume was then increased to 500 µl with distilled water. 1 ml and 2 ml of potassium dichromate and 2 N NaOH reagents were added to each tube respectively. 30 µl of distilled water, 1 ml of potassium dichromate reagent, and 2 ml of 2 N NaOH reagent made up the blank solution. The tubes were

incubated for 30 minutes at 50 ˚C. After cooling, a spectrophotometer was used to measure the absorbance at 600 nm. Based on an ethanol standard curve (Supplementary Figure 2), the amount of bioethanol in the hydrolysate was determined.

2.8. Statistical analysis

Minitab software version 17 was used to conduct an analysis of variance (ANOVA) to determine the impact of the variables under investigation. Significant factors were those with p values < 0.05.

3. Results And Discussion

3.1. Isolation, screening, and molecular identification of yeast isolates

Of sixteen (16) yeast isolates obtained, strain SY4, which showed the most prolific growth in ethanol concentrations of 10 %, was identified using molecular techniques. It had a 99.04 % similarity to *Pichia kudriavzevii* strain ATCC 6258 with accession number NR_131315.1. A phylogenetic tree shows the position of SY4 (Figure 1).

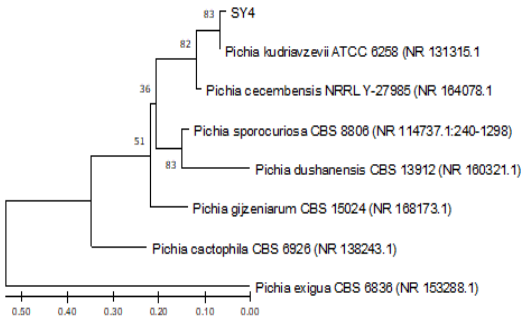

Figure 1: The phylogenetic relationships between yeast isolate SY4 and other closely related species using combined ITS 1 and 2 sequencing analyses. The percentages of replicate trees in which the related taxa clustered together in the bootstrap test are next to the branches. The evolutionary distances utilized to infer the phylogenetic tree have branch lengths scaled at 0.1.

3.2. Impact of mushroom biodegradation on PAP surface structure

Of the four mushrooms investigated, *Ganoderma lucidum* showed the most luxurious growth on PAP (Supplementary Figure 3), while the other mushrooms only grew sparsely. Scanning Electron Microscopy (SEM) analysis was performed to visualize structural changes caused by *G. lucidum* treatment. The PAP's SEM analysis can be used to qualitatively predict how sensitive the substrates will be to subsequent hydrolysis (Xu *et al*., 2017). The pretreatment resulted in more looseness and porosity in the cell wall structure of the PAP (Figure 2). There were visible fiber bundles after pretreatment, indicating that the biomass's structure was considerably broken down, indicating its suitability for hydrolysis.

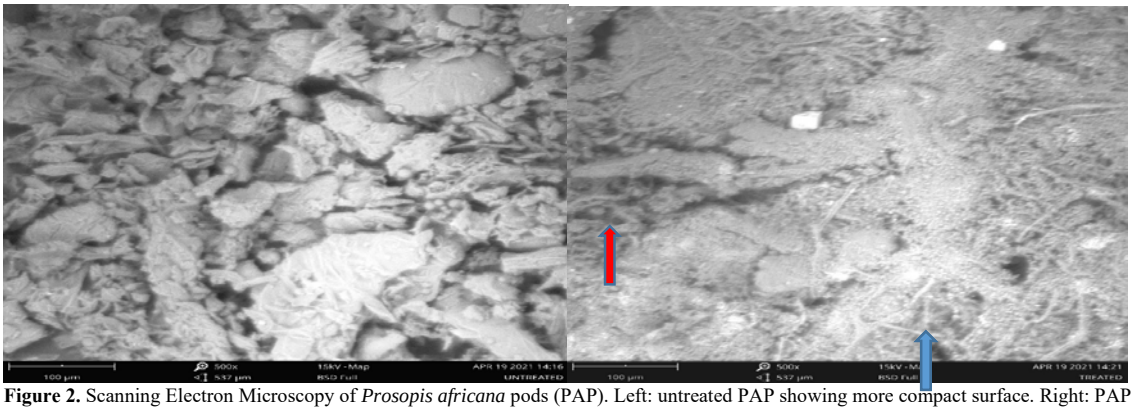

Figure 2. Scanning Electron Microscopy of *Prosopis africana* pods (PAP). Left: untreated PAP showing more compact surface. Right: PAP showing *Ganoderma lucidum*-pretreated PAP with hyphae (blue arrows) and fiber bundles (red arrow)

3.3. Optimisation of Dilute Acid Hydrolysis

The maximum concentration of reducing sugars, 43.37 ± 0.35 g/L, was found to be produced by 5 % HNO_3, 20 % solid loading, and a hydrolysis duration of 15 minutes (Supplementary Table 1). This value exceeds the 18.24 g/L that was obtained from the dilute acid hydrolysis of a similar substrate, *Prosopis juliflora* using 3 % dilute sulfuric acid (Gupta *et al*., 2009).

Figure 3 displays a parity plot that compares the experimental values of the response with those predicted by the statistical model. As a sign of good model fitness, the response points are all grouped together around the linear trendline.

The model's significance is demonstrated by the ANOVA result, which has a high F value of 270.95 and a p-value of 0.000 (Table 4). All the factors investigated had a significant effect on reducing sugar release as they all had p-values < 0.05. The interactions between all the analyzed factors were significant, from 2-way interactions to 4-way interactions.

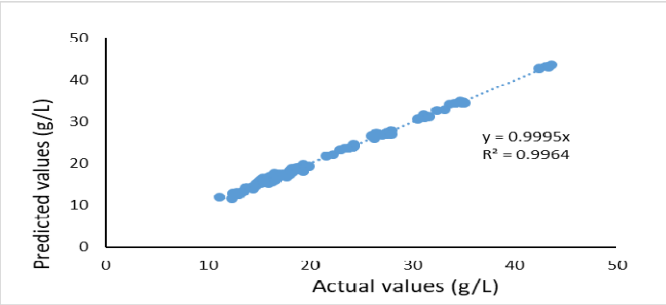

Figure 3: Parity plot of the predicted and actual reducing sugars concentrations from optimized dilute acid hydrolysis of PAP.

Table 4: ANOVA table for FFD model that describes sugar release from *Prosopis africana* pods (PAP) as a function of the chosen coefficient

Source	DF	Adj SS	Adj MS	F-Value	P-Value
Model	54	5900.57	109.27	270.95	0.000
Blocks	1	3.38	3.38	8.39	0.005
Linear	7	3732.52	533.22	1322.18	0.000
Acid type (A)	1	1832.41	1832.41	4543.68	0.000
Conc (%) (B)	2	907.92	453.96	1125.65	0.000
SLR (%) (C)	2	788.38	394.19	977.44	0.000
Time (mins) (D)	2	203.81	101.91	252.69	0.000
2-Way Interactions	18	1215.41	67.52	167.43	0.000
AB	2	305.71	152.85	379.02	0.000
AC	2	432.47	216.24	536.18	0.000
AD	2	7.28	3.64	9.03	0.000
BC	4	263.32	65.83	163.24	0.000
BD	4	83.46	20.87	51.74	0.000
CD	4	123.16	30.79	76.35	0.000
3-Way Interactions	20	617.05	30.85	76.50	0.000
ABC	4	185.63	46.41	115.07	0.000
ABD	4	100.90	25.23	62.55	0.000
ACD	4	95.37	23.84	59.12	0.000
BCD	8	235.14	29.39	72.88	0.000
4-Way Interactions	8	332.21	41.53	102.97	0.000
ABCD	8	332.21	41.53	102.97	0.000
Error	53	21.37	0.40		
Total	107	5921.94			

$R^2 = 0.9964$, R^2 (adj) = 0.9927

Sindhu *et al.* (2014) made similar observations, reporting that temperature, acid concentration, and time significantly affected reducing sugar release from biomass. The R^2 value of 0.9964, which shows that the model can account for 99.64 % of the response's variability, further supported the model's appropriateness.

3.4. Fermentation

A preliminary fermentation revealed that by Day 4 of growth, *P. kudriavzevii* SY4 produced a maximum concentration of ethanol of 27 g/L (data not shown).

3.4.1. Half-factorial screening of factors

A half-factorial design of experiment was used to assess the impact of temperature, inoculum size, pH, agitation speed, and fermentation time on ethanol production in order to increase yields from the preliminary fermentation (Table 2). Table 5 shows the variables, levels, and ethanol concentrations from the 32 runs of the screening fermentation.

Table 5: Half-factorial design screening of variables and outcomes

Run order	Temperature (oC)	Inoculum size (cells/ml)	pH	Agitation speed	Incubation period	Ethanol (g/L)
1	35	1 × 107	7	140	96	28.52
2	25	1 × 105	3	0	96	18.73
3	35	1 × 105	3	0	24	35.12
4	25	1 × 107	3	140	96	24.71
5	35	1 × 107	7	0	24	36.09
6	35	1 × 105	7	0	96	19.05
7	25	1 × 105	7	140	96	19.17
8	25	1 × 107	7	0	96	18.87
9	35	1 × 107	3	0	96	20.72
10	35	1 × 105	7	140	24	18.36
11	35	1 × 107	7	0	24	36.13
12	25	1 × 105	3	140	24	17.90
13	35	1 × 107	3	0	96	19.42
14	25	1 × 107	7	140	24	24.94
15	25	1 × 105	3	0	96	18.76
16	25	1 × 107	3	140	96	25.75
17	35	1 × 105	3	0	24	36.26
18	35	1 × 107	7	140	96	23.33
19	25	1 × 107	3	0	24	35.10
20	25	1 × 105	7	0	24	35.24
21	35	1 × 105	7	140	24	19.75
22	35	1 × 105	3	140	96	22.75
23	25	1 × 107	7	0	96	19.36
24	25	1 × 105	7	140	96	23.09
25	35	1 × 105	3	140	96	27.60
26	25	1 × 105	3	140	24	23.09
27	35	1 × 105	7	0	96	20.23
28	25	1 × 107	7	140	24	17.32
29	35	1 × 107	3	140	24	16.17
30	35	1 × 107	3	140	24	18.48
31	25	1 × 107	3	0	24	36.64
32	25	1 × 105	7	0	24	36.91

The Pareto chart indicated that inoculum size, pH, temperature, and their interactions had no significant effect on ethanol production (Fig. 4). pH not being significant in this screening contrasts with the findings of Dasgupta *et al.* (2013), who screened 9 factors in producing bioethanol from sugarcane bagasse pith hydrolysate and reported pH to be significant. It also differs with results of Wu (2019), who discovered pH to be a significant influence during the fermentation of bagasse hydrolysate that had been treated with an ionic liquid for the purpose of producing bioethanol. The presence of phenolic chemicals in PAP, which may have a buffering effect in the fermentation medium, may be the cause of the discrepancy in the results. Nonetheless, pH was further investigated over a wide range to confirm its influence on ethanol production from PAP hydrolysate.

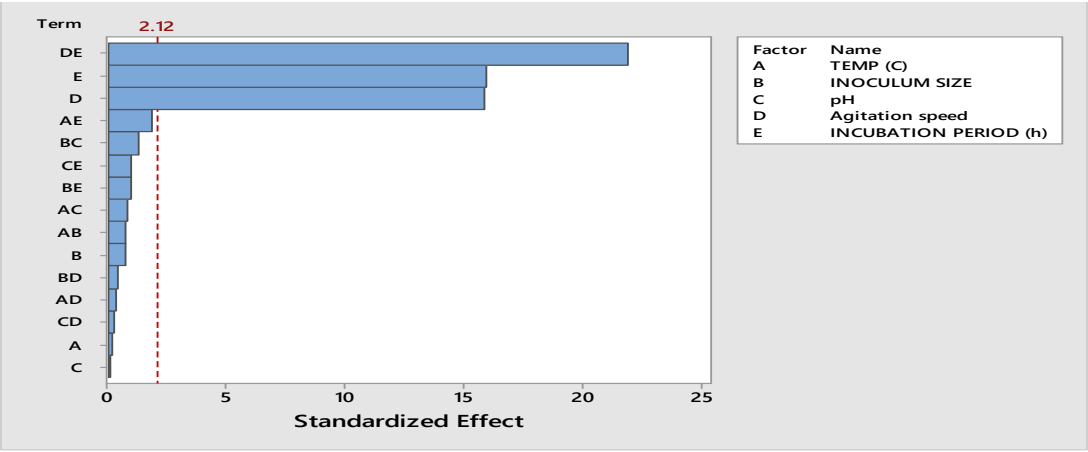

Figure 4. A Pareto chart displaying the factor's in their decreasing order of significance. At a 95% confidence level, bars that go beyond the vertical line represent statistically significant factors.

This study's results are in agreement with those of Karunakaran *et al.* (2013) in that temperature and inoculum size had no discernible impact on ethanol production. Agitation speed and incubation period significantly affected ethanol production (Figure 4), which is similar to the previously reported findings (Dasgupta *et al.*, 2013; Karunakaran *et al.*, 2013). A more effective conversion of carbohydrates to bioethanol is made possible by oxygen's favorable effects on the bioethanol fermentation process (Deniz *et al.*, 2014; Henriques *et al.*, 2018). The model had an R^2 value of 93.15 % with an R^2_{adj} of 91.83 %, implying that it can explain 93.15 % of the variability in ethanol production.

3.4.2. Factor optimization by RSM

RSM based on Box-Behnken design with 30 runs, was used to further analyze the two major components discovered through the screening experiment. pH was included as the third factor as RSM optimizations are accurately performed when three factors are investigated (Ahmed El-Imam *et al*., 2017). The BBD is a unique experimental design because treatment combinations frequently occur towards the edges of the experimental area. As a result, estimating the first and second-order coefficients is made simpler (Oiwoh *et al*., 2018).

The results of RSM optimization showed that pH 7, 70 rpm agitation, and 24 hours of fermentation were the ideal conditions for producing bioethanol from PAP diluted acid hydrolysate using *P. kudriavzevii* strain SY4. This produced a maximum bioethanol concentration of 38.26 ± 0.01 g/L (Table 6).

Table 6. The actual and predicted responses for the Box-Behnken Design matrix for the optimization of ethanol production from *Prosopis africana* pods dilute acid hydrolysate.

Run Order	pH	Agitation speed (rpm)	Incubation period (h)	Ethanol (g/L)	
				Actual	Predicted
1	5	70	60	21.47	21.99
2	5	140	24	34.04	33.70
3	7	140	60	31.28	31.85
4	7	70	96	24.32	24.88
5	5	0	24	32.44	31.78
6	5	70	60	24.68	24.99
7	3	0	60	26.12	26.70
8	3	70	96	29.49	29.16
9	5	0	96	24.61	27.71
10	3	140	60	21.50	22.50
11	3	70	24	27.97	28.72
12	5	70	60	26.55	25.99
13	7	0	60	26.39	26.97
14	7	70	24	38.26	37.62
15	5	140	96	29.94	27.48
16	7	70	96	32.04	31.91
17	5	0	24	29.17	29.81
18	3	70	24	30.94	30.75
19	5	140	24	28.70	27.73
20	5	70	60	24.83	25.01
21	5	140	96	27.02	27.50
22	5	70	60	27.44	26.01
23	3	140	60	22.78	22.52
24	5	70	60	25.03	25.01
25	7	0	60	28.31	27.99
26	5	0	96	31.54	31.74
27	3	70	96	27.61	29.19
28	3	0	60	21.87	21.73
29	7	70	24	38.25	37.64
30	7	140	60	23.88	27.87

Maximum bioethanol concentrations have been obtained under similar conditions (Betiku and Taiwo, 2015; Zani *et al*., 2019). However, the concentrations obtained were higher than those of Sivamani and Baskar (2018) and Dasgupta *et al*. (2013), with 25.59 g/L and 17.44 g/L, respectively, after similar optimization experiments. On the other hand, Techaparin *et al*. (2017) found that following BBD optimization, sweet sorghum juice had higher maximum bioethanol concentrations of 89.32 g/L. The results could differ depending on a number of things, including the biocatalyst, the type of substrate employed, and the fermentation conditions.

In order to determine how each factor affected the response, a quadratic equation was obtained:

$$\text{Ethanol (g/L)} = 34.52 + 0.51A - 0.0063B - 0.2917C + 0.120A^2 - 0.000056B^2 + 0.002926C^2 + 0.00279AB - 0.0195AC - 0.000012BC \quad (4)$$

According to the ANOVA results (Table 7), agitation speed had no discernible influence on bioethanol production, although pH and incubation time did. It was found that the incubation period was significant for the concentration of bioethanol while the square interactions of pH and agitation speed were not. It was also observed that the two-way interactions between all factors had no significant impact on bioethanol concentration. The lack of fit of 0.219 was insignificant, indicating the model's reliability. The model's robustness was measured with the R^2 value, which shows the quality of its prediction of responses. An R^2 value of 97.07 % and an R^2(adj) of 95.73 % indicates the model's suitability, as it can explain 97.07 % variability in response.

Table 7. ANOVA for the quadratic response surface model of ethanol production from *Prosopis africana* pods dilute acid hydrolysate

Source	DF	Adj SS	Adj MS	F-Value	P-Value
Model	10	191.918	19.192	3.87	0.005
Blocks	1	0.602	0.602	0.12	0.731
Linear	3	65.335	21.778	4.39	0.017
pH (A)	1	34.000	34.000	6.85	0.017
Agitation speed (rpm) (B)	1	0.059	0.059	0.01	0.914
Incubation period (h) (C)	1	31.276	31.276	6.31	0.021
Square	3	108.991	36.330	7.32	0.002
A2	1	1.688	1.688	0.34	0.566
B2	1	0.563	0.563	0.11	0.740
C2	1	106.211	106.211	21.41	0.000
2-Way Interaction	3	16.991	5.664	1.14	0.358
AB	1	1.225	1.225	0.25	0.625
AC	1	15.759	15.759	3.18	0.091
BC	1	0.007	0.007	0.00	0.971
Error	19	94.247	4.960		
Lack-of-Fit	15	84.429	5.629	2.29	0.219
Pure Error	4	9.818	2.455		
Total	29	286.165			

$R^2 = 0.9707$, R^2 (adj) = 0.9573

Additionally, three-dimensional response plots were created to display how the parameters affected the concentration of bioethanol (Figure 5)

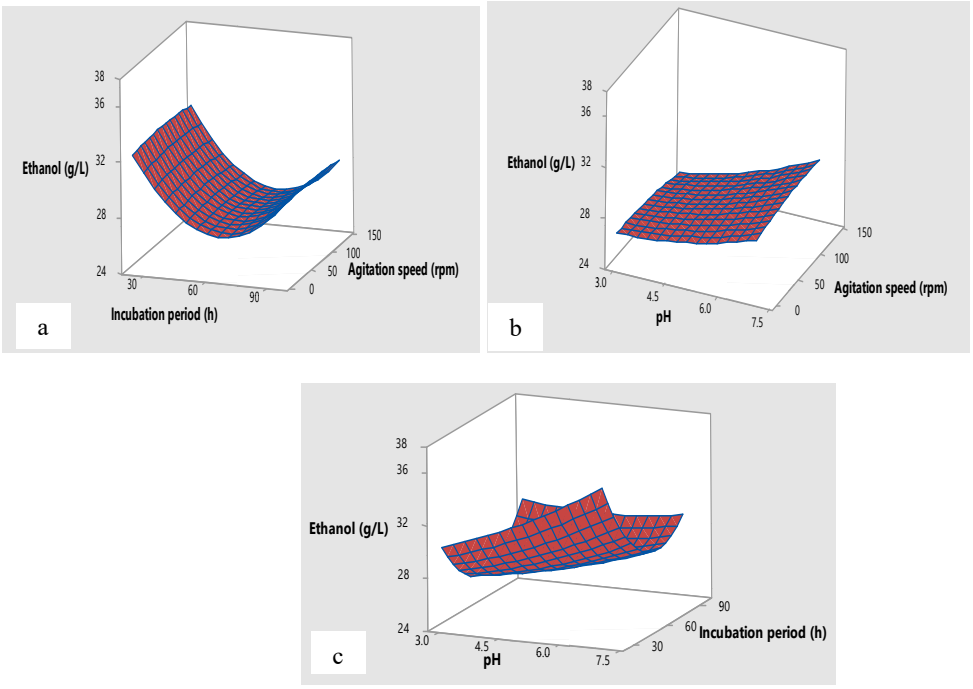

Figure 5: 3D surface plots illustrating how the concentration of bioethanol is affected by (a) incubation period and agitation speed, (b) agitation speed and pH, and (c) incubation period and pH.

The impact of agitation speed and incubation time on bioethanol concentration is depicted in Figure 5a. It was observed that within the range of factor levels tested, bioethanol concentration was higher at lower incubation time and agitation speed, reaching its peak at 24 hours and 70 rpm. Bioethanol concentration decreased with time, suggesting that this strain produces higher ethanol amounts early in the fermentation. The incubation time used in the screening experiments in this study appears to have missed the actual optimal time, which seems to be earlier than 24 hours. This is an advantageous finding as the lowered fermentation duration results in a lower cost of production, making the process economically competitive. A similar study involving the fermentation of hydrolyzed bagasse using a locally isolated yeast showed that peak ethanol concentrations were achieved at times earlier than 24 h (Hosny *et al*., 2016). These authors report that the progressive but minor reduction in ethanol concentration with time could be ascribed to evaporation or consumption of ethanol by the yeast. Higher agitation speeds could also result in faster ethanol evaporation.

Figure 5b shows the effect of pH and agitation speed on bioethanol concentration. It was observed that ethanol concentration increased with increasing pH, reaching its

peak at pH 7. Bioethanol concentration was higher at a lower agitation speed with a maximum concentration of 38.26 g/L at 70 rpm. Thus, higher rotation speed resulted in lower bioethanol concentration. The impact of pH and incubation time on bioethanol concentration is shown in Figure 5c. It was observed that high pH values resulted in higher bioethanol concentration.

Under the optimal conditions (pH 7.0, 70 rpm agitation, and 24 hours incubation time), 38.26 g/L of ethanol was produced, representing a 43.73 % increase in the product compared to unoptimised conditions. This increase can even be improved further at lower incubation times. These results show that PAP is a promising substrate that can be added to the mix of existing feedstocks currently exploited for bioethanol production.

4. Conclusion

Prosopis africana pod is an abundant and under-utilized food processing waste in Nigeria and other regions in Africa. This study showed that the biomass could support the luxurious growth of *Ganoderma lucidum*, which could increase Nigeria's production of the reishi mushroom. The affordable and mild biological pretreatment followed by statistically optimised dilute acid hydrolysis resulted in sugar-rich hydrolysates with up to 43.37 g/ L of sugars. This work is the first report of the hydrolysis requirements for *P. africana* pods and demonstrates its suitability for bioethanol production and other bioprocessing applications. It shows that efforts to exploit less common biomass types to produce bioethanol are still needed, particularly in the light of the Russia-Ukraine war, which has sent petroleum prices soaring globally.

References

Adelabu, B.A., Kareem, S.O., Oluwafemi, F., & Adeogun, I.A. (2017). Bioconversion of corn straw to ethanol by cellulolytic yeasts immobilized in *Mucuna urens* matrix. *J. King Saud Univ. Sci.,* 1-6.

Adelabu, B.A., Kreem, S.O., Adeogun, A.I., & Ademolu, K.O. (2018). Direct Bioconversion of Sorghum Straw to Ethanol in a Single-step Process by *Candida* species. *Jordan J. Biol. Sci.Jordan Journal of Biological Sciences,* **11(1):** 1-7.

Ahmed El-Imam, A., Akoh, P., Saliman, S., & Ighalo, E. (2021). Mushroom-mediated delignification of agricultural wastes for bio-ethanol production. *Niger. J. Biotechnol*., **38(1):** 137-145.

Ahmed El-Imam, A.M. (2017). Fermentative production of value-added products from sorghum bran. PhD thesis, University of Nottingham. Accessed from http://eprints.nottingham.ac.uk/43425/1/PHD%20THESIS.pdf. pp 14.

Ahmed El-Imam, A.M., Darren, G., Chenyu, D., & Paul, S.D. (2019). The development of a biorefining strategy for the production of biofuel from sorghum milling waste. *Biochem. Eng. J*., **150:** 107-288.

Atalla, S.M.M., Ahmed, N.E., Awad, H.M., El Gamal, N.G., & El Shamy, A.R. (2020a). Statistical optimization of xylanase production, using different agricultural wastes by *Aspergillus oryzae* MN894021, as a biological control of faba bean root diseases. *Egypt. J. Biol. Pest Control,* **30:** 125.

Atalla, S.M.M., EL Gamal, N.G., & Awad, H.M. (2020b). Chitinase of Marine *Penicillium chrysogenum* MH745129: Isolation, Identification, Production and Characterization as Controller for Citrus Fruits Postharvest Pathogens. *Jordan J. Biol. Sci.,* **13(1):** 19-28.

Atalla, S.M.M., EL Gamal, N.G., Awad, H.M., & Ali, N.F. (2019). Production of pectin lyase from agricultural wastes by isolated marine *Penicillium expansum* RSW_SEP1 as dye wool fiber. *Heliyon*, **5(8):** e02302.

Awoyale, A.A., & Lokhat, D. (2019). Harnessing the potential of bio-ethanol production from lignocellulosic biomass in Nigeria: A review, *Biofuels, Bioprod. Biorefining,* **13:** 192-207.

Awoyale, A.A., & Lokhat, D. (2021). Experimental determination of the effects of pretreatment on selected Nigerian lignocellulosic biomass in bioethanol production. *Sci. Rep*., **11:** 557.

Beig, B., Riaz, M., Naqvi, S.R., Hassan, M., Zheng, Z., Karimi, K., Pugazhendhi, A., Atabani, A.E., & Chi, N.T.L. (2021). Current challenges and innovative developments in pretreatment of lignocellulosic residues for biofuel production: A review. *Fuel,* **287:** 119670.

Betiku, E., & Taiwo, A.E. (2015). Modeling and Optimization of bioethanol production from breadfruit starch hydrolyzate vis-a-vis response surface methodology and artificial neural network. *Renew. Energ.* **74:** 87-94.

Bhatia, S.K., Kim, S.H., Yoon, J.J., & Yang, Y.H. (2017). Current status and strategies for second generation biofuel production using microbial systems. *Energy Convers. Manag.,* **148:** 1142-1156.

Branco, R.H., Serafim, L.S., & Xavier, A.M. (2019). Second generation bioethanol production: on the use of pulp and paper industry wastes as feedstock. *Fermentation,* **5(1):** 4.

Braz, A., Mateus, M.M., dos Santos, R.G., Machado, R., Bordado, J.M., & Correia, M.J.N. (2019). Modelling of pine wood sawdust thermochemical liquefaction. *Biomass Bioenergy,* **120:** 200-210.

Chang, Y.H., Chang, K.S., Chen, C.Y., Hsu, C.L., Chang, T.C., & Jang, H.D. (2018). Enhancement of the efficiency of bioethanol production by *Saccharomyces cerevisiae* via gradually batch-wise and fed-batch increasing the glucose concentration. *Fermentation,* **4:** 45.

da Silva, C.G.M., Andrade, S.A.C., Schuler, A.R.P., de Souza, E.L., & Stamford, T.L.M. (2011). Production of ethanol from mesquite [*Prosopis juliflora* (SW) D.C.] pods mash by *Zymomonas mobilis* in submerged fermentation. *Sci. Agric*., **68(1):** 124–127.

Dasgupta, D., Suman, S.K., Pandey, D., Ghosh, D., Khan, R., Agrawal, D., Jain, R.K., Vadde, V.T., & Adhikari, D.K. (2013). Design and Optimization of ethanol production from bagasse pith hydrolysate by a thermotolerant yeast *Kluyveromyces* sp. IIPE453 using response surface methodology. *Springerplus,* **2:** 159.

Deniz, I., Imamoglu, E., & Vardar-Sukan, F. (2014). Aeration-enhanced bioethanol production. *Biochem. Eng. J.,* **92:** 41–46.

Gerbens-Leenes, P. (2017). Bioenergy water footprint, comparing first, second and third generation feedstocks for bioenergy supply in 2040. *Eur. Water,* **59:** 373-380.

Ghani, H.U., Silalertruksa, T., & Gheewala, S.H. (2019). Water-energy food nexus of bioethanol in Pakistan: a life cycle approach evaluating footprint indicators and energy performance. *Sci. Total Environ.,* **687:** 867–876.

Gupta, R., Sharma, K.K., & Kuhad, R.C. (2009). Separate hydrolysis and fermentation (SHF) of *Prosopis juliflora*, a woody substrate, for the production of cellulosic ethanol by *Saccharomyces cerevisiae* and *Pichia stipitis*-NCIM 3498. *Bioresour. Technol*., **100(3):** 1214–1220.

Gustin, G. (2022). As Russia's War In Ukraine Disrupts Food Production, Experts Question the Expanding Use of Cropland for

Biofuels. *Inside Climate News.* Retrieved from https://insideclimatenews.org/news/05042022/as-russias-war-in-ukraine-disrupts-food-production-experts-question-the-expanding-use-of-cropland-for-biofuels/ (2022, April 5).

Hamed, E.R., Awad, H.M., Ghazi, E.A., El-Gamal, N.G., & Shehata, H.S. (2015). *Trichoderma asperellum* isolated from salinity soil using rice straw waste as biocontrol agent for cowpea plant pathogens. *J. Appl. Pharm. Sci*., **5(2):** 91–98

Henriques, T.M., Pereira, S.R., Serafim, L.S., & Xavier, A.M.R.B. (2018). Two-Stage Aeration Fermentation Strategy to Improve Bioethanol Production by *Scheffersomyces stipitis*. *Fermentation*, **4(4):** 97.

Hosny, M., Abo-State, M.A., El-Temtamy, S.A., & El-Sheikh, H.H. (2016). Factors affecting bioethanol production from hydrolyzed bagasse. *Int. J. Adv. Res. Biol. Sci.*, **3(9):** 130-138.

I.E.A. (2019). Renewables 2019. Paris: IEA. Document Number)---. (2020). Global Energy Review 2020. Paris: IEA. Document Number)

Ibeto, C., Ofoefule, A., & Agbo, K. (2011). A global overview of biomass potentials for bioethanol production: a renewable alternative fuel. *Trends Appl. Sci. Res.,* **6:** 410-425.

Iticha, T.N. (2016). Isolation and screening of ethanol tolerant yeast for bioethanol production in Ethiopia. *GJLSBR*., **2(2):** 1-7.

Karimi, K., Shafiei, M., & Kumar, R. (2013). Progress in physical and chemical pretreatment of lignocellulosic biomass. Biofuel Technologies. Berlin: Springer, Berlin, Heidelberg.

Karunakaran, S., Ramasamy, G., Duraisamy, S., & Balakrishnan, S. (2013). Screening and Optimization of fermentation media for increased production of ethanol from *Gracilaria* sp. Using Response Surface Methodology. *J. Pure Appl. Microbiol.,* **7(4):** 2641-2652.

Koshy, B.E., Pandey, F.K., & Bhatnagar, T. (2014). Quantitative estimation of bioethanol produced from lignocellulosic & household wastes. *Int. J. Life Sci. Res.* **2(4):** 130-145.

Malik, K., Salama, E., Kim, T.H., & Li, X. (2020). Enhanced ethanol production by *Saccharomyces cerevisiae* fermentation post acidic and alkali chemical pretreatments of cotton stalk lignocellulose. *Int. Biodeterior. Biodegrad.,* **147:** 104869.

Manavalan, T., Manavalan, A., & Heese, K. (2015). Characterization of lignocellulolytic enzymes from white-rot fungi. *Curr. Microbiol.,* **70:** 485-498.

Milano, J., Ong, H., Masjuki, H., Chong, W., Lam, M.K., Loh, P.K., & Vellayan, V. (2016). Microalgae biofuels as an alternative to fossil fuel for power generation. *Renew. Sustain. Energy Rev.,* **58:** 180-197.

Oiwoh, O., Ayodele, B.V., Amenaghawon, N.A., & Okieimen, C.O. (2018). Optimization of bioethanol production from simultaneous saccharification and fermentation of pineapple peels using *Saccharomyces cerevisiae*. *J. Appl. Sci. Environ. Manage.,* **22(1):** 54-59.

Oni, O.D., Oke, M.A., & Sani, A. (2020). Mixing of *Prosopis africana* pods and corn cob exerts contrasting effects on the production and quality of *Bacillus thuringiensis* crude endoglucanase. *Prep. Biochem. Biotechnol.*, 1–10.

Pasiecznik, N.M., Tewari, J.C., Harsh, L.N., Felker, P., Harris, P.J.C., Cadoret, K., Cruz, G., & Maldonado, L.J. (2001). The *Prosopis juliflora - Prosopis pallida* Complex: A Monograph. Henry Doubleday Research Association (HDRA): Coventry, UK.

Raina, N., Slathia, P.S., & Sharma, P. (2020). Response surface methodology (RSM) for Optimisation of thermochemical pretreatment method and enzymatic hydrolysis of deodar sawdust (DS) for bioethanol production using separate hydrolysis and co-fermentation (SHCF). *Biomass Conv. Bioref.* https://doi.org/10.1007/s13399-020-00970-0.

Rani, P., Kalyani, N., & Prathiba, K. (2008). Evaluation of Lignocellulosic Wastes for Production of Edible Mushrooms. *Appl. Biochem. Biotechnol.*, **151:** 151–159.

Rezania, S., Oryani, B., Cho, J., Talaiekhozani, A., Sabbagh, F., Hashemi, B., Rupani, P.F., & Mohammadi, A.A. (2020). Different pretreatment technologies of lignocellulosic biomass for bioethanol production: an overview. *Energy,* 117457.

Sana, H., Kanwal, S., Akhtar, J., Haider, R., Nawaz, S., Sheikh, N., & Munir, S. (2017). Production of ethanol and bio-chars from Pakistani lignocellulosic biomasses. *Energy Sources A: Recovery Util. Environ. Eff.,* **39(5):** 465-472.

Sindhu, R., Binod, P., & Pandey, A. (2016). Biological pretreatment of lignocellulosic biomass–An overview. *Bioresour. Technol.*, **199:** 76-82.

Sindhu, R., Kuttiraja, M., Binod, P., Sukumaran, R.K., & Pandey, A. (2014). Bioethanol production from dilute acid pretreated Indian bamboo variety (*Dendrocalamus* sp.) by separate hydrolysis and fermentation. *Ind. Crops Prod.,* **52:** 169–176.

Sivamani, S., & Baskar, R. (2018). Process design and optimization of bioethanol production from cassava bagasse using statistical design and genetic algorithm. *Prep. Biochem. Biotechnol.*, DOI: 10.1080/10826068.2018.1514512.

Tamura, K., Peterson, D., Peterson, N., Stecher, G., Nei, M., & Kumar, S. (2011). MEGA5: molecular evolutionary genetics analysis using maximum likelihood, evolutionary distance, and maximum parsimony methods. *Mol. Biol. Evol.*, **28(10):** 2731–2739.

Taufikurahman, T., Jessica, S., & Delimanto, W.O. (2020). A comparison of alkali and biological pretreatment methods in napier grass (*Pennisetum purpureum* Scumach.) for reducing lignin content in the bioethanol production process. *J. Biol. Sci. Technol Manag.,* **2(1):** 31-43.

Techaparin, A., Thanonkeo, P., & Klanrit, P. (2017). High-temperature ethanol production using thermotolerant yeast newly isolated from Greater Mekong Subregion. *Braz. J. Microbiol.*, **238:** 1-15.

Wu, Z. (2019). Mixed fermentation of *Aspergillus niger* and *Candida shehatae* to produce bioethanol with ionic-liquid-pretreated bagasse. *3 Biotech* **9:** 41.

Wuryantoro, W., Adinurani, P.G., Wardhani, R.M., Sutrinso, S., Yamin, B.M., & Nur, S.M. (2021). Utilization of "Uwi" Plant (_Dioscorea_ sp.) as a Renewable Bioenergy Resource. *Jordan J. Biol. Sci.Jordan Journal of Biological Science,* **14(5):** 945-951.

Xie, T., Liu, J., Du, K., Liang, B., & Zhang, Y. (2013). Enhanced biofuel production from high-concentrated bioethanol wastewater by a newly isolated heterotrophic microalga, *Chlorella vulgaris* LAM-Q. *J. Microbiol. Biotechnol.,* **23(10):** 1460-1471.

Xu, X., Xu, Z., Shi, S., & Lin, M. (2017). Lignocellulose degradation patterns, structural changes, and enzyme secretion by *Inonotus obliquus* on straw biomass under submerged fermentation. *Bioresour. Technol.,* **241:** 415-423.

Yildirim, O., Ozkaya, B., Altinbas, M., & Demir, A. (2021). Statistical Optimization of dilute acid pretreatment of lignocellulosic biomass by response surface methodology to obtain fermentable sugars for bioethanol production. *Int. J. Energy Res.,* **45(6):** 8882–8899.

Zani, S.H.M., Asri, F.M., Azmi, N.S., Yussof, H.W., & Zahari, M.A.K.M. (2019). Optimization of process parameters for bioethanol production from oil palm frond juice by Saccharomyces cerevisiae using Response Surface Methodology as a tool. Mater. Sci. Eng., 702: 012003.

APPENDIX

Supplementary Table 1: Full-factorial experimental design and results obtained for dilute acid hydrolysis

Run Order	Acid type	Conc (%)	SLR (%)	Time (mins)	Reducing sugars (g/L)	
					Actual	Predicted
1	HNO3	3	10	15	26.23	26.46
2	HNO3	3	10	60	42.38	42.65
3	H3PO4	1	20	15	17.20	17.07
4	HNO3	3	20	15	33.63	34.17
5	HNO3	5	5	15	17.39	17.52
6	H3PO4	1	5	60	12.82	12.65
7	HNO3	3	20	30	34.71	34.97
8	H3PO4	1	10	30	16.72	16.47
9	HNO3	1	20	30	24.25	24.10
10	H3PO4	3	20	15	18.80	18.54
11	HNO3	3	10	30	30.50	30.70
12	HNO3	5	20	30	32.42	32.59
13	H3PO4	5	5	15	22.88	23.17
14	HNO3	5	10	15	34.14	34.38
15	HNO3	3	5	60	14.31	14.34
16	HNO3	5	20	60	31.61	31.20
17	HNO3	5	20	15	43.12	43.19
18	HNO3	1	20	60	17.96	18.23
19	H3PO4	1	20	60	14.45	13.90
20	H3PO4	5	20	60	17.98	17.82
21	H3PO4	5	5	60	12.46	12.88
22	H3PO4	5	10	60	16.27	16.01
23	H3PO4	1	10	15	14.81	15.07
24	H3PO4	3	5	15	17.12	17.00
25	HNO3	1	10	30	21.60	21.74
26	H3PO4	3	5	60	12.37	11.55
27	HNO3	5	10	60	26.26	26.47
28	H3PO4	3	10	30	19.92	19.43
29	HNO3	5	10	30	27.52	27.54
30	H3PO4	3	20	60	13.02	12.55
31	H3PO4	5	20	15	15.35	16.37
32	H3PO4	3	10	15	16.10	16.86
33	H3PO4	1	10	60	15.21	15.29
34	HNO3	3	5	30	23.35	23.52
35	H3PO4	5	5	30	18.80	18.47
36	H3PO4	3	20	30	16.26	16.87
37	H3PO4	5	10	30	17.01	17.49
38	HNO3	1	20	15	18.14	18.71
39	HNO3	3	5	15	17.13	17.39
40	H3PO4	3	5	30	16.83	17.58
41	H3PO4	5	20	30	26.01	26.58
42	HNO3	1	5	30	18.12	18.20
43	HNO3	1	5	60	16.91	16.93
44	HNO3	1	10	15	18.67	18.61
45	HNO3	5	5	30	23.00	23.19
46	HNO3	1	5	15	15.17	15.93
47	H3PO4	5	10	15	18.85	18.80
48	HNO3	1	10	60	14.70	15.03
49	H3PO4	1	5	30	14.99	15.65
50	HNO3	5	5	60	19.12	18.98
51	H3PO4	1	5	15	13.30	13.12
52	H3PO4	1	20	30	15.06	15.69
53	HNO3	3	20	60	26.45	27.38
54	H3PO4	3	10	60	16.51	17.75
55	HNO3	1	5	15	16.34	15.58
56	H3PO4	3	10	15	17.98	17.22
57	HNO3	3	5	60	14.72	14.69
58	HNO3	1	5	60	17.30	17.28
59	HNO3	3	5	30	24.05	23.88
60	HNO3	1	20	30	24.30	24.45
61	H3PO4	5	5	60	12.94	12.52
62	HNO3	3	10	15	26.33	26.10
63	H3PO4	3	20	60	12.44	12.91
64	HNO3	3	10	60	43.28	43.01
65	H3PO4	1	20	30	16.67	16.04
66	H3PO4	5	5	30	18.50	18.83

67	HNO3	5	10	30	27.91	27.89
68	HNO3	3	10	30	31.25	31.05
69	HNO3	5	5	60	18.48	18.62
70	H3PO4	3	5	60	11.09	11.91
71	H3PO4	1	5	60	12.83	13.00
72	H3PO4	5	10	60	16.10	16.36
73	H3PO4	1	10	15	15.68	15.42
74	H3PO4	5	10	15	19.11	19.16
75	H3PO4	1	10	30	16.57	16.82
76	H3PO4	1	5	15	13.48	13.30
77	HNO3	5	20	30	33.12	32.95
78	HNO3	3	20	30	34.87	34.61
79	H3PO4	3	20	30	17.83	17.22
80	H3PO4	5	10	30	18.32	17.84
81	H3PO4	3	10	30	19.30	19.79
82	H3PO4	5	20	30	27.51	26.94
83	H3PO4	3	10	60	19.35	18.11
84	HNO3	5	5	30	23.74	23.55
85	HNO3	3	20	60	27.95	27.02
86	H3PO4	1	5	30	15.96	15.30
87	H3PO4	3	20	15	18.63	18.89
88	H3PO4	5	20	60	18.01	18.17
89	HNO3	1	10	30	22.24	22.10
90	H3PO4	1	10	60	15.72	15.64
91	HNO3	1	10	60	15.72	15.39
92	HNO3	1	20	15	18.93	18.36
93	HNO3	5	20	60	31.14	31.55
94	HNO3	5	10	60	27.04	26.83
95	HNO3	5	20	15	43.62	43.55
96	HNO3	1	10	15	18.90	18.96
97	H3PO4	5	20	15	17.74	16.72
98	H3PO4	1	20	60	13.70	14.25
99	HNO3	3	20	15	35.06	34.52
100	H3PO4	3	5	15	17.23	17.35
101	HNO3	3	5	15	18.01	17.75
102	H3PO4	5	5	15	23.82	23.53
103	HNO3	1	20	60	18.86	18.59
104	HNO3	5	5	15	18.01	17.88
105	H3PO4	3	5	30	17.98	17.23
106	HNO3	5	10	15	34.97	34.73
107	HNO3	1	5	30	18.63	18.55
108	H3PO4	1	20	15	17.29	17.42

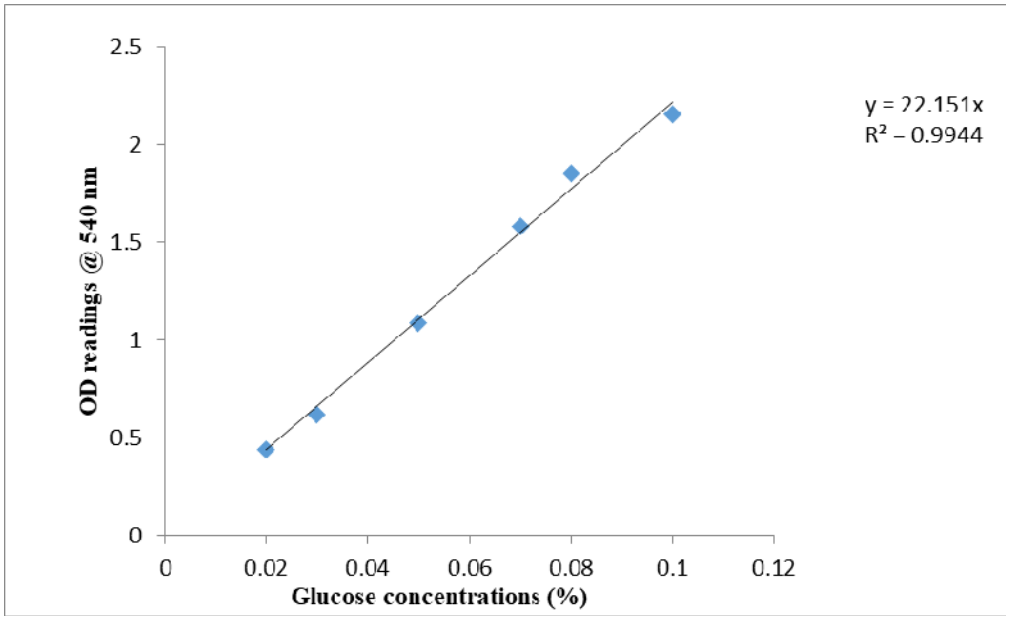

Supplementary Figure 1: Glucose standard curve

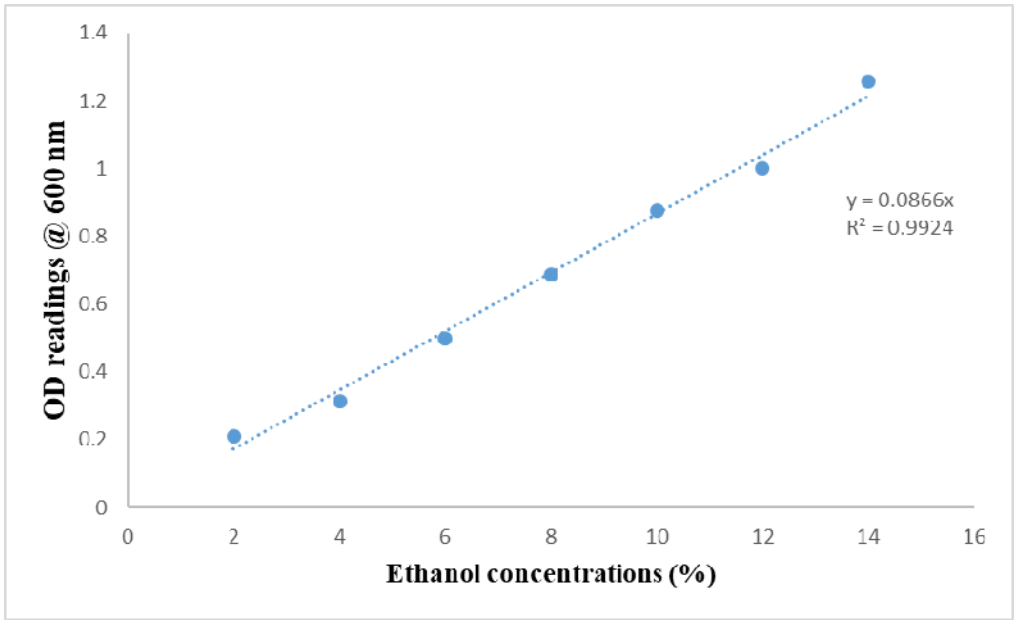

Supplementary Figure 2: Ethanol standard curve

Supplementary Figure 3: Growth pattern of *Ganoderma lucidum* on milled *Prosopis africana* pods.

JJBS

Volume 15, Number 5,December 2022
ISSN 1995-6673
Pages 869 – 877
https://doi.org/10.54319/jjbs/150516

Jordan Journal of Biological Sciences

Bio-guided Fractionation: Optimization of Chemical Profiling, Antioxidant, Anti-inflammatory and Antibacterial Properties of *Vitex doniana* Fruits.

Raymond P. Barry[1], Kiessoun Konaté[1,2,*], Abdoudramane Sanou[1], Yérobessor Dabiré[1] and Mamoudou H. Dicko[1]

[1]*Laboratory Biochemistry, Biotechnology, Food Technology and Nutrition (LABIOTAN), Department of Biochemistry and Microbiology, University Joseph KI-ZERBO, 03 B. P. 7021, Ouagadougou, Burkina Faso;* [2]*Applied Sciences and Technologies Training and Research Unit, Department of Biochemistry and Microbiology, University of Dedougou, B.P.176, Dedougou, Burkina Faso.*

Received: June 2, 2022; Revised: September 17, 2022; Accepted: September 28, 2022

Abstract

This study is an evaluation of the chemical profile of *vitex doniana* fruit as well as its antioxidant, anti-inflammatory and antibacterial properties *in vitro*. For this purpose, bio-guided fractionation was performed and the phytonutrients and antioxidant activity of these fractions were evaluated using standard methods. Then, the anti-inflammatory activity of the different fractions was evaluated by four inhibitory methods: protein denaturation, protienase, A5-LOX and xanthine oxidase. Finally, agar well diffusion and colorimetric microdilution methods were used to determine the antibacterial activity of the two best fractions on 11 reference bacterial strains. The results showed that the ethyl acetate (EAF) fraction presented the best chemical profile and correlated with interesting antioxidant, anti-inflammatory and antibacterial activities. To this end, bio-guided fractionation appears as a method to optimize the chemical profile and therapeutic activities.

KEYWORDS : Phytonutrients, Antibacterial; Anti-inflammatory ; Antioxidant; fruits of *Vitex doniana*

1. Introduction

The human immune system develops several mechanisms to fight infectious and inflammatory diseases (Behl *et al.,* 2021). For the effectiveness of the immune system in this task, antibiotic therapy is used to control microbial and bacterial activity (Valsamatzi *et al.,* 2021) while non-steroidal anti-inflammatory drugs (NSAIDs) are used to relieve fever and pain (Jiang *et al.,* 2018). However, the emergence of antimicrobial resistance, particularly bacterial resistance, is an imminent global threat (Allcock *et al.,* 2017). Indeed, some diseases such as pneumonia, tuberculosis, gonorrhoea and salmonellosis are becoming more difficult to treat with antibiotics and leading to inflammatory diseases (Sonter *et al.,* 2021). In addition, the inadequacy or absence of infection prevention and control methods play an important role in the emergence of antibiotic resistance and the occurrence of inflammatory diseases (Valsamatzi *et al.,* 2021). Also, it is worth noting that reactive oxygen species (ROS) resulting from oxidative stress have been shown to be a key driver of microbial resistance (Martelli and Giacomeini, 2018). To remedy this situation, new approaches are being initiated by scientists to discover and develop natural plant-based products, their analogues as potential therapeutic agents (Najmi *et al.,* 2022). Several studies have also shown a positive correlation between bioactive compounds, antioxidant and anti-inflammatory activities (Bendjedid, 2022). For this purpose, a plant of interest in the search for therapeutics and antimicrobial compounds is *Vitex doniana* (also known as black plum) (Njoku *et al.,* 2019). It is a valued plant for both food and medicinal use (Dadjo *et al.,* 2020). To further illustrate a basis for scientific validation of the medicinal use of *Vitex doniana* in traditional medicine, this study was undertaken to compare the efficacy of different fraction extracts of *Vitex doniana* to determine its phyto-constituents, antioxidant and antibacterial properties against selected microbial strains. To the best of our knowledge, this is the first comparative study on the pharmacological efficacy of different extracts of *Vitex doniana* from bio-guided fractionation.

2. Materials and Methods

2.1. Plant material

The plant material whose fruits of *Vitex doniana* were collected in August 2019 in the Hauts Bassins region, more precisely in Faramana (12°02′53" N and 4°40′02"W) located 120 km from Bobo-Dioulasso, Burkina Faso's economic capital. Dr Lassina TRAORE, botanist at the Laboratory of Biology and Ecology of the Joseph KI ZERBO University, has been working on the identification and authentication of the plant. Consequently, a reference number 20/08/2019/PRB has been deposited in the herbarium of the Life and Earth Sciences Unit of the Joseph KI ZERBO University.

* Corresponding author. e-mail: E-mail: mehekiessoum@yahoo.fr.

2.2. Fractionation of extracts

Fifty grams (50 g) of fruits were sprayed with 400 ml of acetone and 100 ml of distilled water, and the mixture was mechanically stirred for 48 hours at 37°C. After this stirring, the acetone evaporated in a rotavapor at 45°C.Hydroacetonic extracts were then subjected to liquid-liquid fractionation of increasing polarity with n-hexane (n-HF), dichloromethane (DCMF), ethyl acetate (EAF) and n-butanol (n-BF). Each fraction was concentrated and then lyophilized (Konaté *et al.,* 2010).

2.3. Phytonutrient analysis

2.3.1. Evaluation of total alkaloid contents

Total alkaloids contents (TAC) was determined by (Selvakumar *et al.,* 2019) with minor modifications. Thus, 1 ml of 1 mg/ml of the solution of each Fraction extract one summer mixed with 5 ml of green bromocresol solution and 5 ml of phosphate buffer of 4.7 pH. The mixture was vortexed pendant 3 to 5 minutes with 1; 2; 3 and 4 ml of chloroform. Afterwards, the whole mixture was collected in a 10 ml volumetric bottle. The atropine used as a standard, a summer used at the respective concentrations of: 20; 40; 60; 80 and 100 mg/ml. The reading was made at a wavelength of 470 nm. The experiments were carried out in triplicate. The TAC was expressed as mg Atropine Equivalent per 100 mg of dry fraction extract (mgAE/100 mgMS). Reagent blank was prepared in the same manner but without Fraction extract.

2.3.2. Evaluation of total phenolic contents

About this evaluation, the total phenolic contents was determined by using the Folin-Ciocalteu method and gallic acid as the standard as described by Belkacem et al. (2014) with minor modifications. An aliquot of 125µl solution of each methanolic fraction (10 mg/ml) solubilised in 1.5 ml of sodium carbonate solution (7.5%). After a 5 minute incubation, 1.25 ml of Folin-Ciocalteu (0.2 N) was added and vortexed for 2-3 minutes, incubated without light for one hour at 37°C. After this incubation period, the reading has been made at 760 nm against a blank on a UV/visible light spectrophotometer. The experiments were carried out in triplicate. The calibration curve was traced using gallic acid as a positive control. The results were expressed as mg Gallic Acid Equivalent per 100 mg of dry Fraction extract (mgGAE/100 mgMS).

2.3.3. Evaluation of total flavonoid contents

For the determination of total flavonoids contents, we used the method described by Elhanafi et al. (2020) with some modifications. Total flavonoids contents were identified using the aluminium chloride assay. 0.5 ml of methanol of each fraction solubilized (0.1 mg/ml) was mixed with 1.5 mL of $AlCl_3$ (2%) and incubated for 30 min at room temperature after this incubation period. The reading has been made spectrophotometrically on a blank at 415 nm. The experiments were carried out in triplicate. Quercetin was used as the reference standard compound. A standard curve was obtained using quercetin as a standard, and the results were expressed as in mg of equivalent per 100 mg of dry fraction extracted (mgEQ/100 mgMS).

2.4. In vitro Antioxidant activity determination of fraction extracts

2.4.1. Determination of DPPH radical scavenging assay

Radical analysis of DPPH (2, 2-diphenyl-1-picrylhydrazyl) trapping was performed according to Hifnawy et al. (2021) with some modifications. To determine the radical trapping behavior of fraction extract, a DPPH solution was prepared by dissolving 20 mg of DPPH in 100 ml of methanol. The absorbance of 3 ml of this solution was read as a control. For the preparation of stock solutions, 5 mg of each fraction was solubilised in 5 ml of methanol and then different serial dilutions (25; 50; 75 and 100 µL/ml) were prepared. Subsequently, 2 ml of each dilution was mixed with a 2 ml solution of DPPH and the IC_{50s} were determined. The percentage of DPPH free radical inhibition per fraction was determined by following the formula with some modifications.

$$\%\ \text{DPPH inhibition} = (1 - B/A) * 100 \quad (1)$$

Where, B is the absorbance of the sample, and A is the absorbance of the control. The scavenging activity of samples was expressed as IC_{50} value, which represented the inhibitory concentration of fraction/standard essential to scavenge 50% of DPPH radicals.

2.4.2. Determination of ABTS (2,2-azinobis (3-ethylbenzthiazoline) -6-sulfonic acid) free radicals scavenging activity

The antioxidant potential of the fractions was also assessed by ABTS free radical scavenging. An ABTS stock solution was prepared in methanol from ABTS (7 mM) and potassium persulphate (2.45 mM). Each fraction (300 µL) was evaluated in a 3 ml mixture of ABTS solution maintained at 25 °C for 15 min and the optical density was read at 734 nm (Dehimat *et al.,* 2021). The data were collected in triplicate, and the formula used to measure the percentage of ABTS free radical scavenging activity was as follows:

$$\%\text{ABTS scavenging inhibition} = (1 - D/C) * 100 \quad (2)$$

Where, C is the absorbance of the control, and D is the absorbance of the samples.

2.4.3. Determination of FRAP assay

The FRAP assay of fraction extract was studied according Jayanthi et Lalitha. (2011) in some minor modifications. Concentrations of fraction range from 0.2; 0.4; 0.6; 0.8 and 1 mg/ml and l-ascorbic acid at the same concentrations were then mixed with 2 ml of potassium ferricyanide ($K_3Fe(CN)_6$) and 2 ml of buffer phosphate (0.2 M, pH 6.6). The mixture was kept for 20 min at 50ºC. In addition, 2 ml of 10% trichloroacetic acid (TCA) was added to the mixture. The mixture was centrifuged for 10 min to 1000 revolutions per min (rpm). 2 ml of surnageant was sucked in and mixed with 1 ml of 0.1% iron chloride ($FeCl_3$) and 2 ml of distilled water. The reading absorbance was made at spectrophotometry at the wavelength of 700 nm. The median effective concentration (IC_{50}) of each fraction was determined.

2.4.4. Determination of RHS activity

The RHS (Radical Hydroxyl scavenging) was performed according to the method described by Klein et al. (1981) with minor modifications. The reaction medium

was made by adding 2.4 ml of phosphate buffer (pH 7.8), phenanthroline (90 mM), hydrogen peroxide (150 mM), iron (1 mM) and phytexpont (1.5 ml) and standard (l-ascorbic acid) at different concentrations (100%; 10%; 1%; 1% and 0.01%), except in the controls, and then incubated at room temperature for 5 min. The reading was taken at 560 nm, and the RHS activity was calculated using the following formula:

$$\%\,\text{RHS inhibition} = (1 - F/E) * 100 \quad (3)$$

Where F is the absorbance of the sample, and E is the absorbance of the control.

The half maximal inhibitory concentration (IC_{50}) of the fraction extracts was computed from a plot of percentage hydroxyl radical inhibition versus the fraction concentration.

2.5. In vitro anti-inflammatory test of fraction extracts

2.5.1. Evaluation of protein denaturation activity

Inhibition of protein denaturation was determined according to the method of Mizushima et Kobayashi. (1968) with some modifications. The reaction mixture contained the test fraction extracts at the final concentration of 200 µg/mL and 1% BSA (aqueous solution). The reaction mixture will be adjusted taking into account the pH. The fraction extracts will be subjected to different temperature variations, then finally cooled and the reading will be made to 600 nm. The experiment was performed in triplicate. Percent inhibition of protein denaturation was calculated as follows:

$$P\% = (1 - B/A) * 100 \quad (4)$$

With, A = The value of absorbance of control and B = The value of absorbance of test sample.

2.5.2. Evaluation of proteinase inhibitory activity

The reaction was initiated with trypsin (3 µg/mL), Tris HCl buffer (20 mM, pH=7.4), and 1 ml of each fraction (200µg/mL) was tested and incubated at 37°C for 5 min. Subsequently, 1 ml of 0.8% (w/v) casein was added and incubated for 20 min. 2 mL of perchloric acid (70%) was added again, and the cloudy suspension was centrifuged. The reading was taken at 210 nm (Oyedapo and Famurewa, 1995). The mean value of the three observations was noted. The percentage inhibition of PI activity was calculated as follows:

$$P\% = (1 - D/C) * 100 \quad (5)$$

With, D = The value of absorbance of control and C = The value of absorbance of test sample.

2.5.3. Evaluation of A5-LOX activity

A5-LOX (arachidonate 5-lipoxygenase) inhibitory activity of fractions was determined by spectrometric method (Dona *et al.,* 2018). For the reaction mixture, fraction extracts were used at the final concentration of 200µg/mL. Briefly, 10 µL of each fraction solubilised in methanol was added to sodium phosphate buffer (110 µL, 100 mM, pH 8.0) followed by A5-LOX solution (55 µL) and incubated for 10 min at 25 °C. To this reaction mixture, 25 µL of linoleic acid solution was added. The reading was made at 234 nm for a period of 10 min at 25 °C. Baicalein was used as the reference standard. Percentage inhibition of A5-LOX was determined by comparison of reaction rates of fraction relative to control using the formula :

$$P\% = (1 - E/F) * 100 \quad (6)$$

Where, P = Percent inhibition of A5-LOX was calculated as follows F and E are activities of the enzyme with and without fractions, respectively.

2.5.4. Evaluation of xanthine oxidase inhibitory activity

Xanthine oxidase inhibitory activity of fraction was determined by a kinetic method (Nagao *et al.,* 2014) with slight modifications. For the reaction mixture, fraction was used at the final concentration of 200µg/mL. Briefly, sodium phosphate buffer (150 µL, 50 mM, pH 7.4), fraction extract (10 µL) and xanthine oxidase solution (10 µL) were incubated at 25 °C for 10 min. The reaction was then initiated with the addition of xanthine solution (0.1 mM). The reading was made at 295 nm for a period of 10 min at 25 °C. Percentage inhibition of xanthine oxidase was calculated using the formula:

$$P\% = (1 - G/H) * 100 \quad (7)$$

Where, P = Percent inhibition of xanthine oxidase, G is the activity of enzyme without fraction extracts and H is the activity of enzyme with fractions. Allopurinol was used as the reference standard.

2.6. In vitro Antibacterial properties

2.6.1. Bacterial strains used

All microorganisms were provided by Food Technology Department (CNRST/IRSAT/DTA) and Center for Research in Biological, Food and Nutritional Sciences (CRSBAN) of Burkina Faso. Gram-positive ($Gram^+$) reference bacteria strains were : *Bacillus subtilis* ATCC 25923 ; *Bacillus cereus* 13569 ; *Micrococcus luteus* SKN 624 ; *Lysteria monocytogenesis* NCTC 9863; *Staphylococcus aureus* ATCC 2523 and *Bacillus subtilis spizinii* 6051. Gram-negative (Gram) bacterial strains were represented by *Escherichia coli* 25922 ; *Yersinia enterolitica* 8A30 SKN 601 ; *Pseudomonas aeruginosa* ATCC 9027; *shigella dysenteriae* SKN 557 and *Salmonella typhimurium* SKN 1152 were used in this research.

2.6.2. Preparation of inocula

We had used susceptibility tests by the MHA well diffusion method according to Ezoubeiri et al. (2005) with some modifications. Nutrient agar was used as a medium to grow the bacterial strains at 37°C for 24 hours and then the strains were suspended in saline (0.9%, w/v) NaCl and adjusted by a 0.5 standard Mac Farland turbidity test (10^8 CFU/ml). To obtain the inocula we are going to use, suspensions were diluted 100 times in MHB to give 10^6 colony-forming units (CFU)/ml.

2.6.3. Preparation of discs

The EAF and n-BF extracts were dissolved in distilled water containing 10% DMSO at a final concentration of 200 mg/L after a serial two-fold dilution. Each stock solution of the fractions was sterilised by filtration through a sterilising filter (0.22 µm). Sterile discs (6 mm) were impregnated with 10 µL of fraction extracts. Negative controls were prepared using discs impregnated with DMSO (10%) and commercially available antibiotic

diffusion discs used as positive controls for the experiment (Tambekar & Dahikar, 2011).

2.6.4. Determination of diameters of the inhibition zones (DIZ)

The Petri dishes (9 cm) were prepared with 20 ml of a base layer of MHA. Each Petri dish was inoculated with 15 µl of each bacterial suspension (10^6 CFU/ml. After drying in a sterile hood, 6 mm diameter discs soaked with 10 µl of the different solutions of fractions (EAF and n-BF) were then placed on the agar. The discs containing Gen.(30µg) and Cip.(25µg) were used as positive controls against DMSO (10%) as negative control. A 24 h incubation at 37°C of the petri dishes and at 44°C for *Escherichia coli* was performed. The DIZs were evaluated in millimetres. Fraction extracts (EAF and n-BF) inducing a zone of inhibition ≥ 3 mm around the disc were considered antibacterial. All tests were performed in triplicate, and the bacterial activity was expressed as the mean of DIZ (mm) produced (Deabes *et al.,* 2020).

2.6.5. Determination of Minimum Inhibition Concentration (MIC)

MIC was determined by the microdilution method according (Nigussie *et al.,* 2021) with some modifications. Eight twice-series dilutions of EAF and n-BF were prepared as described above, to obtain a final concentration range of 200 to 1.5625µg/ml. Microplates from 96 wells containing 100 µL of MHB were used. For each bacteria strain, three columns of eight wells to the micro-plate were used. Each well has getting: the culture medium + fractions (EAF or n-BF) + inoculum (10 µl of inocula) and INT (50 µl; 0.2 mg/ml). The plates were covered and incubated at 37°C and at 44°C for *Escherichia coli* for 24 h. All tests were performed in triplicate, and the bacterial activity was expressed as the mean of inhibitions produced. Inhibition of bacterial growth was judged by rose or yellow colour. The MIC was defined as the lowest concentration of fractions at which no colony was observed after incubation. So, the MIC was defined as the lowest concentration at which no visible growth was observed.

2.6.6. Determination of Minimum Bactericidal Concentration (MBC)

The lowest concentration of the fractions (EAF or n-BF) capable of neutralising 99.9% of the bacterial inocula after 24 hours of incubation at 37°C are considered MBC. For this purpose, MBCs were determined by inoculating 100 µl of bacterial suspension from the subculture showing no visible growth on nutrient agar. After incubation, MBC was determined with wells with concentrations ≥ MIC (Nigussie *et al.,* 2021). The MBC were determined in MHA medium.

2.6.7. Evaluation of bactericidal and bacteriostatic capacity

The MIC and MBC are the parameters that allow to assess the bacterial activity of a fraction on strains through the MBC/MIC ratio. Indeed, a MBC/MIC ratio equal to 1 or 2 has a bactericidal effect, whereas a MBC/MIC ratio = 4 or 16, the effect is bacteriostatic.

3. Statistical analysis

The R-Studio software version 4.1.3 was used for statistical processing of the data obtained through ANOVA, Tukeys test in order to evaluate the inhibitory effect of the extracts on the bacteria and to judge the efficiency of the different bioactive fractions.

4. Results

4.1. Total phytonutriment contents

Contents of total alkaloids, total phenolics and total flavonoids were determined respectively. Indeed, the phytonutrients showed significant differences for the various fractions. The EAF fraction showed the best contents of total alkaloids (7.28±1.73 mgAE/100 mgMS), total phenolics (48.34± 1.45 mg GAE/100 mgMS) and total flavonoids (14.18±1.01), while the lowest levels were noted for the hexanoic fraction (Figure 1).

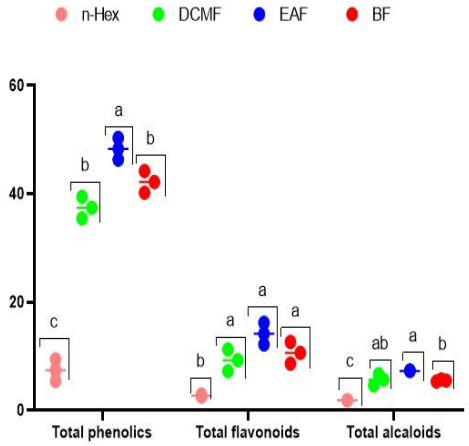

Figure 1. Phytonutrient contents of fraction extracts of fruits from *Vitex doniana*

Values are Mean ±SD (n=3). Different in the same column indicate significant difference (P<0.05) for our different extracts.

4.2. In vitro Antioxidant activity of fraction extracts

Antioxidant activity was assessed by four different methods: Ferric Reducing Antioxidant Power (FRAP) test, DPPH radical scavenging activity, ABTS scavenging test and RHS test. For these different tests, we note that EAF presented the best scavenging activities for 50% of the radicals (IC_{50}): FRAP (70.82±1.71 ug/mL), DPPH (4.42 ± 1.01 µg/mL), RHS (184.12±1.21 µg/mL) and ABTS (53.2 ± 2.51 ug/mL) compared to the other fractions (figure 2). These results show that ethyl acetate extraction consequently optimized its antioxidant power but was slightly lower than the standard ascorbic acid.

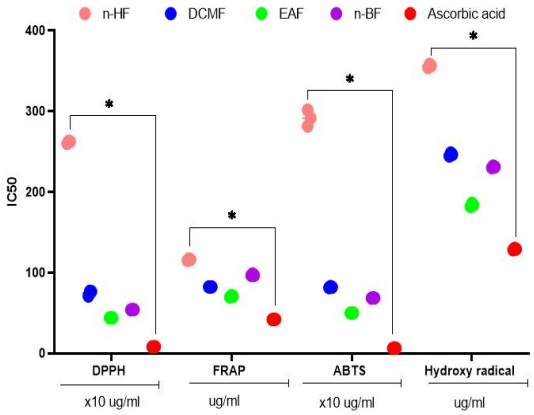

Figure 2. *In vitro* Antioxidant activities of fruits fractions of fruits from *Vitex doniana*

mmoL AAE/g extract: mmol equivalent Ascorbic Acid for 1g dried extracts

Values are Mean ±SD (n=3). Different in the same column indicate significant difference (P<0.05) for the different fractions and to the IC_{50} value of the standard (ascorbic acid) a significant difference with (P<0.001).

4.3. In vitro anti-inflammatory assay

The anti-inflammatory activity was evaluated by 4 inhibitory activities, namely: inhibition of protein denaturation; inhibition of proteinases; inhibition of arachidonate 5-lipoxygenase and inhibition of xanthine oxidase. For these four methods, it appears that the different fractions have an influence on the anti-inflammatory activities. Indeed, EAF showed the best anti-inflammatory activities including denaturation inhibition (70.12±1.02%), proteinase inhibition (69.93±2.00%), A5-LOX inhibition (70.60±1.54%) and xanthine oxidase inhibition (72.12±1.45) while n-HF showed the lowest activities (figure 3). Therefore, the EAF fraction will be used for *in vivo* testing.

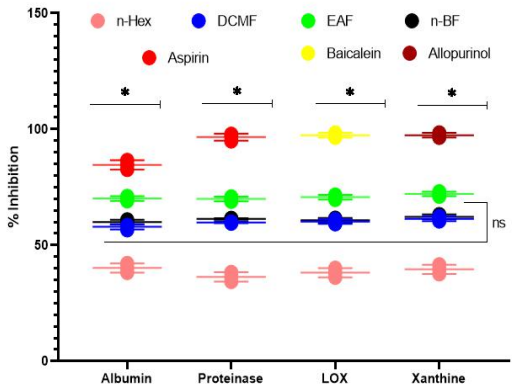

Figure 3. *In vitro* Anti-inflammatory of fraction extracts of fruits from *Vitex doniana.*

Values are Mean ±SD (n=3). Different in the same column indicate significant difference (P<0.05) for our different extracts.

4.4. Antibacterial activity

Antibacterial activities of two fractions (EAF and n-BF) of *Vitex doniana* were tested on 11 reference bacterial strains, of which six $Gram^+$ and five $Gram^-$ bacterial strains were used. In fact, the *in vitro* antibacterial activity was tested by the presence or absence of a zone of inhibition in diameter (DIZ), the minimum inhibitory concentration (MIC) and the minimum bactericidal concentration (MBC) against the reference antibacterial drugs (*gentamicin; cirpofloxacin*). In general, it was observed that both fractions showed anti-bacterial effects against all strains except *Salmonella typhimurium*. For the diameters of the inhibition zones, the EAF fraction showed the best activity on $Gram^+$ and $Gram^-$ bacterial strains similar to the standards. In particular, high bacterial activity of EAF was noted on *E.coli* (24.53±2.74 mm) and *Bacillus subtilis* (20.68 ±0.35 mm) (Table 1 and 2). MIC values ranged from 6.25 to 50 µg/mL for $Gram^+$ bacteria (Table 1), while 12.50 to 50 µg/mL for $Gram^-$ bacteria (Table 2). MBC values ranged from 25 to 50 µg/mL for $Gram^+$ bacteria (Table 1) and also from 25 to 50 µg/mL for $Gram^-$ bacteria (Table 2). These parameters confirm that fractionation has an influence on bacterial activity and, therefore, EAF is the best antibacterial fraction.

Table 1. *In vitro* Antibacterial activity of two fractions of fruits from *Vitex doniana* with Gram$^+$ bacterial strains

Activity	Fractions or Antibiotics	Gram$^+$ bacterial strains					
		B. subtilis	*B.cereus*	*M.luteus.*	*L.monocytogenesis*	*S.aureus*	*B.spizinii*
DIZ (mm)	EAF	20.68±0.35^a	19.58 ±3.09^a	18.77±0.70^a	15.60±0.65^a	20.73±0.25^a	13.30 ±1.25^{bc}
	n-BF	16.41±0.77^b	20.07±0.40^b	13.97±0.35^b	19.93±2.72^b	16.267±0.64^b	13.60 ±0.35^c
	Gen.	39.5± 2.18^a	34.38±1.71^a	39.26±1.10^a	34.96±0.65^a	19.37±0.32^a	34.73±1.62^a
	Cip.	40.83 ±1.75^a	27.67± 1.16^a	38.07±0.90^a	35.73±0.55^a	20.63±0.55^a	23.73±1.81^{ab}
MIC (µg/mL)	EAF	25	6.25	50	25	50	50
	n-BF	6.25	6.25	25	50	25	50
MBC(µg/mL)	EAF	25	12.50	25	50	50	50
	n-BF	12.50	12.50	50	50	50	50
MBC/MIC	EAF	+	+	+	+	+	+
	n-BF	+	+	+	+	+	+

DIZ includes diameter of discs (6 mm).

The results are the means of number of the colonies ± standard deviations.

+: bactericidal effect (MBC/MIC = 1 or 2) and –: bacteriostatic effect (MBC/MIC = 4 or 16).

Table 2: *In vitro* Antibacterial activity of two BF extracts of fruits from *Vitex doniana* with Gram$^-$ bacterial strains

Activity	Fractions or Antibiotics	Gram$^-$ bacterial strains				
		Escherichia coli;	*Yersinia enterolitica*	*Pseudomonas aeruginosa*	*Shigella dysenteriae*	*Salmonella typhimurium*
DIZ (mm)	EAF	24.53 ±2.74^a	16.30± 0.98^a	12.83 ±1.04^{ab}	13.47 ±0.41^b	Nd
	n-BF	16.17±1.25^b	13.37± 0.47^b	13.80± 1.05^b	15.30± 0.32^b	Nd
	Gen.	20.33±0.57^a	36.00±2.64^a	31.33±1.15^a	45.00±1.00^a	Nd
	Cip.	29.33 ±2.08^a	26.67± 1.52^a	26.33±1.52^a	41.00 ±1.00^a	Nd
MIC (µg/mL)	EAF	25	25	12.50	25	50
	n-BF	12.50	12.50	12.50	25	25
MBC(µg/mL)	EAF	50	50	50	50	25
	n-BF	50	50	50	50	25
MBC/MIC	EAF	+	+	-	+	+
	n-BF	-	-	-	+	+

DIZ includes diameter of discs (6 mm).

The results are the means of number of the colonies ± standard deviations.

+: bactericidal effect (MBC/MIC = 1 or 2) and –: bacteriostatic effect (MBC/MIC = 4 or 16).

5. Discussion

Regarding phytonutrient levels, the results obtained are interesting and as shown by the EAF with TPC (48.34 ± 1.45) and TFC (14.18 ± 1.01). Even higher levels were found by Traore et al. (2021) with total polyphenols (202.51 ±4.19 to 259.75 ± 2.81) and flavonoids (75.71 ± 1.03 to 145.55 ± 1.03). In addition, it is widely known that total phenolic compounds are one of the main groups of compounds acting as primary antioxidants or terminators of free radicals (Thakur *et al.,* 2021). Phenolics coumpounds is considered an important indicator of the antioxidant potential of plant extracts (Najmi *et al.,* 2022). Similar results show correlations between phenol content and antioxidant activities of plant extracts (El-chaghaby *et al.,* 2014). In this study, the radical inhibitory activity of the fraction (IC_{50} = 4.42 ± 1.01 µg/mL) was even more interesting than that of the EAF fraction obtained by Adjei et al. (2021) (99.35 ± 0.77µg/mL).

For anti-inflammatory activity *in vitro*, it should be noted that the fractions (EAF and n-BF) showed quite interesting results. When it comes to biological proteins in general, it is known that most biological proteins are denatured by the application of stress or chemicals and lead to the loss of their function. Proteins denaturation is a real and very important cause of inflammation (Flore *et al.,* 2019). Therefore, the anti-inflammatory potential of the extracts inhibited of proteins denaturation. It is well documented that serine proteinase contained in neutrophils play a fairly important role in inflammatory reactions during certain tissue damage, and proteinase inhibition is thought to have a more or less significant protective system (Leelaprakash *et al.,* 2011). In the present study, EAF inhibited protein denaturation and possessed anti-protease activity explaining their anti-inflammatory potential. With respect to the inhibitory activity of A5-LOX, EAF (200 mg/kg) showed very good A5-LOX inhibitory activity compared to that of control (baicalein). Xanthine oxidase also plays a vital role in the metabolic disease known to all and commonly called gout. It is closely linked to inflammation and other inflammatory-mediated diseases because of the formation of certain free radicals. Inhibition of this enzyme is considered to be a starting point for the management of diseases associated with oxidative stress and metabolic diseases (Yumita *et al.,* 2013). In the present study, the extracts studied showed significant inhibitory activity of xanthine oxidase ($P < 0.05$). EAF (200 mg/kg) showed the highest xanthine oxidase inhibitory activity compared to other fractions. In

addition, flavonoids, including quercetin, are recognized as a reference anti-inflammatory molecule, particularly in the treatment of acute inflammation (Li *et al.,* 2019). The EAF showed the highest anti-inflammatory potential, this may be related to the presence of certain secondary metabolites including triterpenes and flavonoids, saponins, tannins, and alkaloids (Qnais *et al.,* 2009). This statement is consistent with the work according to (Han and Bakovic, 2015) who suggest that triterpenoids are biologically active and possess anti-inflammatory properties.

Medicinal plants play a very important role in microbial defense mechanisms, thanks to the various secondary metabolites they contain (Anand *et al.,* 2019). The present study showed a good antibacterial potential of the plant fraction extracts on these different microorganisms studied. Indeed, the results show that the MICs obtained on *B. subtilis*, *S. aureus, P. aeroginosa and S. Typhi* bacteria are better to those obtained by Udeani et al. (2021) who obtained MICs for *B. subtilis* (28.15 mg/mL), *S. aureus* (8.90mg/mL), *P. aeroginosa* (3.84mg/L*) and S. Typhi* (3.80mg/mL) respectively. It is noted that anti-bacterial activity was found to be more pronounced against $Gram^+$ bacteria compared to $Gram^-$ bacteria. Our results would be similar to those obtained by Vlietinck et al. (1995) according to which, plant extracts have a better potential against $Gram^+$ bacteria than $Gram^-$. Indeed, $Gram^+$ and $Gram^-$ bacteria would be different in structure. The outer membrane that surrounds the cell wall is found only in $Gram^-$ bacteria and would be very impermeable for the passage of substances inside the bacterium unlike $Gram^+$ bacteria *(*Gibbons *et al.,* 2000). Studies already carried out show that the antimicrobial potential of plants is due to the different secondary metabolites namely phenols, flavones, flavanols, alkaloids and many others (Stavri *et al.,* 2007). The phytochemical characterisation of the different fractions used showed interesting contents of phenolic compounds, flavonoids and alkaloids. Moreover, flavonoids are known for their excellent antimicrobial properties. According to fairly recent literature, many flavonoids have anti-infectious properties by forming complexes with the different proteins of the walls of bacteria (Mahboubi *et al.,* 2015). In addition, it could be said that foods rich in polyphenols could greatly reduce health risks due to the anti-inflammatory, antioxidant and antibacterial properties that polyphenols possess (Abdel-Mawgoud *et al.,* 2019). Finally, it could also be said that the mechanism of toxicity of phenolic compounds against microorganisms could be explained by hydrolysis due to microbial enzymes including proteases and carbohydrolases or by other mechanisms, namely the action of the microbial andesis or that of transport proteins (Cowan, 1999).

6. Conclusion

The study showed that the EAF fraction of *Vitex doniana* would contain a considerable amount of phenolic compounds and possess interesting antioxidant, anti-inflammatory and antimicrobial properties. This study confirms a high availability of interesting nutrients in these plant extracts for pharmaceutical application. Therefore, chromatographic characterisation of individual compounds to elucidate their different biochemical mechanisms and clinical use. For this purpose, these isolated compounds should be scientifically evaluated using scientific animal models and clinical mechanisms of action in search of bioactive molecules. These results confirm the traditional use of the plant in inflammatory and infectious diseases in Burkina Faso.

Acknowledgments

The authors thank Doctor Lassina TRAORE of the Department of Plant Biology at the University of Ouagadougou (Burkina Faso) for the botanical identification of our study. The West African Biotechnology Network (RABIOTECH, ISP/IPICS project n°172600000) has particularly contributed to the realisation of this study through the financing of sampling, chemicals and laboratory materials. The authors declare no conflicts of interest.

References

Abdel M, Khedr FG and Enas MI. 2019. Phenolic Compounds, Antioxidant and Antibacterial Activities of *Rhus flexicaulis* Baker. *Jordan J. Biol. Sci.,* **12**(1): 17–21.

Adjei S, Kingsley I, Oppong S, Kingsley B, Boadu K, Yeboah A, Kwesi, M and Fosu-mensah G. 2021. Fruits of *Vitex doniana sweet* : toxicity profile , anti-inflammatory and antioxidant activities , and quantification of one of its bioactive constituents oleanolic acid. *Heliyon* **(2021)** e07910. https://doi.org/10.1016/j.heliyon.2021.e07910.

Allcock S, Young EH, Holmes M, Gurdasani D, Dougan G, Sandhu MS, Solomon L and Török ME. (2017). Antimicrobial resistance in human populations: challenges and opportunities, *Glob. Health Epidemiol. Genom.*. **2**(4):1-7. https://doi.org/10.1017/gheg.2017.4

Anand U, Jacobo-herrera N and Altemimi A. 2019. A Comprehensive review on medicinal plants as antimicrobial therapeutics : potential avenues of biocompatible drug discovery. *Metabolites,* **9**(258): 1–13.

Behl T, Kumar K, Brisc C, Rus M, Nistor-cseppento DC, Bustea C, Anca R, Aron C, Pantis C, Zengin G, Sehgal A, Kaur R, Kumar A, Arora S, Setia D, Chandel D and Bungau S. 2021. Exploring the multifocal role of phytochemicals as immunomodulators. *Biomed. Pharmacother.*, **133**(2021), 110959. https://doi.org/10.1016/j.biopha.2020.110959

Belkacem N, Djaziri R, Lahfa Fand Boucherit Z. 2014. Pharmacognosie phytochemical screening and in vitro antioxidant activity of various *Punica granatum l . Peel* extracts from Algeria : A comparative study, *Phytothérapie* **12:**372-379. doi: 10.1007/s10298-014-0850-x

Bendjedid S, Ismahene B, Tadjine A, Djellou R, Abes B and Chawki B. 2022. Analysis of phytochemical constituents by using LC-MS , Antifungal and allelopathic activities of leaves extracts of Aloe. *Jordan J. Biol. Sci.,,* **15**(1): 21–28.

Cowan MM. 1999. Plant Products as Antimicrobial Agents *Clin. Microbiol. Rev.,* **12**(4):564–582.

Dadjo CD, Ssogbadjo AEA, Andohan BF, Akaï RGLK, Hakeredza SC, Ouehanou, TD, Van Damme P. and Sinsin B. 2012. Uses and management of black plum *(Vitex doniana Sweet)* in Southern Benin. *Fruit,* **67**(4):239–248. https://doi.org/10.1051/fruits/2012017

Deabes MM, Allayeh A, Seif MM, Rasmey AH and Naguib KM. 2020. Antiviral, antifungal, and anti-bacterial potential activities of *Ephedra Sinica* in Vitro. *Jordan J. Biol. Sci.,, Sciences,* **13**(3):313–320.

Dehimat A, Azizi I and Bachra VB. 2021.In vitro antioxidant and inhibitory potential of leaf extracts of Varthemia sericea against key enzymes linked to type 2 diabetes. *Jordan J. Biol. Sci.,,***14**(1):97–104.

Dona H, Melshandi S, Koralalage J, Radhika R, Handunnetti SM, Vithanage O, Sisira D, Weerasena J, Weeratunga HD ,Jabeen A, and Choudhary, MI. 2018. In vitro pro-inflammatory enzyme inhibition and anti-oxidant potential of selected Sri Lankan medicinal plants. *BMC Complement Altern. Med.* **(2018**) 18:271. https://doi.org/10.1186/s12906-018-2335-1

El-chaghaby GA, Ahmad AF and Ramis ES. 2014. Evaluation of the antioxidant and antibacterial properties of various solvents extracts of *Annona squamosa* L . leaves. *Arab. J. Chem.,***7**(2):227–233. https://doi.org/10.1016/j.arabjc.2011.06.019

Elhanafi L, Benkhadda ZB, Rais C, Houhou M, Lebtar S, Channo A and Greche H. 2020. Biochemical composition , antioxidant power and anti- inflammatory of Dehulled *Sesamum indicum* Seeds and its coat fraction. *Jordan J. Biol. Sci.,,* **13**(3):289–294.

Ezoubeiri A, Gadhi CA, Fdil N, Benharref A, Jana M and Vanhaelen M. 2005. Isolation and antimicrobial activity of two phenolic compounds from *Pulicaria odora L* . J. Ethnopharmacol. **99**(2):287–292. https://doi.org/10.1016/j.jep.2005.02.015

Flore SND, Tsafack EG, Mbiantcha M, Gilbert A, Atsamo AD, Nana WY, Matah V, Mba M, and Adjouzem CF. 2019. In vitro anti-inflammatory and in vivo anti-arthritic activities of aqueous and ethanolic extracts of *Dissotis thollonii Cogn* . (*Melastomataceae*) in Rats. *J Evid Based Complementary Altern Med* .**019** Nov 15; 2019:3612481.
doi: 10.1155/2019/3612481. eCollection 2019.

Gibbons HS, Lin S, Cotter RJ and Raetz CRH. 2000. Oxygen Requirement for the Biosynthesis of the S -2- Hydroxymyristate Moiety in *Salmonella typhimurium* Lipid A. *J. Biol. Chem.*,**275**(42):32940–32949.
https://doi.org/10.1074/jbc.M005779200

Han N and Bakovic M. 2015. Biologically Active Triterpenoids and Their Cardioprotective and Anti- Inflammatory Effects. **J.** *Bioanal. Biomed*.**2015***, S12* https://doi.org/10.4172/1948-593X.S12-005

Hifnawy MS, Issaa MY, El-Seedi H and Ashour RMS. 2021. Phytochemical study, nutritional evaluation and in vitro anti-obesity potential of fruits pericarp and seeds of *Livistona carinensis* and *Thrinax parviflora*. *Jordan J. Biol. Sci.,,* **14**(1): 163–171.

Jayanthi P and Lalitha P. (2011). Reducing power of the solvent extracts of *eichhornia crassipes* (mart.) Solms. *International J. Pharm. Pharm. Sci*., **3**(3):126-128.

Jiang W, Wang L, Zhang J, Shen H, Dong W, Zhang T, Li X, Wang K and Du J. 2018. Effects of postoperative non-steroidal anti-in fl ammatory drugs on long-term survival and recurrence of patients with non-small cell lung cancer. *Medecine*, **97**:39(e12442). http://dx.doi.org/10.1097/MD.0000000000012442

Konaté K, Souza A, Coulibaly A, Kiendrebeogo M, Lamien-Meda NRTM, LamidiJRM. and Nacoulkma OG. 2010).In vitro antioxidant, lipoxygenase and xanthine oxidase inhibitory activities of fractions from *Cienfuegosia digitata Cav., Sida alba L. and Sida acuta Burn f. (Malvaceae). Pak. J. Biol. Sci.,* **13**(22):1092–1098.

Leelaprakash G, Dass SM. 2011. In vitro anti-inflammatory activity of methanol extract of Enicostemma axillare. *Int. J. Drug Dev. & Res.* **3**(3)**:** 189–196.

Li T, Li F, Liu X, Liu J and Li D. 2019. *S*ynergistic anti - inflammatory effects of quercetin and catechin via inhibiting activation of TLR4 – MyD88 - mediated NF - κ B and MAPK signaling pathways. *Phytother Res.,* **33**(3)*:756-767.* https://doi.org/10.1002/ptr.6268

Klein M, Cohen S, G., & Cederbaum, and A. I. 1981. Production of formaldehyde during metabolsm of dimethyl sulfoxide by hydroxyl radical generating systems. *Biochemistry*, **20**(21)**:** 6006–6012.

Mahboubi A, Asgarpanah J, Sadaghiyani PN and Faizi M. 2015. Total phenolic and flavonoid content and antibacterial activity of *Punica granatum L . var . pleniflora flowers (Golnar*) against bacterial strains causing foodborne diseases. *BMC Complement Altern. Med.*. (**2015**) 15:366. DOI 10.1186/s12906-015-0887-x

Martelli G and Giacomini D. 2018. Antibacterial and antioxidant activities for natural and synthetic dual-active compounds. *Eur. J. Med. Chem.*, **158:**91-105**.**
https://doi.org/10.1016/j.ejmech.2018.09.009

Mizushima Y and Kobayashi M. 1968. Anti-inflammatory drugs with serum proteins, especially with some biologically active protein. *J. Pharm. Pharmacol.* **20**(3):169-73. doi: 10.1111/j.2042-7158.1968.tb09718.x.

Nagao A, Seki M and Kobayashi H. 2014. *I*nhibition of xanthine oxidase by flavonoids. *Biosci. Biotechnol. Biochem.* **63**(10):1787-1790. DOI:. https://doi.org/10.1271/bbb.63.1787.

Najmi A, Javed SA, Al Bratty M and Hasan AA (2022). Modern Approaches in the Discovery and Development of Plant-Based Natural Products and Their Analogues as Potential Therapeutic Agents. *Molecules*, **27**(2): 349. https:// doi.org/10.3390/molecules27020349**.**

Nigussie D, Davey G, Legesse BA, Fekadu A and Makonnen E. 2021. Antibacterial activity of methanol extracts of the leaves of three medicinal plants against selected bacteria isolated from wounds of lymphoedema patients. *BMC Complement Ther Med.*, **21:**2 https://doi.org/10.1186/s12906-020-03183-0.

Njoku OC, Airaodion AI, Awosanya OO and Ekenjoku JA. 2019. *A*ntidiabetic Potential of Alkaloid Extracts from *Vitex doniana and Ficus thonningii* Leaves on Alloxan-induced Diabetic Rats. *International J. Gastroenterol. Hepatol. 2*(2):1–12.

Oyedapo OO and Famurewa AJ. (1995). Antiprotease and membrane stabilizing activities of extracts of *Fagara zanthoxylozdes, Olax subscorpzozdes* and T*etrapleura tetraptera. Int. j. pharmacogn.*, **33**(1):65–69.

Qnais E, Abu-Safieh K, Mohammad HA and Fuad AA. 2009. Antinociceptive Effect of Two Flavonoids from *Aloysia Triphylla L. Jordan J. Biol. Sci.,* **2(**4):167–170.

Selvakumar S, Vimalanban S and Balakrishnan G. 2019. Quantitative determination of phytochemical constituents from *Anisomeles malabaric*a. *MOJ J. Bioequivalence Bioavailab.* **6**(2): 19–21. https://doi.org/10.15406/mojbb.2019.06.00130

Sonter S, Mishra S, Dwivedi MK and Singh PK. 2021. Chemical profiling, in vitro antioxidant, membrane stabilizing and antimicrobial properties of wild growing Murraya paniculata from Amarkantak (M.P.). *Sci. Rep.,* **11**(1): 1–15. https://doi.org/10.1038/s41598-021-87404-7

Stavri M, Piddock LJV and Gibbons S. 2007. Bacterial efflux pump inhibitors from natural sources. *J. Antimicrob. Chemother*. **59**(6):1247–1260. https://doi.org/10.1093/jac/dkl460

Tambekar DH and Dahikar SB. 2011. Antibacterial activity of some Indian Ayurvedic preparations against enteric bacterial pathogens. *J. Adv. Pharm. Technol. Res.* **2**(1): 24–29. https://doi.org/10.4103/2231-4040.79801

Thakur A, Singh S and Puri S. 2021. Nutritional evaluation , phytochemicals, Phytochemicals, Antioxidant and Antibacterial activity of Stellaria monosperma Buch.-Ham. Ex D. Don and Silene vulgaris (Moench) Garcke: wild edible plants of Western Himalayas. *Jordan J. Biol. Sci.,,* ***14***(1): 83–90.

Traore KF, Kone KY, Ahi AP, Soro D, Assidjo NE., Fauconnier ML and Sindic, M. 2021. Phenolic compounds characterisation and antioxidant activity of black plum *(Vitex doniana)* fruit pulp and peel from Côte d'Ivoire. *J. Food Meas. Charact.* ,**15**(2):1281–1293. https://doi.org/10.1007/s11694-020-00719-3

Udeani TK, Ugwu LO, Nnadi CO and Okwuosa CN. 2021. Evaluation of Anti-Microbial Activity and Proximate Composition of Alkaloids from *Vitex doniana* Seed. *J. Pharm. Sci.*. **20**(1): 81-86.

Valsamatzi A, Katya P and Robert BP. 2021. Methods for prevention and constraint of antimicrobial resistance : a review. *Environ. Chem. Lett.* **19**(2021): 2005-2012. https://doi.org/10.1007/s10311-021-01206-x

Vlietinck AJ, VanHoff L Lasur A, Vanden D, Rwangado PC and Mvukiyumwami J. (1995). Screening of hundred Rwandese medicinal plants for anti- microbial and antiviral properties. *J. Ethnopharmacol.* **46**(1): 31-47.

Yumita A, Suganda AG and Sukandar EY. 2013. Xanthine oxidase inhibitory activity of some indonesian medicinal plants and active fraction of selected plants. *Int. J. Pharm. Pharm.* **5**(2):293-296

JJBS

Volume 15, Number 5,December 2022
ISSN 1995-6673
Pages 879 – 886
https://doi.org/10.54319/jjbs/150517

Jordan Journal of Biological Sciences

Potential Utilization of Dried Rice Leftover of Household Organic Waste for Poultry Functional Feed

Rusli Tonda[1,2], Lili Zalizar[1], Wahyu Widodo[1], Roy Hendroko Setyobudi[1], David Hermawan[1], Damat Damat[1,*] , Endang Dwi Purbajanti[3], Hendro Prasetyo[4], Ida Ekawati[5], Yahya Jani[6], Juris Burlakovs[7], Satriyo Krido Wahono[8], Choirul Anam[9], Trias Agung Pakarti[10], Mardiana Sri Susanti[11], Rifa'atul Mahnunin[2], Adi Sutanto[1], Dewi Kurnia Sari[2], Hilda Hilda[12], Ahmad Fauzi[1], Wirawan Wirawan[13], Nico Syahputra Sebayang[14], Hadinoto Hadinoto[15], Eni Suhesti[15], Ulil Amri[16], Yunus Busa[17]

[1]University of Muhammadiyah Malang, Malang, 65145, East Java, Indonesia; [2]PT. Zakiyah Jaya Mandiri, Lumajang 67381, East Java, Indonesia; [3]University of Diponegoro, Semarang 50275, Central Java, Indonesia; [4]University of Brawijaya, Malang 65145, East Java, Indonesia ;[5]University of Wiraraja, Sumenep 69451. East Java, Indonesia; [6]Mälardalen University, 72220 Västerås, Sweden; [7]Institute of the Polish Academy of Sciences, 31261 Kraków, Poland; [8]Research Center for Food Technology and Processing - National Research and Innovation Agency Republic of Indonesia, Special Region of Yogyakarta 55861, Indonesia; [9]Universitas Islam Darul Ulum, Lamongan 62253, Indonesia; [10]Mayantara School, Malang, 65146, East Java, Indonesia; [11]Aura Statistics Consultant, Malang 65141, East Java, Indonesia; [12]CV. Harapan Jaya Abadi, Malang 65144, East Java, Indonesia; [13]University of Tribhuwana Tunggadewi, Malang 65144, East Java, Indonesia; [14]University of Muhammadiyah Palembang, Palembang 30116, South Sumatera, Indonesia; [15]University of Lancang Kuning, Pekanbaru, Riau 28266, Indonesia; [16]University of Muhammadiyah Makassar, Makassar 90221, South Sulawesi, Indonesia; [17]University of Muhammadiyah Enrekang, Enrekang 91712, South Sulawesi Indonesia

Received: Oct 10, 2022; Revised: Nov 10, 2022; Accepted Nov 12, 2022

Abstract

Indonesia produced 30×10^6 t of waste in 2021; 40 % was organic and 276×10^3 t leftover rice. Meanwhile, broiler chicken farmers have been struggling with high feed costs to continue their production. Processing leftover rice into "aking-rice" is environmentally friendly, and it also provides alternative feed for chickens. "Aking-rice" is a type of resistant starch because it has undergone a gelatinization process that works as a synthesis of short-chain fatty acids that positively improve the function of the digestive tract because it increases the villi in the small intestine. This study analyzed the potential of "aking-rice" in broiler chicken productivity. The experimental method was a completely randomized design with three treatments, five replications and 12 chickens in each unit. The treatments are T0 (100 % basal feed), T1 (80 % basal feed + 20 % "aking-rice" spread on top of the basal feed), and T2 (80 % basal feed + 20 % "aking-rice" mix). Statistical analysis used ANOVA, and continued with LSD with observed variables, *i.e.* Feed Intake (FI), Average Daily Gain (ADG), Feed Conversion Ratio (FCR), and Performance Index (PI). The results showed that the highest FI values were T0 (99.02), T1 (97.45), and T2 (96.58). The highest ADG was T1 (40.40) then T0 (37.07) and the lowest was T2 (36.40). T1 has the lowest FCR (2.42) compared to T0 (2.68), T2 (2.66). The lowest FCR is T1 (2.42), then T2 (2.66) and the highest is T0 (2.68). The third variable was not significantly different, but the PI results showed a significant difference with the highest PI value T1 (433.84), while T0 (374.81) and T2 (372.67) were not different. Economic analysis also shows that the highest cost T0 (118 475) is significantly different from T1 (110 541) and T2 (109 558). The highest profit is shown by T1 (2 102) then T2 (1 063) and T0 (507). In conclusion, the use of "aking-rice" can increase the performance index with a higher ADG value and a lower FCR so that the costs are smaller and the profit is greater.

Keywords: Aking-rice, Alternatif feed, Environmentally friendly, Farmer income, Feed cost, Feed substitution, Resistant starch, Waste to feed.

1. Introduction

Based on the data released by the Ministry of Environment and Forestry, Indonesia produced 30×10^6 of waste in 2021 – 40 % was organic, and 40 % of aforementioned organic waste was domestic garbage mostly out of food remains (Setiawan, 2021; Setyobudi *et al.*, 2021a; SISPN, 2022). Anriany *et al.* (2013) stated that the amount of remaining rice in Indonesia per capita per year is an average of 1 000 g. Therefore, if Indonesia's population is 276×10^6, the remaining rice per year is 276×10^3 t. Even Hidayat (2021) explains that food waste in Indonesia is 112×10^6 per year.

Realizing the urgency of handling waste properly, researchers have been studying various attempts on the

* Corresponding author. e-mail: damatumm@gmail.com

matter (Halim *et. al.*, 2019; Monice and Perinov, 2017; Setyobudi *et al.*, 2019, 2022) in accordance with government regulations PP No. 27/2020 on waste management (RI, 2020) and supportive towards waste management program for renewable energy (Abdullah *et al.*, 2020; Ibrahim, 2022; Misna, 2018; Setyobudi *et al*., 2021b, 2022). In particular, Hendroko *et al.* (2013) and Adinurani *et al.* (2017) suggested a two-stage digester for biogas with organic waste feedstocks related to the low pH in the initial process (hydrolysis and acidogenesis process).

Reusing domestic waste for feed is beneficial to not only cut down organic waste, but also reduce feed cost in farming. About 65 % of the current feed cost goes to imported materials (Emiria, 2022; Kemenperin, 2019; Nasution and Kisihandi, 2021), while feed prices tend to hike from year to year (Midaada, 2022; Romdhon, 2022; Suprobo, 2021; Susanto, 2022; Tumion *et al.*, 2017). A staple food in Indonesia, rice contributes a considerably large amount of domestic waste on daily basis; processing it into *nasi aking* (sun-dried waste rice) should solve part of the problems. Once rinsed in clean water, rice leftovers are sundried to reduce the water content up to 14 % before further treatment for poultry feed.

"Aking rice" is characterized as resistant starch (Arshad *et al.*, 2018; Fuentes-Zaragoza *et al*., 2010; Rozali *et al.*, 2018) which is uncommon in other feed materials. Since it is unhydrolyzed and indigestible (Suloi, 2019), it goes to the colon and nourishes apathogenic bacteria when administered in warm temperature (Arshad *et al*., 2018; Fuentes-Zaragoza *et al.*, 2010; Setiarto *et al.*, 2015). Quite popular among duck (*Anas platyrhynchos domesticus* Linnaeus, 1758), swan (*Cygnus cygnus* Linnaeus, 1758), and local chicken (*Gallus gallus domesticus* Linnaeus, 1758) farmers (Nugraha *et al.*, 2012; Prasetyo *et al*., 2018; Saty *et al*., 2014; Yendy *et al.*, 2014), "aking-rice" and its feasibility in poultry industry has been scientifically studied. Roboth (2015) recorded up to 40 % involvement of "aking-rice" in feed for super chicken. Yendy *et al.* (2014) found that using 10 % "aking-rice" and citric acid additive in feed for local male duck was significantly effective ($P < 0.05$) on calcium and phosphor retentions, but not ($P > 0.05$) on feed, calcium, and phosphor consumption rates nor on weight. Maghfiroh *et al.* (2012) stated that utilizing 20 % "aking-rice" and lime additive brought insignificant differences on feed consumption rates, protein digestibility, nitrogen retention, and weight. Khusna (2009) even noted that either feed consisting of 60 % "aking-rice" or 100 % "aking-rice" to substitute corn was viable.

Broiler chicken meat is vastly consumed in Indonesia, and its increase in production goes along with consumption growth rate annually (Pradita *et al*., 2015; Widodo *et al.,* 2019; Yemima, 2014). Since the feed that entails this commodity reaches 70 % of total production cost (Anggitasari *et al.*, 2016; Widodo, 2009; Yendy *et al.*, 2014), a hike in feed price will reduce the farmer's income (Bessei, 2006; Hartono, 2005; Lara and Rostagno, 2013; Ranjan *et al.*, 2019; Tumion *et al.*, 2017). However, "aking-rice" is rarely found in broiler chicken farms despite its benefits. One study by Zulfikar and Sania (2014) concluded that broiler chicken feed containing 10 % "aking-rice" was inconsequential towards foot color, meat cholesterol percentage, and breast meat deposition percentage.

The short list of studies on "aking-rice" for broiler chicken feed calls for more discussions. Until this report was written, no research on an effective "aking-rice" feeding method to boost broiler chicken productivity in warm temperature had been conducted.

2. Materials and Methods

Authorized by the Ethical Commission on Health Studies of the Faculty of Medicine of University of Muhammadiyah Malang (E.5.a/222/KEPK-UMM/X/ 2022), this research was conducted in 2022 in PT. Zakiyah Jaya Mandiri, a broiler chicken farm in Lumajang, East Java, Indonesia (112º-53' to 113º-23' E and 7º-54 to 8-23' S), at an average temperature of 33 °C.

2.1. Materials

Day old chicks (DOC) were of platinum PT. Multibreeder Adirama Indonesia Tbk., adlibitum feed with Wonokoyo BR1 (Indonesia product) at the starter age (1 d to 21 d), transferred to a battery cage at 14 d old for adaptation, and treated at 21 d old.

The experiment was held in dry season at day temperature of between 28 ºC and 33 ºC – lightbulbs of 100 Watt were utilized to keep the temperature at 30 ºC to 33 ºC. Amount of 15 units of battery cages were arranged, and each was occupied by 12 chickens.

"Aking-rice" used as much as 20 % for treatment T1 and T2. The nutrients contained in "aking-rice" are based on the results of a proximate analysis from the nutrition laboratory of the University of Muhammadiyah Malang; water content 12.58 %; dry matter 87.42 %; ash content 0.83 %; crude protein 8.96 %; crude fat 0.43 %; and crude fiber 0.59 %.

2.2. Methods

Corresponding to experimental method of completely randomized design, five replications were performed to make 15 tests, and each test comprised 12 chickens. Three treatments were prepared: T0 (100 % basal feed), T1 (20 % "aking-rice" spread a top 80 % basal feed), and T2 (20 % "aking-rice" evenly mixed with 80 % basal feed). The formula of each treatment is detailed in the following Table 1 on the basis of recommendations SNI 8173.1:2015.

Table 1. Feed formula in treatments

No	Ingredient	T0	T1	T2
1	Corn (%)	69.43	48.91	48.91
2	Wheat pollard (%)	5.31	2.66	2.66
3	Corn gluten meal (CGM) (%)	12.60	12.49	12.49
4	Distillers dried grains with solubles (%)	3.00	5.00	5.00
5	"Aking-rice" (%)	0.00	20.00	20.00
6	Meat bone meal (%)	7.23	8.04	8.04
7	Palm oil (%)	0.20	1.00	1.00
8	L-Lysine HCL (%)	0.96	0.88	0.88
9	Calcium carbonat (CaCO3) (%)	0.65	0.58	0.58
10	Salt (%)	0.17	0.21	0.21
11	DL Methionine (%)	0.15	0.13	0.13
12	Dicalsium phospat (%)	0.30	0.10	0.10
Calculated analyses				
13	Poultry ME (kcal kg^{-1})	3 200.00	3 200.00	3 200.00
14	Crude protein (%)	20.00	20.00	20.00
15	Crude fat (%)	4.75	4.75	4.75
16	Crude fiber (%)	3.84	3.84	3.84
17	Calcium (%)	0.90	0.90	0.90
18	Available phosphorus (%)	0.45	0.45	0.45
19	Na (%)	0.15	0.15	0.15
20	Lysin (%)	1.00	1.00	1.00
21	Metionin (%)	0.38	0.38	0.38

Feed was measured before administered between 10 AM and 4 PM at an average temperature of 32 ºC, and any leftovers were scaled in the following day.

The rates of feed intake (FI), average daily gain (ADG), and feed conversion ratio (FCR) were calculated in order to analyze the effect of "aking-rice" in broiler chicken's performance index and its prospect to prosper its farmers via income analysis.

FI refers to the total amount of feed consumption during the 14 d of treatment (Fijana *et al*., Hasan *et al*., 2013; 2012; Liu *et al.*, 2020), calculated as per Equation (1):

FI = Total feed consumption / Day of treatment (1)

The weights of all chickens were measured at the beginning (21 d old) and the end (35 d old) of the research. Deducting chicken weights when the experiment started from when it concluded should give ADG (Astuti and Jaiman, 2019; Awad *et al.*, 2009; Hoan *et al.*, 2021) in accordance with Equation (2):

ADG = Final body weight – First body weight (2)

FCR should reveal the broiler chicken productivity during treatment (Hoan *et al.*, 2021; Khalifa *et al*., 2014; Rusli, 2012; Sugito, 2016; Umam *et al*., 2015), determined through Equation (3):

FCR= Daily feed consumption / Daily weight gain (3)

Recorded data was then evaluated for its average and standard deviation, then run for analysis of variance (ANOVA) (Adli and Sjofjan, 2018; Kartikaningrum, 2018; Saty, 2014). Should a significant effect be detected, Least Student Differences (LSD) test would follow (Abdulbaqi *et al*., 2018; Adinurani, 2016, 2022; Alwi *et al.*, 2019).

2.3. Performance Index (PI)

PI represents how well the treatment meets its goal. In this experiment, percentage of live chickens, body weight, average harvest age, and FCR are the defining factors (Anggitasari and Sjofjan, 2016; Azis *et al*., 2011; Herlina *et al.*, 2016; Nuryati, 2019; Rusli, 2012) run through Equation (4):

$$PI = \frac{\text{Live chicken (\%)} \times \text{Average weight (kg)}}{\text{FCR} \times \text{Average age} \times 100\ \%} \quad (4)$$

2.4. Income Analysis

Gain/loss analysis is an approach to estimate a farmer's income (Solehah and Halimatus, 2016; Suwarta *et al*., 2012; Tuite *et al*., 1987), so Equation (5) was run to verify whether "aking-rice" is beneficial for farmers:

Gain/loss = Output – input (5)

3. Results and Discussion

3.1. Performance index (PI)

The outcome of consuming "aking-rice" towards FI, ADG, and FCR of broiler chicken is presented in Figure 1. The result of PI analysis is also displayed.

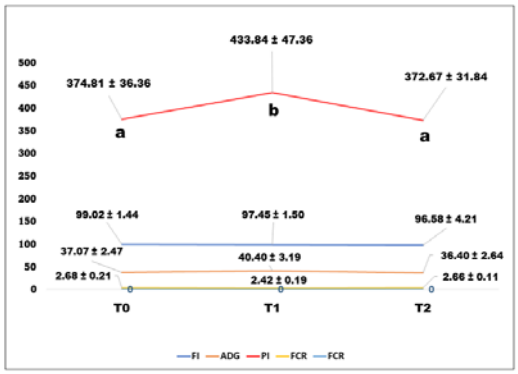

Figure 1. FI, ADG, FCR, and PI of broiler chicken fed with "aking-rice"

Figure 1. Illustrates that the highest FI rate is of P0 (99.02), followed by P1 (97.45) and P2 (96.58). Although only slightly different, the best ADG goes to P1 even with lower intake. P1 also recorded the lowest FCR rate (2.42) compared to P0 (2.68) and P2 (2.66). "Aking-rice" in P1 treatment has performed significantly better ($P < 0.05$) – in other words, "aking-rice" sprinkled on top of the feed is advantageous in enhancing PI when administered at a high temperature.

A bigger ADG rate and a smaller FCR one are keys to a higher PI value (Khalifa, 2014; Syukma, 2016; Umam *et al*., 2015; Yendy, 2014;), and their differences rely on nutrient absorption in broiler feed (Kusnadi, 2006; Nugraha *et al*, 2012; Roboth, 2015). Despite lacking on FI distinctions, P1 proves through its highest ADG rate that the nutrients in it have been better absorbed than in the other two treatments, which is appropriate to a statement by Marinus *et al.* (2020) and Suprayogi (2021) that the more nutrients a chicken absorbed, the heavier it will be (Widodo *et al*. 2019). Factors that may induce low nutrient absorption are low quality feed (Hakim *et al*., 2019; Latif and Sulaksana, 2014; Mansyur and Tangko, 2008; Widiyaningrum and Utami, 2014) or poor digestion as an effect of stress or illness (Setiarto *et al*., 2015; Sugito, 2016; Zalizar, 2010). Since the feed was of good quality and the materials were healthy, it is apparent that the low nutrient absorptions in P0 and P2 were due to stress – heat stress, to be specific (Dayyani and Bakhtiari, 2013; Khalifa, 2014; Kusnadi, 2007; Li *et al*., 2015; Mohammed *et al*., 2021; Tamzil, 2014).

The presence of resistant starch (RS) in "aking-rice" is deduced to be the reason of high IP. RS is not only indigestible but also unhydrolyzed, preventing it from getting absorbed in the small intestine (Setiarto *et al.*, 2015; Suloi, 2019) and, consequently, reducing the organ's metabolic burden (Carvalho *et al*., 2020; Lin *et al.*, 2006; Setiarto *et al.*, 2015; Tamzil, 2014). Sprinkling "aking-rice" on feed ensures its higher consumption, which means more RS intake, since chickens eat more of it on the top layer contrasted to one mixed in the feed. As a result, chickens feel satiated longer and are able to relax despite the heat, enable them to eat normally and maintain stable weight gain. Besides, RS boosts the number of villi in ileum (Damat *et al*. 2020; Fuentes-Zaragoza *et al.*, 2011; Lotfi *et al.*, 2019; Santos *et al.*, 2019; Suprayogi *et al.*, 2021) and maximizes microbial functions there, which is essential in increasing chicken's performance (Astuti *et al.*, 2015; Marinus *et al.*, 2020; Mohammed *et al.*, 2019; Wahyudi, 2008) – organic acids produced in the intestine should ease any heat stress syndromes, particularly in sensitive organs like jejunum (Awad *et al*., 2009; Santos *et al.*, 2019; Sun *et al.*, 2005; Suprayogi *et al.*, 2021). Fast and feed cutdown – two techniques commonly applied to fight heat stress – are against broiler chicken's instincts to eat more in order to increase productivity by gaining weight (Astuti *et al.*, 2015; Raji *et al.*, 2017), adding more stress to the chickens and cost them their ADG (Azis *et al.*, 2011; Khalifa, 2014).

RS also improves the digestive system (Astuti *et al.*, 2015; Rozali *et al.*, 2018) by nourishing the growth of good bacteria in the colon (Arshad *et al.*, 2018; Damat *et al*. 2021a, 2021b; Setiarto *et al.*, 2015). The good bacteria then produce bacterial acid that enhances insulin production in the pancreas which is essential in metabolism (Banjarnahor and Wangko, 2013; Lee *et al.*, 2010; Marinus *et al.*, 2020) as well as supporting the forming of short-chain fatty acid (butirat) (Damat *et al*. 2013; Rozali *et al.*, 2018; Salim *et al.*, 2013; Yendy, 2014) and the suppression of ammonia (Supartini and Darmawan, 2016; Suloi, 2019). Additionally, RS is able to accelerate the recovery process from diarrhea in broiler chicken by reducing the growth of vibrio cholera (Sulistiyanto *et al.*, 2019; Suloi, 2019).

3.2. Income analysis

The potential of "aking-rice" in improving the welfare of broiler chicken farmers was analyzed by comparing feed cost (input) and harvest (output) and calculating profit-and-loss. Figure 2 and Figure 3 below signify the results.

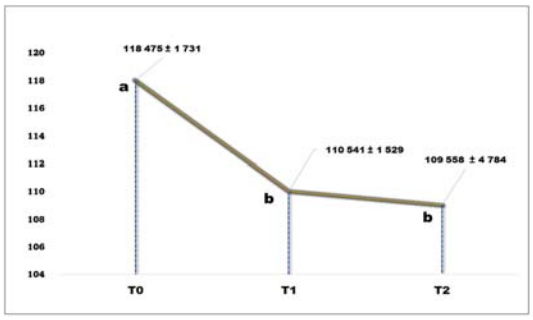

Figure 2. Feed cost (input) of broiler chicken

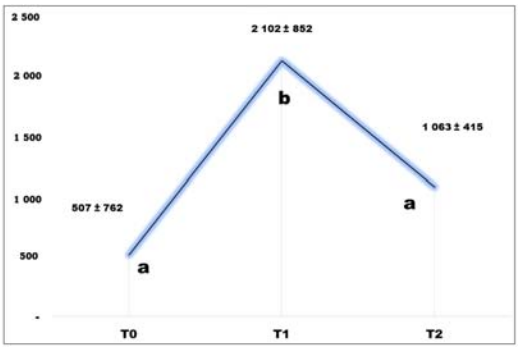

Figure 3. Profit-and-loss of broiler chicken

P1 was quite effective towards both input and profit-and-loss, while P2 was significantly effective towards input but less significant towards profit-and-loss. None of the treatments gave effect towards output, which means that although the harvest remains the same, involving 20 %

"aking-rice" in broiler chicken feed should help in cutting down feed cost, thus increasing the farmer's profit.

Feed cost reduction is made possible since "aking-rice" is cheaper than corn, the broiler chicken basal feed. Since the highest production cost in broiler farming goes to feed (Astuti *et al*., 2019; Solehah and Halimatus, 2016; Suwarta *et al*., 2012) – covering 60 % (Anggitasari and Sjofjan, 2016; Widodo, 2009; Yafi, 2021) even 70 % to 80 % (Ariyadi and Anggraini, 2010; Astuti *et al*., 2015; Yendy, 2014) – lower feed cost should give higher revenue (Hartono, 2005; Hendayana and Wally, 2008; Iyai *et al*., 2020; Jaelani *et al*., 2013; Prasasta, 2018; Solehah, 2016). This study asserts the importance of "aking-rice" for feed efficiency to flourish broiler farming.

4. Conclusion and Suggestion

The use of "aking-rice" can improve the digestive tract so as to increase the performance index with a higher ADG value and lower FCR so that the cost is smaller and the profit is greater.

References

Abdulbaqi NJ, Dheeb BI and Irshad R. 2018. Expression of biotransformation and antioxidant genes in the liver of albino mice after exposure to aflatoxin B1 and an antioxidant sourced from turmeric (*Curcuma longa*). *Jordan J. Biol. Sci.,* **11(1)**: 93–98.

Abdullah K, Saepul UA, Soegeng R, Suherman E, Susanto H, Setyobudi RH, Burlakovs J and Vincē Viča-Gaile Z. 2020. Renewable energy technologies for economic development. *E3S Web Conf.,* **188(00016)**:1–8. https://doi.org/10.1051/e3sconf/202018800016.

Adinurani PG. 2016. **Design and Analysis of Agrotrial Data: Manual and SPSS**. Plantaxia, Yogyakarta, Indonesia

Adinurani PG. 2022. **Agrotechnology Applied Statistics** (compiled according to the emester learning plan). Deepublish, Yogyakarta, Indonesia

Adinurani PG, Setyobudi RH, Wahono SK, Mel M, Nindita A, Purbajanti E, Harsono SS, Malala AR, Nelwan LO and Sasmito A. 2017. Ballast weight review of capsule husk Jatropha curcas Linn. on acid fermentation first stage in two-phase anaerobic digestion. *Proc. Pakistan Acad. Sci.: B.,* **54(1)**: 47–57

Adli DN and Sjofjan O. 2018. Nutrient content evaluation of dried poultry waste urea molasses block (DPW-UMB) on in-vitro analysis. *Sains Peternakan.,* **16(2):**50. https://doi.org/10.20961/sainspet.v16i2.21264.

Alwi MD, Apada AGS and Rell F. 2019. Administration of live-attenuated newcastle disease (ND) vaccines derived from B1 and lasota strain and their effect on broiler antibody titers. *Jurnal Riset Veteriner Indonesia*. **3(2)**:56–60.

Anggitasari S, Sjofjan O and Djunaidi IH. 2016. Effect of some kinds of commercial feed on quantitative and qualitative production performance of broiler chicken. *Buletin Peternakan.* **40(3)**:187–196.

Anriany D. and Martianto D. 2013. Estimation of consumer rice leftovers in several types of restaurants in Bogor City. *Jurnal Gizi dan Pangan*. **8**(1):33. https://doi.org/10.25182/jgp.2013.8.1.33-38.

Ariyadi T and Anggraini H. 2010. Determination of carbohydrate levels in "aking-rice" consumed by the community of Singorojo village, Kendal regency. Prosiding Seminar Nasional UNIMUS. Universitas Muhammadiyah Semarang, East Java, Indonesia. pp. 36–38.

Arshad NH, Zaman S and Rawi M. 2018. Resistant starch evaluation and in vitro fermentation of lemantak (native sago starch), for prebiotic assessment. *Int. Food Res. J.,* **25(3):**951–957.

Astuti FK, Busono W and Sjofjan O. 2015. Effect of addition of liquid probiotics in feed on production appearance in broilers. *Pembangunan dan Alam Lestari.* **6(2)**:99–104.

Astuti FK and Jaiman E. 2019. Comparison of body weight gain of broilers in CV Arjuna Group based on three different heights. *Journal Sains Peternakan.* **7(2)**:75–90.

Awad WA, Ghareeb K, Abdel-Raheem S and Bohm J. 2009. Effects of dietary inclusion of probiotic and synbiotic on growth performance, organ weights, and intestinal histomorphology of broiler chickens. *Poult. Sci.*, **88(1)**:49–55. https://doi.org/10.3382/ps.2008-00244.

Azis A, Abbas H, Heryandi Y and Kusnadi E. 2011. Compensation growth and production efficiency of broilers that are restricted in feeding time. *Media Peternak.*, **34(1)**:50–57. https://doi.org/10.5398/medpet.2011.34.1.50.

Banjarnahor E and Wangko S. 2013. Pancreatic beta cells synthesis and insulin secretion. *Jurnal Biomedik.* **4(3)**:156–162. https://doi.org/10.35790/jbm.4.3.2012.795.

Bessei W. 2006. Welfare of broilers: A review. *World's Poult. Sci. J.,* **62(9)**:455–466. https://doi.org/10.1079/WPS2005108.

RI (Republic of Indonesia). 2020. Government regulation number 27/2020 concerning waste management of specific waste.

http://www.indonesianwaste.org/republic-of-indonesia-government-regulation-number-27-of-2020-concerning-waste-management-of-specific-waste-peraturan-pemerintah-republic-indonesia-nomor-27-tahun-2020-tentang-pengelolaan-sampah-spe/

Carvalho GB, Martins PC, Resende PM, Santos JS, De Oliveira E, De Campos TT, Marins DB and Stringhini JH. 2020. Hematology and serum biochemistry of broilers at the initial and growth stages submitted to different levels of digestible sulfur amino acids. *Cienc. Rural*, **50(5)**:1–9. https://doi.org/10.1590/0103-8478cr20180881.

Damat D. 2013. Effect of butyrylated arrowroot starch to the digesta profile and molar ratio SCFA. *J. Food Sci.,* **2(2)**:144–149.

Damat D, Setyobudi RH, Soni P, Tain A, Handjani H and Chasanah U. 2020. Modified arrowroot starch and glucomannan for preserving physicochemical properties of sweet bread. *Ciência e Agrotecnologia*, **44(014820)**:1–9. https://doi.org/10.1590/1413-7054202044014820.

Damat D, Setyobudi RH, Utomo JS, Gaile ZV, Tain A and Siskawardani DD. 2021a. The characteristics and predicted of glycemic index of rice analogue from modified arrowroot starch (*Maranta arundinaceae* L.). *Jordan J. Biol. Sci.,* **14(3):**389–393. https://doi.org/10.54319/jjbs/140302

Damat D, Setyobudi RH, Burlakovs J, Vincevica-Gaile Z, Siskawardani DD, Anggriani R and Tain A. 2021b. Characterization properties of extruded analog rice developed from arrowroot starch with addition of seaweed and spices. *Sarhad J. Agric.*. **37 (Special issue 1)**:159–170. https://dx.doi.org/10.17582/journal.sja/2021.37.s1.159.170

Dayyani N and Bakhtiari H. 2013. Heat stress in poultry: Background and affective factors. *Int. J. Adv. Biol. Biomed. Res.* **1(11)**:1409–1413.

Emiria DC. 2022. 60% Imported feed ingredients, RI can be threatened by chicken 'doomsday'? CNBC Indonesia. https://www.cnbcindonesia.com/news/20220617162033-4-348088/60-bahan-pakan-impor-ri-bisa-terancam-kiamat-ayam.

Fijana MF, Suprijatna E and Atmomarsono U. 2012. The effect of feeding proportion at midday and night and lighting at night on broiler chicken carcass production. *Animal Agriculture Journal.* **1(1)**:697–710.

Fuentes-Zaragoza E, Riquelme-Navarrete MJ, Sánchez-Zapata E and Pérez-Álvarez, JA. 2010. Resistant starch as functional ingredient: A review. *Food Res. Int.,* **43(4)**:931–942. https://doi.org/10.1016/j.foodres.2010.02.004.

Fuentes-Zaragoza E, Sánchez-Zapata E, Sendra E, Sayas E, Navarro C, Fernández-Lõpez J and Pérez-Alvarez J. 2011. Resistant starch as prebiotic: A review. *Starch.* **63(7)**:406–415.

https://doi.org/10.1002/star.201000099.

Hakim AR, Kurniawan K and Siregar ZA. 2019. Effect of replacement of fish meal with *Hermetia illucens* and *Azolla* sp. on the quality of floating fish feed. *Jurnal Riset Akuakultur*. **14(2)**:77–85.

Halim AK., Hariansyah M and Lutfi M. 2019. Plastic waste management based on renewable energy in realizing sustainable development. *Jurnal Pendidikan dan Pemberdayaan Masyarakat.* **6(2)**:126–147.

Hartono G. 2005. Broiler chicken feed demand analysis using a translog function model. *Agric.* **18(7)**:41–56.

Hasan N, Atmomarsono U and Suprijatna E. 2013. Effect of feeding frequency on feed restriction on final weight, abdominal fat and liver fat content of broilers. *Animal Agriculture Journal.* **2(1)**:336–343.

Hendayana R and Wally F. 2008. Institutional analysis of people's livestock business input and output market. *Socioeconomics of Agriculture and Agribusiness.* **8(1)**:1–10

Hendroko R, Liwang T, Adinurani PG, Nelwan LO, Sakri Y, and Wahono SK. 2013. The modification for increasing productivity at hydrolysis reactor with *Jatropha curcas* Linn. capsule husk as bio-methane feedstocks at two-stage digestion. *Energy Procedia* **32**:47–54.
https://doi.org/10.1016/j.egypro.2013.05.007

Herlina B, Novita R and Karyono T. 2016. Effect of time and ration on the performance growth and broiler production betty. *Jurnal Sain Peternakan Indonesia.* **10(2)**:107–113. https://doi.org/10.31186/jspi.id.10.2.107-113.

Hidayat AAN. 2021. Bapenas: Without policy intervention, food waste is 112 million tons per year. Tempo.Co. June 9, 2021.
https://bisnis.tempo.co/read/1470633/bappenas-tanpa- intervensi-kebijakan-sampah-makanan-112-juta-ton-per-tahun.

Hoan ND, Dung TH, Hoan PD and Thang TV. 2021. Effect of supplementation of green tea extract on blood corticosterone concentration and growth performance in heat-stressed broiler. *Livest. Res. Rural Dev.*, **33(1)**

Ibrahim J. 2022. Manage waste into new renewable energy fuel. Pemerintah Kota Pontianak.
https://www.pontianakkota.go.id/pontianak-hari-ini/berita/Kelola-Sampah-Jadi-Bahan-Bakar-Energi-Baru-Terbarukan.

Iyai D, Mustaqim AI and Sagrim M. 2020. Profile, input and output of livestock systems in the agro-ecological area of Tambrauw, West Papua Province. *Jurnal Pertanian Terpadu.* **8(1)**:1–13. https://doi.org/10.36084/jpt..v8i1.230.

Jaelani A, Suslinawati S and Maslan M. 2013. Feasibility analysis of broiler chicken farming at Tapin Utara subdistrict, Tapin district. *Jurnal Ilmu Ternak.* **13(2)**:42–48.

Kartikaningrum V. 2018. Effect of boiled bay leaf (*Syzygium polyanthum*) on HDL and LDL cholesterol levels in hyperlipidemic male mice (*Mus musculus* L.). *Jurnal Widya Warta.* **42(02)**:149–161.

Kemenperin. 2019. **Analysis of the Structure of the Animal Feed Industry in the Context of Regional Development of Industry**. Final Report. Kementerian Perindustrian, https://kemenperin.go.id/download/24035

Khalifa H, Abougabal M and El-Shafei A. 2014. Mitigating heat stress in broilers: 1-effect of feed restriction and early heat acclimation on productive performance. *Middle East J. Appl. Sci.,* **4(4):**967–982.

Khusna. 2009. The effect of using "aking rice" in feed on the appearance of broiler production. Undergraduated Thesis, Universitas Brawijaya, Malang, Indonesia

Kusnadi E. 2006. Vitamin C supplementation as an antidote to heat stress in broiler chickens. *Jurnal Ilmu Ternak dan Veteriner.* **11(4)**:249–253.

Kusnadi E. 2007. Effect of pegagan (*Centella asiatica*) and vitamin C on blood hemoglobin and hematocrite of heat-stressed broilers. *Jurnal Ilmu Ternak.* **7(2)**:140–144.

Lara LJ and Rostagno MH. 2013. Impact of heat stress on poultry production. *Animals*, **3**:356–369.
https://doi.org/10.3390/ani3020356.

Latif A and Sulaksana SFI. 2014. Increased production and quality of Etawah crossbreed goat's milk as a response to improve feed quality. *Jurnal Ilmiah Ilmu-Ilmu Peternakan.* **26(1)**:15–21.

Lee KW, Lee SH, Lillehoj HS, Li GX, Jang SI, Babu US, Park MS, Kim DK, Lillehoj EP, Neumann AP, Rehberger TG and Siragusa GR. 2010. Effects of direct-fed microbials on growth performance, gut morphometry, and immune characteristics in broiler chickens. *Poult. Sci.,* **89(2)**:203–216.
https://doi.org/10.3382/ps.2009-00418.

Li M, Wu J and Chen Z. 2015. Effects of heat stress on the daily behavior of Wenchang chickens. *Brazilian J. Poul. Sci.,* **17**:559–566.

Lin H, Decuypere E and Buyse J. 2006. Acute heat stress induces oxidative stress in broiler chickens. *Comp. Biochem. Physiol.-A Mol. Integr. Physiol.*, **144(1)**:11–17.
https://doi.org/10.1016/j.cbpa.2006.01.032.

Liu L, Ren M, Ren K, Jin Y and Yan M. 2020. Heat stress impacts on broiler performance: A systematic review and meta-analysis. *Poult. Sci.*, **99(11)**:6205–6211.
https://doi.org/10.1016/j.psj.2020.08.019.

Lotfi K, Mahdavi A, Javan JA, Staji H and Darabighane B. 2019. Effects of different levels of resistant starch on growth performance and ileum morphology in broilers: A comparison to fructooligosaccharide and zinc bacitracin. *Iran. J. Appl. Anim. Sci.,* **9(2)**:315–322.

Maghfiroh K, Mangisah I and Ismadi VDY. 2012. Effect of addition of lime juice (*Citrus aurantifolia*) in ration on crude protein digestibility and nitrogen retention in male Magelang ducks. *Anim. Agric. J.*, **1(1)**:669–683.

Mansyur A and Tangko M. 2008. Probiotics: Their use for low-quality fish feed. *Media Akuakultur*, **3(2)**:145–149.

Marinus FW, Borg R, Buddiger NJH, Wood BJ, Rebel JMJ, Krimpen MMV, Calus MPL, Park JE and Schokker D. 2020. Regulating appetite in broilers for improving body and muscle development – A review. *J. Anim. Physiol. Anim. Nutr.,* **104(6)**:1819–1834. https://doi.org/10.1111/jpn.13407.

Midaada A. 2022. Livestock feed prices continue to rise, laying chicken farmers are restless. Sindonews,
https://ekbis.sindonews.com/read/857407/34/harga-pakan-ternak-terus-naik-peternak-ayam-petelur-resah-1660619315

Misna AF. 2018. The importance of utilizing waste as an energy source. Kementerian Energi dan Sumber Daya Mineral Direktorat Jenderal Energi Baru, Terbarukan dan Konservasi Energi - Republic of Indonesia. https://ebtke.esdm.go.id/post/ 2018/11/ 23/2060/pentingnya.pemanfaatan.sampah.sebagai.sumber.energi

Mohammed A, Mahmoud M, Murugusen R and Cheng HW. 2021. Effect of a synbiotic supplement on fear response and memory assessment of broiler chickens subjected to heat stress. *Animals*, **11(2)**:1–15. https://doi.org/10.3390/ani11020427.

Mohammed AA, Jiang S, Jacobs JA and Cheng HW. 2019. Effect of a synbiotic supplement on cecal microbial ecology, antioxidant status, and immune response of broiler chickens reared under heat stress. *Poult. Sci.,* **98(10)**:4408–4415. https://doi.org/10.3382/ps/pez246.

Monice M and Perinov P. 2017. Analysis of waste potential as raw material for waste power plant (PLTSa) in Pekanbaru. *Jurnal Sains, Energi, Teknologi, dan Industri*, **1(1)**:9–16. https://doi.org/10.31849/sainetin.v1i1.166.

Nasution DD and Kisihandi F. 2021. Government to import poultry feed raw materials. Republica.co.id., https://www.republika.co.id/berita/qwnev9472/pemerintah-akan-impor-bahan-baku-pakan-unggas

Nugraha D, Atmomarsono U and Mahfudz LD. 2012. The effect of fermented water hyacinth (*Eichornia crassipes*) addition in the diet on Tegal duck egg's production. *Animal Agricultural.* **1(1)**:75–85.

Nuryati T. 2019. Performance analysis of broiler in closed house and opened house. *Jurnal Peternakan Nusantara* **5(2)**:77–86.

Pradita D, Sarengat W and Handayani M. 2015. Production efficiency of Riski Jaya Abadi broiler farm at Kebumen regency sighted from management efficiency, technical efficiency, economic efficiency and price efficiency. *Animal Agriculture Journal*. **4**:75–80.

Prasasta H. 2018. Adaptation of laying hens in the face of turmoil in the input and output markets (study on laying hens in Ponggol District, Blitar Regency). Undergraduate Thesis Universitas Brawijaya, Malang, Indonesia.

Prasetyo MS, Jan LR, Rozi T and Kasip LM. 2018. Lombok duck egg production and quality for making salted egg raised intensively in Centre Lombok. *Jurnal Ilmu dan Teknologi Peternakan Indonesia.* **4(1)**:199–206.

Ranjan A, Sinha R, Devi I, Rahim A and Tiwari S. 2019. Effect of heat stress on poultry production and their managemental approaches. *Int. J. Cur. Microbiol. Appl. Sci.,* **8(02)**:1548–1555.

Raji AA, Mohammed B, Oladele SB, Saidu L, Jibril AH and Cazaban C. 2017. Bursa body index as a visual indicator for the assessment of bursa of fabricius. ***J. Vet. Med. Anim. Health.*** **9(2):**32–38. https://doi.org/10.5897/JVMAH2016.0456.

Roboth RH. 2015. The level of adding parched rice in the feed to the body weight gain and feed conversion of starter chicken. Undergraduate Thesis. Universitas Negri Gorontalo, Gorontalo, Indonesia

Romdhon MS. 2022. Expensive feed prices, 30 percent of chicken farmers in Kuningan failed. Kompas Bandung. https://bandung.kompas.com/read/2022/06/08/091523378/harga-pakan-mahal-30-persen-peternak-ayam-di-kuningan-bangkrut?page=all

Rozali ZF, Purwani EY, Iskandariati D, Sri N and Suhartono T. 2018. The potential of rice resistant starch as fungsional food ingredient. *Jurnal Pangan*. **27(3):**215–224.

Rusli R. 2012. Success analysis of chicken farmers (case study of Telur Intan Group breeders partnership pattern in Malang). Undergraduate Thesis, University of Muhammadiyah Malang, Malang, Indonesia

Salim HM, Kang HK, Akter N, Kim DW, Kim JH, Kim MJ, Na JC, Jong HB, Choi HC, Suh OS and Kim WK. 2013. Supplementation of direct-fed microbials as an alternative to antibiotic on growth performance, immune response, cecal microbial population, and ileal morphology of broiler chickens. *Poult. Sci.*, **92(8)**:2084–2090. https://doi.org/10.3382/ps.2012-02947.

Santos RR, Awati A, Roubus-van den Hil PJ, Van Kempen TATG, Tersteeg-Zijderveld PJ, Koolmees PA, Smits C and Fink-Gremmels J. 2019. Effects of a feed additive blend on broilers challenged with heat stress. *Avian Pathol*., **48(6)**:582–601. https://doi.org/10.1080/03079457.2019.1648750.

Saty L, Praseno K and Kasiyati K. 2014. Cholesterol and β-carotene levels of duck eggs from several duck cultivation locations in Java. *Buletin Anatomi dan Fisiologi.* **22(2)**:56–63.

Setiarto RH, Laksmi JBS, Farida DN and Saskiawan I. 2015. Study of development resistant starch contained in food ingredients as prebiotic source. *Jurnal Ilmu Pertanian Indonesia.* **20(3)**:191–200. https://doi.org/10.18343/jipi.20.3.191.

Setiawan A. 2021. Improving national waste management. Portal Informasi Indonesia. https://indonesia.go.id/kategori/indonesia-dalam-angka/2533/membenahi-tata-kelola-sampah-nasional.

Setyobudi RH, Zalizar L, Wahono SK, Widodo W, Wahyudi A, Mel M, Prabowo B, Jani Y, Nugroho YA, Liwang T and Zaebudin A. 2019. Prospect of Fe non-heme on coffee flour made from solid coffee waste: Mini review. *IOP Conf. Ser. Earth Environ. Sci.*, **293 (012035)**:1–24. https://doi.org/10.1088/1755-1315/293/1/012035.

Setyobudi RH, Yandri E, Atoum MFM, Nur SM, Zekker I, Idroes R, Tallei TE, Adinurani PA, Vincēviča-Gaile Z, Widodo W, Zalizar L, Van Minh N, Susanto H, Mahaswa RK, Nugroho YA, Wahono SK and Zahriah Z. 2021a. Healthy-smart concept as standard design of kitchen waste biogas digester for urban households. *Jordan J. Biol. Sci.* **14(3)**: 613 – 620 https://doi.org/10.54319/jjbs/140331

Setyobudi RH, Yandri E, Nugroho YA, Susanti MS, Wahono SK, Widodo W, Zalizar L, Saati EA, Maftuchah M, Atoum MFM, Massadeh MI, Yono D, Mahaswa RK, Susanto H, Damat D, Roeswitawati D, Adinurani PG and Mindarti S. 2021b. Assessment on coffee cherry flour of Mengani Arabica Coffee, Bali, Indonesia as iron non-heme source. *Sarhad J. Agric*., **37(Special issue 1)**: 171–183. https://dx.doi.org/10.17582/journal.sja/2022.37.s1.171.183.

Setyobudi RH, Atoum MFM, Damat D, Yandri E, Nugroho YA, Susanti MS, Wahono SK, Widodo W, Zalizar L, Wahyudi A, Saati EA, Maftuchah M, Hussain Z, Yono D, Harsono SS, Mahaswa RK, Susanto H, Adinurani PG, Ekawati I, Fauzi A, Mindarti S. 2022. Evaluation of coffee pulp waste from some coffee cultivation areas in indonesia as iron booster. *Jordan J. Biol. Sci.,***15(3)**:475–488. https://doi.org/10.54319/jjbs/150318

SISPN. 2022. Waste management performance achievements. Kementrian Lingkungan Hidup dan Kehutanan. https://sipsn.menlhk.go.id/sipsn/

Solehah and Halimatus. 2016. Analysis of the calculation of cost of production of broiler chicken with full costing method on abshar farms as business partners of CV. Mutiara Sinar Abadi of Samarinda. *eJournal Ilmu Administrasi Bisnis.* **4(1)**:1–14.

Sugito and Mira D. 2016. Effect of heat stress on body weight gain, heterophile-lymphocite ratio and body temperature in broiler. *Jurnal Kedokteran Hewan Indonesia.* **3(1)**:218–226. https://doi.org/10.21157/j.ked.hewan.v3i1.3082.

Sulistiyanto B, Kismiati S and Utama CS. 2019. Production performance and immunomodulation effects on broiler given a processed wheat pollard based diet. *J. Vet.*, **20(3)**:352–359. https://doi.org/10.19087/jveteriner.2019.20.3.352.

Suloi ANF. 2019. Potential resisten starch prepared by banana – a review. *Jurnal Penelitian dan Pengembangan Agrokompleks*. **2(1)**:92–96.

Sun X, McElroy A, Webb KE, Sefton AE and Novac C. 2005. Broiler performance and intestinal alterations when fed drug-free diets. *Poult. Sci.,* **84(8)**:1294–1302. https://doi.org/10.1093/ps/84.8.1294.

Supartini N and Darmawan H. 2016. Utilization of rice snail (tutut) as duck feed supplementation to increase layer duck productivity in Simorejo-Bojonegoro village. *Buana Sains*, **16(1)**:1–8.

Suprayogi EJ, Zalizar L and Winaya A. 2021. The effect of grit administration on the macroscopic and microscopic appearance of starter phase broilers digestive tract. *IOP Conf. Ser. Earth Environ. Sci.,* **788(012087)**:1–6. https://doi.org/10.1088/17551315/788/1/012087.

Suprobo HY. 2021. Chicken farmers complain about the high price of feed. Harian Jogya. https://jogjapolitan.harianjogja.com/read/2021/05/06/514/1070958/peternak-ayam-keluhkan-mahalnya-harga-pakan

Susanto H. 2022. Expensive animal feed prices, breeders in Cilacap mix with "aking rice". Inews Jateng, https://jateng.inews.id/berita/harga-pakan-ternak-mahal-peternak-di-cilacap-mencampur-dengan-nasi-aking/2 .

Suwarta S, Irham I and Hartono S. 2012. Cost structure and revenue livestock broiler chickens in Sleman Regency. *Agrika*, **6(1)**:65–85.

Syukma YD. 2016. Cultivation and analysis of broiler chickens using vitamins and chickens that don't use vitamins (herbal chicken). *J. Nas. Ecopedon*, **3(1)**:77–82. https://doi.org/10.1016/j.tetlet.2007.02.128.

Tamzil MH. 2014. Heat stress in poultry: metabolism, effects and countermeasures. *Wartazoa*, **24(2)**:57–66.

Tuite MF, Cox BS and McLaughlin CS. 1987. A ribosome-associated inhibitor of in vitro nonsense suppression in [psi-] strains of yeast. *FEBS Lett.,* **225(1–2)**:205–208. https://doi.org/10.1016/0014-5793(87)81158-4.

Tumion B, Panelewen VVJ, Makalew A and Rorimpandey B. 2017. The effect of feed and labor costs on profits for laying chickens owned by Vony Kanaga in Tawaan village, Bitung city (case study). *Zootec.* **37(2)**:207–215. https://doi.org/10.35792/zot.37.2.2017.15800.

Umam M, Prayogi H and Nurgiartiningsih V. 2015. The performance of broiler rearing in system stage floor and double floor. *Jurnal Ilmu-Ilmu Peternakan.* **24(3)**:79–87.

Wahyudi A. 2008. **Get Fit with Fermented Milk**. UMM Press, Malang, Indonesia

Widiyaningrum P and Utami NR. 2014. Training in intensive drawing management of ducks in Wedung district, Demak regency. *Rekayasa*. **12(1)**:48–56.

Widodo W. 2009. Poultry feed security in the midst of a food crisis. *Jurnal Salam.* **12(1)**:107–125.

Widodo W, Rahayu ID, Sutanto A, Setyobudi RH and Mel M. 2019. The effectiveness of curcuma (*Curcuma xanthorriza* Roxb.) addition in the feed toward super Kampong chicken performances. *Proc. Pak. Acad. Sci.: B*, **56(4):** 39–46

Yafi M. 2021. Imported raw materials contribute 60-75 percent of feed material costs. Poultry Indonesia, https://www.poultryindonesia.com/bahan-baku-impor-menyumbang-60-75-persen-biaya-bahan-pakan/

Yemima Y. 2014. Business analysis of household-scale broiler chicken farms in Karya Bakti Village, Rungan subdistrict, Gunung Mas, Central Kalimantan. *Jurnal Ilmu Hewani Tropika*. **3(1)**:27–32.

Yendy SA, Mangisah I and Sukamto B. 2014. The effect of citric acids addition in diets as acidifier on calcium and phospor retention of the local male ducks. *Anim. Agric. J.*, **3**:70–78.

Zalizar L. 2010. The impact of giving levamisole hydrochloride on antibody titers after avian infulenza virus vaccination in layers. *Jurnal Ilmu-Ilmu Peternakan.* **20(1)**:86–91.

Zulfikar and Sania. 2014. Effect of substituting rice bran with "aking rice" flour in feed on broiler carcass quality. Undergraduate Thesis, Universitas Brawijaya, Malang, Indonesia.

JJBS

Volume 15, Number 5 ,December 2022
ISSN 1995-6673
Pages 887 – 892
https://doi.org/10.54319/jjbs/150518

Jordan Journal of Biological Sciences

The Potential of Cashew Apple Waste as a Slimming Agent

Asmawati Asmawati[1], Marianah Marianah[1], Manar Fayiz Mousa Atoum[2,3], Desy Ambar Sari[1,*], Irum Iqrar[4,5], Zahid Hussain[6], Roy Hendroko Setyobudi[7], and Nurhayati Nurhayati[1]

[1]*Department Agricultural Product Technology, Faculty of Agriculture, University of Muhammadiyah Mataram, Jl. KH. Ahmad Dahlan No. 1 Pagesangan Mataram 83127, West Nusa Tenggara, Indonesia;*[2]*Molecular Biology and Genetics, The Hashemite University, PO Box 330127, 13133 Zarqa, Jordan;*[3]*Department of Medical Laboratory Sciences, The Hashemite University, Zarqa, Jordan;* [4]*Department of Biotechnology, Quaid-i-Azam University, NCB Building Islamabad 45320, Pakistan;* [5]*Pakistan Academy of Sciences, 3 Constitution Ave, G-5/2, Islamabad Capital Territory, Pakistan;* [6]*The University of Agriculture, Peshawar, 25130, Khyber Pakhtunkhwa, Pakistan;*
[7]*Department of Agriculture Science, Postgraduate Program, University of Muhammadiyah Malang, Jl. Raya Tlogo Mas No. 246, Malang, 65145, East Java, Indonesia*

Received: Oct 18, 2022; Revised: Nov 12, 2022; Accepted Nov 17, 2022

ABSTRACT

The cashew apple (*Anacardium occidental* L.) is a tropical fruit that is a byproduct of the cashew nut processing industry. Rich in vitamins, polyphenols, sugars, minerals, amino acids, and dietary fiber, it contains bioactive compounds and several active components (ascorbic acid, anacardic acid, carotenoids, condensed tannins, quercetin, and other phenolic) that serve as antioxidants. This study aims to determine the effect of giving cashew apple juice and its nutritional impact on Wistar rats (*Rattus norvegicus* – Berkenhout 1769). The study adopted 21 male Wistar rats for 7 d fed with AIN 76 (American Institute of Nutrition 1976) diet, divided into three groups of seven rats. The first group was administered with fresh cashew apple juice treatment 0.14 % (CAJT 0.14 %), the second group with cashew apple juice 0.12 % (CAJT 0.12 %), and the last group with aquadest (Placebo) per day orally for 28 d. Employing an experimental method, variables of protein using Kjeldahl method, starch using the direct acid hydrolysis method, and calcium levels in the feces of experimental rats were observed. The data was obtained through analysis of variance, and differences among samples were tested using Least Significant Different (LSD). The results showed that CAJT 0.14 % significantly reduced protein digestibility (11.49 %) and starch feed (0.69 %) as well as weight rate by 78.85 g (38.34 %) while increased calcium excretion (0.44 %). CAJT 0.12 % followed at 11.36 %, 0.68%, 38.64 % (88.74 g), and 0.44 % respectively. Placebo was not affective towards research variables. The effect of consuming cashew apple juice regarding nutrient digestibility shows its potential for a commercial process as a functional food and a slimming agent, which answers the environmental need for waste utilization.

Keywords: *Anacardium occidentale* (L.), Bioactive compound, Caju, Functional food, *In vivo* test, *Rattus norvegicus* (Berkenhout, 1769), Tannin, Waste utilization.

1. Introduction

A tropical plant commonly found at an altitude of about 1 000 m above sea level, a cashew tree or *caju* (*Anacardium occidental* L.) can grow well on various types of soil, even the dry ones with poor nutrients (Runjala and Kella, 2017). The fruit produced by this plant consists of two edible parts: cashew nut and cashew apple – while the first is its actual fruit, the latter is pseudo fruit formed from an enlarged fruit stalk (Balandrán-Quintana *et al.,* 2019). Oliveira *et al*. (2020) have highlighted that cashew nut, the main commodity of the plant, represents only 10 % of the total fruit weight. So far, cashew apple has only been used as animal feed if not disposed of as waste (Aidoo *et al*., 2022). Several researchers (Gadikar *et al*., 2021; Prabhudessai *et al*., 2013; Setyobudi *et al*., 2021a) suggest using this waste as feedstock for biogas. However, considering the low pH, a two-stage digester technology is recommended (Abdullah *et al*., 2020; Hendroko *et al*., 2013).

Cashew apple contains water (83.6 g 100 g^{-1}) and nutritional substances such as vitamin C (126 mg 100 g^{-1} to 372 mg 100 g^{-1}), which is 6 to 7 times higher than in citrus fruits, dietary fiber (312 mg), carbohydrates (11.1 g), and calcium (0.9 mg 100 g^{-1} to 21.4 mg 100 g^{-1}) (Damasceno *et al*., 2008; Bhakyaraj and Singaravad, 2012); cashew apple should be able to serve as a good source of energy (Cristina *et al*., 2012; Honorato *et al*., 2007). Rich in bioactive compounds of polyphenols (gallic acid, protocatechuic acid, cryptoxanthin, zeinoxanthin, and lutein 214.8 mg 100 mL^{-1} to 215.1 mg 100 mL^{-1}) and organic acids (malic, citric, and lactic acids 0.1 g 100 g^{-1} to 0.36 g 100 g^{-1} (Sucupira *et al*., 2020), tannins 0.22 g 100 g^{-1} to 0.58 g 100 g^{-1} (Sobhana and Mathew, 2015), carotene 0.03 mg 100 g^{-1} to 0.74 mg 100 g^{-1} (Lopes *et al*., 2012), anacardic acid 1.1 g (Nambelaa *et al.,* 2022), the fruit is therefore packed with antioxidants (Andayanie *et*

* Corresponding author. e-mail: desyambars@gmail.com.

JJBS

Volume 15, number 5,December 2022
ISSN 1995-6673
Pages 893 – 896
https://doi.org/10.54319/jjbs/150519

Jordan Journal of Biological Sciences

Protein Level Efficacy in Improving Meat Nutritional Contents in Cross-bred Local Chickens Aged 0 Month to 2 Month

Wahyu Widodo[1,*], Aris Winaya[2], Lili Zalizar[3], Apriliana Devi Anggraini[4], Abdul Malik[5], Suyatno Suyatno[6], Muhammad Zahoor[7], and Maizirwan Mel[8]

[1]*Nutrition Laboratory University of Muhammadiyah Malang, Jl. Raya Tlogomas No 246, Malang 65144, East Java, Indonesia;* [2]*Genetic Laboratory University of Muhammadiyah Malang, Jl. Tegal Gondo No 245, Malang 65152, East Java, Indonesia;* [3]*Health Laboratory University of Muhammadiyah Malang, Jl. Raya Tlogomas No 246, Malang 65144, East Java, Indonesia;* [4]*Feed Laboratory University of Muhammadiyah Malang, Jl. Raya Tlogomas No 246, Malang 65144, East Java, Indonesia;* [5]*Poultry Production Laboratory University of Muhammadiyah Malang, Jl. Tegal Gondo No 245, Malang 65152, East Java, Indonesia;* [6]*Breding Laboratory University of Muhammadiyah Malang, Jl. Tegal Gondo No 245, Malang 65152, East Java, Indonesia;* [7]*Department of Biochemistry, University of Malakand, Chakdara, Lower Dir, 18800, Khyber Pakhtunkhwa, Pakistan;* [8]*Postgraduate School, Program Study of Biology, Menara Universitas Nasional Jl. RM. Harsono No.1, Special Region of Jakarta 12550, Indonesia*

Received: Oct 5, 2022; Revised: Dec 17, 2022; Accepted Dec 23, 2022

Abstract

Various types of local chickens (*Gallus gallus domesticus* Linnaeus, 1758) exist in Indonesia and are raised for their meat. Chicken meat is a favorite for its good taste, affordable price, higher protein content compared with other protein-containing agricultural products, and higher essential amino acids compared with non-poultry animals. This research was conducted from 6th December 2021 to 6th February 2022, worked in the cage installed explicitly in the precinct of the University of Muhammadiyah Malang, East Java, Indonesia. The research analyzed the dry meat matter, ash, protein, and fat contents in cross-bred chickens fed with different protein levels when aged 0 mo to 2 mo (mo = month). The research method was the experimental method. The research applied an experimental method with a randomized block design, involving four groups in each of the four treatments. T0, T1, T2, and T3 were fed with protein contents of 17 %, 18 %, 19 %, and 20 %, respectively. Analysis of variance (ANOVA) with a chance of Least Student Differences (LSD) test was employed to analyse the data. Conclusively, different protein levels in feed do not affect the nutrition contents such as dry meat matter, ash, protein, and fat contents formed in cross-bred local chickens. It is therefore suggested that the lowest protein content of 17 % for cross-bred local chickens aged 0 mo to 2 mo should be the most efficient.

Keywords: Domestic fowl, Feed efficiency, *Gallus gallus domesticus* (Linnaeus, 1758), Nutrition efficiency, Nutritional needs, Poultry, Productivity increase, Protein ratio

1. Introduction

Various local chickens, both native and adopted, have existed in Indonesia from tens to hundreds of years ago. Local chickens without special characteristics are referred to as native chickens, and they are generally raised in rural communities for their meat, eggs, or savings (Iriyanti *et al*., 2014). Three classes of local chickens are broiler (*pelung*, *nagrak*, *gaok*, *sedayu*), layer (black *kedu*, white *kedu*, *nusa penida*, *nunukan, merawang*, *wareng*, *sumatra*), and dual-purpose (*sentul, bangkalan, olagan, ayunai, melayu*, *siem*). Some other chickens are considered fighter (*banten, ciparage, tolaki*, *bangkok*) and ornamental (*pelung*, *gaok*, *tukung*, *burgo*, *bekisar*, *walik*) (Diwyanto *et al*., 2007). Finally, there are also cross-bred local chickens, which are the outcomes of cross-breeding male native chickens with female laying local chickens.

Feed is one of the important aspects of poultry (Wahyudi *et al*., 2021). Before this paper was completed, the nutritional needs of cross-bred local chickens were unknown. Since poultry feed quality is determined by its protein contents (Sabate *et al*., 2014; Wahju, 2015), it is safe to assume that adding various protein sources in feeds should help reveal the nutritional needs rates according to age. Bodyweight gain in livestock relies heavily on protein intake, and protein-based feed should contain complete amino acids in a balanced amount to ensure efficiency. The body will then absorb the amino acid to form the meat and increase its mass. The protein efficiency ratio will show the level of the coefficient of chicken to convert every gram of protein consumed into body weight gain (Bai *et al*., 2015; Khan, 2018).

Meat is a food source for humans as it is the most significant protein source compared to other protein-containing agricultural products (Sekhar *et al*., 2020). While chicken meat contains 18.71 % protein, tempeh has 18.44 %, and tofu 13.84 % (Sidadolog, 2006). Chicken meat is one of the people's favorite choices due to its good taste and affordable price, which drives the chicken meat consumption rate higher yearly. Since protein content in meat depends on protein consumption and amino acid balance in the feed (Gultom *et al*., 2016; Parolini *et al*., 2020), this research aims to find out if different protein levels in feed affect meat nutrition contents. Cross-bred

* Corresponding author. e-mail: *wahyu@umm.ac.id*

local chicken has become the focus of it since 2020 as potential laying native chicken, and the age range of 0 mo to 2 mo ((mo = month) is essential in the starter period.

2. Research Methods

This research was conducted from 6th December 2020 to 6th February 2021; worked in the cage installed explicitly in the precinct of the University of Muhammadiyah Malang, East Java, Indonesia, to study poultry. The materials were 80 cross-bred local chickens one-day-old with an average weight of 34.22 g. Variables studied were (i) meat dry matter content, (ii) meat ash content, (iii) meat protein content, and (iv) meat fat content by employing proximate analysis (Widodo, 2019). In detecting the meat dry matter content, the material samples of breast meat were dried in an oven (Memmert UN 30, Germany) at 105 °C to get rid of water and then calculated as per Equation (1):

$$\text{Dry matter content } (\%) = \left({(C - A)}/{B} \right) \times 100 \ \% \quad (1)$$

Descriptions:

A = Weight of empty container (g)
B = Sample weight (g)
C = Weight of container and sample after oven drying (g)

To discover the meat ash content, the material samples were kilned (Furnace Neytech Jff 2000, USA) at a temperature of 600 °C for 1 h and computed according to Equation (2):

$$\text{Ash content} = ((C - A)/B) \times 100 \ \% \quad (2)$$

Description:

A = Weight of empty container (g)
B = Sample weight (g)
C = Weight of container and sample after charring (g)

The three stages of the Kjeldahl method – digestion, distillation, and titration – were performed to observe the meat protein content. First, samples were boiled into solutions, and then the components in the solutions were separated before their concentrations were assessed by the following Equation (3):

$$\text{Crude Protein } (\%) = \text{Nitrogen Content } (N)(\%) \times 6.25 \quad (3)$$

Soxhlet extractor (Apparatus – 64826 Sigma-Aldrich Pte. Ltd.) was employed to determine the meat fat content. Each solvent containing fat was placed in the extractor and then heated in an oven at 105 °C to evaporate the solvent, leaving fat free of it. The crude fat content was then assessed in line with Equation (4):

$$\text{Fat content} = \left({(C - A)}/{B} \right) \times 100 \ \% \quad (4)$$

Descriptions:

A = Weight of empty fat container (g)
B = Sample weight (g)
C = Weight of fat container and sample after heating (g)

The research procedure has been approved by the Ethical Commission of the Faculty of Medicine, University of Muhammadiyah Malang (No.5.a/048.a /KEPK-UMM/III/2022) with an experimental method, randomized block design due to different types of cross-bred local chicken involved.

Four treatments were prepared, detailed as: T0 = feed with 17 % protein content, T1 = feed with 18 % protein content, T2 = feed with 19 % protein content, and T3 = feed with 20 % protein content (Fitasari *et al*., 2016). Each treatment was of four groups: K1 = male *wareng* with female *lurik*, K2 = male *ranupani* with female white *kedu*, K3 = male white *kedu* with female *ranupani*, and K4 = male *ranupani* with female *wareng*. Each group held five chickens. The data obtained were calculated using analysis of variance (ANOVA). Should there be a significant effect, Least Student Differences (LSD) test would be performed (Adinurani, 2016, 2022). The feed compositions for all treatments are detailes as per Table 1.

Table 1. Ingredients and nutrient content of feed

Feed ingredients	Treatment			
	T0	T1	T2	T3
CGM	2.00	3.23	4.45	5.68
DDGS	10.00	8.94	7.87	6.81
Fish meal (Menhaden)	1.90	2.27	2.63	3.00
MBM	5.20	5.13	5.07	5.00
Corn	49.65	47.55	45.45	43.35
Rice bran	22.57	22.32	22.06	21.81
Bone meal	0.10	0.07	0.03	0.00
soy sauce flour	5.20	7.17	9.15	11.12
Metionin	0.41	0.41	0.41	0.41
Lysin	0.29	0.28	0.26	0.25
Cooking oil	0.30	0.30	0.30	0.30
Salt	0.25	0.25	0.25	0.25
Herbal	1.00	1.00	1.00	1.00
Lime	1.13	1.08	1.02	0.97
Dicalcium phosphat	0.00	0.02	0.04	0.06
Total	100 %	100 %	100 %	100 %
Nutrient Feed				
ME	2900	2900	2900	2900
Protein	17.00	18.00	19.00	20.00
Fat	5.00	5.00	5.00	5.00
Crude Fiber	5.00	5.00	5.00	5.00
Ca	1.00	1.00	1.00	1.00
P	0.45	0.45	0.45	0.45
Na	0.15	0.15	0.15	0.15
Arginin	1.20	1.20	1.20	1.20
Histidin	2.00	2.00	2.00	2.00
Feed ingredients	Treatment			
	T0	T1	T2	T3
Isoleusin	0.60	0.60	0.60	0.60
Leusin	1.00	1.00	1.00	1.00
Lisin	1.10	1.10	1.10	1.10
Metionin	0.75	0.75	0.75	0.75
Fenilalanin	0.54	0.54	0.54	0.54
Treonin	0.68	0.68	0.68	0.68
Triptofan	0.17	0.17	0.17	0.17
Valin	0.62	0.62	0.62	0.62

3. Results and Discussion

The meat nutritional content findings in cross-bred local chickens fed with different protein levels are presented in Table 2 below.

Table 2. Meat nutritional contents in cross-bred local chickens fed with different protein levels

	Treatments (%)			
Variable	T1	T2	T3	T4
Dry matter	91.90 ± 1.92	93.95 ± 0.74	93.41 ± 1.42	92.58 ± 0.33
Ash	8.35 ± 2.88	9.19 ± 0.88	8.38 ± 1.40	8.72 ± 1.65
Protein	80.20 ± 2.81	82.06 ± 4.95	82.78 ± 2.46	82.04 ± 1.26
Fat	3.24 ± 2.00	2.41 ± 0.72	2.23 ± 1.03	2.15 ± 0.69

Poultry meat comprises food components, such as protein, fat, carbohydrates, vitamins, water, and minerals (Giannenas *et al.*, 2017). Meat quality depends on the amount of nutrients consumed, and the feed consumption rate is related to the property of the available feed. Moreover, feed compositions and other factors such as age, species, nation, sex, additives, slaughter weight or carcass weight, growth rate, type of livestock, and treatment before and after cutting also affect the meat characteristics. Further, post-cutting handling, storage, and preservation by withering, processing by cooling, freezing, drying, heating or cooking, and additives can influence the change of chemical composition in meat (Grashom and Serini, 2006).

Meat dry matter is the total feed ingredients other than water. Referring to Table 1, feeding with different protein levels does not significantly affect meat dry matter content ($P > 0.05$). The causative factors can be changes in environmental temperature, biosecurity systems, uncomfortable cage conditions, and high humidity. It is in line with Widodo *et al.* (2019) opinion that the most significant factors that affect the number of lymphocytes are high temperature, the environment, and stress. An increase in temperature reduces the weights of lymphoid thymus and bursa Fabricius, resulting in a lower number of lymphocytes which then impedes the digestive tract from working optimally.

Digestible dry matter and absorbable nutrient contents also have some bearing on the value of dry matter content in meat. According to Suryanto *et al.* (2009), the body does not absorb dry matter excreted in the feces. In this study, the amount of dry matter in the ration used was almost the same, so the results of the nutritional content in local chicken meat were relatively the same.

Meat ash is a group of mineral substances found in food or animal tissue determined by burning organic substances and then weighing the rest. Measuring ash content is a way to quantify the amount of mineral content in food (Daniel *et al.*, 2018; Niken, 2012). Table 1 indicates that feeding with different protein levels has no significant effect ($P > 0.05$) on meat ash content. Such an event may occur when the protein content in the feed is of low quality or when the protein mixture is of lower quantity than necessary. Mineral absorption often requires specific carrier proteins, of which synthesis plays an essential role in regulating bodily mineral levels. Transporting and storing minerals also demand specific binding to the carrier proteins; its deficiency should send lots of the minerals to the kidneys, digestive tract, and bile, which are then lost in secretions (Widodo *et al.*, 2021).

The most significant dry matter component in meat (Dhama *et al.*, 2011), protein is a complex organic substance with high molecular weight. Chicken meat contains high-quality protein because it is easily digested and absorbed; it also has a larger number of essential amino acids than non-poultry animals (Bai *et al.*, 2015). As revealed in Table 1, feeding different protein levels has no significant effect ($P > 0.05$) on meat protein content. That the different protein levels suffice to keep all treatments in normal conditions is the apparent cause. Hidayat (2017) and Rana *et al.* (2020) have stated that protein intake goes along with ration consumption, where the higher the protein value, the lower the ration conversion value. Furthermore, Gultom (2016) and Soglia *et al.* (2021) agree that high protein consumption affects protein absorption in meat and provides adequate amino acids to ensure normal cellular metabolism. While low protein treatment results in low meat protein content (Kartikasari *et al.*, 2001; Sutanto *et al.*, 2019), Anang (2017) and Iriyanti *et al.* (2014), it was emphasized that local chicken meat has decent nutritional values and high protein contents.

Meat fat is a high-energy food for every gram provides more energy than carbohydrates or protein (Ruben *et al.*, 2017). Fat also acts as insulation and protection in the tissues of the subcutaneous and around certain organs, solvent vitamins A, D, E, K, and food reserves in the body (Van, 2019). Table 1 shows that feeding different protein levels has no significant effect ($P > 0.05$) on meat fat content. This is due to the nearly identical nutritional content of the feed in each treatment, especially the additional herbs, so the crude fat digestibility levels are similar.

The low rates of crude fat digestibility happen when chickens avoid increasing the ambient temperature. Instead, feed is stored in the cache to be digested gradually later. When the cage is comfortable enough, chickens reduce the burden of digesting fat. While the increase in temperature and heat stress can reduce the digestibility of dry matter, crude protein, and carbohydrates, they are barely effective to fat digestibility (Tolimir *et al.*, 2010).

4. Conclusions and Suggestions

It was concluded that feed with different levels of protein does not present significant changes in dry matter, ash, protein, and fat contents of cross-bred local chicken meat. Therefore, the lowest feed protein content of 17 % for cross-breed local chickens aged 0 mo to 2 mo should be of the highest nutrition contents.

Acknowledgment

The authors would like to express their gratitude to the National Research and Innovation Agency of the Republic of Indonesia (BRIN), the Educational Fund Management Institution (LPDP), and the Ministry of Agriculture for funding this research under the National Research Priority Project Cooperation (7/EI/II/PRN/2020). In addition, the authors also wish to thank the Directorate of Research and Community Service and the Department of Animal Science of the Faculty of Agriculture and Animal Science of the University of Muhammadiyah Malang.

References

Adinurani PG. 2016. **Design and Analysis of Agrotrial Data: Manual and SPSS**. Plantaxia, Yogyakarta, Indonesia

Adinurani, PG. 2022. **Agrotechnology Applied Statistics** (compiled according to the semester learning plan). Deepublish, Yogyakarta, Indonesia

Anang A. and Suharyanto. 2007. **Harvest Chicken in 7 Weeks Free of Avian Influenza**. Penebar Swadaya, Depok, Indonesia.

Bai J, Greene E, Li W, Kidd MT, and Dridi S. 2015. Branched-chain amino acids modulate the expression of hepatic fatty acid metabolism-related genes in female broiler chickens. *Mol. Nutr. Food Res*., **59(6):** 1171–1181.

https://doi.org/10.1002/mnfr.201400918

Daniel S, Razvan-Mihail R, Ioan C and Georghe DM. 2018. Influence of feed particle size on chicken broilers performance. *Annals of the University of Oradea, Fascicle: Ecotoxicology, Animal Husbandry, and Food Science and Technology*, **17/B:** 257–262.

Dhama K, Verma V, Sawant PM, Tiwari R, Vaid RK and Chauhan RS. 2011. Applications of probiotics in poultry: Enhancing immunity and beneficial effects on production performances and health. *J. Immunol. Immunopathol.,* **13(1):** 1–19.

Diwyanto K, Sulandari S, Diwyanto K and Prijono SN. 2007. Diversity of Indonesia's local chicken biological resources: Benefits and potential, In: Diwyanto K and Prijono SN (Eds.). Pusat Penelitian Biologi - LIPI, Jakarta, Indonesia.

Fitasari E, Reo K and Nadia Niswi N. 2016. The use of different levels of protein in native chickens on the performance of protein production and digestibility. *Jurnal Ilmu-Ilmu Peternakan,* **26(2)**: 73–83. https://doi.org/10.21776/ub.jiip.2016.026.02.10

Giannenas I, Bonos E, Anestis V, Filioussis G, Papanastasiou DK, Bartzanas T, Papaioannou N, Tzora A and Skoufos I. 2017. Effects of protease addition and replacement of soybean meal by corn gluten meal on the growth of broilers and on the environmental performances of a broiler production system in Greece. *PloS One* **12(1):** 1–26.

https://doi.org/10.1371/journal.pone.0169511

Grashorn MA and Serini C. 2006. Quality of chicken meat from conventional and organic production. Proceedings of the 12th EPC. Verona, Italy.

Gultom EP, Wahyuni TH and Tafsin M. 2016. Digestibility of crude fiber and crude protein diet containing oil palm frond treated by physical, biological and chemical on sheep. *Jurnal Peternakan Integratif.,* **4(2):** 193–202.

https://doi.org/10.32734/jpi.v4i2.2795

Hidayat Z. 2017. The effect of adding feed additives with different doses in the ration on the performance of laying hens. Undergraduate Thesis. Lampung University, Lampung, Indonesia.

Iriyanti N, Santosa RSS and Rachmawati WS. 2014. Blood profile and performance of native chicken with functional feed. *Int. J. Poult. Sci.*, **13(11):** 645–651.

Kartikasari LR, Soeparno and Setiyono. 2001. Chemical composition and fatty acid studies of broiler breast meat receiving methionine supplementation on low protein feed. *Bulletin of Animal Science*. **25(1):** 33–39.

Khan HS. 2018. Recent advances in role of insects as alternative protein source in poultry nutrition. *J. Appl. Anim. Res.*, **46(1):** 1144–1157.

https://doi.org/10.1080/09712119.2018.1474743

Niken A. 2012. Performance of free-range chicken with broiler concentrate-based ration. *Jurnal Agrisains.* **3(5):** 51–58

Parolini M, Ganzaroli A and Bacenetti J. 2020. Earthworm as an alternative protein source in poultry and fish farming: Current applications and future perspectives. *Sci. Total Environ.*, **734:**1–25. https://doi.org/10.1016/j.scitotenv.2020.139460

Rana P, Tewatia BS, Jyotsana, Kumar R and Panwar VS. 2020. Effect of herbal methionine supplementation on growth performance and economics of broiler chicken. *J. Entomol. Zool. Stud.*, **8(6):** 2076–2081.

Ruben NT, Raphael KJ, Boris NT, Doriane YMD, Herve MK, Serges K, Alexis T and Ami M. 2017. Performances of broiler chicken fed on diet supplemented with thyme and oregano essential oils stabilized in a plant charchoal matrix. *J. World's Poult. Res.,* **7(2):** 79–87.

Sabate J, Sranacharoenpong K, Harwatt H, Wien M and Soret S. 2014. The environmental cost of protein food choices. *Public Health Nutr.*, **18(11):** 2067–2073

https://doi.org/10.1017/S1368980014002377

Sekhar SRM, Matt SG and Manvi SS. 2020. Prediction of protein secondary structure from amino acid sequences by integrating fuzzy, random forest and feature vector methodologies. *Jordan J. Biol. Sci*., **13(4)**: 483–492

Sidadolog P. 2006. Adjustment of different feeding time and protein energy content on feed efficiency and growth of broiler chickens. *Buletin Peternakan*. **30(3):** 126–135.

https://doi.org/10.21059/buletinpeternak.v30i3.1203

Sogila F, Zampiga M, Baldi G, Malila Y, Thanatsang KV, Srimarut Y, Petracci M, Tatiyaborworntham N, Unger O, Klamchuen A, Laghi L, and Sirri F. 2021. Lysine depletion during different feeding phases: Effects on growth performances and meat quality of broiler chickens. *Animals*. **11(6):** 1–16. https://doi.org/10.3390/ani11061499

Suryanto E, Sasongko H, Maryam M and Santosa R. 2009. The effect of type of feed and slaughter age on the performances and carcass characteristic of male Arab chicken. *J. Indones. Trop. Anim. Agric.*, **3(3):** 181–188.

Sutanto A, Widodo W and Rahayu ID. 2019. Developing organic feed stuff as the main component of broiler chickens' feed with canvas model in East Java: A case study of analysis on organic rice and corn in Malang and Tulungagung. *IOP Conf. Ser.: Mater. Sci.Eng*., **532(012022):**1–5**.** http://dx.doi.org/10.1088/1757-899X/532/1/012022

Tolimir N, Peric L, Milosevic N and Bogdanovic V. 2010. The effect of multiphase nutrition on production performances of broilers. *Biotechnol. Anim. Husb.*, **26(1–2):** 83–90

Van DP. 2019. Meat production performances of cay cum chickens in rations with different levels of metabolizable energy and crude protein with probiotics. MSc Theses Laguna State Polytechnic University, Siniloan, Laguna, Philippines .

Wahju J. 2015. **Poultry Nutrition Science.** Universitas Gadjah Mada Press, Yogyakarta, Indonesia

Wahyudi A, Pamungkas D, Setyobudi RH, Hendraningsih L and Vincēviča-Gaile Z. 2021. Organic acid and nutrient composition of lactic acid bacteria inoculated total mixed ration silage under tropical condition: organic acids and nutrients composition of Lactic Acid Bacteria. *Proc. Pak. Acad. Sci.: B*, **54(1):** 41–45.

Widodo W. 2019. **Poultry Livestock Nutrition Science**. UMM Press, Malang, Indonesia.

Widodo W, Rahayu ID, Sutanto A, Setyobudi RH and Mel M. 2019. The effectiveness of curcuma (*Curcuma xanthorriza* Roxb.) addition in the feed toward super Kampong chicken performances. *Proc. Pak. Acad. Sci.: B*, **56(4):** 39–46

Widodo W, Rahayu ID, Sutanto A, Anggraini AD, Sahara H,

Safitri S and Yaro A. 2021. *Curcuma xanthorriza* Roxb. as feed additive on the carcass and fat weight percentage, meat nutrient, and nutrient digestibility of Super Kampong Chicken. *Sarhad J. Agric.*, **37(1):** 41–4

al., 2019; Laddha *et al*., 2020). Specifically, chemically active components of ascorbic acid, anacardic acid, carotenoids, condensed tannins, quercetin, and other phenolic compounds are essential in anti-mutagenic mechanism (Onuh *et al*., 2017; Setyobudi *et al*. 2019) with an ability to stimulate DNA repair or reverse DNA damage. The details above should prove that cashew apple is nutritious and healthy to consume (Tai *et al*., 2020).

The other positive impact of consuming cashew apple juice is that it can reduce the concentration of total cholesterol, LDL triglycerides T6, and increase the concentration of HDL (cholesterol in the blood) (Asmawati *et al*., 2021; Carvalho *et al*., 2018). Several previous researches also reported the presence of tannin, which is known for its capacity to form insoluble complexes with macromolecules (proteins, fats, and carbohydrates) as well as micro-components (vitamins and minerals) to decrease availability and bioavailability (Emmanuelle *et al*., 2016; Setyobudi *et al*., 2021b and 2022; Soltan *et al*., 2013), Total tannin (hydrolysable) in cashew is about 0.64 mg 100 g^{-1} while condensed tannin is about 0.18 mg 100 g^{-1}. Tannins content are commonly known for protein binding and leather-forming activities. Apart from the ability to precipitate protein, tannin equally decreases digestibility and palatability (Aliyu and Hammed, 2008; Dabonne *et al*., 2015). High concentrations of these compounds were discovered in experimental animals' feces, consequently suppressing their growth and weight gain rates, which showed potential as slimming agents (Ebere *et al*., 2015; Menci *et al*., 2021). The above findings have become the bases of research on cashew apple juice's nutritional digestibility, aimed to see if it is possible to be a source of functional food serving as a slimming agent.

2. Materials and Methods

2.1. Materials

2.1.1. Cashew apple juice

The raw material of yellow-orange cashew apples was obtained from North Lombok, Indonesia. After sorted and washed, the fruit was blanched for 1 min to soften the texture and then extracted; the juice served as the first treatment with tannin content of 0.14 % (CAJT 0.14 %). As for the other treatment, the fruit was soaked in a calcium hydroxide solution [$Ca(OH_2)$ 3 %] for 15 min after washed and blanched, then extracted for its juice with tannin content of 0.12 % (CAJT 0.12 %).

Reducing tannin level from 0.14 % to 0.12 % was due to findings of a few researchers. Emmanuelle *et al*. (2016), Aliyu and Hammed (2008), Osagie and Eka (1998) reported that tannin equally decreased digestibility and palatability. Orak *et al*., (2012) and Setyobudi *et al*. (2022) stated that tannin bound protein, suppressed digestion by inhibiting key enzymes, and rendered iron and vitamin B12 unavailable.

2.1.2. Experimental animal

The animals involved in the experiment were Wistar male rats (*Rattus* norvegicus – Berkenhout 1769), 6 wk old with an average body weight of 104 g ± 8 g, obtained from the Experimental Animal Development Unit (UPHP) of Universitas Gadjah Mada, Yogyakarta, Indonesia. The rats were fed under the standard feed set by the American Institute of Nutrition 1976 (AIN 76) made in the nutritional laboratory of the Faculty of Agricultural Technology of Universitas Gadjah Mada, Yogyakarta, Indonesia.

2.2. Research Procedure

The research procedure has been approved by the Ethical Commission of the Faculty of Medicine of Al-Azhar Islamic University, West Nusa Tenggara, Indonesia (Number 29/EC/FK-06/UNIZAR/VIII/2020) and carried out consistent with the steps in Figure 1. First, the AIN 76 standard feed was allotted to determine the levels of protein, carbohydrates, calcium, and initial body weight of experimental rats before treatment administering. Then, 21 male Wistar rats were led to 7 d of adaptation, fed with AIN 76 and distilled drinking water. Once the period was over, the rats were divided into three equal groups:

- **Group 1** was given Cashew Apple Juice Treatment 0.14 % (CAJT 0.14 %) with tannin content.
- **Group 2** was assigned to drinking Cashew Apple Juice Treatment 0.12 % (CAJT 0.12 %) with reduced tannin content.
- **Group 3** was given aquadest (placebo group).

The aforementioned rats received cashew apple juice (0.14 % and 0.12 %) and aquadest of 2 mL d^{-1} two times a day (morning and evening) by force-feeding while still fed with AIN 76 standard meal for 28 d (4 wk). In addition, all rat feces collected during the study (28 d) were analyzed for their protein, carbohydrate, and calcium levels to determine digestibility.

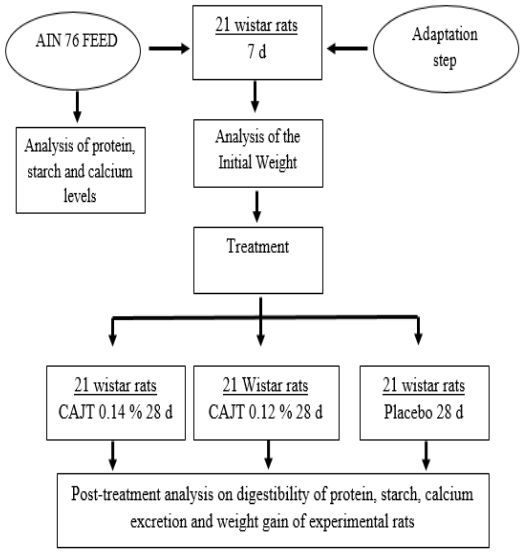

Figure 1. Scheme of the research

2.3. Measurement of research variables

2.3.1. Feed protein digestibility

Feed intake was weighed, and feces samples from the last 3 d (26 d to 28 d) were collected. To determine the effect of tannins on protein digestibility, 1 g of diet and feces samples were analyzed for nitrogen content using the micro Kjeldahl method (% N × 6.25). The 1 g of diet or feces sample was mixed with a digestion flask with 1.9 g ± 0.1 g potassium sulfate, 80 mg ± 10 mg mercuric oxide,

and 2 mL H_2SO_4. Boiling chips were added to digest the sample and turn the solution colorless. Once cooled, the digest was diluted with distilled ammonia-free water before being transferred to the distillation apparatus. The tip of a 10 mL conical flask containing 5 mL boric acid solution and drops of an indicator variant was dipped into the solution, and 10 mL of sodium hydroxide-sodium thiosulphate solution was inserted. The ammonia produced by the boric acid was distilled and collected. The emulsion was then titrated until a violet color appeared at the tip of the condenser and rinsed before the titration process. Next, the reagent blank was run with an equal volume of aqua dest to one of the titration results. Finally, the titration result volume was subtracted from the sample's original volume. The results were calculated per Equation (1) (Kara *et al*., 2018; Mæhre *et al*., 2018).

$$\text{Protein digestibility (\%)} = \frac{\text{N intake} - \text{N feces} \times 100}{\text{N intake}} \quad (1)$$

2.3.2. Feed starch digestibility

Feed intake was weighed, and feces samples from the last 3 d (26 d to 28 d) were collected. To determine the effect of tannins on starch digestibility, diet and feces samples were analyzed for starch content using the direct acid hydrolysis method (Kim *et al*., 2012; Kumar *et al*., 2022). Amount of 15 g dry basis of starch was added in a mixture of sulphuric acid and water (100 mL, 3.16 M), stirred, and left at a temperature of 35 °C for different lengths of time (0 d to 15 d). The solution was then cooled to 5 °C to recover non-hydrolyzed materials and centrifuged (6 000 *x g*) for 15 min. The precipitates formed during the process were rinsed with aqua dest to reach pH 7 (neutral), and the solid products were air-dried at 35 °C for 24 h before being stored in a sealed glass container at 4 °C. The hydrolysis recorded in the form of percentages were of suspended solids and dissolved non-hydrolyzed starch relative to the original starch solids, of which results were calculated as per Equation (2):

$$\text{Digestibility of starch (\%)} = \frac{\text{Starch intake} - \text{starch stool} \times 100}{\text{Starch intake}} \quad (2)$$

2.3.3. Calcium content

Calcium contained in diet and feces was determined quantitatively. 0.5 g of sample and 25 mL of 6 M HCl were mixed in a 250 mL beaker and boiled for approximately 30 men to make a 5 mL reduction. An amount of 5 mL of hot deionized water was added and boiled further, then filtered in a 50 mL volumetric flask. Deionized water was then mixed in to reach a 50 mL end solution. Ca content was analyzed using Buck Scientific 210VGP – Atomic Absorption Spectrophotometric (USA) at a wavelength of 422.2 nm (Nehad *et al*., 2018). This study's chemicals and reagents are classified as of analytical grade, purchased from Sigma Aldrich Chemical Co. (St Louis, Mo, USA).

2.4. Body Weight and Feed Intake

All rats were feed one time a day (morning), Each rat was provided with approximately 15 g fresh feed AIN 76 standard meal for 28 d (4 wk) using feeder jar to prevent it from being tilted or dislodged. Approximately 1 g to 2 g food remained when the feeder jar was removed and another jar provided at the same time on the subsequent day, providing the same amount for each day. During this period, body weight was measured every other day (Wolden *et al*., 2000; Serrano *et al*., 2017).

2.5. Data analysis

This research was conducted in proportion to the experimental method, and the plan was of completely randomized design. The data was obtained through analysis of variance, and differences among samples were tested using Least Significant Different (LSD) with the significance level set at $P < 0.05$ (Adinurani, 2016, 2022).

3. Results and Discussion

The overall results came out positive, meaning that cashew apple juice significantly affected the digestibility of protein and carbohydrates, absorption of calcium, and weight gain of experimental rats.

3.1. Protein digestibility

Table 1 shows how protein digestibility in experimental rats has decreased significantly after drinking cashew apple juice for 28 d.

Table 1. Protein digestibility of experimental rat with cashew apple juice

Treatment	Protein Digestibility Feed (%)	Protein Content Feces (%)
CAJT 0.14 %	33.05 b	11.49 a
CAJT 0.12 %	33.80 b	11.36 a
Placebo	52.39 a	8.17 b

Note: Numbers followed by the same letter in the same column are not significantly different at 5 %
CAJT 0.14 %: Pure Cashew Apple Juice
CAJT 0.12 %: Cashew Apple Juice with tannin reduction
Placebo: aqua dest

Feed's low protein digestibility rates were associated with high fecal protein contents. Cashew apple juice consumption has significantly increased the protein (nitrogen) contents in rat feces per trial due to the presence of tannins (CAJT 0.14 % and CAJT 0.12 %). An insoluble complex formed between protein and tannin inhibits protein digestibility (Osman and Gassem, 2013) and prevented the enzyme from breaking down, resulting in increased nitrogen removal through feces. This statement is compatible with the result of research by Kara *et al*. (2018).

3.2. Starch digestibility

Table 2 demonstrates how carbohydrate digestibility in experimental rats has decreased significantly after drinking cashew apple juice for 28 d. Yet, it is not as high as protein digestibility.

Table 2. Carbohydrate (starch) digestibility of experimental rat with cashew apple juice

Treatment	Carbohydrate digestibility Feed (%)	Carbohydrate content (starch) Feces (%)
CAJT 0.14 %	97.02 b	0.69 a
CAJT 0.12 %	97.05 b	0.68 a
Placebo	97.31 a	0.62 b

Note: Numbers followed by the same letter in the same column are not significantly different at 5 %
CAJT 0.14 %: Pure Cashew Apple Juice
CAJT 0.12 %: Cashew Apple Juice with tannin reduction
Placebo: aqua dest

The significant increases in stool starch in Group 1 and Group 2 are evident in low carbohydrate digestibility rates. That tannic acid essentially inhibits glucose absorption in experimental rats' intestines, thus increasing their fecal starch levels, which was compatible with the results of research conducted by Amoako and Awika (2016) and reported by Saha *et al*. (2018) that tannic acid and catechins could be associated with starch, resulting in decreased digestibility *in vitro*.

3.3. Calcium excretion

Table 3 records the significant increase of fecal calcium levels in experimental rats after drinking cashew apple juice for 28 d.

Table 3. Calcium excretion of experimental rat with cashew apple juice

Treatment	Ca cashew apple juice (%)	Ca content feces (%)
CAJT 0.14 %	0.23	0.44 a
CAJT 0.12 %	0.21	0.43 a
Placebo	-	0.39 b

Note: Numbers followed by the same letter in the same column are not significantly different at 5 %
CAJT 0.14 %: Pure Cashew Apple Juice
CAJT 0.12 %: Cashew Apple Juice with tannin reduction
Placebo: aqua dest

The high levels of calcium in the feces of Group 1 and Group 2 are evident that tannins can bind to calcium to form insoluble calcium-tanate; since the intestinal absorption of experimental rats was unable to absorb it, it was then excreted along with feces. This statement complies with Addisu (2016) that tannic acid could reduce the speed across the intestine due to the anti-nutritional inhibition of tannins. Further, the high loss of calcium through feces was due to decreased calcium absorption in the intestine triggered by the formation of complexes with tannins. This goes along with the assertion of Amalraj and Pius (2015) that calcium is very sensitive to even a tiny amount of tannins in feed or drink.

3.4. Rat weight gain

Table 4 logs the changes and percentages of experimental rats' weight gain after drinking cashew apple juice for 28 d.

Table 4. Weight gain of experimental rats with cashew apple juice

Treatment	Weekly weight gain (g)				
	0	I	II	III	IV
CAJT 0.14 %	126.81	142.37	166.47	186.10	205.66
CAJT 0.12 %	141.03	162.01	189.24	210.09	229.77
Placebo	112.14	133.17	164.69	187.74	213.63

CAJT 0.14 %: Pure Cashew Apple Juice
CAJT 0.12 %: Cashew Apple Juice with tannin reduction
Placebo: aqua dest

The result explains that the rats with cashew apple juice – both control and treatment – have lower weight gain rates than the placebo group. Focusing on the groups administered with cashew apple juice of different tannin contents, it is perceptible that the control group receiving more tannin has gained less weight than the treatment group. The ability of tannins to form insoluble complexes with protein (Table 1) and carbohydrates (Table 2) resulted in lower weight gain in rats. Details on weight gain percentage are revealed further in Table 5 below

Table 5. Weight gain percentage of experimental rats with cashew apple juice

Treatment	Weight Gain		Average Intake Feed (g d–1)
	%	g d–1	
CAJT 0.14 %	62.18 b	2.82 b	11.00 b
CAJT 0.12 %	62.92 b	3.17 ab	11.41 ab
Placebo	90.50 a	3.62 a	11.74 a

Note: Numbers followed by the same letter in the same column are not significantly different at 5 %
CAJT 0.14 %: Pure Cashew Apple Juice
CAJT 0.12 %: Cashew Apple Juice with tannin reduction
Placebo: aqua dest

The lowest weight gain occurred in the group treated with CAJT 0.14 % cashew apple juice at 62.18 % (78.85 g), followed by the group with CAJT 0.12 % at 62.92 % (88.74 g). In comparison, the placebo rat group was 90.50 % (101.49 g) and significantly different ($P < 0.05$). This corresponds to the low digestibility of protein (Table 2) and starch (Table 2) as a result of the occurrence of complexes with anti-nutritional compounds that can bind protein and carbohydrates and reduce the activity of digestive enzymes, causing the rat's body weight gain to be below optimal during the trial. This phenomenon is in line with the study of Rivera-Méndez *et al*. (2017), stating that tannins could affect experimental rats' growth and weight gain (Nwaneri *et al*., 2016).

The rats' feed intake was affected by the rats' weight gain, which was lower on average at 11.00 g (CAJT 0.14 %) and 11.41 g (CAJT 0.12 %), while the placebo rat group was higher at 11.74 g. The low feed intake of the experimental rats is thought to be due to the astringent taste in the cashew juice that affects the experimental rats' appetite.

4. Conclusion

The tannin content in cashew apple juice can cut off protein and starch digestibility, increase calcium excretion, and suppress the rate of weight gain. Therefore, the results confirm cashew apple's potential to be a slimming agent. How cashew apple juice diminishes appetite and how to develop cashew apples from waste to functional food can be subjects for further research.

References

Abdullah K, Uyun AS, Rahadi S, Suherman E, Susanto H., Setyobudi RH., Burlakovs J and Vincēviča-Gaile Z. 2020. Renewable energy technologies for economic development. *E3S Web of Conf.,* **188(00016)**: 1–8. https://doi.org/10.1051/e3sconf/202018800016

Addisu SH. 2016. Effect of dietary tannin source feeds on ruminal fermentation and production of cattle; a review. *Online Journal of Animal and Feed Research*, **6(2):**45–56.

Aidoo R, Kwofie EM and Ngadi MO. 2022. Circularity of cashew apples: examining the product-process pathways, techno-functional, nutritional/phytomolecular qualities for food applications. *ACS Food Sci. Technol*., **2(7)**: 1051–1066.

https://doi.org/10.1021/acsfoodscitech.2c00093

Adinurani PG. 2016. **Design and analysis of agrotrial data: Manual and SPSS**. Plantaxia, Yogyakarta, Indonesia.

Adinurani PG. 2022. **Agrotechnology Applied Statistics** (compiled according to the emester learning plan). Deepublish, Yogyakarta, Indonesia

Aliyu OM and Hammed LA. 2008. Nigerian cashew economy: A review of nut production sector. Paper presented at the International Academy of African Business and Development (IAABD) Conference. University of Florida, Gainesville, USA, May 20 – 24th, 2008.

Amalraj A and Pius A. 2015. In vitro study on the bioavailability of calcium and its absorption inhibitors in raw and cooked pulses commonly consumed in India. *Int. Food Res. J* ., **22(4)**: 1525–1532.

Amoako, DB and Awika JM. 2016. Polymeric tannins significantly alter properties and in vitro digestibility of partially gelatinized intact starch granule. *Food Chem.*, **208**:10–17. https://doi.org/10.1016/j.foodchem.2016.03.096

Andayanie WR, Nuriana W and Ermawaty N. 2019. Bioactive compounds and their their antifeedant activity in the cashew nut (*Anacardium occidentale* L.) shell extract against *Bemisia tabaci*, (Gennadius, 1889) (Hemiptera:Aleyrodidae). *Acta Agric. Slov.***113(2):** 281–288. https://doi.org/10.14720/aas.2019.113.2.9

Asmawati A, Marianah M, Yaro A and Setyobudi RH. 2021. The potential of cashew apple juice as anti hypercholesterol agent on whistar rats (*Rattus norvegicus* Berkenhout, 1769). *E3S Web Conf*., **226(00009**): 1–8. https://doi.org/10.1051/e3sconf/202122600009.

Balandrán-Quintana RR, Mendoza-Wilson AM, Ramos-Clamont MG and Huerta-Ocampo JA. 2019. Plant-based proteins.. In: Galanakis CM (Ed.). Chapter 4. **Proteins: Sustainable Source, Processing and Applications**. Academic Press, Cambridge, Massachusetts, USA. pp. 97–130 https://doi.org/10.1016/B978-0-12-816695-6.00004-0.

Bhakyaraj R and Singaravad K. 2012. Minerals and bioactive compounds in cashew apple (*Anacardium occidentale* L.) *J. Food Resour. Sci.,* **1(2)**: 32–36. https://doi.org/10.3923/jfrs.2012.32.36.

Carvalho DV, Santos FA, Lima RP, Viana AFSC, Fonseca SGC, Nunes PIG, de Melo T., Gallão, MI and de Brito ES. 2018. Influence of low molecular weight compounds associated to cashew (Anacardium occidentale L.) fiber on lipid metabolism, glycemia and insulinemia of normal mice. *Bioact. Carbohydr. Diet. Fibre*., **13***:*1–6. https://doi.org/10.1016/j.bcdf.2017.12.001.

Cristina F, Luiz HSF, Palmeira GJ and Mariano SNJ. 2012. Chemical composition of the cashew apple bagasse and potential use for ethanol production. *Adv. Chem. Engineer. Sci*., **(4):**519–523. https://doi.org/10.4236/aces.2012.24064

Damasceno LF, Fernandes FAN, Magalhães, MMA and Brito ES. 2008. Evaluation and optimization of non enzymatic browning of "cajuina" during thermal treatment. *Braz. J. Chem. Eng*.**25(2)**: 313–320. https://doi.org/10.1590/S0104-66322008000200010.

Ebere CO, Emelike NJT and Kiin-Kabari DB. 2015. Physico-chemical and sensory properties of cookies prepared from wheat flour and cashew-apple residue as a source of fibre. *Asian J. Agric. Sci*., **3(2)**: 213–218.

Emmanuelle D, Joseph D, Victor, A and Mohamed MS. 2016. A review of cashew (*Anacardium occidentale* L.) apple: Effects of processing techniques, properties and quality of juice. *Afr. J. Biotechnol*., **15(47)**: 2637–2648. https://doi.org/10.5897/ajb2015.14974

Gadikar AA, Gadade SR, and Mohod AG. 2021. Study of biogas generation from cashew apple waste. *MSIBM Interdisciplinary Journal of Management & Research*, 1:42–47

Hendroko R, Liwang T, Adinurani PG, Nelwan LO, Sakri Y and Wahono SK. 2013. The modification for increasing productivity at hydrolysis reactor with *Jatropha curcas* Linn. capsule husk as bio-methane feedstocks at two-stage digestion. *Energy Procedia* **32**:47–54. https://doi.org/10.1016/j.egypro.2013.05.007

Honorato TL, Rabelo MC, Gonçalves LRB, Pinto GAS and Rodrigues S. 2007. Fermentation of cashew apple juice to produce high added value products. *World J. Microbiol. Biotechnol*., **23**:1409–1415. https://doi.org/10.1007/s11274-007-9381-z

Kara K, Guclu BK, Baytok E, Aktug E, Oguz FK, Kamalak A and Atalay AI. 2018. Investigation in terms of digestive values, silages quality and nutrient content of the using pomegranate pomace in the ensiling of apple pomace with high moisture contents. *J. Appl. Anim. Res*., **46(1)**:1233–1241. https://doi.org/10.1080/09712119.2018.1490300.

Kim HY, Lee JH, Kim JY, Lim WJ and Lim ST. 2012. Characterization of nanoparticles prepared by acid hydrolysis of various starches. Starch/Stärke, **64**: 367–373.

Kumar A, Lal MK, Nayak S, Sahoo U, Behera A, Bagchi TB, Parameswaran C, Swain P and Sharma S. 2022. Effect of parboiling on starch digestibility and mineral bioavailability in rice (*Oryza sativa* L.). *LWT*, **156(113026)**:1–9.. https://doi.org/10.1016/j.lwt.2021.113026.

Laddha AP, Adki KM, Gaikwad AB and Kulkarni YA. 2020. Beneficial effects of nuts from india in cardiovascular disorders. In: Preedy VR and Watson RR (Eds.). Chapter 32, **Nuts and Seeds in Health and Disease Prevention** (Second Edition). Academic Press Cambridge, Massachusetts, USA pp. 453-469. https://doi.org/10.1016/B978-0-12-818553-7.00032-2

Lopes MM, De A, Miranda MRA, Moura CFH and Enéas FJ. 2012. Bioactive compounds and total antioxidant capacity of cashew apples (Anacardium occidentale L.) during the ripening of early dwarf cashew clones. *Cienc. e Agrotecnologia*, **36(3)**:325–332. https://doi.org/10.1590/s1413-70542012000300008.

Mæhre HK, Dalheim L, Edvinsen GK, Elvevoll EO and Jensen IJ. 2018. Protein determination—method matters. *Foods*, **7(5):**1–11. https://doi.org/10.3390/foods7010005.

Menci R, Coppa M, Torrent A, Natalello A, Valenti B, Luciano G, Priolo, A, and Niderkorn V. 2021. Effects of two tannin extracts at different doses in interaction with a green or dry forage substrate on in vitro rumen fermentation and biohydrogenation *Anim. Feed Sci. Technol*., **278:**114977.
https://doi.org/10.1016/j.anifeedsci.2021.114977.

Nambelaa L, Haulea LV and Mgani QA. 2022. Anacardic acid isolated from cashew nut shells liquid: A potential precursor for the synthesis of anthraquinone dyes. *Cleaner Chemical Engineering* **3(100056)**:1–10.

https://doi.org/10.1016/j.clce.2022.100056

Nehad KA, Luma AM and Amal MS. 2018. Determination of macro and microelements in medicinal plant purslane (*Portulaca oleracea* L.) by atomic absorption spectrophotometric (AAS) and flame photometric techniques. *Al Mustansiriyah Journal of Pharmaceutical Sciences*, **18(2):**51–57.
https://doi.org/10.32947/ajps.18.02.0374.

Nwaneri CVO, Idoko VO and Salemcity AJ. 2016. Assessment of antioxidant activity of ethanol and n-hexane seed extracts of *Annona muricata* in rats. *Jordan J. Biol. Sci*, **9(4):** 234–241.

Oliveira NN, Mothé CG, Mothé MG and Oliveira LG. 2020. Cashew nut and cashew apple: a scientific and technological monitoring worldwide review. *J. Food Sci. Technol*., **57(1):** 12–21. https://doi.org/10.1007/s13197-019-04051-7.

Onuh OJ, Idoko G, Yusufu P and Onuh F. 2017. Comparative Studies of the Phytochemical, antioxidant and antimicrobial properties of cashew leaf, bark and fruits extracts. *American Journal of Food and Nutrition*, **5(4):** 115–120. https://doi.org/:10.12691/ajfn-5-4-1.

Orak HH, Yagar H and Isbilir SS. 2012. Comparison of antioxidant activities of juice, peel, and seed of pomegranate (Punica granatum L.) and inter-relationships with total phenolic, tannin, anthocyanin, and flavonoid contents. *Food Sci. Biotechnol*., **21(2):** 373–387. https://doi.org/10.1007/s10068-012-0049-

Osagie AU and Eka OU. 1998. **Nutritional Qualities of Plant Foods**. University of Benin, Benin City, Nigeria.

Osman MA and Gassem M. 2013. Effects of domestic processing on trypsin inhibitor, phytic, acid, tannins and in-vitro protein digestibility of three sorghum varieties. *J. Agric. Sci. Technol*., **9(5):**1187–1198.

Prabhudessai, V, Ganguly A and Mutnuri S. 2013. Biochemical methane potential of agro wastes. *J. Energy*, **ID 350731**: 1–7. https://doi.org/10.1155/2013/350731

Rivera MC, Plascencia A, Torrentera N and Zinn RA. 2017. Effect of level and source of supplemental tannin on growth performance of steers during the late finishing phase. *J. Appl. Anim. Res*.**45(1)**: 199–203.

https://doi.org/10.1080/09712119.2016.1141776

Runjala S and Kella L. 2017. Cashew apple (Anacardium occidentale L.) therapeutic benefits, processing and product development: An over view. *J. Pharm. Innov*., **69(7)**: 260–264.

Saha S, Islam Z, Islam S, Hassan MF, Hossain MS and Islam SMS. 2018. Determination of antioxidant properties and the bioactive compounds in wheat (*Triticum aestivum* L.). *Jordan J. Biol. Sci*., **11(3)**: 315–321.

Serrano J, Casanova MÀ, Gual A, Pérez-Vendrell AM, Blay MT, Terra X, Ardévol A and Pinent M. 2017. A specific dose of grape seed-derived proanthocyanidins to inhibit body weight gain limits food intake and increases energy expenditure in rats. *European Journal of Nutrition*, ***56*(4)**, 1629–1636.
https://doi.org/10.1007/s00394-016-1209-x

Setyobudi RH, Zalizar L, Wahono SK, Widodo W, Wahyudi A, Mel M, Prabowo B, Jani Y, Nugroho YA, Liwang T and Zaebudin A. 2019. Prospect of Fe non-heme on coffee flour made from solid coffee waste: Mini review. *IOP Conf. Ser. Earth Environ. Sci*., **293 (012035)**:1–24. https://doi.org/10.1088/1755-1315/293/1/012035

Setyobudi RH, Yandri E, Atoum MFM, Nur SM, Zekker I, Idroes R, Tallei TE, Adinurani PA, Vincēviča-Gaile Z, Widodo W, Zalizar L, Van Minh N, Susanto H, Mahaswa RK, Nugroho YA, Wahono SK and Zahriah Z. 2021a. Healthy-smart concept as standard design of kitchen waste biogas digester for urban households. *Jordan J. Biol. Sci*. **14(3):** 613–620
https://doi.org/10.54319/jjbs/140331

Setyobudi RH, Yandri E, Nugroho YA, Susanti MS, Wahono SK, Widodo W, Zalizar L, Saati EA, Maftuchah M, Atoum MFM, Massadeh MI, Yono D, Mahaswa RK, Susanto H, Damat D, Roeswitawati D, Adinurani PG and Mindarti S. 2021b. Assessment on coffee cherry flour of Mengani Arabica Coffee, Bali, Indonesia as iron non-heme source. *Sarhad J. Agric*., **37(Special issue 1)** : 171–183.
https://dx.doi.org/10.17582/journal.sja/2022.37.s1.171.183

Setyobudi HS, Atoum MFM, Damat D, Yandri E, Nugroho YA, Susanti MS, Wahono SK, Widodo W, Zalizar L, Wahyudi A, Saati EA, Maftuchah M, Hussain Z, Yono D, Harsono SS, Mahaswa RK, Susanto H, Adinurani PA, Ekawati I, Fauzi A and Mindarti S. 2022. Evaluation of coffee pulp waste from coffee cultivation areas in Indonesia as iron booster. *Jordan J. Biol. Sci*., **15(3):**475– 488. https://doi.org/10.54319/jjbs/150318

Sobhana A and Mathew J. 2015. Vinegar production from cashew apple. *International Journal of Processing and Post Harvest Technology*, **6(2**): 150–156.

Soltan YA, Morsy AS, Sallam SMA, Lucas RC, Louvandini H, Kreuzer M and Abdalla AL. 2013. Contribution of condensed tannins and mimosine to the methane mitigation caused by feeding *Leucaena leucocephala*. *Arch. Anim. Nutr*., **67(3)**: 169–184. https://doi.org/10.1080/1745039X.2013.801139

Sucupira NR, Sabino LB. de S, Gondim NL, Gouveia ST, Figueiredo RW, de Maia GA and Sousa PHM. 2020. Evaluation of cooking methods on the bioactive compounds of cashew apple fibre and its application in plant-based foods. *Heliyon*, **6(11)**:1–9**.** https://doi.org/10.1016/j.heliyon.2020.e05346

Tai VA, Tuan BQ, Thuy VTT and Trach N X. 2020. Use of cashew apple fruit silage in the cattle fattening diet. *Livest. Res. Rural. Dev*., **32(5).**

Wolden-Hanson T, Mitton DR, McCants RL, Yellon SM, Wilkinson CW, Matsumoto AM, and Rasmussen, DD. 2000. Daily melatonin administration to middle-aged male rats suppresses body weight, intraabdominal adiposity, and plasma leptin and insulin independent of food intake and total body fat. *Endocrinology*, **141(2)**, 487–497.
https://doi.org/10.1210/endo.141.2.7311.

JJBS

Volume 15, number 5,December 2022
ISSN 1995-6673
Pages 893 – 896
https://doi.org/10.54319/jjbs/150519

Jordan Journal of Biological Sciences

Protein Level Efficacy in Improving Meat Nutritional Contents in Cross-bred Local Chickens Aged 0 Month to 2 Month

Wahyu Widodo[1,*], Aris Winaya[2], Lili Zalizar[3], Apriliana Devi Anggraini[4], Abdul Malik[5], Suyatno Suyatno[6], Muhammad Zahoor[7], and Maizirwan Mel[8]

[1]*Nutrition Laboratory University of Muhammadiyah Malang, Jl. Raya Tlogomas No 246, Malang 65144, East Java, Indonesia;* [2]*Genetic Laboratory University of Muhammadiyah Malang, Jl. Tegal Gondo No 245, Malang 65152, East Java, Indonesia;* [3]*Health Laboratory University of Muhammadiyah Malang, Jl. Raya Tlogomas No 246, Malang 65144, East Java, Indonesia;* [4]*Feed Laboratory University of Muhammadiyah Malang, Jl. Raya Tlogomas No 246, Malang 65144, East Java, Indonesia;* [5]*Poultry Production Laboratory University of Muhammadiyah Malang, Jl. Tegal Gondo No 245, Malang 65152, East Java, Indonesia;* [6]*Breding Laboratory University of Muhammadiyah Malang, Jl. Tegal Gondo No 245, Malang 65152, East Java, Indonesia;* [7]*Department of Biochemistry, University of Malakand, Chakdara, Lower Dir, 18800, Khyber Pakhtunkhwa, Pakistan;* [8]*Postgraduate School, Program Study of Biology, Menara Universitas Nasional Jl. RM. Harsono No.1, Special Region of Jakarta 12550, Indonesia*

Received: Oct 5, 2022; Revised: Dec 17, 2022; Accepted Dec 23, 2022

Abstract

Various types of local chickens (*Gallus gallus domesticus* Linnaeus, 1758) exist in Indonesia and are raised for their meat. Chicken meat is a favorite for its good taste, affordable price, higher protein content compared with other protein-containing agricultural products, and higher essential amino acids compared with non-poultry animals. This research was conducted from 6th December 2021 to 6th February 2022, worked in the cage installed explicitly in the precinct of the University of Muhammadiyah Malang, East Java, Indonesia. The research analyzed the dry meat matter, ash, protein, and fat contents in cross-bred chickens fed with different protein levels when aged 0 mo to 2 mo (mo = month). The research method was the experimental method. The research applied an experimental method with a randomized block design, involving four groups in each of the four treatments. T0, T1, T2, and T3 were fed with protein contents of 17 %, 18 %, 19 %, and 20 %, respectively. Analysis of variance (ANOVA) with a chance of Least Student Differences (LSD) test was employed to analyse the data. Conclusively, different protein levels in feed do not affect the nutrition contents such as dry meat matter, ash, protein, and fat contents formed in cross-bred local chickens. It is therefore suggested that the lowest protein content of 17 % for cross-bred local chickens aged 0 mo to 2 mo should be the most efficient.

Keywords: Domestic fowl, Feed efficiency, *Gallus gallus domesticus* (Linnaeus, 1758), Nutrition efficiency, Nutritional needs, Poultry, Productivity increase, Protein ratio

1. Introduction

Various local chickens, both native and adopted, have existed in Indonesia from tens to hundreds of years ago. Local chickens without special characteristics are referred to as native chickens, and they are generally raised in rural communities for their meat, eggs, or savings (Iriyanti *et al*., 2014). Three classes of local chickens are broiler (*pelung*, *nagrak*, *gaok*, *sedayu*), layer (black *kedu*, white *kedu*, *nusa penida*, *nunukan, merawang*, *wareng*, *sumatra*), and dual-purpose (*sentul, bangkalan, olagan, ayunai, melayu*, *siem*). Some other chickens are considered fighter (*banten, ciparage, tolaki*, *bangkok*) and ornamental (*pelung*, *gaok*, *tukung*, *burgo*, *bekisar*, *walik*) (Diwyanto *et al*., 2007). Finally, there are also cross-bred local chickens, which are the outcomes of cross-breeding male native chickens with female laying local chickens.

Feed is one of the important aspects of poultry (Wahyudi *et al*., 2021). Before this paper was completed, the nutritional needs of cross-bred local chickens were unknown. Since poultry feed quality is determined by its protein contents (Sabate *et al*., 2014; Wahju, 2015), it is safe to assume that adding various protein sources in feeds should help reveal the nutritional needs rates according to age. Bodyweight gain in livestock relies heavily on protein intake, and protein-based feed should contain complete amino acids in a balanced amount to ensure efficiency. The body will then absorb the amino acid to form the meat and increase its mass. The protein efficiency ratio will show the level of the coefficient of chicken to convert every gram of protein consumed into body weight gain (Bai *et al*., 2015; Khan, 2018).

Meat is a food source for humans as it is the most significant protein source compared to other protein-containing agricultural products (Sekhar *et al*., 2020). While chicken meat contains 18.71 % protein, tempeh has 18.44 %, and tofu 13.84 % (Sidadolog, 2006). Chicken meat is one of the people's favorite choices due to its good taste and affordable price, which drives the chicken meat consumption rate higher yearly. Since protein content in meat depends on protein consumption and amino acid balance in the feed (Gultom *et al*., 2016; Parolini *et al*., 2020), this research aims to find out if different protein levels in feed affect meat nutrition contents. Cross-bred

* Corresponding author. e-mail: *wahyu@umm.ac.id*

local chicken has become the focus of it since 2020 as potential laying native chicken, and the age range of 0 mo to 2 mo ((mo = month) is essential in the starter period.

2. Research Methods

This research was conducted from 6th December 2020 to 6th February 2021; worked in the cage installed explicitly in the precinct of the University of Muhammadiyah Malang, East Java, Indonesia, to study poultry. The materials were 80 cross-bred local chickens one-day-old with an average weight of 34.22 g. Variables studied were (i) meat dry matter content, (ii) meat ash content, (iii) meat protein content, and (iv) meat fat content by employing proximate analysis (Widodo, 2019). In detecting the meat dry matter content, the material samples of breast meat were dried in an oven (Memmert UN 30, Germany) at 105 °C to get rid of water and then calculated as per Equation (1):

$$\text{Dry matter content } (\%) = \left({(C - A)}/{B} \right) \times 100 \ \% \quad (1)$$

Descriptions:

A = Weight of empty container (g)
B = Sample weight (g)
C = Weight of container and sample after oven drying (g)

To discover the meat ash content, the material samples were kilned (Furnace Neytech Jff 2000, USA) at a temperature of 600 °C for 1 h and computed according to Equation (2):

$$\text{Ash content} = ((C - A)/B) \times 100 \ \% \quad (2)$$

Description:

A = Weight of empty container (g)
B = Sample weight (g)
C = Weight of container and sample after charring (g)

The three stages of the Kjeldahl method – digestion, distillation, and titration – were performed to observe the meat protein content. First, samples were boiled into solutions, and then the components in the solutions were separated before their concentrations were assessed by the following Equation (3):

$$\text{Crude Protein } (\%) = \text{Nitrogen Content } (N)(\%) \times 6.25 \quad (3)$$

Soxhlet extractor (Apparatus – 64826 Sigma-Aldrich Pte. Ltd.) was employed to determine the meat fat content. Each solvent containing fat was placed in the extractor and then heated in an oven at 105 °C to evaporate the solvent, leaving fat free of it. The crude fat content was then assessed in line with Equation (4):

$$\text{Fat content} = \left({(C - A)}/{B} \right) \times 100 \ \% \quad (4)$$

Descriptions:

A = Weight of empty fat container (g)
B = Sample weight (g)
C = Weight of fat container and sample after heating (g)

The research procedure has been approved by the Ethical Commission of the Faculty of Medicine, University of Muhammadiyah Malang (No.5.a/048.a /KEPK-UMM/III/2022) with an experimental method, randomized block design due to different types of cross-bred local chicken involved.

Four treatments were prepared, detailed as: T0 = feed with 17 % protein content, T1 = feed with 18 % protein content, T2 = feed with 19 % protein content, and T3 = feed with 20 % protein content (Fitasari *et al*., 2016). Each treatment was of four groups: K1 = male *wareng* with female *lurik*, K2 = male *ranupani* with female white *kedu*, K3 = male white *kedu* with female *ranupani*, and K4 = male *ranupani* with female *wareng*. Each group held five chickens. The data obtained were calculated using analysis of variance (ANOVA). Should there be a significant effect, Least Student Differences (LSD) test would be performed (Adinurani, 2016, 2022). The feed compositions for all treatments are detailes as per Table 1.

Table 1. Ingredients and nutrient content of feed

Feed ingredients	Treatment			
	T0	T1	T2	T3
CGM	2.00	3.23	4.45	5.68
DDGS	10.00	8.94	7.87	6.81
Fish meal (Menhaden)	1.90	2.27	2.63	3.00
MBM	5.20	5.13	5.07	5.00
Corn	49.65	47.55	45.45	43.35
Rice bran	22.57	22.32	22.06	21.81
Bone meal	0.10	0.07	0.03	0.00
soy sauce flour	5.20	7.17	9.15	11.12
Metionin	0.41	0.41	0.41	0.41
Lysin	0.29	0.28	0.26	0.25
Cooking oil	0.30	0.30	0.30	0.30
Salt	0.25	0.25	0.25	0.25
Herbal	1.00	1.00	1.00	1.00
Lime	1.13	1.08	1.02	0.97
Dicalcium phosphat	0.00	0.02	0.04	0.06
Total	100 %	100 %	100 %	100 %
Nutrient Feed				
ME	2900	2900	2900	2900
Protein	17.00	18.00	19.00	20.00
Fat	5.00	5.00	5.00	5.00
Crude Fiber	5.00	5.00	5.00	5.00
Ca	1.00	1.00	1.00	1.00
P	0.45	0.45	0.45	0.45
Na	0.15	0.15	0.15	0.15
Arginin	1.20	1.20	1.20	1.20
Histidin	2.00	2.00	2.00	2.00
Feed ingredients	Treatment			
	T0	T1	T2	T3
Isoleusin	0.60	0.60	0.60	0.60
Leusin	1.00	1.00	1.00	1.00
Lisin	1.10	1.10	1.10	1.10
Metionin	0.75	0.75	0.75	0.75
Fenilalanin	0.54	0.54	0.54	0.54
Treonin	0.68	0.68	0.68	0.68
Triptofan	0.17	0.17	0.17	0.17
Valin	0.62	0.62	0.62	0.62

3. Results and Discussion

The meat nutritional content findings in cross-bred local chickens fed with different protein levels are presented in Table 2 below.

Table 2. Meat nutritional contents in cross-bred local chickens fed with different protein levels

	Treatments (%)			
Variable	T1	T2	T3	T4
Dry matter	91.90 ± 1.92	93.95 ± 0.74	93.41 ± 1.42	92.58 ± 0.33
Ash	8.35 ± 2.88	9.19 ± 0.88	8.38 ± 1.40	8.72 ± 1.65
Protein	80.20 ± 2.81	82.06 ± 4.95	82.78 ± 2.46	82.04 ± 1.26
Fat	3.24 ± 2.00	2.41 ± 0.72	2.23 ± 1.03	2.15 ± 0.69

Poultry meat comprises food components, such as protein, fat, carbohydrates, vitamins, water, and minerals (Giannenas *et al.*, 2017). Meat quality depends on the amount of nutrients consumed, and the feed consumption rate is related to the property of the available feed. Moreover, feed compositions and other factors such as age, species, nation, sex, additives, slaughter weight or carcass weight, growth rate, type of livestock, and treatment before and after cutting also affect the meat characteristics. Further, post-cutting handling, storage, and preservation by withering, processing by cooling, freezing, drying, heating or cooking, and additives can influence the change of chemical composition in meat (Grashom and Serini, 2006).

Meat dry matter is the total feed ingredients other than water. Referring to Table 1, feeding with different protein levels does not significantly affect meat dry matter content ($P > 0.05$). The causative factors can be changes in environmental temperature, biosecurity systems, uncomfortable cage conditions, and high humidity. It is in line with Widodo *et al.* (2019) opinion that the most significant factors that affect the number of lymphocytes are high temperature, the environment, and stress. An increase in temperature reduces the weights of lymphoid thymus and bursa Fabricius, resulting in a lower number of lymphocytes which then impedes the digestive tract from working optimally.

Digestible dry matter and absorbable nutrient contents also have some bearing on the value of dry matter content in meat. According to Suryanto *et al.* (2009), the body does not absorb dry matter excreted in the feces. In this study, the amount of dry matter in the ration used was almost the same, so the results of the nutritional content in local chicken meat were relatively the same.

Meat ash is a group of mineral substances found in food or animal tissue determined by burning organic substances and then weighing the rest. Measuring ash content is a way to quantify the amount of mineral content in food (Daniel *et al.*, 2018; Niken, 2012). Table 1 indicates that feeding with different protein levels has no significant effect ($P > 0.05$) on meat ash content. Such an event may occur when the protein content in the feed is of low quality or when the protein mixture is of lower quantity than necessary. Mineral absorption often requires specific carrier proteins, of which synthesis plays an essential role in regulating bodily mineral levels. Transporting and storing minerals also demand specific binding to the carrier proteins; its deficiency should send lots of the minerals to the kidneys, digestive tract, and bile, which are then lost in secretions (Widodo *et al.*, 2021).

The most significant dry matter component in meat (Dhama *et al.*, 2011), protein is a complex organic substance with high molecular weight. Chicken meat contains high-quality protein because it is easily digested and absorbed; it also has a larger number of essential amino acids than non-poultry animals (Bai *et al.*, 2015). As revealed in Table 1, feeding different protein levels has no significant effect ($P > 0.05$) on meat protein content. That the different protein levels suffice to keep all treatments in normal conditions is the apparent cause. Hidayat (2017) and Rana *et al.* (2020) have stated that protein intake goes along with ration consumption, where the higher the protein value, the lower the ration conversion value. Furthermore, Gultom (2016) and Soglia *et al.* (2021) agree that high protein consumption affects protein absorption in meat and provides adequate amino acids to ensure normal cellular metabolism. While low protein treatment results in low meat protein content (Kartikasari *et al.*, 2001; Sutanto *et al.*, 2019), Anang (2017) and Iriyanti *et al.* (2014), it was emphasized that local chicken meat has decent nutritional values and high protein contents.

Meat fat is a high-energy food for every gram provides more energy than carbohydrates or protein (Ruben *et al.*, 2017). Fat also acts as insulation and protection in the tissues of the subcutaneous and around certain organs, solvent vitamins A, D, E, K, and food reserves in the body (Van, 2019). Table 1 shows that feeding different protein levels has no significant effect ($P > 0.05$) on meat fat content. This is due to the nearly identical nutritional content of the feed in each treatment, especially the additional herbs, so the crude fat digestibility levels are similar.

The low rates of crude fat digestibility happen when chickens avoid increasing the ambient temperature. Instead, feed is stored in the cache to be digested gradually later. When the cage is comfortable enough, chickens reduce the burden of digesting fat. While the increase in temperature and heat stress can reduce the digestibility of dry matter, crude protein, and carbohydrates, they are barely effective to fat digestibility (Tolimir *et al.*, 2010).

4. Conclusions and Suggestions

It was concluded that feed with different levels of protein does not present significant changes in dry matter, ash, protein, and fat contents of cross-bred local chicken meat. Therefore, the lowest feed protein content of 17 % for cross-breed local chickens aged 0 mo to 2 mo should be of the highest nutrition contents.

Acknowledgment

The authors would like to express their gratitude to the National Research and Innovation Agency of the Republic of Indonesia (BRIN), the Educational Fund Management Institution (LPDP), and the Ministry of Agriculture for funding this research under the National Research Priority Project Cooperation (7/EI/II/PRN/2020). In addition, the authors also wish to thank the Directorate of Research and Community Service and the Department of Animal Science of the Faculty of Agriculture and Animal Science of the University of Muhammadiyah Malang.

References

Adinurani PG. 2016. **Design and Analysis of Agrotrial Data: Manual and SPSS**. Plantaxia, Yogyakarta, Indonesia

Adinurani, PG. 2022. **Agrotechnology Applied Statistics** (compiled according to the semester learning plan). Deepublish, Yogyakarta, Indonesia

Anang A. and Suharyanto. 2007. **Harvest Chicken in 7 Weeks Free of Avian Influenza**. Penebar Swadaya, Depok, Indonesia.

Bai J, Greene E, Li W, Kidd MT, and Dridi S. 2015. Branched-chain amino acids modulate the expression of hepatic fatty acid metabolism-related genes in female broiler chickens. *Mol. Nutr. Food Res*., **59(6):** 1171–1181.

https://doi.org/10.1002/mnfr.201400918

Daniel S, Razvan-Mihail R, Ioan C and Georghe DM. 2018. Influence of feed particle size on chicken broilers performance. *Annals of the University of Oradea, Fascicle: Ecotoxicology, Animal Husbandry, and Food Science and Technology*, **17/B:** 257–262.

Dhama K, Verma V, Sawant PM, Tiwari R, Vaid RK and Chauhan RS. 2011. Applications of probiotics in poultry: Enhancing immunity and beneficial effects on production performances and health. *J. Immunol. Immunopathol.,* **13(1):** 1–19.

Diwyanto K, Sulandari S, Diwyanto K and Prijono SN. 2007. Diversity of Indonesia's local chicken biological resources: Benefits and potential, In: Diwyanto K and Prijono SN (Eds.). Pusat Penelitian Biologi - LIPI, Jakarta, Indonesia.

Fitasari E, Reo K and Nadia Niswi N. 2016. The use of different levels of protein in native chickens on the performance of protein production and digestibility. *Jurnal Ilmu-Ilmu Peternakan,* **26(2)**: 73–83. https://doi.org/10.21776/ub.jiip.2016.026.02.10

Giannenas I, Bonos E, Anestis V, Filioussis G, Papanastasiou DK, Bartzanas T, Papaioannou N, Tzora A and Skoufos I. 2017. Effects of protease addition and replacement of soybean meal by corn gluten meal on the growth of broilers and on the environmental performances of a broiler production system in Greece. *PloS One* **12(1):** 1–26.

https://doi.org/10.1371/journal.pone.0169511

Grashorn MA and Serini C. 2006. Quality of chicken meat from conventional and organic production. Proceedings of the 12th EPC. Verona, Italy.

Gultom EP, Wahyuni TH and Tafsin M. 2016. Digestibility of crude fiber and crude protein diet containing oil palm frond treated by physical, biological and chemical on sheep. *Jurnal Peternakan Integratif.,* **4(2):** 193–202.

https://doi.org/10.32734/jpi.v4i2.2795

Hidayat Z. 2017. The effect of adding feed additives with different doses in the ration on the performance of laying hens. Undergraduate Thesis. Lampung University, Lampung, Indonesia.

Iriyanti N, Santosa RSS and Rachmawati WS. 2014. Blood profile and performance of native chicken with functional feed. *Int. J. Poult. Sci.*, **13(11):** 645–651.

Kartikasari LR, Soeparno and Setiyono. 2001. Chemical composition and fatty acid studies of broiler breast meat receiving methionine supplementation on low protein feed. *Bulletin of Animal Science*. **25(1):** 33–39.

Khan HS. 2018. Recent advances in role of insects as alternative protein source in poultry nutrition. *J. Appl. Anim. Res.*, **46(1):** 1144–1157.

https://doi.org/10.1080/09712119.2018.1474743

Niken A. 2012. Performance of free-range chicken with broiler concentrate-based ration. *Jurnal Agrisains.* **3(5):** 51–58

Parolini M, Ganzaroli A and Bacenetti J. 2020. Earthworm as an alternative protein source in poultry and fish farming: Current applications and future perspectives. *Sci. Total Environ.*, **734:**1–25. https://doi.org/10.1016/j.scitotenv.2020.139460

Rana P, Tewatia BS, Jyotsana, Kumar R and Panwar VS. 2020. Effect of herbal methionine supplementation on growth performance and economics of broiler chicken. *J. Entomol. Zool. Stud.*, **8(6):** 2076–2081.

Ruben NT, Raphael KJ, Boris NT, Doriane YMD, Herve MK, Serges K, Alexis T and Ami M. 2017. Performances of broiler chicken fed on diet supplemented with thyme and oregano essential oils stabilized in a plant charchoal matrix. *J. World's Poult. Res.,* **7(2):** 79–87.

Sabate J, Sranacharoenpong K, Harwatt H, Wien M and Soret S. 2014. The environmental cost of protein food choices. *Public Health Nutr.*, **18(11):** 2067–2073

https://doi.org/10.1017/S1368980014002377

Sekhar SRM, Matt SG and Manvi SS. 2020. Prediction of protein secondary structure from amino acid sequences by integrating fuzzy, random forest and feature vector methodologies. *Jordan J. Biol. Sci*., **13(4)**: 483–492

Sidadolog P. 2006. Adjustment of different feeding time and protein energy content on feed efficiency and growth of broiler chickens. *Buletin Peternakan*. **30(3):** 126–135.

https://doi.org/10.21059/buletinpeternak.v30i3.1203

Sogila F, Zampiga M, Baldi G, Malila Y, Thanatsang KV, Srimarut Y, Petracci M, Tatiyaborworntham N, Unger O, Klamchuen A, Laghi L, and Sirri F. 2021. Lysine depletion during different feeding phases: Effects on growth performances and meat quality of broiler chickens. *Animals*. **11(6):** 1–16. https://doi.org/10.3390/ani11061499

Suryanto E, Sasongko H, Maryam M and Santosa R. 2009. The effect of type of feed and slaughter age on the performances and carcass characteristic of male Arab chicken. *J. Indones. Trop. Anim. Agric.*, **3(3):** 181–188.

Sutanto A, Widodo W and Rahayu ID. 2019. Developing organic feed stuff as the main component of broiler chickens' feed with canvas model in East Java: A case study of analysis on organic rice and corn in Malang and Tulungagung. *IOP Conf. Ser.: Mater. Sci.Eng*., **532(012022):**1–5**.** http://dx.doi.org/10.1088/1757-899X/532/1/012022

Tolimir N, Peric L, Milosevic N and Bogdanovic V. 2010. The effect of multiphase nutrition on production performances of broilers. *Biotechnol. Anim. Husb.*, **26(1–2):** 83–90

Van DP. 2019. Meat production performances of cay cum chickens in rations with different levels of metabolizable energy and crude protein with probiotics. MSc Theses Laguna State Polytechnic University, Siniloan, Laguna, Philippines .

Wahju J. 2015. **Poultry Nutrition Science.** Universitas Gadjah Mada Press, Yogyakarta, Indonesia

Wahyudi A, Pamungkas D, Setyobudi RH, Hendraningsih L and Vincēviča-Gaile Z. 2021. Organic acid and nutrient composition of lactic acid bacteria inoculated total mixed ration silage under tropical condition: organic acids and nutrients composition of Lactic Acid Bacteria. *Proc. Pak. Acad. Sci.: B*, **54(1):** 41–45.

Widodo W. 2019. **Poultry Livestock Nutrition Science**. UMM Press, Malang, Indonesia.

Widodo W, Rahayu ID, Sutanto A, Setyobudi RH and Mel M. 2019. The effectiveness of curcuma (*Curcuma xanthorriza* Roxb.) addition in the feed toward super Kampong chicken performances. *Proc. Pak. Acad. Sci.: B*, **56(4):** 39–46

Widodo W, Rahayu ID, Sutanto A, Anggraini AD, Sahara H,

Safitri S and Yaro A. 2021. *Curcuma xanthorriza* Roxb. as feed additive on the carcass and fat weight percentage, meat nutrient, and nutrient digestibility of Super Kampong Chicken. *Sarhad J. Agric.*, **37(1):** 41–4

JJBS

Volume 15, Number 5,December 2022
ISSN 1995-6673
Pages 897 – 904
https://doi.org/10.54319/jjbs/150520

Jordan Journal of Biological Sciences

Chemical Compounds, Antioxidant Properties, and Enzyme Inhibitory Activities of Kitolod Leaf and Fruit Hexane Extracts as Antidiabetic

Sukardi Sukardi[1,*], Damat Damat[1], Manar Fayiz Mousa Atoum[2], Lili Zalizar[3], Rahayu Relawati[4], Asad Jan[5], Zane Vincēviča-Gaile[6], Effendi Andoko[7], and Warkoyo Warkoyo[1]

[1]Department of Food Technology, Faculty of Agriculture and Animal Science, University of Muhammadiyah Malang, Jl. Raya Tlogomas No 246, Malang 65144, East Java, Indonesia; [2]Department of Medical Laboratory Sciences, The Hashemite University, Zarqa, Jordan; [3]Department of Animal Science, Faculty of Agriculture and Animal Science, University of Muhammadiyah Malang, Indonesia; [4]Department of Agribisnis, Faculty of Agriculture and Animal Science, University of Muhammadiyah Malang, Indonesia; [5]Institute of Biotechnology Genetic Engineering, The University of Agriculture, Peshawar, 25130, Khyber Pakhtunkhwa, Pakistan; [6]Department of Environmental Science, University of Latvia, Jelgavas Street 1, Room 302, Riga LV-1004, Latvia; [7]College of Agriculture and Natural Resources, National Chung Hsing University, Agricultural Environment Science Building, South District, Taichung City, Taiwan 402

Received: Oct 5, 2022; Revised: Dec 17, 2022; Accepted Dec 23, 2022

Abstract

Diabetes (DMT 2) is one of the most common free radicals-incited conditions, and its treatment calls for natural antioxidants fit for daily administration with minimum burden to the bodily system. Traditionally used to treat eye disease in Indonesia, kitolod [*Isotoma longiflora* (L) Presl.] was studied for its antidiabetic prospect. Hexane extracts from the leaves and fruit were analyzed for their non-polar chemical compounds, antioxidant properties, and α-amylase and α-glucosidase enzyme inhibition activities. Liquid chromatography (LC)-mass spectrometry (MS) identified 29 compounds out of the leaf and 36 compounds out of the fruit. The extracts showed moderate antioxidant activity with IC_{50} values of (90.586 ± 0.663) μg mL^{-1} and (92.832 ± 1.042) μg mL^{-1}. Their inhibitory against α-amylase was very strong, with IC_{50} values of (38.511 ± 0.068) mL^{-1} and (39.790 ± 0.233) mL^{-1}, while ones against α-glucosidase were strong to moderate with IC_{50} value of leaf extract (40.833 ± 0.571) μg mL^{-1} and of fruit extract (65.383 ± 0.511) μg mL^{-1}. Seeing the high potential in kitolod extracts to inhibit α-amylase and α-glucosidase enzymes, they should correspond with functional food for people with diabetes.

Keywords: Antioxidant, Diabetes herbal medicine, Environmentally friendly, Functional food, *Isotoma longiflora* (L) Presl., Medicinal plant, Phytochemical, Sangkobak

1. Introduction

While technology improves human welfare, its practices emit free radicals into the environment. Add them up with ones naturally released by living organisms, and their levels can be too high to tolerate (Kaewseejan and Siriamornpun, 2015). In such cases of environmental imbalance, free radicals can interfere with the work of various cellular elements, such as proteins, lipids, carbohydrates, and nucleic acids (Sies, 2015). Moreover, at the cellular level, excessive free radicals can cause oxidative stress (Dando *et al*., 2015). Such activities, in the long run, can affect human physiological conditions (Damat *et al.*, 2021a; Ma, 2014) by triggering ailments like inflammation, diabetes, cardiovascular, a neuro degenerative disorder, and cancer (Elmakawy *et al*., 2019; Pingitore *et al.,* 2015; Setyobudi *et al*., 2019 and 2021).

With reported prevalence rate of diabetes in adults in 2021 to reach 537 × 10^6 (IDF, 2021), Diabetes mellitus type 2 (DMT 2) is a global issue. Indonesia is ranked fourth place with 21 000 000 – still higher than Mexico at 13 100 000 – yet lower than China at 89 500 000, India at 67 800 000 and USA at 30 700 000 (Lin *et al*., 2020). As one of the most common free radicals-incited conditions, DMT 2 treatment calls for natural antioxidants fit for daily administration with minimum burden to the bodily system.

Antioxidants can protect cells from the damage caused by free radicals by developing safe interactions with them (Gupta and Gupta, 2015; Setyobudi *et al*., 2022) and terminating any reactions before the molecular interference stage (Elmakawy, 2019). Chemically-processed medicine containing synthetic antioxidants works fast in neutralizing free radicals, but long-term consumption is detrimental to health. Besides, the production process itself discharges more free radicals into the environment. Therefore, plant-based supplements and functional foods containing phytochemicals and secondary metabolites should help improve human health and prevent the forming of problems due to free radicals (Abdel-Mawgoud *et al*., 2019; Ahmed *et al*., 2015; Damat *et al*., 2019). Furthermore, natural means are environmentally friendly

* Corresponding author. e-mail: *sukardi@umm.ac.id*

since additional free radicals from the production process will be low.

People with diabetes need regular antioxidant intake to keep free radicals at bay. Based on the results of epidemiological studies, it is known that antioxidants can reduce diabetes-related complications and restore insulin sensitivity (Rajendiran *et al*., 2018). This situation calls for herbal medicine fit for daily administration with minimum burden to the bodily system. Easy to grow and cultivate, Kitolod – Sangkobak, Javanese local name [*Isotoma longiflora* (L) Presl.] is a medicinal plant traditionally used to treat eye disease in Indonesia that has been known to contain secondary metabolites. Previous studies had screened alkaloid, terpenoid, and phenol contents (which showed antioxidant activity and worked as an anticancer against the MCF7 breast cancer cell line) in the leaf, stem, and fruit (Egarani *et al*., 2020). Terpenoid compounds are found in many organisms, especially in green and flowering plants. The leaves, fruit, flowers, stems, and roots of the kitolod plant contained flavonoid compounds of (10.48 ± 0.10) mg kg^{-1}, (2.27 ± 0.23) mg kg^{-1} , (1.10 ± 0.11) mg kg^{-1}, (0.72 ± 0.12) mg kg^{-1}, and (0.53 ± 0.13) mg kg^{-1}, respectively (Enggarani *et al*., 2020). Fruits and flowers are known to have very strong antioxidant activity. Kitolod leaf parts have strong antioxidant activity, while the stem and roots have weak antioxidant activity.

Plants containing terpenoids have been used for medicine in the Middle East (Pichersky and Raguso., 2016). Furthermore, Hapsari *et al*. (2016) underlined its ability to treat respiratory diseases like bronchitis and asthma due to its anti-inflammatory and analgesic functions. Furthermore, its ethanol extract inhibits the growth of several microorganisms, such as candida fungus and tuberculosis bacteria (*Mycobacterium tuberculosis*). In order to see the plant's prospect as a source of natural antioxidants to treat diabetics, this research explores the bioactive components in kitolod hexane extracts. It identifies their antioxidant properties and their α-amylase and α-glucosidase enzyme inhibitory through an *in-vitro* assay.

2. Materials and Methods

2.1. Plant extraction

Leaves and fruit of kitolod were collected from natural populations in Karangploso, Pendem, Batu, East Java, Indonesia. Preparatory steps involved washing under running water, draining for 2 h, and drying in a dryer cabinet (GETRA, FJ-15C, China) at 50 °C for 36 h. Voucher specimens have been deposited at the Herbarium of Bali Botanic Garden, National Research and Innovation Agency, Bedugul, Bali, Indonesia. The dried leaves and fruit were each ground to powder, sifted with 40 mesh filters, packaged in a closed glass beaker, and stored at -20 °C (LG, GN 304SL, South Korea) in the dark prior to use.

Powdered leaves (200 g) were macerated with 1 L hexane (Merck, USA) for 48 h at room temperature (on temperature 27 ºC) and separated from its filtrate in a Buchner funnel layered with Whatman No.2 filter paper connected to a vacuum pump. The fruit specimen also received the same treatments. Ethanol 99.9 %, Merck USA filtrates were fractionated successively with n-hexane and ethyl acetate with purity ≥ 99 %. Each fraction was then concentrated using a vacuum rotary evaporator (Heidolph RE-502, Germany) at a temperature of 40 °C until one-fifth of the volume was reached and transferred into a clean bottle. The solvent is separated by flowing nitrogen gas into the erlenmeyer. The process will end when the solvent is no longer smelled.

2.2. Liquid chromatography (LC)-mass spectrometry (MS)

LC/MS analysis to identify bioactive compounds employed Shimadzu LCMS-8040 LC/MS, Shimadzu Column, and FC-ODS Shim Pack (2 mm × 150 mm, 3 μm). The column temperature was maintained at 35 °C, and the injection volume was fixed at 1 μL. The flow gradients were programmed on 0/0 or 0 min, 15/85 at 5 min, 20/80 at 20 min, and 90/10 at 24 min. The flow rate was 0.5 mL min^{-1} (90 % methanol in water) with disolvation at 350 °C. Low-energy CID induced fragmentation (Salih *et al*., 2017). Other chemicals and reagents used in this research were classified as an analytical grade, purchased from Sigma Aldrich Chemical Co. (St Louis, Mo, USA).

2.3. Antioxidant activity test

2.3.1. DPPH (1, 1-diphenyl-2-picryl-hydroxyl) radical scavenging activity

IC_{50} method (Damat *et al*., 2021b; Liu *et al*., 2014) was brought to determine the level of extracts regarding the ability to inhibit 50 % of free radicals added. The hexane (Merck, Canada) extracts were prepared in six different concentrations [(0, 20, 40, 60, 80, 100) μg mL^{-1})]. Each kitolod leaf and fruit sample in methanol (100 μL) and DPPH in ethanol (1.9 mL of 0.1 mM) was mixed and homogenized, then stored in a tightly-lidded container and allowed to stand for 30 min at room temperature in the dark. The positive control comprised quercetin. The blanks included all the reaction reagents except the extract and the positive control substances. The purple to yellow colour formed in the test solution was measured at 517 nm. The tests were carried out in triplicates. IC_{50} was determined from percent inhibition vs. concentration plots. The capacity to scavenge the DPPH radical was based on Equation (1):

$$\text{DPPH}^{\bullet}\text{ scavenging activity \%} = [(A_C - A_S) / A_C] \times 100 \quad (1)$$

(A_C) is the absorbance of the negative control reaction, and (A_S) is the absorbance in the presence of plant extracts. The results were conveyed as IC_{50} [the concentration (μg mL^{-1}) of the hexane extract that scavenges 50 % of $DPPH^{\bullet}$ radical].

2.3.2. Inhibition of α-amylase assay

Following the standard method, α-amylase inhibitory activities of kitolod hexane extracts were performed (Chelladurai and Chinnachamy, 2018). The substrate was of starch solution (0.5 % w v^{-1}), gained after boiling potato starch in distilled water for 15 min. The enzyme solution was 1 mg of porcine pancreatic α-amylase dissolved in 20 mM phosphate buffer (100 mL, pH 6.9). The sample solutions prepared in Dimethyl sulfoxide (Merck, USA) were of various concentrations (10 to 100) mg mL^{-1}. DNS solution (Merck, USA) (20 mL of 96 mM 3,5-dinitro salicylic acid, 12 g sodium potassium tartrate (Merck,

USA) in 8 mL of 2 M NaOH (Merck, USA), and 12 mL deionized water) served as the colouring reagent.

Three experiments– test, blank, and control – were conducted. For tests, enzyme solutions were added in 1 mL of each test in a test tube and incubated at 25 °C for 30 min. 1 mL taken from each mixture was then mixed with 1 mL starch solution and incubated at 25 °C for 3 min. After that, 1 mL of DNS solution was added. The tube was then covered and heated in a water bath at 85 °C for 15 min. Once the tube cooled, the reaction mixture was diluted with distilled water (9 mL). The absorbance was finally recorded at 540 nm. For blanks, DNS solution was added prior to starch solution. As of control, the procedure was the same as tests outside of replacing plant extracts with 1 mL Dimethyl Sulfoxide. Acarbose (Glyco AC 50 acarbose, Mumbai India), a well-known antidiabetic medicine, was selected as the positive control. The percentage of inhibition was calculated as per Equation (2):

$$\text{Inhibition (\%)} = [(A_C - A_S) / A_C] \times 100 \quad (2)$$

Ac was the absorbance of the control, and AS was the absorbance in the presence of the plant extracts. The results were recorded as IC_{50} [the hexane extract concentration (µg mL^{-1}) inhibiting 50 % of α-amylase activity].

2.3.3. Inhibition of α-glucosidase assay

Samples were prepared in varying concentrations from (2 to 200) µg mL^{-1} of hexane extract dissolved in Dimethyl Sulfoxide. In a microplate with a 30 µL sample, quasi-phosphate 36 µL phosphate buffer of pH 6.9 and 17 µl 4 mM substrate of p-nitrophenyl-α-D-glucopyranose (p-NPG) were added (Sigma-Aldrich, Switzerland). After incubation for 5 min at 39 °C, 25 µL enzyme solution α-glucosidase (Saccharomyces cerevisiae, Sigma-Aldrich-Germany) of 0.8 unit L^{-1} was added and incubated again for 15 min at 39 °C to reduce the substrate. The reaction was then stopped by adding 100 µL of Na_2CO_3 200 mM solution (Merck, USA). To measure the amount of p-nitrophenol released from p-NPG, a microplate reader (Versamax ELISA Microplate Reader, USA) at 400 nm was utilized to determine the inhibition rates of alpha-glucosidase. The reading of the results was carried out three times. Acarbose became the positive control. Substrate + enzyme solution (no extract added) served as blank, and substrate (no enzyme added) acted as control (Mahayasih *et al*., 2017). The inhibition percentage was calculated referring to Equation (3):

$$\text{Inhibition (\%)} = [(\text{blank absorption} - \text{sample absorption}) / \text{blank absorption}] \times 100 \quad (3)$$

The results were expressed as IC_{50} [the concentration (µg mL^{-1}) of the hexane extracts that inhibited 50 % of α-glucosidase activity].

2.4. Data analysis

All experiments were performed in triplicate, of which data were then analysed on Microsoft Excel, noted as mean ± standard deviation (n = 3). The IC_{50} values were computed using GraphPad Prism 7 for Windows, GraphPad Software, La Jola, California, USA. Differences were regarded as significant when the rates hit $P < 0.05$ (Adinurani, 2016, 2022).

3. Results and Discussion

3.1. Chemical Compounds

Samples were of 200 g kitolod leaf powder and fruit powder in hexane macerations for 72 h. LC-MS discovered 29 compounds out of 22.064 g hexane extract from the leaf and 36 compounds out of 37.126 g from the fruit. The results of compound spectrum analysis are displayed in Table 1 and Table 2, respectively. The components contained in both hexane extracts were grouped into three: (i) ones of > 5.000 %, (ii) between 3.000 % and 5.000 %, and (iii) lower than 3.000 %.

Components in the leaf sample that belong to Group 1 are β Caryophyllene (7.296 %), Chrysandiol (7.175 %), Chrysartemin B (6.499 %), Chrysartemin A (6.337 %), and 5 Ethylidene 5,6 dihydro 3,6,6 trimethyl 2 pyranone (6.329 %); Santamarine (5.764 %) is in sesquiterpene category. Components in Group 2 are Myrcene (3.690 %), Thymol (4.118 %), Capelin (3.929 %), β Farnesene (3.238 %), α-Cardinal (3.562 %), Nerolidol (4.374 %) and Stigmasterol (4.864 %). Components listed in Group 3 include Benzaldehyde, Benzoicacid, Sabinene, Camphene, Nojigiku alcohol, Germacrene D, cis Spiro ketalenol etherpolyne, Kikkanol B, Clovane 2 β.9 α diols, Kikkanol C, Kikkanol D, Chrysartemin A, Arteglasin A, β Cyclopyrethrosin, and Flavoxanthin.

As of the fruit sample, Apigenin (10.081 %), Chrysetunone (6.387 %), and Chrysandiol (5.297 %) are incorporated in Group 1. Group 2 consists of Chrysanthenone, Thymol, Linalool,5 Ethylidene 5.6 dihydro 3,6,6 trimethyl 2 pyranones, Bornylacetate, β Caryophyllene, Chrysartemin A, Chrysartemin B, and β Sitosterol. The remaining 27 compounds are gathered in Group 3.

A total of 80.343 % of chemical components found in the leaf extract and 72.830 % in the fruit extract are classified as sesquiterpenes – or those that have shown antioxidant activities. Yu *et al*. (2013) pointed out that β-farnesene had the potential to control plant-angels ticks and influence genetic engineering. Francomano *et al*. (2019) stated that β-caryophyllene proved anti-inflammatory activity by inhibiting major inflammatory mediators such as nitrite oxide synthase. Su *et al*. (2015) reported that α-cardinal contained in *Diospyros discolor* Willd essential oil exhibited cytotoxic activity against human colon, liver, and lung cancer cells. An alcoholic sesquiterpene, Nerolidol, was indicative of anti-inflammatory, antioxidant, and anticancer properties (Ni *et al*., 2019). Chrysandiol belongs to a sesquiterpene group widely found in flowers and leaves with antidiabetic activity (Jiang *et al*., 2021). Santamarine was also classified as a sesquiterpene that has antioxidant activity (Oh *et al*., 2021). Betha-sitosterol is widely found in traditional medicines since many plants produce it; despite its role in prostate enlargement, the compound showed antioxidant activities (Vo *et al*., 2020).

3.2. Antioxidant properties

Antioxidant potential can be measured by various methods, including hydrogen atom transfer, single electron transfer, or targeted scavenging activity (Christodoulou *et*

al., 2022). The antioxidant activity test method for DPPH radicals is widely used to analyze the antioxidants of extracts of natural ingredients (Mishra *et al*., 2019). Antioxidant activity capacity test (DPPH) was carried out on hexane extracts from kitolod fruit and leaves and compared with quercetin standards.

The results of DPPH radical scavenging assay towards leaf hexane extract, fruit hexane extract, and quercetin are summarized in Table 3. The differences in activity were due to the amount of hydrogen or electron thrown to free radicals (Makasana *et al*., 2017). A smaller IC_{50} value indicates a higher radical scavenging capability, and that means a higher effectiveness (Promprom and Chatan, 2017). It is therefore conclusive that kitolod hexane extracts – containing potent antioxidants Myrcene and β-caryophyllene (Noriega *et al*., 2019) – have better performance compared to the controls. Moreover, nerolidol, a sesquiterpene also contained in kitolod, had been recommended by Chan *et al*. (2016) to prevent oxidation of unsaturated fatty acids.

Table 1. Phyto components of kitolod leaf identified by LC-MS

Peak No.	RT (min)	Exact Mass (g mol^{-1})	Molecular Weight (g mol^{-1})	Compound	Chemical Formula	Composition (%)
1	1.230	106.041	106.124	Benzaldehyde	C_7H_6O	1.923
2	1.289	122.036	122.123	Benzoic acid	$C_7H_6O_2$	1.165
3	1.483	136.125	136.238	Sabinene	$C_{10}H_{16}$	1.314
4	1.497	136.125	136.238	Camphene	$C_{10}H_{16}$	1.913
5	1.500	136.125	136.238	Myrcene	$C_{10}H_{16}$	3.690
6	1.611	150.104	150.221	Thymol	$C_{10}H_{14}O$	4.118
7	1.626	152.120	152.237	Nojigiku alcohol	$C_{10}H_{16}O$	1.314
8	2.800	166.099	166.220	5 Ethylidene 5,6 dihydro 3,6,6 trimethyl two pyranone	$C_{10}H_{14}O_2$	6.329
9	2.812	168.057	168.195	Capelin B-Caryophyllene	$C_{12}H_8O$	3.929
10	5.494	204.187	204.357	B-Farnesene	$C_{15}H_{24}$	7.296
11	5.498	204.187	204.357	Germacrene D	$C_{15}H_{24}$	3.238
12	5.507	204.187	204.357	cis Spiroketalenolether polyyne	$C_{15}H_{24}$	2.643
13	5.852	214.099	214.264	α-Cardinal	$C_{14}H_{14}O_2$	2.643
14	6.947	222.198	222.372	Nerolidol	$C_{15}H_{26}O$	3.562
15	6.950	222.198	222.372	Kikkanol B	$C_{15}H_{26}O$	4.374
16	7.979	236.177	236.355	Chrysandiol	$C_{15}H_{24}O_2$	1.904
17	8.001	252.172	252.354	Clovane 2 β,9 α diol	$C_{15}H_{24}O_3$	7.175
18	8.007	238.193	238.371	Santamarine	$C_{15}H_{26}O_2$	2.513
19	8.018	248.141	248.322	Kikkanol C	$C_{15}H_{20}O_3$	5.764
20	8.245	252.172	252.354	Kikkanol A	$C_{15}H_{24}O_3$	2.188
21	8.298	254.188	254.370	Kikkanol D	$C_{15}H_{26}O_3$	2.498
22	8.303	254.188	254.370	Chrysartemin A	$C_{15}H_{26}O_2$	1.283
23	9.938	278.115	278.304	Chrysartemin B	$C_{15}H_{18}O_5$	6.337
24	9.940	278.115	278.304	Arteglasin A	$C_{15}H_{18}O_5$	6.499
25	11.496	304.131	304.342	β Cyclopyrethrosin	$C_{17}H_{20}O_5$	3.535
26	11.525	306.146	306.358	Stigmasterol	$C_{17}H_{22}O_5$	1.927
27	15.048	412,370	412.702	β Sitosterol	$C_{29}H_{48}O$	2.643
28	15.638	414.386	414.718	Flavoxanthin	$C_{29}H_{50}O$	4.864
29	33.604	584.422	584.885		$C_{40}H_{56}O_3$	1.419

RT: Retention Time

Table 2. Phyto components of kitolod fruit identified by LC-MS

Peak No	RT (min)	Exact Mass (g mol^{-1})	Molecular Weight (g mol^{-1})	Compound	Chemical Formula	**Composition (%)**
1	1.230	106.042	106.124	Benzaldehyde	C_7H_6O	1.309
2	1.289	122.037	122.123	Benzoic acid	$C_7H_6O_2$	0.757
3	1.471	134.110	134.222	p Cymene	$C_{10}H_{14}$	0.492
4	1.476	136.125	136.238	α Terpinene	$C_{10}H_{16}$	2.067
5	1.477	136.125	136.238	α Pinene	$C_{10}H_{16}$	1.631
6	1.479	136.125	136.238	β Pinene	$C_{10}H_{16}$	2.401
7	1.483	136.125	136.238	Sabinene	$C_{10}H_{16}$	4.588
8	1.497	136.125	136.238	Camphene	$C_{10}H_{16}$	3.238
9	1.500	136.125	136.238	Myrcene	$C_{10}H_{16}$	2.726
10	1.599	150.105	150.221	Chrysanthenone	$C_{10}H_{14}O$	4.319
11	1.611	150.105	150.221	Thymol	$C_{10}H_{14}O$	3.247
12	1.635	154.136	154.253	Borneol	$C_{10}H_{18}O$	1.958
13	1.637	154.136	154.253	Linalool	$C_{10}H_{18}O$	3.248
14	2.800	166.099	166.220	5 Ethylidene 5,6 dihydro 3,6,6 trimethyl 2 pyranone	$C_{10}H_{14}O_2$	0.973
15	2.810	168.042	168.148	2,6 Dimethoxy p benzoquinone	$C_8H_8O_4$	1.082
				Bornyl acetate		
16	5.156	196.146	196.290	Calacorene	$C_{12}H_{20}O_2$	2.708
17	5.233	200.157	200.325	Calamine	$C_{15}H_{20}$	4.331
18	5.284	202.172	202.341	α Copaene	$C_{15}H_{22}$	1.851
19	5.488	204.188	204.357	β Caryophyllene	$C_{15}H_{24}$	2.646
20	5.494	204.188	204.357	β Farnesene	$C_{15}H_{24}$	2.709
21	5.498	204.188	204.357	α Selinene	$C_{15}H_{24}$	1.476
22	5.500	204.188	204.357	β Element	$C_{15}H_{24}$	2.646
23	5.504	204,188	204.357	Germacrene D	$C_{15}H_{24}$ $C_{15}H_{24}$	2.709
24	5.507	204,188	204.357	α Cardinal	$C_{15}H_{26}O$	1.957
25	6.947	222.198	222.372	t Muurolol	$C_{15}H_{26}O$	1.742
26	6.956	222.198	222.372	Kikkanol B	$C_{15}H_{24}O_2$	0.973
27	7.979	236.178	236.355	Chrysandiol	$C_{15}H_{24}O_3$	5.297
28	8.001	252.173	252.354	Santamarina	$C_{15}H_{20}O_3$	3.237
29	8.018	248.141	248.322	Chrysetunone	$C_{15}H_{24}O_3$	6.387
30	8.243	252.173	252.354	Kikkanol A	$C_{15}H_{26}O_3$	1.082
31	8.298	254.188	254.370	Apigenin	$C_{15}H_{10}O_5$	1.082
32	9.365	270.053	270.240	Chrysartemin A	$C_{15}H_{18}O_5$	10.081
33	9.938	278.115	278.304	Chrysartemin B	$C_{15}H_{10}O_5$	3.248
34	9.940	278,115	278.304	Stigmasterol	$C_{29}H_{48}O$	4.253
35	15.048	412.371	412.702	β Sitosterol	$C_{29}H_{50}O$	2.836
36	15.638	414.386	414.718			3.734

RT: Retention Time

Table 3. Radical scavenging activity, α-amylase activity, andα-glucosidase activity inhibitions of kitolod leaf and fruit hexaneextract

Materials	Radical scavenging activity IC_{50} (μg mL^{-1})	Inhibition of α-amylase activity IC_{50} (mg mL^{-1})	Inhibition of α-glucosidase activity IC_{50} (μg mL^{-1})
Leaf	92.832 ± 1.042[a]	39.790 ± 0.233[a]	40.833 ± 0.571[b]
Fruit	90.586 ± 0.663[a]	38.511 ± 0.068[a]	65.383 ± 0.511[c]
Quercetin	111.923 ± 0.676[b]	184.677 ± 1.480[b]	87.051 ± 0.430[d]
Acarbose	-	231.647 ± 0.593[c]	14.289 ± 0.112[a]

Note: The above value is mean ± sd. Subcritp shows a meaningful difference with $P < 0.05$

3.3. Enzyme inhibitory

3.3.1. α-amylase inhibitory activity

The inhibitory activity of the alpha-amylase enzyme was carried out in vitro. As a comparison, inhibition uses acarbose and quercetin. The α-amylase enzyme has a role in inhibiting the breakdown of oligosaccharides and disaccharides into monosaccharides so that it will delay glucose absorption (Jemaa *et al*., 2017). This mechanism will efficiently reduce postprandial sugar levels (Duarte *et al*., 2020).

Referring to Table 3, since the extracts came out with lower IC_{50} values – (39.790 ± 0.233) μg mL^{-1} and (38.511 ± 0.068) μg mL^{-1} for leaf and fruit correspondingly – than acarbose and quercetin, their α-amylase inhibitory activities are equally proven higher than the latter two. The potential of the hexane extract in inhibiting α-amylase is more likely due to the presence of β-sitosterol. The fact that α-amylase inhibition plays a role in the process of starch and glycogen digestion is the basic idea to treat carbohydrate absorption disorders in people with diabetes (Sales *et al*., 2012). The active compounds in both extracts are of the same type of inhibitory activity and only differ in concentrations. Rufino *et al*. (2015) said that myrcene had an antidiabetic effect, and Sales *et al.* (2012) supported the finding that terpenoids had high bioactivity against hyperglycemia. The reason behind choosing hexane extraction is due to previous discoveries that hexane extractfrom plants (*Cinnamomum zeylanicum* Blume, *Crataegus oxyacantha* (Ram Tulsi), *Hibiscus sabdariffa* L.*, Morus alba* L.*, Portulaca oleracea* L., *Rubus fruticosus, Syzygium aromaticum* (L.) Merrill and Perry, *Teucrium polium* L., *Trigonella foenum-graecum* L., and *Vaccinium arctostaphylos* L.) are able to inhibit α-amylase enzyme (Salehi *et al.*, 2013) and that bioactive compounds in hexane fraction are able to inhibit the activity of α-amylase hydrolyzed polysaccharides into end products containing mixtures of maltose, malt triose, and oligosaccharides (6-8 glucose units) (Sales *et al*., 2012).

3.3.2. α-glucosidaseinhibitory activity

The enzyme α-glucosidase hydrolyzes oligosaccharides into monosaccharides. Furthermore, monosaccharides are absorbed by the small intestine to increase blood glucose levels (Sallau *et al*., 2018). The activity of the α-glucosidase enzyme can be inhibited by the hexane extract of kitolod leaves and fruit *in vitro*. Positive comparators were from acarbose and quercetin. Terpene compounds found in various medicinal plants contribute to the inhibition of alpha-glucosidase enzyme activity (Al Kury *et al*., 2022). Terpenes obtained from plants show inhibition of α-glucosidase and prove their potential in the management of diabetes (Panigrahy *et al*., 2020).

Signification from Table 3 shows that the IC value of$_{50}$ acarbose drugs is smaller compared to hexane extracts from kitolod leaves and fruits as well as quercetin positive standards. This suggests that the inhibitory activity of the enzyme alpha-glucosidase acarbose > hexane extract from the leaves > the hexane extract from the fruit > quercetin. The content of sesquiterpene (capelin) has a role in inhibiting the activity of the enzyme alpha-glucosidase. Capelin, a component in the hexane extract, apparently plays an active role in antidiabetics (Islam *et al.*, 2016). Myrcene, one of the terpenoids predominant components that serves as an antioxidant (Wang *et al*., 2019), should support the process. Capelinand capillinol have shown the ability to inhibit α-glucosidase, so Islam *et al*. (2016) agreed that the keto group in capelin should be a significant determinant on anti-diabetes potential.

4. Conclusion

In conclusion, spanning over 38 substances combined, the main chemical compounds in kitolod leaf and kitolod fruit hexane extracts are predominated by sesquiterpenes. Their lowest IC_{50} values of antioxidant inhibitory activity, lowest IC_{50} values of α-amylase inhibitory activity, and fairly low IC_{50} values of α-glucosidase inhibitory activity should prove that kitolod leaf and kitolod fruit hexane extract showed potential as antioxidants and that they can function as antidiabetic.

Acknowledgments

The authors wish to thank the Ministry of Research and Technology, Republic of Indonesia, for funding this research (E.5c/092/DPPM/L/IV/2019).

References

Abdel-Mawgoud M, Khedr FG and Mohammed EI. 2019. Phenolic compounds, antioxidant and antibacterial activities of *Rhus flexicaulis* Baker. *Jordan J. Biol. Sci*., **12(1)**:17–21.

Adinurani PG. 2016. **Design and Analysis of Agrotrial Data: Manual and SPSS**. Plantaxia, Yogyakarta, Indonesia

Adinurani, PG. 2022. **Agrotechnology Applied Statistics** (compiled according to thesemester learning plan). Deepublish, Yogyakarta, Indonesia.

Ahmed D, Saeed R, Shakeel N, Fatima K and Arshad A. 2015. Antimicrobial activities of methanolic extract of *Carissa opaca* roots and its fractions and compounds isolated from the most active ethyl acetate fraction. *Asian Pac. J. Trop. Biomed*., **5(7)**: 541–545. https://doi.org/10.1016/j.apjtb.2015.05.006

Al Kury LTA, Abdoh A, Ikbariah A, Sadek B and Mahgoub M. (2022). In vitro and in vivo antidiabetic potential of

monoterpenoids: An update. *Molecules* 27(182) :1–29. https://doi.org/10.3390/molecules27010182

Chan WK, Tan LTH, Chan KG, Lee LH and Goh BH. 2016. Nerolidol: A sesquiterpene alcohol with multi-faceted pharmacological and biological activities. *Molecules*, **21(5)**259: 1-40. https://doi.org/10.3390/molecules21050529

Chelladurai GRM and Chinnachamy C. 2018. Alpha amylase and alpha glucosidase inhibitory effects of aqueous stem extract of *Salacia oblonga* and its GC-MS analysis. *Brazilian J. Pharm. Sci*., **54(1)**:1–10. https://doi.org/10.1590/s2175-97902018000117151

Christodoulou MC, Palacios JCO, Golnaz H, Jafarzadeh S, Lorenzo JM, Dominguez R, Moreno A and Hadidi M. 2022. Spectrophotometric methods for measurement of antioxidant activity in food and pharmaceuticals. *Antioxidants* **11(2213)** :1–33. https://doi.org/10.3390/antiox11112213

Damat D, Anggriani R, Setyobudi RH and Soni P. 2019. Dietary fiber and antioxidant activity of gluten-free cookies with coffee cherry flour addition. *Coffee Sci*., **14(4)**:493–500. http://dx.doi.org/10.25186/cs.v14i4

Damat D, Setyobudi RH, Utomo JS, Gaile ZV, Tain A and Siskawardani DD. 2021a. The characteristics and predicted of glycemic index of rice analogue from modified arrowroot starch (*Maranta arundinaceae* L.). *Jordan J. Biol. Sci.,* **14(3):**389–393. http://jjbs.hu.edu.jo/vol14.htm

Damat D, Setyobudi RH, Burlakovs J, Gaile ZV, Siskawardani DD, Anggriani R and Tain A. 2021b. Characterization properties of extruded analog rice developed from arrowroot starch with addition of seaweed and spices. *Sarhad J. Agric*, **37(Special issue 1)**: 159–170. https://dx.doi.org/10.17582/journal.sja/2021.37.s1.159.170

Dando I, Cordani M, Pozza ED, Biondani G, Donadelli M and Palmieri M. 2015. Antioxidant mechanisms and ROS-related MicroRNAs in cancer stem cells. *Oxid Med Cell Longev*, **2015(ID 425708)** :1–13. https://doi.org/10.1155/2015/425708

Duarte AM, Guarino MP, Barroso S and Gil MM. 2020. Phytopharmacological strategies in the management of type 2 Diabetes Mellitus.*Foods***9(271)** :1–31. https://doi.org/10.3390/foods9030271

Egarani GR, Kasmiyati S, and Kristiani EBE. (2020). The antioxidant content and activity of various plant organs of kitolod (*Isotoma longiflora). J. Biol. Educ*.. **12(3)**:297–303. http://dx.doi.org/10.15294/biosaintifika.v12i3.23888

Elmakawy AI, Ibrahim FM and Abdel-Azeim S. 2019. Assessment of *Satureja montana* L. and *Mentha piperita* L. antioxidant activity, cytotoxicity and pattern of apoptotic gene expression in hepatoma cells. *Jordan J. Biol. Sci*., **12(3)**:251–258.

Francomano F, Caruso A, Barbarossa A, Fazio A, Torre C, Ceramella J, Mallamaci R, Saturnino C, Iacopetta D and Sinicropi MS. 2019. Aplied sciences β -Caryophyllene: A sesquiterpene with countless biological properties. *Appl. Sci.,* **9(5420)** :1–19. https://doi.org/10.3390/app9245420

Gupta J and Gupta A. 2015. Isolation and extraction of flavonoid from the leaves of *Rauwolfia serpentina* and evaluation of DPPH-scavenging antioxidant potential. *Orient. J. Chem*., **31** :231–235. https://doi.org/10.13005/ojc/31.Special-Issue1.28

Hapsari A, Asti D, Selviana, Hidayati R, Kumalla N and Suhendi A. 2016. The potency of Kitolod (*Isotoma longiflora* (L) Presl.) herb extract as a cure for cervical cancer an in vitro study of hela cells. Proceeding ISETH (International Conference on Science, Technology, and Humanity), Universitas Muhamadiyah Surakarta, Surakarta, Indonesia. pp.108–114.

IDF (International Diabetes Federation) 2021. Diabetes now affects one in 10 adults worldwide. https://www.idf.org/news/240:diabetes-now-affects-one-in-10-adults-worldwide.html

Islam N, Joo R, Hyun C, Jung A and Choi JS. 2016. Promising anti-diabetic potential of capillin and capillinol isolated from *Artemisia capillaris*. *Arch. Pharm. Res*., **39(3)**:340–349. https://doi.org/10.1007/s12272-016-0715-y

Jemaa HB, Jemia AB, Khlifi S, Halima BA, Fethi BS, Anis B, Elati J, and Aouidet A. 2017. Antioxidant activity and α-amylase inhibitory potential of *Rosa canina* L. *Afr. J. Tradit. Complement. Altern. Med*. **14(2)**:1–8. https://doi.org/ 10.21010/ajtcam.v14i2.1

Jiang S, Wang M, Jiang Z, Zafar S, Xie Q, Yang Y, Liu Y, Yuan H, Jian Y and Wang W. 2021. Chemistry and pharmacological activity of sesquiterpenoids from the *Chrysanthemum* Genus. *Molecules*. **26 (3038)**: 1–14. https://doi.org/ 10.3390/molecules26103038

Kaewseejan N and Siriamornpun S. 2015. Bioactive components and properties of ethanolic extract and its fractions from *Gynura procumbens* leaves. *Ind. Crops Prod*., **74**: 271–278. https://doi.org/10.1016/j.indcrop.2015.05.019

Liu X, Zhu L, Tan J, Zhou X, Xiao L, Yang X and Wang B. 2014. Glucosidase inhibitory activity and antioxidant activity of flavonoid compound and triterpenoid compound from *Agrimonia Pilosa* Ledeb. *BMC Complement Altern Med*., **14(12)**:1–10. https://doi.org/10.1186/1472-6882-14-12

Lin X, Xu Y, Pan X, Xu J, Ding Y, Sun X, Song X, Ren Y, and Shan PF. 2020. Global, regional, and national burden and trend of diabetes in 195 countries and territories: An analysis from 1990 to 2025. *Sci Rep*., **10(14790)**:1–11. 1.https://doi.org/10.1038/s41598-020-71908-9

Ma Q. 2014. Advances in mechanisms of anti-oxidation. *Discov Med*., **17(93)**:121–130.

Mahayasih PGMW, Elya B and Hanafi M. 2017. Alpha-glucosidase inhibitory activity of *Garcinia lateriflora* Blume leaves. *J. Appl. Pharm. Sci*., **7(10)**:100–104. https://doi.org/10.7324/JAPS.2017.71014

Makasana J, Dholakiya BZ, Gajbhiye NA and Raju S. 2017. Extractive determination of bioactive flavonoids from Butterfly Pea (*Clitoria ternatea* Linn.). *Rev. Chem. Intermed*., **43(2)**:783–799. https://doi.org/10.1007/s11164-016-2664-y

Mishra K, Ojha H and Chaudhury NK. 2012. Estimation of antiradical properties of antioxidants using DPPH assay: A critical review and results. *J.Food Chem*. **130(4)**:1036–1043. https://doi.org/10.1016/j.foodchem.2011.07.127

Ni YL, Shen HT, Su CH, Chen WY, Huang-Liu R, Chen CJ, Chen SP and Kuan YH. 2019. Nerolidol suppresses the inflammatory response during lipopolysaccharide-induced acute lung injury via the modulation of antioxidant enzymes and the AMPK/NRf-2/HO-1 pathway. *Oxid. Med. Cell. Longev*., **2019 (ID 9605980)**:1–10. https://doi.org/10.1155/2019/9605980

Noriega P, Guerrini A, Sacchetti G, Grandini A, Ankuash E and Manfredini S. 2019. Chemical composition and biological activity of five essential oils from the Ecuadorian Amazon rain forest. *Molecules*,**24(1637)**:1–12. https://doi.org/10.3390/molecules24081637

Oh JH, Kim J, Karadeniz F, Kim HR, Park SY, Seo Y, Kong C-S. 2021. Santamarine shows anti-photoaging properties via inhibition of MAPK/AP-1 and stimulation of TGF-β/Smad Signaling in UVA-IrradiatedHDFs.*Molecules.***26(3585)**:1–16. https://doi.org/10.3390/molecules26123585

Panigrahy SK, Bhatt R and Kumar A. 2020. Targeting type II diabetes with plant terpenes: The new and promising antidiabetic therapeutics.*Biologia*,**76(1)**:241–254. https://doi.org/10.2478/s11756-020-00575-y

Pichersky E and Raguso RA. 2016. Why do plants produce so many terpenoid compounds? New Phytol., **220**:692–702. https://doi.org/10.1111/nph.14178

Pingitore A, Lima GPP, Mastorci F, Quinones A, Iervasi G and Vassalle C. 2015. Exercise and oxidative stress: Potential effects of antioxidant dietary strategies in sports. Nutrition, **31(8)**: 916–922. https://doi.org/10.1016/j.nut.2015.02.005

Promprom W and Chatan W. 2017. GC-MS analysis and antioxidant activity of *Bauhinia nakhonphanomensis* leaf ethanolic extract. Pharmacogn. Mag., **9(5)**:663–667. https://doi.org/10.5530/pj.2017.5.105

Rufino AT, Ribeiro M, Sousa C, Judas F, Salgueiro L, Cavaleiro C and Mendes AF. 2015. Evaluation of the anti-inflammatory, anti-catabolic and pro-anabolic effects of E-caryophyllene, myrcene and limonene in a cell model of osteoarthritis. *Eur. J. Pharmacol.*, **750**:141–150. https://doi.org/10.1016/j.ejphar.2015.01.018

Salehi P, Asghari B, Esmaeili MA, Dehghan HIG. 2013. α-Glucosidase and α-amylase inhibitory effect and antioxidant activity of ten plant extracts traditionally used in Iran for diabetes. *J. Med. Plant Res*., **7(6)**:257–266. https://doi.org/DOI: 10.5897/JMPR11.1320

Sales PM, Souza PM, Simeoni LA, Magalhães PO and Silveira D. 2012. α-amylase inhibitors: A review of raw material and isolated compounds from plant source. *J. Pharm. Pharm. Sci*., **15(1)**:141–183. https://doi.org/10.18433/j35s3k

Salih EYA, Fyhrquist P, Abdalla AMA, Abdelgadir AY, Kanninen M, Sipi M, Luukkanen O, Fahmi MKM, Elamin MH and Ali HA. 2017. LC-MS/MS tandem mass spectrometry for analysis of phenolic compounds and pentacyclic triterpenes in antifungal extracts of *Terminalia brownii* (Fresen). *Antibiotics,* **6(4)**:1–18. https://doi.org/10.3390/antibiotics6040037

Sallau AB, Yakubu RN, Aliyu M, Salihu A, and Boniface BY. 2018. *In vitro* effect of terpenoids - rich extract of *Momordica charantia* on alpha glucosidase activity. *J. Vitae* **25(3):**148–153. http://dx.doi.org/10.17533/udea.vitae.v25n3a05

Setyobudi RH, Zalizar L, Wahono SK, Widodo W, Wahyudi A, Mel M, Prabowo B, Jani Y, Nugroho YA, Liwang T and Zaebudin A. 2019. Prospect of Fe non-heme on coffee flour made from solid coffee waste: Mini review. *IOP Conf. Ser. Earth Environ. Sci*., **293 (012035):**1–24. https://doi.org/10.1088/1755-1315/293/1/012035

Setyobudi RH, Yandri E, Nugroho YA, Susanti MS, Wahono SK, Widodo W, Zalizar L, Saati EA, Maftuchah M, Atoum MFM, Massadeh MI, Yono D, Mahaswa RK, Susanto H, Damat D, Roeswitawati D, Adinurani PG and Mindarti S. 2021. Assessment on coffee cherry flour of Mengani Arabica Coffee, Bali, Indonesia as iron non-heme source. *Sarhad J. Agric*., **37(Special issue 1)** : 171–183. https://dx.doi.org/10.17582/journal.sja/2022.37.s1.171.183

Setyobudi HS, Atoum MFM, Damat D, Yandri E, Nugroho YA, Susanti MS, Wahono SK, Widodo W, Zalizar L, Wahyudi A, Saati EA, Maftuchah M, Hussain Z, Yono D, Harsono SS, Mahaswa RK, Susanto H, Adinurani PA, Ekawati I, Fauzi A and Mindarti S. 2022. Evaluation of coffee pulp waste from coffee cultivation areas in Indonesia as iron booster. *Jordan J. Biol. Sci*., **15(3):**475– 488. https://doi.org/10.54319/jjbs/150318

Sies H. 2015. Oxidative stress: A concept in redox biology and medicine.*Redox.Biol*.,**4**:180–183. https://doi.org/10.1016/j.redox.2015.01.002

Su YC, Hsu KP, Wang EIC and Ho CL. 2015. Composition, in vitro cytotoxic, and antimicrobial activities of the flower essential oil of diospyros discolor from Taiwan. *Nat. Prod. Commun*., **10(7)**:1311–1314. https://doi.org/10.1177/1934578x1501000744

Vo KT, Ta QTH, Chu QT, Nguyen TT, and Vo VG. 2020. Anti-hepatocellular-cancer activity exerted by β-sitosterol and β-sitosterol-glucoside from *Indigo ferazollingeriana* Miq. *Molecules* **25(3021)**:1–14. https://doi.org/10.3390/molecules25133021

Wang CY, Chen YW and Hou, C. Y. (2019). Antioxidant and antibacterial activity of seven predominant terpenoids. *Int. J. Food Prop*., **22(1)**: 230–238. https://doi.org/10.1080/10942912.2019.1582541

Yu X, Zhang Y, Ma Y, Xu Z, Wang G and Xia L. 2013. Expression of an (E)-β-farnesene synthase gene from Asian peppermint in tobacco affected aphid infestation. *Crop J.,* **1(1)**:50–60. https://doi.org/10.1016/j.cj.2013.07.005

Subscription

Jordan Journal of Biological Sciences

An International Peer – Reviewed Research Journal

Published by the Deanship of Scientific Research, The Hashemite University, Zarqa, Jordan

Name: ..... الاسم:

Specialty: ..... التخصص:

Address: ..... العنوان:

P.O. Box: ..... صندوق البريد:

City &Postal Code:..... المدينة: الرمز البريدي:

Country: ..... الدولة:

Phone: ..... رقم الهاتف

Fax No.: ..... رقم الفاكس:

E-mail: ..... البريد الإلكتروني:

Method of payment: ..... طريقة الدفع:

Amount Enclosed: ..... المبلغ المرفق:

Signature: ..... التوقيع:

Cheque should be paid to Deanship of Research and Graduate Studies – The Hashemite University.

I would like to subscribe to the Journal

For

- ☐ One year
- ☐ Two years
- ☐ Three years

One Year Subscription Rates

	Inside Jordan	Outside Jordan
Individuals	JD10	$70
Students	JD5	$35
Institutions	JD 20	$90

Correspondence

Subscriptions and sales:

The Hashemite University
P.O. Box 330127-Zarqa 13115 – Jordan
Telephone: 00 962 5 3903333
Fax no. : 0096253903349
E. mail: jjbs@hu.edu.jo

المجلة الأردنية للعلوم الحياتية
Jordan Journal of Biological Sciences (JJBS)

http://jjbs.hu.edu.jo

المجلة الأردنية للعلوم الحياتية: مجلة علمية عالمية محكمة ومفهرسة ومصنفة، تصدرعن الجامعة الهاشمية وبدعم من صندوق دعم البحث العلمي والإبتكار – وزراة التعليم العالي والبحث العلمي.

ترسل البحوث الى العنوان التالي:

رئيس تحرير المجلة الأردنية للعلوم الحياتية
الجامعة الهاشمية
ص.ب , 330127 , الزرقاء, 13115 , الأردن
هاتف: 0096253903333
E-mail: jjbs@hu.edu.jo, Website: www.jjbs.hu.edu.jo

المملكة الأردنية الهاشمية

المجلة الأردنية

للعلوم الحياتية

مجلة علمية عالمية محكمة

تصدر بدعم من صندوق دعم البحث العلمي و الابتكار

http://jjbs.hu.edu.jo/